Hydrogeologic Controls on Bioactive Zone Development in Biostimulated Aquifers

by

Peter Curtis Schillig
B.S. (Dept. Hons), Ohio University, 2005
M.S. (Honors), University of Kansas, 2008

Submitted to the Department of Geology
and the Faculty of the Graduate School of The University of Kansas
in partial fulfillment of the requirements for the degree of
Doctor of Philosophy
2012

_____

Dr. J.F. Devlin, Chair

_____

Dr. Jennifer Roberts, Committee Member

_____

Dr. George Tsoflias, Committee Member

_____

Dr. Robert Goldstein, Committee Member

_____

Dr. Edward Peltier, Committee Member

_____

Dr. David Rudolph, Committee Member

Date Defended: ____9/27/2012_____

The Dissertation Committee for Peter Schillig certifies that this is the approved version of the following dissertation:

Hydrogeologic Controls on Bioactive Zone Development in Biostimulated Aquifers

_____

Dr. J.F. Devlin, Chair

_____

Dr. Jennifer Roberts, Committee Member

_____

Dr. George Tsoflias, Committee Member

_____

Dr. Robert Goldstein, Committee Member

_____

Dr. Edward Peltier, Committee Member

_____

Dr. David Rudolph, Committee Member

Date Approved: ___9/27/2012_____

Abstract

This study investigates the hydrogeological factors that control the feedback between bioactive zone formation and groundwater flow, as well as developing and assessing tools useful for making these investigations. The interaction between groundwater flow and bioactive zone development was investigated in both a subsurface biostimulation study and a laboratory experiments. Prior to the investigation, necessary advances were made in point velocity probe (PVP) technology to ensure successful observation in the field. Advances in these areas allowed for high resolution site characterization of an aquifer to undergo biostimulation for the removal of nitrate contamination. Heterotrophic denitrification was stimulated through daily pulses of acetate into the aquifer. With the onset of acetate delivery, decreases in groundwater velocity magnitude and flow redirection were correlated with permeable zones of relatively finer grain-size and poorer-sorting. In contrast, adjacent well-sorted and relatively coarse zones with initially high groundwater velocities indicated relatively little or no change in groundwater velocity after biostimulation. Superimposed onto these results, greater changes in groundwater velocity were noted where individual acetate pulses mixed through dispersive processes. In contrast, locations up-gradient of acetate pulse mixing indicated a higher variability in measured groundwater velocity. In total, changes in groundwater velocity in the biostimulated zone were in excess of those anticipated by analysis of the hydraulic gradient. Sediment-attached viable cell populations were interpreted to be partially responsible for the measured changes in velocity. Variables of grain-size and initial groundwater velocity were tested in controlled laboratory column experiments to evaluate the most favorable conditions for a bioactive zone to develop, subsequently leading to preferential bioclogging. Results from these experiments supported field observations that transition zones where relatively fine-grained, permeable sediments that lie adjacent to discontinuous coarser sediments - where the high velocities would lead to the highest flux of injected nutrients – represents the likely starting place for bioactive zone development, but may also be at greater risk for bioclogging. Further work was conducted to show that ground penetrating radar could noninvasively detect zones of relatively high bioactivity in granular material.

Acknowledgements

I am forever indebted to numerous individuals whose friendship and support were imperative to the completion of this work. Foremost, this dissertation may not have been possible without the love and support of my wife, Tricia. You've given so much to help see me through my graduate work that I cannot begin to express my gratitude. I look forward to the next stage of our lives together. To my family, I thank you for your understanding of the frequent sacrifices and absences I've made to complete this work. To my dogs, Cody and Belle: Thank you for always being there to lend a sympathetic, floppy ear. I owe you both a lifetime of pork chops and ice cream.

A very special "Thank you" is given to Julie Retrum whose mentorship and friendship has gotten me through many a trying time since we met in 2005. I have been extremely fortunate to have such a good friend and sincerely doubt that I could have finished my Ph.D. without her guidance.

I need to thank the faculty and staff of the KU Geology Dept. who've offered countless hours of help and advice (career, personal, and academic) over these years to ensure that I was on the right track to success. To use an African proverb, it truly "takes a village". To Rick Devlin, Jennifer Roberts, George Tsoflias, Bob Goldstein, and Ted Peltier: I thank you for all the time and effort in reviewing this document and agreeing to see me through this journey. I want to especially thank Rick Devlin, Jennifer Roberts, and George Tsoflias. Your countless hours of mentorship and friendship have been an invaluable hallmark of my time at Kansas. I cannot thank you enough for all that you have given me over these years. I sincerely hope our paths will cross again beyond our work together at KU. I look forward to hearing of your future successes.

I need to acknowledge University of Waterloo's Dave Rudolph for allowing me to work on the Woodstock site with your students. Woodstock has truly been a lesson in modesty and triumph and I appreciate the applied challenges it provided. I want to thank Jim Butler, Don Whittemore, Ed Reboulet, and Masato Ueshima from the Kansas Geological Survey for their expertise in various aspects of my projects.

Many hours of field work were required in this study. None of it would have been possible without Ian Bowen (Kansas), Kate Critchley (Waterloo), Jane Shaw (Waterloo), Bob Ingleton (Waterloo), and Paul Johnson (Waterloo). I want to also thank the many wonderful people at KU whom have been there for me over the years, through thick and thin: Brian Platt, Cori Myers, Wes Gapp, Erin Saupe, Karla Leslie, Paul Kenward, Ezra Kulczycki, Arne Sturm, Kevin Walter, Brian Gibson, Rubina Firdous, Angela Eichler, Huang Bei, Curtis Congreve, Brian Finley, Rob Moyle, and Hunter Harlow to name but a few. I also would be remiss if I didn't acknowledge my wonderful neighbors in De Soto, the Zahner family, who were there to provide a voice of reason over the years. I will greatly miss our fence-side beers.

Finally, I need to acknowledge the many funding sources that made this work possible. The professional development program and financial support from The Madison and Lila Self Graduate Fellowship has provided me with such unique and eye-opening experiences. I also thank the County of Oxford, Ontario, Canada for funding our field work at Woodstock. Additional financial support from The Geological Society of America, The University of Kansas Dept. of Geology, and Sigma Xi were instrumental to the successes of this project.

Contents

Abstract iii
Acknowledgements iv
Figures ix
Introduction 1
1.0: Bioactive Zone Development in Aquifer Remediation 1
1.1: Hypotheses for Establishing the Controls of Biogeochemical Hot Spot Formation 2
1.2: The Effects of Biological Activity on Flow in Porous Media 3
1.3: Modeling the Formation of Bioactive Zones 4
1.4: Denitrification and Biostimulation for In-Situ Denitrification 5
1.5: Outline of the Study 8
1.5.1: Statement of Goals and Objectives 8
1.5.2: Overview of the Dissertation 9
References 11
VelProbePE: An Automated Spreadsheet Program for Interpreting Point Velocity Probe Breakthrough Curves 17
2.0: Introduction 17
2.1 Method of Breakthrough Curve Interpretation and Velocity Vector Calculation 20
2.2: Set up and Data Importation 22
2.3: Calculating Apparent Velocities from Breakthrough Curves 25
2.4: Calculating the Direction and Magnitude of the Average Linear Groundwater Velocity Vector 27
2.5 Summary and Conclusions 29
References 30
Assessment of Density Induced Tracer Movement in Groundwater Velocity Measurements With Point Velocity Probes (PVPs) 44
3.0 Introduction 44
3.1: Theory 45
3.2: Methods 48
3.3: Results and Discussion 50
3.4: Designing PVP Tests 52
3.5: Conclusions 54
References 55

Assessment of Site Characterization with Direct Groundwater Velocity Measurements 63
4.0: Introduction 63
4.0.1 Challenges in Site Characterization 63
4.02: Estimating Groundwater Velocity with PVPs 66
4.03: Geological Setting 67
4.1 Methods 68
4.1.1 Determination of Hydraulic Conductivity 68
4.1.2: Determination of Hydraulic Gradient 68
4.1.3: PVP Installation 69
4.1.4 Tracer Tests 71
4.2: Results and Discussion 72
4.2.1 Hydraulic Conductivity Estimates 72
4.2.2: Hydraulic Gradient Estimate 73
4.2.3: Groundwater Velocities From Multilevel PVPs 1 and 2 and From The CIS Tracer Test 74
4.2.4: Groundwater Velocities from Multilevel PVPs 3, 4, and 5 74
4.3: Conclusions 77
References 78
Hydrological Factors Affecting the Bioclogging of a Heterogeneous Aquifer 89
5.0: Introduction 89
5.0.1 Site Description 91
5.0.2: Biostimulation at Woodstock 92
5.1: Methods 93
5.1.1: Determination of Hydraulic Gradient 93
5.1.2: Groundwater Velocities from PVPs 94
5.1.3: CIS Injections 96
5.1.4: Geochemical Sampling 98
5.1.5: Aqueous CO_2, N2O, and CH_4 Concentrations 99
5.1.6: Biomass Estimation 100
5.1.7: Numerical Modeling 101
5.2: Results and Discussion 102
5.2.1: Effect of Biostimulation on Flow Determined from Darcy's Law 102
5.2.2: Effects of Sediment Texture and Sorting on Changes in Velocity 103

5.2.3: Effects of Nutrient Pulsing on Changes in Velocity 105
5.2.4: Mechanism for Velocity Changes 108
5.3: Conclusions 111
References 113
Evaluation of groundwater velocity and grain-size for preferential clogging of porous media. 129
6.0: Introduction 129
6.1: Methods 131
6.1.1: Manifold Apparatus Construction 131
6.1.2: Sediment and Groundwater Preparation 132
6.1.3: Monitoring Hydraulic Response 134
6.1.4: Geochemistry 135
6.1.5: Total Lipid Biomass 137
6.2: Results and Discussion 138
6.2.1:The Effect of Velocity on Bioclogging 138
6.2.2: Grain-Size Experiments 139
6.2.3: Mechanism for Clogging 140
6.3: Summary and Implications 142
References 144
Ground Penetrating Radar Observations of Enhanced Biological Activity in a Sandbox Reactor 151
7.0: Introduction 151
7.1: Methods 154
7.1.1 Reactor Construction and Setup 154
7.1.2. Geochemical Sampling and Biomass Analysis 156
7.1.3: Ground Penetrating Radar Data Acquisition and Analysis 158
7.2 Results 160
7.2.1 Electrical Conductivity and pH 160
7.2.2 Changes in Daily Average GPR Two-way Travel Times and Maximum Amplitudes 161
7.2.3 Sediment Mineralogy 162
7.2.4 Changes in Total Lipid Biomass 163
7.2.5 Spatial Changes of GPR Arrival Times 163
7.3: Discussion 164

7.4: Conclusions and Implications 170
References 172
Conclusions and Recommendations 181
8.0: Conclusions 181
8.1: Recommendations 185
8.1.1: Additional Modeling 185
8.1.2: Improved PVP Design 187
*8.1.*3: *Available Organic Carbon Analysis* 188
8.1.4: Quantifying Extracellular Polysaccharides 188
8.1.5: Independent Confirmation of Secondary Mineral Formation 189
8.1.6: A Reductionist Experiment to Investigate the Relationship Between Biomass Growth and GPR Signal 189
8.1.7: Laboratory Examination of Transient Heterogeneity with the Biostimulation of Stratified Sediments 189
Appendices 191

Figures

Figure 2.01
A labeled profile schematic of a PVP and a plan-view of the PVP in a hypothetical flow field. 32
Figure 2.02
An example of a simplex movement across an RSS response surface for an equation of a line. 33
Figure 2.03
Screen-capture images of the welcoming screen (Top) and the file directory used to locate datalogger files for processing (bottom). 34
Figure 2.04
Screen capture of the user form that requires input of the PVP tracer launch times. 35
Figure 2.05
Screen capture of a spreadsheet with PVP detector data stored in columns A (Observed Time) and B (Observed Electrical Conductivity). A graph is automatically created showing the BTC. 36
Figure 2.06
Data adjustment user form to perform any of four different data adjustment operations. 37
Figure 2.07
An example of using the "Data Adjustment" user form's linear detrend operation on an example BTC. 38
Figure 2.08
Input box for tracer distance and "First Approximation" user form to input estimated tracer transport parameters and weighting preference. 39
Figure 2.09
Example of spreadsheet output. 40
Figure 2.10
Manual version of the "First Approximation" user form. 41
Figure 2.11
Analysis user form to assign optimized apparent velocities to a unique probe name and calculate the precise angle from the injection port to the detectors. 42
Figure 2.12
Screen capture of the "Results" worksheet that displays dispersivity, gamma (γ), and apparent velocity (v_{app}) for each worksheet used in the calculation of alpha (α) and average linear velocity (v_{∞}) for a given probe. 43
Figure 3.01
Schematic of a PVP shown in a porous medium with a saline tracer bead on the surface and hypothetical manometer. 57
Figure 3.02
NeST design for achieving horizontal flow in a gravel packed bin (inner bin 2). 58
Figure 3.03
Theoretical and experimental percent of vertical flow in the NeST experiments. 59
Figure 3.04
Relationship between mass of NaCl added to site groundwater in a PVP tracer and the magnitude of the imposed vertical flow as a function of the ambient horizontal flow gradient. 60

Figure 4.01
Location of the field site southwest of Woodstock, Ontario, Canada and locations of wells used for monitoring water-levels, multilevel PVPs, and multilevel sampling. 83
Figure 4.02
Water-table map using water-levels collected December, 2010, superimposed on geologic layers. 84
Figure 4.03
Schematic of three multilevel probes with detectors to the left of the injection port to monitor horizontal groundwater velocity and detectors above and below the injection port to ascertain vertical groundwater velocity. 85
Figure 4.04
Comparison of *K* profiles from slug testing and grain-size analyses and groundwater velocity magnitudes from multilevel PVPs 1 and 2 and those from the CIS. 86
Figure 4.05
Horizontal flow directions determine from all three-point estimators that satisfied the b:h and head-drop requirements and those from PVPs where $\alpha < 110°$. 87
Figure 4.06
Profiles of resultant groundwater velocity magnitudes plotted with elevation from multilevel PVPs 3, 4, and 5 and geologic layers. 88
Figure 5.01
Map of the field area depicting surficial geology with potentiometric surface and instrumentation immediately around the treatment area. 119
Figure 5.02
Cross section parallel to flow showing general hydrostratigraphy and the hydraulic window. 120
Figure 5.03
Transects indicating resultant PVP and CIS Tracer Testing velocity magnitude profiles for pre and post biostimulated conditions as well as their percent difference. 121
Figure 5.04
Compiled multilevel PVP horizontal and vertical flow directions for pre and post biostimulated datasets. 122
Figure 5.05
Transect showing significant changes from prebiostimulated conditions in the variance of both horizontal and vertical components of velocity magnitude from multilevel PVPs 3, 4, and 5. Transect indicating bromide mass profiles from tracer testing the CIS system at ML5 and ML7 for pre and post biostimulated conditions. 123
Figure 5.06
Bromide breakthrough curves on day 55 of biostimulation and projected 2 days into the future at ML5 and ML7. Breakthrough curves shown represent conditions from the well-sorted gravel in the high velocity zone (290.25 m) and the poorly-sorted sediments below it (288.50 m). 124
Figure 5.07
Concentration of DO and nitrate over the 55 days of biostimulation alongside fluctuations of nitrate on the final day of biostimulation. 125
Figure 5.08

A profile of zero-order denitrification rates for ML5 and ML7 plotted with interpreted denitrification zones similar to those described by Critchley 2010. 126
Figure 5.09
Total lipid biomass profiles taken for multilevel PVPs 3 and 4 before and after biostimulation. 127
Figure 6.01
Manifold apparatus with three columns used in the velocity and grain-size stages of the experiment. Each column was set to have either a unique velocity or grain-size. 147
Figure 6.02
Time lapse graphs indicating the response of the duplicate columns to the addition of growth nutrients..... 148
Figure 6.03
Changes in total head along the length of varying velocity columns at the beginning and end of biostimulation. 149
Figure 6.04
Changes in total head along the length of varying grain-size columns at the beginning and end of biostimulation. 150
Figure 7.01
Schematic of the flow-through tank, or sandbox, showing the GPR data acquisition grids along with the location of the injection wells and sampling ports..... 176
Figure 7.02
Comparison of up-gradient and down-gradient portions of the tank..... 177
Figure 7.03
Powder XRD patterns of sand used in the experiment. 178
Figure 7.04
Average biomass measured in the sand used in the experiment. 179
Figure 7.05
Side panel view of the sandbox showing spatial changes in two-way travel times..... 180

Tables

Table 3.1: Solution density estimation as a function of temperature. 61
Table 3.2: Deviations in PVP measured horizontal velocities from expected values as a function of NaCl tracer concentration. 62
Table 5.1: Saturation indicies for calcite and dissolved gasses (CO_2, N_2O, CH_4). 128

This Page Intentionally Left Blank

1

Introduction

1.0: Bioactive Zone Development in Aquifer Remediation

Biostimulation is an accepted approach to *in-situ* groundwater treatment. It involves the stimulation of bacteria through nutrient additions until the number of cells and associated bioactivity are sufficient to consume pollutants at a desired rate. The primary objective of this research is to identify and quantify the hydrogeological factors that foster microbial activity in aquifers receiving nutrient additions. Although bioremediation has been employed to treat a variety of pollutants over the past several decades, including petroleum hydrocarbons, chlorinated solvents, perchlorate, and nitrate (Alvarez and Illman 2006), the efforts are not always successful, in large part because of hydrogeological constraints (Kinzelbach and Schafer 1994). For example, it has been demonstrated in lab and numerical studies that enhanced microbial activity (cell and extracellular polysaccharide accumulation, gas production, and mineral precipitation) leads to the development of heterogeneities that affect flow, particularly by causing permeability reductions (Baveye et al. 1998; Seki et al. 2006; Thullner 2010) and flow redirection (Seki et al. 2006; Kildsgaard and Engesgaard 2002). Recently, field evidence for these effects was reported to cause flow redirection and transient heterogeneity (Schillig *et al*., 2011; Englert *et al*., 2009)

Despite recognition of the importance of hydrogeology in biostimulation programs, research in the field has been dominated by the microbiological aspects of the problem. There

has been surprisingly little systematic work done to elucidate the chief hydrogeological factors that influence, or perhaps control, biological treatment zones in aquifers. Flow and transport modeling has been used extensively to investigate ways of overcoming the constraints. However, the models in use tend to rely on existing knowledge and simplifying assumptions that need experimental verification.

1.1: Hypotheses for Establishing the Controls of Biogeochemical Hot Spot Formation

A logical conceptual model for bioactive zone development, is that it begins in localized patches, termed 'hot spots', and then spreads to form full treatment zones. In most cases where localized microbial growth is known to have occurred the availability of organic carbon was most commonly responsible for determining hot spot formation (McClain et al. 2003; Vidon and Hill 2004; Starr and Gillham 1993). Many aquifers are oligotrophic environments, and therefore low in organic carbon, which becomes rate limiting. In such cases, injections of soluble carbon in a biostimulation program can impose the carbon distribution in an aquifer, a distribution that can be engineered to be as uniform as possible. Thus, in this increasingly common scenario, the hot spots that initiate a treatment zone are unlikely to be carbon controlled. Instead, hydrogeologic factors may feature prominently because they determine the rate of carbon delivery to organisms, or offer the organisms some advantage as a surface on which to grow. In this work, carbon-stimulated bioactive zones were created in idealized laboratory experiments and in a non-ideal heterogeneous aquifer. Conventional hydrogeological methods and direct velocity measurements were used to assess locations in the porous media where bioactivity a) exerted an effect on the pollutant distribution, and b)

exerted an effect on the flow system. Experiments were performed to assess the relative importance of two hydrogeological variables hypothesized to be primary controls on where microbial growth would occur in an aquifer (i.e., control the locations of hot spots), 1) groundwater velocity and 2) grain-size. Second, it was hypothesized that hot spots alter flow patterns in a porous medium by redirecting flow away from pores where growth (or secondary effects of bioactivity such as gas formation and the formation of chemical precipitates). This may be an important link in gaining an understanding of how full bioactive treatment zones become established.

1.2: The Effects of Biological Activity on Flow in Porous Media

Hot spot occurrence is likely related to background, and later transient, variations in aquifer permeability. Geesey and Mitchell (2008) describe a conceptual feedback mechanism in which a high flow setting was associated with biological activity that subsequently caused flow impedance and redirection to secondary pathways. A similar feedback loop was proposed by Englert *et al.* (2009). Changes in permeability and flow direction, i.e., transient heterogeneity attributed in part to microbial activity, were observed by Schillig et al. (2011) in a controlled field study after biostimulation. A contributing cause of the transient heterogeneity was independently found to be the accumulation of microbial cells which appeared to have directly or indirectly lead to a partial clogging of the aquifer. Partial clogging and flow redirection have been reported in biostimulation laboratory tank experiments, however, local (i.e., point) changes in discharge, gradient, or hydraulic conductivity are difficult to estimate in such experiments, leaving the details of the associated hydrogeology (Kildsgaard and Engesgaard 2002; Seki et al. 2006). Previous bioclogging experiments using 1D columns allow for the

quantification of discharge, gradient, hydraulic conductivity, and solute transport parameters but inevitably result in nearly complete clogging since flow is maintained despite the development of potentially large backpressures; flow redirection is not possible (Seifert and Engesgaard 2007; Holm 2001; Taylor and Jaffe 1990; Baveye et al. 1998; Delozada et al. 1994; Vandevivere and Baveye 1992a, 1992b; Thullner 2010). Beyond the work of Schillig et al. (2011), relatively little work has been done to directly measure the effects of bioclogging in the field. Typical field studies have been limited to assessing bioclogging near well screens (McCarty et al. 1998; Oberdorfer and Peterson 1985). Field studies of bioclogging performed in open aquifers typically involve spatially averaged measurements dependent upon the uncertainties of hydraulic conductivity (Fleming et al. 1999), or they *infer* temporal changes in biomass based on tracer progress and reactive transport modeling (Li et al. 2010; Li et al. 2009; Englert et al. 2009). The introduction of the point velocity probe (PVP) has made more detailed, *in situ* bioclogging studies possible (Labaky et al., 2007; Schillig et al., 2011).

1.3: Modeling the Formation of Bioactive Zones

Biological clogging of porous media has been investigated with numerical simulations. In the majority of the models, microbial growth is triggered by the addition of substrate/nutrient loads, usually assuming a uniform biomass initially (Ham et al., 2007; Kildsgaard and Engesgaard 2001; Chen-Charpentier and Kojouharov 2001; MacDonald et al., 1999; Clement et al., 1996). However, a uniform biomass is an arbitrary condition chosen for modeling simplicity and due to a lack of data on which to base a nonuniform distribution. Initial biomass distributions have been demonstrated to impact the simulated rate and patterns of biological clogging (Brovelli et al., 2009), so the assumption of uniformity can result in misleading modeling outcomes.

Attempts have been made to model bioactive systems at the pore scale, sometimes referred to as the micro-scale. Some of these efforts suggest the possibility of a grain-size control on microbial colony development (Clement et al., 1996). Thullner et al. (2002), using a pore network model, came to a similar conclusion to that of Vandevivere et al. (1995), who reviewed experimental and modeled data to conclude that porous media with grain diameters less than 1 mm were preferentially associated with biomass growth in discrete colonies. In contrast, grains larger than 1 mm favored the development of more uniform biofilms. Not surprisingly, clogging of relatively small pore throats in aggregates was found to occur more quickly in microbial colony modeling by Dupin et al. (2001). Similarly, MacDonald et al., (1999) determined numerically that biofilm growth in coarse grained material was limited due to greater distances needed for mass transfer of dissolved nutrients. The degree of granular heterogeneity was also found to influence the extent of bioclogging. However, the modeling based research on bioclogging has not yet reached consensus. For example, early numerical experiments by Taylor et al. (1990) predicted that as an aquifer approaches homogeneity, a higher degree of permeability reduction is expected. In contrast, Thullner et al. (2002) found the opposite to be true. Ultimately, experimental work is needed to resolve these discrepancies and extend the comparisons to scales ranging from field sites to pore-scale studies. This thesis will focus on comparing the field and laboratory column scales.

1.4: Denitrification and Biostimulation for In-Situ Denitrification

Denitrification refers to the conversion of $NO_{3(aq)}^{-}$ to $N_{2(aq)}$. It occurs as the cumulative result of nitrate respiration, nitrite respiration combined with nitric oxide reduction, and nitrous oxide respiration carried out by autotrophic (Smith et al. 2001), chemolithotrophic

(Zumft 1997; Bohlke et al. 2002), and heterotrophic bacteria (Zumft 1997). The processes can be summarized through the following progression:

$$NO_3 \rightarrow NO_2 \rightarrow NO \rightarrow N_2O \rightarrow N_2$$

Bacteria that participate in the above processes, collectively referred to as denitrifiers, are nearly ubiquitous in aquifers, and were selected as subjects for this study in part due to their ability to transform nitrate to dinitrogen gas in the subsurface. They play an important role in environmental health since nitrate in drinking water has been linked to methemoglobinemia (blue baby syndrome) and the formation of nitrosamines in the body which are known to be carcinogenic, mutagenic, and teratogenic (Powlson et al. 2008). Another reason for selecting denitrifiers is that they are facultative anaerobes, i.e., they transform nitrate anaerobically but are able to survive in the presence of molecular oxygen. This characteristic simplifies experimental designs since a temporary compromise to the anaerobic conditions of an experiment will not be catastrophic.

Nitrate is one of the most common groundwater contaminants in the United States and Canada (Goss et al. 1998; Rudolph et al. 1998). There are several common point and non-point sources for nitrate contamination that are often attributed to agricultural fertilizers, human and animal wastes (Starr and Gillham 1993; Goss et al. 1998; Rudolph et al. 1998; McMahon et al. 2008), urea-based deicing agents (Tartakovsky et al. 2002), and the oxidation of naturally occurring ammonium (Hendry et al. 1984).

Nitrate can be removed from groundwater through a variety of processes such as incorporation into microbial biomass, the dissimilatory reduction of nitrate into ammonium, uptake by phreatophytes, and, as alluded to above, denitrification (Rivett et al. 2008). In

bioremediation programs, denitrification is the preferred method for nitrate removal through either autotrophic or heterotrophic means. While denitrification can be supported with ferrous iron as an electron donor (Devlin et al. 2000), these reactions are considered minor in comparison to those conducted by heterotrophic bacteria (Rivett et al. 2008).

In most aquifers adversely impacted by nitrate, oligotrophic conditions predominate and engineered denitrification must be stimulated by supplying a suitable amount of electron donor. Given the nonpoint source nature of most nitrate contamination, passive or semi passive remediation schemes may be preferred due to their overall lower cost compared to active methods such as pump-and-treat. Labile organic carbon delivered as either an injectable soluble compound or a cellulose matrix in a permeable reactive barrier (PRB) is the most common type of electron donor supplied for denitrification. PRBs have the advantage of being a nearly entirely passive technology once the barrier is in place. However, they are subject to failure if flow directions are not steady or if prevailing geochemical conditions cause clogging of the barrier material (Schipper et al. 2004; Robertson et al. 2005; van Driel et al. 2006; Gibert et al. 2008).

The injection of labile organic carbon into an aquifer may be a preferred way to foster denitrification where variable gradients or installation challenges would render a PRB unfavorable. Several means of accomplishing carbon injections have been described, including single well push-pull tests (Istok et al. 1997), dipole well injections (Wilson et al. 2006), re-circulation systems (Burbery and Wang 2010) and the cross-injection system (CIS) (Devlin and Barker, 1994; Gierczack et al. 2009). The latter method was adopted for this work and involves an injection-extraction well pair that injects organic carbon in discrete pulses that are pulled

transverse to the natural gradient. The discrete pulses establish a spatially continuous, carbon rich zone between the two wells that is allowed to migrate with ambient flow between pumping episodes. The pulses mix with the groundwater by dispersion, establishing an optimized treatment zone some small distance downstream of the injection-extraction wells. Pulsing of nutrients in this manner is done to maximize treatment, minimize pumping costs, and limit the potential of bioclogging near the well screens (Gierczak et al. 2007; Critchley 2010). Full-scale, multi-well injection-withdrawl systems have been employed to address municipal supply wells impacted with nitrate. For example, the Daisy Well System centers a series of carbon injection wells around a central municipal supply extraction well (Khan and Spalding 2004).

1.5: Outline of the Study

1.5.1: Statement of Goals and Objectives

This study expands the conceptual model of Geesey and Mitchell (2008) to include hydrogeological factors in the feedback between bioactive zone formation and groundwater flow. The notion of transient heterogeneity is introduced and investigated in a subsurface biostimulation context. Therefore, the first objective of this study is to evaluate the hydrogeological factors most important in determining the evolution and growth of a bioactive zone in an aquifer. A second objective is to quantify the changes in flow that develop in saturated granular media under both field and laboratory conditions following biostimulation. The second objective was partially addressed in an earlier field study involving a near homogeneous sand aquifer (Schillig et al. 2011), so a third objective was to document the feedback between bioactive zone development and flow in a heterogeneous aquifer. Finally, an

objective of this thesis is to introduce new tools suitable for investigating groundwater flow in saturated, transiently heterogeneous porous media.

1.5.2: Overview of the Dissertation

This thesis is presented in six chapters. Chapter 2 addresses the need for a standard processing protocol for interpreting data from point velocity probes (PVP), which were used extensively in the work. This chapter describes the development of an automated Visual Basic program that couples a nonlinear simplex optimizer, a 1D solution to the advection-dispersion equation, and PVP theory to interpret breakthrough curves generated by the PVPs.

Chapter 3 continues with tool development. PVPs operate on the basis of small-scale tracer tests on the probe surfaces. This chapter addresses the magnitude of density driven flow of the tracer used in PVP tests, provides a framework for correcting measurements affected by this process, and offers guidance for the selection of appropriate tracer salinities. Laboratory testing coupled with variable density fluid modeling evaluates saline tracer transport at the scale of the PVP measurement.

Chapter 4 applies PVPs to the characterization of a nitrate-contaminated municipal well field site near Woodstock, Ontario, Canada. This study compares PVP-derived groundwater velocities with velocities determined using more conventional techniques, in particular those based on head measurements from multiple wells, and Darcy's Law.

Chapter 5 utilizes groundwater velocities presented in Chapter 3 to design a CIS biostimulation system and interpret the results of a pilot scale trial. Particular attention was focused on documenting changes to the flow system and the distribution of denitrifying

bacteria. In addition, these changes were examined in relation to the local hydrostratigraphic setting.

Chapter 6 examines two hydrogeological factors considered to be of first importance in determining where bioactive zones may first become established: groundwater velocities and sediment grain size. This chapter describes laboratory experiments that systematically evaluate the hypothesis that there are optimal velocities and grain sizes that promote microbial growth, all other factors being equal.

Chapter 7 addresses the need to develop techniques of obtaining data that can fill in the blanks between point measurements with instruments like the PVPs. Specifically, a laboratory experiment is described in which GPR is used to identify zones of stimulated bioactivity.

References

Alvarez, P.J.J., and W.A. Illman. 2006. *Bioremediation and natural attenuation: process fundamentals and mathematical models*. Hoboken, N.J.: Wiley-Interscience. 609p.

Baveye, P., P. Vandevivere, B.L. Hoyle, P.C. DeLeo, and D.S. de Lozada. 1998. Environmental impact and mechanisms of the biological clogging of saturated soils and aquifer materials. *Critical Reviews in Environmental Science and Technology* 28 no. 2: 123-191.

Bekeris, L. 2007. Field-scale evaluation of enhanced agricultural management practices using a novel unsaturated zone nitrate mass load approach. M.Sc. Thesis,Department of Earth and Environmental Sciences, University of Waterloo, Waterloo, ON. 217 p.

Bohlke, J.K., R. Wanty, M. Tuttle, G. Delin, and M. Landon. 2002. Denitrification in the recharge area and discharge area of a transient agricultural nitrate plume in a glacial outwash sand aquifer, Minnesota. *Water Resources Research* 38 no. 7: 1105.

Brusseau, M.L., M.Q. Hu, J.M. Wang, and R.M. Maier. 1999. Biodegradation during contaminant transport in porous media. 2. The influence of physicochemical factors. *Environmental Science & Technology* 33 no. 1: 96-103.

Burbery, L.F., and F.L. Wang. 2010. A Re-Circulating Tracer Well Test method for measuring reaction rates in fast-flowing aquifers: Conceptual and mathematical model. *Journal of Hydrology* 382 no. 1-4: 163-173.

Chen-Charpentier, B.K., H.V. 2001. Modeling of subsurface biobarrier formation. *Journal of Hazardous Substance Research* 3: 1-14.

Clement, T.P., B.S. Hooker, and R.S. Skeen. 1996. Macroscopic models for predicting changes in saturated porous media properties caused by microbial growth. *Ground Water* 34 no. 5: 934-942.

Critchley, K. 2010. Stimulating In Situ Denitrification in an Aerobic, Highly Conductive Municipal Drinking Water Aquifer. M.Sc. Thesis,Department of Earth and Environmental Sciences, University of Waterloo, Waterloo, ON. 249 p.

Delozada, D.S., P. Vandevivere, P. Baveye, and S. Zinder. 1994. Decrease of the hydraulic conductivity of sand columns by Methanosarcina-barkeri. *World Journal of Microbiology & Biotechnology* 10 no. 3: 325-333.

Devlin, J.F. 1994. Enhanced in situ biodegradation of carbon tetrachloride and trichloroethene using a premeable wall injection system. Ph.D. Dissertation, Department of Earth and Environmental Sciences, University of Waterloo, Waterloo, ON. 633 p.

Devlin, J.F., R. Eedy, and B.J. Butler. 2000. The effects of electron donor and granular iron on nitrate transformation rates in sediments from a municipal water supply aquifer. *Journal of Contaminant Hydrology* 46 no. 1-2: 81-97.

Dupin, H.J., P.K. Kitanidis, and P.L. McCarty. 2001. Simulations of two-dimensional modeling of biomass aggregate growth in network models. *Water Resources Research* 37 no. 12: 2981-2994.

Englert, A., S.S. Hubbard, K.H. Williams, L. Li, and C.I. Steefel. 2009. Feedbacks Between Hydrological Heterogeneity and Bioremediation Induced Biogeochemical Transformations. *Environmental Science & Technology* 43 no. 14: 5197-5204.

Fleming, I.R., R.K. Rowe, and D.R. Cullimore. 1999. Field observations of clogging in a landfill leachate collection system. *Canadian Geotechnical Journal* 36 no. 4: 685-707.

Geesey, G.G., and A.C. Mitchell. 2008. Need of direct measurements of coupled microbiological and hydrological processes at different scales in porous media systems. *Journal of Hydrologic Engineering* 13 no. 1: 28-36.

Gierczak, R., J.F. Devlin, and D.L. Rudolph. 2007. Field test of a cross-injection scheme for stimulating in situ denitrification near a municipal water supply well. *Journal of Contaminant Hydrology* 89 no. 1-2: 48-70.

Gierczak, R.F.D., J.F. Devlin, and D.L. Rudolph. 2006. Combined use of field and laboratory testing to predict preferred flow paths in an heterogeneous aquifer. *Journal of Contaminant Hydrology* 82 no. 1-2: 75-98.

Gibert, O., S. Pomierny, I. Rowe, and R.M. Kalin. 2008. Selection of organic substrates as potential reactive materials for use in a denitrification permeable reactive barrier (PRB). *Bioresource Technology* 99 no. 16: 7587-7596.

Goss, M.J., D.A.J. Barry, and D.L. Rudolph. 1998. Contamination in Ontario farmstead domestic wells and its association with agriculture: 1. Results from drinking water wells. *Journal of Contaminant Hydrology* 32 no. 3-4: 267-293.

Ham, Y.J., S.B. Kim, and S.J. Park. 2007. Numerical experiments for bioclogging in porous media. *Environmental Technology* 28 no. 10: 1079-1089.

Hand, V.L., J.R. Lloyd, D.J. Vaughan, M.J. Wilkins, and S. Boult. 2008. Experimental studies of the influence of grain size, oxygen availability and organic carbon availability on bioclogging in porous media. *Environmental Science & Technology* 42 no. 5: 1485-1491.

Haslauer, C.P. 2005. Hydrogeologic analysis of a complex aquifer system and impacts of changes in agricultural practices on nitrate concentrations in a municipal well field, Woodstock, Ontario. M.Sc. Thesis, Department of Earth and Environmental Sciences, University of Waterloo, Waterloo, ON. 185 p.

Hendry, M.J., R.G.L. McCready, and W.D. Gould. 1984. Distribution, source and evolution of nitrate in a glacial till of southerm Alberta, Canada. *Journal of Hydrology* 70 no. 1-4: 177-198.

Holm, J. 2001. Effect of biomass growth on the hydrodynamic properties of groundwater aquifers. *Series Paper - Department of Hydrodynamics and Water Resources, Technical University of Denmark* 72.

Istok, J.D., M.D. Humphrey, M.H. Schroth, M.R. Hyman, and K.T. Oreilly. 1997. Single-well, ''push-pull'' test for in situ determination of microbial activities. *Ground Water* 35 no. 4: 619-631.

Istok, J.D., J.M. Senko, L.R. Krumholz, D. Watson, M.A. Bogle, A. Peacock, Y.J. Chang, and D.C. White. 2004. In situ bioreduction of technetium and uranium in a nitrate-contaminated aquifer. *Environmental Science & Technology* 38 no. 2: 468-475.

Khan, I.A., and R.F. Spalding. 2004. Enhanced in situ denitrification for a municipal well. *Water Research* 38 no. 14-15: 3382-3388.

Kildsgaard, J., and P. Engesgaard. 2001. Numerical analysis of biological clogging in two-dimensional sand box experiments. *Journal of Contaminant Hydrology* 50 no. 3-4: 261-285.

Kildsgaard, J., and P. Engesgaard. 2002. Tracer tests and image analysis of biological clogging in a two-dimensional sandbox experiment. *Ground Water Monitoring and Remediation* 22 no. 2: 60-67.

Kinzelbach, W., and W. Schafer. 1994. Modelling and design of in-situ bioremediation measures. In *Groundwater Quality Management* vol. 220, 399-412. Tallinn, Estonia: IAHS.

Labaky, W., J.F. Devlin, and R.W. Gillham. 2007. Probe for measuring ground water velocity at the centimeter scale. *Environmental Science & Technology* 41 no. 24: 8453-8458.

Levy, J., K. Sun, R.H. Findlay, F.T. Farruggia, J. Porter, K.L. Mumy, J. Tomaras, and A. Tomaras. 2007. Transport of Escherichia coli bacteria through laboratory columns of glacial-outwash sediments: Estimating model parameter values based on sediment characteristics. *Journal of Contaminant Hydrology* 89 no. 1-2: 71-106.

Li, L., C.I. Steefel, M.B. Kowalsky, A. Englert, and S.S. Hubbard. 2010. Effects of physical and geochemical heterogeneities on mineral transformation and biomass accumulation during biostimulation experiments at Rifle, Colorado. *Journal of Contaminant Hydrology* 112 no. 1-4: 45-63.

Li, L., C.I. Steefel, K.H. Williams, M.J. Wilkins, and S.S. Hubbard. 2009. Mineral Transformation and Biomass Accumulation Associated With Uranium Bioremediation at Rifle, Colorado. *Environmental Science & Technology* 43 no. 14: 5429-5435.

MacDonald, T.R., P.K. Kitanidis, P.L. McCarty, and P.V. Roberts. 1999. Mass-transfer limitations for macroscale bioremediation modeling and implications on aquifer clogging. *Ground Water* 37 no. 4: 523-531.

McCarty, P.L., M.N. Goltz, G.D. Hopkins, M.E. Dolan, J.P. Allan, B.T. Kawakami, and T.J. Carrothers. 1998. Full scale evaluation of in situ cometabolic degradation of trichloroethylene in groundwater through toluene injection. *Environmental Science & Technology* 32 no. 1: 88-100.

McClain, M.E., E.W. Boyer, C.L. Dent, S.E. Gergel, N.B. Grimm, P.M. Groffman, S.C. Hart, J.W. Harvey, C.A. Johnston, E. Mayorga, W.H. McDowell, and G. Pinay. 2003. Biogeochemical hot spots and hot moments at the interface of terrestrial and aquatic ecosystems. *Ecosystems* 6 no. 4: 301-312.

McGlashan, M.A., G.P. Tsoflias, P.C. Schillig, J.F. Devlin, and J.A. Roberts. 2012. Field GPR monitoring of biostimulation in saturated porous media. *Journal of Applied Geophysics* 78 no. 0: 102-112.

McMahon, P.B., J.K. Bohlke, L.J. Kauffman, K.L. Kipp, M.K. Landon, C.A. Crandall, K.R. Burow, and C.J. Brown. 2008. Source and transport controls on the movement of nitrate to public supply wells in selected principal aquifers of the United States. *Water Resources Research* 44 no. 4: 17.

Musslewhite, C.L., M.J. McInerney, H.L. Dong, T.C. Onstott, M. Green-Blum, D. Swift, S. Macnaughton, D.C. White, C. Murray, and Y.J. Chien. 2003. The factors controlling microbial distribution and activity in the shallow subsurface. *Geomicrobiology Journal* 20 no. 3: 245-261.

Musslewhite, C.L., D. Swift, J. Gilpen, and M.J. McInerney. 2007. Spatial variability of sulfate reduction in a shallow aquifer. *Environmental Microbiology* 9 no. 11: 2810-2819.

Oberdorfer, J.A., and F.L. Peterson. 1985. Watewater injection-Geochemical and biogeochemical clogging processes. *Ground Water* 23 no. 6: 753-761.

Powlson, D.S., T.M. Addisott, N. Benjamin, K.G. Cassman, T.M. de Kok, H. van Grinsven, J.L. L'hirondel, A.A. Avery, and C. van Kessel. 2008. When does nitrate become a risk for humans? *Journal of Environmental Quality* 37 no. 2: 291-295.

Rivett, M.O., S.R. Buss, P. Morgan, J.W.N. Smith, and C.D. Bemment. 2008. Nitrate attenuation in groundwater: A review of biogeochemical controlling processes. *Water Research* 42 no. 16: 4215-4232.

Robertson, W.D., N. Yeung, P.W. van Driel, and P.S. Lombard. 2005. High-permeability layers for remediation of ground water; Go wide, not deep. *Ground Water* 43 no. 4: 574-581.

Rudolph, D.L., D.A.J. Barry, and M.J. Goss. 1998. Contamination in Ontario farmstead domestic wells and its association with agriculture: 2. Results from multilevel monitoring well installations. *Journal of Contaminant Hydrology* 32 no. 3-4: 295-311.

Schillig, P.C., J.F. Devlin, J.A. Roberts, G.P. Tsoflias, and M.A. McGlashan. 2011. Transient Heterogeneity in an Aquifer Undergoing Bioremediation of Hydrocarbons. *Ground Water* 49 no. 2: 184-196.

Schipper, L.A., G.F. Barkle, J.C. Hadfield, M. Vojvodic-Vukovic, and C.P. Burgess. 2004. Hydraulic constraints on the performance of a groundwater denitrification wall for nitrate removal from shallow groundwater. *Journal of Contaminant Hydrology* 69 no. 3-4: 263-279.

Seifert, D., and P. Engesgaard. 2007. Use of tracer tests to investigate changes in flow and transport properties due to bioclogging of porous media. *Journal of Contaminant Hydrology* 93 no. 1-4: 58-71.

Seki, K., M. Thullner, J. Hanada, and T. Miyazaki. 2006. Moderate bioclogging leading to preferential flow paths in biobarriers. *Ground Water Monitoring and Remediation* 26 no. 3: 68-76.

Smith, R.L., D.N. Miller, M.H. Brooks, M.A. Widdowson, and M.W. Killingstad. 2001. In situ stimulation of groundwater denitrification with formate to remediate nitrate contamination. *Environmental Science & Technology* 35 no. 1: 196-203.

Starr, R.C., and R.W. Gillham. 1993. Denitrification and Organic-Carbon Availability in 2 Aquifers. *Ground Water* 31 no. 6: 934-947.

Tartakovsky, B., D. Millette, S. Delisle, and S.R. Guiot. 2002. Ethanol-stimulated bioremediation of nitrate-contaminated ground water. *Ground Water Monitoring and Remediation* 22 no. 1: 78-87.

Taylor, S.W., and P.R. Jaffe. 1990. Biofilm growth and the related changes in the physical properties of a porous medium. 1. Experimental investigations

Water Resources Research 26 no. 9: 2153-2159.

Taylor, S.W., P.C.D. Milly, and P.R. Jaffe. 1990. Biofilm growth and the related changes in the physical-properties of a porous medium. 2. Permeability. *Water Resources Research* 26 no. 9: 2161-2169.

Thullner, M. 2010. Comparison of bioclogging effects in saturated porous media within one- and two-dimensional flow systems. *Ecological Engineering* 36 no. 2: 176-196.

Thullner, M., J. Zeyer, and W. Kinzelbach. 2002. Influence of microbial growth on hydraulic properties of pore networks. *Transport in Porous Media* 49 no. 1: 99-122.

Vandevivere, P., and P. Baveye. 1992a. Effect of bacterial extracellular polymers on the saturated hydraulic conductivity of sand columns *Applied and Environmental Microbiology* 58 no. 5: 1690-1698.

Vandevivere, P., and P. Baveye. 1992b. Saturated hydraulic conductivity reduction caused by aerobic-bacteria in sand columns. *Soil Science Society of America Journal* 56 no. 1: 1-13.

van Driel, P.W., W.D. Robertson, and L.C. Merkley. 2006. Upflow reactors for riparian zone denitrification. *Journal of Environmental Quality* 35 no. 2: 412-420.

Vidon, P., and A.R. Hill. 2004. Denitrification and patterns of electron donors and acceptors in eight riparian zones with contrasting hydrogeology. *Biogeochemistry* 71 no. 2: 259-283.

Wilson, R., D. McKnight, D. Lerner, N. Thomson, S. Banwart, S. Thornton, and M. Mohamed. 2006. The dipole flow and reactive tracer test. In *Arid Land Hydrogeology: In Search of a Solution to a Threatened Resource*, 79-83. Taylor & Francis.

Zumft, W.G. 1997. Cell biology and molecular basis of denitrification. *Microbiology and Molecular Biology Reviews* 61 no. 4: 533-+.

2

VelProbePE: An Automated Spreadsheet Program for Interpreting Point Velocity Probe Breakthrough Curves

2.0: Introduction

Groundwater velocity is one of the most important parameters for assessing the fate and transport of solutes and contaminants (Ballard, 1996; Kearl, 1997; Labaky et al., 2007). Effective remediation strategies, particularly passive methods, require accurate estimates of groundwater velocity during aquifer characterization in order to anticipate contaminant pathways, loadings, and residence times in selected portions of aquifers (Schillig, 2008). Point velocity probes (PVPs) were recently developed to provide direct, centimeter-scale estimates of groundwater velocity by tracking the progression of a small, saline tracer along the cylindrical probe surface (Figure 2.01a). While other direct groundwater velocity techniques exist, PVPs are advantageous in that they are inexpensive to construct (Devlin et al., 2009), function without a well and therefore do not require an empirical calibration factor to correct for a converging flow field, and can resolve centimeter-scale velocity profiles (Labaky et al., 2007).

Recent studies with PVPs have demonstrated its usefulness in aquifer characterization. Labaky et al. (2009) compared the PVP with other established methods of flow characterization in a forced gradient field-experiment. Vertical profiles of groundwater velocity from the PVP compared well with those from the Geoflo® meter (Kerfoot and Massard 1985) and a large scale tracer test, and the velocity profile was qualitatively similar to the hydraulic conductivity profile determined by high resolution slug testing (Zemansky and McElwee, 2005; Labaky et al., 2009).

Point velocity probes were also used in laboratory tests to characterize solute velocity profiles across the water table and through the capillary fringe (Berg and Gillham, 2010). Velocity measurements using the PVP within the capillary fringe compared well to the expected values determined from the hydraulic gradient and unsaturated hydraulic conductivity values up to 75% of saturation (Berg and Gillham, 2010). Devlin et al. (2009) described in practical detail the construction of a multilevel array of PVPs to characterize flow in the cross-section in a sheet pile gate. By using a multilevel array of PVPs in a bioremediating portion of a well-sorted, fine sand aquifer, Schillig et al. (2011) observed time lapse changes in groundwater velocity direction and magnitude attributed to enhanced biological activity that lead to partial clogging of the aquifer. Point velocity probes outfitted with detectors to measure groundwater velocity in both the horizontal and vertical directions, accurately characterized a dipole flow field surrounding pumping and injection well screens (Bowen, 2010).

The algorithms used to analyze PVP data are based on idealized flow around a submerged circular cylinder (Bird et al., 1960). Briefly, the average linear velocity beyond the influence of the probe can be calculated from the measured apparent velocity of a small injected saline tracer (typically 0.01 - 0.5 mL in sandy aquifer material) along the circumference of a cylindrical probe (Figure 2.01b). Apparent horizontal velocities on the probe surface are converted to ambient velocity magnitude by fitting tracer breakthrough curves (BTCs) from the detectors. Direction of flow is also obtainable if two or more detectors are used (Figure 2.01a) (Berg and Gillham, 2010; Bowen, 2010; Devlin et al., 2009; Labaky et al., 2007, 2009; Schillig et al., 2011).

Analysis of the PVP BTCs was originally accomplished using the Fortran program PULSEPE, a parameter estimation code written by Devlin (1994), adapted from the SIMPLX Fortran code of Jurs (1986). During operation, PULSEPE required the user to manually import and edit BTCs in a spreadsheet then later generate input files to be read by the program. Once the input file was loaded into the program, an iterative process of estimating transport parameters, running the program, graphing the results from the output file, and evaluating the fit between observed and calculated data was required to obtain the best optimized transport parameters. If the user were required to analyze multiple BTCs, the above process, though accurate, was repetitive and time intensive, taking an experienced user approximately an hour to complete a pair of BTCs. Once satisfied with the parameter estimation of the BTC, additional calculations were necessary to convert the apparent velocities from PULSEPE to average linear velocity vectors using theory presented by Labaky et al. (2007).

With the continuing application of PVPs to investigate a variety of hydrogeological problems, a need exists to streamline the data processing procedures. The objectives of creating VelProbePE were to 1) customize and adapt the PULSEPE source code specifically for analyzing PVP BTCs using Visual Basic for Applications (VBA) in an Excel® spreadsheet environment; 2) provide subroutines that allowed the user to edit and detrend BTC data and graphically display the results; 3) incorporate theoretical equations necessary to convert apparent velocities measured at the probe surface to average linear ground water velocity directions and magnitudes beyond the influence of the probe. Data presented as examples in this manuscript were collected from PVPs installed in the well-studied Borden aquifer (Mackay

et al., 1986). Specific information regarding data acquisition, PVP construction, and geologic setting can be found in Devlin et al. (2009) and Schillig et al. (2011).

2.1 Method of Breakthrough Curve Interpretation and Velocity Vector Calculation

In order to calculate apparent groundwater velocities from PVP BTCs, VelProbePE uses a non-linear optimizer program adapted from Jurs (1986) and Devlin (1994) to fit a calculated transport equation to observed data by adjusting the value(s) of user defined parameters. The best fit is obtained by minimizing the residual sum of squares (RSS) between the observed and calculated data points,

$$RSS = \sum_{i=1}^{n} \left[y_i - f(x_i) \right]^2 \qquad [1]$$

where y_i is the ith observed relative conductance and $f(x_i)$ is the calculated relative electrical conductance from a 1-D solution to the advection-dispersion equation adapted from Devlin and Barker (1996):

$$C(x,t) = \frac{C_O}{2}\left[erfc \frac{x - w/(2R) - v_{app}t/R}{2(Dt/R)^{1/2}} - erfc \frac{x + w/(2R) - v_{app}t/R}{2\left[D\left(t - w/v_{app}\right)/R\right]^{1/2}} \right] \qquad [2]$$

where

$$D = v_{app}\alpha_L + D^* \qquad [3]$$

$C(x,t)$ is the solute relative conductance (V/L^3), C_O is the injection relative conductance (V/L^3), x is the distance from the injection port to the farthest wire on a given detector (L), w is the pulse-width of the tracer (L), v_{app} is the apparent velocity for the tracer at a given detector (L/T), t is time (T), R is the retardation factor (dimensionless), D is the hydrodynamic dispersion

coefficient (L^2/T), α_L is the dispersivity (L), and D^* is the effective diffusion coefficient of the tracer (L^2/T).

Simplex optimization works when a simplex, or geometric shape with N +1 verticies (N is the total number of variable parameters in Equation 2) is created on an RSS response surface. Initial estimates given to each parameter serve as the initial vertex values. The simplex moves on the RSS response surface by changing one of the values of the verticies at a time over several iterations until a sufficiently low RSS between the observed and calculated data are reached (Devlin, 1994; Jurs, 1986). Once a user determined, minimal RSS is reached (default = 0.0001 as ERRMIN variable in VelProbePE userforms 4 and 5 code), optimized parameter estimates are taken as the final vertex values. Figure 2.02 illustrates the manipulations of a two dimensional simplex searching for the global minimum RSS on the RSS response surface. Details of the code responsible for these manipulations are given in Jurs (1986) and Devlin (1994). As is the case for all nonlinear optimizers, it is imperative that good initial guesses are assigned to vertex (parameter) values so convergence occurs on the global RSS minima rather than a local RSS minima.

Using the apparent velocity from two horizontal flow detectors of the same tracer injection, the angle of the injection port to the flow direction (α) can be determined as follows (Labaky et al., 2007):

$$\alpha = \tan^{-1}\left[\frac{v_{app1}\gamma_1(\cos\gamma_2 - 1) + v_{app2}\gamma_2(1-\cos\gamma_1)}{v_{app1}\gamma_1\sin\gamma_2 - v_{app2}\gamma_2\sin\gamma_1}\right] \quad [4]$$

where v_{app1} and v_{app2} represent apparent velocities optimized from Equation 2 for the first and second detector, respectively. The fixed angles between the injection port and detectors 1 and 2 are γ_1 and γ_2, respectively. Radian values for γ_1 and γ_2 are determined by

$$\gamma = x/r \quad [5]$$

where γ represents the γ-angle of interest (either γ_1 or γ_2) and r is the radius taken from ½ the outer diameter of the probe casing. With v_{app} and γ known for a given detector and α known, the average linear groundwater velocity, beyond the influence of the probe (v_∞), can be calculated using Equation 6 below (Labaky et al., 2007):

$$v_\infty = \frac{v_{app}\,\gamma}{2(\cos\alpha - \cos(\alpha+\gamma))} \quad [6]$$

Where PVPs are designed with detectors oriented to measure flow in the vertical direction (d_3 and d_4 in Figure 2.01a), v_∞ is assumed to be equal to v_{app} from Equation 2 (taken directly from the optimizing step) since the tracer travels a straight vertical path on the probe casing to reach the detector. In situations where flow creates high amplitude BTCs on both vertical and horizontal detectors, the groundwater velocity vector should be calculated as the resultant vector using velocities from both vertical and horizontal detectors as respective components.

2.2: Set up and Data Importation

VelProbePE code is written in VBA and requires Microsoft® Excel® version 2003 or later. Installation is performed by simply moving the "VelProbePE" Excel® file to the user's hard drive. The current version of VelProbePE is configured to automate PVP BTC processing for data collected from a Campbell CR1000 datalogger where each electrical conductivity detector is wired in a half bridge configuration. Half bridge table definitions for the CR1000 are supplied in

the example CRBasic Code. This ensures that the acquired data from each half bridge (detector) will be correctly placed in predetermined cells within the workbook program. The program contains macros, therefore security settings within Excel® should be adjusted accordingly (with macros enabled).

Upon opening the VelProbePE workbook, the welcoming screen user form prompts the user to "Import External Data" where a file directory allows the user to select the target datalogger text file (DAT file) for processing (Figure 2.03). Once the desired datalogger file has been selected, VelProbePE will execute a macro that will open the text file in a new Excel® workbook, copy, paste, and auto format the data within the VelProbePE workbook. Once the data are successfully brought into VelProbePE, the user is prompted with a second user form to assign the date along with a designated name and launch time for up to 16 detectors (Figure 2.04). The program automatically calculates elapsed time for each BTC based on datalogger timestamps. The code then creates 16 additional spreadsheets, one for each detector. The observed data are converted from relative values of electrical resistivity to relative values of electrical conductivity and their respective BTCs are plotted within each spreadsheet (Figure 2.05).

The code next selects the first BTC on the datalogger and launches a mobile user form titled "Data Adjustment" (Figure 2.06). The advantage of a mobile user form is that the user has the capability to view and edit any data within the spreadsheet while the user form is open. "Data Adjustment" was designed to auto-calculate baseline adjustments on BTCs prior to analysis.

To begin editing data, the user simply switches the “Baseline Adjustment” radio button from the default of “No” to “Yes” at the top of the user form. This will automatically create a backup of the data from Rows A and B to Rows E and F in case the user wishes to undo the manual data adjustments at a later time. Additionally, switching the “Baseline Adjustment” radio button from “No” to “Yes” activates checkboxes for four optional data adjustment operations. The four operations can be executed any number of times on the same BTC. These operations include “Bulk Vertical Shift”, “Remove Unnecessary Initial Data”, “Remove Unnecessary Final Data”, and “Linear Detrend” (Figure 2.06). To select the next or previous worksheet within the workbook to continue data adjustment, the user may select the “Previous” or “Next” buttons at the bottom of the user form.

Selecting the check box beside “Bulk Vertical Shift” activates the adjacent textbox for data entry. The purpose of this function is to apply a constant vertical shift in relative electrical conductivity (hereafter, units reported as mV). The changes are made once the “Apply” button at the bottom of the user form is selected.

Sometimes data at the beginning or end of a BTC may contain undesired departures from the baseline, or extended times at the baseline. Such data are undesirable since they increase run times, or compromise the ability of the optimizer to accurately fit the BTC. To delete unnecessary initial or final data, select either “Remove Unnecessary Initial Data” or “Remove Unnecessary Final Data” checkboxes. By entering a given elapsed time (hr) in the “Remove Unnecessary Initial Data” textbox, the user can specify the last timestamp to be removed. Similarly, by entering a given elapsed time (hr) in the “Remove Unnecessary Final Data” textbox, the user is specifying the first timestamp (measured to the end of the data set)

to be removed. The changes are made once the “Apply” button at the bottom of the user form is selected.

A linear drift in the baseline can be removed with the “Linear Detrend” feature. To activate it, four adjacent textboxes labeled “X1”, “Y1”, “X2”, “Y2” are completed. The program then systematically subtracts from each data point, the Y value determined by a straight line connecting the two points (X1,Y1 and X2,Y2) (Figure 2.07). The changes are made once the “Apply” button near the bottom of the user form is selected.

2.3: Calculating Apparent Velocities from Breakthrough Curves

Once the user is satisfied with the data adjustments for all the BTCs in the spreadsheet, the “Run VelprobePE” button is selected on the “Data Adjustment” user form to launch the “First Approximation” user form (Figure 2.08). The “First Approximation” user form is designed to automatically optimize all BTCs in the workbook with the same initial parameters and provide the user with a first attempt to fit the BTCs. The “First Approximation” input screen allows the user to make initial guesses of the diffusion coefficient (cm^2/s), apparent groundwater velocity (cm/d), dispersivity (cm), pulse width (cm), retardation factor (DIM), and injection relative conductance (mV). Any parameter, with the exception of diffusion coefficient, can be held constant or varied. To hold a parameter value constant during optimization, the user simply selects the “Fix” check box next to the respective parameter textbox. By default, “Retardation Factor” is fixed since the tracer is assumed to be conservative. Weighting options are taken from PULSEPE and allow the user to select between “Relative”, “Bisquared”, or “No” weighting. The “No” weighting option simply fits the data as they appeared from the datalogger. The “Relative” weighting option calculates the residuals and then divides them by

their corresponding conductances so that large residuals on high conductance measurements receive the same proportionate weighting as lower residuals on low conductances. This option is appropriate for signals with relative error. The purpose of the "Bisquare" weighting is to give anomalous spikes in the observed data (locations of high RSS) less emphasis on the curve fitting process (Duggleby 1981). Once the "Run" button is selected, the initial guesses entered in the user form are applied to all BTCs in the workbook. The user is then prompted to enter the distance from the injection point to the detector. Clicking on the "OK" button then initiates the simplex optimizer routine for that spreadsheet. Once convergence is achieved, the optimizer proceeds to the next detector's spreadsheet and again prompts the user to enter the injector to detector distance. This process continues until all detector breakthrough curves have been fit with a calculated curve.

Once a BTC has been fitted with a calculated BTC, VelProbePE displays the following output data within the spreadsheet: observed data, calculated data, residuals, optimized parameter estimates, initial guesses of input parameters including velocity, RSS, which input parameters are fixed, 95% confidence intervals for optimized parameters, critical RSS value used in calculating the confidence intervals, and a graph illustrating the fit between the observed and calculated data (Figure 2.09). Unsatisfactory fits may occur, often as a result of improper guesses of initial parameters, and further optimization may be required. To facilitate this, VelprobePE automatically launches a manual version of the "First Approximation" user form after optimization, with an input screen that only applies changes to the active spreadsheet (Figure 2.10). Note that in this second dialogue box the "Distance from source" parameter is by default the distance entered by the user in the first dialogue box. However, the

distance from source can be edited if the adjacent radio button is selected to enable the textbox. Once the parameters are adjusted to better characterize the observed BTC, the "Run" button is selected, the changes are then applied with the optimizer routine, and optimization is attempted again. The user can apply changes in an iterative fashion until satisfied with the fit between the observed and calculated data. This process can be repeated any number of times for any BTC within the workbook. Once complete, the "Finished" button is selected to launch the "Analysis" user form needed to convert the apparent velocities from the optimizer stage to the average linear velocity (direction and magnitude) beyond the influence of the probe.

2.4: Calculating the Direction and Magnitude of the Average Linear Groundwater Velocity Vector

The "Analysis" user form, which is automatically launched once the "Finished" button is selected at the end of the optimization process, is designed to allow the user maximum flexibility in probe assignment, detector pairings (for flow orientation estimation), and apparent velocity selection within the 95% confidence range Eight text boxes allow the user to uniquely label the specific probe from which the apparent velocities were acquired. Underneath the heading "Select half bridge parings" are two list boxes per probe name. Each list box contains a dropdown menu for all the named worksheets in the workbook, i.e., for each detector from which a breakthrough curve was obtained (Figure 2.11). The user selects the worksheet that is named for the desired detector (i.e. half bridge), and the corresponding data are assigned to the v_{app1} and v_{app2} variables for use in Equation 4, the estimation of α. Following the selection of the desired detector pairings, the user is required to enter the probe outside diameter to ensure an exact angle is calculated between the injection port and the two detectors (γ_1 and γ_2)

by using Equation 5. This method of calculating γ_1 and γ_2 utilizes the "Distance to Source" variable from the optimization process and eliminates the need for a separate input of directly measured γ_1 and γ_2 which will vary as a result of individual probe construction.

On occasion, especially when BTC peaks exhibit relatively high dispersion, an optimized BTC will reach a peak earlier or later than the peak of the observed BTC. Radio buttons under the "Select Apparent Velocity" heading allow the user to choose the optimized, high, or low estimates within the calculated 95% confidence interval. The purpose of this option is to allow the user to manually select the estimate that best describes the apparent velocity as calculated by the optimizer. The default setting is "optimized". Once the preferred apparent velocity for an individual probe is selected, the apparent velocity value from each selected detector will be applied to Equation 6 to generate a corresponding v_∞ estimate. Thus, two v_∞ values are calculated for each probe.

When finished, the user selects "View Results" to see the output of the analysis. The user is prompted with a message box to either save the project under a unique name for archival purposes or to skip the save and proceed directly to the results. To continue to view the results, the user selects "OK". A new spreadsheet titled "Results" is created with the summary of the analysis (Figure 2.12). Results are organized according to the probe names and reported dispersivity for each detector, calculated γ_1 and γ_2 angles for each half bridge, the orientation of the probe in the flow field (α), apparent velocities for each detector, the v_∞ as calculated for each detector, and the percent difference between the two v_∞ values. For a successful calculation, the percent difference value should be low or near zero.

2.5 Summary and Conclusions

Point Velocity Probes are a recently developed aquifer characterization tool designed to provide direct measurements of centimeter-scale groundwater velocities. With this new technology, there was a need to develop software to streamline data processing. VelProbePE is a newly developed Visual Basic code imbedded in the Microsoft® Excel® environment. It is used specifically to process data collected from PVPs. The code is organized in modular userforms that automatically launch to guide the user through the data processing steps. VelProbePE organizes PVP data collected from a specific model and manufacturer of datalogger, but the code can be modified for other manufacturers or models. The data are imported to a single workbook that allows the user to edit/detrend BTCs on the fly with instant graphical updates. The program interprets BTCs using a simplex optimization process, which is among the most robust of the nonlinear optimizers. Since VelProbePE uses an adaptation of the simplex optimizer used in PULSEPE, the apparent velocity calculation is identical between the two programs. However, VelProbePE extends on PULSEPE by performing the additional calculations needed to relate apparent velocities from BTCs acquired at the probe surface to the average linear groundwater velocity direction and magnitude, beyond the influence of the probe.

References

Ballard, S., 1996. The In Situ Permeable Flow Sensor: A ground-water flow velocity meter. Ground Water 34, 231-240.

Berg, S.J., Gillham, R.W., 2010. Studies of water velocity in the capillary fringe: The Point Velocity Probe. Ground Water 48, 59-67.

Bird, W.E., Stewart, R.B., Lightfoot, E.N., 1960. Transport Phenomena. John Wiley & Sons, New York, 123-140 pp.

Bowen, I.R., 2010. Characterization of a dipole flow system using Point Velocity Probes. M.Sc Thesis. Department of Geology. University of Kansas, Lawrence, 102pp.

Devlin, J.F., 1994. A simple and powerful method of parameter-estimation using simplex optimization. Ground Water 32, 323-327.

Devlin, J.F., Barker, J.F., 1996. Field investigation of nutrient pulse mixing in an in situ biostimulation experiment. Water Resources Research 32, 2869-2877.

Devlin, J.F., Tsoflias, G., McGlashan, M., Schillig, P., 2009. An inexpensive multilevel array of sensors for direct ground water velocity measurement. Ground Water Monitoring and Remediation 29, 73-77.

Duggleby, R.G., 1981. A nonlinear regression program for small computers. Analytical Biochemistry 110, 9-18.

Jurs, P.C., 1986. Computer Software Applications in Chemistry. John Wiley & Sons, New York, 125-140 pp.

Kearl, P.M., 1997. Observations of particle movement in a monitoring well using the colloidal borescope. Journal of Hydrology 200, 323-344.

Kerfoot, W.B., Massard, V.A., 1985. Monitoring well screen influences on direct flowmeter measurements. Ground Water Monitoring & Remediation 5, 74-77.

Labaky, W., Devlin, J.F., Gillham, R.W., 2007. Probe for measuring ground water velocity at the centimeter scale. Environmental Science & Technology 41, 8453-8458.

Labaky, W., Devlin, J.F., Gillham, R.W., 2009. Field comparison of the point velocity probe with other groundwater velocity measurement methods. Water Resources Research 45 W00D30, 1-9. doi:10.1029/2008WR007066.

Mackay, D.M., Freyberg, D.L., Roberts, P.V. 1986. A natural gradient experiment on solute transport in a sand aquifer 1. approach and overview of plume movement. Water Resources Research 22, 2017-2029.

Schillig, P. C., 2008. Microbial activity during biodegradation and its effects on groundwater velocity in a contaminated aquifer. Department of Geology, University of Kansas, Lawrence, 225 pp.

Schillig, P.C., Devlin, J.F., Roberts, J.A., Tsoflias, G.P., McGlashan, M.A. 2011. Transient heterogeneity in an aquifer undergoing bioremediation of hydrocarbons. Ground Water 49, 184-196.

Zemansky, G.M., McElwee, C.D. 2005. High-resolution slug testing. Ground Water 43, 222-230.

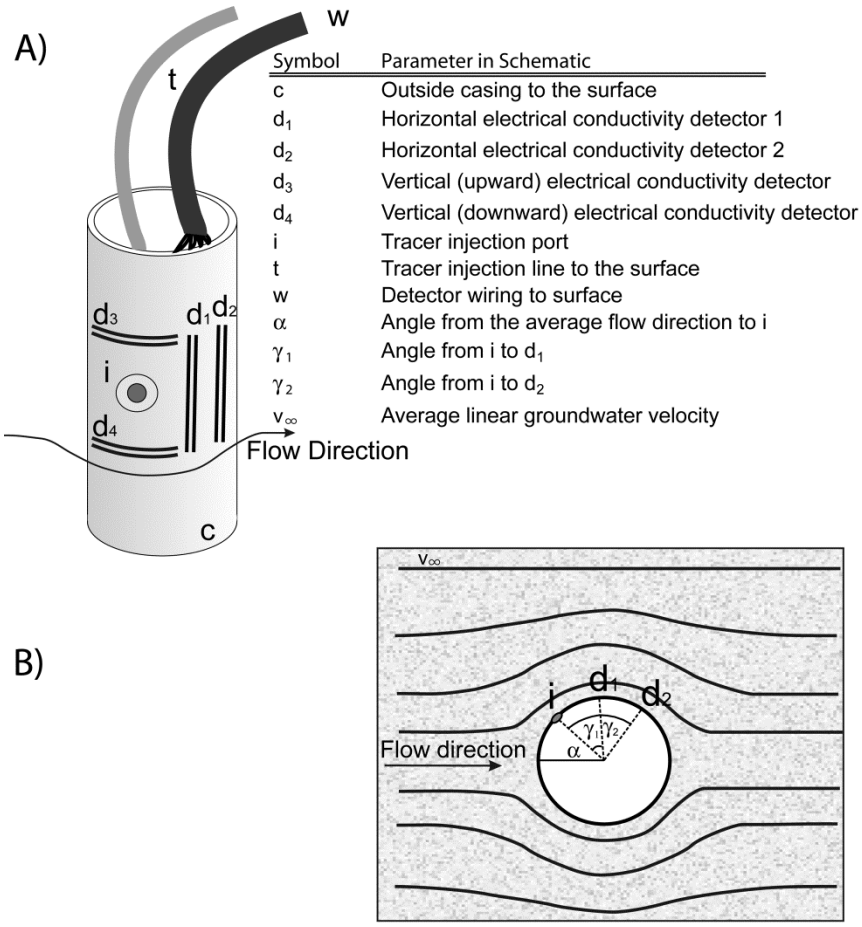

Symbol	Parameter in Schematic
c	Outside casing to the surface
d_1	Horizontal electrical conductivity detector 1
d_2	Horizontal electrical conductivity detector 2
d_3	Vertical (upward) electrical conductivity detector
d_4	Vertical (downward) electrical conductivity detector
i	Tracer injection port
t	Tracer injection line to the surface
w	Detector wiring to surface
α	Angle from the average flow direction to i
γ_1	Angle from i to d_1
γ_2	Angle from i to d_2
v_∞	Average linear groundwater velocity

Figure 2.01: A labeled profile schematic of a PVP and a plan-view of the PVP in a hypothetical flow field is shown in (B) where the detection of a single tracer on both d_1 and d_2 are required to determine α (Modified from Labaky et al., 2007).

.

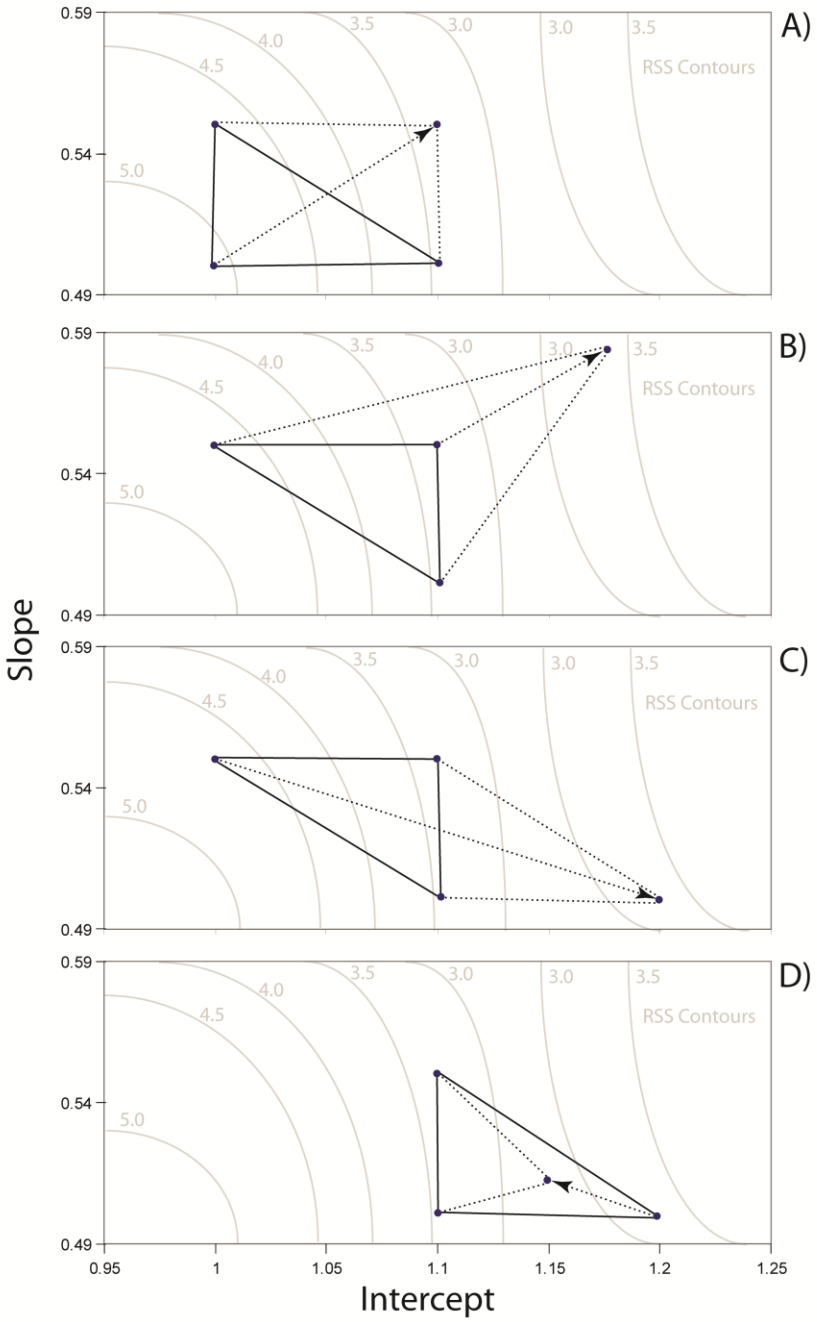

Figure 2.02: An example of a simplex movement across an RSS response surface for an equation of a line (values for slope and intercept to be determine- requires three verticies). The simplex can move across the surface by reflection (A and C), extension (B), and retraction (D) of the highest RSS vertex.

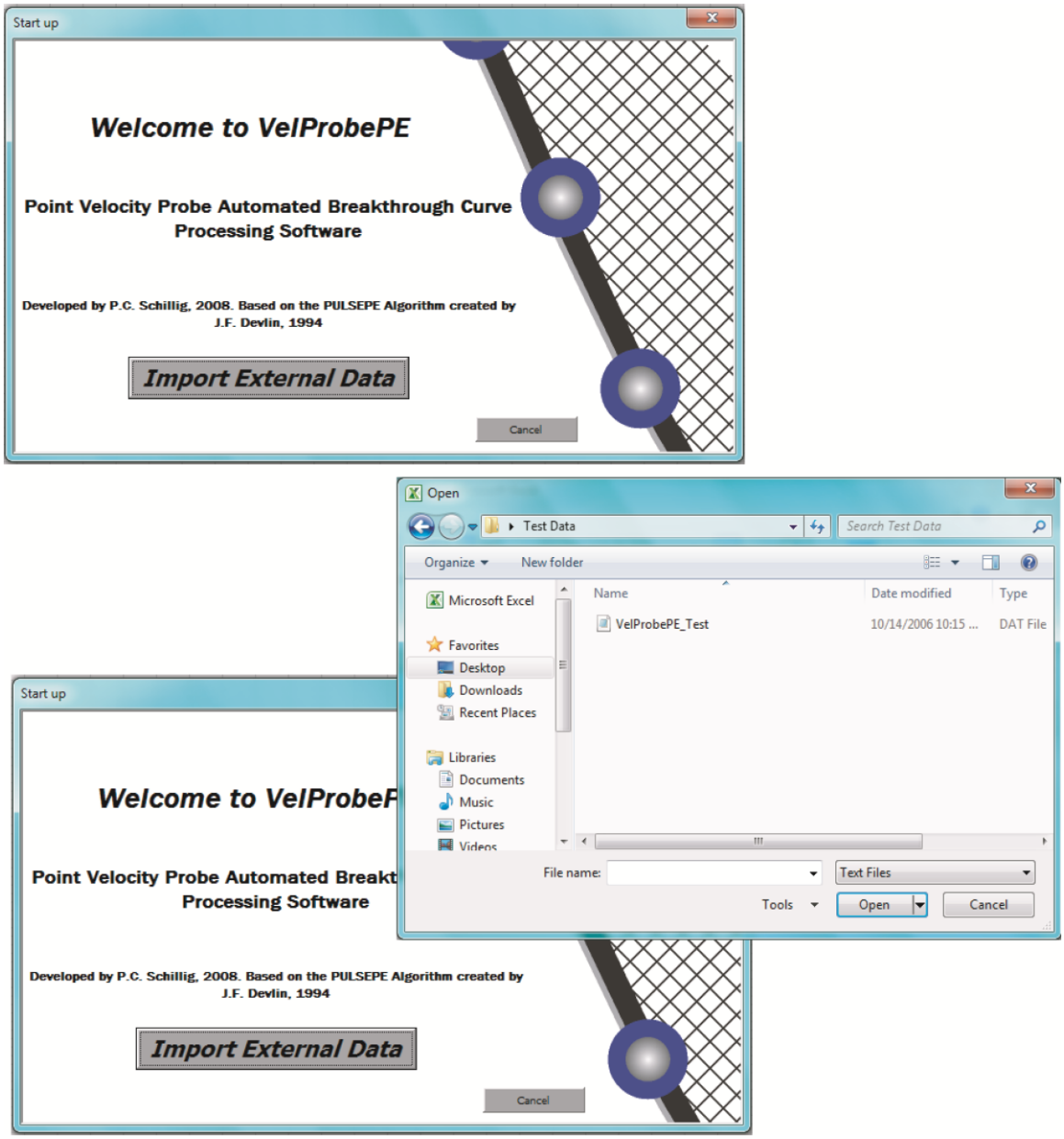

Figure 2.03: Screen-capture images of the welcoming screen (Top) and the file directory used to locate datalogger files for processing (bottom).

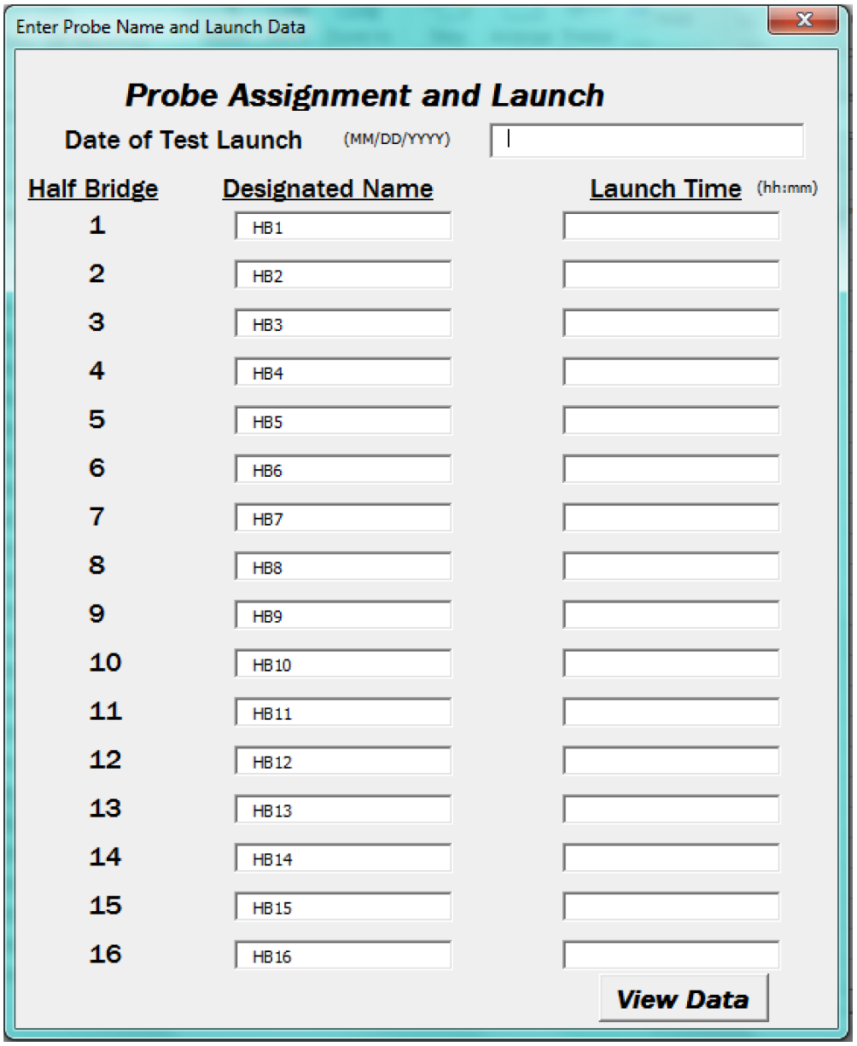

Figure 2.04: Screen capture of the user form that requires input of the PVP tracer launch times. This user form will separate and graph up to 16 PVP detectors into individual spreadsheets. Note that each half bridge circuit at the datalogger corresponds to a separate detector on the probe surface.

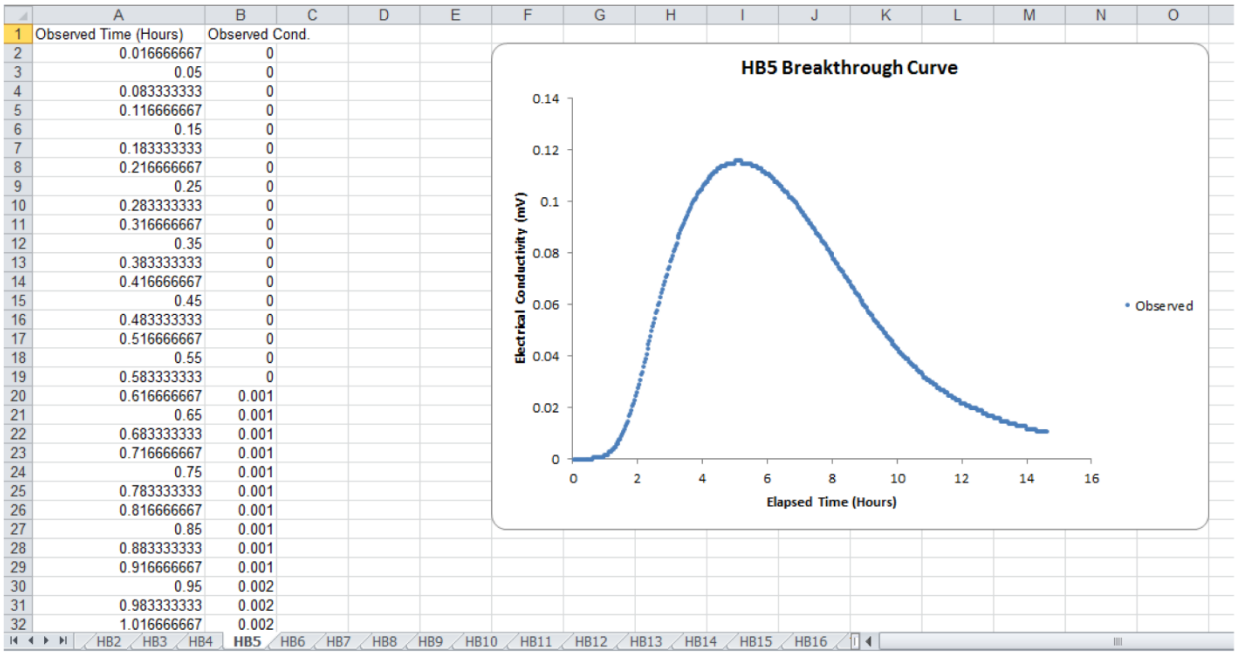

	A	B
1	Observed Time (Hours)	Observed Cond.
2	0.016666667	0
3	0.05	0
4	0.083333333	0
5	0.116666667	0
6	0.15	0
7	0.183333333	0
8	0.216666667	0
9	0.25	0
10	0.283333333	0
11	0.316666667	0
12	0.35	0
13	0.383333333	0
14	0.416666667	0
15	0.45	0
16	0.483333333	0
17	0.516666667	0
18	0.55	0
19	0.583333333	0
20	0.616666667	0.001
21	0.65	0.001
22	0.683333333	0.001
23	0.716666667	0.001
24	0.75	0.001
25	0.783333333	0.001
26	0.816666667	0.001
27	0.85	0.001
28	0.883333333	0.001
29	0.916666667	0.001
30	0.95	0.002
31	0.983333333	0.002
32	1.016666667	0.002

HB2 HB3 HB4 **HB5** HB6 HB7 HB8 HB9 HB10 HB11 HB12 HB13 HB14 HB15 HB16

Figure 2.05: Screen capture of a spreadsheet with PVP detector data stored in columns A (Observed Time) and B (Observed Electrical Conductivity). A graph is automatically created showing the BTC.

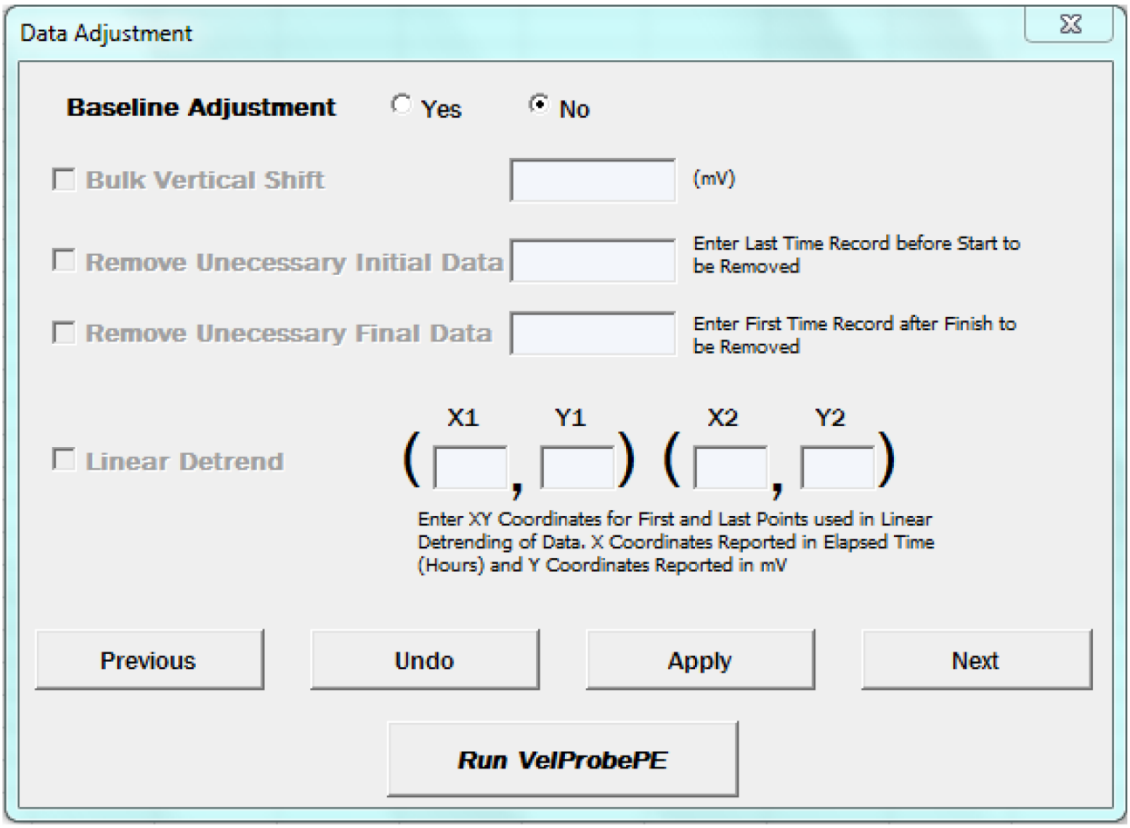

Figure 2.06: Data adjustment user form to perform any of four different data adjustment operations (bulk vertical shift, removal of unnecessary initial data, removal of unnecessary final data, and linear detrend) prior to the optimization process. The user form is also used to navigate through spreadsheets in the workbook as well as undo unfavorable data adjustments.

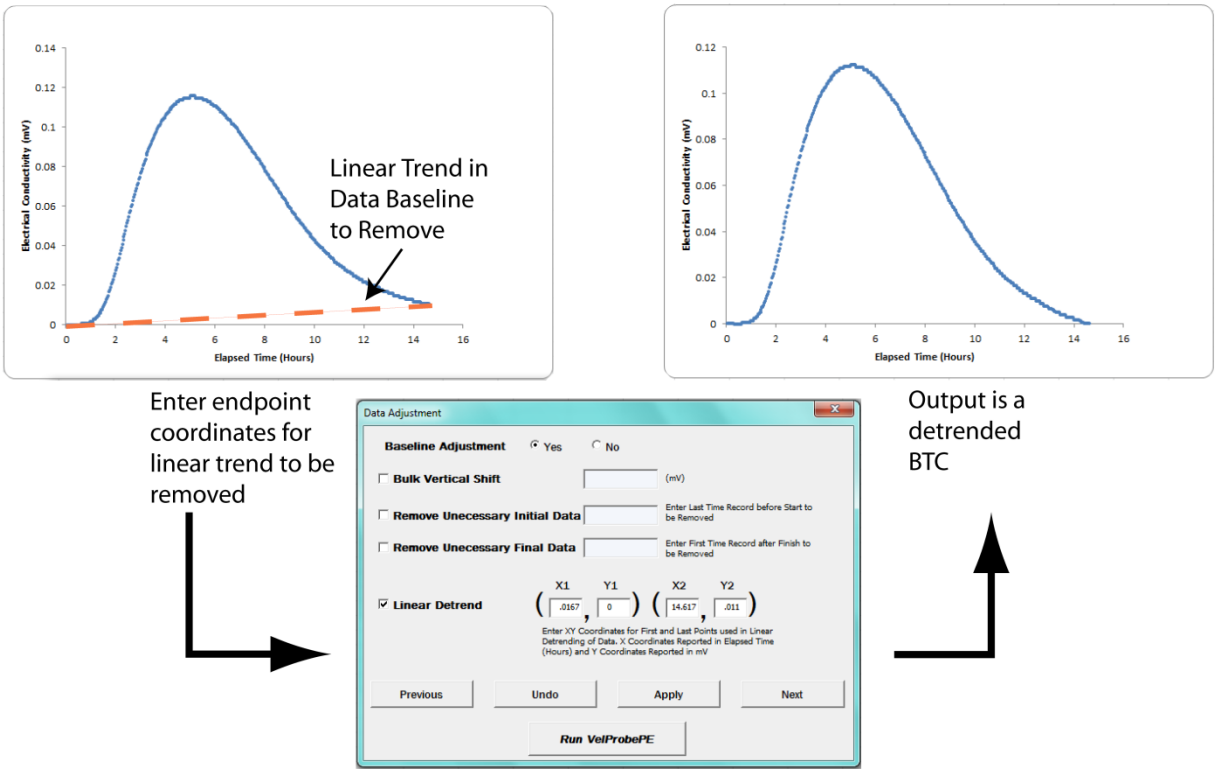

Figure 2.07: An example of using the "Data Adjustment" user form's linear detrend operation on an example BTC.

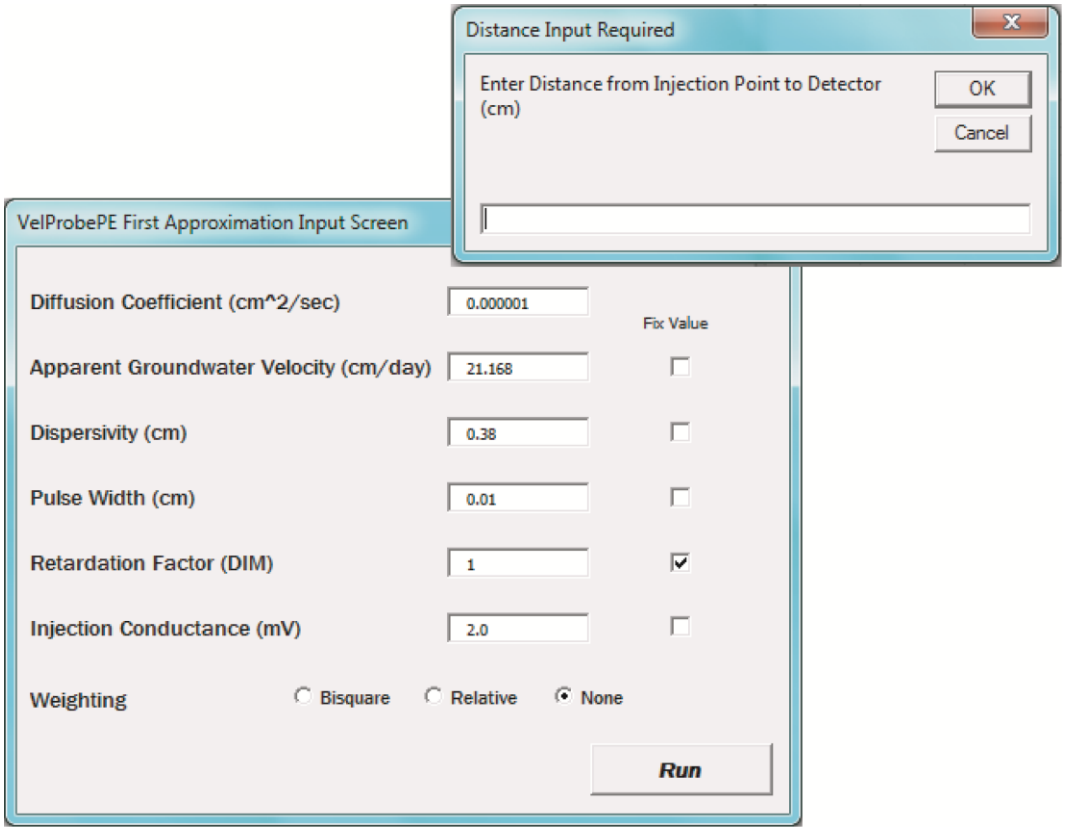

Figure 2.08: Input box for tracer distance and "First Approximation" user form to input estimated tracer transport parameters and weighting preference.

Observed Time (Hours)	Observed Cond.	Calculated Cond	Residuals
0.61666667	0.0002	9.4786E-13	0.0002
0.65	0.00019481	4.876E-12	0.00019481
0.68333333	0.00018961	2.1236E-11	0.00018961
0.71666667	0.00018442	8.0158E-11	0.00018442
0.75	0.00017922	2.6733E-10	0.00017922
0.78333333	0.00017403	8.0041E-10	0.00017403
0.81666667	0.00016883	2.1806E-09	0.00016883
0.85	0.00016364	5.4663E-09	0.00016363
0.88333333	0.00015844	1.2731E-08	0.00015843
0.91666667	0.00015325	2.7771E-08	0.00015322
0.95	0.00014805	5.7139E-08	0.00014799
0.98333333	0.00014286	1.1156E-07	0.00014275
1.01666667	0.00013766	2.078E-07	0.00013745
1.05	0.00013247	3.7092E-07	0.0001321
1.08333333	0.00012727	6.3703E-07	0.00012664
1.11666667	0.00012208	1.0564E-06	0.00012102
1.15	0.00011688	1.6968E-06	0.00011519
1.18333333	0.00011169	2.647E-06	0.00010904
1.21666667	0.00010649	4.0204E-06	0.00010247
1.25	0.0001013	5.9584E-06	9.534E-05
1.28333333	9.6104E-05	8.6335E-06	8.747E-05
1.31666667	0.00109091	1.2252E-05	0.00107866
1.35	0.00108571	1.7055E-05	0.00106866
1.38333333	0.00108052	2.3321E-05	0.0010572
1.41666667	0.00107532	3.1366E-05	0.00104396
1.45	0.00107013	4.1544E-05	0.00102859
1.48333333	0.00106494	5.4242E-05	0.00101069
1.51666667	0.00105974	6.9883E-05	0.00098986
1.55	0.00105455	8.8918E-05	0.00096563
1.58333333	0.00104935	0.00011183	0.00093752
1.61666667	0.00104416	0.00013911	0.00090504
1.65	0.00103896	0.00017129	0.00086767
1.68333333	0.00203377	0.0002089	0.00182487
1.71666667	0.00202857	0.00025247	0.0017761
1.75	0.00202338	0.00030254	0.00172083
1.78333333	0.00201818	0.00035965	0.00165853
1.81666667	0.00201299	0.00042432	0.00158867
1.85	0.00200779	0.00049705	0.00151075
1.88333333	0.0020026	0.00057832	0.00142428
1.91666667	0.0019974	0.0006686	0.0013288
1.95	0.00199221	0.0007683	0.00122391
1.98333333	0.00298701	0.00087782	0.0021092
2.01666667	0.00298182	0.00099749	0.00198433
2.05	0.00297662	0.00112763	0.00184899
2.08333333	0.00297143	0.0012685	0.00170293
2.11666667	0.00296623	0.0014203	0.00154594
2.15	0.00296104	0.00158319	0.00137785
2.18333333	0.00295584	0.00175729	0.00119856
2.21666667	0.00395065	0.00194265	0.002008
2.25	0.00394545	0.00213929	0.00180617
2.28333333	0.00394026	0.00234715	0.00159311
2.31666667	0.00393506	0.00256616	0.00136891
2.35	0.00392987	0.00279616	0.00113371
2.38333333	0.00392468	0.00303697	0.00088771
2.41666667	0.00491948	0.00328835	0.00163113
2.45	0.00491429	0.00355003	0.00136425
2.48333333	0.00490909	0.0038217	0.00108739
2.51666667	0.0049039	0.00410299	0.0008009
2.55	0.0048987	0.00439352	0.00050518

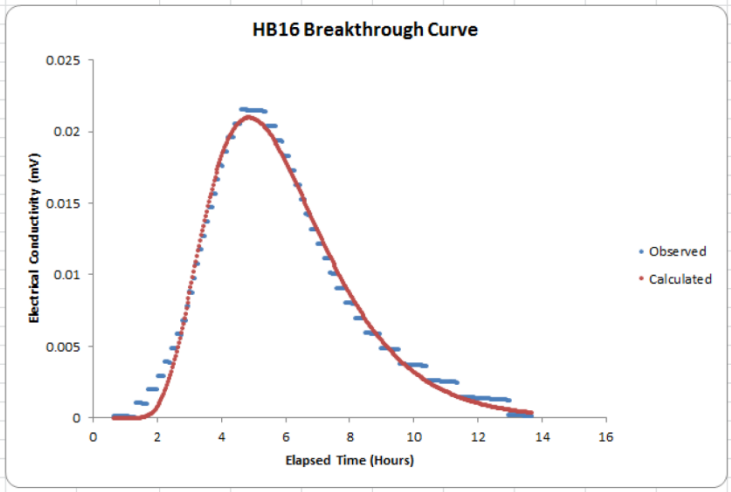

OPTIMIZED PARAMETER ESTIMATES

VELOCITY(cm/d)		13.11873	
DISPERSIVITY (cm)		0.203654	
PULSE WIDTH (cm)		0.015542	
RF		1	
Co (mV)		3.574597	
RESDIUAL SUM OF SQUARES =		0.000185	
INITIAL GUESSES AND INPUT OF PARAMETERS			
			FIX
VELOCITY(cm/d)		5	
DISPERSIVITY (cm)		0.38	
PULSE WIDTH (cm)		0.01	
RF		1	Y
Co (mV)		2	
DISTANCE FROM SOURCE (cm)		3.05	Y
DIFFUSION COEFF (cm^2/sec)		0.000001	Y
95% CONFIDENCE INTERVALS FOR ESTIMATED PARAMETERS			
Parameter	Low	Optimized	High
VELOCITY(cm/d)	13.11873	13.11873	13.11873
DISPERSIVITY(cm)	0.197545	0.203654	0.209764
PULSE WIDTH (cm)	0.015387	0.015542	0.015698
Co(mV)	3.538851	3.574597	3.610343
CRITICAL RSS VALUE =		0.000192	

Figure 2.09: Example of spreadsheet output containing observed data, calculated fit data from simplex optimization, input estimates, optimized estimates, graph of observed (blue series) and calculated data (red series), and 95% confidence intervals for estimated parameters.

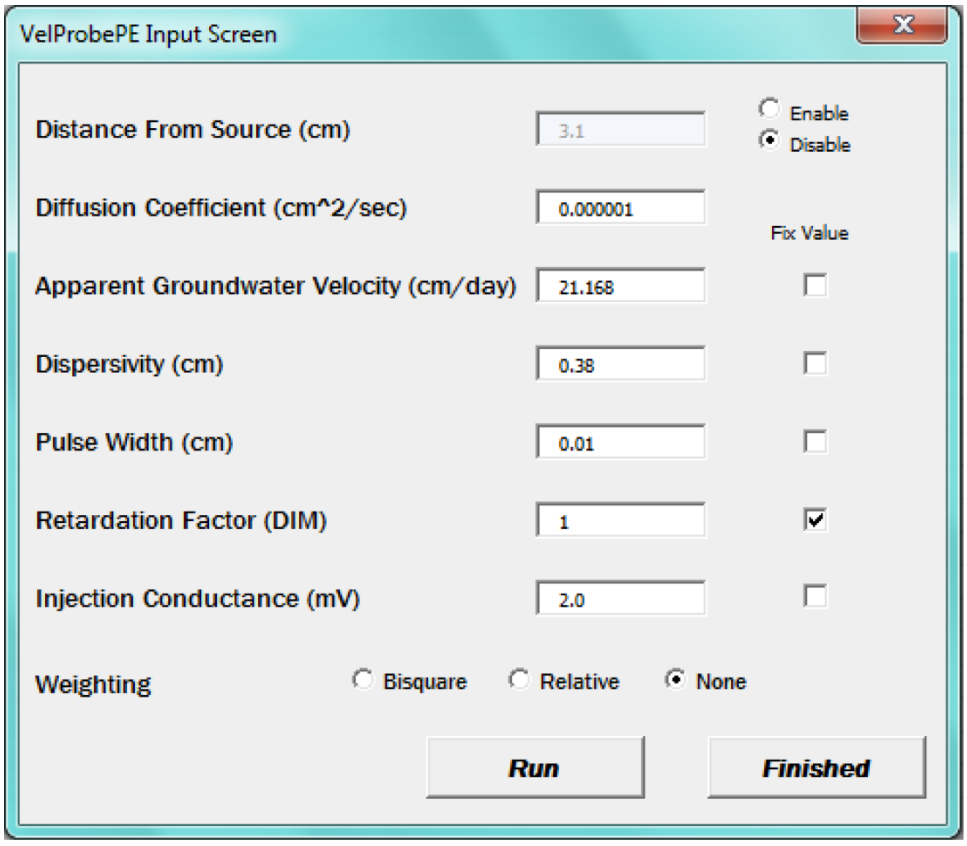

Figure 2.10: Manual version of the “First Approximation” user form to fine tune optimization if necessary. Distance from source is assumed the same from the First Approximation process and its input box is inactive by default.

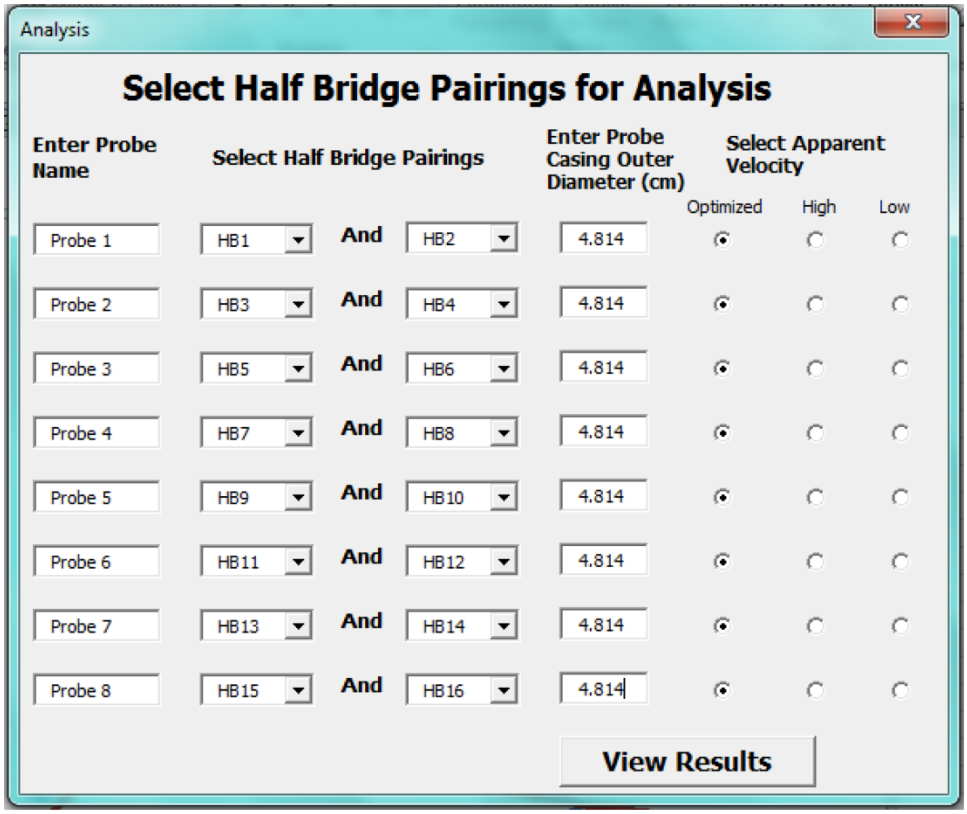

Figure 2.11: Analysis user form to assign optimized apparent velocities to a unique probe name and calculate the precise angle from the injection port to the detectors. Option radio buttons are designed to allow the user to select which apparent velocity to use for analysis in the 95% confidence interval.

Probe Name	Dispersivity 1 (cm)	Dispersivity 2 (cm)	Gamma 1 (Degrees)	Gamma 2 (Degrees)	Alpha (Degrees)	Apparent Velocity 1 (cm/d)	Apparent Velocity 2 (cm/d)	Average Linear Velocity 1 (cm/d)	Average Linear Velocity 2 (cm/d)	Percent Difference
Probe 1	0.354112965	0.219636239	47.61661	72.6153304	28.2685286	6.637877	7.310249	4.331485	4.331485	0
Probe 2	0.299141496	0.180390296	44.045364	69.0440846	41.0745353	4.977604	5.212706	2.861036	2.861036	1.1641E-14
Probe 3	0.272840329	0.205402534	46.426195	73.8057457	74.2404846	7.982352	7.196031	4.137234	4.137234	1.0734E-14
Probe 4	0.272516079	0.278299308	49.997441	74.9961609	94.0979787	9.690439	7.964259	5.723596	5.722473	0.00490542
Probe 5	0.37278355	0.274885912	46.426195	71.4249152	26.7696957	6.283344	7.0045	4.217145	4.217145	5.2653E-15
Probe 6	0.268826096	0.199628467	46.426195	71.4249152	35.6651208	8.169407	8.705651	4.905056	4.905056	0
Probe 7	0.239738792	0.162017461	46.426195	71.4249152	46.4497466	8.029162	8.166322	4.401211	4.401211	0
Probe 8	0.317118902	0.211218007	47.61661	72.6153304	22.6848394	11.5332	13.1097	8.185328	8.185328	5.4254E-15

Figure 2.12: Screen capture of the "Results" worksheet that displays dispersivity, gamma (γ), and apparent velocity (v_{app}) for each worksheet used in the calculation of alpha (α) and average linear velocity (v_{∞}) for a given probe. Percent difference between average linear velocity values is also reported.

3

Assessment of Density Induced Tracer Movement in Groundwater Velocity Measurements With Point Velocity Probes (PVPs)

3.0 Introduction

Recently, point velocity probes (PVPs) have been used to characterize groundwater velocities in aquifers composed of sand or sand and gravel (Labaky et al. 2007; Labaky et al. 2009; Berg et al. 2010; Schillig et al. 2011; Devlin et al. 2012). The PVP operates by injecting a small volume of tracer – usually saline – on the surface of a cylindrical probe. The analysis of tracer breakthrough curves provides information about the ambient velocity (direction in 3 dimensions, and magnitude). Previous PVP studies have used a variety of tracers ranging from deionized (DI) water to a solution of 6000 mg L^{-1} of NaCl, prepared in ambient groundwater (Labaky et al. 2007; Berg and Gillham 2010; Schillig et al. 2011). Since it is well known that tracers with solution densities that differ from the groundwater undergo buoyancy-driven transport (Schincariol and Schwartz 1990; Beinhorn et al. 2005; Tenchine and Gouze 2005; Mastrocicco et al. 2011), the possibility of biases in PVP measurements due to this effect needs to be evaluated. The goal of this work was to assess the magnitude of density driven flow in PVP tests, to provide a framework for correcting measurements affected by this process, and to provide guidance for the selection of appropriate tracer salinities for PVP tests.

3.1: Theory

Consider a static system in which a bead of saline tracer rests on the surface of a PVP surrounded by a saturated porous medium (Figure 3.01). Water at a discrete point (*i*) within the tracer bead can be defined as point water in a fashion similar to that described by Lusczynski (1961). The formulation for hydraulic head at a given point *i* is:

$$H_i = z_i + \frac{P_i}{\rho_i g} \qquad [4]$$

where H_i represents the total head of the tracer fluid (L) in the bead , z_i represents the elevation head (L), P_i represents tracer fluid pressure ($ML^{-1}T^{-2}$), ρ_i represents the density of the tracer (ML^{-3}), and g is gravitational acceleration (LT^{-2}). For simplicity, the hydrostatic pressure of water above the bead can be ignored in this analysis since it is a constant that later cancels by subtraction.

The concept of freshwater head ($H_{i,f}$) is defined as the equivalent fluid pressure of freshwater density (ρ_f) at a given point, *i*,

$$H_{i,f} = z_i + \frac{P_i}{\rho_f g} \qquad [5]$$

Since P_i must be the same in equations 4 and 5, (Post et al. 2007):

$$H_{i,f} = z_i + \frac{[\rho_i g(H_i - z_i)]}{\rho_f g} \qquad [6]$$

Differentiating equation 6,

$$\frac{\partial H_{i,f}}{\partial z_i} = 1 + \frac{\rho_i}{\rho_f}\frac{\partial H_i}{\partial z_i} - \frac{\rho_i}{\rho_f}$$

If static conditions exist within the tracer bead, $\partial H_i/\partial z_i = 0$ and the equivalent freshwater hydraulic gradient driving the bead to move along the PVP surface vertically due to buoyancy forces is

$$\frac{\partial H_{i,f}}{\partial z_i} = \left(\frac{\rho_f - \rho_i}{\rho_f}\right) \qquad [8]$$

This equivalent freshwater gradient applies across the entire bead (and everywhere inside). It will be assumed that this is the driving force for the bead to move along the PVP surface. Since the radius of a bead is normally expected to be smaller than the distance from the injection port to the detectors (1.9 cm in Figure 3.01), the gradient from equation 8 should be conservatively large. Nevertheless, since the bead diameter is a somewhat arbitrary distance, the assumption needs verification through laboratory testing.

In a system dominated by horizontal flow (Q_H), the vertical movement of tracer caused by a density difference with the ambient groundwater (Q_v) could be mistaken for ambient vertical flow. To quantify the magnitude of density driven flow, a ratio of vertical flow (*VF*) to the total of the individual contributions from the horizontal and vertical directions can be defined as:

$$\%VF = \frac{Q_v}{Q_H + Q_v} X\ 100\% \qquad [9]$$

Substitute Darcy's Law for *Q*

$$\%VF = \frac{-KA\left(\frac{dH_{i,f}}{dz}\right)_v}{-KA\left(\frac{dH}{dx}\right)_H - KA\left(\frac{dH_{i,f}}{dz}\right)_v} \times 100\% \qquad [10]$$

where the subscript *H* indicates horizontal and *v* indicates vertical. Dividing the numerator and denominator by porosity, the *%VF* is given in terms of horizontal and vertical velocities, which are directly measureable with PVPs,

$$\%VF = \frac{v_v}{v_H + v_v} \times 100\% \qquad [11]$$

Alternatively, the term *–KA* in equation 10 can be cancelled,

$$\%VF = \frac{\left(\frac{dH_{i,f}}{dz}\right)_v}{\left(\frac{dH}{dx}\right)_H + \left(\frac{dH_{i,f}}{dz}\right)_v} \times 100\% \qquad [12]$$

The *%VF* is seen to depend only on the horizontal and vertical gradients, assuming homogeneous and isotropic conditions around the PVP injection port. Horizontal gradients can be estimated from available water level data (see Devlin, 2003 for example), and the magnitude of the vertical gradient due to tracer density is given by equation 8. Therefore, equation 12 can be used as the basis for deciding on the maximum concentration of salt to use in a PVP tracer for a given aquifer.

Equation 8 requires knowledge of the ambient groundwater density and the tracer solution density. When these values are not readily available, they can be estimated as follows. Solution density and total dissolved solids (*TDS* in mg L^{-1}) are linearly related for simple NaCl solutions. Using data from Weast (1978) it was found that at 1 atmosphere and 20 ^{o}C, solutions of NaCl could be described by the following linear relationship

$$\rho_s = mTDS + b \qquad [13]$$

where ρ_s is the density of the solution, m = 7.07 X 10^{-7} (L g (mg^{-1} mL^{-1}) is the slope of the line, and b = 0.99823 g mL^{-1} is the intercept and the density of pure water, so

$$\frac{\rho_f - \rho_i}{\rho_f} = \frac{TDS_{ambient} - TDS_{tracer}}{TDS_{ambient} + \frac{b}{m}} \approx -\frac{m}{b}(M_{NaCl}) \qquad [14]$$

where TDS_{tracer} is the total dissolved solids of the tracer (mg L^{-1}), $TDS_{ambient}$ is the total dissolved solids of the background water (mg L^{-1}) *b/m* = 1.41 X 10^6 mg L^{-1}, *m/b* = 7.09 X 10^{-7} and M_{NaCl} is the mass of salt in mg added to one liter of ambient groundwater to form the tracer solution. The sign in equation 14 indicates direction, and is consistent with the sign that would apply in Darcy's Law. Usually in freshwater aquifers, *b/m* >> $TDS_{ambient}$ so the approximation given above is valid in those cases. The approximation in equation 14 can be very convenient since it eliminates the need for *TDS* measurements to make the buoyancy assessment. To account for temperature, the approximate formula for estimating water density as a function of temperature and salinity given by McCutcheon et al (1993) was used to produce temperature specific versions of equations 13 and 14 (Table 1). The estimates of *m/b* from the experimental data of Weast (1978) and the approximate value from Table 1 for 20 ^oC agree to within 7%, so the values given in Table 1 are expected to be of value in practical applications.

3.2: Methods

Aquifer conditions were simulated in the laboratory using the NeST design (Bowen et al., in review) to create a horizontal flow system in a gravel porous medium (Figure 3.02). Briefly, the NeST design consists of an outer plastic storage bin containing two inner bins. Water is pumped into the first inner bin, which contains open water. It passes through several screened connectors into the second inner bin, which is packed with granular material. It

passes out of the second bin and into the outer bin through numerous screened holes located on the down-gradient side of the packed bin. Water is pumped from the outer bin back into the first inner bin to complete the cycle. The system has been shown to produce a predictable and uniform flow regime within a granular porous medium, is simple to assemble and operate, and is inexpensive to construct (Bowen et al., in review). Here, gravel was chosen as the porous medium since a high *K* would permit more rapid tracer movement and faster tests than could be achieved in less permeable material.

A PVP was installed in the middle of the second inner bin during packing. The orientation of the injection port was set at 22° (= α) from the expected flow direction for the majority of tests. A second orientation of 42° was also tested in the 60 mg L^{-1} NaCl tracer salinity experiments. The PVP was constructed from a 3.8 cm schedule-40 PVC pipe. Electrical conductivity (EC) sensors were placed on both sides of the injection port to track horizontal flow, and above and below the injection port to track vertical flow. Tracer solutions that were tested included DI water and solutions with salinities of 60, 130, 250, 500, 1000, and 2000 mg NaCl L^{-1}. All saline tracer solutions were prepared using DI water that had previously been equilibrated with the gravel in the NeST. Tests were conducted with injection volumes of 0.5 mL and 1.0 mL for each tracer with 0.5 mL injections conducted in duplicate. A Campbell Scientific CR1000 was used to record all PVP measurements (mV) at 4 bytes per reading and 7 digit precision.

PVP breakthrough data were interpreted using VelProbePE, a Visual Basic enhanced spreadsheet program freely available online (Schillig, 2012). Briefly, a nonlinear optimizer fits the observed EC breakthrough curve data with a 1 dimensional solution to the advection-

dispersion equation to determine an apparent velocity of the tracer (Devlin, 1994). Apparent velocities are used to calculate the average linear velocity (horizontal flow) and α angle as described by Labaky et al. (2007). Vertical velocities were taken directly from the breakthrough curve fits from the vertical detectors.

All experiments were conducted using wet packed Quickrete® 1151 all-purpose gravel. The gravel (10 mm grain size, density (ρs) of 2.14 g mL^{-1}) was flushed with DI water prior to experimentation. The gravel-packed storage bin had a cross sectional area, A, of 867 cm^2. Flow between the inner and outer bins was maintained at a rate, Q, of between 34 and 50 mL min^{-1}. At the end of the experiments, the bulk dry density, ρb (= 1.33 g mL^{-1}) of the gravel was determined gravimetrically from three saturated core samples (~ 500 mL) taken from the gravel-packed bin. These values were converted to a volumetric water content, n, of 0.38 ± 0.001 ($n=\rho b/\rho s$ -1). The K of the gravel was found to be 3.1 x 10^{-2} ms^{-1} based on a constant head permeameter test. With A, n, and Q known, the horizontal hydraulic gradient across the gravel-packed bin in each PVP test could be determined from

$$\frac{\Delta H}{\Delta x} = \frac{Q}{AK} \qquad [15]$$

Vertical gradients due to density contrasts were estimated from equation 8.

3.3: Results and Discussion

Tracers containing more than 60 mg NaCl L^{-1} exhibited vertical transport in all cases, despite flow in the packed bin being dominantly horizontal. This finding shows that saline tracer density exerted a measureable downward effect on flow on the PVP surface even with dilute NaCl tracer solutions. Upward vertical flow was found to occur when DI water was used

as the tracer, again supporting the notion that buoyancy forces were important in the experiments. With increasingly concentrated NaCl tracers, and correspondingly increased flow perturbations, the accuracy of the PVP velocity estimates in both the α and velocity magnitude values declined (Table 1). This was partially because the amount of tracer that reached the horizontal detectors diminished as vertical transport became more pronounced, and the reliability of the breakthrough curves declined accordingly. The average percent difference between the expected velocities and the PVP estimates was found to be $\pm$14% for tracers containing less than 500 mg NaCl L^{-1}, which is comparable to the $\pm$9% uncertainty reported for laboratory experiments conducted by Labaky et al. (2007) in sand and a 600 mg NaCl L^{-1} tracer. For tracers > 500 mg NaCl L^{-1}, the average difference increased to about $\pm$36% (Table 1). The difference in flow direction, as given by α, was $\pm$14° or less for tracers consisting of less than 250 mg NaCl L^{-1}. This compares well with the 15° error reported for the experiments conducted by Labaky et al. (2007) in sand. For tracers more concentrated than 250 mg NaCl L^{-1}, the average differences increased to $\pm$53° (Table 1). Clearly, unaccounted for buoyancy effects have the potential to significantly bias groundwater directions inferred from PVP measurements.

The horizontal and vertical velocities measured with the PVP were used to determine *%VF* (equation 11), and compared with the theoretical relationship predicted from equations 12, 14 and 15 (Figure 3.03). Initially, the measured values of K (0.031 ms^{-1}) and n (0.38) were used in equation 15 to obtain the horizontal gradient (2.2 X 10^{-3}). The fit to the experimental data points was then optimized by adjusting K using the Solver add-in in Excel®. In the course

of improving the fit, the *K* was changed from 0.031 ms^{-1} to 0.033 ms^{-1}, indicating that the experimentally determined value was quite accurate.

3.4: Designing PVP Tests

The theoretical development presented above can be used to provide guidelines for the preparation of site specific PVP tracers. If a tracer solution is prepared by adding NaCl to site groundwater, then the equivalent freshwater gradient that develops across a tracer bead on a PVP, due to buoyancy forces, can be estimated using equation 14. Combining this with equation 12, a family of curves was calculated to indicate the tracer strength required to remain within a desired limit on *%VF* for various horizontal hydraulic gradients (Figure 3.04). For example, a site with an horizontal hydraulic gradient of 1 X 10^{-3} could be examined using a 1000 mg NaCl L^{-1} tracer with the expectation that density driven vertical flow transporting the tracer would account for about 40% of the total flow affecting the measurements (equation 11). Measured vertical velocities leading to higher % VF (downward in this case) would be an indication of true, ambient vertical flow in the aquifer. Vertical velocities less than this % VF would suggest ambient flow in the other vertical direction. If 30% vertical flow is chosen as an acceptable limit, then the maximum tracer strength for a site with an ambient horizontal gradient of 1 X 10^{-3} would be about 700 mg L^{-1}, prepared in the site groundwater (Figure 3.04).

This analysis provides guidance for the preparation of PVP tracers, but, as suggested above, it can also be used to correct or gain insight into existing data that have been affected by the density difference between the tracer and the groundwater. Note that only the measured vertical velocities need correction; horizontal velocities may be used as measured, except in

extreme cases where the tracer is so dense (or buoyant) that it travels vertically away from the detector area before reaching the horizontal flow detectors.

As an example of revisiting existing data sets, consider the case reported by Labaky et al. (2009) who reported using a 6000 mg NaCl L^{-1} PVP tracer solution in the CFB Borden aquifer. The test was conducted in a sheet-pile alley where flow was maintained artificially (cross-sectional area = 4.6 X 10^4 cm^2; Q = 216 mL min^{-1}; K_{avg} = 0.48 cm min^{-1}). The horizontal gradient was estimated to be 1 X 10^{-2}, and the background $TDS_{ambient}$ was approximately 210 mg L^{-1} based on electrical conductance (*EC*) measurements of 350 μS cm^{-1} (*TDS* ≈ 0.6 *EC,* Freeze and Cherry, 1979). Examination of Figure 3.04 shows that a tracer of about 6000 mg NaCl L^{-1} would exhibit a *%VF* of 30% under these conditions, which is notable but not severe. To illustrate why this is so, imagine a PVP with a horizontal detector located 2 cm from the injection port. In the time it would take for the tracer to reach the detector, it would descend on the PVP surface about 0.7 cm (30% of 2 cm). As long as the horizontal detector was constructed in a way that would enable it to sense a tracer that had descended that far on the PVP surface, the horizontal velocity could be measured without a detailed consideration of the density driven movement of the tracer.

Schillig et al. (2011) also performed PVP experiments in the Borden aquifer to measure horizontal velocities, this time with a tracer strength of 1000 mg NaCl L^{-1}. Their experiment was similarly conducted between sheet-piles, but an average gradient of about 5 X 10^{-3} existed in the test zone. Once again, examination of Figure 3.04 indicates a low *%VF* prevailed, this time only about 14%, making consideration of density driven flow non-essential in that case.

It is common for aquifers to exhibit vertical anisotropy in *K*. When this is the case, downward or upward tracer movement is impeded and more concentrated tracers (or DI water) can be used with the advantage of easier detection and a diminished effect of density related tracer movement. At the Borden site mentioned above, the vertical anisotropy ratio was estimated to be quite small (factor of 1.3, favoring horizontal flow) (Sudicky, 1986). However, anisotropy ratios up to 100 have been reported (Freeze and Cherry, 1979).

3.5: Conclusions

Density related flow affecting PVP measurements is primarily a function of the relative magnitudes of the hydraulic gradients, horizontal and vertical. Where strong vertical anisotropy exists at the scale of the PVP measurement, the *K* ratios should also be considered.

The salinity of a tracer can affect the accuracy of velocities measured with PVPs. Unaccounted buoyancy effects can bias vertical velocity estimates, but do not compromise horizontal velocity estimates for cases where the fraction of flow that is vertical does not exceed 30%, judged to be a conservative limit based on laboratory testing. In the laboratory tests performed here, horizontal velocity was determined with reasonable accuracy with a tracer concentration of 500 mg L^{-1} NaCl, which induced a vertical flow of 60%. We suggest that tracer strength be estimated using Figure 3.04, which accounts for buoyancy forces and ambient horizontal flow to estimate a maximum salt concentration for PVP applications.

Density imposed vertical velocities can be corrected in existing data sets using the framework developed in this chapter. In a more proactive sense, site specific tracer concentrations can be formulated using site groundwater to minimize the effects of density driven flow.

References

Beinhorn, M., P. Dietrich, and O. Kolditz. 2005. 3-D numerical evaluation of density effects on tracer tests. *Journal of Contaminant Hydrology* 81 no. 1-4: 89-105.

Berg, S.J., and R.W. Gillham. 2010. Studies of Water Velocity in the Capillary Fringe: The Point Velocity Probe. *Ground Water* 48 no. 1: 59-67.

Bowen, I.R., Devlin, J.F., Schillig, P.C. (in review). Design and Testing of a Convenient Bench-top Sandbox for Controlled Flow Experiments. Submitted to Ground Water Monitoring and Remediation.

Devlin, J.F., Schillig, P.C., Bowen, I., Critchley, C.E., Rudolph, D.L., Thomson, N.R., Tsoflias,G.P., Roberts, J.A. 2012. Applications and implications of direct groundwater velocity measurement at the centimetre scale, Journal of Contaminant Hydrololology, doi:10.1016/j.jconhyd.2011.06.007

Devlin, J.F. 1994. A simple and powerful method of parameter estimation using simplex optimization, Ground Water, v. 32, no. 2, 323-327.

Diersch, H.J.G., and O. Kolditz. Variable-density flow and transport in porous media: approaches and challenges. *Advances in Water Resources* 25 no. 8-12: 899-944.

Freeze, R.A., Cherry, J.A. 1979. Groundwater. Prentice Hall, Englewood Cliffs, N.J.

Labaky, W., J.F. Devlin, and R.W. Gillham. 2007. Probe for measuring ground water velocity at the centimeter scale. *Environmental Science & Technology* 41 no. 24: 8453-8458.

Labaky, W., Devlin, J.F., Gillham, R.W. 2009. Field comparison of the point velocity probe with other groundwater velocity measurement methods, Water Resources Research, 45, W00D30, doi:10.1029/2008WR007066.

Lusczynski, N.J. 1961. Head and Flow of Ground Water of Variable Density. *J. Geophys. Res.* 66 no. 12: 4247-4256.

Mastrocicco, M., H. Prommer, L. Pasti, S. Palpacelli, and N. Colombani. 2011. Evaluation of saline tracer performance during electrical conductivity groundwater monitoring. *Journal of Contaminant Hydrology* 123 no. 3-4: 157-166.

McCutcheon, S.C., Martin, J.L., Barnwell, T.O. jr. 1993. Water quality. Chapter 11 in Handbook of Hydrology, D.R. Maidment ed., McGraw-Hill Inc., New York,

Post, V., H. Kooi, and C. Simmons. 2007. Using hydraulic head measurements in variable-density ground water flow analyses. *Ground Water* 45 no. 6: 664-671.

Schillig, P.C. 2012. VelprobePE: An automated spreadsheet program for interpreting point velocity probe breakthrough curves. *Computers & Geosciences* 39: 161-170.

Schillig, P.C., J.F. Devlin, J.A. Roberts, G.P. Tsoflias, and M.A. McGlashan. 2011. Transient Heterogeneity in an Aquifer Undergoing Bioremediation of Hydrocarbons. *Ground Water* 49 no. 2: 184-196.

Schincariol, R.A., and F.W. Schwartz. 1990. An experimental investigation of variable density flow and mixing in homogeneous and heterogeneous media. *Water Resour. Res* 26 no. 10: 2317–2329.

Sudicky, A. E. 1986. A natural gradient experiment on solute transport in a sand aquifer: Spatial variation of hydraulic conductivity and its role in the dispersion process. Water Resources. Research, 22 no. 13, 2069-2082.

Tenchine, S., and P. Gouze. 2005. Density contrast effects on tracer dispersion in variable aperture fractures. *Advances in Water Resources* 28 no. 3: 273-289.

Weast, R.C. ed. 1978. CRC Handbook of chemistry and physics. CRC Press, Inc., Boca Raton, Florida, p. D-299.

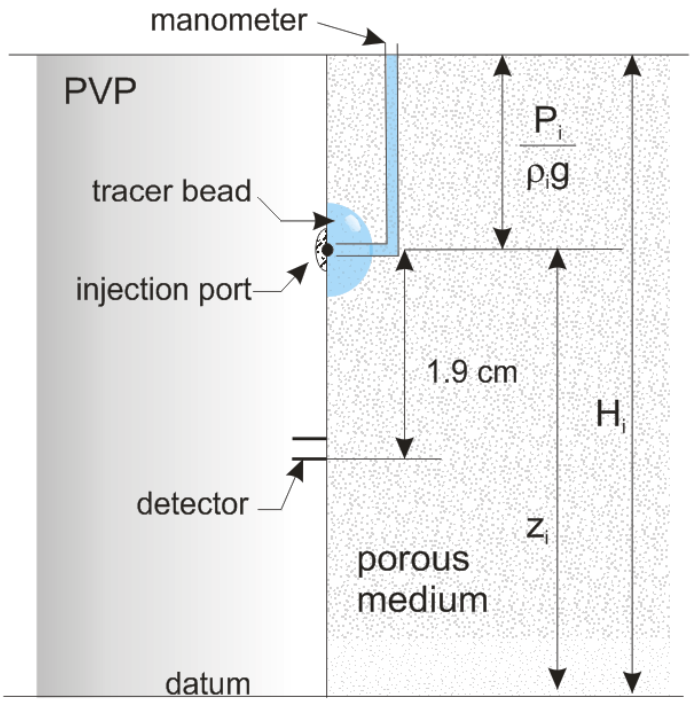

Figure 3.01: Schematic of a PVP shown in a porous medium with a saline tracer bead on the surface and hypothetical manometer.

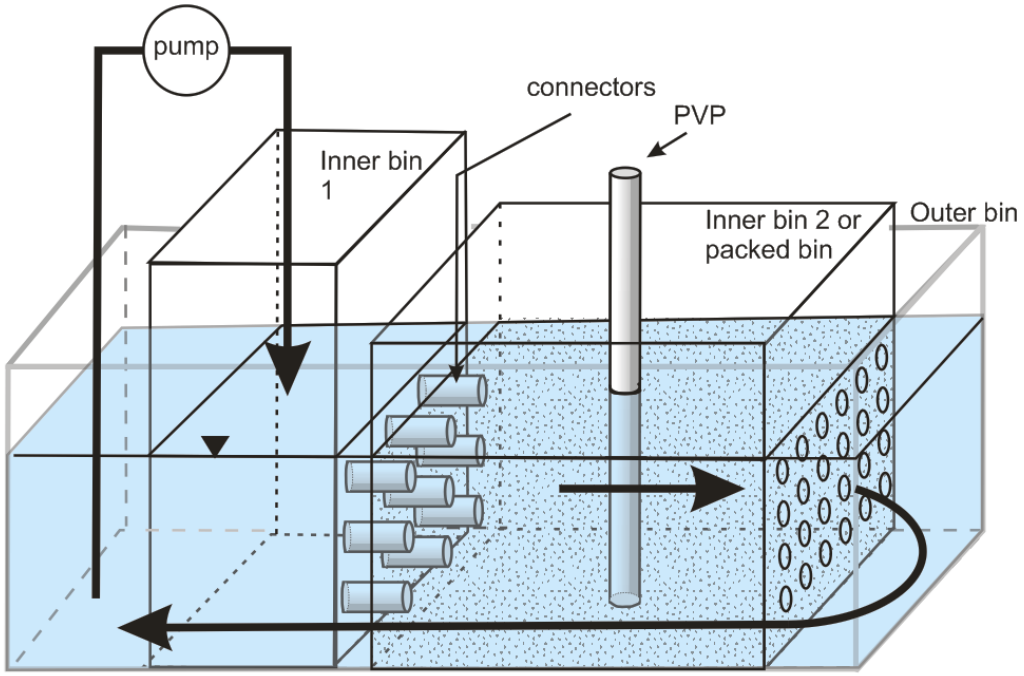

Figure 3.02: NeST design for achieving horizontal flow in a gravel packed bin (inner bin 2).

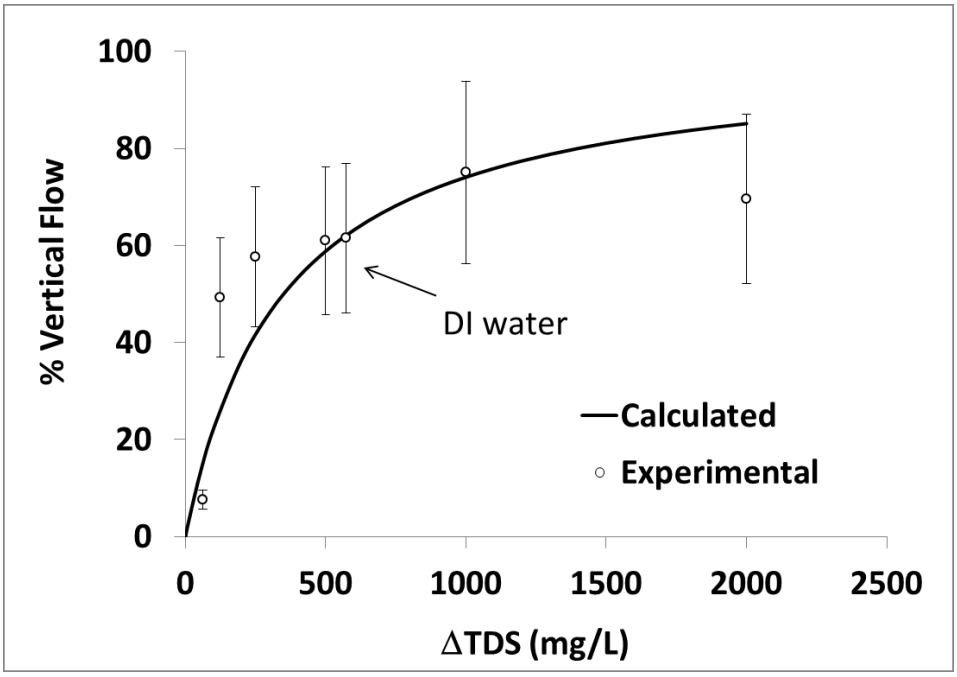

Figure 3.03: Theoretical (equations 8 and 12) and experimental (equations 12, 14 and 15) percent of vertical flow in the NeST experiments. All vertical flow was due to density differences between the tracer and the simulated groundwater. Experimental points shown represent averages of tests at specific tracer concentrations (n = 2 to 6). ΔTDS represents the mass of NaCl added to 1 L of simulated groundwater except in the DI water test, where it represents the mass of salt dissolved by 1 L of DI water as it equilibrated with the gravel. Error bars represent one standard deviation on the averages (±25%).

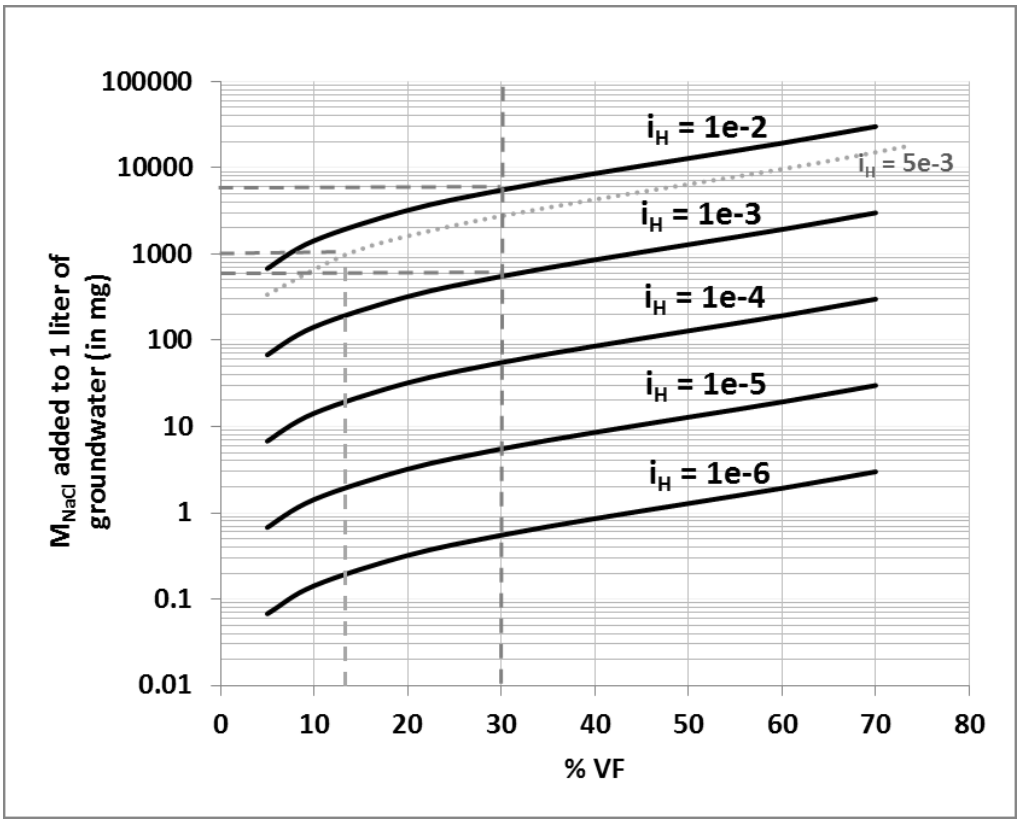

Figure 3.04: Relationship between mass of NaCl added to site groundwater in a PVP tracer and the magnitude of the imposed vertical flow as a function of the ambient horizontal flow gradient. A value of m/b for 10 ^{o}C from Table 3.1 was used to generate these curves.

Table 3.1: Solution density estimation as a function of temperature.

Temperature (^{o}C)	**Regression equation 13 for ρ_s in g/mL from *TDS* in mg L^{-1}**	**m/b for equation 14 approximation**
5	$7.9374 \times 10^{-7}(TDS) + 1.0000$	7.9374×10^{-7}
10	$7.7960 \times 10^{-7}(TDS) + 0.99974$	7.7980×10^{-7}
15	$7.6795 \times 10^{-7}(TDS) + 0.99914$	7.6861×10^{-7}
20	$7.5836 \times 10^{-7}(TDS) + 0.99824$	7.5970×10^{-7}
25	$7.5051 \times 10^{-7}(TDS) + 0.99709$	7.5270×10^{-7}

Table 3.2: Deviations in PVP measured horizontal velocities from expected values as a function of NaCl tracer concentration.

Salt as ΔTDS (mg/L)	± %v	± α (^{o})
62.5	19.6	14
125	12.5	8
250	14.5	13
500	6.9	22
573	42.1	57
1000	14.0	49
2000	36.4	84

4

Assessment of Site Characterization with Direct Groundwater Velocity Measurements

4.0: Introduction

4.0.1 Challenges in Site Characterization

During the initial phases of aquifer characterization, hydraulic conductivity (*K*), porosity (*n*), and hydraulic gradient (*i*) are commonly used to obtain estimates of groundwater velocity (*v*) and parameterize models. Estimates of *K* are obtained through a variety of techniques, including aquifer tests, slug tests, laboratory analysis of core, borehole flowmeters, dipole tests, direct-push profiling, and hydraulic tomography (Butler, 2005). In order to obtain reliable estimates of groundwater velocity, the spatial distribution of *K* is an important consideration. As a result, much attention has been given in the literature regarding the accuracy, uncertainty, and spatial distribution in *K* (Russo and Bresler 1981; Sudicky 1986; Woodbury and Sudicky 1991; Ritzi et al. 2000; Butler 2005; Zemansky and McElwee 2005; Bohling et al. 2007; Sudicky et al. 2010; Alexander et al. 2011). It has been noted that this consideration is especially important where passive remediation efforts are underway (Hemsi and Shackelford 2006). In spite of recent improvements in site characterization methods, it remains widely recognized that *K* is the largest source of uncertainty in estimating groundwater velocity (Devlin *et al.*, 2012).

Relative to *K*, considerably less attention has been given to the uncertainty in the orientation and magnitude of *i*. One method of determining *i* approximates the piezometric

surface or water table as a plane using a least-squares fitting routine. The equation of the plane is then used to estimate the gradient magnitude and orientation (Kelly and Bogardi 1989; Devlin 2003). Devlin and McElwee (2005) used this technique to show that in highly permeable aquifers, *i* could introduce considerable uncertainty into groundwater velocity estimates. A similar approach illustrated the difficulties in measuring vertical gradients accurately (Silliman and Mantz 2000). To minimize uncertainty in *i*, they recommended that 1) 5-10 monitoring wells be used, 2) the monitored area maintain an aspect ratio (ratio of the length of any two sides bounding the area) near 1, and 3) the monitored area should be large enough to measure a head drop greater than three times the uncertainty on the water level measurements.

Other investigations have attempted to minimize error and local uncertainty by conducting a large number of three-point estimations of *i* (Pinder et al. 1981; Abriola and Pinder 1982; Silliman and Frost 1998; McKenna and Wahi 2006). The most reliable three-point estimators have been found to be geometrically constrained with base to height ratios between 0.5 and 5.0 (McKenna and Wahi 2006). Three-point estimators have also been used to identify single wells that bias estimates of *i* due to the presence of local heterogeneities (Silliman and Frost 1998).

For the purposes of this chapter, the term 'direct velocity measurement' refers to techniques that permit velocity estimation by following tracer movement or other sensing methods not reliant on hydraulic heads. Natural gradient tracer testing provides direct groundwater velocity information without prior knowledge of *K* or *i*, but can be fairly resource intensive (Sudicky 1986; Leblanc et al. 1991). Direct groundwater velocity measurements from single wells offer a similar advantage. Point-dilution techniques have received attention as a

groundwater velocity measurement method (Drost et al. 1968). However, because point dilution provides no indication of the flow direction it is actually a speed measurement technique (Moore et al. 1992). Various borehole/well velocimeters such as the Colloidal Borescope (Kearl 1997), Geoflo® Meter (Melville et al. 1985), and Laser Doppler Velocimeter (Momii et al. 1993) provide direct measurements of groundwater velocity (speed and direction), but are generally limited to measuring horizontal flow, and require calibration steps to compensate for flow perturbations due to gravel packs and well screens (Bayless et al. 2011). A thermal device that is installed in direct contact with aquifer materials, called the Vector Technology and formerly known as the In Situ Permeable Flow Sensor (ISPFS), is sensitive to thermal heterogeneities of the aquifer material, and yields velocities representative of scales on the order of approximately 1.0 vertical meter (Ballard 1996). A relatively new technology for determining groundwater velocity is the point velocity probe (PVP). The probes are simple to construct, inexpensive, and can be installed in direct contact with the aquifer material, circumventing the need for empirical correction factors. Point velocity probes have performed well in both laboratory (Labaky et al. 2007; Bowen et al. in review) and field settings (Labaky et al. 2009; Devlin et al. 2009; Schillig et al. 2011; Devlin et al. 2012). Their measurements are at the centimeter scale, so the issue of scale compatibility with other independent methods has yet to be fully resolved. The purpose of this study is to determine if the PVP-derived velocities can be directly compared to the conventional larger scale velocity estimates, in particular those based head measurements from multiple wells, and Darcy's Law. Given the importance of *K* in the conventional velocity estimates, several methods of estimating *K* were utilized to bracket the range of values that might be obtained in standard investigations. The methods included

slug tests and grain-size analysis of core material, and a review of aquifer testing results previously conducted on the site.

4.02: Estimating Groundwater Velocity with PVPs

Velocities from PVP measurements are calculated from equations that describe fluid flow around a cylinder (Bird et al. 1960). The apparent velocity of water at any point along a cylinder's surface can be related to the average linear velocity beyond the influence of the probe. By injecting a small, saline tracer from a discrete source on the surface of the cylinder, and collecting breakthrough data at sensors positioned downstream on the cylinder surface, the direction and magnitude of the groundwater velocity vector can be determined (Labaky et al. 2007). Apparent velocities (v_{app}) are calculated by fitting measured breakthrough curves to the advection-dispersion equation and are used in equations (1) and (2) to calculate the orientation angle of the injection port with respect to the flow direction (α) and the average linear groundwater velocity (v_∞) beyond the influence of the probe (Labaky et al. 2007):

$$\alpha = \tan^{-1}\left[\frac{v_{app1}\,\gamma_1\,(\cos\gamma_2 - 1) + v_{app2}\,\gamma_2(1-\cos\gamma_1)}{v_{app1}\,\gamma_1\sin\gamma_2 - v_{app2}\,\gamma_2\sin\gamma_1}\right] \quad [1]$$

$$v_\infty = \frac{v_{app}\,\gamma}{2(\cos\alpha - \cos(\alpha+\gamma))} \quad [2]$$

where v_{app1} and v_{app2} are the apparent velocities for detectors 1 and 2, respectively. The fixed angles between the injection port and horizontal detectors 1 and 2 are γ_1 and γ_2, respectively. Laboratory testing and modeling have indicated that PVPs are accurate to within 9% of the expected water speed and about 8° in direction (Labaky et al. 2007). Results from field PVP testing compared well with velocity estimations based on Darcy calculations in a test conducted

in a sandy aquifer with flow constrained by a sheet-pile alleyway (Labaky et al. 2009). Individual PVPs, stacked as multilevels, were utilized to show a 2-dimensional profile of flow velocities through the sheet-pile alleyway (Devlin et al. 2009; Schillig et al. 2011). In that work the PVPs indicated temporal changes in flow related to biostimulation. Point velocity probes have also been used to map velocities in 3-dimensions, defining the flow field surrounding a recirculating (dipole) well (Bowen 2010; Devlin et al. 2012).

4.03: Geological Setting

The study area consists of an unconfined sand and gravel aquifer located to the south of Woodstock, Ontario, Canada (Figure 4.01). The surficial geology comprises primarily Quaternary tills deposited approximately 15,000 years ago near an interlobate zone between two ice-sheets (Cowan 1978; Piotrowski 1987; Krzyszkowski 2001). During the Quaternary, multiple ice advances and retreats resulted in the deposition of alternating till and outwash sequences (Krzyszkowski 2001). The complex depositional history at the site is evident by the heterogeneous nature of the aquifer (Haslauer 2005). The field area for this study is located in a glacialfluvial outwash channel, bounded by drumlinized Tavistock Till (Figure 4.02). Groundwater flows generally south of east, toward the Thorton Well Field that supplies water to the municipality (Figure 4.02), with *K*s ranging from 4.8×10^{-4} to 1.9×10^{-2} m/s (Critchley 2010) at an average speed of about 1 m/day (Devlin et al. 2012).

4.1 Methods

4.1.1 Determination of Hydraulic Conductivity

Hydraulic conductivity was determined from slug tests using solid, PVC slugs of varying volume in wells WO75 S, WO74 S, WO74 M, and WO74 D (Figure 4.01). Details regarding well construction and development can be found in Critchley (2010). A minimum of four rising and four falling head tests were conducted for each well. The head response in each test was fitted using the solution of Springer and Gelhar (1991), developed exclusively for unconfined aquifers.

Hydraulic conductivity estimates were also acquired from grain-size analyses of core extracted during the installation of multilevel PVPs 1 and 2. In total, 57 samples were collected from the two cores at 20-30 cm intervals. The *K* determinations were based on the d_{10} values of the sediments (grain-size diameter at which 10% of the particles are finer) using the method of Terzaghi (1925). Additional core samples were collected during the installation of multilevels 3, 4, and 5, at the depths corresponding to the placement of the PVPs. Particle-size and sorting descriptions at these locations were determined using the method of Blott and Pye (2001).

4.1.2: Determination of Hydraulic Gradient

Hydraulic gradients were calculated using eight wells from the 'WO' series (Figure 4.01), excluding WO74 S and WO74 M as they were screened at a lower elevation than the other wells in the series. Hydraulic gradient calculations were based on manual water-level measurements collected while the PVP data collection was also underway. Water-levels were

measured six times over three consecutive days. Since the water-level measurements occurred close together in time, differential barometric effects between head measurements at different wells were assumed to be negligible. The hydraulic gradient magnitude and orientation was characterized by two techniques: first, the water table was represented by a best-fit plane using data from the entire well network. Six such planes were calculated, one for each water level snapshot, using the method of Devlin (2003).

Second, the gradients from all possible three-point estimators in the well network were again determined for each snapshot, providing a data set suitable for statistical analysis (Pinder et al. 1981; Silliman and Frost 1998; McKenna and Wahi 2006). The three-point estimator data were filtered to exclude cases where the maximum head drop between wells was less than three times the error of the water-level measurement (< 3 cm with ± 1 cm error) (Devlin and McElwee 2007) and cases with base to height ratios outside the range of 0.5 to 5.0 (McKenna and Wahi 2006) (Appendix 6). Gradient magnitudes and orientation for each estimator were calculated according to Devlin (2003). Uncertainties in all gradient calculations were reported as 1 standard deviation from the dataset population.

4.1.3: PVP Installation

Five PVP multilevel stands were assembled using 4.81 cm O.D. schedule 40 flush-thread PVC pipe using the design given by Devlin et al. (2009). Detector wires were soldered to solid conductor CAT-5E wire crimped with an RJ45 jack at the surface to facilitate setup and take down. Multilevel PVPs 1 and 2 consisted of six PVPs each, equally spaced from elevations 292.00 to 287.00 masl. Each probe contained four detectors, placed at 40° and 70° on either side of the injection port. A second injection port added to each PVP 120° from the first. With

two injection ports, the PVPs were capable of measuring velocities anywhere inside a maximum arc of about 260^{o}. Three additional PVP multilevel stands, designated PVPs 3, 4, and 5, were later constructed with seven probes each. These latter probes were constructed with additional detectors 3 cm above and below a single injection port, to detect vertical flow. The horizontal flow detectors were limited to one side of the injection ports to leave cable capacity for extra multilevel probe units (Figure 4.03). The measurable arc of detection for these units was about 110^{o}. Individual PVPs on multilevels 3, 4, and 5 were installed at elevations 294.00, 291.30, 290.00, 289.75, 289.50, 288.50, and 286.75 masl.

PVP multilevels were installed by advancing a 5.72 cm O.D. casing to a depth of 15.25 m below ground surface (BGS) (elevation 285.45 masl) using a direct push rig. Continuous cores were recovered for later analysis. Following core extraction, a 6.35 cm I.D. x 8.26 cm O.D. casing with an expendable point was advanced to 15.25 m BGS down the same borehole. Multilevel PVP stacks with tracer lines prefilled with sodium chloride tracer solution (concentrations were adjusted for the groundwater salinity and aquifer texture, see below) were lowered into the direct push casing with the injection ports oriented ~ N30°W. The exact orientation was later determined to within ±1^{o}. Thus, velocities could be measured with flow directions between N150°E and N40°W. The direct push casing was filled with site groundwater immediately prior to its removal to promote aquifer collapse around the PVP multilevel.

Both deionized water (PVPs 1 and 2) and a 0.0625 g/L solution of NaCl (in site groundwater; PVPs 3, 4, and 5) were tested as PVP tracers. Typically, 3-7 mLs of injected tracer were required to produce a measurable signal. This volume exceeded those reported in previous studies partly because the tracer solutions had to be sufficiently dilute to avoid density

driven flow, which we observed was more noticeable in the gravel units than in the sand (Devlin et al. 2009. Labaky et al. 2009, Schillig et al. 2011). All multilevel PVPs were tested within four to five days of installation. Tracer breakthrough at each detector was monitored at 10 second intervals using a Campbell CR1000 datalogger. Breakthrough curves were interpreted using Equations 1 and 2 (Labaky et al. 2007; Schillig 2012).

4.1.4 Tracer Tests

Conservative (Br^-) tracer testing from a cross-injection system (CIS), similar to the one described by Gierczak et al. (2007), yielded groundwater velocity estimates through the same zones monitored by the PVPs. The Br^- tracer pulse was created by extracting groundwater from WO78 (screened from elevations 294.37 to 283.70 meters above mean sea-levels(masl)) at an average rate of approximately 190 L/minute, amending the groundwater with a 250,000 mg/L Br^- solution and re-injecting it into WO79 (screened from elevations 294.47 to 285.32 masl) (Figure 4.01). The amendment was mixed with the groundwater in-line at a rate of 0.20 L/min for a period of just under 4 hours, yielding an injection concentration of approximately 263 mg/L. Following the injection period, the circulation cycle was continued for an additional 2.5 hours to flush the wells. Samples were collected during and following the injection for a total period of 17 hours from down-gradient multilevel wells ML5, ML6, ML7, and ML8. Samples were analyzed for Br^- using a Dionex ICS 3000 ion chromatograph and Dionex IonPac AS18 analytical column. Groundwater velocities were calculated by fitting the observed Br^- breakthrough data to a 1-dimensional solution to the advection-dispersion equation (Devlin 1994; Devlin and Barker 1996).

4.2: Results and Discussion

4.2.1 Hydraulic Conductivity Estimates

Hydraulic conductivity estimates from slug testing at WO75 S, WO74 S, WO74 M, and WO74 D were examined for vertical trends in *K* (Figure 4.04). The highest *K* measured in any single well was considered the most reliable at that location because dynamic skin effects tend to bias *K* estimates low (Butler et al. 1996). The highest overall *K* from the slug test profile was estimated to be 2.00 X 10^{-3} m/s, at WO74 M (screened from 287.02 to 288.24 masl).

Grain-size analyses from two cores recovered during the installation of multilevel PVPs 1 and 2 yielded a depth-averaged *K*, over the interval 286.00 to 296.00 masl, of 1.28 X 10^{-3} m/s and 1.48 X 10^{-3} m/s (Figure 4.04). These values agree reasonably well with the overall average *K* from the slug test profile, 1.54 X 10^{-3} m/s (Figure 4.04). The higher sampling resolution of the grain-size analyses reveals greater variability in *K* compared to slug testing, as would be expected. In the case of the PVP 1 core, three relatively high *K* zones were observed. The first was over the elevation range 288.25-288.51 (6.40 X 10^{-3} m/s), the second at about 290.03 (4.77 X 10^{-3} m/s), and the third at 294.35 (2.97 X 10^{-3} m/s) masl (Figure 4.04). The multilevel PVP 2 core indicated four high *K* zones, at elevations 286.21 (8.26 X 10^{-3} m/s), 289.79 (5.29 X 10^{-3}m/s), 294.04 (4.28 X 10^{-3} m/s), and 296.15 (4.77 X 10^{-3} m/s) masl (Figure 4.04). Grain-size analyses also indicated that the aquifer was composed primarily of gravel-rich sediments, with grains > 2 mm making up 52% of the mass in the PVP 1 core and 64% of the mass in the multilevel PVP 2 core. In total, *K* estimates from grain-size analyses and slug tests varied from 1.27 x 10^{-5} to 8.26

x 10^{-3} m/s, leading to an expected range of groundwater velocities of 0.01 m/d to 4.33 m/d, with an average of 0.72 m/d, assuming a hydraulic gradient of 0.002. Justification for this estimate of *i* is provided below.

4.2.2: Hydraulic Gradient Estimate

The three-point estimator method produced a total of 25 acceptable (out of 56 possible) combinations of three wells, using the eight wells in the network. This was repeated for each of the six measurement times, i.e., snapshots. The orientation of *i* was characterized by a bimodal distribution with one maximum toward the east and another toward the southeast at N117°E ± 21°. There was a maximum range of 76° in flow directions between estimators, from N90°E to N166°E (Figure 4.05). However, further examination of the data indicated that all of the estimators with due east flow directions included WO75 S as one of the three wells. By removing WO75 S from the analysis, the site-wide orientation of *i* became unimodal in distribution, with a flow direction of N134°E ± 14°. This result was found to be similar to that obtained when only the wells nearest the PVPs were used in the three-point estimator analysis. These wells are all those shown in the lower right inset of Figure 4.01 (24% of all viable estimators). In that analysis, the gradient exhibited a near normal distribution with a mean direction of N139°E and a standard deviation of about 8°. A survey error at WO75 S was ruled out as a cause of the previously mentioned bimodal distribution since several surveys of well locations were conducted at the site over several years with the same results. A similar problem was observed by Silliman and Frost (1998) where three-point estimator analysis indicated that a single well caused a secondary flow direction 50-60° from the primary one. Those authors suggested that local heterogeneity surrounding that well may have contributed

to the unrepresentative heads at the anomalous well. It is possible that the same cause existed at WO75 S in this study.

The best-fit plane method yielded an average flow direction of N99°E ± 2° when WO75 S was included in the analysis, and N137°E ± 3° when it was excluded. Both the three-point estimator and best-fit plane methods yielded similar *i* magnitudes, 0.002 ± 2.5 x 10^{-4} and 0.002 ± 3.0 x 10^{-5}, respectively.

4.2.3: Groundwater Velocities From Multilevel PVPs 1 and 2 and From The CIS Tracer Test

Horizontal groundwater velocity magnitudes from multilevel PVPs 1 and 2 coincided well. Both showed a high velocity zone at 289.00 masl with a magnitude of 26.41 to 27.84 m/d, respectively (Figure 4.04). Weak, highly asymmetric breakthrough curves at the horizontal flow detectors were observed at the probes located above 289.00 masl, which was hypothesized to be caused by vertical transport of the tracer. Tracer testing conducted from the CIS wells indicated high groundwater velocities at elevations 290.40 (28.03 m/d), 290.06 (27.24 m/d), and 290.04 masl (37.05 m/d) at ML5, ML6, and ML7, respectively (Figure 4.04). These velocities are consistent in magnitude and depth of occurrence with those reported above for multilevel PVPs 1 and 2. Moreover they are the most important to take into account in treatment calculations because they represent the pathways that conduct the greatest proportion of nitrate mass to potential receptors, such as the municipal wells.

4.2.4: Groundwater Velocities from Multilevel PVPs 3, 4, and 5

Multilevel PVPs 3, 4, and 5 were installed to confirm the occurrence of high horizontal velocities, and to test the hypothesis that an important vertical component to flow might also

be present in some locations. The testing indicated that the highest groundwater velocities from multilevels 3, 4, and 5 occurred at elevations 290.00 (15.38 m/d), 289.75 (35.57 m/d), and 289.50 masl (32.81 m/d), respectively, which is consistent with previous findings (Figure 4.06). A high velocity was observed at the PVP 3 probe located at 288.50 masl (9.07 m/d), corresponding to a sand unit (Figure 4.06). Multilevel PVP 4 was found to have high velocities at 294.00 masl (24.21 m/d) and 291.30 masl (27.10 m/d), associated with well-sorted gravel and moderately-sorted sandy gravel units, respectively. PVP 5 detected a high velocity layer consisting of gravel at 289.00 masl (34 m/d).

Taken together, the PVP derived velocities averaged about 12 m/d. The highest Darcy-calculated velocity from grain-size analyses and slug testing was about 4 m/d (Section 3.1). This discrepancy cannot easily be explained by uncertainties in either *n* or *i* alone, leaving uncertainty in *K* as the likely source of the disagreement. Since the CIS tracer test validated the PVP measurements, it would seem that the conventional velocity estimation, based on Darcy calculations, is the method with the largest bias in this case. Previous studies of PVPs in granular aquifers and in laboratory sand tanks showed better agreement between PVP velocities and those from Darcy calculations (Labaky et al. 2009; Schillig et al. 2011; Bowen 2010). Therefore, the differences at the Woodstock site must reflect conditions in the aquifer that differ from those in the previous investigations. Given that the degree of heterogeneity of the aquifer greatly exceeds that in earlier PVP work, the differences are perhaps not surprising (Alexander et al. 2011). Notably, the differences illustrate how PVP measurements can provide valuable additional insight to a site characterization program by providing an independent validation on Darcy-derived velocities.

A vertical component to flow was detected at most probe locations, supporting the hypothesis for flow at the site. The exceptions were probes at 290.00 masl and 288.50 masl on PVP 3; 290.00 masl, 289.50 masl on PVP 4; and 294.00 masl and 290.00 masl on PVP 5 (Figure 4.06). Vertical flow was typically found to exist in finer and/or mixed sediment zones. Where the core record was complete, velocities in these units indicated vertical flow tended to converge on coarser sediment textures (including zones where recovery was poor, suggesting non-cohesive, coarse-grained material) and/or layers with a high degree of relative sorting. The complex glacio-fluvial and till origins of the site sediments – shown to be highly variable in texture by grain-size analyses – would be expected to produce locally discontinuous strata consistent with the observed flow patterns (Haslauer 2005). In summary, the observed flow directions appear to make hydrogeologic sense. The converging vertical flow in both up and down directions at PVPs 3, 4, and 5, indicate that density-driven transport of the NaCl tracer was not a major factor in these experiments.

Directional data determined using the horizontal flow detectors on the PVPs were compiled to indicate an average flow azimuth (direction) of N123°E ± 28°, ranging from N53°E to N152°E, a 99° variation in direction (Figure 4.05). Overall, 66% of the horizontal flow directions measured satisfied the requirement that $\alpha < 110°$ from the injection port, making magnitude and direction estimations possible. The southeasterly flow direction is in agreement with both the *i* estimates, reported in Section 3.2 (Figure 4.05) and a water-table map generated from water-levels collected two weeks after testing of multilevel PVPs 3, 4, and 5 (Figure 4.02). The agreement between measured velocity direction and that predicted by the hydraulic gradient suggests that anisotropy at the site is minimal. The 99° range in flow

directions, as determined with the PVPs is undeniably large. Since PVPs sample flow velocities at the centimeter-scale, the observed range in measured flow directions is thought to be related to the scale of the measurement. However, the agreement between the average PVP velocity direction and that determined from the conventional methods supports the validity of the PVP measurements.

4.3: Conclusions

It is concluded that PVPs generated estimates of groundwater velocity in a heterogeneous, sand and gravel aquifer that were in close agreement with natural gradient (CIS) tracer testing. PVP datasets exhibited notable variability in both magnitude and direction from location to location, but the velocities were generally reproducible on a probe by probe basis, indicating the tests were not simple artifacts of the probes. The directional variations (N53^{o}E to N152^{o}E) were attributed to natural variability at the centimeter scale, but this could not be definitively verified. Directions determined by three-point estimators also showed high variability (N90°E to N166°E), but this was primarily due to anomalous head measurements from a single well. Removing that well from the analysis resulted in much reduced variability in *i*-from estimator to estimator. The relatively low variability is attributable to the scale of the measurements, which are on the order of the well screen lengths (several meters). It is further concluded that PVPs enhanced the characterization of flow systems due to their ability to detect narrow zones of high velocity, and vertical flow components in addition to horizontal ones.

References

Abriola, L.M., and G.F. Pinder. 1982. Calculation of velocity in 3 space dimensions from hydraulic-head measurements. Ground Water 20 no. 2: 205-213.

Alexander, M., S.J. Berg, and W.A. Illman. 2011. Field Study of Hydrogeologic Characterization Methods in a Heterogeneous Aquifer. Ground Water 49 no. 3: 365-382.

Ballard, S. 1996. The In Situ Permeable Flow Sensor: A ground-water flow velocity meter. Ground Water 34 no. 2: 231-240.

Bayless, E.R., W.A. Mandell, and J.R. Ursic. 2011. Accuracy of flowmeters measuring horizontal groundwater flow in an unconsolidated aquifer simulator. Ground Water Monitoring and Remediation 31 no. 2: 48-62.

Bird, W.E., R.B. Stewart, and E.N. Lightfoot. 1960. Transport Phenomena. New York: John Wiley & Sons.

Blott, S.J., and K. Pye. 2001. GRADISTAT: A grain size distribution and statistics package for the analysis of unconsolidated sediments. *Earth Surface Processes and Landforms* 26 no. 11: 1237-1248.

Bohling, G.C., J.J. Butler, X.Y. Zhan, and M.D. Knoll. 2007. A field assessment of the value of steady shape hydraulic tomography for characterization of aquifer heterogeneities. Water Resources Research 43 no. 5: W05430. DOI:10.1029/2006wr004932.

Bowen, I.R. 2010. Characterization of a Dipole Flow System Using Point Velocity Probes. M.Sc. Thesis, Department of Geology, University of Kansas, Lawrence.

Bowen, I.R., Devlin, J.F., Schillig, P.C.(in review). Design and testing of a convenient benchtop sandbox for controlled flow experiments. Submitted to Ground Water Monitoring and Remediation.

Butler, J.J., Jr. , C.D. McElwee, and W.Z. Liu. 1996. Improving the quality of parameter estimates obtained from slug tests. *Ground Water* 34 no. 3: 480-490.

Butler, J.J., Jr. 2005. Hydrogeological methods for estimation of spatial variations in hydraulic conductivity. In Hydrogeophysics, ed. Y. Rubin and S. S. Hubbard, 23-58. Dordrecht, The Netherlands: Springer.

Corporation of the County of Oxford. 2001. Quaternary Geology: The Corporation of the County of Oxford, Woodstock, Ontario, Canada.

Corporation of the County of Oxford. 2003 A. Municipal Water Wells: The Corporation of the County of Oxford, Woodstock, Ontario, Canada.

Corporation of the County of Oxford. 2003 B. Roads: The Corporation of the County of Oxford, Woodstock, Ontario, Canada.

Cowan, W.R. 1978. Trend surface analysis of major late Wisconsinan till sheets, Brantford-Woodstock area, southern Ontario. Canadian Journal of Earth Sciences 15 no. 6: 1025-1036.

Critchley, K. 2010. Stimulating In Situ Denitrification in an Aerobic, Highly Conductive Municipal Drinking Water Aquifer. M.Sc. Thesis, Department of Earth Sciences, University of Waterloo, Waterloo, Ontario, Canada.

Devlin, J.F. 1994. A Simple and Powerful Method of Parameter-Estimation Using Simplex Optimization. *Ground Water* 32 no. 2: 323-327.

Devlin, J.F., and J.F. Barker. 1996. Field investigation of nutrient pulse mixing in an in situ biostimulation experiment. *Water Resources Research* 32 no. 9: 2869-2877.

Devlin, J.F. 2003. A spreadsheet method of estimating best-fit hydraulic gradients using head data from multiple wells. Ground Water 41 no. 3: 316-320.

Devlin, J.F., and C.D. McElwee. 2007. Effects of measurement error on horizontal hydraulic gradient estimates. Ground Water 45 no. 1: 62-73.

Devlin, J.F., G. Tsoflias, M. McGlashan, and P. Schillig. 2009. An Inexpensive Multilevel Array of Sensors for Direct Ground Water Velocity Measurement. Ground Water Monitoring and Remediation 29 no. 2: 73-77.

Devlin, J.F., Schillig, P.C., Bowen, I., Critchley, C.E., Rudolph, D.L., Thomson, N.R., Tsoflias,G.P., Roberts, J.A. (in revision) Applications and Implications of Direct Groundwater Velocity Measurement at the Centimetre Scale. Journal of Contaminant Hydrology.

Drost, W., D. Klotz, A. Koch, H. Moser, F. Neumaier, and W. Rauert. 1968. Point dilution methods of investigating ground water flow by means of radio isotopes. Water Resources Research 4 no. 1: 125-146.

Gierczak, R., J.F. Devlin, and D.L. Rudolph. 2007. Field test of a cross-injection scheme for stimulating in situ denitrification near a municipal water supply well. Journal of Contaminant Hydrology 89 no. 1-2: 48-70.

Haslauer, C.P. 2005. Hydrogeologic analysis of a complex aquifer system and impacts of changes in agricultural practices on nitrate concentrations in a municipal well field, Woodstock, Ontario. M.Sc. Thesis, Department of Earth Sciences, University of Waterloo, Waterloo, Ontario, Canada.

Hemsi, P.S., and C.D. Shackelford. 2006. An evaluation of the influence of aquifer heterogeneity on permeable reactive barrier design. Water Resources Research 42 no. 3: W03402. DOI: 10.1029/2005wr004629.

Johnson, R.L., R.B. Thoms, R.O. Johnson, and T. Krug. 2008. Field evidence for flow reduction through a zero-valent iron permeable reactive barrier. Ground Water Monitoring and Remediation 28 no. 3: 47-55.

Kearl, P.M. 1997. Observations of particle movement in a monitoring well using the colloidal borescope. Journal of Hydrology 200 no. 1-4: 323-344.

Kelly, W.E., and I. Bogardi. 1989. Flow directions with a spreadsheet. Ground Water 27 no. 2: 245-247.

Krzyszkowski, D.K.P.F. 2001. Wisconsinan inter-lobal stratigraphy in three quarries near Woodstock, Ontario. Géographie physique et Quaternaire 55 no. 1: 3-22.

Labaky, W., J.F. Devlin, and R.W. Gillham. 2007. Probe for measuring ground water velocity at the centimeter scale. Environmental Science & Technology 41 no. 24: 8453-8458.

Labaky, W., J.F. Devlin, and R.W. Gillham. 2009. Field comparison of the point velocity probe with other groundwater velocity measurement methods. Water Resources Research 45: 9.

Leblanc, D.R., S.P. Garabedian, K.M. Hess, L.W. Gelhar, R.D. Quadri, K.G. Stollenwerk, and W.W. Wood. 1991. Large-scale natural gradient tracer test in sand and gravel, Cape-Cod, Massachussetts. 1. Experimental-design and observed tracer movement. Water Resources Research 27 no. 5: 895-910.

McKenna, S.A., and A. Wahi. 2006. Local hydraulic gradient estimator analysis of long-term monitoring networks. Ground Water 44 no. 5: 723-731.

Melville, J.G., F.J. Molz, and O. Guven. 1985. Laboratory investigation and analysis of a groundwater flowmeter. Ground Water 23 no. 4: 486-495.

Momii, K., K. Jinno, and F. Hirano. 1993. Laboratory studies on a new laser doppler-velocimeter system for horizontal groundwater velocity-measurements in a borehole. Water Resources Research 29 no. 2: 283-291.

Moore, Y.H., R.K. Stoessell, and D.H. Easley. 1992. Fresh-water sea-water relationship within a ground-water flow system, northeastern coast of the Yucatan Peninsula. Ground Water 30 no. 3: 343-350.

Pinder, G.F., M. Celia, and W.G. Gray. 1981. Velocity calculation from randomly located hydraulic heads. Ground Water 19 no. 3: 262-264.

Piotrowski, J.A. 1987. Genesis of the Woodstock Drumlin Field, Southern Ontario, Canada. Boreas 16 no. 3: 249-265.

Ritzi, R.W., D.F. Dominic, A.J. Slesers, C.B. Greer, E.C. Reboulet, J.A. Telford, R.W. Masters, C.A. Klohe, J.L. Bogle, and B.P. Means. 2000. Comparing statistical models of physical heterogeneity in buried-valley aquifers. Water Resources Research 36 no. 11: 3179-3192.

Russo, D., and E. Bresler. 1981. Soil hydraulic-properties as stochastic-processes. 1. An analysis of field spatial variability. Soil Science Society of America Journal 45 no. 4: 682-687.

Schillig, P.C., J.F. Devlin, J.A. Roberts, G.P. Tsoflias, and M.A. McGlashan. 2011. Transient Heterogeneity in an Aquifer Undergoing Bioremediation of Hydrocarbons. Ground Water 49 no. 2: 184-196.

Schillig, P.C. 2012. VelProbePE: An Automated Spreadsheet Program for Interpreting Point Velocity Probe Breakthrough Curves. Computers & Geosciences 39: 161-170.

Silliman, S.E., and C. Frost. 1998. Monitoring hydraulic gradient using three-point estimator. Journal of Environmental Engineering 124 no. 6: 517-523.

Silliman, S.E., and G. Mantz. 2000. The effect of measurement error on estimating the hydraulic gradient in three dimensions. Ground Water 38 no. 1: 114-120.

Springer, R.K., and L.W. Gelhar. 1991. Characterization of Large-Scale Aquifer Heterogeneity in Glacial Outwash by Analysis of Slug Tests with Oscillatory Response, Cape Cod, Massachusetts. . U.S. Geological Survey Water Resources Investigation Report 91-4034: 36-40.

Sudicky, E.A. 1986. A natural gradient experiment on solute transport in a sand aquifer-Spatial variability of hydraulic conductivity and its role in the dispersion process. Water Resources Research 22 no. 13: 2069-2082.

Sudicky, E.A., W.A. Illman, I.K. Goltz, J.J. Adams, and R.G. McLaren. 2010. Heterogeneity in hydraulic conductivity and its role on the macroscale transport of a solute plume: From measurements to a practical application of stochastic flow and transport theory. Water Resources Research 46: W01508. DOI: 10.1029/2008wr007558.

Terzaghi, K. 1925. Erdbaumechanik auf Bodenphysikalischer Grundlage. Leipzig: Franz Deuticke.

Woodbury, A.D., and E.A. Sudicky. 1991. The geostatistical characteristics of the Borden aquifer. Water Resources Research 27 no. 4: 533-546.

Zemansky, G.M., and C.D. McElwee. 2005. High-resolution slug testing. Ground Water 43 no. 2: 222-230.

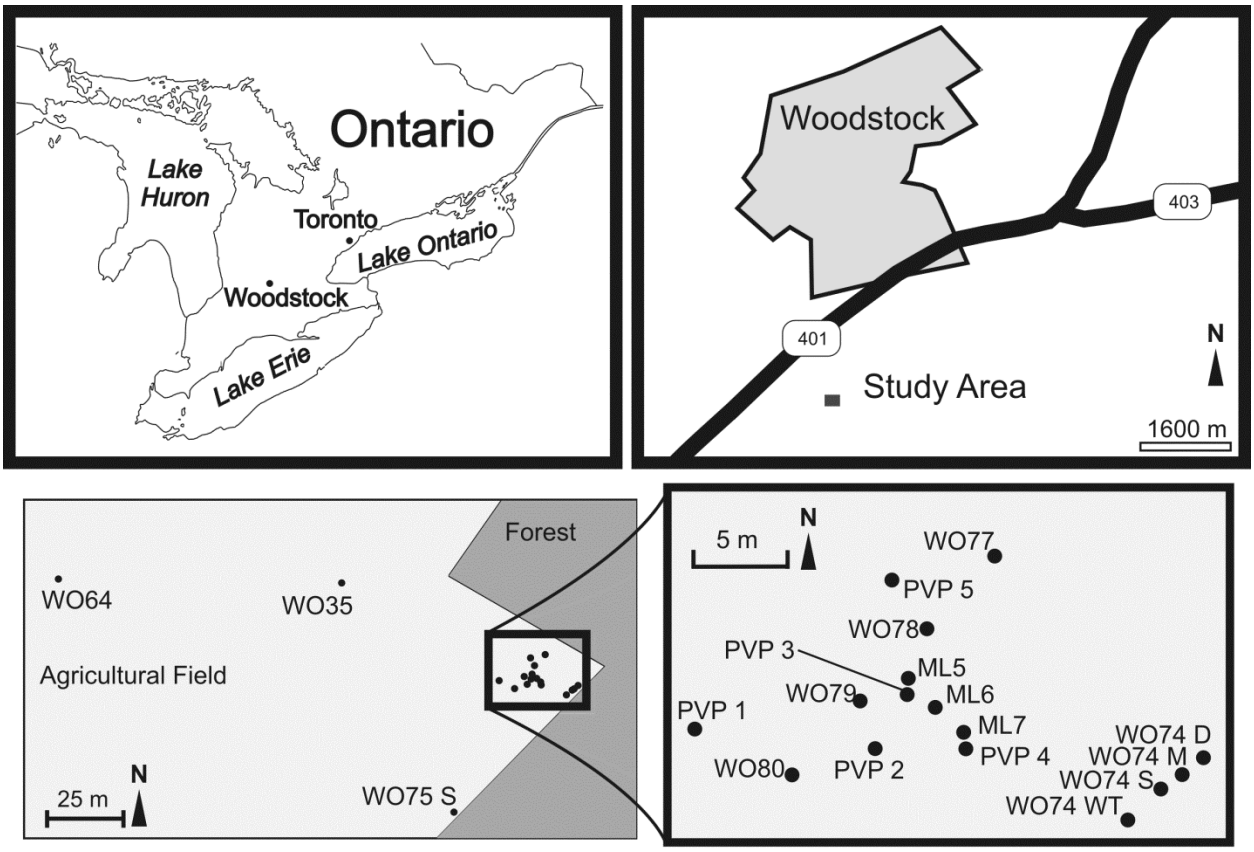

Figure 4.01: Location of the field site southwest of Woodstock, Ontario, Canada (top left and top right) and locations of wells used for monitoring water-levels, multilevel PVPs, and multilevel sampling (bottom left and bottom right).

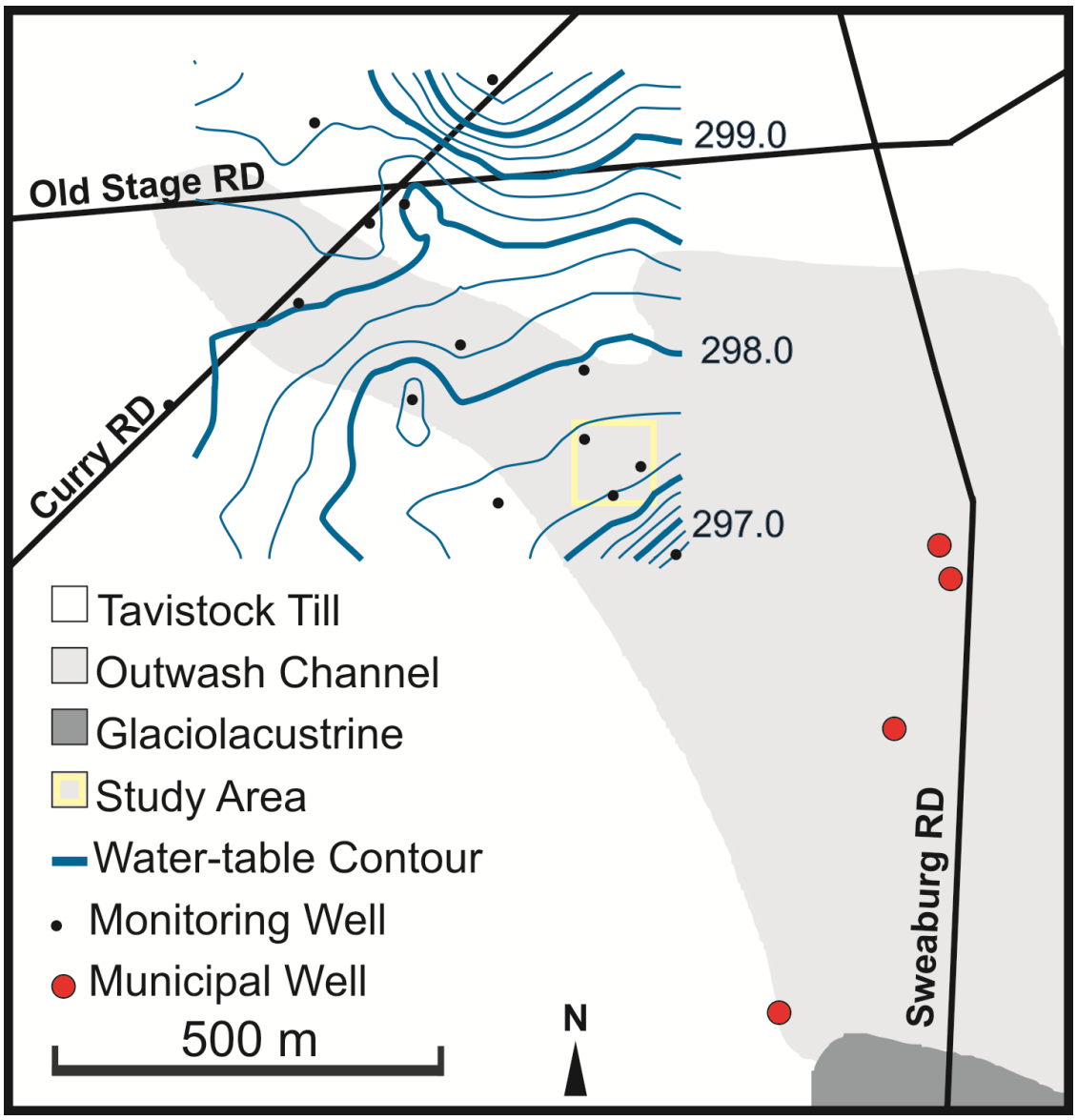

Figure 4.02: Water-table map using water-levels collected December, 2010, superimposed on geologic layers. Groundwater flows to the southeast and south into the outwash channel, toward the municipal well field. The study encompasses wells WO35 to the north, WO74 WT to the east, and WO75 S to the west (Figure 4.01). This map was generated using data acquired from The Corporation of the County of Oxford 2001, 2003 A, and 2003 B.

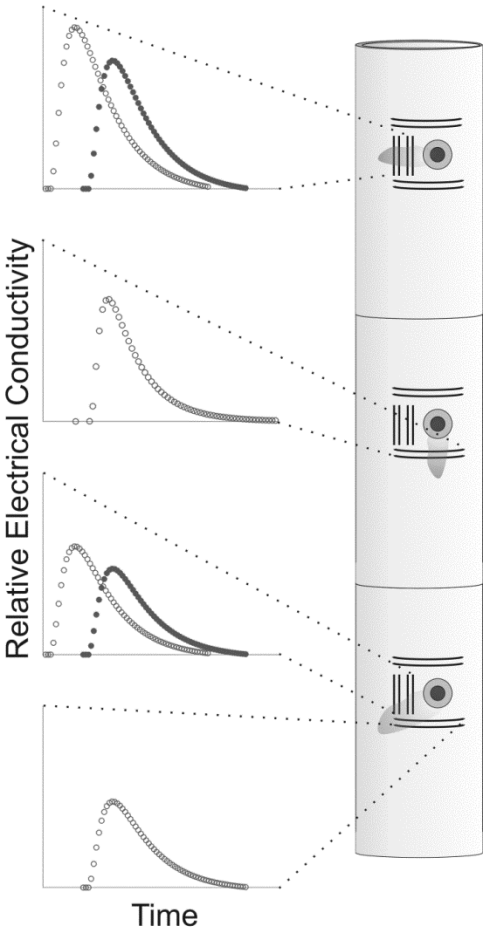

Figure 4.03: Schematic of three multilevel probes with detectors to the left of the injection port to monitor horizontal groundwater velocity and detectors above and below the injection port to ascertain vertical groundwater velocity. This was the design of multilevel PVPs 3, 4, and 5. Hypothetical breakthrough curve responses by the detectors are shown. The top PVP shows two breakthrough curves from the two detectors to the left of the injection port (open circles for the first horizontal flow detector and the solid circles are for the second horizontal flow detector). The middle PVP shows a breakthrough curve indicating downward vertical flow of an injected tracer (open circles). The bottom PVP shows the response to a combination of horizontal and vertical flow components.

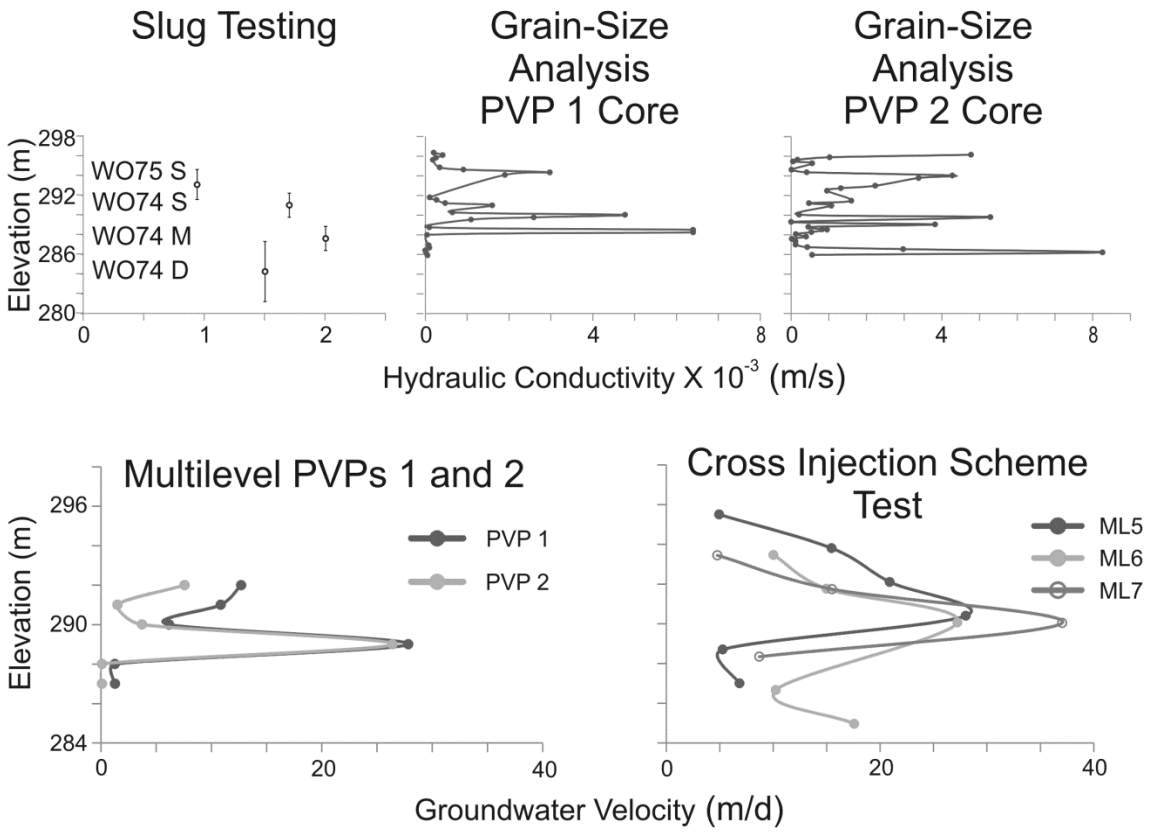

Figure 4.04: Comparison of *K* profiles from slug testing and grain-size analyses (top graphs) and groundwater velocity magnitudes from multilevel PVPs 1 and 2 and those from the CIS (bottom graphs).

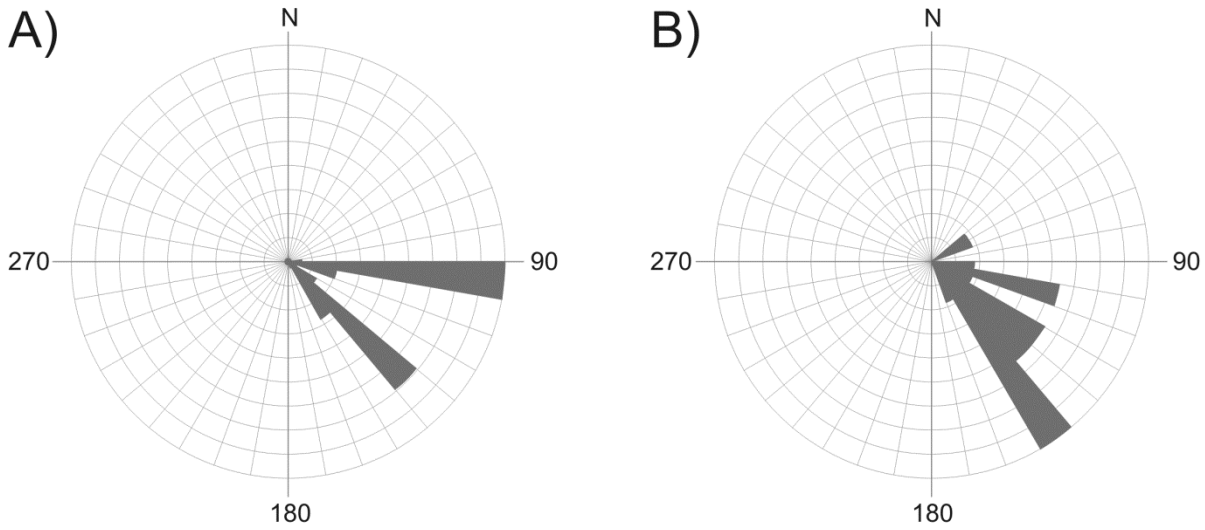

Figure 4.05: Horizontal flow directions determine from all three-point estimators that satisfied the b:h and head-drop requirements (A) and those from PVPs where $\alpha < 110°$. Note the bimodal distribution in A that indicates eastern and southeastern flow.

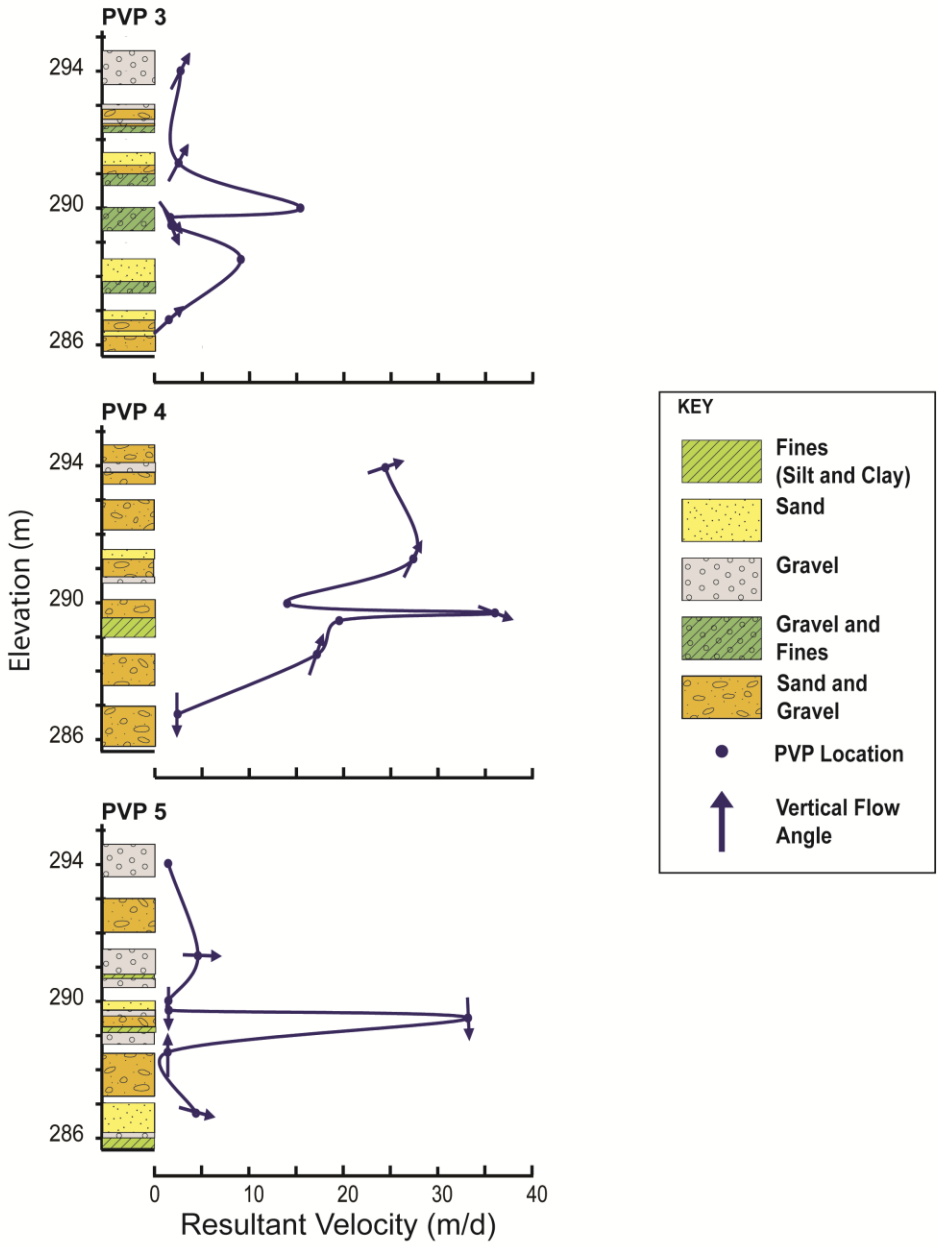

Figure 4.06: Profiles of resultant groundwater velocity magnitudes plotted with elevation from multilevel PVPs 3 (top profile), 4 (middle profile) and 5 (bottom profile). Geologic layers are plotted beside each velocity profile for comparison. Where vertical flow was measured, arrows indicate the calculated angle of flow.

5

Hydrological Factors Affecting the Bioclogging of a Heterogeneous Aquifer

5.0: Introduction

Over the past several decades, biostimulation has been employed to treat a variety of pollutants including petroleum hydrocarbons, chlorinated solvents, perchlorate, and nitrate (Alvarez and Illman 2006). Lab and modeling studies have demonstrated that biostimulation enhances microbial activity and may ultimately lead to the development of heterogeneities that affect flow (Baveye et al. 1998; Seki et al. 2006; Thullner 2010) and cause flow redirection (Seki et al. 2006; Kildsgaard and Engesgaard 2002). Permeability losses occur in response to cell and extracellular polysaccharide accumulation, gas production, and mineral precipitation. Geesey and Mitchell (2008) proposed that a feedback exists between microbial growth and groundwater flow.

Various studies provide insight on how geological and hydrogeological considerations such as sediment texture (Sinclair and Ghiorse 1989; Fontes et al. 1991; Albrechtsen and Winding 1992; Albrechtsen 1994; Vandevivere et al. 1995; Dong et al. 2002; Levy et al. 2007; Hand et al. 2008), sorting (Thullner et al. 2002; Musslewhite et al. 2003; Levy et al. 2007), and groundwater velocity (Brusseau et al. 1999; Nakhla and Niaz 2002; Gu et al. 2007) may affect subsurface microbial distributions and clogging potential. However, there are presently few well controlled field studies that examine these interplays *in situ*. Currently, most field studies that investigate bioclogging have examined its effects on injection wells (Oberdorfer and

Peterson 1985; McCarty et al. 1998) or the formation of biobarriers (Ross and Bickerton 2002), some have documented evidence for clogging within aquifers, beyond near-well environments, based on tracer testing (Luo et al. 2007; Faybishenko et al. 2008). In a recent investigation at the Rifle Site, Colorado, 100 days of biostimulation resulted in different spatial patterns of chemically reduced electron acceptors compared with a bromide tracer and acetate (reactive). The differences were attributed to changes in groundwater velocity, in particular flow direction (Englert et al. 2009). Transport modeling indicated a likely cause for the differences was transience in the aquifer heterogeneity thought to result from biomass accumulation and mineral precipitation (Li et al. 2010).

Changes in groundwater flow following biostimulation were also observed by Schillig et al. (2011), in a petroleum contaminated sandy aquifer treated with dissolved oxygen from ORC®. Point velocity probes (PVPs), were installed along a fence 0.3 m down gradient of the oxygen source, and documented changes in groundwater velocity were interpreted to be caused by biomass accumulation in the pores. Evidence in support of this interpretation included a measured increase in biomass of approximately one order of magnitude in the biostimulated zone compared to unstimulated, background locations. The spatial and temporal changes in groundwater velocity constitute strong support for the idea of waxing and waning preferential flow paths, redirection of groundwater flow, and the development of a transient heterogeneity in response to oxygen amendments. However, many details concerning this phenomenon are poorly understood, including the factors that control the where in an aquifer the process of bioactive zone development begins, and ultimately where biomass build-up occurs affecting flow.

The purpose of this study was to evaluate the hydrogeological factors that influenced bioactive zone development in a biostimulated sand and gravel aquifer contaminated with nitrate. Evidence for flow redirection and changing groundwater speeds at the centimeter and meter scales was gathered with multilevel PVPs capable of measuring flow in 3-dimensions, and tracer testing across the site. The physical factors given special attention included distance from the biostimulation wells, groundwater velocity, sediment texture, and sorting.

5.0.1 Site Description

The study area consists of a series of unconfined sand and gravel aquifers located to the south of Woodstock, Ontario, Canada. The surficial geology comprises primarily Quaternary tills, deposited approximately 15,000 years ago, near an interlobate zone between two ice-sheets (Cowan 1978; Piotrowski 1987; Krzyszkowski 2001). During the Quaternary, multiple ice advances and retreats resulted in the deposition of alternating till and outwash sequences (Krzyszkowski 2001). The aquifer consists of a surficial glacialfluvial outwash channel, bounded by drumlinized Tavistock Till (Haslauer 2005) (Figure 5.01 A). Saturated hydraulic conductivities (*K*) were reported to range from 4.8×10^{-4} to 1.9×10^{-2} m/s (Critchley 2010). The average linear groundwater speed on the site is about 1 m/d (Devlin et al. 2012) though velocities approaching 30 m/d were reproducibly recorded within a thin, coarse-grained stratum between elevations 289 - 290 masl (10 - 11 m bgs) (Chapter 4) (Figure 5.02). Groundwater flows generally southeast, with a slight downward gradient toward the Thorton Well Field, which supplies water to the surrounding municipality (Haslauer 2005). Earlier studies identified a regional aquitard of poorly-sorted gravel and fine textured sediments separating a surficial aquifer from the deeper water supply aquifer (Padusenko 2001; Haslauer 2005) (Figure 5.02). Locally, the

aquitard is thin (< 0.5 m) and discontinuous, and a hydraulic window exists between the surficial and deeper aquifers below the study area (Padusenko 2001; Haslauer 2005; Bekeris 2007; Koch 2009; Critchley 2010) (Figure 5.02). The connection between the upper and lower aquifers is considered an important pathway for agriculturially-derived nitrate to reach the production wells. Concentrations of nitrate have steadily increased since the 1970s, exceeding the 10 mg/L-N regulatory limit at the wells by the mid-1990s (Padusenko 2001). To address this problem, best management practices (BMPs) have been adopted by farmers since 2003 to limit the over-application of nutrients within the capture zone of the Thornton Well Field. Despite these efforts, long lag times, on the scale of a decade or more, are expected before nitrate returns to acceptable levels in the aquifer (Meissner et al. 2002; Tomer and Burkart 2003; McMahon et al. 2006). To enable continued use of the water supply while BMPs exert their effects, the municipal government explored an integrated approach which augmented the BMPs with *in situ* denitrification. This form of bioremediation had previously been shown to be effective in an aquifer in the neighboring town of Baden, Ontario (Devlin et al. 2000; Gierczak et al. 2006; Gierczak et al. 2007).

5.0.2: Biostimulation at Woodstock

To remove excess nitrate, a pilot-scale cross injection scheme (CIS), similar to the design used in the denitrification feasability study of Baden, Ontario (Gierczak et al. 2007), was installed within the hydraulic window, upgradient of the municipal wells. Based on the principal of the nutrient injection wall (NIW) of Devlin and Barker (1996), the CIS operates by utlilizing a recirculating injection-extraction well-pair, oriented perpendicular to the hydraulic gradient (*i*), to emplace a a soluble wall of reactants in a targeted portion of an aquifer. Following the

injection phase, the wells are turned off and the nutrient pulse migrates through the aquifer under natural gradient conditions (Devlin and Barker 1996; Gierczak et al. 2007; Critchley 2010). Dispersion is relied upon to mix the contaminated groundwater with the injected pulses.

Acetate was used as an electron donor for the denitrification (Devlin et al. 2000; Istok et al. 2004; Khan and Spalding 2004; Gierczak et al. 2007; Englert et al. 2009; Critchley 2010). Stoichiometrically, the anticipated reaction requires 10 moles of carbon to remove 8 moles of nitrate if all the carbon is used for denitrification (Devlin et al. 2000):

$$5CH_3COO^-_{(aq)} + 8NO_3^-_{(aq)} + 3H^+_{(aq)} \leftrightarrow 10HCO_3^-_{(aq)} + 4N_{2(g)} + 4H_2O_{(l)} \quad (1)$$

In the presence of dissolved oxygen (DO), an additional 0.5 moles of carbon are required for every mole of O_2 present, to promote anaerobic conditions needed for denitrification:

$$CH_3COO^-_{(aq)} + 2O_{2\,(aq)} \leftrightarrow 2HCO_3^-_{(aq)} + H^+_{(aq)} \quad (2)$$

Even accounting for the presence of dissolved oxygen, previous experimentation using daily pulsed carbon injections at the Woodstock aquifer did not yield complete denitrification (Critchley 2010). However, concurrent studies of the Woodstock aquifer indicated higher than expected groundwater velocities (5 to 30 m/d), suggesting the daily flux of DO and nitrate through the treatment zone exceeded the loadings assumed in the earlier CIS design calculations (Critchley 2010, Chapter 4).

5.1: Methods

5.1.1: Determination of Hydraulic Gradient

Hydraulic gradients were calculated using nine wells from the 'WO' series (Figure 5.01 B and C). Details regarding well geometry and installation can be found in Critchley (2010). Hydraulic gradient calculations were based on manual water-level measurements collected while the groundwater velocity data were being collected with point velocity probes (PVPs, see below). Water-levels were measured for over a period of 84 days, which included the 55 day biostimulation experiment. The hydraulic gradient magnitude, *i*, and orientation were characterized from all possible three-point estimators (i.e., all possible combinations of 3 wells) in the well network (Pinder et al. 1981; Silliman and Frost 1998; McKenna and Wahi 2006). These estimates were filtered to exclude 1) gradients less than their respective uncertainties, i.e., where the maximum head drop between wells was less than three times the error on a water-level measurement (~ ± 1 cm) (Devlin and McElwee 2007) and 2) cases with base to height ratios outside the range of 0.5 to 5.0 (McKenna and Wahi 2006). Gradient magnitudes and orientation for each estimator were calculated as described by Devlin (2003). Uncertainties in all *i* calculations were reported as 1 standard deviation from the dataset population.

5.1.2: Groundwater Velocities from PVPs

Three PVP multilevel stands, designated multilevel PVPs 3, 4, and 5 were constructed with seven probes each using the design given by Devlin et al. (2009). Design and installation specifics are detailed in Chapter 4. Each probe was constructed with detectors placed at 40° and 70° from the injection port to detect horizontal flow. Additional detectors were constructed 3 cm above and below the injection ports to detect vertical flow. Horizontal and vertical velocities were treated as independent components of flow and used to estimate a resultant velocity. Thus, each PVP was capable of monitoring a groundwater velocity in 3-

dimensions. Multilevel PVPs 3 and 4 were installed near multilevel samplers ML5 and ML7, down-gradient of the carbon injection wells, WO78 and WO79, which make up the CIS (Figure 5.01). Multilevel PVP 5 was installed up-gradient and east of the CIS to monitor conditions in the aquifer in a non-biostimulated zone.

PVP multilevels were installed with the injection ports oriented ~ N30°W $\pm 1^{o}$. This set up permitted velocities to be measured as long as flow directions were between N150°E and N40°W. Data were acquired during non-CIS pumping periods. Typically, 3-7 mLs of tracer (1 g NaCl/14 L site groundwater) were required to produce a measurable signal on the PVP detectors. These volumes are higher than normal and suggest most of the injected tracer volume moved away from the probe surface, possibly facilitated by the coarse nature of the sediments. Tracer breakthrough at each detector was monitored at 10 second intervals using a Campbell CR1000 datalogger. Breakthrough curves were interpreted using a nonlinear optimizer coupled with a 1-dimensional solution to the advection dispersion equation (Schillig, 2012, Chapter 2) and theory developed by Labaky et al. (2007). In total, three to four individual probes were tested daily during the 55 days of biostimulation and each probe was tested at least three times prior to biostimulation.

During the multilevel PVP installation, continuous cores were recovered for grain-size analysis using the method of Blott and Pye (2001). Briefly, for a given grain-size distribution, sorting was determined from the standard deviation calculated from the geometrical method of moments and described using the scheme of Folk and Ward (1957). Textural classes were assigned based upon the relative proportion of grain-sizes as described by Folk (1954). Individual PVPs on each multilevel were installed specifically to monitor velocities in poorly-

sorted sediments (typically encountered at 290.0 and 289-288 masl, bounding the high velocity zone) and well-sorted gravels (typically encountered at 294.0, 291.3, 290-289, and 286.8 masl) (Chapter 4).

5.1.3: CIS Injections

The CIS system injected daily carbon pulses (as anhydrous sodium acetate) for a period of 55 days to stimulate heterotrophic denitrification. The required daily flux of acetate was calculated assuming the six-layered hydrostratigraphic model of Critchley (2010) supported with tracer testing-derived velocities from Chapter 4 and using the stoichiometrically required carbon mass (as acetate) to remove a 24-hour cumulative flux of DO and nitrate (equations 1 and 2):

$$M_{acetate} = \frac{M_m}{N_c} \sum_{j=1}^{6} \left(1.25\ V_j\ \Delta Z_j\ \Delta Y\ C_j^{Nitrate}\right) + \left(0.5\ V_j\ \Delta Z_j\ \Delta Y\ C_j^{DO}\right) \qquad [3]$$

where $M_{acetate}$ is the mass of acetate needed for the required moles of carbon (M), M_m is the molar mass of acetate (M/Mol), N_c is the number of carbon molecules in acetate (dim), j is the number of layers in the Critchley (2010) hydrostratigraphic model (dim), V_j is the prebiostimulated groundwater velocity of layer j (L/T), ΔZ_j is the thickness of layer j (L), ΔY is the distance between WO78 and WO79 (L), $C_j^{Nitrate}$ is the molar concentration of nitrate in layer j (Mol/L3), and C_j^{DO} is the molar concentration of DO in layer j (Mol/L3).

The acetate pulses were created by extracting groundwater from WO78 at an average rate of 190 L/minute, amending the groundwater with a 267,880 mg/L sodium acetate solution and re-injecting into WO79. The amendment was mixed with groundwater in-line at a rate of 0.20 L/min for a period of 5 hours, yielding an injection concentration of approximately 203

mg/L acetate. Following the injection period, the circulation cycle was continued for an additional hour to flush the wells and discourage clogging of the screens.

On two occasions, immediately before and after the treatment period (55 days), the acetate pulses were accompanied by pulses of bromide, a conservative tracer. Bromide breakthrough data at the multilevel wells provided information on flow paths and velocities in the treatment zone, and an independent check on PVP estimates of velocity. The bromide tracer pulse was created by amending the pumped groundwater stream with a 353,400 mg/L NaBr solution at a rate of 0.20 L/min for a period of 5 hours, yielding an injection concentration of approximately 224 mg/L. Samples were collected during and following the injection for a total period of 17-28 hours from down-gradient multilevel wells ML5 and ML7.

Groundwater velocities were calculated by fitting the observed Br^- breakthrough data to a 1-dimensional solution to the advection-dispersion equation (Devlin and Barker 1996):

$$C(x,t) = \frac{C_0}{2}\left[erfc\frac{x-\frac{w}{2R}-\frac{vt}{R}}{2\sqrt{\frac{DT}{R}}} - erfc\frac{x+\frac{w}{2R}-\frac{vt}{R}}{2\sqrt{\frac{D\left(t-\frac{w}{v}\right)}{R}}}\right] \qquad [4]$$

where

$$D = v\,\alpha_L + D^* \qquad [5]$$

C(x,t) is the solute concentration (M/L^3), C_O is the injection concentration (M/L^3), *x* is the distance from the midpoint of the tracer pulse (assumed to be directly between the CIS well pair) to the multilevel sampling well (L), *w* is the pulse-width of the tracer (L), *v* is the average linear groundwater velocity (assumed the same as tracer velocity) (L/T), *t* is time (T), *R* is the retardation factor (dimensionless), *D* is the hydrodynamic dispersion coefficient (L^2/T), α_L is the dispersivity (L), and *D** is the effective diffusion coefficient of the tracer (L^2/T).

Using the same bromide breakthrough data above, time independent tracer mass was calculated from the following equation from Devlin and Barker (1996):

$$C\ (x,t) = \frac{\frac{M}{\theta R}}{\sqrt{\frac{4\pi Dt}{R}}}\ exp\left(\frac{-(x-\frac{vt}{R})^2}{\frac{4Dt}{R}}\right) \qquad [6]$$

where *M* is the mass of tracer passing by a given multilevel sampling port (M) and θ is the porosity (dimensionless). Fitting observed breakthrough curves to obtain tracer mass and groundwater velocity at the individual sample ports was accomplished using a simplex optimizer to reduce the residual sum of squares between the calculated and observed data (Devlin 1994).

5.1.4: Geochemical Sampling

Sampling was conducted at multilevel wells ML5 and ML7 over a 17-28 hour period on days 1 and 55 of the treatment period. Sampling for anions, temperature, DO, alkalinity, and pH from ML5 and ML7 was conducted immediately following the acetate injections and approximately every 7-10 days during the entire biostimulation period, with more frequent anion and pH sampling during tracer testing (every 0.5 – 3.0 hrs) . Further details regarding sample handling and analysis can be found in Shaw (2012). Samples collected for anions during the biostimulated and tracer testing periods were analyzed for nitrate, nitrite, acetate, bromide, sulfate, and chloride. All anion samples were collected in 25 mL scintillation vials and frozen as soon as possible to minimize biological activity. Sample analysis was performed on a Dionex ICS 3000 ion chromatograph with a Dionex IonPac AS18 analytical column. Prior to analysis, samples were thawed completely in the refrigerator and mixed before analysis to avoid stratification due to freezing. One duplicate sample was analyzed for approximately every

14 samples. Alkalinity was measured using Hach field titration kits prior to the final tracer testing in September, 2011. For the final tracer test in September, 2011, filtered (0.45 µm) groundwater samples were collected with zero headspace in 60 mL high density polyethylene bottles that were stored on ice until analyzed within 3 days using a digital titration system. Given the inherent difficulty in accurately measuring carbonate alkalinity in high acetate waters, alkalinity was also estimated assuming HCO_3^- was the predominant anion needed for charge-balance. Cation samples were analyzed for sodium, potassium, magnesium, calcium, iron, and manganese. Samples were collected approximately every 5-17 hrs during tracer testing and field-filtered (0.45 µm) into 60 mL high density polyethylene bottles and preserved with 1.2 mL of concentrated nitric acid to maintain a pH of about 2. Cations were analyzed at the Plasma Analytical Laboratory (KU-PAL) at the University of Kansas using inductively coupled plasma atomic emission spectrometry (ICPAES). Based on cation concentrations, alkalinity, and pH temperature-specific saturation indices (*SI*) for calcite were calculated from

$$SI = \log \frac{[Ca^{+2}][CO_3^{-2}]}{K_{sp}\ CaCO_3} \qquad [7]$$

Where K_{sp} $CaCO_3$ at 10°C = $10^{-8.41}$. The $[CO_3^{-2}]$ was estimated using both measured and charge balance-derived alkalinity values, pH, and K_{sp} CO_3^{-2} at 10°C ($10^{-10.49}$) as follows:

$$CO_3^{-2} = \frac{[HCO_3^-][K_{sp}CO_3^-]}{10^{-pH}} \qquad [8]$$

5.1.5: Aqueous CO_2, N_2O, and CH_4 Concentrations

Samples for dissolved gases were collected from ML5 and ML7 during tracer testing, before and after the treatment period. Samples were collected in 70 mL serum bottles and

preserved with mercuric chloride. Both water and the associated degassed bubbles were collected to ensure all dissolved gases were retained. Sample collection consisted of placing the sealed serum bottles under a vacuum created by twice withdrawing the plunger from a 60 mL syringe. Following a 120 mL purge, the samples were collected from the multilevel samplers into 60 ml syringes and immediately transferred into the evacuated serum bottles. The bottles were filled until the vacuum in each was dissipated. The serum bottles were then immediately sealed with silicone cement and inverted to minimize the loss of headspace gases through the septa, stored on ice in the dark, and analyzed within five days of collection for CO_2, N_2O, and CH_4.

Analyses were performed on a gas chromatograph equipped with a Haysept Q 80/100 1/8 in x 6 ft stainless steel column using the thermal conductivity detector (TCD). Henry's law was used to calculate the aqueous concentrations from measured headspace gas concentrations. To determine if any of the above mentioned species existed as bubbles under the conditions in the aquifer, aqueous concentrations were compared to their respective solubilities (Appendix 27).

5.1.6: Biomass Estimation

Prior to and after the treatment time, core samples were extracted from the locations near the PVP stands 3 and 4 to characterize the biomass distribution vertically. Core extracted prior to biostimulation was analyzed to establish background cell numbers. Biomass concentrations were determined based on total lipid biomass analysis. Aseptic methods were used in the handling of core materials and tools (Barbaro et al. 1994). Cores were extracted,

sampled at elevations corresponding to the placement of individual PVPs, homogenized, freeze dried and stored in the dark at -80° C to prevent phospholipid degradation. All samples were analyzed in duplicate using the methods for extraction and lipid-phosphate separation given by Findlay et al., (1989). Concurrently, orthophosphate standards made from glycerol phosphate were processed in duplicate. In preparation for analysis, samples and standards were combined with ammonium molybdate and malachite green solutions and decanted into a cuvette where absorbance was recorded at 610 nm with a Spectronic GENESYS 20 spectrophotometer. The phosphate content of each sample was related to cell mass using the average of a range of conversion factors reported by Dobbs and Findlay (1993) (3.4×10^7 to 2.0×10^9 cells/nmol PO_4) and the average concentration of cells/gram dry weight aquifer material (core) was estimated for each sample. Conversion factors used to characterize microbial consortia with lipid based approaches vary in the literature (Findlay et al. 1989; Dobbs and Findlay 1993; Green and Scow 2000). Therefore, an average was used in this study and biomass comparisons made to other studies are limited to those which used lipid-based approaches.

5.1.7: Numerical Modeling

To identify the effects of *i* on the groundwater velocities determined by tracer testing and PVPs, a 3-dimensional flow model, based on the 5 layer hydrostratigraphic model of Critchley (2010) was constructed with Visual Modflow Pro 2.82. The model domain was 100 m x 100 m centered on the CIS with a total of 129,360 nodes. Two simulations were conducted to model conditions representing the July and September, 2011 tracer tests. Constant head

boundaries were assigned based on an average of all viable three-point estimators for the July (*i* = 0.0034) and September (*i* = 0.0032), 2011 tracer tests, respectively. Average observed pumping rates from the July and September, 2011 tracer tests were measured to be 203 L/min and 187 L/min, respectively. Each simulation was conducted to steady-state with 4 time steps representing the 4 hours of active pumping and 4 time steps representing 36 hours of non-pumping.

5.2: Results and Discussion

5.2.1: Effect of Biostimulation on Flow Determined from Darcy's Law

While velocity reductions were observed at MLs 5 and 7 and multilevel PVPs 3 and 4, analysis of *i* is needed to ascertain these changes. The site specific effect of *i* on velocity in this case can be assessed in a preliminary fashion by assuming porosity and *K* remained constant for the duration of the experiment. Under these conditions, variations in *i* would be the major controlling factor determining groundwater velocity. The gradients calculated from 59 acceptable estimators over 44 days of water level measurements, ranged from 0.0036 to 0.0031, resulting in a maximum percent difference of 14%. This interval included the times during which tracer tests were performed and pumping rates at the CIS varied from 203 L/min to 187 L/min. Numerical modeling that accounted for the regional changes in *i* of the test area before and during the treatment time predicted velocity variations from -9 to +18%, indicating that any flow variations estimated from Darcy's Law were explainable on the basis of regional flow. An attempt was made to make a similar evaluation in the immediate vicinity of the biostimulated zone of the CIS. However, an analysis of *i* from the three-point estimators surrounding the CIS (wells WO77, WO78, WO79, WO80, WO74WT, and WO74S) indicated no

statistically significant change in the direction of the hydraulic gradient (~ N127°E) over the treatment time, based on t-test of average directions before and after biostimulation. (Appendix 14).

The data presented above clearly show that conventional methods of evaluating flow across a bioactive treatment zone were unable to discern any associated flow changes. However, the wells were designed with screens 1.22 to 10.67 m in length, which probably limited the sensitivity of analysis. As shown below, a very different story emerged when high definition measurements were used to make the same assessment.

5.2.2: Effects of Sediment Texture and Sorting on Changes in Velocity

Centimeter-scale PVP velocities (incorporating both horizontal and vertical components), averaged at each probe over all measurements before biostimulation (prebiostimulation) and after biostimulation (post biostimulation), and horizontal velocities from CIS tracer testing were examined for evidence of flow changed by biostimulation (Figure 5.03). Qualitatively, the variations of velocity with depth were similar before and after biostimulation in both cases (Figure 5.03). Velocity profiles from the PVPs indicated that shallow velocities were relatively unchanging, but an abrupt increase occurred in conjunction with a stratum of high gravel content between 289 -290 masl (Figure 5.03 A). Below that stratum, velocities returned to magnitudes similar to the shallow levels, but a second increase occurred at the bottom of the monitored zone, near multilevel PVP 4 (Figure 5.03 A).

Comparing averaged pre- and post-biostimulation datasets, results from multilevel PVP 5, located up-gradient of the CIS, indicated a general increase in groundwater velocity at the site over the treatment period. The largest increases in velocity at multilevel PVP 5 were noted

in high velocity zones at 289 – 290 masl and 286.8 masl, both locations identified to have well-sorted gravels.

The results from the PVP 5 stand contrasted sharply with overall declines in velocity that were observed at multilevel PVPs 3 and 4 (except the high velocity zone at 289 - 290 masl). An examination of the velocities before and after biostimulation shows changes at various depths that are statistically significant at a 67% level of confidence (one standard deviation) (Figure 5.03 A-C). Similar trends in velocity with depth were obtained from the CIS tracer testing (Figure 5.03 D-F). Moreover, the magnitudes of the velocities obtained from the independent tests were comparable, typically within a factor of two.

Relatively large decreases in CIS tracer velocities at ML7 and at multilevel PVPs 3 and 4 were consistently observed at elevations 290 masl and 288 - 289 masl, immediately above and below the high velocity zone (Figure 5.03 C and F). Core extracted at multilevel PVPs 3 and 4 at these elevations indicated both locations to consist of poorly-sorted sands with 12% and 4% gravel, respectively. Other locations that reported large decreases in velocity (between 41% and 132%) include: 291.3 - 292.1 masl at multilevel PVP 3 and ML5 where a mixed sand and gravel unit contacts a well-sorted gravel unit (Figure 5.03 C and F) and 295.2 masl at ML7 where, unfortunately, no core material was recovered. This observation is in agreement with Vandivevere et al. (1995) who found finer-grained sediments are more efficiently clogged than coarser sediments because a smaller fraction of biomass is needed to cause considerable changes in permeability.

Consistent with the findings of Vandivevere et al. (1995), well-sorted gravels associated with relatively high velocities before biostimulation consistently tended to experience minor

declines or increases in velocity magnitude after biostimulation. Examples of these cases include probes on multilevel PVPs 3 and 4 within the well-sorted gravel at 289 - 290 masl, multilevel PVP 4 near the contact of a moderately-sorted sand and gravel unit at 291.3 masl, and a well-sorted gravel unit at MLs 5 and 7 between 293.5 - 293.8 masl (Chapter 4).

Previous study has shown that significant vertical flow can exist in low velocity units when they are adjacent to high velocity units (Chapter 4). With the observed velocity declines following biostimulation, the potential exists for flow redirection into adjacent high velocity units. Accordingly, evidence for vertical flow redirection toward the high velocity zone was observed at multilevel PVP 3 (Figure 5.04) at elevations 288.5 and 289.5 masl (Figure 5.04).

In summary, the greatest changes to groundwater velocity effect of texture in the biostimulated zone of the aquifer occurred in the finer grained, poorly sorted sediments. This result was in contrast to that in coarser, well-sorted sediments where smaller declines or increases in groundwater velocity were observed in the biostimulated zone. This finding suggests that the biological activity that would eventually grow into the bioactive zone was probably initiated in the poorly sorted sediments at the interface of the highly conductive stratum 2.7 to 5.6 meters down-gradient from the CIS injection wells. The reason for the down-gradient offset is likely related to the CIS pulsing rather than textural characteristics, and this is explored below.

5.2.3: Effects of Nutrient Pulsing on Changes in Velocity

Nutrient pulsing for biostimulation is a strategy that has been used to limit bioclogging of injection wells (Devlin and Barker 1996; Khan and Spalding 2004; Gierczak et al. 2007; Critchley 2010). Daily pulses of acetate were designed to mix by dispersion within about 5

meters of the CIS couplet, at the approximate location of ML7, based on the velocities previously reported (Chapter 4). Measured breakthrough curves, superimposed to reflect repeated pulsing, confirmed that mixing had occurred (Figure 5.06). These data indicate that a constant supply of acetate was available to subsurface bacteria between the CIS and ML7, with the locations of the onset of mixing (at a level sufficient to stimulate microbial activity) likely being depth specific. Multilevel PVP 4 and ML7 marked the locations with the greatest measured decreases in velocity, while velocities nearest to the CIS, at multilevel PVP 3, ML5, and the background multilevel PVP 5 were least affected by the CIS operation (Figure 5.03 C and F). The availability of nutrients has been shown to greatly influence temporal and spatial variability in microbial activity (McClain et al. 2003), particularly in pulsed delivery systems (Devlin and Barker 1996). Time-lapse monitoring of the PVPs before and after biostimulation provided evidence for variations in flow related to the pulsing of nutrients (Figure 5.05 A). For example, it was remarked that the probes in well-sorted gravels on multilevel PVPs 4 and 5 exhibited an increase in the variance of velocity magnitudes (considering both horizontal and vertical components) after biostimulation (Figure 5.05 A). This observation suggests that the factors affecting flow were dynamic during the experiment, evidence for truly transient heterogeneity. The increases in variance, in particular those associated with the vertical components of velocity, were found to be statistically significant ($\rho < 0.10$) at multilevel PVP 3, near the source of the injections, based on a two-tailed F-test (Figures 5.04 and 5.05 A). This phenomenon can be explained if the pulsing caused intermittent periods of bioactivity – while the nutrients were present – followed by periods of inactivity between nutrient pulses. In contrast, the horizontal flow measured at multilevel PVPs 4 and 5, as well as those calculated

on the basis of the three point estimators, exhibited no changes in variance, possibly because the nutrient delivery was more even in time at those locations. At PVP stand 5 this would be so because the stand was located upgradient of the CIS, at multilevel PVP 4 it would be so because of the mixing achieved by dispersion.

Flow redirection would be expected to cause changes in tracer delivery to monitoring points in the treatment zone, providing an independent assessment of the importance of the flow variances above. To conduct this assessment, profiles of the tracer mass that passed ML5, near the injection source, were calculated from equation 6 and found to be essentially unchanged by the treatment process (Figure 5.05 B). This indicates that although flow was variable in this area, there was no permanent flow redirection. However, the same analysis at ML7, located in the intended nutrient mixing zone, indicated notable differences at elevations 293.5 and 288.4 masl that could not be linked to differences in sediment texture, sorting, or changes in velocity (Figure 5.05 B). Clearly, flow redirection was indicated at ML7, and was sufficiently important at some depths that differences could be measured in tracer mass breakthrough. Since the probes at multilevel PVP 4, near ML7, did not indicate notable flow direction changes, the flow redirection observed at ML7 must have actually occurred upgradient of the monitor, but down-gradient of ML5.

In summary, the nutrient pulsing was designed to achieve a constant feed to nutrients several meters down-gradient of the injection system, between ML5 and ML7. Where mixing was incomplete, near the injection area (ML5), groundwater velocity was observed to be highly variable. Between ML5 and ML7 mixing was better achieved and groundwater flow was altered in a more stable way, both in magnitude and direction. In this way, nutrient pulsing of the CIS

exerted a control on the down-gradient location of bioactive zone development. The associated biological activity was shown to remove nitrate from the groundwater at rates sufficient to approach or surpass the goals for the project.

5.2.4: Mechanism for Velocity Changes

If dispersive mixing really localized the bioactivity, and the measured velocity changes were really reflective of biomass accumulation, or related secondary processes, it would be expected that the various signatures of oxygen utilization and denitrification (geochemical and microbiological) would be similarly localized. In fact, within the first day of acetate injection, the disappearance of oxygen and nitrate was observed between ML5 and ML7. At ML5, aerobic conditions tended to persist at most depths, though nitrate concentrations exhibited high variability with depth (Figure 5.07). At ML7, where pulse mixing was well established and microbial growth continuously supported, a generally more reducing environment prevailed and observed nitrate concentrations remained at or below the regulatory limit of 10 mg/L-N at all depths above 285.0 masl (Figure 5.07). Heterotrophic denitrification was interpreted to be the mechanism for nitrate removal as indicated by the disappearance of nitrate with the limited production of nitrite, and nitrous oxide. This conclusion was further supported by the appearance of nitrous oxide in the acetylene block experiments on core material collected at the end of the 55 days of injection (Appendix 25). These data support the notion that biostimulation was localized in large part due to the dispersive mixing zone created by the CIS.

Strata with relatively large fractions of gravel, located at 289 – 290 masl and, less dramatically at 286.8 m, exhibited a limited tendency to support denitrification, based on

nitrate persistence. The highest fluxes of nitrate were associated with these strata both before and during treatment (Appendix 23). In addition, these strata were assessed as having relatively low approximate zero-order denitrification rates (Figure 5.08), calculated from

$$\text{Denitrification Rate} = \frac{M_{pre} - M_{post}}{T_{res}} \qquad [9]$$

Where M_{pre} and M_{post} represent the mass determined from measured nitrate concentrations normalized to the assumed volume (4900 L) of aquifer represented by the monitoring point at ML5 or 7 before and after biostimulation, respectively. T_{res} represents the residence time calculated by dividing the distance from the CIS by the post-biostimulated velocity measured at ML5 and 7 for bromide. The highest zero-order denitrification rates (Figure 5.08) were found at elevations with notable differences in bromide mass delivery (Figure 5.05 B). The lower denitrification rates were found in the coarse-grained, high velocity sediments (Figure 5.08). The relative intensities of denitrification were in agreement with those determined by Critchley (2010) below 293.00 masl.

After the 55 days of biostimulation, microbial numbers increased by about a factor of five, with the greatest increases occurring in the high velocity zone at 289 - 290 masl (Figure 5.09). Above this elevation, microbial concentrations near at multilevel PVPs 3 and 4 changed in a similar fashion, suggesting the observed changes did not depend on the dispersive mixing of the acetate pulses to the degree that nitrate removal did. The relatively high and continuous DO flux through these layers almost certainly led to some biomass production. This explains at least in part how the lower denitrification rates coincided with the highest overall increases in microbial populations, as shown in Figure 5.09.

Biomass concentrations decreased in only two locations: near multilevel PVP 3 at elevation 288.5 masl, and near multilevel PVP 4 at 286.8 masl, both corresponding to high pre-biostimulation velocities (Figure 5.09). This unexpected result could have been an artifact of the methods used to measure biomass, since the clasts at this depth (87% gravel at the PVP 4 location) could have biased the mass-normalized total lipid biomass estimates downward. Biogenic gas accumulation or mineral precipitation could potentially influence groundwater velocity, however these parameter revealed little change in the aquifer over the treatment time. Concentrations of $CO_{2\ (aq)}$ were found to range between 13 and 30% of solubility while less than 6 mg/L of $N_2O_{\ (aq)}$ and no $CH_{4\ (aq)}$ were detected on days 0 and 55 (Table 5.1) (Appendix 27). Mineral precipitation was evaluated through saturation index calculations from samples collected on days 0 and 55 (Appendix 22). Calcium and bicarbonate were the predominant cation and anion with concentration ranges of 4.3-6.9 meq/L and 4.6-9.5 meq/L, respectively (total solution ionic strength =3.3 X 10^{-5} to 3.4 x 10^{-4} mol/L). Calcite was found to be undersaturated with saturation indices ranging from 0.21 to 0.51 in prebiostimulated samples and 0.39 to 0.86 in post biostimulated samples (Table 5.1).

In summary, both the microbiological and geochemical indicators of denitrification suggested widespread bioactivity throughout the treatment zone from ML5 to ML7 – consistent with measureable flow variations, but more widespread than indicated by sustained flow redirection. The frequent pulsing of acetate was apparently sufficient to sustain biological activity at a level that could drive denitrification and intermittently affect flow in the sediments low in gravel content. More complete mixing of the acetate pulse by dispersion, near ML7, led to denitrification in the coarser sediments and sustained flow redirection. With chemical

precipitation and free-phase gas formation ruled out as causes of pore space occlusion, the growth of biomass, and possibly nonviable (dead) cell accumulation or associated extracellular polysaccharides (EPS) (Hand et al. 2008), is thought to be the cause of changes in the flow system indicated by the PVPs and CIS tracer tests.

5.3: Conclusions

This study is the first to evaluate changes in groundwater velocity in a biostimulated aquifer to sediment texture and sorting, and nutrient pulse mixing. Conventional methods of site characterization would not likely detect these changes in flow, even if efforts were highly focused in the bioactive zone. Using PVPs in tandem with tracer testing it was determined that poorly-sorted, fine-grained sediments were most susceptible to decreases in groundwater velocity during biostimulation. Coarser sediments were found to change little or increase in velocity, possibly as a result of capturing flow from adjacent zones undergoing a decrease in velocity. Superimposed onto the velocity changes related to sediment texture and sorting were variances in flow linked to the variability of acetate. A high degree of flow variation was found primarily up-gradient of where individual acetate pulses were expected to mix from dispersion. However, the pulse interval was small enough to allow continuous biological activity at the CIS. Further down-gradient of the CIS, consistent decreases in groundwater velocity and evidence for flow redirection were found where pulse mixing occurred. After biostimulation, changes in the mean and variance in flow direction and the variance of velocity magnitude were found to be most sensitive to the vertical component. Ultimately, all changes in velocity were linked to the accumulation of biomass and possibly nonviable biomass (EPS and dead cells) from

biostimulation. Due to the overall coarse nature of the sediments and relatively high initial velocities, the observed decreases in velocity after 60 days of biostimulation are not thought to detrimentally impact the treatment of nitrate at the Woodstock site. These results indicate that aquifers are susceptible to the development of a biologically-induced transient heterogeneity, even when nutrients are pulsed. This work further shows that nutrient pulsing can be successfully applied in the remediation of a high velocity aquifer when the contaminant flux per pulse interval is considered in the treatment calculation.

References

Albrechtsen, H.J. 1994. Distribution of bacteria, estimated by a viable count method, and heterotrophic activity in different size fractions of aquifer sediment. *Geomicrobiology Journal* 12 no. 4: 253-264.

Albrechtsen, H.J., and A. Winding. 1992. Microbial Biomass and Activity in Subsurface Sediments from Vejen, Denmark. *Microbial Ecology* 23 no. 3: 303-317.

Alvarez, P.J.J., and W.A. Illman. 2006. *Bioremediation and natural attenuation: process fundamentals and mathematical models*. Hoboken, N.J.: Wiley-Interscience.

Barbaro, S.E., H.J. Albrechtsen, B.K. Jensen, C.I. Mayfield, and J.F. Barker. 1994. Relationships between aquifer properties and microbial-populations in the borden aquifer. *Geomicrobiology Journal* 12 no. 3: 203-219.

Baveye, P., P. Vandevivere, B.L. Hoyle, P.C. DeLeo, and D.S. de Lozada. 1998. Environmental impact and mechanisms of the biological clogging of saturated soils and aquifer materials. *Critical Reviews in Environmental Science and Technology* 28 no. 2: 123-191.

Bekeris, L. 2007. Field-scale evaluation of enhanced agricultural management practices using a novel unsaturated zone nitrate mass load approach. Department of Earth Sciences, University of Waterloo, Waterloo, Ontario, Canada.

Blott, S.J., and K. Pye. 2001. GRADISTAT: A grain size distribution and statistics package for the analysis of unconsolidated sediments. *Earth Surface Processes and Landforms* 26 no. 11: 1237-1248.

Brusseau, M.L., M.Q. Hu, J.M. Wang, and R.M. Maier. 1999. Biodegradation during contaminant transport in porous media. 2. The influence of physicochemical factors. *Environmental Science & Technology* 33 no. 1: 96-103.

Cowan, W.R. 1978. Trend surface analysis of major late Wisconsinan till sheets, Brantford-Woodstock area, southern Ontario. *Canadian Journal of Earth Sciences* 15 no. 6: 1025-1036.

Critchley, K. 2010. Stimulating In Situ Denitrification in an Aerobic, Highly Conductive Municipal Drinking Water Aquifer. Department of Earth Sciences, University of Waterloo, Waterloo, Ontario, Canada.

Devlin, J.F. 1994. A Simple and Powerful Method of Parameter-Estimation Using Simplex Optimization. *Ground Water* 32 no. 2: 323-327.

Devlin, J.F. 2003. A spreadsheet method of estimating best-fit hydraulic gradients using head data from multiple wells. *Ground Water* 41 no. 3: 316-320.

Devlin, J.F., and J.F. Barker. 1996. Field investigation of nutrient pulse mixing in an in situ biostimulation experiment. *Water Resources Research* 32 no. 9: 2869-2877.

Devlin, J.F., R. Eedy, and B.J. Butler. 2000. The effects of electron donor and granular iron on nitrate transformation rates in sediments from a municipal water supply aquifer. *Journal of Contaminant Hydrology* 46 no. 1-2: 81-97.

Devlin, J.F., and C.D. McElwee. 2007. Effects of measurement error on horizontal hydraulic gradient estimates. *Ground Water* 45 no. 1: 62-73.

Devlin, J.F., P.C. Schillig, I. Bowen, C.E. Critchley, D.L. Rudolph, N.R. Thomson, G.P. Tsoflias, and J.A. Roberts. 2012. Applications and implications of direct groundwater velocity measurement at the centimetre scale. *Journal of Contaminant Hydrology* 127 no. 1-4: 3-14.

Devlin, J.F., G. Tsoflias, M. McGlashan, and P. Schillig. 2009. An Inexpensive Multilevel Array of Sensors for Direct Ground Water Velocity Measurement. *Ground Water Monitoring and Remediation* 29 no. 2: 73-77.

Dobbs, F.C., and R.H. Findlay. 1993. Analysis of microbial lipids to determine biomass and detect the response of sedimentary microorganisms to disturbance. In *Handbook of methods in aquatic microbial ecology*, ed. P. F. Kemp, B. F. Sherr, E. B. Sherr and J. J. Cole, 347-358. Boca Raton: Lewis Publishers.

Dong, H.L., T.C. Onstott, M.F. Deflaun, M.E. Fuller, T.D. Scheibe, S.H. Streger, R.K. Rothmel, and B.J. Mailloux. 2002. Relative dominance of physical versus chemical effects on the transport of adhesion-deficient bacteria in intact cores from South Oyster, Virginia. *Environmental Science & Technology* 36 no. 5: 891-900.

Englert, A., S.S. Hubbard, K.H. Williams, L. Li, and C.I. Steefel. 2009. Feedbacks Between Hydrological Heterogeneity and Bioremediation Induced Biogeochemical Transformations. *Environmental Science & Technology* 43 no. 14: 5197-5204.

Faybishenko, B., T.C. Hazen, P.E. Long, E.L. Brodie, M.E. Conrad, S.S. Hubbard, J.N. Christensen, D. Joyner, S.E. Borglin, R. Chakraborty, K.H. Williams, J.E. Peterson, J.S. Chen, S.T. Brown, T.K. Tokunaga, J.M. Wan, M. Firestone, D.R. Newcomer, C.T. Resch, K.J. Cantrell, A. Willett, and S. Koenigsberg. 2008. In Situ Long-Term Reductive Bioimmobilization of Cr(VI) in Groundwater Using Hydrogen Release Compound. *Environmental Science & Technology* 42 no. 22: 8478-8485.

Findlay, R.H., G.M. King, and L. Watling. 1989. Efficacy of phospholipids analysis in determining microbial biomass in sediments *Applied and Environmental Microbiology* 55 no. 11: 2888-2893.

Folk, R.L. 1954. The distinction between grain size and mineral composition in sedimentary-rock nomenclature. *Journal of Geology* 62 no. 4: 344-359.

Folk, R.L., and W.C. Ward. 1957. Brazos river bar ; a study in the significance of grain size parameters. *Journal of Sedimentary Petrology* 27: 3-26.

Fontes, D.E., A.L. Mills, G.M. Hornberger, and J.S. Herman. 1991. Physical and chemical factors influencing transport of microorganisms through porous-media. *Applied and Environmental Microbiology* 57 no. 9: 2473-2481.

Geesey, G.G., and A.C. Mitchell. 2008. Need of direct measurements of coupled microbiological and hydrological processes at different scales in porous media systems. *Journal of Hydrologic Engineering* 13 no. 1: 28-36.

Gierczak, R., J.F. Devlin, and D.L. Rudolph. 2007. Field test of a cross-injection scheme for stimulating in situ denitrification near a municipal water supply well. *Journal of Contaminant Hydrology* 89 no. 1-2: 48-70.

Gierczak, R.F.D., J.F. Devlin, and D.L. Rudolph. 2006. Combined use of field and laboratory testing to predict preferred flow paths in an heterogeneous aquifer. *Journal of Contaminant Hydrology* 82 no. 1-2: 75-98.

Green, C.T., and K.M. Scow. 2000. Analysis of phospholipid fatty acids (PLFA) to characterize microbial communities in aquifers. *Hydrogeology Journal* 8 no. 1: 126-141.

Gu, C.H., G.M. Hornberger, A.L. Mills, J.S. Herman, and S.A. Flewelling. 2007. Nitrate reduction in streambed sediments: Effects of flow and biogeochemical kinetics. *Water Resources Research* 43 no. 12: 10.

Hand, V.L., J.R. Lloyd, D.J. Vaughan, M.J. Wilkins, and S. Boult. 2008. Experimental studies of the influence of grain size, oxygen availability and organic carbon availability on bioclogging in porous media. *Environmental Science & Technology* 42 no. 5: 1485-1491.

Haslauer, C.P. 2005. Hydrogeologic analysis of a complex aquifer system and impacts of changes in agricultural practices on nitrate concentrations in a municipal well field. Department of Earth Sciences, University of Waterloo, Waterloo, Ontario, Canada.

Istok, J.D., J.M. Senko, L.R. Krumholz, D. Watson, M.A. Bogle, A. Peacock, Y.J. Chang, and D.C. White. 2004. In situ bioreduction of technetium and uranium in a nitrate-contaminated aquifer. *Environmental Science & Technology* 38 no. 2: 468-475.

Khan, I.A., and R.F. Spalding. 2004. Enhanced in situ denitrification for a municipal well. *Water Research* 38 no. 14-15: 3382-3388.

Kildsgaard, J., and P. Engesgaard. 2002. Tracer tests and image analysis of biological clogging in a two-dimensional sandbox experiment. *Ground Water Monitoring and Remediation* 22 no. 2: 60-67.

Koch, J. 2009. Evaluating regional aquifer vulnerability and BMP performance in an agricultural environment using a multi-scale data integration approach. Department of Earth Sciences, University of Waterloo, Waterloo, Ontario, Canada.

Krzyszkowski, D.K.P.F. 2001. Stratigraphie interlobaire du Wisconsinien dans trois carrières des environs de Woodstock, en Ontario Translated Title: Wisconsinan inter-lobal stratigraphy in three quarries near Woodstock, Ontario. *Géographie physique et Quaternaire* 55 no. 1: 3-22.

Labaky, W., J.F. Devlin, and R.W. Gillham. 2007. Probe for measuring ground water velocity at the centimeter scale. *Environmental Science & Technology* 41 no. 24: 8453-8458.

Levy, J., K. Sun, R.H. Findlay, F.T. Farruggia, J. Porter, K.L. Mumy, J. Tomaras, and A. Tomaras. 2007. Transport of Escherichia coli bacteria through laboratory columns of glacial-outwash sediments: Estimating model parameter values based on sediment characteristics. *Journal of Contaminant Hydrology* 89 no. 1-2: 71-106.

Li, L., C.I. Steefel, M.B. Kowalsky, A. Englert, and S.S. Hubbard. 2010. Effects of physical and geochemical heterogeneities on mineral transformation and biomass accumulation during biostimulation experiments at Rifle, Colorado. *Journal of Contaminant Hydrology* 112 no. 1-4: 45-63.

Luo, J., W.M. Wu, J. Carley, C.M. Ruan, B.H. Gu, P.M. Jardine, C.S. Criddle, and P.K. Kitanidis. 2007. Hydraulic performance analysis of a multiple injection-extraction well system. *Journal of Hydrology* 336 no. 3-4: 294-302.

McCarty, P.L., M.N. Goltz, G.D. Hopkins, M.E. Dolan, J.P. Allan, B.T. Kawakami, and T.J. Carrothers. 1998. Full scale evaluation of in situ cometabolic degradation of trichloroethylene in groundwater through toluene injection. *Environmental Science & Technology* 32 no. 1: 88-100.

McKenna, S.A., and A. Wahi. 2006. Local hydraulic gradient estimator analysis of long-term monitoring networks. *Ground Water* 44 no. 5: 723-731.

McMahon, P.B., K.F. Dennehy, B.W. Bruce, J.K. Bohlke, R.L. Michel, J.J. Gurdak, and D.B. Hurlbut. 2006. Storage and transit time of chemicals in thick unsaturated zones under

rangeland and irrigated cropland, High Plains, United States. *Water Resources Research* 42 no. 3.

Meissner, R., J. Seeger, and H. Rupp. 2002. Effects of agricultural land use changes on diffuse pollution of water resources. *Irrigation and Drainage* 51 no. 2: 119-127.

Musslewhite, C.L., M.J. McInerney, H.L. Dong, T.C. Onstott, M. Green-Blum, D. Swift, S. Macnaughton, D.C. White, C. Murray, and Y.J. Chien. 2003. The factors controlling microbial distribution and activity in the shallow subsurface. *Geomicrobiology Journal* 20 no. 3: 245-261.

Nakhla, G., and M. Niaz. 2002. Pilot-scale in situ bioremediation of gasoline-contaminated groundwater: Impact of process parameters. *Environmental Progress* 21 no. 1: 37-46.

Oberdorfer, J.A., and F.L. Peterson. 1985. Watewater injection-Geochemical and biogeochemical clogging processes. *Ground Water* 23 no. 6: 753-761.

Padusenko, G. 2001. Regional hydrogeologic evaluation of a complex glacial aquifer system in an agricultural landscape: Implications for nitrate distribution. Department of Earth Sciences, University of Waterloo, Waterloo, Ontario, Canada.

Pinder, G.F., M. Celia, and W.G. Gray. 1981. Velocity calculation from randomly located hydraulic heads. *Ground Water* 19 no. 3: 262-264.

Piotrowski, J.A. 1987. Genesis of the Woodstock Drumlin Field, Southern Ontario, Canada. *Boreas* 16 no. 3: 249-265.

Ross, N., and G. Bickerton. 2002. Application of Biobarriers for Groundwater Containment at Fractured Bedrock Sites. *Remediation Journal* 12 no. 3: 5-21.

Schillig, P.C. 2012. VelProbePE: An automated spreadsheet program for interpreting point velocity probe breakthrough curves. *Computers & Geosciences* 39: 161-170.

Schillig, P.C., J.F. Devlin, J.A. Roberts, G.P. Tsoflias, and M.A. McGlashan. 2011. Transient Heterogeneity in an Aquifer Undergoing Bioremediation of Hydrocarbons. *Ground Water* 49 no. 2: 184-196.

Seki, K., M. Thullner, J. Hanada, and T. Miyazaki. 2006. Moderate bioclogging leading to preferential flow paths in biobarriers. *Ground Water Monitoring and Remediation* 26 no. 3: 68-76.

Shaw, H.J. 2012. Assessment of enhanced *in situ* denitrification through improved carbon amendment strategies. A report to the University of Waterloo. 89p.

Silliman, S.E., and C. Frost. 1998. Monitoring hydraulic gradient using three-point estimator. *Journal of Environmental Engineering* 124 no. 6: 517-523.

Sinclair, J.L., and W.C. Ghiorse. 1989. Distribution of aerobic bacteria, protozoa, algae, and fungi in deep subsurface sediments. *Geomicrobiology Journal* 7 no. 1-2: 15-31.

Thullner, M. 2010. Comparison of bioclogging effects in saturated porous media within one- and two-dimensional flow systems. *Ecological Engineering* 36 no. 2: 176-196.

Thullner, M., J. Zeyer, and W. Kinzelbach. 2002. Influence of microbial growth on hydraulic properties of pore networks. *Transport in Porous Media* 49 no. 1: 99-122.

Tomer, M.D., and M.R. Burkart. 2003. Long-term effects of nitrogen fertilizer use on ground water nitrate in two small watersheds. *Journal of Environmental Quality* 32 no. 6: 2158-2171.

Vandevivere, P., P. Baveye, D.S. Delozada, and P. Deleo. 1995. Microbial clogging of saturated soils and aquifer materials-Evaluation of mathematical models. *Water Resources Research* 31 no. 9: 2173-2180.

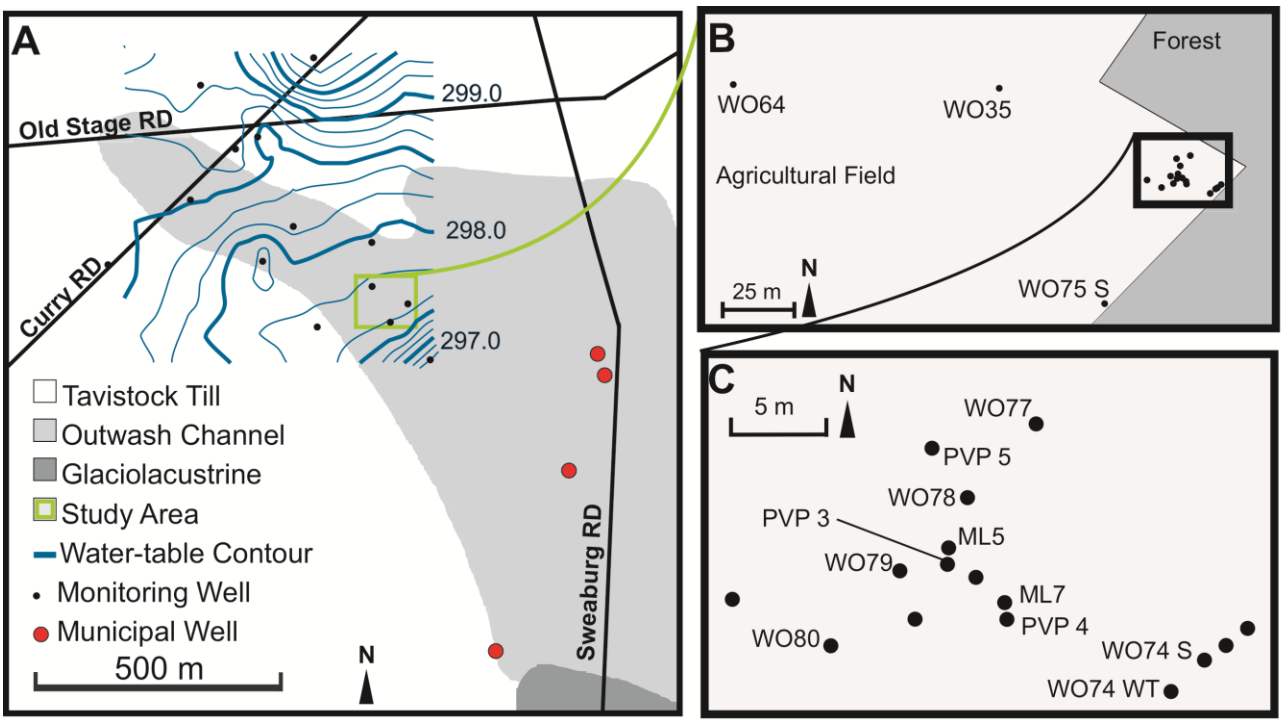

Figure 5.01: Map of the field area depicting surficial geology with potentiometric surface (A), inset within the glacial fluvial outwash channel (B), and instrumentation immediately around the treatment area (C).

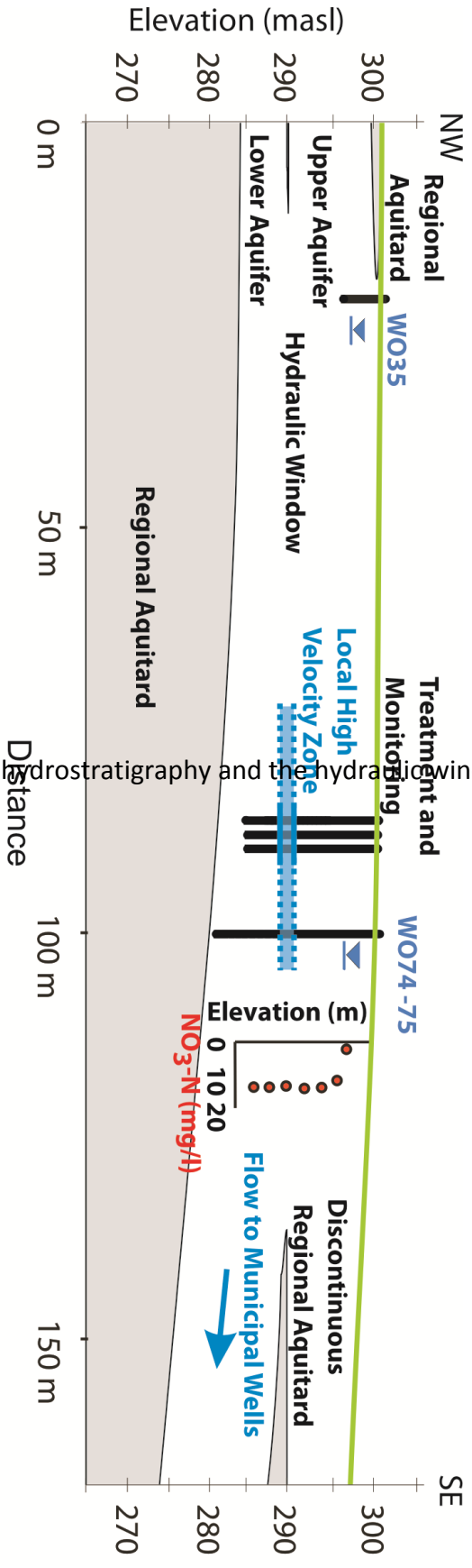

Cross section parallel to flow showing general hydrostratigraphy and the hydraulic window.

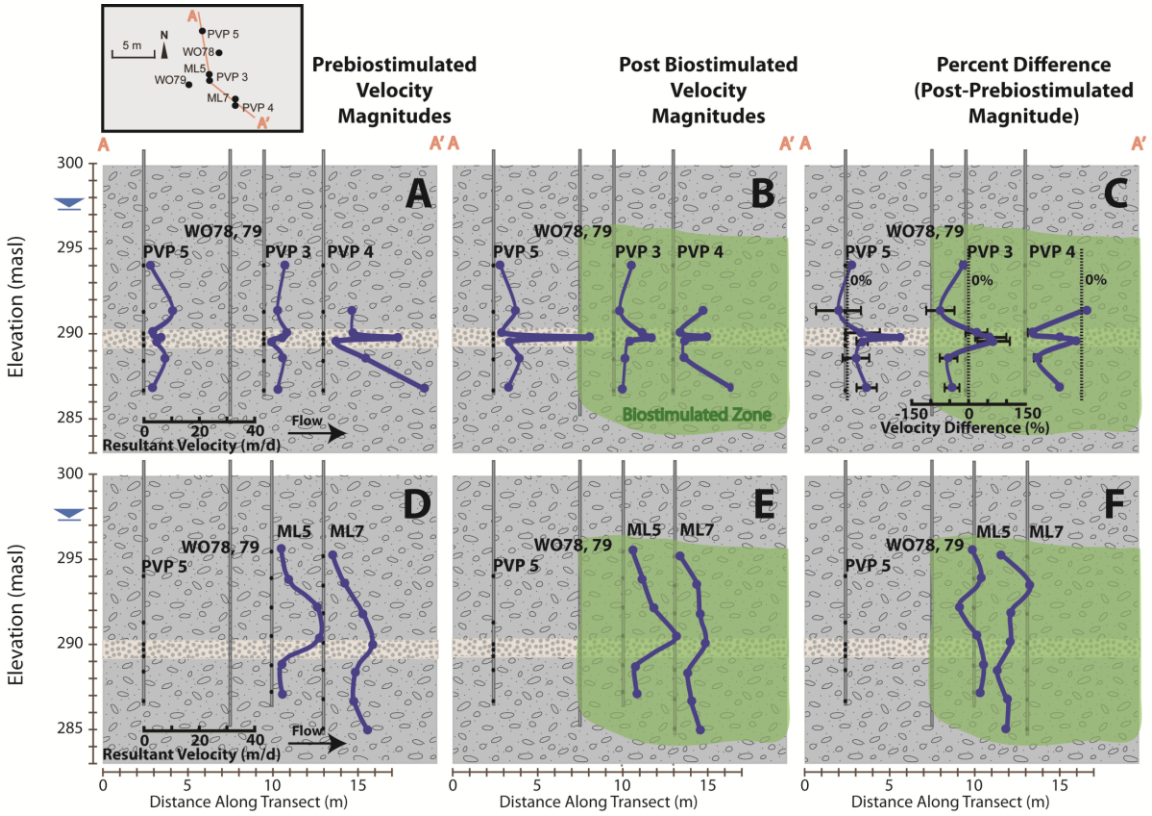

Figure 5.03: Transects indicating resultant PVP velocity magnitude profiles averaged during pre and post biostimulated conditions (A and B, respectively), the percent difference of post subtracted from pre biostimulated average resultant PVP velocity magnitude (C), pre and post biostimulated velocities from tracer testing of the CIS (D and E, respectively), and the percent difference of post subtracted from pre biostimulated velocity (F). Error bars on profile C represent changes in one standard deviation of the percent difference. The high velocity zone from elevation 289-290 m is highlighted in the cross section.

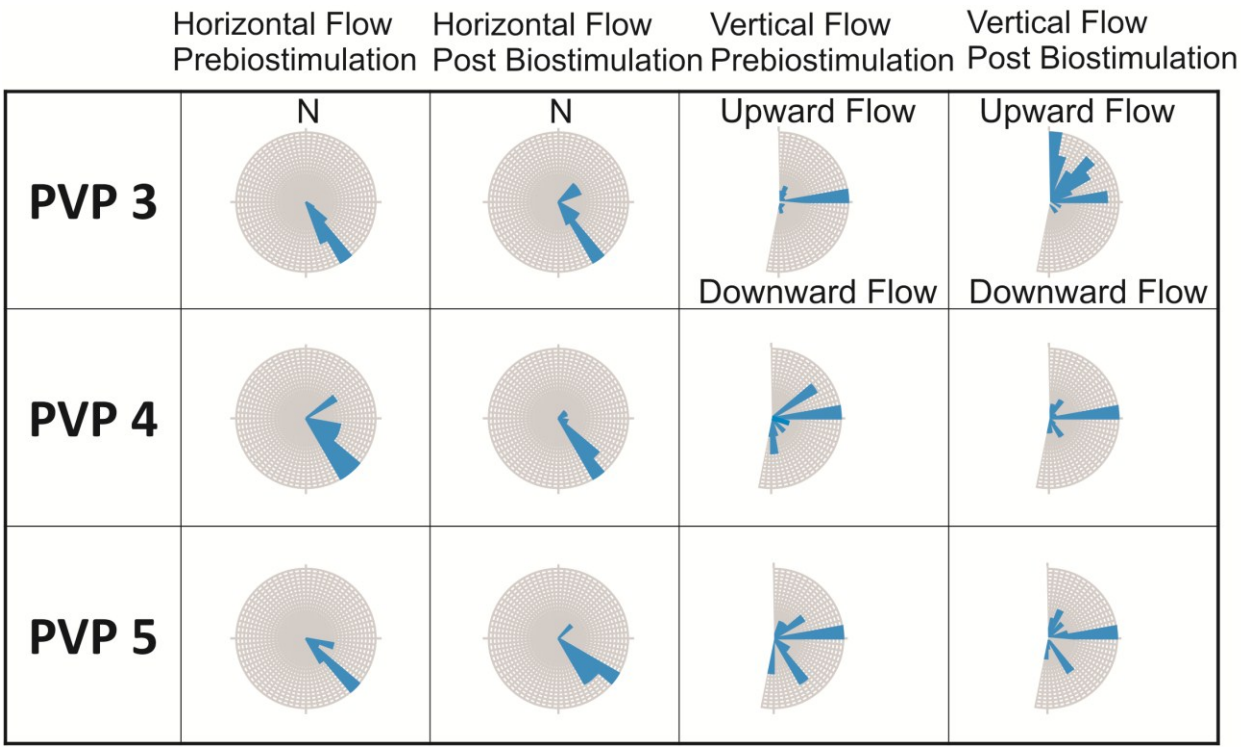

Figure 5.04: Compiled multilevel PVP horizontal and vertical flow directions for pre and post biostimulated datasets.

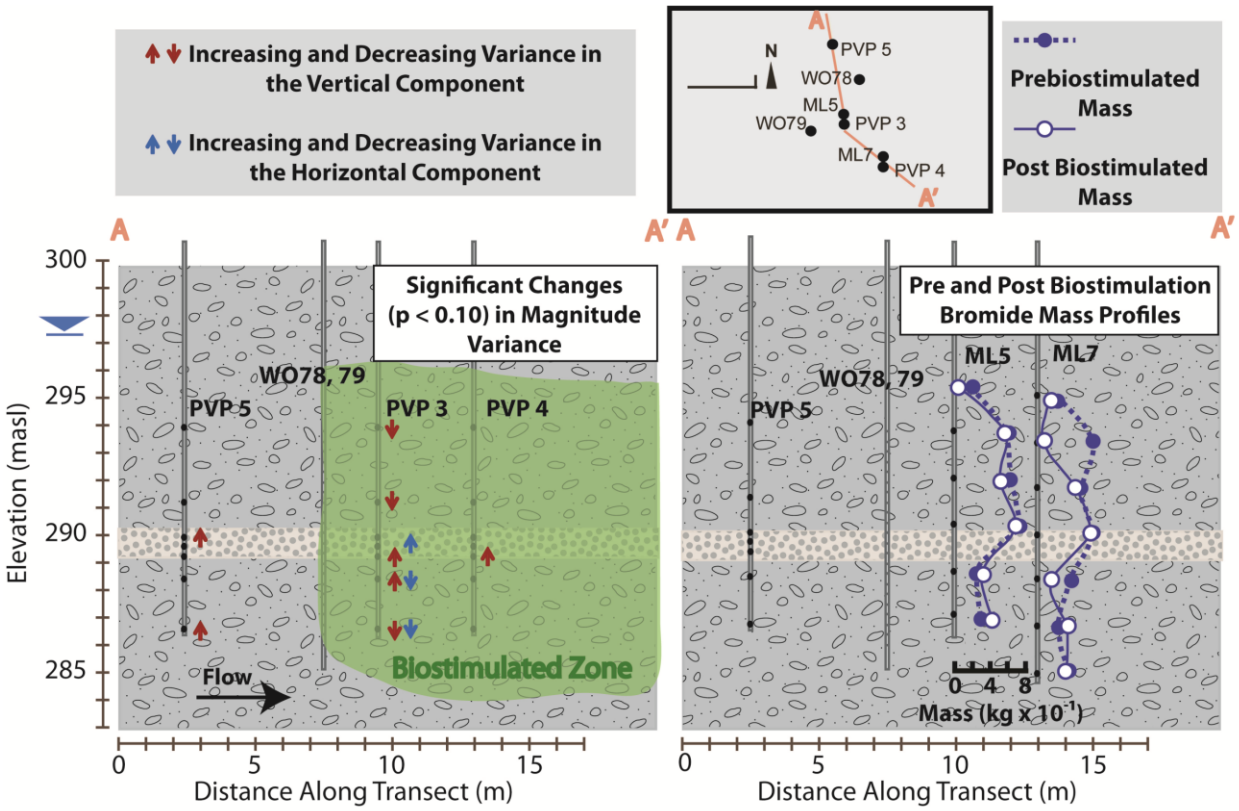

Figure 5.05: Transect showing significant changes from prebiostimulated conditions in the variance of both horizontal and vertical components of velocity magnitude from multilevel PVPs 3, 4, and 5 (A). Transect indicating bromide mass profiles from tracer testing the CIS system at ML5 and ML7 for pre and post biostimulated conditions (B).

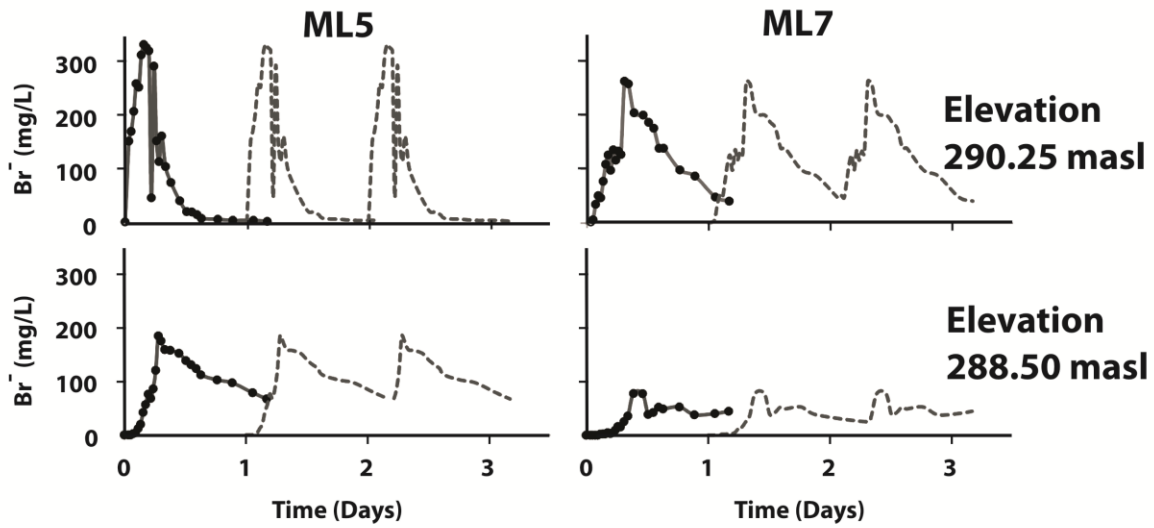

Figure 5.06: Bromide breakthrough curves on day 55 of biostimulation (solid) and projected 2 days into the future (dashed) at ML5 and ML7. Breakthrough curves shown represent conditions from the well-sorted gravel in the high velocity zone (290.25 m) and the poorly-sorted sediments below it (288.50 m).

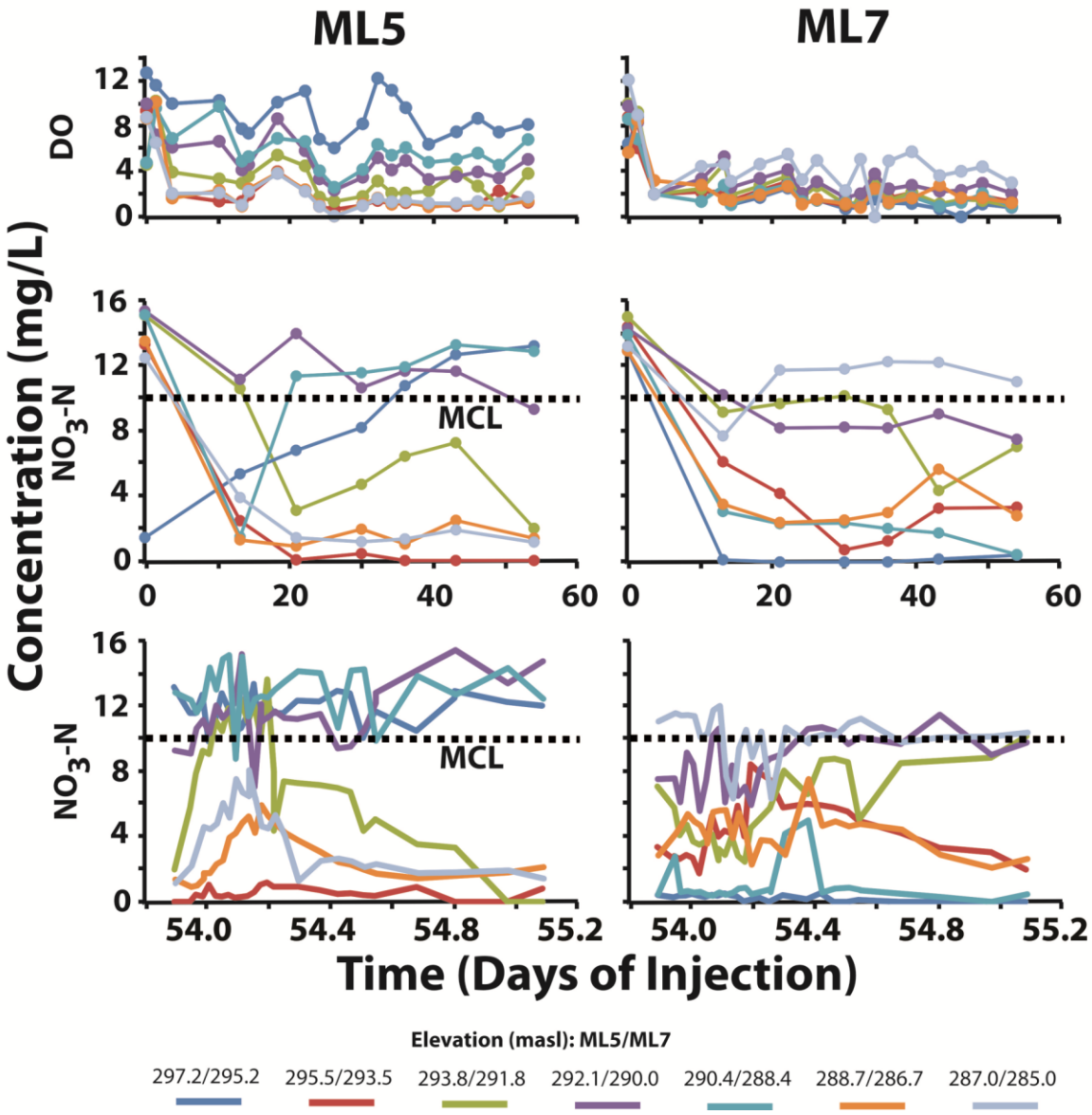

Figure 5.07: Concentration of DO (Top) and nitrate (Center) over the 55 days of biostimulation. The bottom panel shows fluctuations of nitrate on the final day of biostimulation. The maximum contamination level (MCL) for nitrate is shown.

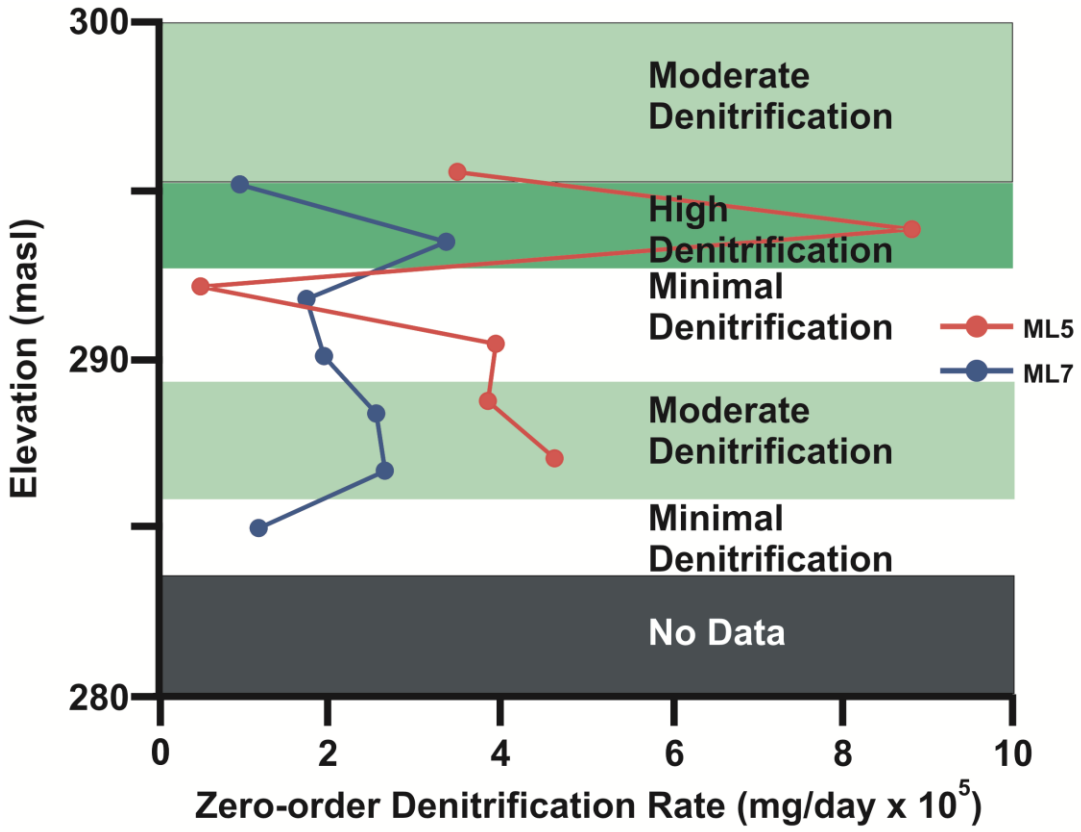

Figure 5.08: A profile of zero-order denitrification rates for ML5 and ML7 plotted with interpreted denitrification zones similar to those described by Critchley 2010.

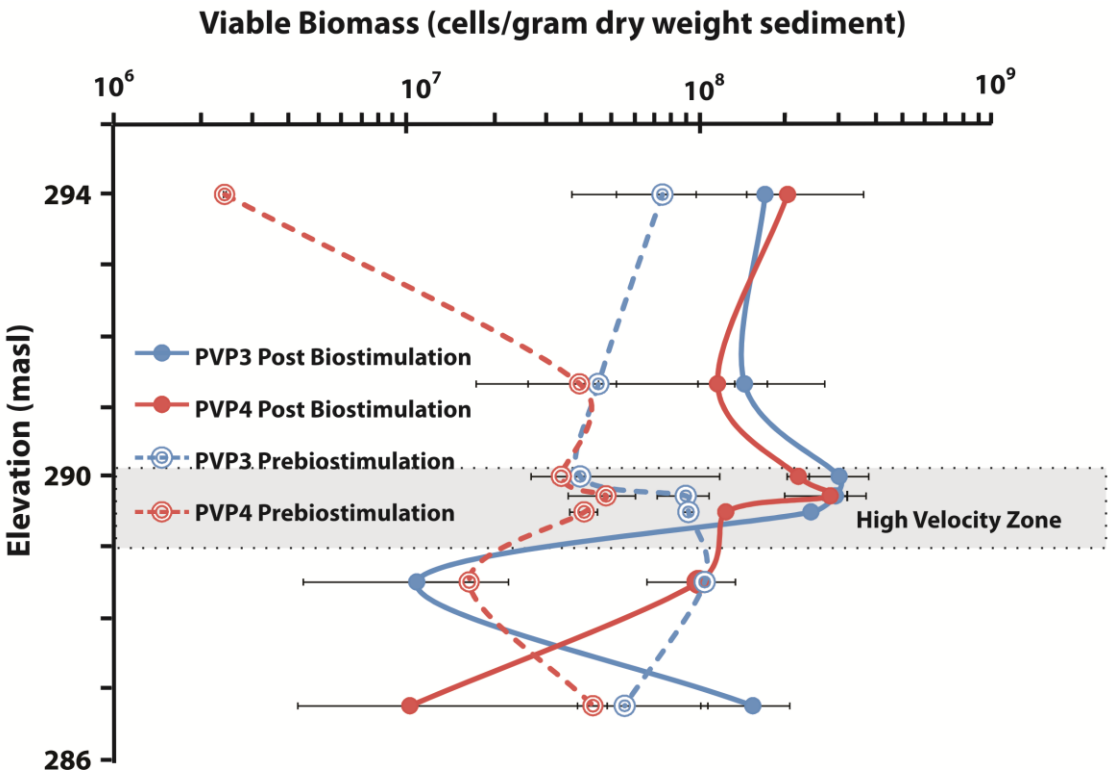

Figure 5.09: Total lipid biomass profiles taken for multilevel PVPs 3 and 4 before and after biostimulation. Error bars represent values measured from duplicate samples.

Table 5.1: Saturation indicies for calcite and dissolved gasses CO_2, N_2O, and CH_4 (Appendix 27). Values greater than 1 represent supersaturated conditions. Calcite saturation indicies were calculated from measured and calculated values for alkalinity and values reported represent an average between the two methods with error bars covering the extremes in the estimate (see data in Appendix 22 and Equations 7 and 8.

	ML5					ML7			
	Saturation Index					Saturation Index			
Elevation (m)	Calcite	CO_2	N_2O	CH_4	Elevation (m)	Calcite	CO_2	N_2O	CH_4
297.2	0.49 ± 0.005	0.28	0.00	0.00	295.2	0.61 ± 0.071	0.30	0.00	0.00
295.5	0.68 ± 0.026	0.20	0.00	0.00	293.5	0.71 ± 0.043	0.23	0.00	0.00
293.8	0.72 ± 0.054	0.23	0.00	0.00	291.8	0.61 ± 0.018	0.18	0.00	0.00
292.1	0.59 ± 0.003	0.20	0.00	0.00	290.1	0.60 ± 0.021	0.20	0.00	0.00
290.4	0.60 ± 0.012	0.23	0.00	0.00	288.4	0.71 ± 0.037	0.22	0.00	0.00
288.7	0.68 ± 0.036	0.19	0.00	0.00	286.7	0.66 ± 0.034	0.16	0.00	0.00
287.0	0.74 ± 0.027	0.17	0.00	0.00	285.0	0.59 ± 0.006	0.17	0.00	0.00

6

Evaluation of groundwater velocity and grain-size for preferential clogging of porous media.

6.0: Introduction

The biological clogging (bioclogging) of saturated, uniform sediments has been recognized in laboratory studies for decades (Slichter 1905; Allison 1947; Baveye et al. 1998; Thullner 2010). Laboratory and modeling studies with 1-D columns indicate that clogging can occur in sediments up to gravel in size (Paksy et al. 1998; Cooke et al. 2005), though the clogging efficiency of biomass was shown to be greatest in finer-grained sediments (Vandevivere et al. 1995). While bioclogging has also been observed to occur faster in finer-grained sediments, the maximum reduction in hydraulic conductivity (*K*) does not necessarily correlate with grain-size (Bielefeldt et al. 2002a; Bielefeldt et al. 2002b). Another important consideration for bioclogging potential is velocity (*v*), which is the primary control for the transport of dissolved nutrients for microbial growth in homogenous systems that are not diffusion controlled (McClain et al. 2003). However, *v* is also often investigated in bioclogging experiments as a contributing parameter in the shearing of biofilms as they become established (Baveye et al. 1998; Thullner 2010). Few bioclogging studies examine the effect of *v* as a function of nutrient flux. Those that directly examine *v* as a parameter for microbial growth report mixed results where higher (Paksy et al. 1998) and lower (Brusseau et al. 1999; Bielefeldt et al. 2002a; Bielefeldt et al. 2002b) flow rates have been demonstrated to lead to a

greater degree of bioclogging. While valuable insight can be gained from these experiments, none directly replicate a natural system's heterogeneity where groundwater can be redirected into preferential flowpaths with the onset of bioclogging.

Review articles concerned with bioclogging describe the occurrence of a feedback mechanism in which a high flow setting was associated with biological activity that subsequently caused flow impedance and redirection to secondary pathways (Geesey and Mitchell 2008; Thullner 2010). To date, this feedback has been difficult to quantify with traditional experimentation because 1-D columns allow for the quantification of discharge (Q), hydraulic gradient (i), K, and solute transport parameters but are susceptible to the development of large back-pressures leading to unrealistic velocities. Furthermore, measuring flow redirection is difficult in single columns (Kildsgaard and Engesgaard 2002; Thullner et al. 2002; Seki et al. 2006). Partial clogging and flow redirection have been reported in 2-D biostimulation laboratory tank experiments. However, local (i.e., point) changes in Q, i, or K are difficult to estimate in such experiments, leaving the details of the associated hydrogeology unknown at the scale of bioactive zone development (Kildsgaard and Engesgaard 2002; Thullner et al. 2002; Seki et al. 2006).

Until recently, field verification of bioclogging has been restricted to near-well environments (Oberdorfer and Peterson 1985). Recent field studies have attributed changes in permeability and flow within aquifers, away from wells, to partial bioclogging of the sediments as a result of biostimulation (Wu et al. 2006; Faybishenko et al. 2008; Englert et al. 2009; Schillig et al. 2011). In Chapter 5, changes in v and flow redirection during the biostimulation of a heterogeneous aquifer were related to grain-size and prebiostimulated v. A need remains to

design a controlled, laboratory experiment that can accurately evaluate the role of grain-size and *v* in bioclogging, obtain accurate measurements of changing hydrogeological parameters, and allow for subsequent flow redirection.

In this study, multiple vertical columns attached to a common manifold are used to observe and quantify changes in permeability, flow, and flow direction with the onset of biostimulation (Figure 6.01). This apparatus, adapted from Dambacher (2005), combines the advantages of a 1-D column experiment with those of a tank experiment by providing the opportunity to quantify changes in parameters used in Darcy's Law, as well as *v*, while permitting flow to be redirected (through the manifold) during biostimulation. For the purposes of this experiment, nitrate serves as the model contaminant for heterotrophic denitrification. The experiment was conducted in two stages. The first stage of this experiment examines the effects of *v* on the feedback between biostimulation and flow redirection. The second stage of this experiment examines the importance of grain-size in promoting permeability changes.

6.1: Methods

6.1.1: Manifold Apparatus Construction

Each experimental stage was conducted with duplicate 2.54 cm diameter manifolds; each connected to three columns. Columns were approximately 50 cm long and constructed from vinyl tubing with an average cross-sectional area of 4.85 cm^2. To isolate the portion of the column most affected by biological activity, manometers were placed at 5.5 cm, 25.5 cm, and 47 cm above the bottom screen, within the porous media. Additional manometers were placed 2.8 cm below the bottom screen and 2.8 cm above the top screen. Each column contained two

sample ports located at 7 cm and 44 cm above the bottom screen. Electrodes located 46 cm above the bottom screen were used for monitoring changes in electrical conductivity breakthrough curves from injected tracers. A gravity-fed Mariotte system supplied groundwater collected from the Geohydrologic Experimental and Monitoring Site (GEMS) near Lawrence, KS to each manifold and gradients were controlled by adjusting the effluent elevation of each column. Prior to packing, the entire assembled flow system was sterilized by flushing a 1:19 bleach solution for eight hours, followed by repeatedly draining and rinsing 10 times with deionized (DI) water, and allowed to dry.

6.1.2: Sediment and Groundwater Preparation

To limit the mineral phase as an active variable for biomass growth, all columns were packed with selected sieved fractions of quartz sand and gravel (Agsco classified silica sands-formerly known as Accusand). For the velocity stage, all three columns were packed with an identical median grain-size of 0.254 mm (#50-70 sieve-size). For the grain-size stage, each column was packed with a unique median grain-size of 0.254 mm (#50-70 sieve-size), 0.508 mm (#30-40 sieve-size), or 3.57 mm (#4-8 sieve-size). Individual sieved fractions of sand and gravel were rinsed with DI water and sonicated for 30 min to remove fine sediments. This process was repeated until the rinse water ran clear. To remove any organic carbon, the sediments were baked at 450°C for 4 hours before packing.

The Packing of columns was conducted by saturating each manifold with water from the Mariotte assembly until water reached the bottom screen in each column. The valve that separated the column to the manifold was then closed (Figure 6.01). The columns were wet packed with DI water and sediment was incrementally added into the column approximately 5-

8 cm at a time. Columns were repeatedly tapped until the sediment settled after each addition. Average porosity for each column was calculated as the ratio of the volume of DI water needed to wet pack the column to the total column volume. The average porosity calculated from all columns was 0.32 ± 0.03. Once the columns were completely packed, the valves were opened to allow water from the Mariotte assembly to pass through the system.

Groundwater for this experiment was collected from GEMS well 0-6, screened in the Kansas River alluvial aquifer. Prior to collection, the 5" well was purged for 15 min at approximately 10 GPM. Collected groundwater was stored in HDPE carboys under dark conditions until transferred to glass Mariotte carboys for delivery into the manifolds. A total of 15L of unfiltered GEMS groundwater was used for inoculation of the packed columns during the prebiostimulation phase. Flow through each column was held at a constant rate of 1.2 mL/min for the velocity stage and 0.24 mL/min for the grain-size stage. After inoculation, 20 L of GEMS groundwater was passed through a UV filter (Crystal Quest 1 GPM Water Sterilization System with 253.7 nM wavelength) to remove suspended biomass. During the biostimulation phase the UV-filtered groundwater was subsequently amended with 1.735 g potassium nitrate and 2.054 g sodium acetate trihydrate per carboy. This mass of carbon from the sodium acetate trihydrate was the stoichiometric optimal amount to fully consume 10 mg/L DO and 15 mg/L NO_3-N as amended by the potassium nitrate as follows (Eby 2004; Devlin et al. 2000):

$$CH_3COO^-_{(aq)} + 2O_{2\,(aq)} \leftrightarrow 2HCO_3^-{}_{(aq)} + H^+_{(aq)} \qquad [1]$$

$$5CH_3COO^-_{(aq)} + 8NO_3^-{}_{(aq)} + 3H^+_{(aq)} \leftrightarrow 10HCO_3^-{}_{(aq)} + 4N_{2(g)} + 4H_2O_{(l)} \qquad [2]$$

Background conditions were established by monitoring flow and head measurements for 14 days prior to biostimulation using UV-filtered groundwater. After the background phase, UV-filtered groundwater, amended with carbon and nitrate, was introduced into the manifold. To minimize growth and activity up-gradient of the columns, the carboys were disconnected, sterilized three times with 100% ethanol, rinsed with DI water, and refilled with UV-filtered, amended groundwater every 2-3 days during biostimulation. All columns and manifolds were operated in the dark to prevent phototrophic growth.

6.1.3: Monitoring Hydraulic Response

After the inoculation phase, the effluent head of each column was adjusted to reach their respective target initial *v* as calculated from *Q* measurements (see equation 3 below). During the velocity stage, each column was set to a unique initial *v* of 1200 cm/d, 100 cm/d, or 50 cm/d (*Q* measured to be approximately 1.23, 0.10, and 0.05 mL/min, respectively). During the grain-size stage, the elevation of each column's effluent was constantly adjusted throughout the experiment to maintain a calculated *v* of 200 cm/d (*Q* measured to be approximately 0.24 mL/min). Velocity (*v*) [LT^{-1}] was calculated from:

$$V = \frac{Q}{A\,n} \qquad [3]$$

Where *Q* [L^3T^{-1}] represents discharge, *A* is the average cross-sectional area of the columns [L^2] and *n* is porosity (dimensionless). Accuracy of calculated velocities was confirmed from tracer testing conducted prior to biostimulation. Briefly, 3 mL of a 1 g NaCl L^{-1} unfiltered GEMS groundwater was injected into the bottom sample port and breakthrough was monitored by electrodes near the top of the column approximately 38 cm down-gradient from the injection

source. Breakthrough curves were interpreted with a 1-D solution to the advection-disperision equation coupled with a nonlinear optimizer described by Devlin (1994).

Discharge from each column was monitored daily during the prebiostimulation phase and up to twice daily during the biostimulation phase for both stages of the experiment. Water was collected for *Q* measurements for 30-45 min during the velocity stage and 10 min during the grain-size stage. Water-levels in each manometer were also monitored during this time using a digital caliper and a leveled board 90.5 cm above the floor serving as the datum. Apparent hydraulic conductivity (K_{app}) was calculated to determine how permeability changed as a result of the bioclogging process as follows:

$$K_{app} = \frac{Q}{A\frac{\Delta h}{\Delta L}} \qquad [4]$$

Where Δ*h* [L] is the change in total head across the column measured by calibrated differential pressure transducers (Omega PX26 1 PSI) and Δ*L* [L] represents the distance (55 cm) between the transducer measuring points (Figure 6.01).

6.1.4: Geochemistry

Evidence for biological activity was acquired through detailed geochemical sampling immediately after the first addition of acetate to the columns and immediately prior to column disassembly. Unfiltered samples were collected for DO, pH, EC, and temperature. DO was analyzed immediately following collection with a Chemetrics kits while pH, EC, and temperature were acquired with handheld meters. Filtered (0.22 µm) anion samples were collected in 25 mL scintillation vials and immediately frozen to minimize biological activity. Samples collected for anions were analyzed for nitrate, nitrite, acetate, bromide, sulfate, and chloride. Analysis was

performed within 40 days of collection and storage. Sample analysis was performed on a Dionex ICS 3000 ion chromatograph featuring a Dionex IonPac AS15 analytical column and AG15 guard column. Prior to analysis, samples were thawed completely in the refrigerator and agitated to prevent stratification due to freezing. Duplicate samples were collected and analyzed approximately every 10 samples. Filtered (0.22 µm) alkalinity samples were collected with zero headspace in 25 mL scintillation vials and stored on ice until analyzed within 1-3 days using Fisher Scientific Titrimeter II Automatic Titration System. Filtered (0.22 µm) cation samples were analyzed for sodium, potassium, magnesium, calcium, iron, strontium, and manganese. Samples were collected into 25 mL scintillation vials, acidified with 100 µL of concentrated nitric acid and refrigerated until analysis, which was competed within 40 days of collection. Samples were analyzed using a Perkin Elmer Optima 5300DV ICS-OES. Using cation and alkalinity, pH and temperature data, a range of saturation indices for calcite were reported using

$$\log \frac{[Ca^{+2}][CO_3^{-2}]}{K_{sp}\ CaCO_3} \qquad [5]$$

Where K_{sp} $CaCO_3$ at 25°C = $10^{-8.48}$. The $[CO_3^{-2}]$ was speciated from measured alkalinity values, pH, and K_{sp} CO_3^{-2} at 25°C ($10^{-10.33}$).

Immediately prior to the disassembly of the columns, samples for dissolved gas analysis were collected in sealed 70 mL serum bottles. Sample collection included water and any exolving gases. A total of 0.25 mL of concentrated cyanide solution (carbonyl cyanide m-chlorophenylhydrazone) was added to serum bottles as a preservative. Sample collection consisted of placing the sealed serum bottles under vacuum by removing 120 mL of air using a 60 mL syringe. With other columns and manometers closed (valved) off, water was transferred

directly from the column of interest into the serum bottles from the syringe using the internal vacuum previously created in the bottles, until atmospheric pressure was reached. This procedure ensured no gas loss during sample collection. Serum bottles were then immediately sealed with silicone cement and inverted to prevent headspace gas loss through the septa, stored on ice in the dark, and the headspace gas was analyzed for CO_2, N_2O, and CH_4 on a gas chromatograph equipped with a Haysept Q 80/100 1/8 in x 6 ft stainless steel column using the thermal conductivity detector (TCD). Henry's Law was used to calculate the aqueous concentrations from measured headspace gas concentrations using Henry's Law. To determine if any of the above mentioned species existed as bubbles under the conditions in the columns, aqueous concentrations were compared to their respective solubilities at 25°C.

6.1.5: Total Lipid Biomass

At the end of the experiment, the most clogged column was sampled for biomass concentrations determine by total lipid biomass analysis. A sample from the inlet of the duplicate column on the second manifold was also removed for analysis. Aseptic methods were used in the handling of sediment materials and tools (Barbaro et al. 1994). Sampled sediments were homogenized, freeze dried and stored in the dark at -80° C to prevent phospholipid degradation. All samples were analyzed in duplicate. Phospholipid extraction from sediment samples and the liberation of lipids from phosphate was achieved using methods for colorimetric analysis described by Findlay et al., (1989). Concurrently, orthophosphate standards made from glycerol phosphate were processed in duplicate with the samples. In preparation for analysis, samples and standards were combined with ammonium molybdate and

malachite green solutions and decanted into a cuvette where absorbance was recorded at 610 nm by a Spectronic GENESYS 20 spectrophotometer. The phosphate content of each sample was related to cell mass using the average of a range of conversion factors reported by Dobbs and Findlay (1993) (3.4×10^7 to 2.0×10^9 cells/nmol PO_4) and the average concentration of cells/gram dry weight aquifer material (core) was estimated for each sample. Conversion factors used to characterize microbial consortia with lipid based approaches vary in the literature (Findlay et al. 1989; Dobbs and Findlay 1993; Green and Scow 2000). Therefore, an average was used in this study and biomass comparisons made to other studies are limited to those which used lipid-based approaches.

6.2: Results and Discussion

6.2.1:The Effect of Velocity on Bioclogging

For the duration of the experiment, duplicates of 50, 100, and 1200 cm/d columns behaved consistently. Velocity was found to vary little during the 15 days before biostimulation in all columns. Tracer testing performed prior to biostimulation yielded *v* magnitudes within 15% of those calculated with equation 3 for four of the six columns tested. Two of the six columns (a 50 cm/d and 100 cm/d column) were as high as 60% difference. With the amendment of acetate and nitrate in the feed water, *v* rapidly declined in the two 1200 cm/d columns while increases occurred in the 100 and 50 cm/d columns after 2 days of biostimulation (Figure 6.02A). After 3 days of biostimulation, *Q* was greater in the 50 and 100 cm/d columns than the 1200 cm/d column on both duplicate manifolds. These increases in the 100 cm/d and 50 cm/d columns were likely a result of flow redirection as *Q* decreased in the 1200 cm/d columns and water was diverted to the other columns. After 4 days of continuous

biostimulation, the 50 and 100 cm/d columns also began to decrease in *v* (Figure 6.02A). These results show that clogging preferentially occurred in the higher *v* columns but eventually spread to the lower *v* columns, duplicating the growth of a bioactive zone in an aquifer *v* (Figure 6.02A). At the end of the experiment, the averaged K_{app} from the duplicate columns was calculated to decline by 99% (1.88×10^{-2} to 2.71×10^{-4} cm/s) in the 1200 cm/d columns while increases of 197% (1.20×10^{-2} to 3.57×10^{-2} cm/s) and 534% (1.11×10^{-2} to 7.04×10^{-2} cm/s) were calculated in the 100 and 50 cm/d columns, respectively. Temporary Increases in *K* above the initial condition have also been reported in other bioclogging studies (Allison 1947; Okubo and Matsumoto 1979; Seki et al. 2006; Thullner 2010). In this study, the average change in K_{app} was proportional to, and similar in magnitude to the changes in average *Q* for the columns, suggesting the changes in *v* (and Q) were related to inherent changes in *K* due to biostimulation.

This work showed that, as expected, a higher nutrient delivery rate will promote microbial activity faster than a lower nutrient delivery rate. In these experiments there was evidence that biological activity caused flow redirection and subsequent enhanced biostimulation along new pathways, lending experimental evidence in support of the conceptual model for bioactive zone development in aquifers.

6.2.2: Grain-Size Experiments

For the duration of these experiments, *v*, as calculated with equation 1, was held constant at 200 cm/d by varying the effluent head and monitoring *Q*. The primary evidence for the occurrence of bioclogging was taken as the *i* needed to maintain a flow *v* of 200 cm/d. Columns were monitored for 15 days prior to biostimulation with little change needed in *i* to

maintain 200 cm/d (Figure 6.02B). Small daily changes were particularly needed in the 3.57 mm grain-size columns since small changes in barometric pressure in these high *K* columns lead to proportionally large changes in *v*. Tracer testing performed prior to biostimulation yielded velocity values within 20% to those calculated with equation 3.

Over the course of the experiment, duplicate columns of median grain-sizes 0.254, 0.508, and 3.57 mm behaved consistently, though one manifold responded to the amendments a little more rapidly than the other (Figure 6.02B and Figure 6.04). With the amendment of acetate and nitrate in the feed water, increases in *i* were needed in the 0.254 and 0.508 mm grain-size columns to maintain 200 cm/d *v* after 2 days of biostimulation (Figure 6.02B). Little to no change in *i* was needed in the 3.57 mm grain-size columns (Figure 6.02B). These results indicate that clogging had preferentially occurred in the finer grain-size columns, through little distinction could be made between the clogging results for these two textures. Despite these differences in clogging, the declines in K_{app} were between 90-95% for all columns, consistent with Bielefeldt et al. (2002a,b).

The similarity in K_{app} decreases across columns packed with different grain-sizes suggests that more biomass accumulated in the coarser grained column, effecting the greatest change in *K*. Despite this, it was the finer grained columns that clogged first. This result indicates that although nutrient flux controls the rate of biomass growth or activity (previous experiment) grain-size controls the first expression of clogging.

6.2.3: Mechanism for Clogging

With the onset of biostimulation, anaerobic conditions developed in all columns. At the same time, nitrate concentrations declined from 52.9 mg/L to 0.9 mg/L. There was no evidence

for iron or sulfate reduction throughout the experiment. Prior to biostimulation, gas bubbles trapped in the effluent lines were not observed for both velocity and grain-size stages. After biostimulation, the effluent lines were repeatedly flushed with DI water to remove gas bubbles that escaped from the porous media. During the velocity stage, zones of desaturation were first noted in the 1200 cm/d columns and were eventually detected in all columns by the end of the experiment. These zones corresponded to locations where increases in total hydraulic head were observed, based on the manometer readings along the columns (Figure 6.03). During the grain-size stage, zones of desaturation were observed in all columns within two days of biostimulation, most notably in 0.254 and 0.507 mm grain-sizes. However, the observed zones of desaturation had little effect on *i* from day 0 (Figure 6.04). Headspace gas analysis of water samples confirmed that CO_2 concentrations were super-saturated for all six columns at the end of the velocity stage, with concentrations between 140% and 230% in excess of solubility. Though lower during the grain-size stage, CO_2 concentrations were above 70% solubility in 5 of the 6 columns. Therefore, presence of free-phase CO_2 gas likely contributed to reductions in K_{app} *and Q*.

Total lipid biomass analyses was conducted with sediment collected at the inlet of the 1200 cm/d and 0.254 mm grain-size columns, where the greatest head losses were found (Figures 6.03 and 6.04). Attached biomass concentrations increased by approximately 1.5 orders of magnitude from $5.18 \times 10^7 \pm 3.01 \times 10^6$ cells/gram dry weight sediment during prebiostimulated conditions to $1.43 \times 10^9 \pm 8.48 \times 10^7$ and $1.16 \times 10^9 \pm 3.42 \times 10^8$ cells/gram dry weight sediment for 1200 cm/d and 0.254 mm grain-size columns, respectively. An order of magnitude increase in biomass alone has been shown to reduce hydraulic conductivity upwards

of 80-90% in previous laboratory studies (Vandevivere and Baveye 1992; Holm 2001; Nakhla and Niaz 2002). Saturation indices for calcite from pre-and post-biostimulated samples were similar in magnitude, and near saturation. However, given the degree of biomass growth and gas production observed in these columns, calcite precipitation was unlikely to have been the major contributor to the clogging.

6.3: Summary and Implications

Multiple columns attached to a common manifold were used to observe and quantify bioclogging as a function of *v* and *i,* in separate experiments. Both experimental stages resulted in K_{app} reductions that began within 2-4 days of continuous biostimulation for sediment of 0.254 mm grain-size. During the variable *v* stage, the high *v* (1200 cm/d) column preferentially clogged relative to 50 and 100 cm/d columns. During the variable grain-size stage, the 0.254 and 0.508 mm median grain-sizes required unrealistically high gradients to maintain a calculated *v* of 200 cm/d. These data indicate that higher velocities and finer grain-sizes promoted clogging conditions more rapidly. Results indicate 50 and 100 cm/d columns behaved in a similar manner, as did columns with 0.254 and 0.508 mm grain-sizes. As expected, initial conditions that differed by up to approximately a factor of two had similar bioclogging behaviors in contrast to initial conditions that differed by approximately one order of magnitude.

In aquifers, large grain-size geologic units of uniform sorting tend to have the highest velocities due to the proportionality between grain-size and *K*. However this work indicates that clogging occurs preferentially in finer grained sediments to such a degree that bioactive zone

formation is more likely to begin in these sediments and spread to coarser sediments with the onset of bioclogging. Transition zones in natural aquifers where fine-grained or poorly-sorted sediments that lie adjacent to discontinuous coarser sediments - where the high velocities would lead to the highest flux of injected nutrients - may be the most likely place where biologically induced transience in the heterogeneity leads to the spreading of the bioactive zone.

References

Allison, L.E. 1947. Effect of microorganisms on permeability of soil under prolonged submergence. *Soil Science* 63 no. 6: 439-450.

Barbaro, S.E., H.J. Albrechtsen, B.K. Jensen, C.I. Mayfield, and J.F. Barker. 1994. Relationships between aquifer properties and microbial-populations in the borden aquifer. *Geomicrobiology Journal* 12 no. 3: 203-219.

Baveye, P., P. Vandevivere, B.L. Hoyle, P.C. DeLeo, and D.S. de Lozada. 1998. Environmental impact and mechanisms of the biological clogging of saturated soils and aquifer materials. *Critical Reviews in Environmental Science and Technology* 28 no. 2: 123-191.

Bielefeldt, A.R., T. Illangasekare, M. Uttecht, and R. LaPlante. 2002a. Biodegradation of propylene glycol and associated hydrodynamic effects in sand. *Water Research* 36 no. 7: 1707-1714.

Bielefeldt, A.R., C. McEachern, and T. Illangasekare. 2002b. Hydrodynamic changes in sand due to biogrowth on naphthalene and decane. *Journal of Environmental Engineering-Asce* 128 no. 1: 51-59.

Brusseau, M.L., M.Q. Hu, J.M. Wang, and R.M. Maier. 1999. Biodegradation during contaminant transport in porous media. 2. The influence of physicochemical factors. *Environmental Science & Technology* 33 no. 1: 96-103.

Cooke, A.J., R.K. Rowe, J. VanGulck, and B.E. Rittmann. 2005. Application of the BioClog model for landfill leachate clogging of gravel-packed columns. *Canadian Geotechnical Journal* 42 no. 6: 1600-1614.

Dambacher, M.L. 2005. Permeability versus surface reactivity on the longevity of granular iron reactive barriers. M.S. Thesis, Dept. of Geology, University of Kansas, Lawrence, KS.

Devlin, J.F. 1994. A Simple and Powerful Method of Parameter-Estimation Using Simplex Optimization. *Ground Water* 32 no. 2: 323-327.

Devlin, J.F., R. Eedy, and B.J. Butler. 2000. The effects of electron donor and granular iron on nitrate transformation rates in sediments from a municipal water supply aquifer. *Journal of Contaminant Hydrology* 46 no. 1-2: 81-97.

Dobbs, F.C., and R.H. Findlay. 1993. Analysis of microbial lipids to determine biomass and detect the response of sedimentary microorganisms to disturbance. In *Handbook of*

methods in aquatic microbial ecology, ed. P. F. Kemp, B. F. Sherr, E. B. Sherr and J. J. Cole, 347-358. Boca Raton: Lewis Publishers.

Eby, G.N. 2004. *Principles of environmental geochemistry*. Pacific Grove, CA: Thomson-Brooks/Cole.

Englert, A., S.S. Hubbard, K.H. Williams, L. Li, and C.I. Steefel. 2009. Feedbacks Between Hydrological Heterogeneity and Bioremediation Induced Biogeochemical Transformations. *Environmental Science & Technology* 43 no. 14: 5197-5204.

Faybishenko, B., T.C. Hazen, P.E. Long, E.L. Brodie, M.E. Conrad, S.S. Hubbard, J.N. Christensen, D. Joyner, S.E. Borglin, R. Chakraborty, K.H. Williams, J.E. Peterson, J.S. Chen, S.T. Brown, T.K. Tokunaga, J.M. Wan, M. Firestone, D.R. Newcomer, C.T. Resch, K.J. Cantrell, A. Willett, and S. Koenigsberg. 2008. In Situ Long-Term Reductive Bioimmobilization of Cr(VI) in Groundwater Using Hydrogen Release Compound. *Environmental Science & Technology* 42 no. 22: 8478-8485.

Findlay, R.H., G.M. King, and L. Watling. 1989. Efficacy of phospholipids analysis in determining microbial biomass in sediments *Applied and Environmental Microbiology* 55 no. 11: 2888-2893.

Geesey, G.G., and A.C. Mitchell. 2008. Need of direct measurements of coupled microbiological and hydrological processes at different scales in porous media systems. *Journal of Hydrologic Engineering* 13 no. 1: 28-36.

Green, C.T., and K.M. Scow. 2000. Analysis of phospholipid fatty acids (PLFA) to characterize microbial communities in aquifers. *Hydrogeology Journal* 8 no. 1: 126-141.

Holm, J. 2001. Effect of biomass growth on the hydrodynamic properties of groundwater aquifers. *Series Paper - Department of Hydrodynamics and Water Resources, Technical University of Denmark* 72.

Kildsgaard, J., and P. Engesgaard. 2002. Tracer tests and image analysis of biological clogging in a two-dimensional sandbox experiment. *Ground Water Monitoring and Remediation* 22 no. 2: 60-67.

McClain, M.E., E.W. Boyer, C.L. Dent, S.E. Gergel, N.B. Grimm, P.M. Groffman, S.C. Hart, J.W. Harvey, C.A. Johnston, E. Mayorga, W.H. McDowell, and G. Pinay. 2003. Biogeochemical hot spots and hot moments at the interface of terrestrial and aquatic ecosystems. *Ecosystems* 6 no. 4: 301-312.

Nakhla, G., and M. Niaz. 2002. Pilot-scale in situ bioremediation of gasoline-contaminated groundwater: Impact of process parameters. *Environmental Progress* 21 no. 1: 37-46.

Oberdorfer, J.A., and F.L. Peterson. 1985. Watewater injection-Geochemical and biogeochemical clogging processes. *Ground Water* 23 no. 6: 753-761.

Okubo, T., and J. Matsumoto. 1979. Effect of infiltration-rate on biological clogging and water quality changes during artifical recharge. *Water Resources Research* 15 no. 6: 1536-1542.

Paksy, A., W. Powrie, J.P. Robinson, and L. Peeling. 1998. A laboratory investigation of anaerobic microbial clogging in granular landfill drainage media. *Geotechnique* 48 no. 3: 389-401.

Schillig, P.C., J.F. Devlin, J.A. Roberts, G.P. Tsoflias, and M.A. McGlashan. 2011. Transient Heterogeneity in an Aquifer Undergoing Bioremediation of Hydrocarbons. *Ground Water* 49 no. 2: 184-196.

Seki, K., M. Thullner, J. Hanada, and T. Miyazaki. 2006. Moderate bioclogging leading to preferential flow paths in biobarriers. *Ground Water Monitoring and Remediation* 26 no. 3: 68-76.

Slichter, C.S. 1905. Field measurements of the rate of movement of underground waters. United States Geological Survey Water-Supply and Irrigation Paper 140.

Thullner, M. 2010. Comparison of bioclogging effects in saturated porous media within one- and two-dimensional flow systems. *Ecological Engineering* 36 no. 2: 176-196.

Thullner, M., L. Mauclaire, M.H. Schroth, W. Kinzelbach, and J. Zeyer. 2002. Interaction between water flow and spatial distribution of microbial growth in a two-dimensional flow field in saturated porous media. *Journal of Contaminant Hydrology* 58 no. 3-4: 169-189.

Vandevivere, P., and P. Baveye. 1992. Saturated hydraulic conductivity reduction caused by aerobic-bacteria in sand columns. *Soil Science Society of America Journal* 56 no. 1: 1-13.

Vandevivere, P., P. Baveye, D.S. Delozada, and P. Deleo. 1995. Microbial clogging of saturated soils and aquifer materials-Evaluation of mathematical models. *Water Resources Research* 31 no. 9: 2173-2180.

Wu, W.M., J. Carley, M. Fienen, T. Mehlhorn, K. Lowe, J. Nyman, J. Luo, M.E. Gentile, R. Rajan, D. Wagner, R.F. Hickey, B.H. Gu, D. Watson, O.A. Cirpka, P.K. Kitanidis, P.M. Jardine, and C.S. Criddle. 2006. Pilot-scale in situ bioremediation of uranium in a highly contaminated aquifer. 1. Conditioning of a treatment zone. *Environmental Science & Technology* 40 no. 12: 3978-3985.

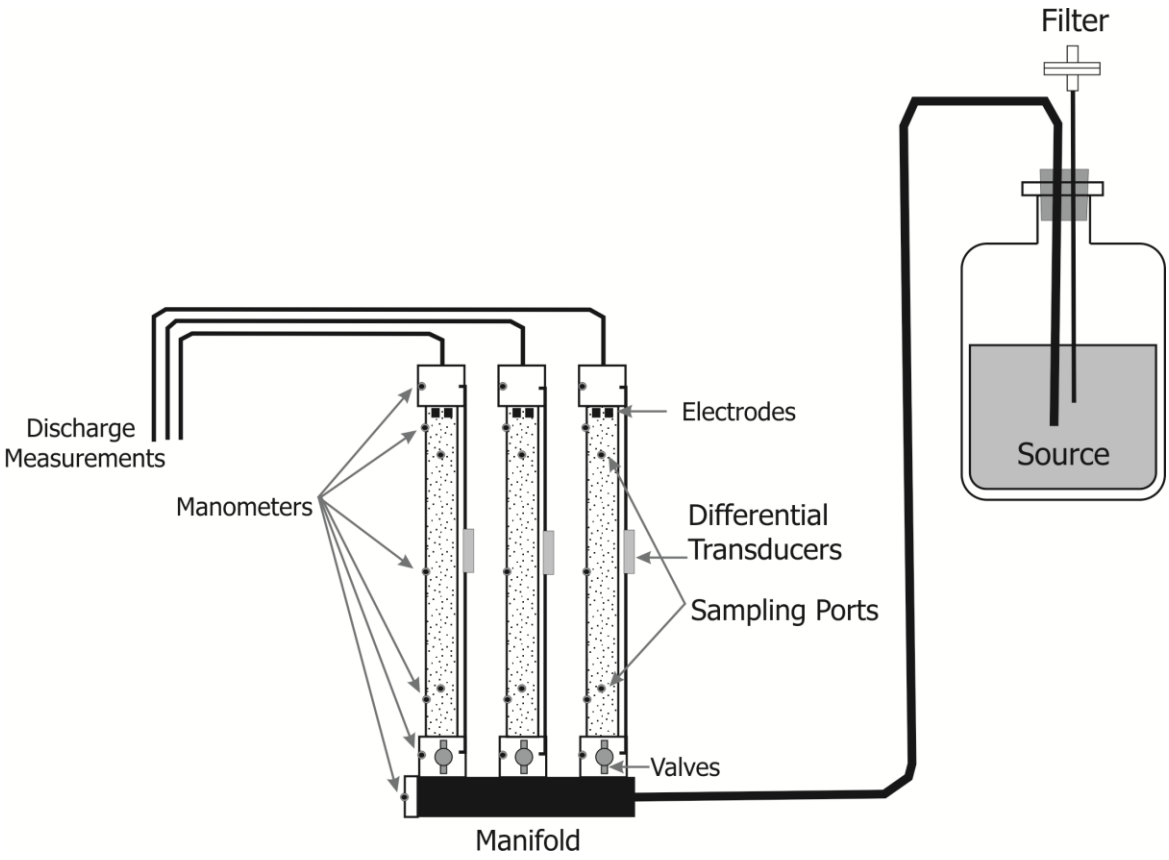

Figure 6.01: Manifold apparatus with three columns used in the velocity and grain-size stages of the experiment. Each column was set to have either a unique velocity or grain-size.

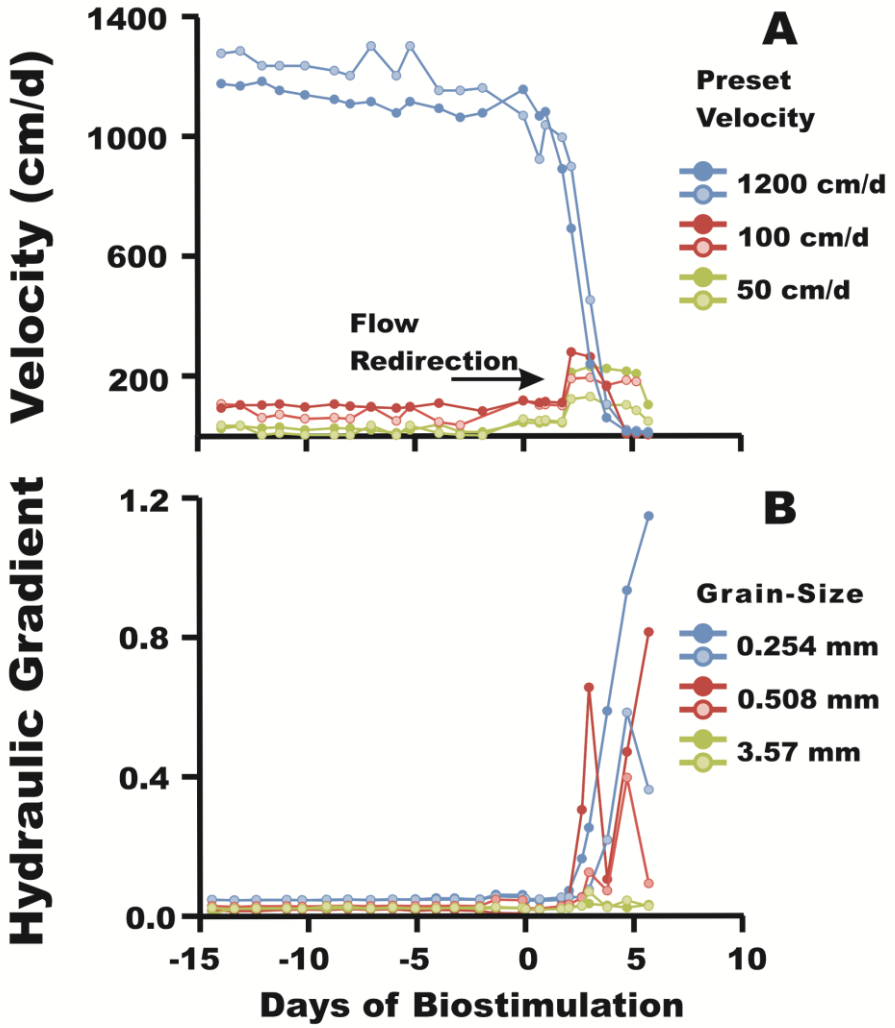

Figure 6.02: Time lapse graphs indicating the response of the duplicate columns to the addition of growth nutrients on Day 0. Changes in velocity (A) also indicate flow redirection to the 50 and 100 cm/d columns as the 1200 cm/d columns decrease in velocity. Temporal changes in hydraulic gradient in response to the addition of growth nutrients were used to indicate bioclogging in the varying grain-size stage (B).

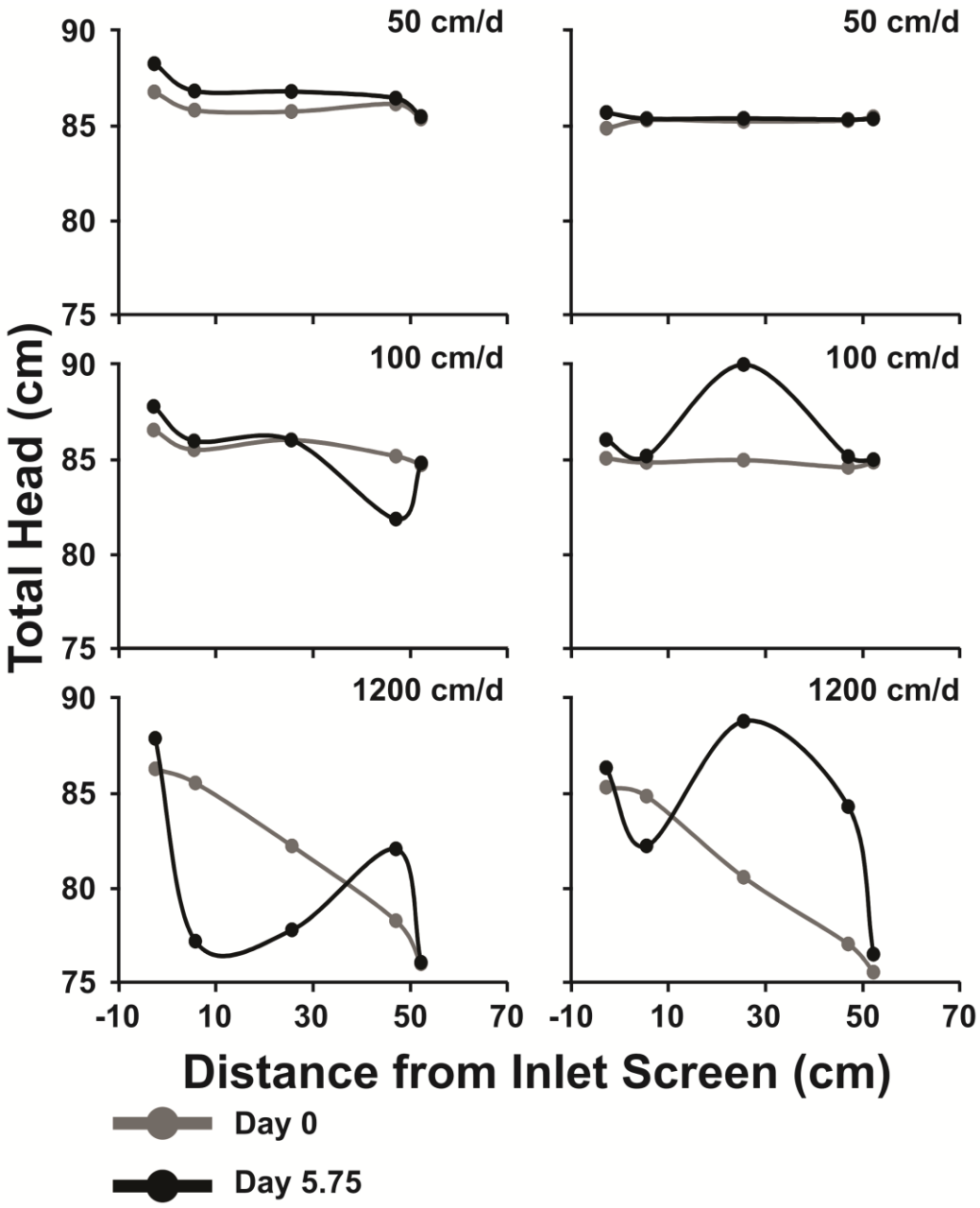

Figure 6.03: Changes in total head along the length of varying velocity columns at the beginning and end of biostimulation.

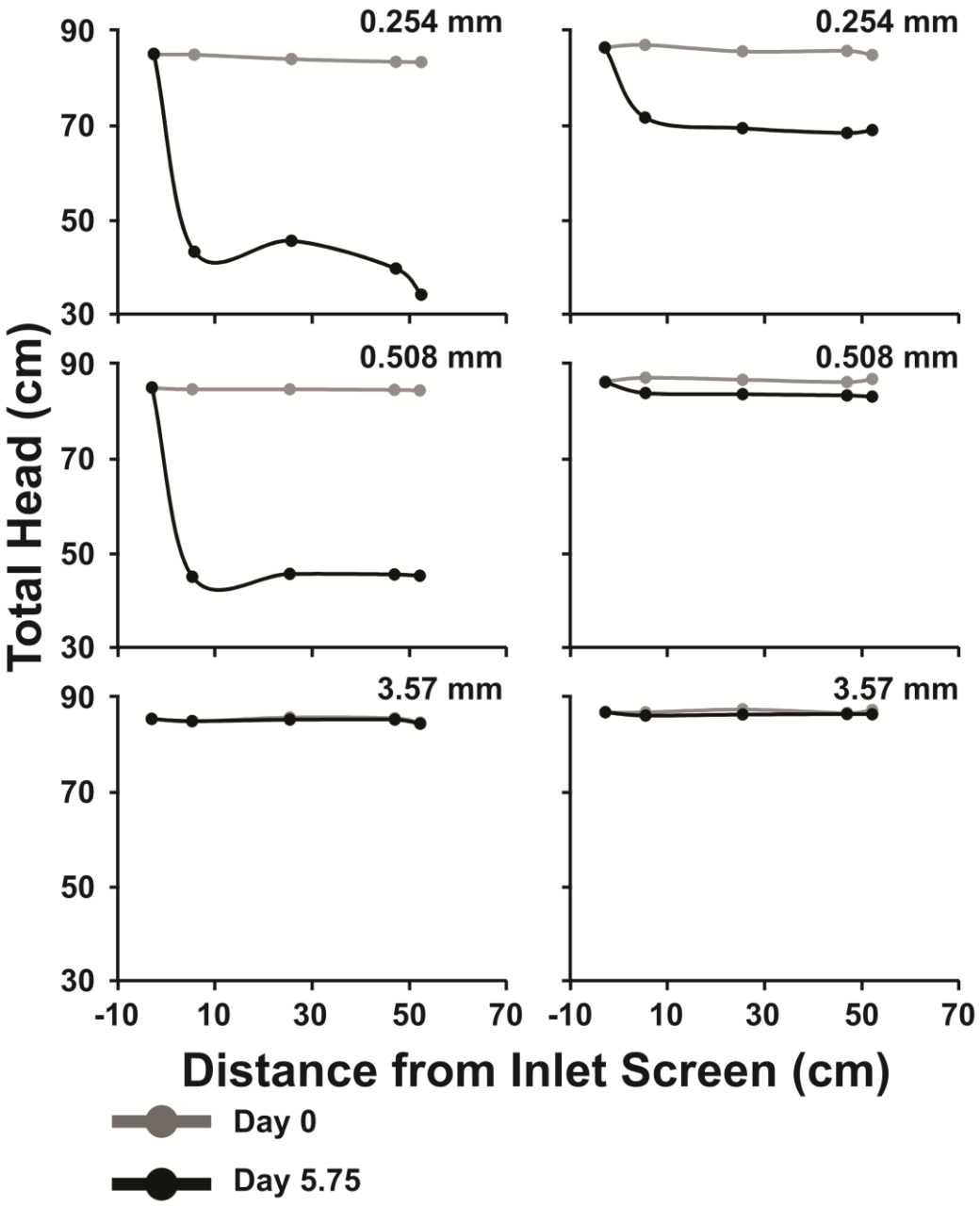

Figure 6.04: Changes in total head along the length of varying grain-size columns at the beginning and end of biostimulation.

7

Ground Penetrating Radar Observations of Enhanced Biological Activity in a Sandbox Reactor

7.0: Introduction

Bioremediation and natural attenuation are widely used methods for removing contaminants from the subsurface. For effective contaminant removal, both approaches rely on the development of an enhanced bioactive zone relative to the surrounding area. Zones of enhanced biological activity can cause changes to the bulk petrophysical and pore-water properties of a saturated porous medium, for example, by the production of cells [*Baveye et al.*, 1998], extracellular polysaccharides [*Vandevivere and Baveye*, 1992a], biogenic gases [*Delozada et al.*, 1994], secondary minerals [*Williams et al.*, 2005; *DeJong et al.*, 2006], inorganic and organic acids that lead to mineral dissolution [*Welch et al*., 2002], and redox processes that dissolve or precipitate minerals [*Rinck-Pfeiffer et al.,* 2000]. Recently, investigators began studying the responses of geophysical methods applied to sediments in which biological activity was enhanced by the presence of a growth nutrient. The use of geophysical techniques to investigate biological activity has formed a new field of study called biogeophysics. Biogeophysical studies have shown that enhanced biological activity in hydrocarbon contaminated sediments cause increased pore-water conductivity (due to mineral dissolution) and increased bulk electrical conductivities (due to mineral dissolution and possibly surface conduction) [*Sauck*, 2000; *Cassidy et al.*, 2001; *Atekwana et al.*, 2004a; *Atekwana et al.*, 2004b]. Building upon these results, other laboratory studies provided evidence that supports a more

complex conceptual model in which the interfacial electrical properties of porous media are altered due to cell attachment and biofilm formation [*Ntarlagiannis et al.*, 2005; *Abdel Aal et al.*, 2006; *Abdel Aal et al.*, 2009].

By suspending cells in a fluid medium, their passive electrical properties can be isolated from the earth environment and characterized by examining the suspension's frequency dependent dielectric behavior. Methods such as dielectric spectroscopy and dielectrophoresis have demonstrated that by examining the frequency dependant dielectric response of cell suspensions, information regarding cell morphology [*Bone et al.*, 1996], cell wall characteristics (e.g. Gram stain; [*Sanchis et al.*, 2007]), viability and biomass [e.g. *Patel and Markx*, 2008] can be ascertained. The contrast between the dielectric constant of cell suspensions and that of the surrounding fluid has been shown to be frequency dependent, where with increasing frequency the dielectric constant of the cells decreases, approaching that of the suspending fluid [*Carstensen*, 1967; *Asami et al.*, 1980; *Prodan et al.*, 2004]. This phenomenon is thought to occur as a result of numerous dispersions caused by the dielectric properties of membranes (MHz range), the relaxation of biopolymers and bound water (MHz to GHz range), and reorientation of water and other molecules (> 1 GHz) [*Miller et al.*, 2005]. In the frequency range of ground penetrating radar (GPR) (MHz to GHz), dielectric spectroscopy studies of cell suspensions show that small increases in dielectric constant relative to the suspending fluid can be measured [*Carstensen*, 1967; *Asami et al.*, 1980]. These studies provide encouraging indications that high frequency electromagnetic (EM) methods such as GPR may be capable of detecting changes in cell concentration in porous media. If so, it is expected that only small

changes in EM wave velocity of propagation and resulting travel time would be observed from the anticipated small increase in dielectric constant.

Previous studies show that GPR has been used in the field successfully to characterize biological activity. Field GPR observations have provided evidence relating increases and decreases in dielectric constant to changes in volumetric water content (i.e. saturation porosity) due to the dissolution, and down-gradient re-precipitation of calcite, respectively. Such was the case for a Cr(VI) contaminated aquifer subjected to hydrogen release compound treatments to stimulate microbial activity [*Hubbard et al.*, 2008]. Mineral dissolution was also inferred on the basis of GPR measurements at the field scale. Increases in electrical conductivity, primarily attributed to an increase in dissolved ionic constituents during biodegradation of light non-aqueous phase liquids (LNAPL), were shown to increase GPR wave attenuation [*Sauck et al.,* 1998; *Bradford* 2007; *Cassidy*, 2007]. Similarly, in a biostimulation experiment with vegetable oil emulsion, borehole GPR amplitude observations, together with electrical logs, were used to track spatial and temporal changes in pore-water electrical conductivity, which resulted in GPR wave attenuation further down-gradient than the injected emulsion [*Lane et al.*, 2006]. In a multi-year field monitoring study, decreases in pore-water electrical conductivity and mass removal of hydrocarbon in a LNAPL contaminated aquifer was suggested as a possible explanation for increased signal strength from GPR reflections [*Che-Alota et. al.*, 2009]. In another study, biogenic CH_4 and CO_2 gas distributions in peatlands were mapped by interpreting surface and borehole GPR responses with direct gas and soil moisture probe data [*Comas et al.*, 2005]. The authors presented evidence suggesting that zones of relatively low reflectivity, identified by surface GPR, were correlated with the accumulation of biogenic gas.

Anomalously high EM wave velocities, as measured by borehole GPR, were attributed to a decrease in dielectric constant caused by up to a 10% loss in saturation. Both zones of high EM wave velocities and low reflectivity were correlated with high CH_4 and CO_2 gas production [*Comas et al.*, 2005].

Previous field studies show that GPR can be used to detect the products of microbial activity in the subsurface, such as changes in bulk electrical conductivity, mineral dissolution and precipitation, and the formation of biogenic gas. Laboratory studies indicate that the dielectric constant of cell suspensions is frequency dependent and generally different than that of the suspending fluid. However, there remains a need to determine if GPR is a viable method for investigating the effects of microbial activity and accompanying changes in an earth environment. The purpose of this study is to investigate spatial and temporal changes in GPR signal travel time and amplitude associated with enhanced biological activity in water-saturated sand. The results from this study provide novel insights regarding radar wave response to biostimulated, saturated, granular porous media.

7.1: Methods

7.1.1 Reactor Construction and Setup

A flow-through tank packed with sand, hereafter referred to as the sandbox, was subjected to time-lapse GPR reflection to monitor electromagnetic wave two-way travel time and amplitude changes during biostimulation. The sandbox measured 1.0 m x 1.0 m x 0.3 m and was constructed of 12.7 mm (0.5 inch) thick sheets of polycarbonate (Figure 7.01). Two screens, constructed from a composite frame and 200 µm Nytex mesh, established the up- and

down-gradient ends of the sand filled portion of the tank, creating open water reservoirs at the two ends of the tank. This design made it possible to maintain a uniform hydraulic gradient across the water saturated sand. Three fully screened wells positioned half way down the long axis of the tank (between gridlines 3 and 4 in Figure 7.01) were used for the injection of a nutrient solution to stimulate microbial growth in the down-gradient section of the tank, whereas microbial growth was not actively stimulated in the up-gradient section. Two 0.5 cm diameter high-density polyethylene monitors, placed in the center of each of the up- and down-gradient sections, allowed for the collection of aqueous samples. Prior to the addition of sand, all internal sandbox components were rinsed with deionized water and cold-sterilized with 100% methanol. Both down- and up-gradient sections of the sandbox were imaged by 21-point GPR reflection grids on the side of the tank (Figure 7.01). An aluminum sheet was placed on the side of the sandbox opposite the grid, to serve as a reflector for transmitted GPR energy. Fine-grained silica sand (Quickcrete® No. 1961) was dry-sterilized at 400ºC for 8 hours and wet packed with deionized water. Native groundwater was acquired from an oligotrophic, uncontaminated portion of the Kansas River alluvial aquifer [*McVay*, 2000] and served as an inoculum. The groundwater has been characterized as circum-neutral in pH (6.9 – 7.4), with a mean pore-water electrical conductivity (EC) of 628 μS cm^{-1}. Oxygen, nitrate and sulfate are available as terminal electron acceptors (TEAs). However, sulfate is the dominant TEA with concentrations of about 35 mg L^{-1} [*McElwee et al*., 1995]. The groundwater inoculum was supplied to the tank from a Mariotte assembly, and allowed to flow through the sand with a constant flow rate of ~ 7 mL min^{-1}. The sandbox was monitored for 39 days before the injection of any nutrient solutions, to establish background conditions. Microbial growth was stimulated

on day 40 with an autoclaved nutrient solution containing 10 grams of Tryptic Soy Broth (TSB) and 10 grams of sodium acetate, dissolved in one liter of deionized water and diluted to three liters. As an all purpose medium, TSB contains 57% pancreatic digest of casein, 10% papaic digest of soybean meal, 17% NaCl, 8% dipotassium phosphate, and 8% dextrose. The acetate was supplied as a carbon source associated with stimulated denitrification and sulfate reduction [*Devlin, and Barker* 1996; *Gierczaket et al*., 2007]. The electrical conductivity of the diluted nutrient solution at the time of injection was 3850 µS cm^{-1}. Between days 40-60, the nutrient solution was injected once per week. After day 60, nutrient injections increased to twice per week. The experiment ran for a total of 90 days.

7.1.2. Geochemical Sampling and Biomass Analysis

Aqueous samples were collected daily from the monitors in both the up-gradient and down-gradient locations. Samples of pore-water (100 mL) were analyzed for EC, pH, and temperature twice daily. Electrical conductivity was measured using an Accumet AP75 conductivity Data Meter that was calibrated with 12.88 mS and 1413 µS solutions of KCl at 25 °C. The pH meter was calibrated prior to each use with three-point calibration lines (pH = 4, 7, and 10). At the completion of the experiment (day 90), three cores were collected from two locations down-gradient and one location up-gradient of the nutrient injection wells, to assess biomass growth. Core material was recovered to a depth of 40 to 50 cm below the sand surface in the tank. The cores were sectioned at 10 cm intervals and freeze dried in preparation for total lipid biomass analysis. Phospholipids were extracted by delivering 2.0 g of sediment into a single-phase solution containing 7.5 mL $CHCl_3$, 15.0 mL CH_3OH, and 5.0 mL of 50 mM

phosphate buffer. The single-phase solution was split into two phases by adding 7.5 mL deionized water and 7.5 mL of $CHCl_3$ to remove the CH_3OH and concentrate the phospholipids in the $CHCl_3$ phase. The phospholipids containing $CHCl_3$ phase was withdrawn, passed through a $NaSO_4$ glass-fiber filter to remove particulate and water, and evaporated in a 37^{O} C water-bath to concentrate the phospholipids. Concurrently, orthophosphate standards (0 nM, 1.5 nM, 3 nM, 6 nM, 10 nM, and 15 nM) made from glycerol phosphate were processed in duplicate with samples. The samples and standards were then digested by combining the extracted/prepared phospholipids with 2.0 mL potassium persulfate (5 g K-persulfate in 99 mLs deionized water and 1 mL 0.36N H_2SO_4.) and reacted at 95^{O} C overnight. In preparation for analysis, samples and standards were combined with 0.5 mL ammonium molybdate (2.5 g $(NH_4)Mo_7O_{24}$-$4H_2O$ in 84 mLs deionized water and 16 mLs 0.36N H_2SO_4) and 2.0 mL malachite green solutions (1.11 g polyvinyl alcohol and 0.11 g malachite green in 1 L deionized water) and decanted into a cuvette where absorbance was recorded at 610 nm by a Spectronic GENESYS 20 spectrophotometer. The phosphate content of each sample was related to cell mass per gram dry weight aquifer material, and was obtained using the average of a range of conversion factors reported by *Dobbs and Findlay* [1993] (3.4×10^7 to 2.0×10^9 cells/nmol PO_4).

To estimate total lipid biomass levels after the inoculation phase but before the biostimulation phase, duplicate columns constructed from 1.27 cm vinyl tubing were wet packed with deionized water and the same sterilized sand used in the sandbox experiment. A total of 20 liters of groundwater collected from the same well used in the sandbox experiment was fed through each column using a Mariotte assembly for a period of seven days. After seven

days, columns were freeze dried and analyzed for total lipid biomass. Sterilized sand was also analyzed for total lipid biomass to ensure sterility of the material.

Sand representing depths 10 to 20 cm from core samples, along with a subset of sterilized sand, was powdered and analyzed by X-ray powder diffraction (XRD) on a Bruker AXS D8 Advance X-ray diffractometer equipped with a xyz stage, and a Cu-Ks beam to characterize the bulk mineralogy. A subset of powdered samples from the above mentioned core locations were also analyzed in duplicate for total inorganic carbon concentration to quantify the fraction of carbonate minerals within the sand using a UIC Coulometrics TC/TIC/TOC carbon analyzer with CM5230 acidification module and CM5015 CO_2 coulometer.

7.1.3: Ground Penetrating Radar Data Acquisition and Analysis

Ground penetrating radar with 1200 MHz antennas (Sensors & Software Inc. pulseEKKO 1000) was employed to examine porous medium changes over time in response to biostimulation. Ground penetrating radar data were acquired by transmitting through the front side of the sandbox and receiving the energy reflected by the aluminum reflector at the back side of the sandbox. The metallic reflector returns nearly all the GPR energy from the back wall of the reactor. In this set-up, the EM energy travels through the saturated porous medium twice, simulating the effect of a longer travel path, and enhancing potential arrival time and amplitude signal changes. Ground penetrating radar data were acquired twice daily through the saturated sand at 21 up-gradient, and 21 down-gradient grid locations as well as through the open air portion of the polycarbonate box (top) (Figure 7.01). EM wave transmission through air was used to monitor instrument response during the 90-day experiment. On the

days of active biostimulation, GPR data were acquired prior to the addition of growth nutrient. Eight radar pulses were transmitted and summed (stacked) for each recorded trace, using a 25 ns time window and 0.01 ns sample interval with no gain. Reflected signal two-way travel times were determined by the time difference between the maximum amplitude of the direct air-wave arrival and the first break of the reflected wave. Two-way travel time and maximum amplitude of the reflected signals were determined for analysis.

Dielectric properties of the medium, as well as GPR instrument response, can vary temporally as a function of ambient temperature, and instrument timing drift (time zero drift). Generally, those sources of arrival time change are considered negligible in typical GPR field investigations. However, to investigate the effects of biostimulation in this experiment, arrival time changes accurate to within a fraction of a nanosecond needed to be assessed. The design of the experiment allowed the determination of daily relative changes between baseline observations (up-gradient) and biostimulated sand (down-gradient). Comparison between up-gradient and down-gradient GPR measurements, which were similarly affected by any temperature variations, ensured that observed changes in radar signals could be distinguished from simple temperature effects.

The GPR observations were examined in two ways. First, a comparison was made of the (21 grid-point) average daily responses from each of the up- and down-gradient sections of the sandbox. Differences in two-way travel times and maximum amplitudes were used to examine relative changes between the two sides of the tank. Examining travel time data in this fashion has the advantage of removing the effects of instrument drift, and water's dielectric constant dependence to temperature. Next, in order to compare spatial variations within the sandbox

over the 90-day experiment, the mean up-gradient two-way travel time (9.06 ns) was used as a baseline to calculate the calibration needed to remove the effects of daily instrument drift and temperature. Two-way travel times for each one of the 42 GPR monitoring grid points were computed for the 90-day experiment in this fashion. The local variations in box geometry, such as bulging in the center due to packing, were corrected by subtracting the background (each grid point's mean two-way travel time for pre-biostimulation days 22-40) from each grid point's respective two-way travel time.

7.2 Results

The sandbox was monitored during an initial 20 day equilibration phase when groundwater from the Kansas River aquifer was flushed through the reactor, replacing the initial (deionized) pore-water. Background data were collected for an additional 20 days to establish and record pre-biostimulation up- and down-gradient conditions. The experiment then proceeded with 20 days of weekly nutrient additions followed by 30 days of twice weekly nutrient additions.

7.2.1 Electrical Conductivity and pH

Water samples were collected daily from the monitors in the up- and down-gradient sides of the sandbox. Pore-water temperature (Figure 7.02A), electrical conductivity (Figure 7.02B) and pH (Figure 7.02C) were monitored in the saturated sand over time. Data prior to day 20 are considered unrepresentative of background since during this time the initial pore water was being replaced with groundwater. By days 22 through 40, pH and EC had achieved

steady baselines. Pore-water EC, down-gradient of the nutrient injection wells, continuously increased after biostimulation (day 41), due in part to the nutrient solutions themselves. Immediately prior to biostimulation, both up- and down-gradient pHs were roughly 7.4. As biostimulation progressed, pH became more variable, but remained similar in magnitude in both ends of the tank.

7.2.2 Changes in Daily Average GPR Two-way Travel Times and Maximum Amplitudes

Daily average changes in two-way travel times between the down- and up-gradient portions of the tank were evaluated by plotting the difference in the daily means of the down-gradient values from the up-gradient values (Figure 7.02D). Prior to biostimulation (days 22-40), a weak upward trend in the data exists, with a slope of 0.00058 (Figure 7.02D). After beginning the weekly addition of nutrients (days 41-60), the fitted trend line slope doubles to 0.0015 (Figure 7.02D). This resulted from the mean down-gradient two-way travel time increasing relative to that associated with the up-gradient end of the tank. Increased nutrient loading (twice per week) after day 60, coincided with the observed formation of gas bubbles in the down-gradient portion of the box and a sharp decrease in down-gradient GPR arrival times. These occurrences are marked by a reversal in trend line slope in Figure 7.02D (slope = -0.0046).

Amplitude observations exhibit greater variability than arrival time observations. The difference in the daily average GPR maximum amplitude between the down- and up-gradient sides of the tank indicate a generally decreasing trend, beginning at approximately day 40,

which correlates to the rise in electrical conductivity (Section 3.1) and the onset of nutrient delivery (Figures 7.02B and 7.02E).

7.2.3 Sediment Mineralogy

To examine changes in bulk sediment mineralogy, post-biostimulated sediment samples collected from core on day 90 were analyzed by XRD and compared to pre-biostimulated sediments. Both pre- and post-biostimulated XRD patterns exhibited mineralogy dominated by quartz and anorthoclase (e.g. $(Na,K)AlSi_3O_8$; Figure 7.03). Ordered quartz peaks were observed at 2-theta angles of 20.87º and 26.63º as well as peaks observed above 35º. A doublet peak at 2-theta angles of 27.48º and 27.85º is consistent with anorthoclase. A small peak that was present only in the pre-biostimulated sediment sample, at a 2-theta angle of 30.57º, could not be uniquely identified. Because it did not correspond to peaks from any of the common minerals or a readily soluble phase, it was treated as an anomalous substance present in unrepresentative amounts in the pre-biostimulated sand sample. Further work is needed to identify the peak conclusively. Any other minerals in the samples were present in insufficient quantities to identify or detect with the instrument. Powdered sediments from the same core locations used in the XRD analysis were analyzed to determine the fraction of inorganic carbon. Duplicate samples from pre- and post-biostimulated sediments each comprised an average of 0.007 % (± 0.001% and ± 0.004%, respectively) carbonate by mass.

Following the addition of the nutrient solution to the tank water, a black precipitate was observed at the down-gradient end of the tank. Although visible on the sediment that was cored, this precipitate was not identifiable by XRD. This may have been due to insufficient

coating thicknesses on the grains, or an amorphous structure of the precipitate. Given the reducing conditions of the experiment, it is likely that dissimilatory iron- and sulfate reduction were occurring concomitantly [*Jakobsen et al.,* 1998]. This would be expected to result in the subsequent rapid precipitation of amorphous iron sulfides [*Rickard* 1995]. The formation of the black precipitate is consistent with this expectation. Further support comes from the observation that the precipitate converted to a rust colored solid (probably an iron oxide or oxyhydroxide) when it was allowed to oxidize at the end of the experiment.

7.2.4 Changes in Total Lipid Biomass

Initial biomass of the sterilized sand was found to be below the detection limit of the method (< 10^4 cells g^{-1} dry weight sediment). Column experiments representing biomass levels after the inoculation phase but before the biostimulation phase were between 10^7 and 10^8 cells g^{-1} dry weight sediment. After inoculation and 50 days of growth nutrient application (day 90), biomass increased to 10^8 - 10^9 cells g^{-1} dry weight sediment in both down- and up-gradient locations within the sandbox (Figure 7.04).

7.2.5 Spatial Changes of GPR Arrival Times

Spatial changes in GPR two-way travel time from background (where background was again considered the mean of travel times between days 22 and 40) at each of the 42 grid locations were compared against the corresponding averages of days 28 to 32, reflecting times of no change, days 58 to 62 and days 88 to 90, corresponding to times of maximum change

between up- and down-gradient sandbox conditions (Figure 7.05). Specifically, days 58 to 62 showed an increase in two-way travel time difference (more negative) down-gradient from the nutrient supply wells. Days 88 to 90 coincide with the appearance of gas bubbles at the base of the tank, down-gradient of the nutrient release wells. Two-way travel times were noted to decrease (more positive) in this area, consistent with gas formation. About this same time, two-way travel times began to increase in the up-gradient end of the tank, above 45 cm depth, suggesting a spreading of the effects of nutrient injection to that area (Figure 7.05). Gas bubbles were not observed in the up-gradient portion of the tank.

7.3: Discussion

The pH and electrical conductivity data were used to help assess changes in the sandbox due to increased microbial activity, and to help interpret changes in GPR data. Fluctuations in pore-water temperature were a result of changes in air temperature within the building. Such changes would likely affect the growth rate of bacteria to some degree, but the outcome would be increased biomass, regardless. Early time variations in the pH are thought to be due to replacement of the original pore-water with groundwater, and equilibration of the ground water with the porous medium. The pH dataset was collected in part to serve as an indicator of microbial metabolism (i.e., production of CO_2) and water-rock interaction. However, after the first 21 days of the experiment, the variability of pH over time was never greater than 0.25 pH units. This relatively small pH variation throughout pre- and post-biostimulation times indicates either that enhanced microbial growth did not affect the pH of the system greatly, or that the pore-water was adequately buffered to mask the effects. As no potential buffers existed in the

sediment mineralogy, as evidenced by XRD analysis, we hypothesize that the solution was buffered by TSB (manufacturer specified set point pH of 7.3).

The injection of dissolved carbon and nutrients increased the electrical conductivity of the groundwater and this was expected to attenuate the radar signal amplitude. Furthermore, metabolic products of biological activity have been shown to increase electrical conductivity through mineral weathering and cause attenuation of radar waves [*Sauck et al.,*1998]. In fact, the signal was attenuated by a mean of 18 % during the entire period of biostimulation (days 40 to 90) in the down-gradient portion of the sandbox, confirming the GPR's amplitude responsiveness to changes in bulk electrical conductivity. However, it is not possible with the current experimental design to differentiate the competing mechanisms of radar signal attenuation.

Biomass measured from core sediments was shown to vary over 1.5 orders of magnitude from sample to sample. This high degree of biomass variability between depth-specific samples is not surprising since only 10 g of sediment was homogenized for lipid biomass analysis, therefore spatial variability was unavoidable. Nevertheless, the total biomass observed after biostimulation was about one order of magnitude greater than the inferred biomass before biostimulation (after inoculation) (Figure 7.04). Using the same method of biomass enumeration, *Schillig et al.* [*in press*] reported similar total biomass magnitudes (10^9 cells g^{-1} dry weight sediment) and changes (one order of magnitude) as a result of adding dissolved oxygen to a petroleum contaminated aquifer. In that case, localized decreases in groundwater velocity and flow redirection resulted from the biomass growth. Other studies have shown similar behaviors, albeit under very different experimental conditions. For

example, in laboratory tests an 80-90% decrease in hydraulic conductivity was observed with an increase in biomass of one order of magnitude leading to a final concentration of 10^8 - 10^9 cells g^{-1} dry weight sediment [*Vandevivere and Baveye*, 1992b; *Holm*, 2001].

Following the change to twice weekly nutrient injections, it is likely that the accumulation of biomass and production of gas down-gradient of the nutrient injection wells both contributed to decreases in the hydraulic conductivity of the porous medium. This may have resulted in nutrient delivery into the up-gradient portion of the sandbox late in the experiment. Evidence for up-gradient nutrient delivery and biostimulation is shown in Figure 7.02C where the up-gradient pore-water electrical conductivity begins to increase from baseline after day 60. By day 88, two-way travel times were noted to increase by 0.1 ns relative to the background in the up-gradient portion of the sandbox (Figure 7.05C).

Increasing two-way travel times observed after biostimulation indicate an increasing bulk dielectric constant of the porous medium, which could be caused by either an increased porosity due to dissolution of mineral grains and/or possibly an increase in biomass. Changes in dielectric constant reported by *Hubbard et al.* [2008] were attributed to the dissolution of calcite minerals near the injection well and further down-gradient precipitation. Data reported by *McGlashan* [2007] at a petroleum contaminated aquifer indicated that the bulk dielectric constant increased as a result of biostimulation. One of the mechanisms postulated by *McGlashan* [2007] to cause the increase in the bulk dielectric constant was an increase in saturated porosity by 1 - 3% (i.e. from an initial value of 0.38 to 0.41) through mineral dissolution. This increase from 1 – 3% in saturated porosity assumes the dielectric constant of biomass is equal to that of water. To estimate the change in porosity required to explain the

travel time changes observed in this study, the two-way travel times were corrected for the thickness of the polycarbonate, and converted to bulk dielectric constants by:

$$\varepsilon_m = \left(\frac{ct}{x}\right)^2 \quad [1]$$

where ε_m is the bulk dielectric constant, c is propagation velocity of electromagnetic waves in free space (0.3 m ns^{-1}), t is the two-way travel time corrected for the time required to propagate EM energy four times through 0.0127 m thick polycarbonate with a dielectric constant of 3, and x is the total travel distance (0.6 m). Finally, ε_m was converted into a volumetric water content or saturated porosity (θ_v) using the equation by *Topp et al.* [1980]:

$$\theta_v = -5.3x10^{-2} + 2.92x10^{-2}(\varepsilon_m) - 5.5x10^{-4}(\varepsilon_m^2) + 4.3x10^{-6}(\varepsilon_m^3) \quad [2]$$

Two-way travel time increases, using both raw and drift-corrected data, can be explained by a total porosity increase of less than 1% (i.e. 0.340 to 0.349), which is below the standard error of the method (0.013 or 1.3%). Even so, the negligible presence of carbonate or other soluble minerals in the porous medium, and the circum-neutral pH that persisted throughout the experiment, argue against mineral dissolution as a cause of the observed travel time changes. Thus, the growth of biomass can be considered as a possible cause of the radar wave velocity changes.

By assuming a constant porosity, an increase in two-way travel time from biomass accumulation would suggest that the biomass had a bulk dielectric constant (at 1200 MHz frequency) that was greater than that of the pore-water. There is little in the literature to support this hypothesis presently. However, the idea is consistent with the findings of *Zhang*

and Van Geel [2007] who reported dielectric constants greater than expected when they made TDR measurements in peat biofilters. They attributed their results to the growth of bacteria.

The rapid decrease in two-way travel time observed after day 60 (Figure 7.02D and Figure 7.05) was coincident with the observation of gas bubbles accumulating on the down-gradient side of the tank. The total change in saturation caused by gas bubble accumulation was estimated using the complex refractive index method (CRIM), a dielectric mixing formula that relates changes in bulk dielectric constant to changes in air, soil, or water content [*Wharton et al.*, 1980]:

$$\sqrt{\varepsilon_m} = \theta_v S_w \sqrt{\varepsilon_w} + (1-\theta_v)\sqrt{\varepsilon_s} + \theta_v (1-S_w)\sqrt{\varepsilon_a} \qquad [3]$$

where ε_m is the observed bulk dielectric constant calculated from Equation 1, ε_w is the temperature dependent dielectric constant of water according to *Wraith and Or* [1999], ε_s is the dielectric constant of dry geologic material, ε_a is the dielectric constant of air (ε_a =1), and S_w is water saturation. The average porosity of the sandbox, prior to biostimulation, was estimated to be 0.34 using Equation 2 for data collected on day 32. The dielectric constant of the dry silica sand was calculated to be 4.53 by calibrating ε_m from day 32 with Equation 2 and Equation 3. By using Equation 3, and assuming no change in total porosity, the maximum decrease in saturation observed on day 88 (gridline 3, 50 cm below the surface in Figure 7.05), compared to background conditions on day 32, was 7.5%. Therefore, 7.5% of the pore-volume occupied by gas (i.e. saturated porosity changes from 0.340 to 0.265) could explain the GPR response.

The changes observed in two-way travel time in this study were small in magnitude, though consistent in nature. Two-way travel times measured in zones receiving nutrients were shown to increase slightly relative to background, as depicted by the increasing slope in Figure 7.02D, representative of days 41 to 60. These changes are relative differences between down- and up-gradient average measurements and are free of water temperature or instrument drift caused variations. Furthermore, by doubling the weekly nutrient delivery on day 60, another measurable change in slope (negative) occurred which was explainable from direct observations (appearance of bubbles) and theoretical calculations (Figure 7.02D). Temporal changes in mean EM propagation velocity from background conditions (days 22 to 40) were determined by dividing the known travel distance by the up- or down-gradient mean two-way travel time. Between days 41 to 60, mean velocity decreased relative to background by 0.23% (0.001 m ns^{-1}) in down-gradient locations, whereas up-gradient locations decreased by less than 0.04% (0.00003 m ns^{-1}). Between days 61 to 90, mean velocity increased relative to background by 0.54% (0.004 m ns^{-1}) in down-gradient locations, whereas mean velocity of up-gradient locations remained unchanged from days 41 to 60. By applying the mean two-way travel times described above to Equation 1, average changes in ε_m can also be calculated for the experiment. Background conditions representing days 22-40 were calculated to have a mean ε_m of 19.43 and 19.13 for down- and up-gradient locations, respectively. Between days 41 to 60, mean ε_m increased to 19.53 in down-gradient locations, whereas up-gradient locations increased to 19.14. Between days 61 to 90, mean ε_m decreased to 19.22 in down-gradient locations, while up-gradient location mean ε_m remained unchanged from days 41 to 60. Down-

gradient ε_m decrease coincides with the visual observation of gas bubbles in the sandbox. The computed ε_m increase is consistent with dielectric spectroscopy studies conducted in the frequency range of GPR where only small increases in dielectric constant relative to the suspending fluid were measured [*Carstensen*, 1967; *Asami et al.*, 1980]. However, in order to calculate the dielectric constant of bacteria using GPR in this experiment, further study would be needed to determine the portion of the pore-space occupied by the biomass itself.

7.4: Conclusions and Implications

Daily changes in GPR two-way travel times were observed in this study as a result of enhanced biostimulation. From this it is concluded that stimulated microbial activity can produce small, but measurable effects on the bulk dielectric properties in saturated silicate sands. Relative decreases in GPR signal two-way travel time and increases in attenuation observed at the end of the experiment were coincident with the observed formation of biogenic gas bubbles. However, earlier increases in two-way travel time and attenuation were also observed in this study, apparently the direct result of biostimulation. Given the pH conditions observed in the experiment and the mineralogical composition of the sand, mineral dissolution to the extent required to alter two-way travel time is thought to be unlikely over the duration of the experiment. It is suggested here that an alternative explanation, directly related to the presence of biomass, exists to account for the increase in two-way travel time reported in this study.

From the above, the results of this study indicate that GPR is sensitive to porous medium changes indirectly, and possibly directly, related to the biostimulation of sand-sized granular porous media. The changes that were detected correspond to biomass concentrations that may be sufficient to alter groundwater flow, and may therefore be of practical concern. By furthering our understanding of the petrophysical changes that occur during biostimulation in controlled environments, the ability to detect and correctly interpret biological transformations and processes in the subsurface with GPR can be better developed for field-scale applications. However, further research is needed to ascertain the mechanistic cause for the changes observed in GPR signals.

References

Abdel Aal, G. Z., L. D. Slater, and E. A. Atekwana (2006), Induced-polarization measurements on unconsolidated sediments from a site of active hydrocarbon biodegradation, Geophysics, 71(2), H13-H24.

Abdel Aal, G., E.A. Atekwana, S. Radzikowski, and S. Rossbach, (2009), Effect of bacterial adsorption on low frequency electrical properties of clean quartz sands and iron-oxide coated sands, Geophys. Res. Lett., 36, L04403, doi:10.1029/2008GL036196

Asami, K., T. Hanai, and N. Koizumi (1980), Dielectric Analysis of Escherichia-Coli Suspensions in the Light of the Theory of Interfacial Polarization, Biophys. J., 31(2), 215-228.

Atekwana, E. A., R. S. Rowe, D. D. Werkema, and F. D. Legall (2004a), The relationship of total dissolved solids measurements to bulk electrical conductivity in an aquifer contaminated with hydrocarbon, J. Appl. Geophys., 56(4), 281-294.

Atekwana, E. A., D. D. Werkema, J. W. Duris, S. Rossbach, W. A. Sauck, D. P. Cassidy, J. Means, and F. D. Legall (2004b), In-situ apparent conductivity measurements and microbial population distribution at a hydrocarbon-contaminated site, Geophysics, 69(1), 56-63.

Baveye, P., P. Vandevivere, B. L. Hoyle, P. C. DeLeo, and D. S. de Lozada (1998), Environmental impact and mechanisms of the biological clogging of saturated soils and aquifer materials, Crit. Rev. Environ. Sci. Technol., 28(2), 123-191.

Bone, S., B. Z. Ginzburg, H. Morgan, G. Wilson, and B. Zaba (1996), Time-domain reflectometry studies on Halobacterium halobium and Halobacterium marismortui, Phys. Med. Biol., 41(1), 45-54.

Bradford, J.H., (2007), Frequency-dependent attenuation analysis of ground-penetrating radar data, Geophysics, 72(3), J7-J16.

Carstensen, E. (1967), Passive Electrical Properties of Microorganisms .2. Resistance of Bacterial Membrane, Biophys. J., 7(5), 493-503.

Cassidy, D. P., D. D. Werkema, W. Sauck, E. Atekwana, S. Rossbach, and J. Duris (2001), The effects of LNAPL biodegradation products on electrical conductivity measurements, J. Environ. Eng. Geophys., 6(1), 47-52.

Cassidy, N. J. (2007), Evaluating LNAPL contamination using GPR signal attenuation analysis and dielectric property measurements: Practical implications for hydrological studies, J. Contam. Hydrol., 94(1-2), 49-75.

Che-Alota, V., E.A. Atekwana, E.A. Atekwana, W.A. Sauk, and D.D Werkema (2009), Temporal geophysical signatures from contaminant-mass remediation, Geophysics, 74(4), B113-B123.

Comas, X., L. Slater, and A. Reeve (2005), Spatial variability in biogenic gas accumulations in peat soils is revealed by ground penetrating radar (GPR), Geophys. Res. Lett., 32(8).

DeJong, J. T., M. B. Fritzges, and K. Nüsslein (2006), Microbially Induced Cementation to Control Sand Response to Undrained Shear, Journal of Geotechnical & Geoenvironmental Engineering, 132(11), 1381-1392.

Delozada, D. S., P. Vandevivere, P. Baveye, and S. Zinder (1994), Decrease of the hydraulic conductivity of sand columns by Methanosarcina-barkeri, World J. Microbiol. Biotechnol., 10(3), 325-333.

Devlin, J.F. and J.F. Barker (1996), Field investigation of nutrient pulse mixing in an in situ biostimulation experiment, Water Resour. Res., 32(9), 2869-2877.

Dobbs, F. C., and R. H. Findlay (1993), Analysis of microbial lipids to determine biomass and detect the response of sedimentary microorganisms to disturbance, in Handbook of methods in aquatic microbial ecology, edited by P. F. Kemp, et al., pp. 347-358, Lewis Publishers, Boca Raton.

Gierczak, R.F.D., J.F. Devlin, D.L. Rudolph, (2007), Field test of a cross-injection scheme for stimulating in situ denitrification near a municipal water supply well. J. Contam. Hydrol., 89(1-2), 48-70.).

Holm, J. (2001), Effect of biomass growth on the hydrodynamic properties of groundwater aquifers, Series Paper - Department of Hydrodynamics and Water Resources, Technical University of Denmark, 72.

Hubbard, S. S., K. Williams, M. E. Conrad, B. Faybishenko, J. Peterson, J. Chen, P. Long, and T. Hazen (2008), Geophysical Monitoring of Hydrological and Biogeochemical Transformations Associated with Cr(VI) Bioremediation, Environ. Sci. Technol., 42(10), 3757-3765.

Jakobsen, R., Albrechtsen, H.-J., Rasmussen, M., Bay, H., Bjerg, P.L., and T.H. Christensen (1998), H2 Concentrations in a Landfill Leachate Plume (Grindsted, Denmark): In Situ Energetics of Terminal Electron Acceptor Processes, Environ. Sci. Technol., 32 (14), 2142-2148.

Lane, J. W., F. D. Day-Lewis, and C. C. Casey (2006), Geophysical monitoring of a field-scale biostimulation pilot project, Ground Water, 44(3), 430-443.

McElwee, C.D., J.J. Butler, G.L. Macpherson, G.C. Bohling, R.D. Miller, C.M. Mennicke, T.J. Huettl, M. Zenner, Z. Hyder, W. Liu, M. Orcutt, M.L. Beilfuss, and S. Gonuguntla (1995),

Characterization of heterogeneities controlling transport and fate of pollutants in unconsolidated sand and gravel aquifers, final report, Open-file Report no. 95-16, 559 pp. Kansas Geological Survey.

McGlashan, M. A. (2007), Monitoring dielectric property changes and groundwater velocity changes in a contaminated aquifer using borehole ground penetrating radar and multi-level point velocity probes (PVPs), M.S. Thesis, 148 pp, Univ. of Kan, Lawrence.

McVey, S. (2000), Geomicrobial denitrifying and nitrifying characteristics of a nitrate-contaminated alluvial aquifer, northeastern Kansas, M.S. Thesis, 116 pp, Univ. of Kan, Lawrence.

Miller, J. H., D. Nawarathna, D. Warmflash, F. A. Pereira, and W. E. Brownell (2005), Dielectric properties of yeast cells expressed with the motor protein prestin, J. Biol. Phys., 31(3-4), 465-475.

Ntarlagiannis, D., N. Yee, and L. Slater (2005), On the low-frequency electrical polarization of bacterial cells in sands, Geophys. Res. Lett., 32(24), L24402, doi: 10.1029/2005GL024751.

Patel, P., and G. H. Markx (2008), Dielectric measurement of cell death, Enzyme and Microbial Technology, 43(7), 463-470.

Prodan, C., F. Mayo, J. R. Claycomb, J. H. Miller, and M. J. Benedik (2004), Low-frequency, low-field dielectric spectroscopy of living cell suspensions, J. Appl. Phys., 95(7), 3754-3756.

Rickard, D. (1995), Kinetics of FeS precipitation: Part 1. Competing reaction mechanisms, Geochim. Cosmochim. Acta, 59 (21), 4367-4379.

Rinck-Pfeiffer, S., S. Ragusa, P. Sztajnbok, and T. Vandevelde (2000), Interrelationships between biological, chemical, and physical processes as an analog to clogging in aquifer storage and recovery (ASR) wells, Water Res., 34(7), 2110-2118.

Sanchis, A., A. P. Brown, M. Sancho, G. Martinez, J. L. Sebastian, S. Munoz, and J. M. Miranda (2007), Dielectric characterization of bacterial cells using dielectrophoresis, Bioelectromagnetics, 28(5), 393-401.

Sauck, W.A., E.A. Atekwana, and M.S. Nash, (1998), High conductivities associated with an LNAPL plume imaged by integrated geophysical techniques, J. Environ. Eng. Geophys., 2(3), 203-212.

Sauck, W. A. (2000), A model for the resistivity structure of LNAPL plumes and their environs in sandy sediments, J. Appl. Geophys., 44(2-3), 151-165.

Schillig, P.C., J.F. Devlin, J.A. Roberts, G.P. Tsoflias, and M.A. McGlashan (In Press) Transient Heterogeneity in an Aquifer Undergoing Bioremediation of Hydrocarbons. Submitted to Ground Water.

Topp, G. C., J. L. Davis, and A. P. Annan (1980), Electromagnetic determination of soil water content: Measurements in coaxial transmission-lines, Water. Resour. Res., 16(3), 574-582.

Vandevivere, P., and P. Baveye (1992a), Effect of bacterial extracellular polymers on the saturated hydraulic conductivity of sand columns, Appl. Environ. Microbiol., 58(5), 1690-1698.

Vandevivere, P., and P. Baveye (1992b), Saturated hydraulic conductivity reduction caused by aerobic-bacteria in sand columns, Soil Sci. Soc. of Am. J., 56(1), 1-13.

Welch, S.A., A.E. Taunton, and J.F. Banfield (2002), Effect of microorganisms and microbial metabolites on apatite dissolution, Geomicrobiol. J., 19(3) 343-367.

Wharton, R. P., G. A. Hazen, R. N. Rau, and D. L. Best (1980), Electromagnetic propagation logging: Advances in technique and interpretation, in 55th Annual Fall Technical Conference and Exhibition of the Society of Petroleum Engineers, edited, p. 12, Dallas, TX.

Williams, K. H., D. Ntarlagiannis, L. D. Slater, A. Dohnalkova, S. S. Hubbard, and J. F. Banfield (2005), Geophysical imaging of stimulated microbial biomineralization, Environ. Sci. Technol., 39(19), 7592-7600.

Wraith, J. M., and D. Or (1999), Temperature effects on soil bulk dielectric permittivity measured by time domain reflectometry: Experimental evidence and hypothesis development, Water Resour. Res., 35(2), 361-369.

Zhang, X. Y., and P. J. Van Geel (2007), Development of a vertical TDR probe to evaluate the vertical moisture profile in peat columns to assess biological clogging, J. Environ. Eng. Sci., 6(6), 629-642.

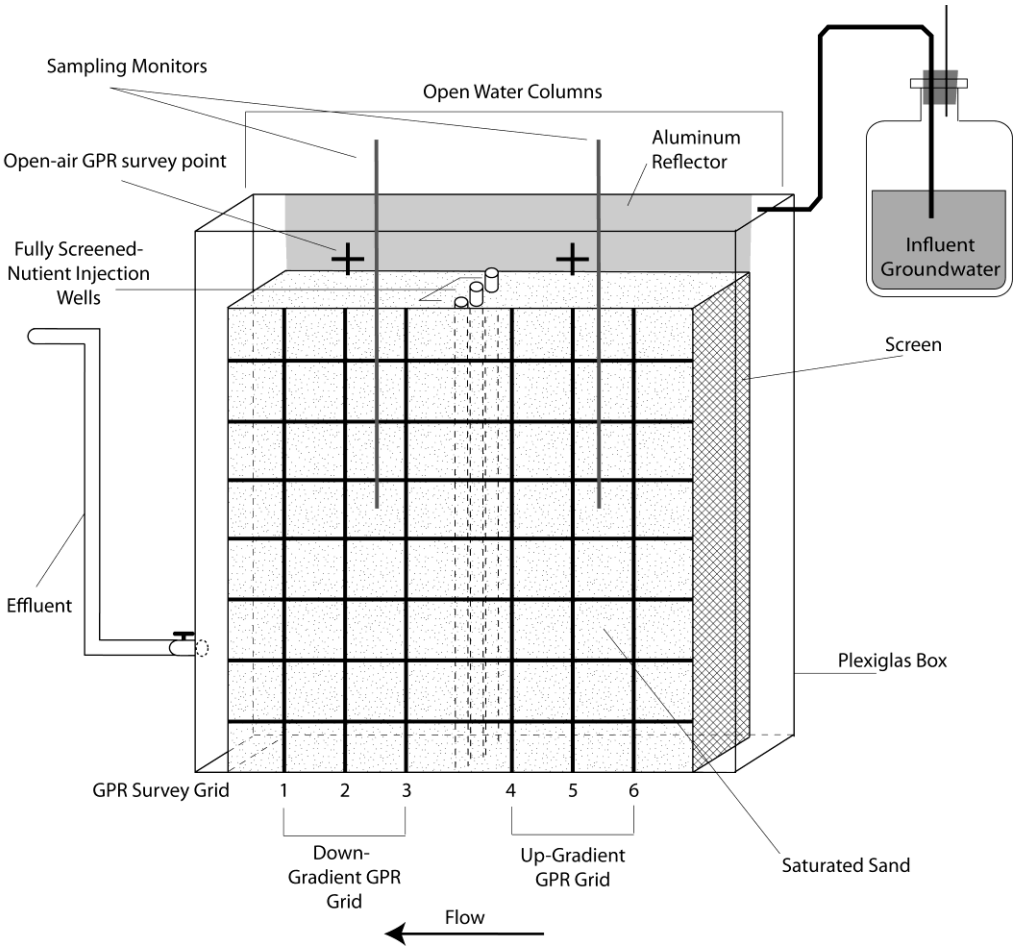

Figure 7.01: Schematic of the flow-through tank, or sandbox, showing the GPR data acquisition grids along with the location of the injection wells and sampling ports.

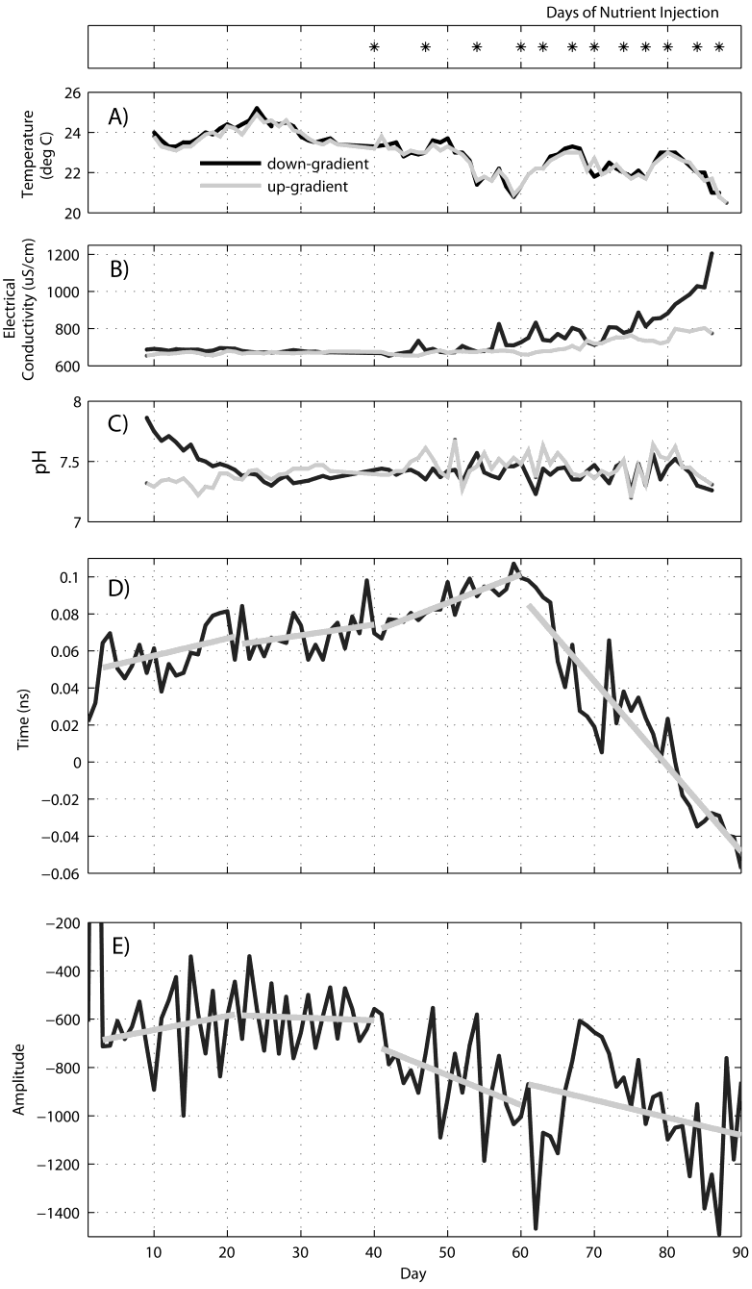

Figure 7.02: Comparison of up-gradient and down-gradient (A) pore-water temperature, (B) pore-water electrical conductivity, (C) pH, (D) differences in mean two-way travel time (down-gradient minus up-gradient), and (E) differences in mean maximum amplitude (down-gradient minus up-gradient). Initial biostimulation with weekly nutrient additions began on day 40, whereas twice weekly nutrient additions began on day 60, as shown above plot A. Trends lines (grey) on plots D and E are fitted to data during the reactor's equilibration phase (< day 21), background phase (days 22-40), weekly biostimulation phase (days 41-60), and twice weekly biostimulation phase (days 61-90)

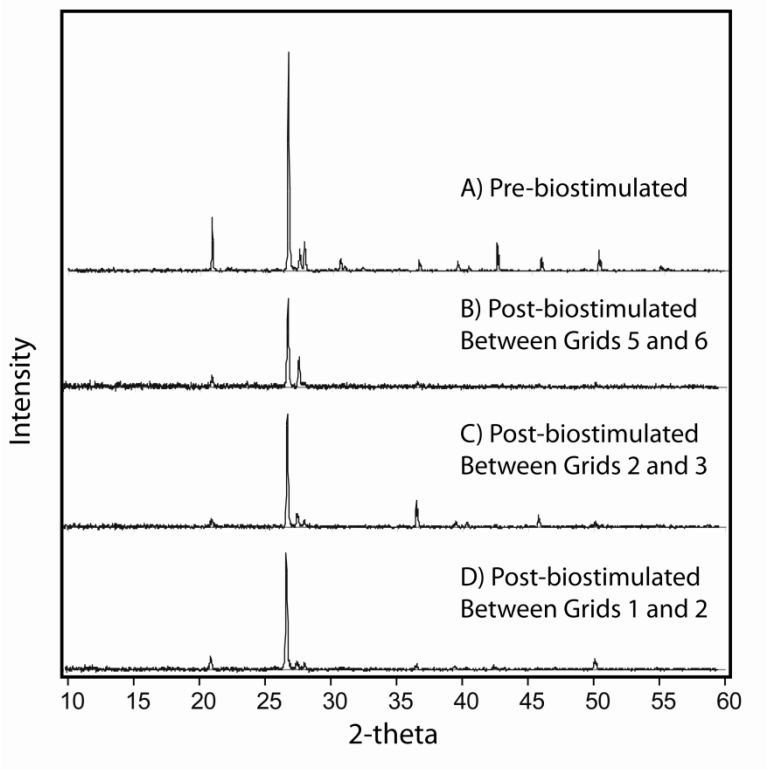

Figure 7.03: Powder XRD patterns of sand used in the experiment (A) prior to being packed into the sandbox, and (B) from core located between grids 5 and 6, (C) grids 2 and 3, and (D) grids 1 and 2. All samples from the core represent depths of 10 – 20 cm below the sand surface. All observed peaks of 2-theta greater than 35º are interpreted as secondary quartz peaks.

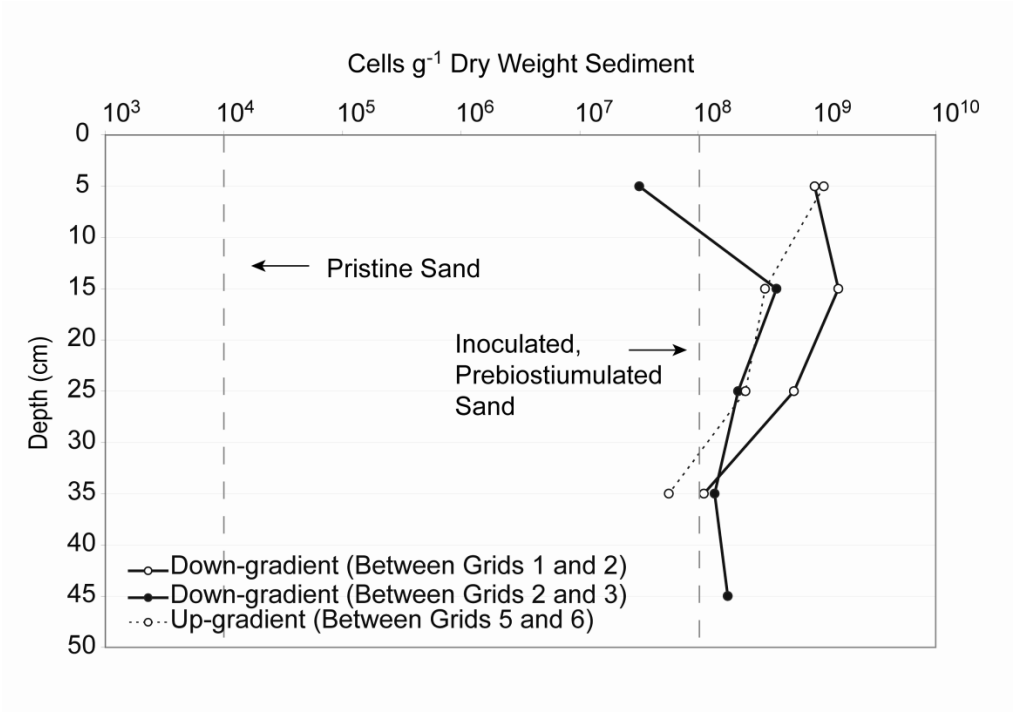

Figure 7.04: Average biomass measured in the sand used in the experiment. Pre-biostimulation conditions, shown as vertical dashed lines, were determined in samples not from the sandbox, but handled identically to those collected from the sandbox. Samples of post-biostimulation sand from the up-gradient end of the sand box, at the end of the experiment, are shown as points connected with a dotted line, and down-gradient samples are shown as points connected by solid lines. Note that by the end of the experiment, nutrient additions had affected both sides of the sandbox.

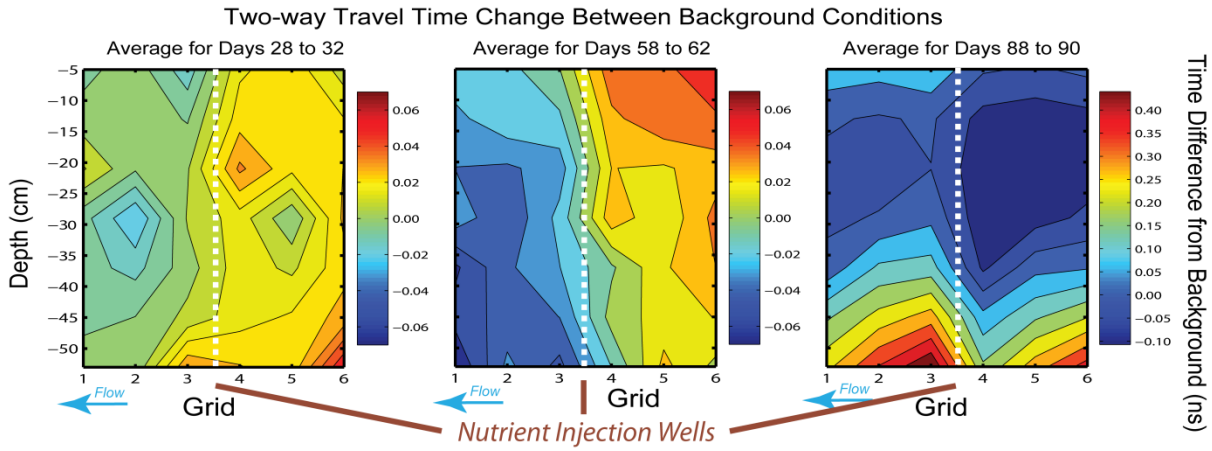

Figure 7.05: Side panel view of the sandbox showing spatial changes in two-way travel times (i.e., average background travel time minus measured travel times, in nanoseconds) for days 28-32, days 58-62 and days 88-90. Cooler colors indicate negative changes corresponding to increased two-way travel times, whereas warmer colors indicate positive changes associated with decreased two-way travel times. The location of the nutrient injection wells is shown by the vertical white dashed lines. Note the decrease in two-way travel time change down-gradient of the nutrient injection wells on days 58-62, following biostimulation, and the increase in two-way travel time change relative to the background down-gradient of the nutrient injection wells on days 88-90. Note also that an expanded color scale is used for days 88-90.

8

Conclusions and Recommendations

8.0: Conclusions

This study investigates the hydrogeological factors that control the feedback between bioactive zone formation and groundwater flow, as well as developing and assessing tools useful for making these investigations. The notion of transient heterogeneity follows directly from the recognition that the waxing and waning of biological activity changes groundwater flow. This phenomenon was investigated experimentally in both a subsurface biostimulation study and a laboratory experiments. Prior to the investigation of this phenomenon, necessary advances were made in point velocity probe (PVP) technology to ensure successful observation. Point velocity probe technology was advanced with a unique data processing software and further work was required in the interpretation of 3-D data in light of variable density flow.

With PVPs capable of measuring flow in 3-D, both the horizontal and vertical components of velocity can be successfully interpreted as either a response to natural flow in heterogeneous media, transient heterogeneity formed during bioactive zone development, or variable density flow from the saline tracer. The latter effect was investigated in detail in the laboratory to avoid introducing biases when investigating the former phenomena. Density related flow affecting PVP measurements was found to be a function of the relative magnitudes of the equivalent freshwater hydraulic gradients, horizontal and vertical. During laboratory study, unaccounted buoyancy effects were found to bias vertical velocity estimates, but did not

compromise horizontal velocity estimates for cases where the fraction of flow that is vertical did not exceed 30%. This is a conservative limit.

During site characterization of the Woodstock aquifer, agreement between the flow directions determined with tracer testing, multiple PVPs and predictions based on the orientation of the hydraulic gradient calculated from viable three-point estimators indicated that with respect to horizontal flow the aquifer is isotropic in nature at the regional scale. Vertical flow converges toward well-sorted, coarse sediments of high velocity, which makes hydrologic sense given the discontinuous, heterogeneous nature of the aquifer. Point velocity probe datasets exhibited notable variability in both magnitude and direction from location to location, but the velocities were generally reproducible on a probe by probe basis (i.e., good precision), indicating the variability was not due to noise inherent in the equipment. The variability was interpreted to be a result of natural variability in groundwater velocities at the centimeter scale. The relatively fine-scale measurement of the PVPs enhanced the characterization of flow systems due to their ability to detect 1) narrow zones where high groundwater velocities existed, and 2) vertical flow components in addition to horizontal ones. This level of characterization from a single instrument allows for unprecedented detail that cannot be attained from current, conventional methods based on Darcy's Law. High resolution data are needed for the detection of transient heterogeneity in immature bioactive zones and the associated sedimentary variables that correlate.

Biostimulation was conducted in the Woodstock aquifer based on the need to remove excess nitrate from the groundwater impacting a municipal well field. Denitrification of the aquifer was successful at most depths after sufficient amounts of soluble organic carbon were

injected to treat the daily flux of dissolved oxygen and nitrate. Changes in velocity occurred after biostimulation that could not be attributed to changes in the natural hydraulic gradient. It was determined that poorly-sorted, relatively fine-grained sandy sediments were most susceptible to decreases in groundwater velocity during biostimulation. During the biostimulation of Woodstock, coarser sediments with initially high velocities were found to change little or increase in velocity, possibly as a result of capturing flow from adjacent zones undergoing a decrease in velocity. Superimposed onto these velocity changes were variances in the temporal variability of soluble organic carbon related to the dispersive mixing of the carbon pulses, which indirectly affected flow by intermittently contributing to bioactivity, including growth. The vertical component of the resultant velocity vector was shown to have the highest degree of sensitivity with prominent changes in the mean and variance in flow direction and the variance of velocity magnitude. Attached viable biomass was shown to increase by approximately a factor of five as a result of biostimulation, with the highest concentration noted in a well-sorted gravel. While high velocities promote high nutrient flux, stimulating a greater degree of microbial growth, the relatively coarse nature of these sediments ultimately inhibits the onset of clogging, or may preclude clogging altogether. In either case, bioclogging as interpreted from the increase in attached biomass was at least partially responsible for changes in velocity.

Controlled laboratory experimentation was conducted with a series (stages) of experiments simulating the range of velocity and grain-size observed at the Woodstock site. Both experimental stages, testing velocity and grain-size variables, indicated that the major causes of clogging within fine sand and high velocity columns were biomass and free-phase

biogenic gas accumulation that resulted in decreases in apparent hydraulic conductivity by upwards of 90%. During the velocity stage, preferential clogging was noted first in the high initial velocity (1200 cm/d) columns with flow being redirected to lower initial velocity columns (50 and 100 cm/d) as seen from their measured higher relative discharges. Shortly after experiencing these higher flow rates, the 50 and 100 cm/d columns began decreasing in flow as the bioactive zone spread. While it cannot be directly ascertained whether the spreading of the bioactive zone into the slower velocity columns was a result of delayed growth or flow redirection, the progressive nature of bioactive zone growth has been demonstrated.

During the grain-size stage, preferential clogging was noted to occur in finer-grained sand columns (0.254 and 0.508 mm median grain-size) as indicated by the need to increase the hydraulic gradient to maintain a constant discharge rate in these columns to compensate for the decreases in hydraulic conductivity. On this basis, finer-grained, lower hydraulic conductivity sands, were shown to preferentially clog relative to gravelly sediments. Unless local gradients are unrealistically increased, as required during the grain-size stage to maintain a constant discharge, flow would be redirected to more permeable units.

The results above were consistent with the observations during the Woodstock biostimulation experiment. Transition zones in natural aquifers where relatively fine-grained or poorly-sorted sediments that lie adjacent to discontinuous coarser sediments - where the high velocities would lead to the highest flux of injected nutrients – represents the likely starting place for bioactive zone development, but may also be at greater risk for bioclogging. These results indicate that heterogeneous aquifers are susceptible to the development of a biologically-induced transient heterogeneity. The bioclogging of transition zones between

coarse (gravely) and less coarse (sandy) sediments implies that 1) High permeability zones targeted for biostimulation are unlikely to be the first locations in an aquifer to exhibit the desired biodegradation reactions. Early evaluations of biostimulation efforts should focus on the transition zones to verify the desired processes are occurring; 2) Significantly different permeability zones with in a treatment area should have their nutrient injection rates adjusted to minimize clogging potential and applying excess injectate; 3) High resolution site characterization should be conducted throughout the treatment process, with data interpreted in real-time, to evaluate if any major changes in flow are occurring.

Preliminary field tests showed that ground penetrating radar (GPR) may be capable of detecting small, but measureable changes in the dielectric properties coincident with bioactive zone development from background. Together with PVP data, this raises the possibility of non-invasively obtaining a near-continuous picture of the subsurface showing zones at risk of redirected flow and altered treatment efficiencies. Controlled laboratory testing performed here confirmed that changes in GPR two-way travel times and attenuation do occur as a result of increased biomass and gas accumulation.

8.1: Recommendations

8.1.1: Additional Modeling

Further numerical modeling work is necessary for the Woodstock Site. By comparing PVP, Br^- tracer testing, hydraulic head data, and biogeochemical data, it is the interpretation from the Woodstock biostimulation study that changes in hydraulic conductivity likely occurred between July and September, 2011. While changes in velocity were reported, changes in hydraulic conductivity were not directly measured nor the magnitude of their changes

interpreted. High resolution slug testing and perhaps hydraulic tomography conducted before and after biostimulation may provide a continuous picture of changes in hydraulic conductivity. However, this would require that the developed transient heterogeneity is of a large enough scale and magnitude to be successfully measured by the tests. Of course, to accomplish this, many additional wells should be installed.

Given the uncertainties in hydraulic conductivity and the anticipated difficulty in obtaining a reliable measurement of partially clogged sediment, numerical modeling is needed to estimate the changes. It is suggested here that separate calibrated flow and transport models be developed for the July and September datasets to calculate changes in hydraulic conductivity that occurred from partial bioclogging. Software packages such as PEST (Parameter ESTimation) would be needed to calibrate hydraulic conductivity from borehole-measured heads and MODLFOW as well as measured Br^- concentrations from multilevel samplers and MT3D. Results from this analysis would provide a calculation of the magnitude in which hydraulic conductivity may have changed. Further modeling work is suggested to investigate the variance in velocity due to gradient changes alone. This information would be relevant to identify how changes in regional hydraulic gradient alone could impact vertical, horizontal, and resultant velocities. To accomplish this, a Monte Carlo analysis of the recorded gradient range should be used to modify the direction and orientation of constant head boundaries in a coupled with a numerical flow model. By coupling with a numerical flow model, local changes in velocity can be calculated and compared to the observed variance data. This would serve as additional complimentary evidence to confirm if the observed changes in variance could not be accounted for by changes in regional hydraulic gradient as opposed to microbial growth.

8.1.2: Improved PVP Design

PVPs used in this study were constructed from custom ordered lengths of 1.5” schedule 40 flush-thread PVC casing. Planning and construction of these probes was time consuming and detailed records were needed since distances from the injection port to detectors varied for each probe. Since custom lengths of casing were required, there was minimal flexibility in adjusting the depths of probes if difficulties or changes in the site conceptual model were made during the installation process. While Cat 5E cable was used for the detectors and a quick connect system possible to incorporate into the design, the eight available wires limited the number of detectors that could be incorporated onto each probe. Injection ports constructed from porous stones limit the available space inside the PVC casing and hence the number of PVPs that can be installed on a single multilevel stand. In addition, this also reduces the number of injection ports on an individual probe, therefore limiting the effective range of flow directions that can be measured. It is therefore recommended that new, faster ways of constructing PVPs be explored.

A PVP construction method adopted immediately following the Woodstock PVP installations was based on rapid prototype tool technology (3D printing). This technology overcomes several problems cited above, including 1) Printed PVPs do not require custom lengths of PVC casing and therefore are considerably more flexible for plan changes during installation; 2) These PVPs can be designed to fit any diameter casing desired by the user and may be optimized to limit the aquifer collapse during installation; 3) All PVPs will be practically identical in their respective injection port and detector geometries, ensuring better comparability between PVP measurements; and 4) Three injection ports staggered 120° from

each other with common horizontal flow detectors spaced at 50 and 70° between each injection port would enable a user to theoretically install a PVP without prior knowledge of the flow direction at the site and be able to obtain, accurate and reliable results.

Continued work with the prototype printer PVPs could benefit from the following design changes, which take advantage of the strengths of the hand-made design used in this dissertation, and offer potential improvements in construction time and flexibility of use. It is recommended that further models use a hollow design to reduce the amount of ABS plastic consumed, hence the cost of production, allow more internal space for ease of construction and the stacking of additional multilevel probes, and to eliminate the need for epoxy sealing the injection line or creation of internal wire channels.

8.1.3: *Available Organic Carbon Analysis*

Additional work is needed here to characterize the naturally occurring organic carbon content of the Woodstock aquifer sediments for completeness of this study. While the bioavailable organic content is interpreted to be low in the monitored area based on the persistence of aerobic conditions, a considerable body of literature exists that relates hot spots and hot moments of biological activity to the presence of solid, bioavailable organic carbon. Therefore a more direct of the aquifer materials for natural organic matter or other electron donors (e.g. sulfides) should be performed.

8.1.4: Quantifying Extracellular Polysaccharides

While the number of viable cells were enumerated in this dissertation by total lipid biomass, the content of extracellular polysaccharides (EPS) was not accounted for and may

have significantly contributed to the clogging process. Future bioclogging studies should account for EPS production since their role in associated flow changes cannot be concluded. Furthermore, nonviable biomass in the form of deceased cells should also be accounted for if possible.

8.1.5: Independent Confirmation of Secondary Mineral Formation

Testing of sediments from Chapter 6 was not complete in time for the defense of this dissertation. While aqueous geochemistry provides evidence to suggest the likelihood of secondary mineral precipitation, it is not conclusive. Sediments from pre and post-biostimulated conditions could be analyzed with x-ray diffraction (XRD) or electron energy loss spectroscopy (TEM/EELS) to find comparative evidence that indicates secondary mineral precipitation.

8.1.6: A Reductionist Experiment to Investigate the Relationship Between Biomass Growth and GPR Signal

Additional work must be done to examine the mechanistic cause for the observed changes in GPR signal during biostimulation. Time lapse dielectric spectroscopy conducted at high frequencies of different growing pure cultures would provide valuable information to help interpret changes in the waveform and examine both real and imaginary components of their dielectric constant.

8.1.7: Laboratory Examination of Transient Heterogeneity with the Biostimulation of Stratified Sediments

Column experimentation with a common manifold provided results that could be directly related to the Woodstock biostimulation experiment. However, sorting was not explicitly tested as an active variable, and its effects were indirectly interpreted from the grain-size experiment, where finer grain-sizes would be analogous to poorer sorting. It is recommended here that for completeness, another stage testing sorting as an active variable be conducted using different mixed fractions of sieved grain-sizes.

As previously described, column experiments do not necessary reflect conditions representative in natural aquifers. It is suggested here that water velocity, grain-size, sorting, and nutrient pulsing be further tested in a tank setting, complete with stratified sediments. This design would allow for the integration of the sensitive hydrologic variables identified in this dissertation in a controlled setting. Sediments can be wet packed in the tank to represent conditions found in natural aquifers (discontinuous units, coarse sediments, fine sediments, poorly sorted sediments). A network of ports into the side of the tank can be installed to allow for differential pressure transducers (1 PSI sensitivity) that can monitor changes in the horizontal and vertical gradients within specific units of interest, or their interfaces, as a result of biostimulation. Multileveled electrodes spaced throughout the tank can monitor the progression of tracers injected at various stages of the experiment. It is also recommended that detailed chemical analysis and microscopy be conducted of the attached biomass and EPS to verify their respective roles in the clogging process. This design could test the effects of nutrient pulsing or continuous feed on the timing and location where the bioactive zone develops.

Appendices

Appendix 1: VelprobePE Code 193

Appendix 2: Pinder Algorithm for Three-Point Estimators……239

Appendix 3: Woodstock PVP CR1000 Code……246

Appendix 4: High Resolution PVP CR1000 Code……250

Appendix 5: Differential Pressure Transducer CR1000 Code……254

Appendix 6: Base to Height Calculation for Three-Point Estimators……257

Appendix 7: Woodstock PVP Location and Coordinates……259

Appendix 8: Woodstock Well Coordinates (From Critchley 2010)……261

Appendix 9: Velocities for PVPs 1 and 2 with 2009 Tracer Testing……268

Appendix 10: Hydraulic Conductivity from PVPs 1 and 2 Core……270

Appendix 11: 2010 Site Characterization Testing of PVPs 3, 4, and 5……272

Appendix 12: Slug Testing Results……276

Appendix 13: Pre and Post Biostimulation PVP Data……278

Appendix 14: Pre and Post Biostimulation Flow Direction Rose Diagrams……283

Appendix 15: CLOUDPE Output Files from Biostimulation CIS Tracer Testing……287

Appendix 16: PULSEPE Results from Biostimulation CIS Tracer Testing……301

Appendix 17: Summary Table of CIS Biostimulation Tracer Testing……329

Appendix 18: Co-Authored Manuscript in Preparation Regarding Woodstock Site Characterization……334

Appendix 19: Field Core Logs from PVP 3, 4, 5, Biomass and Acetylene Block Cores……372

Appendix 20: Hydraulic Conductivity From Grain-Size Analysis of PVP 3, 4, and 5 Cores……375

Appendix 21: Grain-Size Analysis Details from PVP 3, 4, and 5 Core……377

Appendix 22: Woodstock Biostimulation Aqueous Geochemistry……404

Appendix 23: Acetate Delivery Rate Calculation for Woodstock CIS……417

Appendix 24: Zero-Order Denitrification Rate Calculation……419

Appendix 25: Relevant Acetylene Block Results……421

Appendix 26: Total Lipid Biomass Data for Woodstock……424

Appendix 27: Headspace Gas Analysis for Woodstock……429

Appendix 28: Tracer Breakthrough Curves for Column Experiments……432

Appendix 29: Transducer Calibration for Column Experiments……444

Appendix 30: Total Lipid Biomass for Column Experiments……457

Appendix 31: Aqueous Geochemistry for Column Experiments……459

Appendix 32: Total Lipid Biomass for GPR Sandbox Experiment……463

Appendix 1: VelprobePE Code

User form 1 code

```
Private Sub CommandButton1_Click()

Dim FileToOpen
Dim FileName As String
Dim WkbkName As Object

10  FileToOpen = Application.GetOpenFilename("Text Files (*.DAT), *.DAT")
   FileName = ActiveWorkbook.Path + "\" + ActiveWorkbook.NAME
   If FileToOpen = False Then Exit Sub
   If FileToOpen <> "" Then

      Msg = "Do you want to open " & FileToOpen & " ?"  ' Define message.
      Style = vbYesNo + vbDefaultButton1  ' Define buttons.
      Title = "Workbook to Open"  ' Define title.
      Response = MsgBox(Msg, Style, Title)

         If Response = vbYes Then    ' User chose Yes.
         Workbooks.Open (FileToOpen)    ' Perform some action.
         Else: GoTo 10   ' User chose No.
         End If

End If


Application.Run ("ImportFromDatalogger")
UserForm1.Hide
UserForm2.Show



End Sub


Private Sub CommandButton2_Click()
   Unload Me
End Sub
```

Module 1 code

```
Sub ImportFromDatalogger()
'
' ImportFromDatalogger Macro
' Macro recorded 1/25/2008 by Peter Schillig
'

'
   Application.ScreenUpdating = False
    Columns("A:A").Select
    Selection.TextToColumns Destination:=Range("A1"), DataType:=xlDelimited, _
       TextQualifier:=xlDoubleQuote, ConsecutiveDelimiter:=False, Tab:=True, _
       Semicolon:=False, Comma:=True, Space:=False, Other:=False, FieldInfo _
       :=Array(Array(1, 1), Array(2, 1), Array(3, 1), Array(4, 1), Array(5, 1), Array(6, 1), _
       Array(7, 1), Array(8, 1), Array(9, 1), Array(10, 1), Array(11, 1), Array(12, 1), Array(13, 1 _
       ), Array(14, 1), Array(15, 1), Array(16, 1), Array(17, 1), Array(18, 1), Array(19, 1)), _
       TrailingMinusNumbers:=True
```

```
Range("A1").Select
Range("B5:C5").Select
Range(Selection, Selection.End(xlDown)).Select
Range(Selection, Selection.End(xlDown)).Select
Selection.ClearContents
Range("B1:C1").Select
Range(Selection, Selection.End(xlDown)).Select
Selection.ClearContents
Columns("E:E").Select
Selection.Insert Shift:=xlToRight
Columns("G:G").Select
Selection.Insert Shift:=xlToRight
Columns("I:I").Select
Selection.Insert Shift:=xlToRight
Columns("K:K").Select
Selection.Insert Shift:=xlToRight
Columns("M:M").Select
Selection.Insert Shift:=xlToRight
Columns("O:O").Select
Selection.Insert Shift:=xlToRight
ActiveWindow.SmallScroll ToRight:=13
Columns("Q:Q").Select
Selection.Insert Shift:=xlToRight
Columns("S:S").Select
Selection.Insert Shift:=xlToRight
Columns("U:U").Select
Selection.Insert Shift:=xlToRight
Columns("W:W").Select
Selection.Insert Shift:=xlToRight
Columns("Y:Y").Select
Selection.Insert Shift:=xlToRight
Columns("AA:AA").Select
Selection.Insert Shift:=xlToRight
Columns("AC:AC").Select
Selection.Insert Shift:=xlToRight
Columns("AE:AE").Select
Selection.Insert Shift:=xlToRight
Columns("AG:AG").Select
Selection.Insert Shift:=xlToRight
Range("C2").Select
ActiveCell.FormulaR1C1 = "Elapsed Time (Hrs) HB1"
Range("E2").Select
ActiveCell.FormulaR1C1 = "Elapsed Time (Hrs) HB2"
Range("G2").Select
ActiveCell.FormulaR1C1 = "Elapsed Time (Hrs) HB3"
Range("I2").Select
ActiveCell.FormulaR1C1 = "Elapsed Time (Hrs) HB4"
Range("K2").Select
ActiveCell.FormulaR1C1 = "Elapsed Time (Hrs) HB5"
Range("M2").Select
ActiveCell.FormulaR1C1 = "Elapsed Time (Hrs) HB6"
Range("O2").Select
ActiveCell.FormulaR1C1 = "Elapsed Time (Hrs) HB7"
Range("Q2").Select
ActiveCell.FormulaR1C1 = "Elapsed Time (Hrs) HB8"
Range("S2").Select
```

```
    ActiveCell.FormulaR1C1 = "Elapsed Time (Hrs) HB9"
    Range("U2").Select
    ActiveCell.FormulaR1C1 = "Elapsed Time (Hrs) HB10"
    Range("W2").Select
    ActiveCell.FormulaR1C1 = "Elapsed Time (Hrs) HB11"
    Range("Y2").Select
    ActiveCell.FormulaR1C1 = "Elapsed Time (Hrs) HB12"
    Range("AA2").Select
    ActiveCell.FormulaR1C1 = "Elapsed Time (Hrs) HB13"
    Range("AC2").Select
    ActiveCell.FormulaR1C1 = "Elapsed Time (Hrs) HB14"
    Range("AE2").Select
    ActiveCell.FormulaR1C1 = "Elapsed Time (Hrs) HB15"
    Range("AG2").Select
    ActiveCell.FormulaR1C1 = "Elapsed Time (Hrs) HB16"
    Cells.Select
    Selection.Copy
    Windows("VelProbePE_2.2.2.xls").Activate
    ActiveWindow.WindowState = xlNormal
    ActiveWindow.WindowState = xlNormal
    Range("A1").Select
    ActiveSheet.Paste
    Range("A1").Select
    Range("C4").Select
    Selection.ClearContents
    ActiveWindow.WindowState = xlNormal
    ActiveWindow.WindowState = xlNormal
    ActiveWindow.WindowState = xlNormal

For Each WkbkName In Application.Workbooks()
        If WkbkName.NAME <> "VelProbePE_2.2.2.xls" Then WkbkName.Close (False)
    Next
End Sub
```

User form 2 code

```
Private Sub CommandButton1_Click()


 Dim DateLaunch, DateandTime, FDateandTime As Date
 Dim R, foundcell As Range
 Dim LastRow, LastRowNewSheet, HeaderOffset, NumRows As Integer
 Dim sheetdate, testime As Date
 Dim Graph As ChartObject
 Dim cw, rh As Long
 Dim HBLaunchTime(16) As String
 Dim TextBoxHB(16) As String

'makes userform input for HB name into variable for code
TextBoxHB(1) = TextBoxHB1Name.Text
TextBoxHB(2) = TextBoxHB2Name.Text
TextBoxHB(3) = TextBoxHB3Name.Text
TextBoxHB(4) = TextBoxHB4Name.Text
TextBoxHB(5) = TextBoxHB5Name.Text
TextBoxHB(6) = TextBoxHB6Name.Text
TextBoxHB(7) = TextBoxHB7Name.Text
```

```
TextBoxHB(8) = TextBoxHB8Name.Text
TextBoxHB(9) = TextBoxHB9Name.Text
TextBoxHB(10) = TextBoxHB10Name.Text
TextBoxHB(11) = TextBoxHB11Name.Text
TextBoxHB(12) = TextBoxHB12Name.Text
TextBoxHB(13) = TextBoxHB13Name.Text
TextBoxHB(14) = TextBoxHB14Name.Text
TextBoxHB(15) = TextBoxHB15Name.Text
TextBoxHB(16) = TextBoxHB16Name.Text

'makes userform input for HB launch time into variable for code
HBLaunchTime(1) = TextBoxHB1LaunchTime.Text
HBLaunchTime(2) = TextBoxHB2LaunchTime.Text
HBLaunchTime(3) = TextBoxHB3LaunchTime.Text
HBLaunchTime(4) = TextBoxHB4LaunchTime.Text
HBLaunchTime(5) = TextBoxHB5LaunchTime.Text
HBLaunchTime(6) = TextBoxHB6LaunchTime.Text
HBLaunchTime(7) = TextBoxHB7LaunchTime.Text
HBLaunchTime(8) = TextBoxHB8LaunchTime.Text
HBLaunchTime(9) = TextBoxHB9LaunchTime.Text
HBLaunchTime(10) = TextBoxHB10LaunchTime.Text
HBLaunchTime(11) = TextBoxHB11LaunchTime.Text
HBLaunchTime(12) = TextBoxHB12LaunchTime.Text
HBLaunchTime(13) = TextBoxHB13LaunchTime.Text
HBLaunchTime(14) = TextBoxHB14LaunchTime.Text
HBLaunchTime(15) = TextBoxHB15LaunchTime.Text
HBLaunchTime(16) = TextBoxHB16LaunchTime.Text


Application.ScreenUpdating = False

 HeaderOffset = 4
 Sheets("Sheet1").NAME = "Datalogger File"
 Range("B3").Select
 ActiveCell = "Delta Time (Hrs)"
 LastRow = Sheets("Datalogger File").Range("A10").End(xlDown).Row 'cell A10 is an arbitrary cell expected to
contain data
 DateLaunch = DateTextBox.Text
 On Error Resume Next

'Loop calculates elapsed time and makes separate worksheets for 16 HBs
For i = 1 To 16

 Sheets("Datalogger File").Activate
 DateandTime = DateLaunch & "  " & HBLaunchTime(i)
 FDateandTime = Format(DateandTime, "ddddd  hh:mm:ss AMPM")
 NumRows = LastRow - HeaderOffset
 ActiveSheet.Range("B4:B" & LastRow).Clear

 'looping through rows to find first time larger than launch time
   For n = 1 To NumRows
   If ActiveSheet.Cells(n + 4, 1).Value > FDateandTime Then
      ActiveSheet.Cells(n + 4, 2).Value = (ActiveSheet.Cells(n + 4, 1).Value - FDateandTime) * 24
   End If
   Next
```

```
'copying elapsed time and pasting it into the respective half bridge elapsed time column
    Range("B3").End(xlDown).End(xlDown).Select
    Range(Selection, Selection.End(xlUp)).Copy
    Range("B1").End(xlDown).End(xlDown).Offset(0, 2 * i - 1).Select
    ActiveCell.PasteSpecial

'pasting elapsed time and electrical resitivity measurments into a new spreadsheet with the half bridge name.
Elelctrical resitivity is converted to electrical conductivity
    Range(ActiveCell, ActiveCell.Offset(0, 1)).Select
    Range(Selection, Selection.End(xlDown)).Select
    Range(Selection, Selection.End(xlDown)).Copy
    Worksheets.Add(After:=Worksheets(Worksheets.Count)).NAME = TextBoxHB(i)
    ActiveCell.Offset(1, 0).Select
    ActiveSheet.Paste
    LastRowNewSheet = Range("B5").End(xlDown).Row
    Range("C2").Select
    ActiveCell = "=(B2-$B$2)*-1"
    Selection.AutoFill Destination:=Range("C2:C" & LastRowNewSheet)
    ActiveSheet.Range("C2:C" & LastRowNewSheet).Copy
    ActiveSheet.Range("B2:B" & LastRowNewSheet).PasteSpecial Paste:=xlValues, Operation:=xlNone,
SkipBlanks:=False, Transpose:=False
    ActiveSheet.Range("C2:C" & LastRowNewSheet).Clear
    ActiveSheet.Range("A1").Select
    ActiveCell = "Observed Time (Hours)"
    ActiveCell.Offset(0, 1).Select
    ActiveCell = "Observed Cond."

'graph is created for the observed data. statements identifies size and location, title, chart type, series selection, axes
formatting, plot area formatting, title formatting
    cw = Columns(1).Width
    rh = Rows(1).Height
    Set Graph = ActiveSheet.ChartObjects.Add(cw * 5, rh * 1, cw * 10, rh * 25)
    Graph.NAME = TextBoxHB(i) & " Breakthrough Curve"
    Graph.Chart.ChartType = xlXYScatter

Graph.Chart.SeriesCollection.NewSeries
 With Graph.Chart.SeriesCollection(1)
        .Values = ActiveSheet.Range("B2:B" & LastRowNewSheet)
        .XValues = ActiveSheet.Range("A2:A" & LastRowNewSheet)
        .NAME = "Observed"
        .MarkerSize = 2
        .MarkerStyle = xlMarkerStyleCircle
End With

'    Graph.Chart.SeriesCollection.Add Source:=ActiveSheet.Range("B2:B" & LastRowNewSheet)

    With Graph.Chart.Axes(xlCategory)
        .HasTitle = True
        .AxisTitle.Caption = "Elapsed Time (Hours)"
        .CategoryNames = Range("A2:A" & LastRowNewSheet)
    End With

    With Graph.Chart.Axes(xlValue)
        .HasTitle = True
    With .AxisTitle
        .Caption = "Electrical Conductivity (mV) "
```

```
    End With
    End With

    Graph.Chart.Axes(xlValue).HasMajorGridlines = False
    Graph.Chart.Axes(xlCategory).HasMajorGridlines = False
    Graph.Chart.ChartArea.Interior.Color = RGB(255, 255, 255)
    Graph.Chart.PlotArea.Interior.Color = RGB(255, 255, 255)
    Graph.RoundedCorners = True
    With Graph.Chart.ChartTitle
        .Caption = TextBoxHB(i) & " Breakthrough Curve"
        .Font.Size = 14
        .Font.Bold = True
    End With

If TextBoxHB(i) = Null Then Sheets(TextBoxHB(i)).delete
    'If TextBoxHB(i) = Null Then Worksheet.Name = TextBoxHB(i).delete
Next

'Deleting Excess Worksheets and activating screen update
For Each ws In ThisWorkbook.Worksheets
    If Application.WorksheetFunction.CountA(ws.Cells) = 0 Then
    Application.DisplayAlerts = False
    ws.delete
    Application.DisplayAlerts = True
End If
Next

Application.ScreenUpdating = True

' maximize window, set active sheet to lowest HB, launch userform 3, and hide userform 2

ActiveWindow.WindowState = xlMaximized
Worksheets(2).Activate
UserForm2.Hide
UserForm3.Show

End Sub
```

User form 3 code

```
Private Sub UserForm_Initialize()

Applymsgbox = MsgBox("Please Remove Extra Worksheets With No Data Before Selecting Run VelprobePE",
vbInformation, "Program Request")

End Sub

Private Sub BaselineAdjYes_Click()

Dim endrows As Integer

ActiveSheet.Range("E2").Select
If Application.CountA(Selection) = 0 Then
    endrows = ActiveSheet.Range("A2").End(xlDown).Row
    ActiveSheet.Range("A2:B" & endrows).Copy
    ActiveSheet.Range("E2").Select
```

```
    ActiveCell.PasteSpecial
End If


If UserForm3.BaselineAdjYes.Value = True Then
    BulkVertShift.Enabled = True
    RemoveInitialData.Enabled = True
    RemoveFinalData.Enabled = True
    LinearDetrend.Enabled = True
End If



End Sub

Private Sub BulkVertShift_Click()

Dim White As String
White = "&H80000005"

If UserForm3.BulkVertShift.Value = True Then
    TextBoxBulkVertShift.BackColor = White
    TextBoxBulkVertShift.Enabled = True
End If


End Sub



Private Sub RemoveInitialData_Click()

Dim White As String
White = "&H80000005"

If UserForm3.RemoveInitialData.Value = True Then
    TextBoxInitialData.BackColor = White
    TextBoxInitialData.Enabled = True
End If
End Sub


Private Sub RemoveFinalData_Click()

Dim White As String
White = "&H80000005"

If UserForm3.RemoveFinalData.Value = True Then
    TextBoxFinalData.BackColor = White
    TextBoxFinalData.Enabled = True
End If


End Sub

Private Sub LinearDetrend_Click()
```

```
Dim White As String
White = "&H80000005"

If UserForm3.LinearDetrend.Value = True Then
   TextBoxX1.BackColor = White
   TextBoxX1.Enabled = True
   TextBoxX2.BackColor = White
   TextBoxX2.Enabled = True
   TextBoxY1.BackColor = White
   TextBoxY1.Enabled = True
   TextBoxY2.BackColor = White
   TextBoxY2.Enabled = True
End If

End Sub


Private Sub Apply_Click()

Dim TextBxRemoveInitial, TextBxRemoveFinal, TextBxBulkShift, TextBxX1, TextBxY1, TextBxX2, TextBxY2,
Slope, Interc As Double
Dim i, n, m, endrows  As Integer

ScreenUpdating = False
endrows = ActiveSheet.Range("A2").End(xlDown).Row


'performs bulk vertical shift by looping through the B column and making adjustments in the C column. Final values
from C are copied and pasted over B. As a final Step, the C column is deleted.

If UserForm3.BulkVertShift.Value = True Then

   Application.ScreenUpdating = False
   TextBxBulkShift = CDbl(TextBoxBulkVertShift.Text)
   For i = 2 To endrows
      ActiveSheet.Cells(i, 3).Value = (ActiveSheet.Cells(i, 2)) + TextBxBulkShift
   Next

   ActiveSheet.Range("C2:C" & endrows).Copy
   ActiveSheet.Range("B2:B" & endrows).Select
   ActiveSheet.Range("B2:B" & endrows).PasteSpecial
   ActiveSheet.Range("C2:C" & endrows).Clear

End If

'performs initial data reduction based on entered time

If UserForm3.RemoveInitialData.Value = True Then

   Application.ScreenUpdating = False
   TextBxRemoveInitial = CDbl(TextBoxInitialData.Text)
   ActiveSheet.Range("A2").Select
   For n = 2 To endrows
      If ActiveSheet.Cells(n, 1).Value < (TextBxRemoveInitial) Then
```

```
            ActiveSheet.Range(ActiveCell, ActiveCell.Offset(0, 1)).Select
            Selection.delete
        End If
    Next
End If

'performs final data reduction

If UserForm3.RemoveFinalData.Value = True Then

    Application.ScreenUpdating = False
    TextBxRemoveFinal = CDbl(TextBoxFinalData.Text)
    For m = 2 To endrows
        If ActiveSheet.Cells(m, 1).Value > (TextBxRemoveFinal) Then
            ActiveSheet.Cells(m, 1).Select
            ActiveSheet.Range(ActiveCell, ActiveCell.Offset(0, 1)).Select
            Selection.Clear
        End If
    Next
    ActiveSheet.Range("A2").Select
End If

' performs linear detrend

If UserForm3.LinearDetrend.Value = True Then

    Application.ScreenUpdating = False
    TextBxX1 = TextBoxX1.Text
    TextBxY1 = TextBoxY1.Text
    TextBxX2 = TextBoxX2.Text
    TextBxY2 = TextBoxY2.Text


    Slope = (TextBxY2 - TextBxY1) / (TextBxX2 - TextBxX1)
    Interc = TextBxY2 - Slope * TextBxX2

    For n = 2 To endrows
    If ActiveSheet.Cells(n, 1).Value > CDbl(TextBxX1) Then
            ActiveSheet.Cells(n, 3).Value = Slope * (ActiveSheet.Cells(n, 1)) + Interc
            ActiveSheet.Cells(n, 4).Value = ActiveSheet.Cells(n, 2).Value - ActiveSheet.Cells(n, 3).Value
    End If

    If Str(ActiveSheet.Cells(n, 1).Value) = " " Then n = endrows
    Next

    ActiveSheet.Range("D2:D" & endrows).Copy
    ActiveSheet.Range("B2:B" & endrows).Select
    ActiveSheet.Range("B2:B" & endrows).PasteSpecial
    ActiveSheet.Range("C2:D" & endrows).Clear


End If

ScreenUpdating = True

End Sub
```

```
Private Sub BaselineAdjNo_Click()

Dim Gray As String
Gray = "&H8000000B"


If UserForm3.BaselineAdjNo.Value = True Then

    BulkVertShift.Value = False
    RemoveInitialData.Value = False
    RemoveFinalData.Value = False
    LinearDetrend.Value = False
    BulkVertShift.Enabled = False
    RemoveInitialData.Enabled = False
    RemoveFinalData.Enabled = False
    LinearDetrend.Enabled = False
    TextBoxBulkVertShift.Enabled = False
    TextBoxInitialData.Enabled = False
    TextBoxFinalData.Enabled = False
    TextBoxX1.Enabled = False
    TextBoxY1.Enabled = False
    TextBoxX2.Enabled = False
    TextBoxY2.Enabled = False
    TextBoxBulkVertShift.BackColor = Gray
    TextBoxInitialData.BackColor = Gray
    TextBoxFinalData.BackColor = Gray
    TextBoxX1.BackColor = Gray
    TextBoxY1.BackColor = Gray
    TextBoxX2.BackColor = Gray
    TextBoxY2.BackColor = Gray

End If


End Sub



Private Sub Undo_Click()

Dim endrows As Integer

endrows = ActiveSheet.Range("E2").End(xlDown).Row
ActiveSheet.Range("E2:F" & endrows).Copy
ActiveSheet.Range("A2").Select
ActiveCell.PasteSpecial

ActiveSheet.ChartObjects(ActiveSheet.NAME & " Breakthrough Curve").Activate
ActiveChart.SeriesCollection(1).XValues = ActiveSheet.Range("A2:A" & endrows)
ActiveChart.SeriesCollection(1).Values = ActiveSheet.Range("B2:B" & endrows)
End Sub


Private Sub PreviousSheet_Click()

On Error Resume Next
```

```
ActiveSheet.Previous.Select
UserForm3.BaselineAdjNo.Value = True
TextBoxBulkVertShift.Value = ""
TextBoxInitialData.Value = ""
TextBox.FinalData.Value = ""
TextBoxX1.Value = ""
TextBoxX2.Value = ""
TextBoxY1.Value = ""
TextBoxY2.Value = ""

End Sub

Private Sub NextSheet_Click()

On Error Resume Next
ActiveSheet.Next.Select
UserForm3.BaselineAdjNo.Value = True
TextBoxBulkVertShift.Value = ""
TextBoxInitialData.Value = ""
TextBoxFinalData.Value = ""
TextBoxX1.Value = ""
TextBoxX2.Value = ""
TextBoxY1.Value = ""
TextBoxY2.Value = ""


End Sub

Private Sub RunVELPORBEPE_Click()

UserForm4.Show
UserForm3.Hide

End Sub
```

Public Variables

```
Public Z(10) As Double
Public R(10) As Double
Public X(10) As Double
Public Data(20000, 10) As Double
Public Resi(20000) As Double
Public U(20000) As Double
Public W(20000) As Double
Public YCALC(20000) As Double
Public Phix(10) As Double
Public NP As Integer
Public NP1 As Integer
Public BSW As Integer
Public Kount As Integer
Public NOBS As Integer
Public manip As String
```

User form 4 code

```
Private Sub Run_Click()

Dim NSIM As Integer
Dim NumSheets As Integer
Dim MaxCnt As Integer
Dim ILO As Integer
Dim IHI As Integer
Dim Scal As Double
Dim ERRMIN As Double
Dim ERPCNT As Double
Dim C(10) As Double
Dim E(10) As Double
Dim P(10, 10) As Double
Dim F(32, 10) As Double
Dim Dstar As Double
Dim Dist As Double
Dim RSS As Double
Dim OLDNOBS As Double
'Dim Phix(10) As Double
'Dim X(10) As Double
'Dim Data(20000, 10) As Double
'Dim Resi(20000) As Double
'Dim U(20000) As Double
'Dim W(20000) As Double
'Dim YCALC(20000) As Double
'Dim R(10) As Double
'Dim NP As Integer
'Dim NP1 As Integer
'Dim NOBS As Integer
'Dim bsw As Integer
'Dim Kount As Integer
'dimensions that are commented out are available in the "Public_Variables" Module for use as an array transfer to a public function

NP = 6
NP1 = NP + 1
manip = "" 'manip is a debugging variable used to denote which manipulation is going on (reflection, expansion, contraction)
NSIM = 1
MaxCnt = 500
ER = 1
ERRMIN = 0.0001
Dstar = CDbl(DiffusionCoeff.Text) * 3600
X(1) = CDbl(ApparentVel.Text) / 24
X(2) = CDbl(Disper.Text)
X(3) = CDbl(PulseWidth.Text)
X(4) = CDbl(Retardation.Text)
X(5) = CDbl(InjectionConc.Text)
X(6) = 0 'first order decay is assumed to be 0
    'X(6) = CDbl(FirstOrderDecay.Text) * 3600 'Version 2.2 code where the tracer first order decay constant was a parameter

If X(6) > 0 Then X(6) = Log(X(6))
```

```
For i = 1 To 10
   Phix(i) = 0
Next

' fix input sets values negative to allow code to hold negative parameter constant
If GWV.Value = True Then Phix(1) = 1
If Dis.Value = True Then Phix(2) = 1
If PW.Value = True Then Phix(3) = 1
If RF.Value = True Then Phix(4) = 1
If IC.Value = True Then Phix(5) = 1
   'If FODC.Value = True Then Phix(6) = 1 'Version 2.2 code where the tracer first order decay constant was a
parameter
If X(6) = 0 Then Phix(6) = 1 'if a zero is entered for the first order decay constant, then it is automatically fixed

'count total sheets to process and set up loop to go through them all with PULSEPE code

NumSheets = Worksheets.Count
For q = 2 To NumSheets
   Worksheets(q).Activate

Dist = CDbl(InputBox("Enter Distance from Injection Point to Detector (cm)", "Distance Input Required"))

   NOBS = ActiveSheet.Range("A2").End(xlDown).Row - 1
   OLDNOBS = ActiveSheet.Range("E2").End(xlDown).Row
   'clearing data from Columns E&F from "undo" function in userform 3
   ActiveSheet.Range("E2:F" & OLDNOBS).Clear

   'clearing data array to remove previous data

   For i = 1 To 20000
      For j = 1 To NP1
         Data(i, j) = 0#
      Next
   Next

   For i = 1 To NOBS
         Data(i, 1) = ActiveSheet.Cells(i + 1, 1)
         Data(i, 2) = ActiveSheet.Cells(i + 1, 2)
   Next

'starting error function value
 E(1) = ErrorFun(X, Dstar, Data, NOBS, Kount, Resi, U, W, YCALC, Dist, NP, BSW, manip)

   'INITIALIZE THE SIMPLEX
   Kount = 0

   For j = 1 To NP
      P(1, j) = X(j)
   Next

   For i = 2 To NP1

      For j = 1 To NP
         P(i, j) = X(j)
      Next
```

```
    P(i, i - 1) = 1.1 * X(i - 1)
       If (Phix(i - 1) = 1) Then P(i, i - 1) = X(i - 1)
       If (Abs(X(i - 1)) < 0.000000000001) Then P(i, i - 1) = 0.0001
       If (X(6) = 0#) Then P(7, 6) = 0#
       Next

'Find PLOW Ad PHIGH / BEST = PLOW / WORST = PHIGH
31   ILO = 1
     IHI = 1

      For i = 1 To NP1

          For j = 1 To NP
             X(j) = P(i, j)
          Next

         E(i) = ErrorFun(X, Dstar, Data, NOBS, Kount, Resi, U, W, YCALC, Dist, NP, BSW, manip)
         If (E(i) < E(ILO)) Then ILO = i
         If (E(i) > E(IHI)) Then IHI = i
      Next

'FIND PNHI THE NEXT HIGHEST NEXT=PNHI

41    NHI = ILO
     For i = 1 To NP1
         If (E(i) >= E(NHI) And i <> IHI) Then NHI = i
43    Next

'COMPUTE THE CENTROID
     For j = 1 To NP
         C(j) = -P(IHI, j)
         For i = 1 To NP1
             C(j) = C(j) + P(i, j)
44         Next
         C(j) = C(j) / NP
46    Next

i = 1

51 GoTo 52

52 'STOPPING CRITERION
     If (Kount > MaxCnt) Then
       UserForm4.Hide
       UserForm5.Show
          If MsgBox("EXECUTION TERMINATED; MAXCOUNT EXCEEDED. Please Enter Correct Distance
from Source and Retry Manually", vbCritical) = vbOK Then
             Exit Sub
     End If
     End If

ERPCNT = Abs(E(ILO) - E(IHI)) / E(ILO) * 100

If (Abs(E(ILO) - E(IHI)) / E(ILO) < ERRMIN) Then GoTo 200
If Kount = 0 Then GoTo 61
```

```
If (ER < 0.000001) Then GoTo 200

GoTo 61

'REFLECTION
61    For j = 1 To NP
          R(j) = 1.9985 * C(j) - 0.9985 * P(IHI, j)
62    Next
      manip = "REFLECT"
      ER = ErrorFun(R, Dstar, Data, NOBS, Kount, Resi, U, W, YCALC, Dist, NP, BSW, manip)

'REFLECTION AGAIN IF SUCCESSFUL
      If (ER < E(ILO)) Then GoTo 91
      If (ER >= E(IHI)) Then GoTo 122

'REPLACE WORST VERTEX WITH NEW ONE
79    For j = 1 To NP
          P(IHI, j) = R(j)
80    Next

      NSIM = NSIM + 1
      E(IHI) = ER
      If (ER > E(NHI)) Then GoTo 51
      IHI = NHI
      GoTo 41

'EXPAND THE SIMPLEX
91    ILO = IHI
      IHI = NHI
      For j = 1 To NP
          X(j) = 1.95 * R(j) - 0.95 * C(j)
93    Next
      manip = "EXPAND"
      EX = ErrorFun(X, Dstar, Data, NOBS, Kount, Resi, U, W, YCALC, Dist, NP, BSW, manip)
      If (EX < ER) Then GoTo 104

'R IS BETTER THAN X
      For j = 1 To NP
          P(ILO, j) = R(j)
99    Next

      NSIM = NSIM + 1
      E(ILO) = ER
      GoTo 110

'X IS BETTER THAN R
104   For j = 1 To NP
          P(ILO, j) = X(j)
105   Next

      'IF(IDB > 0) then EX,(X(j),j=1,NP)
      NSIM = NSIM + 1
      E(ILO) = EX
110   GoTo 41

i = 1
```

```
'CONTRACT THE SIMPLEX
122   For j = 1 To NP
          R(j) = 0.5015 * C(j) + 0.4985 * P(IHI, j)
123   Next
      manip = "CONTRACT"
      ER = ErrorFun(R, Dstar, Data, NOBS, Kount, Resi, U, W, YCALC, Dist, NP, BSW, manip)
      If (ER < E(ILO)) Then GoTo 91
      If (ER < E(IHI)) Then GoTo 79

'Scale
Scal = CDbl(InputBox("Enter Scale to Continue: <0 Expands, >0 Shrinks, =0 Stops", "Scale Factor Required"))
If (Scal = 0#) Then GoTo 200
137   For i = 1 To NP1
          For j = 1 To NP
              P(i, j) = P(i, j) + Scal * (P(ILO, j) - P(i, j))
138       Next
139   Next
      GoTo 31

'WRITING THE OUTPUT

200

ActiveSheet.Range("C1") = "Calculated Cond"
ActiveSheet.Range("D1") = "Residuals"

For i = 1 To NOBS
    ActiveSheet.Cells(i + 1, 3) = YCALC(i)
    ActiveSheet.Cells(i + 1, 4) = Resi(i)
Next

ActiveSheet.Range("A1:D" & NOBS + 1).Select 'Follwowing With statement formats A through D columns for
headers and data alignment
With Selection
    .ColumnWidth = 10
    .NumberFormat = "General"
    .HorizontalAlignment = xlCenter
    .VerticalAlignment = xlCenter
    .WrapText = True
End With

'places text in spreadsheet to identify output parameters
ActiveSheet.Range("G28") = "OPTIMIZED PARAMETER ESTIMATES"
ActiveSheet.Range("G30") = "VELOCITY(cm/d)"
ActiveSheet.Range("G31") = "DISPERSIVITY (cm)"
ActiveSheet.Range("G32") = "PULSE WIDTH (cm)"
ActiveSheet.Range("G33") = "RF"
ActiveSheet.Range("G34") = "Co (mV)"
    'ActiveSheet.Range("G35") = "FODC ( /sec)" 'Version 2.2 code where the tracer first order decay constant was a
parameter
ActiveSheet.Range("G37") = "RESDIUAL SUM OF SQUARES ="
ActiveSheet.Range("G39") = "INITIAL GUESSES AND INPUT OF PARAMETERS"
ActiveSheet.Range("G41") = "VELOCITY(cm/d)"
ActiveSheet.Range("G42") = "DISPERSIVITY (cm)"
ActiveSheet.Range("G43") = "PULSE WIDTH (cm)"
```

```
ActiveSheet.Range("G44") = "RF"
ActiveSheet.Range("G45") = "Co (mV)"
   'ActiveSheet.Range("G46") = "FODC ( /sec)" 'Version 2.2 code where the tracer first order decay constant was a
parameter
   'ActiveSheet.Range("G47") = "DISTANCE FROM SOURCE (cm)" 'Version 2.2 code where the tracer first order
decay constant was a parameter
   'ActiveSheet.Range("G48") = "DIFFUSION COEFF (cm^2/sec)" 'Version 2.2 code where the tracer first order
decay constant was a parameter
ActiveSheet.Range("G46") = "DISTANCE FROM SOURCE (cm)"
ActiveSheet.Range("G47") = "DIFFUSION COEFF (cm^2/sec)"
ActiveSheet.Range("M40") = "FIX"
ActiveSheet.Range("G1").ColumnWidth = 10 ' allows all text to be seen


ActiveSheet.ChartObjects(ActiveSheet.NAME & " Breakthrough Curve").Activate
For Each Series In ActiveChart.SeriesCollection
       Series.delete
   Next Series 'deletes all series to prevent more than two series from being added to the same chart

ActiveChart.SeriesCollection.NewSeries 'replots observed data
 With ActiveChart.SeriesCollection(1)
       .Values = ActiveSheet.Range("B2:B" & NOBS + 1)
       .XValues = ActiveSheet.Range("A2:A" & NOBS + 1)
       .NAME = "Observed"
       .MarkerSize = 2
       .MarkerStyle = xlMarkerStyleCircle
   End With

ActiveChart.SeriesCollection.NewSeries 'plots calculated data
 With ActiveChart.SeriesCollection(2)
       .Values = ActiveSheet.Range("C2:C" & NOBS + 1)
       .XValues = ActiveSheet.Range("A2:A" & NOBS + 1)
       .NAME = "Calculated"
       .MarkerSize = 2
       .MarkerStyle = xlMarkerStyleCircle
   End With
'places values for optimized parameter estimates
ActiveSheet.Range("J30") = X(1) * 24
ActiveSheet.Range("J31") = X(2)
ActiveSheet.Range("J32") = X(3)
ActiveSheet.Range("J33") = X(4)
ActiveSheet.Range("J34") = X(5)
   'ActiveSheet.Range("J35") = X(6) / 3600 'Version 2.2 code where the tracer first order decay constant was a
parameter
ActiveSheet.Range("K37") = E(ILO)
' places values for initial guesses
ActiveSheet.Range("J41") = CDbl(ApparentVel.Text)
ActiveSheet.Range("J42") = CDbl(Disper.Text)
ActiveSheet.Range("J43") = CDbl(PulseWidth.Text)
ActiveSheet.Range("J44") = CDbl(Retardation.Text)
ActiveSheet.Range("J45") = CDbl(InjectionConc.Text)
   'ActiveSheet.Range("J46") = CDbl(FirstOrderDecay.Text) 'Version 2.2 code where the tracer first order decay
constant was a parameter
   'ActiveSheet.Range("J47") = Dist
   'ActiveSheet.Range("J48") = CDbl(DiffusionCoeff.Text)
ActiveSheet.Range("J46") = Dist
```

```
ActiveSheet.Range("J47") = CDbl(DiffusionCoeff.Text)

'denoting parameters fixed at input
If GWV.Value = True Then ActiveSheet.Range("M41") = "Y"
If Dis.Value = True Then ActiveSheet.Range("M42") = "Y"
If PW.Value = True Then ActiveSheet.Range("M43") = "Y"
If RF.Value = True Then ActiveSheet.Range("M44") = "Y"
If IC.Value = True Then ActiveSheet.Range("M45") = "Y"
   'If FODC.Value = True Then ActiveSheet.Range("M46") = "Y"'Version 2.2 code where the tracer first order
decay constant was a parameter
If GWV.Value = False Then ActiveSheet.Range("M41") = " "
If Dis.Value = False Then ActiveSheet.Range("M42") = " "
If PW.Value = False Then ActiveSheet.Range("M43") = " "
If RF.Value = False Then ActiveSheet.Range("M44") = " "
If IC.Value = False Then ActiveSheet.Range("M45") = " "
   'If FODC.Value = False Then ActiveSheet.Range("M46") = " " 'Version 2.2 code where the tracer first order
decay constant was a parameter
   'ActiveSheet.Range("M47:M48") = "Y" 'distance and diffusion coeff never varied 'Version 2.2 code where the
tracer first order decay constant was a parameter
ActiveSheet.Range("M46:M47") = "Y" 'distance and diffusion coeff never varied

'code for confidence int
Confit = CONFINT(X, Dstar, Data, NOBS, Kount, Resi, U, W, YCALC, Dist, NP, BSW, Phix, R, C)

Next

UserForm5.Show
UserForm4.Hide

End Sub

Public Function ErrorFun(X, Dstar As Double, Data, NOBS As Integer, Kount As Integer, Resi, U, W, YCALC,
Dist As Double, NP As Integer, BSW As Integer, manip As String) As Double

  'COMPUTES THE ERROR FUNCTION FOR THE DATA SET
   'SMALLER VALUE IS BETTER

Dim SMRESI As Double
Dim u1 As Double
Dim u2 As Double
     u1 = 0#
     u2 = 0#
     ErrorFun = 0#
     SMRESI = 0#

If Bisquare.Value = True Then BSW = 1
If Relative.Value = True Then BSW = 2
If None.Value = True Then BSW = 0

'Sometimes negative values are predicted by the optimizer that are not real and will cause VBA run time errors.
'The following function simply converts them to positive values prior to evaluating the error function
 For j = 1 To NP - 1
      If X(j) < 0 Then X(j) = -X(j)
 Next

If (X(6) <> 0#) Then X(6) = Exp(X(6))
```

```
For i = 1 To 20000
   Resi(i) = 0#
   U(i) = 0#
   W(i) = 0#
10 Next

For i = 1 To NOBS

'CHANGE THE NEXT STATEMENT TO CHANGE THE FUNCTION BEING FIT

    SOURC = Exp(-X(6) * Data(i, 1))
    DCOEF = (X(1) * X(2) + Dstar)

    If (Data(i, 1) <= 0#) Then
        ERFCU1 = 0#
        GoTo 20
    Else
        u1 = (Dist - X(3) / (2 * X(4)) - X(1) * Data(i, 1) / X(4)) / (2 * (DCOEF * Data(i, 1) / X(4)) ^ 0.5)
        ERFCU1 = ERFC(u1)
    End If

20   If (Data(i, 1) <= X(3) / X(1)) Then
        ERFCU2 = 0#
        GoTo 30
     Else
        u2 = (Dist + X(3) / (2 * X(4)) - X(1) * Data(i, 1) / X(4)) / (2 * (DCOEF * (Data(i, 1) - X(3) / X(1)) / X(4)) ^
0.5)
        ERFCU2 = ERFC(u2)
    End If

30   GoTo 40

40   YCALC(i) = 0.5 * X(5) * SOURC * (ERFCU1 - ERFCU2)
    Resi(i) = Data(i, 2) - YCALC(i)
    SMRESI = SMRESI + Abs(Resi(i))
60   Next

    If (BSW = 1) Then
        C = 6# * SMRESI / CDbl(NOBS)
        For i = 1 To NOBS
            U(i) = Resi(i) / C
            W(i) = (1 - U(i) * U(i)) ^ 2
            If (U(i) > 1#) Then W(i) = 0#
            ErrorFun = ErrorFun + W(i) * Resi(i) * Resi(i)
70       Next
    End If

    If (BSW = 2) Then
        For i = 1 To NOBS
            If (Data(i, 2) = 0#) Then
                W(i) = 0#
            Else
                W(i) = 1# / (Data(i, 2) ^ 2#)
            End If
            ErrorFun = ErrorFun + W(i) * Resi(i) * Resi(i)
```

```
75        Next
      End If

      If (BSW = 0) Then
        For i = 1 To NOBS
            ErrorFun = ErrorFun + Resi(i) * Resi(i)
80      Next
      End If

      Kount = Kount + 1

      If (X(6) > 0#) Then X(6) = Log(X(6))


'fills calculated data and residuals into spreasheet for debugging purposes. X(1) through X(6) units are converted to
those used in PULSEPE for comparison

      'ActiveSheet.Cells(Kount, 17) = X(1) * 24 / 8640000
      'ActiveSheet.Cells(Kount, 18) = X(2) / 100
      'ActiveSheet.Cells(Kount, 19) = X(3) / 100
      'ActiveSheet.Cells(Kount, 20) = X(4)
      'ActiveSheet.Cells(Kount, 21) = X(5)
      'ActiveSheet.Cells(Kount, 22) = X(6)
      'ActiveSheet.Cells(Kount, 23) = manip
      'ActiveSheet.Cells(Kount, 24) = ErrorFun



End Function


Public Function ERFC(arg As Double)


'COMPLIMENTARY ERROR FUNCTION SUBROUTINE REAL*8 FUNCTION ERFC(ARG)
'COMPUTES THE COMPLIMENTARY ERROR FUNCTIOn FOR AN ARGUMENT
'IMPLICIT REAL*8 (A-H,L,M,O-Z)
'PARAMETER (P=0.3275911, A1=0.254829592, A2=-0.284496736,
'    1          A3=1.421413741, A4=-1.453152027, A5=1.061405429)
'TU = 1 / (1 + p * Abs(ARG))

'     ERFC=(A1*TU+A2*TU**2+A3*TU**3+A4*TU**4+A5*TU**5)
'    1      *EXP(-(ARG**2))
'     IF(ARG .LT. 0) ERFC=2-ERFC

'     RETURN
'     END


Dim P As Double
Dim A1 As Double
Dim A2 As Double
Dim A3 As Double
Dim A4 As Double
Dim A5 As Double
Dim TU As Double
```

```
P = 0.3275911
A1 = 0.254829592
A2 = -0.284496736
A3 = 1.421413741
A4 = -1.453152027
A5 = 1.061405429


TU = 1 / (1 + P * Abs(arg))

    ERFC = (A1 * TU + A2 * TU ^ 2 + A3 * TU ^ 3 + A4 * TU ^ 4 + A5 * TU ^ 5) * Exp(-(arg ^ 2))

    If (arg < 0) Then ERFC = 2 - ERFC


'********** FUNCTION DERFC(ARG)
'  ROUTINE FOR ERFC (ARG) BY SERIES EXPANSION
'  DOUBLE PRECISION VERSION


 '    Dim IL As Integer
 '    Dim LJL As Integer
 '    Dim JLJ As Integer
 '    Dim XOX As Double
 '    Dim SUMXOX As Double
 '    Dim Fact As Double
 '    Dim UOX As Double
 '    Dim US As Double
 '    Dim ZOZ As Double
 '    Dim TXOX As Double
 '    Dim OLDFACT As Double


  '    Pi = 3.14159265358
  '    SUMXOX = 1#
  '    XOX = Abs(arg)
  '    If (XOX > 3.4) Then GoTo 5160

'  THIS SERIES EXPANSION IS FOR ARG <= 3.4

   '    Fact = 1#
    '   IL = 1
     '  UOX = XOX * XOX
     '  US = UOX
'5085  Fact = Fact * IL
'      ZOZ = -1#
'      If ((IL / 2) * 2 = IL) Then ZOZ = 1#
'      TXOX = UOX / ((2# * IL + 1#) * Fact)
'      SUMXOX = SUMXOX + ZOZ * TXOX
'      UOX = UOX * US
'      IL = IL + 1


'     STOP THIE SUMMATION WHEN THE CURRENT TERM
'     IS LESS THAN 1E-20
```

```
'    If (TXOX > 1E-20) Then GoTo 5085
'    ERFC = 1# - 2# * XOX / (Pi) ^ 0.5 * SUMXOX
'    If (arg < 0#) Then ERFC = 2# - ERFC
'    GoTo 5430
'5160  If (XOX > 14#) Then GoTo 5410

'   THIS SERIES EXPANSION IS FOR ARG>3.4

 '    UOX = 2# * XOX * XOX
 '    LJL = 1
 '    JLJ = 1
 '    Fact = 1#
'5300  OLDFAC = Fact
'     Fact = Fact / UOX * JLJ

'  STOP THE SUMMATION WHEN THE CURRENT TERM BECOMES LARGER THAN
'  THE PREVIOUS TERM

'     If (Fact > OLDFAC) Then GoTo 5333
'     ZOZ = -1#
'     If ((LJL / 2) * 2 = LJL) Then ZOZ = 1#
'     TXOX = ZOZ * Fact
'     SUMXOX = SUMXOX + TXOX
'     LJL = LJL + 1
'     JLJ = JLJ + 2
'5333  ERFC = Exp(-XOX * XOX) / (Pi) ^ 0.5 / XOX * SUMXOX
'     GoTo 5420
'5410  ERFC = 0#
'5420  If (arg < 0#) Then ERFC = 2# - ERFC
5430 End Function

Public Function CONFINT(X, Dstar As Double, Data, NOBS As Integer, Kount As Integer, Resi, U, W, YCALC,
Dist As Double, NP As Integer, BSW As Integer, Phix, R, C) As Double

Dim NME(6) As String

NME(1) = "VELOCITY(cm/d)"
NME(2) = "DISPERSIVITY(cm)"
NME(3) = "PULSE WIDTH (cm)"
NME(4) = "RF"
NME(5) = "Co(mV)"
NME(6) = "FODC(1/sec)"


ActiveSheet.Range("G50:K60").Clear

 'DEFINING NPP TO BE THE NUMBER OF PARAMETERS BEING FIT
    NPP = 0
    For i = 1 To NP
        If Phix(i) = 0 Then NPP = NPP + 1
10   Next
    If NPP = 0 Then GoTo 300

  'DETERMINING THE CRITICAL RESIDUAL SUM OF SQUARES
```

```
  'WHICH DEFINES THE UPPER AND LOWER CONFIDENCE INTERVAL

     ER = ErrorFun(X, Dstar, Data, NOBS, Kount, Resi, U, W, YCALC, Dist, NP, BSW, manip)
     'FESTI = FESTIM(NOBS, NPP, IDB) alternative below
     ActiveSheet.Range("G51") = NOBS 'allows NOBS to be used in Excel's FINV function
     ActiveSheet.Range("G50") = "=FInv(0.05, G51-6, 6)" '0.05 = 95% confidence interval, G51 = NOBS, 6 = NP,
degrees of freedom = NOBS-NP, NP
     FESTI = ActiveSheet.Range("G50").Value
     'Fnpp = float(NPP)
     'FNOBS = float(NOBS)
     'RSSCRIT = ER * (1 + Fnpp / (FNOBS - Fnpp) * FESTI)
      RSSCRIT = ER * (1 + NPP / (NOBS - NPP) * FESTI)

'    LOOPING THROUGH THE PARAMETERS TO DETERMINE CONFIDENCE INTERVALS

For i = 1 To NP
   For j = 1 To NP
     R(j) = X(j)
     C(j) = X(j)
90  Next

    If Phix(i) = 1 Then GoTo 199

'   LOOKING FOR THE UPPER LIMIT
        NCOUNT = 1
100

    'IF(FLOAT(I) .EQ. 6. .AND. X(I) .LT. 0.) THEN
     If i = 6 And X(i) < 0 Then
           R(i) = R(i) - 0.1 * X(i)
        Else
           R(i) = R(i) + 0.1 * X(i)
        End If
        ER = ErrorFun(R, Dstar, Data, NOBS, Kount, Resi, U, W, YCALC, Dist, NP, BSW, manip)
        If R(6) < -100 Or R(6) > 100 Then GoTo 120
        If NCOUNT > 1 Then
           If Abs((ERCHK - ER) / ER * 100) < 0.001 Then
              R(i) = -1#
              GoTo 120
           End If
        Else
           NCOUNT = 2
        End If
        ERCHK = ER
        If ER < RSSCRIT Then GoTo 100

110

      'IF(FLOAT(I) .EQ. 6. .AND. X(I) .LT. 0.) THEN
      If i = 6 And X(i) < 0 Then

         R(i) = R(i) + 0.01 * X(i)
         Else
         R(i) = R(i) - 0.01 * X(i)
      End If
```

```
   ER = ErrorFun(R, Dstar, Data, NOBS, Kount, Resi, U, W, YCALC, Dist, NP, BSW, manip)
      If ER > RSSCRIT Then GoTo 110

     'LOOKING FOR THE LOWER LIMIT
120
      'IF(FLOAT(I) .EQ. 6. .AND. X(I) .LT. 0.) THEN
       If i = 6 And X(i) < 0 Then
           C(i) = C(i) + 0.1 * X(i)
        Else
           C(i) = C(i) - 0.1 * X(i)
        End If
       'IF(C(I) .LT. 0. .AND. FLOAT(I) .NE. 6.) THEN
       If C(i) < 0 And i <> 6 Then
           C(i) = C(i) + 0.1 * X(i)
125          C(i) = C(i) - 0.01 * X(i)
           If C(i) < 0 Then
              C(i) = 0#
              GoTo 249
           End If
        End If

        ER = ErrorFun(C, Dstar, Data, NOBS, Kount, Resi, U, W, YCALC, Dist, NP, BSW, manip)
        If C(6) < -100 Or C(6) > 100 Then GoTo 249
        If ER < RSSCRIT Then GoTo 120

130
        'IF(FLOAT(I) .EQ. 6. .AND. X(I) .LT. 0.) THEN
        If i = 6 And X(i) < 0 Then
           C(i) = C(i) - 0.01 * X(i)
        Else
           C(i) = C(i) + 0.01 * X(i)
        End If

        ER = ErrorFun(C, Dstar, Data, NOBS, Kount, Resi, U, W, YCALC, Dist, NP, BSW, manip)
        If ER > RSSCRIT Then GoTo 130

249
        If i = 6 Then
           X(i) = Exp(X(i))
           If R(i) < -99 Then
              R(i) = 0#
           Else
              R(i) = Exp(R(i))
           End If
           C(i) = Exp(C(i))
        End If

259  'Writing to the output file

        ActiveSheet.Range("G50") = "95% CONFIDENCE INTERVALS FOR ESTIMATED PARAMETERS"
        ActiveSheet.Range("G51") = "Parameter"
        ActiveSheet.Range("I51") = "Low"
        ActiveSheet.Range("J51") = "Optimized"
        ActiveSheet.Range("K51") = "High"
        ActiveSheet.Range("G60") = "CRITICAL RSS VALUE ="
        ActiveSheet.Range("J60") = RSSCRIT
```

```
      If R(i) > 0 Then

         ActiveSheet.Cells(i + 52, 7) = NME(i)
         ActiveSheet.Cells(i + 52, 9) = C(i) 'lower limit
         ActiveSheet.Cells(i + 52, 10) = X(i) 'optimized
         ActiveSheet.Cells(i + 52, 11) = R(i) 'upper limit

            If i = 1 Then 'converts velocity to cm/d
               ActiveSheet.Cells(i + 52, 9) = C(i) * 24 'lower limit
               ActiveSheet.Cells(i + 52, 10) = X(i) * 24 'optimized
               ActiveSheet.Cells(i + 52, 11) = R(i) * 24 'upper limit
            End If

            If i = 6 Then ' converts FODC to /sec
               ActiveSheet.Cells(i + 52, 9) = C(i) / 3600 'lower limit
               ActiveSheet.Cells(i + 52, 10) = X(i) / 3600 'optimized
               ActiveSheet.Cells(i + 52, 11) = R(i) / 3600 'upper limit
            End If

         Else
          ActiveSheet.Range("G52") = "No Convergence"
         End If
199
200   Next

      If R(i) = 0 Then

         ActiveSheet.Cells(i + 52, 7) = ""
         ActiveSheet.Cells(i + 52, 9) = ""
         ActiveSheet.Cells(i + 52, 10) = ""
         ActiveSheet.Cells(i + 52, 11) = ""
      End If

299
300
    If X(6) > 0 Then
        X(6) = Log(X(6))
    Else
        X(6) = 0#
    End If

End Function
```

User form 5 code

```
Private Sub EnableButton_Click()

Dim White As String
Dim Grey As String

White = "&H80000005"
Grey = "&H8000000B"
```

```
If UserForm5.EnableButton.Value = True Then
   SourceDistance.BackColor = White
   SourceDistance.Enabled = True
End If

End Sub

Private Sub DisableButton_Click()


Dim White As String
Dim Grey As String

White = "&H80000005"
Grey = "&H8000000B"

If UserForm5.DisableButton.Value = True Then
   SourceDistance.BackColor = Grey
   SourceDistance.Enabled = False
End If

End Sub

Private Sub Run_Click()

Dim NSIM As Integer
Dim NumSheets As Integer
Dim MaxCnt As Integer
Dim ILO As Integer
Dim IHI As Integer
Dim Scal As Double
Dim ERRMIN As Double
Dim ERPCNT As Double
Dim C(10) As Double
Dim E(10) As Double
Dim P(10, 10) As Double
Dim F(32, 10) As Double
Dim Dstar As Double
Dim Dist As Double
Dim RSS As Double
Dim OLDNOBS As Double
'Dim Phix(10) As Double
'Dim X(10) As Double
'Dim Data(20000, 10) As Double
'Dim Resi(20000) As Double
'Dim U(20000) As Double
'Dim W(20000) As Double
'Dim YCALC(20000) As Double
'Dim R(10) As Double
'Dim NP As Integer
'Dim NP1 As Integer
'Dim NOBS As Integer
'Dim bsw As Integer
'Dim Kount As Integer
'dimensions that are commented out are available in the "Public_Variables" Module for use as an array transfer to a
public function
```

```
NP = 6
NP1 = NP + 1
manip = "" 'manip is a debugging variable used to denote which manipulation is going on (reflection, expansion, contraction)
NSIM = 1
MaxCnt = 500
ER = 1
ERRMIN = 0.0001

If SourceDistance.Enabled = True Then
   Dist = CDbl(SourceDistance.Text)
Else
      'Dist = ActiveSheet.Range("J47") 'Version 2.2 code where the tracer first order decay constant was a parameter
   Dist = ActiveSheet.Range("J46")
End If

Dstar = CDbl(DiffusionCoeff.Text) * 3600
X(1) = CDbl(ApparentVel.Text) / 24
X(2) = CDbl(Disper.Text)
X(3) = CDbl(PulseWidth.Text)
X(4) = CDbl(Retardation.Text)
X(5) = CDbl(InjectionConc.Text)
X(6) = 0 'first order decay is assumed to be 0
   'X(6) = CDbl(FirstOrderDecay.Text) * 3600 'Version 2.2 code where the tracer first order decay constant was a parameter


If X(6) > 0 Then X(6) = Log(X(6))

For i = 1 To 10
   Phix(i) = 0
Next

' fix input sets values negative to allow code to hold negative parameter constant
If GWV.Value = True Then Phix(1) = 1
If Dis.Value = True Then Phix(2) = 1
If PW.Value = True Then Phix(3) = 1
If RF.Value = True Then Phix(4) = 1
If IC.Value = True Then Phix(5) = 1
   'If FODC.Value = True Then Phix(6) = 1 'Version 2.2 code where the tracer first order decay constant was a parameter
If X(6) = 0 Then Phix(6) = 1 'if a zero is enetered for the first order decay constant, then it is automatically fixed

   NOBS = ActiveSheet.Range("A2").End(xlDown).Row - 1
   OLDNOBS = ActiveSheet.Range("E2").End(xlDown).Row
   'clearing data from Columns E&F from "undo" function in userform 3
   ActiveSheet.Range("E2:F" & OLDNOBS).Clear

   'clearing data array to remove previous data

   For i = 1 To 20000
      For j = 1 To NP1
         Data(i, j) = 0#
      Next
```

```
    Next

    For i = 1 To NOBS
          Data(i, 1) = ActiveSheet.Cells(i + 1, 1)
          Data(i, 2) = ActiveSheet.Cells(i + 1, 2)
    Next

'starting error function value
 E(1) = ErrorFun(X, Dstar, Data, NOBS, Kount, Resi, U, W, YCALC, Dist, NP, BSW, manip)

    'INITIALIZE THE SIMPLEX
    Kount = 0

    For j = 1 To NP
       P(1, j) = X(j)
    Next

    For i = 2 To NP1

       For j = 1 To NP
          P(i, j) = X(j)
       Next

    P(i, i - 1) = 1.1 * X(i - 1)
       If (Phix(i - 1) = 1) Then P(i, i - 1) = X(i - 1)
       If (Abs(X(i - 1)) < 0.000000000001) Then P(i, i - 1) = 0.0001
       If (X(6) = 0#) Then P(7, 6) = 0#
       Next

'Find PLOW Ad PHIGH / BEST = PLOW / WORST = PHIGH
31   ILO = 1
     IHI = 1

      For i = 1 To NP1

         For j = 1 To NP
            X(j) = P(i, j)
         Next

        E(i) = ErrorFun(X, Dstar, Data, NOBS, Kount, Resi, U, W, YCALC, Dist, NP, BSW, manip)
        If (E(i) < E(ILO)) Then ILO = i
        If (E(i) > E(IHI)) Then IHI = i
      Next

'FIND PNHI THE NEXT HIGHEST NEXT=PNHI

41    NHI = ILO
     For i = 1 To NP1
         If (E(i) >= E(NHI) And i <> IHI) Then NHI = i
43   Next

'COMPUTE THE CENTROID
     For j = 1 To NP
        C(j) = -P(IHI, j)
        For i = 1 To NP1
           C(j) = C(j) + P(i, j)
```

```
44          Next
          C(j) = C(j) / NP
46      Next

i = 1

51 GoTo 52

52 'STOPPING CRITERION
      If (Kount > MaxCnt) Then
           UserForm5.Show
           If MsgBox("EXECUTION TERMINATED; MAXCOUNT EXCEEDED. Please Update Parameters and
Retry", vbCritical) = vbOK Then
              Exit Sub
      End If
      End If
ERPCNT = Abs(E(ILO) - E(IHI)) / E(ILO) * 100

If (Abs(E(ILO) - E(IHI)) / E(ILO) < ERRMIN) Then GoTo 200
If Kount = 0 Then GoTo 61
If (ER < 0.000001) Then GoTo 200

GoTo 61

'REFLECTION
61    For j = 1 To NP
          R(j) = 1.9985 * C(j) - 0.9985 * P(IHI, j)
62    Next
      manip = "REFLECT"
      ER = ErrorFun(R, Dstar, Data, NOBS, Kount, Resi, U, W, YCALC, Dist, NP, BSW, manip)

'REFLECTION AGAIN IF SUCCESSFUL
      If (ER < E(ILO)) Then GoTo 91
      If (ER >= E(IHI)) Then GoTo 122

'REPLACE WORST VERTEX WITH NEW ONE
79    For j = 1 To NP
          P(IHI, j) = R(j)
80    Next

      NSIM = NSIM + 1
      E(IHI) = ER
      If (ER > E(NHI)) Then GoTo 51
      IHI = NHI
      GoTo 41

'EXPAND THE SIMPLEX
91    ILO = IHI
      IHI = NHI
      For j = 1 To NP
          X(j) = 1.95 * R(j) - 0.95 * C(j)
93    Next
      manip = "EXPAND"
      EX = ErrorFun(X, Dstar, Data, NOBS, Kount, Resi, U, W, YCALC, Dist, NP, BSW, manip)
      If (EX < ER) Then GoTo 104
```

```
'R IS BETTER THAN X
    For j = 1 To NP
        P(ILO, j) = R(j)
99  Next

    NSIM = NSIM + 1
    E(ILO) = ER
    GoTo 110

'X IS BETTER THAN R
104 For j = 1 To NP
        P(ILO, j) = X(j)
105 Next

    'IF(IDB > 0) then EX,(X(j),j=1,NP)
    NSIM = NSIM + 1
    E(ILO) = EX
110 GoTo 41

i = 1

'CONTRACT THE SIMPLEX
122 For j = 1 To NP
        R(j) = 0.5015 * C(j) + 0.4985 * P(IHI, j)
123 Next
    manip = "CONTRACT"
    ER = ErrorFun(R, Dstar, Data, NOBS, Kount, Resi, U, W, YCALC, Dist, NP, BSW, manip)
    If (ER < E(ILO)) Then GoTo 91
    If (ER < E(IHI)) Then GoTo 79

'Scale
Scal = CDbl(InputBox("Enter Scale to Continue: <0 Expands, >0 Shrinks, =0 Stops", "Scale Factor Required"))
If (Scal = 0#) Then GoTo 200
137 For i = 1 To NP1
        For j = 1 To NP
            P(i, j) = P(i, j) + Scal * (P(ILO, j) - P(i, j))
138     Next
139 Next
    GoTo 31

'WRITING THE OUTPUT

200

ActiveSheet.Range("C1") = "Calculated Cond"
ActiveSheet.Range("D1") = "Residuals"

For i = 1 To NOBS
   ActiveSheet.Cells(i + 1, 3) = YCALC(i)
   ActiveSheet.Cells(i + 1, 4) = Resi(i)
Next

ActiveSheet.Range("A1:D" & NOBS + 1).Select 'Follwowing With statement formats A through D columns for
headers and data alignment
With Selection
   .ColumnWidth = 10
```

```
    .NumberFormat = "General"
    .HorizontalAlignment = xlCenter
    .VerticalAlignment = xlCenter
    .WrapText = True
End With

'places text in spreadsheet to identify output parameters
ActiveSheet.Range("G28") = "OPTIMIZED PARAMETER ESTIMATES"
ActiveSheet.Range("G30") = "VELOCITY(cm/d)"
ActiveSheet.Range("G31") = "DISPERSIVITY (cm)"
ActiveSheet.Range("G32") = "PULSE WIDTH (cm)"
ActiveSheet.Range("G33") = "RF"
ActiveSheet.Range("G34") = "Co (mV)"
    'ActiveSheet.Range("G35") = "FODC ( /sec)" 'Version 2.2 code where the tracer first order decay constant was a
parameter
ActiveSheet.Range("G37") = "RESDIUAL SUM OF SQUARES ="
ActiveSheet.Range("G39") = "INITIAL GUESSES AND INPUT OF PARAMETERS"
ActiveSheet.Range("G41") = "VELOCITY(cm/d)"
ActiveSheet.Range("G42") = "DISPERSIVITY (cm)"
ActiveSheet.Range("G43") = "PULSE WIDTH (cm)"
ActiveSheet.Range("G44") = "RF"
ActiveSheet.Range("G45") = "Co (mV)"
    'ActiveSheet.Range("G46") = "FODC ( /sec)" 'Version 2.2 code where the tracer first order decay constant was a
parameter
    'ActiveSheet.Range("G47") = "DISTANCE FROM SOURCE (cm)" 'Version 2.2 code where the tracer first order
decay constant was a parameter
    'ActiveSheet.Range("G48") = "DIFFUSION COEFF (cm^2/sec)" 'Version 2.2 code where the tracer first order
decay constant was a parameter
ActiveSheet.Range("G46") = "DISTANCE FROM SOURCE (cm)"
ActiveSheet.Range("G47") = "DIFFUSION COEFF (cm^2/sec)"
ActiveSheet.Range("M40") = "FIX"
ActiveSheet.Range("G1").ColumnWidth = 10 ' allows all text to be seen


ActiveSheet.ChartObjects(ActiveSheet.NAME & " Breakthrough Curve").Activate
For Each Series In ActiveChart.SeriesCollection
        Series.delete
    Next Series 'deletes all series to prevent more than two series from being added to the same chart

ActiveChart.SeriesCollection.NewSeries 'replots observed data
 With ActiveChart.SeriesCollection(1)
        .Values = ActiveSheet.Range("B2:B" & NOBS + 1)
        .XValues = ActiveSheet.Range("A2:A" & NOBS + 1)
        .NAME = "Observed"
        .MarkerSize = 2
        .MarkerStyle = xlMarkerStyleCircle
    End With

ActiveChart.SeriesCollection.NewSeries 'plots calculated data
 With ActiveChart.SeriesCollection(2)
        .Values = ActiveSheet.Range("C2:C" & NOBS + 1)
        .XValues = ActiveSheet.Range("A2:A" & NOBS + 1)
        .NAME = "Calculated"
        .MarkerSize = 2
        .MarkerStyle = xlMarkerStyleCircle
    End With
```

```
'places values for optimized parameter estimates
ActiveSheet.Range("J30") = X(1) * 24
ActiveSheet.Range("J31") = X(2)
ActiveSheet.Range("J32") = X(3)
ActiveSheet.Range("J33") = X(4)
ActiveSheet.Range("J34") = X(5)
   'ActiveSheet.Range("J35") = X(6) / 3600 'Version 2.2 code where the tracer first order decay constant was a
parameter
ActiveSheet.Range("K37") = E(ILO)
' places values for initial guesses
ActiveSheet.Range("J41") = CDbl(ApparentVel.Text)
ActiveSheet.Range("J42") = CDbl(Disper.Text)
ActiveSheet.Range("J43") = CDbl(PulseWidth.Text)
ActiveSheet.Range("J44") = CDbl(Retardation.Text)
ActiveSheet.Range("J45") = CDbl(InjectionConc.Text)
   'ActiveSheet.Range("J46") = CDbl(FirstOrderDecay.Text) 'Version 2.2 code where the tracer first order decay
constant was a parameter
   'ActiveSheet.Range("J48") = CDbl(DiffusionCoeff.Text)
ActiveSheet.Range("J47") = CDbl(DiffusionCoeff.Text)

If SourceDistance.Enabled = True Then
   ActiveSheet.Range("J46") = CDbl(SourceDistance.Text)
      'ActiveSheet.Range("J47") = CDbl(SourceDistance.Text)'Version 2.2 code where the tracer first order decay
constant was a parameter
End If

'denoting parameters fixed at input
If GWV.Value = True Then ActiveSheet.Range("M41") = "Y"
If Dis.Value = True Then ActiveSheet.Range("M42") = "Y"
If PW.Value = True Then ActiveSheet.Range("M43") = "Y"
If RF.Value = True Then ActiveSheet.Range("M44") = "Y"
If IC.Value = True Then ActiveSheet.Range("M45") = "Y"
   'If FODC.Value = True Then ActiveSheet.Range("M46") = "Y"'Version 2.2 code where the tracer first order
decay constant was a parameter
If GWV.Value = False Then ActiveSheet.Range("M41") = " "
If Dis.Value = False Then ActiveSheet.Range("M42") = " "
If PW.Value = False Then ActiveSheet.Range("M43") = " "
If RF.Value = False Then ActiveSheet.Range("M44") = " "
If IC.Value = False Then ActiveSheet.Range("M45") = " "
   'If FODC.Value = False Then ActiveSheet.Range("M46") = " " 'Version 2.2 code where the tracer first order
decay constant was a parameter
   'ActiveSheet.Range("M47:M48") = "Y" 'distance and diffusion coeff never varied 'Version 2.2 code where the
tracer first order decay constant was a parameter
ActiveSheet.Range("M46:M47") = "Y" 'distance and diffusion coeff never varied

'code for confidence int

Confit = CONFINT(X, Dstar, Data, NOBS, Kount, Resi, U, W, YCALC, Dist, NP, BSW, Phix, R, C)

End Sub

Public Function ErrorFun(X, Dstar As Double, Data, NOBS As Integer, Kount As Integer, Resi, U, W, YCALC,
Dist As Double, NP As Integer, BSW As Integer, manip As String) As Double

  'COMPUTES THE ERROR FUNCTION FOR THE DATA SET
  'SMALLER VALUE IS BETTER
```

```
Dim SMRESI As Double
Dim u1 As Double
Dim u2 As Double
      u1 = 0#
      u2 = 0#
      ErrorFun = 0#
      SMRESI = 0#

If Bisquare.Value = True Then BSW = 1
If Relative.Value = True Then BSW = 2
If None.Value = True Then BSW = 0

'Sometimes negative values are predicted by the optimizer that are not real and will cause VBA run time errors.
'The following function simply converts them to positive values prior to evaluating the error function
 For j = 1 To NP - 1
       If X(j) < 0 Then X(j) = -X(j)
 Next

If (X(6) <> 0#) Then X(6) = Exp(X(6))

For i = 1 To 20000
   Resi(i) = 0#
   U(i) = 0#
   W(i) = 0#
10 Next

For i = 1 To NOBS

'CHANGE THE NEXT STATEMENT TO CHANGE THE FUNCTION BEING FIT

     SOURC = Exp(-X(6) * Data(i, 1))
     DCOEF = (X(1) * X(2) + Dstar)

     If (Data(i, 1) <= 0#) Then
        ERFCU1 = 0#
        GoTo 20
     Else
        u1 = (Dist - X(3) / (2 * X(4)) - X(1) * Data(i, 1) / X(4)) / (2 * (DCOEF * Data(i, 1) / X(4)) ^ 0.5)
        ERFCU1 = ERFC(u1)
     End If

20    If (Data(i, 1) <= X(3) / X(1)) Then
        ERFCU2 = 0#
        GoTo 30
      Else
        u2 = (Dist + X(3) / (2 * X(4)) - X(1) * Data(i, 1) / X(4)) / (2 * (DCOEF * (Data(i, 1) - X(3) / X(1)) / X(4)) ^
0.5)
        ERFCU2 = ERFC(u2)
     End If

30    GoTo 40

40    YCALC(i) = 0.5 * X(5) * SOURC * (ERFCU1 - ERFCU2)
     Resi(i) = Data(i, 2) - YCALC(i)
     SMRESI = SMRESI + Abs(Resi(i))
```

```
60    Next

    If (BSW = 1) Then
        C = 6# * SMRESI / CDbl(NOBS)
        For i = 1 To NOBS
            U(i) = Resi(i) / C
            W(i) = (1 - U(i) * U(i)) ^ 2
            If (U(i) > 1#) Then W(i) = 0#
            ErrorFun = ErrorFun + W(i) * Resi(i) * Resi(i)
70      Next
    End If

    If (BSW = 2) Then
        For i = 1 To NOBS
            If (Data(i, 2) = 0#) Then
                W(i) = 0#
            Else
                W(i) = 1# / (Data(i, 2) ^ 2#)
            End If
            ErrorFun = ErrorFun + W(i) * Resi(i) * Resi(i)
75      Next
    End If

    If (BSW = 0) Then
      For i = 1 To NOBS
          ErrorFun = ErrorFun + Resi(i) * Resi(i)
80    Next
    End If

    Kount = Kount + 1

    If (X(6) > 0#) Then X(6) = Log(X(6))


'fills calculated data and residuals into spreasheet for debugging purposes. X(1) through X(6) units are converted to
those used in PULSEPE for comparison

    'ActiveSheet.Cells(Kount, 17) = X(1) * 24 / 8640000
    'ActiveSheet.Cells(Kount, 18) = X(2) / 100
    'ActiveSheet.Cells(Kount, 19) = X(3) / 100
    'ActiveSheet.Cells(Kount, 20) = X(4)
    'ActiveSheet.Cells(Kount, 21) = X(5)
    'ActiveSheet.Cells(Kount, 22) = X(6)
    'ActiveSheet.Cells(Kount, 23) = manip
    'ActiveSheet.Cells(Kount, 24) = ErrorFun



End Function


Public Function ERFC(arg As Double)


'COMPLIMENTARY ERROR FUNCTION SUBROUTINE REAL*8 FUNCTION ERFC(ARG)
```

```
'COMPUTES THE COMPLIMENTARY ERROR FUNCTIOn FOR AN ARGUMENT
'IMPLICIT REAL*8 (A-H,L,M,O-Z)
'PARAMETER (P=0.3275911, A1=0.254829592, A2=-0.284496736,
'    1          A3=1.421413741, A4=-1.453152027, A5=1.061405429)
'TU = 1 / (1 + p * Abs(ARG))

'     ERFC=(A1*TU+A2*TU**2+A3*TU**3+A4*TU**4+A5*TU**5)
'    1      *EXP(-(ARG**2))
'     IF(ARG .LT. 0) ERFC=2-ERFC

'     RETURN
'     END


Dim P As Double
Dim A1 As Double
Dim A2 As Double
Dim A3 As Double
Dim A4 As Double
Dim A5 As Double
Dim TU As Double

P = 0.3275911
A1 = 0.254829592
A2 = -0.284496736
A3 = 1.421413741
A4 = -1.453152027
A5 = 1.061405429


TU = 1 / (1 + P * Abs(arg))

    ERFC = (A1 * TU + A2 * TU ^ 2 + A3 * TU ^ 3 + A4 * TU ^ 4 + A5 * TU ^ 5) * Exp(-(arg ^ 2))

    If (arg < 0) Then ERFC = 2 - ERFC


'********** FUNCTION DERFC(ARG)
'   ROUTINE FOR ERFC (ARG) BY SERIES EXPANSION
'   DOUBLE PRECISION VERSION


 '     Dim IL As Integer
 '     Dim LJL As Integer
 '     Dim JLJ As Integer
 '     Dim XOX As Double
 '     Dim SUMXOX As Double
 '     Dim Fact As Double
 '     Dim UOX As Double
 '     Dim US As Double
 '     Dim ZOZ As Double
 '     Dim TXOX As Double
 '     Dim OLDFACT As Double


  '    Pi = 3.14159265358
```

```
  '    SUMXOX = 1#
  '    XOX = Abs(arg)
  '    If (XOX > 3.4) Then GoTo 5160

'  THIS SERIES EXPANSION IS FOR ARG <= 3.4

  '    Fact = 1#
   '   IL = 1
    '  UOX = XOX * XOX
    '  US = UOX
'5085  Fact = Fact * IL
'      ZOZ = -1#
'      If ((IL / 2) * 2 = IL) Then ZOZ = 1#
'      TXOX = UOX / ((2# * IL + 1#) * Fact)
'      SUMXOX = SUMXOX + ZOZ * TXOX
'      UOX = UOX * US
'      IL = IL + 1


'     STOP THIE SUMMATION WHEN THE CURRENT TERM
'     IS LESS THAN 1E-20


  '    If (TXOX > 1E-20) Then GoTo 5085
  '    ERFC = 1# - 2# * XOX / (Pi) ^ 0.5 * SUMXOX
  '    If (arg < 0#) Then ERFC = 2# - ERFC
  '    GoTo 5430
'5160  If (XOX > 14#) Then GoTo 5410

'   THIS SERIES EXPANSION IS FOR ARG>3.4

  '    UOX = 2# * XOX * XOX
  '    LJL = 1
  '    JLJ = 1
  '    Fact = 1#
'5300  OLDFAC = Fact
'      Fact = Fact / UOX * JLJ

'  STOP THE SUMMATION WHEN THE CURRENT TERM BECOMES LARGER THAN
'  THE PREVIOUS TERM

'      If (Fact > OLDFAC) Then GoTo 5333
'      ZOZ = -1#
'      If ((LJL / 2) * 2 = LJL) Then ZOZ = 1#
'      TXOX = ZOZ * Fact
'      SUMXOX = SUMXOX + TXOX
'      LJL = LJL + 1
'      JLJ = JLJ + 2
'5333  ERFC = Exp(-XOX * XOX) / (Pi) ^ 0.5 / XOX * SUMXOX
'      GoTo 5420
'5410  ERFC = 0#
'5420  If (arg < 0#) Then ERFC = 2# - ERFC
5430 End Function

Public Function CONFINT(X, Dstar As Double, Data, NOBS As Integer, Kount As Integer, Resi, U, W, YCALC,
Dist As Double, NP As Integer, BSW As Integer, Phix, R, C) As Double
```

```
Dim NME(6) As String

NME(1) = "VELOCITY(cm/d)"
NME(2) = "DISPERSIVITY(cm)"
NME(3) = "PULSE WIDTH (cm)"
NME(4) = "RF"
NME(5) = "Co(mV)"
NME(6) = "FODC(1/sec)"

ActiveSheet.Range("G50:K60").Clear


 'DEFINING NPP TO BE THE NUMBER OF PARAMETERS BEING FIT
    NPP = 0
    For i = 1 To NP
       If Phix(i) = 0 Then NPP = NPP + 1
10   Next
    If NPP = 0 Then GoTo 300

  'DETERMINING THE CRITICAL RESIDUAL SUM OF SQUARES
  'WHICH DEFINES THE UPPER AND LOWER CONFIDENCE INTERVAL

    ER = ErrorFun(X, Dstar, Data, NOBS, Kount, Resi, U, W, YCALC, Dist, NP, BSW, manip)
    'FESTI = FESTIM(NOBS, NPP, IDB) alternative below
    ActiveSheet.Range("G51") = NOBS 'allows NOBS to be used in Excel's FINV function
    ActiveSheet.Range("G50") = "=FInv(0.05, G51-6, 6)" '0.05 = 95% confidence interval, G51 = NOBS, 6 = NP,
degrees of freedom = NOBS-NP, NP
    FESTI = ActiveSheet.Range("G50").Value
    'Fnpp = float(NPP)
    'FNOBS = float(NOBS)
    'RSSCRIT = ER * (1 + Fnpp / (FNOBS - Fnpp) * FESTI)
     RSSCRIT = ER * (1 + NPP / (NOBS - NPP) * FESTI)

'   LOOPING THROUGH THE PARAMETERS TO DETERMINE CONFIDENCE INTERVALS

For i = 1 To NP
   For j = 1 To NP
     R(j) = X(j)
     C(j) = X(j)
90  Next

   If Phix(i) = 1 Then GoTo 199

'  LOOKING FOR THE UPPER LIMIT
       NCOUNT = 1
100

   'IF(FLOAT(I) .EQ. 6. .AND. X(I) .LT. 0.) THEN
    If i = 6 And X(i) < 0 Then
          R(i) = R(i) - 0.1 * X(i)
       Else
          R(i) = R(i) + 0.1 * X(i)
       End If
       ER = ErrorFun(R, Dstar, Data, NOBS, Kount, Resi, U, W, YCALC, Dist, NP, BSW, manip)
       If R(6) < -100 Or R(6) > 100 Then GoTo 120
```

```
        If NCOUNT > 1 Then
            If Abs((ERCHK - ER) / ER * 100) < 0.001 Then
                R(i) = -1#
                GoTo 120
            End If
        Else
            NCOUNT = 2
        End If
        ERCHK = ER
        If ER < RSSCRIT Then GoTo 100

110

      'IF(FLOAT(I) .EQ. 6. .AND. X(I) .LT. 0.) THEN
      If i = 6 And X(i) < 0 Then

         R(i) = R(i) + 0.01 * X(i)
         Else
         R(i) = R(i) - 0.01 * X(i)
      End If

   ER = ErrorFun(R, Dstar, Data, NOBS, Kount, Resi, U, W, YCALC, Dist, NP, BSW, manip)
      If ER > RSSCRIT Then GoTo 110

    'LOOKING FOR THE LOWER LIMIT
120
      'IF(FLOAT(I) .EQ. 6. .AND. X(I) .LT. 0.) THEN
       If i = 6 And X(i) < 0 Then
            C(i) = C(i) + 0.1 * X(i)
        Else
            C(i) = C(i) - 0.1 * X(i)
        End If
       'IF(C(I) .LT. 0. .AND. FLOAT(I) .NE. 6.) THEN
       If C(i) < 0 And i <> 6 Then
            C(i) = C(i) + 0.1 * X(i)
125           C(i) = C(i) - 0.01 * X(i)
            If C(i) < 0 Then
                C(i) = 0#
                GoTo 249
            End If
        End If

        ER = ErrorFun(C, Dstar, Data, NOBS, Kount, Resi, U, W, YCALC, Dist, NP, BSW, manip)
        If C(6) < -100 Or C(6) > 100 Then GoTo 249
        If ER < RSSCRIT Then GoTo 120

130
        'IF(FLOAT(I) .EQ. 6. .AND. X(I) .LT. 0.) THEN
        If i = 6 And X(i) < 0 Then
            C(i) = C(i) - 0.01 * X(i)
        Else
            C(i) = C(i) + 0.01 * X(i)
        End If

        ER = ErrorFun(C, Dstar, Data, NOBS, Kount, Resi, U, W, YCALC, Dist, NP, BSW, manip)
        If ER > RSSCRIT Then GoTo 130
```

```
249
        If i = 6 Then
            X(i) = Exp(X(i))
            If R(i) < -99 Then
                R(i) = 0#
            Else
                R(i) = Exp(R(i))
            End If
            C(i) = Exp(C(i))
        End If

259  'Writing to the output file

       ActiveSheet.Range("G50") = "95% CONFIDENCE INTERVALS FOR ESTIMATED PARAMETERS"
       ActiveSheet.Range("G51") = "Parameter"
       ActiveSheet.Range("I51") = "Low"
       ActiveSheet.Range("J51") = "Optimized"
       ActiveSheet.Range("K51") = "High"
       ActiveSheet.Range("G60") = "CRITICAL RSS VALUE ="
       ActiveSheet.Range("J60") = RSSCRIT

       If R(i) > 0 Then

          ActiveSheet.Cells(i + 52, 7) = NME(i)
          ActiveSheet.Cells(i + 52, 9) = C(i) 'lower limit
          ActiveSheet.Cells(i + 52, 10) = X(i) 'optimized
          ActiveSheet.Cells(i + 52, 11) = R(i) 'upper limit

             If i = 1 Then 'converts velocity to cm/d
                ActiveSheet.Cells(i + 52, 9) = C(i) * 24 'lower limit
                ActiveSheet.Cells(i + 52, 10) = X(i) * 24 'optimized
                ActiveSheet.Cells(i + 52, 11) = R(i) * 24 'upper limit
             End If

             If i = 6 Then ' converts FODC to /sec
                ActiveSheet.Cells(i + 52, 9) = C(i) / 3600 'lower limit
                ActiveSheet.Cells(i + 52, 10) = X(i) / 3600 'optimized
                ActiveSheet.Cells(i + 52, 11) = R(i) / 3600 'upper limit
             End If

          Else
           ActiveSheet.Range("G52") = "No Convergence"
          End If
199
200   Next

       If R(i) = 0 Then

          ActiveSheet.Cells(i + 52, 7) = ""
          ActiveSheet.Cells(i + 52, 9) = ""
          ActiveSheet.Cells(i + 52, 10) = ""
          ActiveSheet.Cells(i + 52, 11) = ""
       End If

299
```

```
300
    If X(6) > 0 Then
        X(6) = Log(X(6))
    Else
        X(6) = 0#
    End If


End Function

Private Sub Finished_Click()
UserForm6.Show
UserForm5.Hide
End Sub
```

User form 6 code

```
Private Sub UserForm_Initialize()

For Each Worksheet In ActiveWorkbook.Sheets
            ComboBox1.AddItem Worksheet.NAME
            ComboBox2.AddItem Worksheet.NAME
            ComboBox3.AddItem Worksheet.NAME
            ComboBox4.AddItem Worksheet.NAME
            ComboBox5.AddItem Worksheet.NAME
            ComboBox6.AddItem Worksheet.NAME
            ComboBox7.AddItem Worksheet.NAME
            ComboBox8.AddItem Worksheet.NAME
            ComboBox9.AddItem Worksheet.NAME
            ComboBox10.AddItem Worksheet.NAME
            ComboBox11.AddItem Worksheet.NAME
            ComboBox12.AddItem Worksheet.NAME
            ComboBox13.AddItem Worksheet.NAME
            ComboBox14.AddItem Worksheet.NAME
            ComboBox15.AddItem Worksheet.NAME
            ComboBox16.AddItem Worksheet.NAME

        Next
End Sub

Private Sub ViewResults_Click()

Dim Gamma(16) As Double
Dim AppVel(16) As Double
Dim Disper(16) As Double
Dim VelInf(16) As Double
Dim Alpha(8) As Double
Dim Err(8) As Double
Dim Part1 As Double
Dim Part2 As Double
Dim Part3 As Double
Dim Part4 As Double
Dim ProbeName(8) As Variant
Dim ComboBox(16) As Variant
Dim OuterD(16) As Variant
Dim Opt(16) As Variant
```

```
Dim High(16) As Variant
Dim Low(16) As Variant


ComboBox(1) = ComboBox1.Value
ComboBox(2) = ComboBox2.Value
ComboBox(3) = ComboBox3.Value
ComboBox(4) = ComboBox4.Value
ComboBox(5) = ComboBox5.Value
ComboBox(6) = ComboBox6.Value
ComboBox(7) = ComboBox7.Value
ComboBox(8) = ComboBox8.Value
ComboBox(9) = ComboBox9.Value
ComboBox(10) = ComboBox10.Value
ComboBox(11) = ComboBox11.Value
ComboBox(12) = ComboBox12.Value
ComboBox(13) = ComboBox13.Value
ComboBox(14) = ComboBox14.Value
ComboBox(15) = ComboBox15.Value
ComboBox(16) = ComboBox16.Value

OuterD(1) = TextBox1.Value
OuterD(2) = TextBox1.Value
OuterD(3) = TextBox2.Value
OuterD(4) = TextBox2.Value
OuterD(5) = TextBox3.Value
OuterD(6) = TextBox3.Value
OuterD(7) = TextBox4.Value
OuterD(8) = TextBox4.Value
OuterD(9) = TextBox5.Value
OuterD(10) = TextBox5.Value
OuterD(11) = TextBox6.Value
OuterD(12) = TextBox6.Value
OuterD(13) = TextBox7.Value
OuterD(14) = TextBox7.Value
OuterD(15) = TextBox8.Value
OuterD(16) = TextBox8.Value

ProbeName(1) = TextBox9.Value
ProbeName(2) = TextBox10.Value
ProbeName(3) = TextBox11.Value
ProbeName(4) = TextBox12.Value
ProbeName(5) = TextBox13.Value
ProbeName(6) = TextBox14.Value
ProbeName(7) = TextBox15.Value
ProbeName(8) = TextBox16.Value

Opt(1) = Opt1.Value
Opt(2) = Opt1.Value
Opt(3) = Opt2.Value
Opt(4) = Opt2.Value
Opt(5) = Opt3.Value
Opt(6) = Opt3.Value
Opt(7) = Opt4.Value
Opt(8) = Opt4.Value
Opt(9) = Opt5.Value
```

```
Opt(10) = Opt5.Value
Opt(11) = Opt6.Value
Opt(12) = Opt6.Value
Opt(13) = Opt7.Value
Opt(14) = Opt7.Value
Opt(15) = Opt8.Value
Opt(16) = Opt8.Value

High(1) = High1.Value
High(2) = High1.Value
High(3) = High2.Value
High(4) = High2.Value
High(5) = High3.Value
High(6) = High3.Value
High(7) = High4.Value
High(8) = High4.Value
High(9) = High5.Value
High(10) = High5.Value
High(11) = High6.Value
High(12) = High6.Value
High(13) = High7.Value
High(14) = High7.Value
High(15) = High8.Value
High(16) = High8.Value

Low(1) = Low1.Value
Low(2) = Low1.Value
Low(3) = Low2.Value
Low(4) = Low2.Value
Low(5) = Low3.Value
Low(6) = Low3.Value
Low(7) = Low4.Value
Low(8) = Low4.Value
Low(9) = Low5.Value
Low(10) = Low5.Value
Low(11) = Low6.Value
Low(12) = Low6.Value
Low(13) = Low7.Value
Low(14) = Low7.Value
Low(15) = Low8.Value
Low(16) = Low8.Value

On Error Resume Next

' if the combo box has a value, then fill apparent velocity dispersivity, and gamma arrays
For i = 1 To 16
   If ComboBox(i) <> "" Then
   Worksheets(ComboBox(i)).Activate
   Disper(i) = ActiveSheet.Range("J31").Value
   Gamma(i) = ActiveSheet.Range("J47").Value / (CDbl(OuterD(i)) / 2)
      If Opt(i) = True Then
         AppVel(i) = ActiveSheet.Range("J30").Value
         End If
      If High(i) = True Then
         AppVel(i) = ActiveSheet.Range("K53").Value
         End If
```

```
      If Low(i) = True Then
         AppVel(i) = ActiveSheet.Range("I53").Value
         End If
   End If
Next
'create results worksheet
Worksheets.Add(After:=Worksheets(Worksheets.Count)).NAME = "Results"

'loop to calculate alphas, average linear velocities, and report the findings in the Results worksheet
For i = 1 To 8

'alpha calculation
   Part1 = (AppVel(2 * i - 1) * Gamma(2 * i - 1) * (Cos(Gamma(2 * i)) - 1))
   Part2 = (AppVel(2 * i) * Gamma(2 * i) * (1 - Cos(Gamma(2 * i - 1))))
   Part3 = (AppVel(2 * i - 1) * Gamma(2 * i - 1) * Sin(Gamma(2 * i)))
   Part4 = (AppVel(2 * i) * Gamma(2 * i) * Sin(Gamma(2 * i - 1)))
   Alpha(i) = Atn((Part1 + Part2) / (Part3 - Part4))
   If Alpha(i) < 0 Then Alpha(i) = Alpha(i) + 3.141

'average linear velocity calculation from apparent velocities and alpha
   VelInf(2 * i - 1) = AppVel(2 * i - 1) * Gamma(2 * i - 1) / (2 * (Cos(Alpha(i)) - Cos(Alpha(i) + Gamma(2 * i -
1))))
   VelInf(2 * i) = AppVel(2 * i) * Gamma(2 * i) / (2 * (Cos(Alpha(i)) - Cos(Alpha(i) + Gamma(2 * i))))
   Err(i) = (VelInf(2 * i - 1) - VelInf(2 * i)) ^ 2

'converts alpha and gammas from radians to degrees
   Alpha(i) = Alpha(i) * (180 / 3.141)
   Gamma(2 * i - 1) = Gamma(2 * i - 1) * (180 / 3.141)
   Gamma(2 * i) = Gamma(2 * i) * (180 / 3.141)

'writting to the output worksheet
   ActiveSheet.Cells(i + 1, 1) = ProbeName(i)
   ActiveSheet.Cells(i + 1, 2) = Disper(2 * i - 1)
   ActiveSheet.Cells(i + 1, 3) = Disper(2 * i)
   ActiveSheet.Cells(i + 1, 4) = Gamma(2 * i - 1)
   ActiveSheet.Cells(i + 1, 5) = Gamma(2 * i)
   ActiveSheet.Cells(i + 1, 6) = Alpha(i)
   ActiveSheet.Cells(i + 1, 7) = AppVel(2 * i - 1)
   ActiveSheet.Cells(i + 1, 8) = AppVel(2 * i)
   ActiveSheet.Cells(i + 1, 9) = VelInf(2 * i - 1)
   ActiveSheet.Cells(i + 1, 10) = VelInf(2 * i)
   ActiveSheet.Cells(i + 1, 11) = Err(i)
Next
ActiveSheet.Range("A1") = "Probe Name"
ActiveSheet.Range("B1") = "Dispersivity 1 (cm)"
ActiveSheet.Range("C1") = "Dispersivity 2 (cm)"
ActiveSheet.Range("D1") = "Gamma 1 (Degrees)"
ActiveSheet.Range("E1") = "Gamma 2 (Degrees)"
ActiveSheet.Range("F1") = "Alpha (Degrees)"
ActiveSheet.Range("G1") = "Apparent Velocity 1 (cm/d)"
ActiveSheet.Range("H1") = "Apparent Velocity 2 (cm/d)"
ActiveSheet.Range("I1") = "Average Linear Velocity 1 (cm/d)"
ActiveSheet.Range("J1") = "Average Linear Velocity 2 (cm/d)"
ActiveSheet.Range("K1") = "Error"
ActiveSheet.Range("A1").Select
Range(Selection, Selection.End(xlToRight)).Select
```

```
Selection.Font.Bold = True
Range("A1").Select
Range(Selection, Selection.End(xlDown)).Select
Selection.Font.Bold = False
Selection.Font.Bold = True
Selection.Borders(xlDiagonalDown).LineStyle = xlNone
Selection.Borders(xlDiagonalUp).LineStyle = xlNone
Selection.Borders(xlEdgeLeft).LineStyle = xlNone
Selection.Borders(xlEdgeTop).LineStyle = xlNone
Selection.Borders(xlEdgeBottom).LineStyle = xlNone
With Selection.Borders(xlEdgeRight)
        .LineStyle = xlContinuous
        .Weight = xlThin
        .ColorIndex = xlAutomatic
End With
Selection.Borders(xlInsideHorizontal).LineStyle = xlNone
Range("A1").Select
Range(Selection, Selection.End(xlToRight)).Select
Selection.Borders(xlDiagonalDown).LineStyle = xlNone
Selection.Borders(xlDiagonalUp).LineStyle = xlNone
Selection.Borders(xlEdgeLeft).LineStyle = xlNone
Selection.Borders(xlEdgeTop).LineStyle = xlNone
With Selection.Borders(xlEdgeBottom)
        .LineStyle = xlDouble
        .Weight = xlThick
        .ColorIndex = xlAutomatic
End With
Selection.Borders(xlEdgeRight).LineStyle = xlNone
Range("A1").Select
Range(Selection, Selection.End(xlToRight)).Select
    With Selection
        .HorizontalAlignment = xlCenter
        .VerticalAlignment = xlCenter
        .WrapText = True
        .Orientation = 0
        .AddIndent = False
        .IndentLevel = 0
        .ShrinkToFit = False
        .ReadingOrder = xlContext
        .MergeCells = False
    End With
Range("A2").Select
Range(Selection, Selection.End(xlDown)).Select
    With Selection
        .HorizontalAlignment = xlCenter
        .VerticalAlignment = xlCenter
        .WrapText = False
        .Orientation = 0
        .AddIndent = False
        .IndentLevel = 0
        .ShrinkToFit = False
        .ReadingOrder = xlContext
        .MergeCells = False
    End With
Columns("B:B").ColumnWidth = 11.43
Columns("B:B").ColumnWidth = 13.14
```

```
Columns("C:C").ColumnWidth = 11.43
Columns("C:C").ColumnWidth = 13.29
Columns("D:D").ColumnWidth = 9.57
Columns("E:E").ColumnWidth = 10
Columns("F:F").ColumnWidth = 10
Response = MsgBox("Analysis Complete. Do you wish to save your project with a unique name?", vbYesNo)

If Response = vbYes Then    ' User chose Yes.
        NewName = InputBox("Enter New File Name", "Save As")
        ActiveWorkbook.SaveAs FileName:=ThisWorkbook.Path & NewName, FileFormat:=xlNormal,
Password:="", WriteResPassword:="", ReadOnlyRecommended:=False, CreateBackup:=False
        Else: GoTo 999    ' User chose No.
   End If

999 End Sub
```

Appendix 2: Pinder Algorithm for Three-Point Estimators

```
Private Sub CommandButton1_Click()

Dim NumWells, i, j, k, l, m, n As Integer
Dim MinX, MinY As Double

Application.ScreenUpdating = False
'calculates number of wells
NumWells = ActiveSheet.Range("A2").End(xlDown).Row - 1

ActiveSheet.Range("i1") = "Well A"
ActiveSheet.Range("j1") = "Well B"
ActiveSheet.Range("k1") = "Well C"
ActiveSheet.Range("l1") = "Gradient"
ActiveSheet.Range("m1") = "Flow Direction from North (X Direction)"
ActiveSheet.Range("f1") = "Adjusted X-Coordinate"
ActiveSheet.Range("g1") = "Adjusted Y-Coordinate"

'calculation for adjusting well coordinates into smaller, more managable number for Gradient
spreadsheet
'If UTM coordinates are used, the spreadsheet will have difficulty calculating an accurate gradient from
them

Set XRange = Worksheets("Sheet1").Range("B2:B" & NumWells + 1)
Set YRange = Worksheets("Sheet1").Range("C2:C" & NumWells + 1)

MinX = Application.WorksheetFunction.Min(XRange)
```

```
MinY = Application.WorksheetFunction.Min(YRange)

For m = 1 To NumWells

   ActiveSheet.Cells(m + 1, 6) = ActiveSheet.Cells(m + 1, 2) - MinX
   ActiveSheet.Cells(m + 1, 7) = ActiveSheet.Cells(m + 1, 3) - MinY

Next

'factorial code goes here

'l is the counter which indicates where to paste the output for each calculation
l = 2

'Series of For loops to determine all the possible configurations of 3 wells without repetition
For i = 1 To NumWells - 2
For j = 2 To NumWells - 1
   If j <= i Then j = i + 1 'forces j>i - eliminates repetition
For k = 3 To NumWells
   If k <= j Then k = j + 1 'forces k>j - eliminates repetition

Application.ScreenUpdating = False

'Moves Well A name  and pastes to output
      ActiveSheet.Cells(i + 1, 1).Copy
```

```
        ActiveSheet.Cells(l, 9).PasteSpecial
    'Copies hydraulic head and XY location data from Wells ABC and pastes into gradient formula
        ActiveSheet.Next.Select
        ActiveSheet.Range("A7").PasteSpecial
        ActiveSheet.Previous.Select
        ActiveSheet.Cells(i + 1, 6).Copy
        ActiveSheet.Next.Select
        ActiveSheet.Range("B7").PasteSpecial
        ActiveSheet.Previous.Select
        ActiveSheet.Cells(i + 1, 7).Copy
        ActiveSheet.Next.Select
        ActiveSheet.Range("C7").PasteSpecial
        ActiveSheet.Previous.Select
        ActiveSheet.Cells(i + 1, 4).Copy
        ActiveSheet.Next.Select
        ActiveSheet.Range("D7").PasteSpecial
        ActiveSheet.Previous.Select

'Moves Well B name and pastes to output
        ActiveSheet.Cells(j + 1, 1).Copy
        ActiveSheet.Cells(l, 10).PasteSpecial
    'Copies hydraulic head and XY location data from Wells ABC and pastes into gradient formula of
Devlin 2003
        ActiveSheet.Next.Select
        ActiveSheet.Range("A8").PasteSpecial
        ActiveSheet.Previous.Select
```

```
        ActiveSheet.Cells(j + 1, 6).Copy
        ActiveSheet.Next.Select
        ActiveSheet.Range("B8").PasteSpecial
        ActiveSheet.Previous.Select
        ActiveSheet.Cells(j + 1, 7).Copy
        ActiveSheet.Next.Select
        ActiveSheet.Range("C8").PasteSpecial
        ActiveSheet.Previous.Select
        ActiveSheet.Cells(j + 1, 4).Copy
        ActiveSheet.Next.Select
        ActiveSheet.Range("D8").PasteSpecial
        ActiveSheet.Previous.Select

'Moves Well C name and pastes to output
        ActiveSheet.Cells(k + 1, 1).Copy
        ActiveSheet.Cells(l, 11).PasteSpecial
    'Copies hydraulic head and XY location data from Wells ABC and pastes into gradient formula
        ActiveSheet.Next.Select
        ActiveSheet.Range("A9").PasteSpecial
        ActiveSheet.Previous.Select
        ActiveSheet.Cells(k + 1, 6).Copy
        ActiveSheet.Next.Select
        ActiveSheet.Range("B9").PasteSpecial
        ActiveSheet.Previous.Select
        ActiveSheet.Cells(k + 1, 7).Copy
```

```
        ActiveSheet.Next.Select
        ActiveSheet.Range("C9").PasteSpecial
        ActiveSheet.Previous.Select
        ActiveSheet.Cells(k + 1, 4).Copy
        ActiveSheet.Next.Select
        ActiveSheet.Range("D9").PasteSpecial

'Copies gradient magnitude and direction and pastes it to output

ActiveSheet.Range("g3:h3").Copy
ActiveSheet.Previous.Select
ActiveSheet.Cells(l, 12).PasteSpecial Paste:=xlPasteValues

l = l + 1 'advances l counter

Next
Next
Next

'copies data for all wells and places them into gradient spreadsheet
For n = 1 To NumWells

    ActiveSheet.Cells(n + 1, 1).Copy
    ActiveSheet.Next.Select
    ActiveSheet.Cells(n + 6, 1).PasteSpecial
```

```
    ActiveSheet.Previous.Select
    ActiveSheet.Cells(n + 1, 6).Copy
    ActiveSheet.Next.Select
    ActiveSheet.Cells(n + 6, 2).PasteSpecial
    ActiveSheet.Previous.Select
    ActiveSheet.Cells(n + 1, 7).Copy
    ActiveSheet.Next.Select
    ActiveSheet.Cells(n + 6, 3).PasteSpecial
    ActiveSheet.Previous.Select
    ActiveSheet.Cells(n + 1, 4).Copy
    ActiveSheet.Next.Select
    ActiveSheet.Cells(n + 6, 4).PasteSpecial
    ActiveSheet.Previous.Select

Next

Application.ScreenUpdating = True


End Sub
```

Appendix 3: Woodstock PVP CR1000 Code

```
'CR1000

'Created by SCWIN (2.3)


'Declare Variables and Units

Public Batt_Volt

Public HalfBR(16)


Units Batt_Volt=Volts

Units HalfBR=mV


'Define Data Tables

DataTable(Oct12,True,-1)

        DataInterval(0,5,sec,10)

        Minimum(1,Batt_Volt,FP2,False,False)

        Sample(1,HalfBR(1),FP2)

        Sample(1,HalfBR(2),FP2)

        Sample(1,HalfBR(3),FP2)

        Sample(1,HalfBR(4),FP2)

        Sample(1,HalfBR(5),FP2)

        Sample(1,HalfBR(6),FP2)

        Sample(1,HalfBR(7),FP2)

        Sample(1,HalfBR(8),FP2)

        Sample(1,HalfBR(9),FP2)

        Sample(1,HalfBR(10),FP2)

        Sample(1,HalfBR(11),FP2)
```

```
        Sample(1,HalfBR(12),FP2)
        Sample(1,HalfBR(13),FP2)
        Sample(1,HalfBR(14),FP2)
        Sample(1,HalfBR(15),FP2)
        Sample(1,HalfBR(16),FP2)
EndTable

'Main Program
BeginProg
        Scan(1,Sec,25,0)
                'Default Datalogger Battery Voltage measurement Batt_Volt:
                Battery(Batt_Volt)
                'Generic Half Bridge measurements HalfBR(1):
                BrHalf(HalfBR(1),1,mV2500,1,1,1,2500,True,0,_60Hz,1.0,0.0)
                BrHalf(HalfBR(2),1,mV2500,2,1,1,2500,True,0,_60Hz,1.0,0.0)
                BrHalf(HalfBR(3),1,mV2500,3,1,1,2500,True,0,_60Hz,1.0,0.0)
                BrHalf(HalfBR(4),1,mV2500,4,1,1,2500,True,0,_60Hz,1.0,0.0)
                BrHalf(HalfBR(5),1,mV2500,5,1,1,2500,True,0,_60Hz,1.0,0.0)
                BrHalf(HalfBR(6),1,mV2500,6,1,1,2500,True,0,_60Hz,1.0,0.0)
                BrHalf(HalfBR(7),1,mV2500,7,1,1,2500,True,0,_60Hz,1.0,0.0)
                BrHalf(HalfBR(8),1,mV2500,8,1,1,2500,True,0,_60Hz,1.0,0.0)
                BrHalf(HalfBR(9),1,mV2500,9,1,1,2500,True,0,_60Hz,1.0,0.0)
                BrHalf(HalfBR(10),1,mV2500,10,1,1,2500,True,0,_60Hz,1.0,0.0)
                BrHalf(HalfBR(11),1,mV2500,11,1,1,2500,True,0,_60Hz,1.0,0.0)
                BrHalf(HalfBR(12),1,mV2500,12,1,1,2500,True,0,_60Hz,1.0,0.0)
```

```
        BrHalf(HalfBR(13),1,mV2500,13,1,1,2500,True,0,_60Hz,1.0,0.0)
        BrHalf(HalfBR(14),1,mV2500,14,1,1,2500,True,0,_60Hz,1.0,0.0)
        BrHalf(HalfBR(15),1,mV2500,15,1,1,2500,True,0,_60Hz,1.0,0.0)
        BrHalf(HalfBR(16),1,mV2500,16,1,1,2500,True,0,_60Hz,1.0,0.0)
        CallTable(Oct12)
    NextScan

EndProg
```

Appendix 4: High Resolution PVP CR1000 Code

```
'CR1000

'Created by SCWIN (2.3)


'Declare Variables and Units

Public Batt_Volt

Public HalfBR(16)


Units Batt_Volt=Volts

Units HalfBR=mV


'Define Data Tables

DataTable(Oct12,True,-1)

        DataInterval(0,10,sec,10)

        Minimum(1,Batt_Volt,FP2,False,False)

        Sample(1,HalfBR(1),IEEE4)

        Sample(1,HalfBR(2),IEEE4)

        Sample(1,HalfBR(3),IEEE4)

        Sample(1,HalfBR(4),IEEE4)

        Sample(1,HalfBR(5),IEEE4)

        Sample(1,HalfBR(6),IEEE4)

        Sample(1,HalfBR(7),IEEE4)

        Sample(1,HalfBR(8),IEEE4)

        Sample(1,HalfBR(9),IEEE4)

        Sample(1,HalfBR(10),IEEE4)

        Sample(1,HalfBR(11),IEEE4)
```

```
        Sample(1,HalfBR(12),IEEE4)
        Sample(1,HalfBR(13),IEEE4)
        Sample(1,HalfBR(14),IEEE4)
        Sample(1,HalfBR(15),IEEE4)
        Sample(1,HalfBR(16),IEEE4)
EndTable

'Main Program
BeginProg
        Scan(1,Sec,25,0)
                'Default Datalogger Battery Voltage measurement Batt_Volt:
                Battery(Batt_Volt)
                'Generic Half Bridge measurements HalfBR(1):
                BrHalf(HalfBR(1),1,mV2500,1,1,1,2500,True,0,_60Hz,1.0,0.0)
                BrHalf(HalfBR(2),1,mV2500,2,1,1,2500,True,0,_60Hz,1.0,0.0)
                BrHalf(HalfBR(3),1,mV2500,3,1,1,2500,True,0,_60Hz,1.0,0.0)
                BrHalf(HalfBR(4),1,mV2500,4,1,1,2500,True,0,_60Hz,1.0,0.0)
                BrHalf(HalfBR(5),1,mV2500,5,1,1,2500,True,0,_60Hz,1.0,0.0)
                BrHalf(HalfBR(6),1,mV2500,6,1,1,2500,True,0,_60Hz,1.0,0.0)
                BrHalf(HalfBR(7),1,mV2500,7,1,1,2500,True,0,_60Hz,1.0,0.0)
                BrHalf(HalfBR(8),1,mV2500,8,1,1,2500,True,0,_60Hz,1.0,0.0)
                BrHalf(HalfBR(9),1,mV2500,9,1,1,2500,True,0,_60Hz,1.0,0.0)
                BrHalf(HalfBR(10),1,mV2500,10,1,1,2500,True,0,_60Hz,1.0,0.0)
                BrHalf(HalfBR(11),1,mV2500,11,1,1,2500,True,0,_60Hz,1.0,0.0)
                BrHalf(HalfBR(12),1,mV2500,12,1,1,2500,True,0,_60Hz,1.0,0.0)
```

```
        BrHalf(HalfBR(13),1,mV2500,13,1,1,2500,True,0,_60Hz,1.0,0.0)
        BrHalf(HalfBR(14),1,mV2500,14,1,1,2500,True,0,_60Hz,1.0,0.0)
        BrHalf(HalfBR(15),1,mV2500,15,1,1,2500,True,0,_60Hz,1.0,0.0)
        BrHalf(HalfBR(16),1,mV2500,16,1,1,2500,True,0,_60Hz,1.0,0.0)
        CallTable(Oct12)
    NextScan

EndProg
```

Appendix 5: Differential Pressure Transducer CR1000 Code

```
'CR1000

'Created by Short Cut (2.5)


'Declare Variables and Units

Public Batt_Volt

Public DiffVolt(8)


Units Batt_Volt=Volts

Units DiffVolt=mV


'Define Data Tables

DataTable(Table1,True,-1)

        DataInterval(0,30,min,10)

        Sample(1,DiffVolt(1),FP2)

        Sample(1,DiffVolt(2),FP2)

        Sample(1,DiffVolt(3),FP2)

        Sample(1,DiffVolt(4),FP2)

        Sample(1,DiffVolt(5),FP2)

        Sample(1,DiffVolt(6),FP2)

        Sample(1,DiffVolt(7),FP2)

        Sample(1,DiffVolt(8),FP2)

EndTable


DataTable(Table2,True,-1)

        DataInterval(0,1440,sec,1)
```

```
        Minimum(1,Batt_Volt,FP2,False,False)
EndTable


'Main Program
BeginProg
        Scan(1,Sec,1,0)
                'Default Datalogger Battery Voltage measurement Batt_Volt:
                Battery(Batt_Volt)
                'Generic Differential Voltage measurements DiffVolt(1):
                VoltDiff(DiffVolt(1),8,mV25,1,True,0,_60Hz,1.0,0.0)
                'Call Data Tables and Store Data
                CallTable(Table1)
                CallTable(Table2)
        NextScan
EndProg
```

Appendix 6: Base to Height Calculation for Three-Point Estimators

Determining base to height ratios in three point estimators

In any three-point estimator, there are three possible base to height ratios, depending on which side is chosen as the base. Therefore, for each estimator the base to height ratios were recalculated in turn assuming each side as the base. For example, assuming a triangular estimator with vertices A, B, and C (Figure A1-1), an initial base was defined by the distance between Wells A and C ($\overline{AC}$).

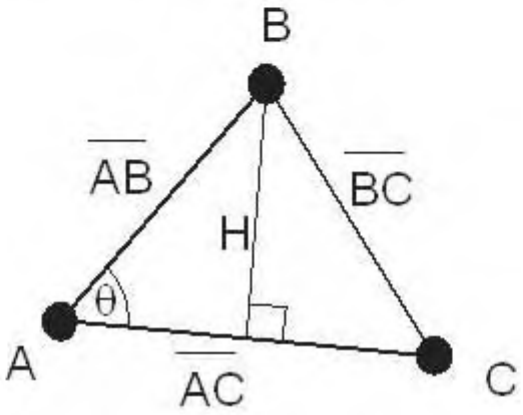

Figure A1-1: Three wells, A, B, and C, making up a three point estimator.

The interior angle of the estimator at Well A (θ) formed by the lines $\overline{AB}$ and $\overline{AC}$ was determined using the Law of Cosines:

$$\theta = \cos^{-1} \frac{\overline{AB}^2 + \overline{AC}^2 - \overline{BC}^2}{2\,\overline{AB}\;\overline{AC}} \qquad [3]$$

With the interior angle θ known, the height of the triangle (H) with $\overline{AC}$ as the base was calculated from:

$$H = \overline{AB} \sin\theta \qquad [4]$$

This process was repeated for all interior angles, using each side as the base, for each three-point estimator. Any estimator for which one of the base to height ratios failed the screening criteria was eliminated from further consideration.

Appendix 7: Woodstock PVP Location and Coordinates

Multilevel PVP	Distance to Well (cm)						
	ML5	ML6	ML7	ML8	ML12	WO78	WO79
PVP3	81	164				346	243
PVP4		253	74	133			
PVP5	530				530	340	624

Multilevel PVP	UTM (Zone 17)				
	Northing (m)		Easting (m)		Ground Surface Elevation (masl)
PVP1	4770157.50		520030.15		301.02
PVP2	4770156.45		520039.34		300.72

Appendix 8: Woodstock Well Coordinates (From Critchley 2010)

Table A.1: Construction and location information for the injection-extraction wells.

Well ID	[UTM NAD 83 17 N]		Ground Surface Elevation (masl)	Top of Casing Elevation (masl)	Total Depth (masl)	Top of Screen Depth (masl)	Length of Screen (m)
	Easting (m)	Northing (m)					
WO77	520045.40	4770166.24	300.47	300.69	283.90	294.56	10.67
WO78	520041.97	4770162.58	300.52	301.15	283.70	294.37	10.67
WO79	520038.57	4770158.89	300.67	301.31	285.32	294.47	9.14
WO80	520035.13	4770155.04	300.85	301.21	284.00	294.66	10.67

Table A.2: Construction and location information for the multi-level monitoring wells installed in 2008.

Well ID	[UTM NAD 83 17 N]		Ground Surface Elevation (masl)	Top of Casing Elevation (masl)	Port ID	Depth to Centre of Screen (mbgs)	Depth to Centre of Screen (masl)
	Easting (m)	Northing (m)					
ML1	520030.78	4770156.59	301.01	301.70	1	3.88	297.13
					2	5.38	295.63
					3	6.88	294.13
					4	8.38	292.63
					5	9.88	291.13
					6	11.38	289.63
					7	12.88	288.13
ML2	520046.05	4770165.48	300.52	301.02	1	5.89	294.62
					2	7.59	292.92
					3	9.29	291.22
					4	10.99	289.52
					5	12.69	287.82
					6	14.39	286.12
					7	16.09	284.42
					8	17.79	282.72
ML3	520047.44	4770164.16	300.53	301.12	1	5.93	294.59
					2	7.63	292.89
					3	9.33	291.19
					4	11.03	289.49
					5	12.73	287.79
					6	14.43	286.09
					7	16.13	284.39
					8	17.83	282.69
ML4	520048.89	4770162.76	300.54	301.12	1	6.07	294.47
					2	7.77	292.77
					3	9.47	291.07
					4	11.17	289.37
					5	12.87	287.67
					6	14.57	285.97
					7	16.27	284.27
					8	17.97	282.57

Table A.2: (continued)

Well ID	[UTM NAD 83 17 N]		Ground Surface Elevation (masl)	Top of Casing Elevation (masl)	Port ID	Depth to Centre of Screen (mbgs)	Depth to Centre of Screen (masl)
	Easting (m)	Northing (m)					
ML5	520041.03	4770160.03	300.64	301.19	1	3.40	297.24
					2	5.10	295.54
					3	6.80	293.84
					4	8.50	292.14
					5	10.20	290.44
					6	11.90	288.74
					7	13.60	287.04
					8	15.30	285.34
ML6	520042.42	4770158.54	300.67	301.29	1	5.51	295.15
					2	7.21	293.45
					3	8.91	291.75
					4	10.61	290.05
					5	12.31	288.35
					6	14.01	286.65
					7	15.71	284.95
					8	17.41	283.25
ML7	520043.83	4770157.27	300.69	301.28	1	5.52	295.17
					2	7.22	293.47
					3	8.92	291.77
					4	10.62	290.07
					5	12.32	288.37
					6	14.02	286.67
					7	15.72	284.97
					8	17.42	283.27
ML8	520045.07	4770156.28	300.73	301.35	1	6.19	294.54
					2	7.89	292.84
					3	9.59	291.14
					4	11.29	289.44
					5	12.99	287.74
					6	14.69	286.04
					7	16.39	284.34
					8	18.09	282.64

Table A.2: (continued)

Well ID	[UTM NAD 83 17 N]		Ground Surface Elevation (masl)	Top of Casing Elevation (masl)	Port ID	Depth to Centre of Screen (mbgs)	Depth to Centre of Screen (masl)
	Easting (m)	Northing (m)					
ML9	520036.00	4770154.31	300.85	301.70	1	5.07	295.78
					2	6.77	294.08
					3	8.47	292.38
					4	10.17	290.68
					5	11.87	288.98
					6	13.57	287.28
					7	15.27	285.58
					8	17.02	283.83
ML10	520037.37	4770153.01	300.92	301.45	1	6.33	294.59
					2	8.03	292.89
					3	9.73	291.19
					4	11.43	289.49
					5	13.13	287.79
					6	14.83	286.09
					7	16.53	284.39
					8	18.23	282.69
ML11	520038.80	4770151.82	300.91	301.35	1	6.38	294.53
					2	8.08	292.83
					3	9.78	291.13
					4	11.48	289.43
					5	13.18	287.73
					6	14.88	286.03
					7	16.58	284.33
					8	18.28	282.63
ML12	520044.84	4770165.49	300.49	301.20	1	5.71	294.78
					2	7.41	293.08
					3	9.11	291.38
					4	10.81	289.68
					5	12.51	287.98
					6	14.21	286.28
					7	15.91	284.58
					8	17.61	282.88

Table A.3: Construction and location information for the Solinst® CMT Multi-level Systems.

Well ID	[UTM NAD 83 17 N]		Ground Surface Elevation (masl)	Top of Casing Elevation (masl)	Port ID	Depth to Centre of Screen (mbgs)	Depth to Centre of Screen (masl)
	Easting (m)	Northing (m)					
WO74-ML	520051.31	4770151.86	300.81	301.28	1	4.17	296.64
					2	5.49	295.32
					3	7.01	293.80
					4	8.53	292.28
					5	10.36	290.45
					6	12.80	288.01
					7	14.63	286.18
WO75-ML	520014.39	4770113.06	302.82	303.22	1	3.81	299.01
					2	5.03	297.79
					3	7.47	295.35
					4	9.30	293.52
					5	11.13	291.69
					6	12.95	289.87
					7	14.78	288.04

Table A.4: Construction and location information for larger diameter, single-screen, existing monitoring wells.

Well ID	[UTM NAD 83 17 N]		Ground Surface Elevation	Top of Casing Elevation (masl)	Total Depth (masl)	Top of Screen Depth (masl)	Length of Screen (m)
	Easting (m)	Northing (m)					
WO74-S	520053.90	4770154.28	300.75	301.64	290.39	291.61	1.22
WO74-WT	520052.33	4770152.75	300.75	301.64	294.81	297.70	2.89
WO74-M	520055.03	4770154.97	300.74	301.63	287.02	288.24	1.22
WO74-D	520056.14	4770155.97	300.75	301.62	282.77	285.81	3.04
WO75-S	520015.09	4770112.00	302.68	303.58	292.32	293.84	1.52
WO75-D	520013.59	4770112.04	302.80	303.62	281.46	284.51	3.05
WO35	519977.82	4770190.29	302.57	303.00	295.87	297.39	1.52
WO02-D-14	520134.99	4770065.73	300.89	301.08	286.74	289.24	2.50

Appendix 9: Velocities for PVPs 1 and 2 with 2009 Tracer Testing

Ground Water Velocity Estimates for Chapter 4

Probe	Elevation	Injection Volume (mL)	Alpha (degrees)	Horizontal Velocity (cm/d)
1-1A#3&4	292	1		1270.99
1-2A#3&4	291	1		1085.01
1-3A#3&4	290	1		618.44
1-4A#3&4	289	1	123.89	2783.96
1-5A#3&4	288	5	44.62	126.08
1-6A#3&4	287	5	120.21	128.13
2-1A#3&4	292	5	13.52	758.05
2-2A#3&4	291	1	2.56	150.11
2-3A#3&4	290	1	6.43	372.53
2-4A#3&4	289	1	129.32	2640.88
2-5A#3&4	288			10*
2-6A#3&4	287			10*

* No breakthrough curve detectable, assumed 10 cm/d for plotting purposes

Multilevel	Elevation (masl)	Velocity (m/s)	Velocity (cm/d)
ML5-2	295.50	5.73E-05	495
ML5-3	293.80	1.79E-04	1547
ML5-4	292.10	2.42E-04	2092
ML5-5	290.40	3.24E-04	2803
ML5-6	288.70	6.12E-05	529
ML5-7	287.00	7.93E-05	685
ML6-2	293.46	1.16E-04	1003
ML6-3	291.76	1.74E-04	1499
ML6-4	290.06	3.15E-04	2724
ML6-6	286.66	1.19E-04	1026
ML6-7	284.96	2.04E-04	1760
ML7-2	293.44	5.54E-05	478
ML7-3	291.74	1.80E-04	1552
ML7-4	290.04	4.29E-04	3705
ML7-5	288.34	1.01E-04	871

Appendix 10: Hydraulic Conductivity from PVPs 1 and 2 Core

Grain-Size Analysis for PVP 1 and 2 Core

Core ID	Sample Elevation (masl)	Terzaghi Arithmetic Mean K (m/s)
Core 1-1	296.36	2.01E-04
Core 1-1	296.10	4.14E-04
Core 1-1	295.85	2.56E-04
Core 1-1	295.62	1.81E-04
Core 1-2	294.86	3.44E-04
Core 1-2	294.63	9.11E-04
Core 1-2	294.35	2.97E-03
Core 1-2	294.09	1.90E-03
Core 1-4	291.81	1.04E-04
Core 1-4	291.55	2.68E-04
Core 1-4	291.22	4.76E-04
Core 1-4	291.00	1.60E-03
Core 1-5	290.28	6.48E-04
Core 1-5	290.03	4.77E-03
Core 1-5	289.78	2.59E-03
Core 1-5	289.55	1.09E-03
Core 1-6	288.76	9.64E-05
Core 1-6	288.51	6.40E-03
Core 1-6	288.25	6.40E-03
Core 1-6	288.00	4.28E-05
Core 1-7	286.93	8.26E-05
Core 1-7	286.68	9.64E-05
Core 1-7	286.42	0.00E+00
Core 1-7	286.17	1.90E-05
Core 1-7	285.92	5.29E-05

Core ID	Sample Elevation (masl)	Terzaghi Arithmetic Mean K (m/s)
Core 2-1	296.15	4.77E-03
Core 2-1	295.89	1.02E-03
Core 2-1	295.64	1.71E-04
Core 2-1	295.46	5.29E-05
Core 2-1	295.28	5.58E-04
Core 2-2	294.62	1.27E-05
Core 2-2	294.37	4.14E-04
Core 2-2	294.04	4.28E-03
Core 2-2	293.78	3.38E-03
Core 2-3	293.00	2.23E-03
Core 2-3	292.74	1.32E-03
Core 2-3	292.49	9.55E-04
Core 2-4	291.47	1.60E-03
Core 2-4	291.22	4.76E-04
Core 2-4	290.96	1.07E-03
Core 2-5	290.05	2.11E-04
Core 2-5	289.80	5.29E-03
Core 2-5	289.31	0.00E+00
Core 2-5	289.06	3.82E-03
Core 2-5	288.80	4.60E-04
Core 2-5	288.55	8.25E-04
Core 2-6	288.53	9.55E-04
Core 2-6	288.27	5.41E-04
Core 2-6	288.07	1.27E-04
Core 2-6	287.81	4.00E-04
Core 2-6	287.59	1.90E-05
Core 2-6	287.33	1.17E-04
Core 2-7	287.00	1.19E-04
Core 2-7	286.75	4.29E-04
Core 2-7	286.54	2.97E-03
Core 2-7	286.21	8.26E-03
Core 2-7	285.96	5.58E-04

Appendix 11: 2010 Site Characterization Testing of PVPs 3, 4, and 5

PVP	Probe Depth (ft)	Estimated Probe Elevation (masl)	Horizontal Velocity (cm/d)	Alpha	Vertical Velocity (cm/d)- negative value is downward flow and positive is upward flow	Resultant Flow Magnitude (cm/d)	Measured Injection Port Orientation (Degrees from N)	Flow Direction (Degrees from N)	Vertical flow angle from horizontal	Launch time	mL Injected	Type of Tracer
3-1	22.00	293.99	157.26	49.20	229.38	278.11	336	286.80	55.57	11/6 @ 1035	1	DI Tracer
3-1	22.00	293.99	138.21	48.88	229.48	267.89	336	287.12	58.94	11/6 @ 13:00	1	DI Tracer
3-2	30.80	291.31	181.66	NA	201.40	271.22	336	NA	47.95	11/6 @ 13:00	1	DI Tracer
3-2	30.80	291.31	134.92	26.85	207.68	247.66	336	309.15	56.99	11/6 @ 13:50	5	DI Tracer
3-2	30.80	291.31	127.82	NA	0.00	127.82	336	NA	0.00	11/7 @ 8:30	5	NaClTracer
3-2	30.80	291.31	145.10	7.79	194.61	242.75	336	328.21	53.29	11/7 @ 10:20	7	NaClTracer
3-3	35.10	290.00	175.34	NA	187.15	256.45	336	NA	46.86	11/6 @ 13:00	1	DI Tracer
3-3	35.10	290.00	484.77	NA	165.56	512.26	336	NA	18.86	11/6 @ 13:50	5	DI Tracer
3-3	35.10	290.00	145.78	3.62	0.00	145.78	336	332.38	0.00	11/7 @ 8:30	5	NaClTracer
3-3	35.10	290.00	680.34	136.67	0.00	680.34	336	199.33	0.00	11/7 @ 10:20	7	NaClTracer
3-3	35.10	290.00	1538.7206	na	0.00	1538.72	336	NA	0.00	11/7 @ 12:20	10	NaClTracer
3-4	36.00	289.73	48.74	55.94	278.97	283.19	336	280.06	80.09	11/6 @ 13:00	1	DI Tracer
3-4	36.00	289.73	0.00	NA	410.47	410.47	336	NA	90.00	11/6 @ 13:50	5	DI Tracer
3-4	36.00	289.73	175.33	NA	0.00	175.33	336	NA	0.00	11/7 @ 8:30	5	NaClTracer
3-4	36.00	289.73	0.00	NA	-179.88	179.88	336	NA	90.00	11/7 @ 10:20	7	NaClTracer
3-4	36.00	289.73	103.39	11.62	-122.538	160.33	336	324.38	-49.85	11/7 @ 12:20	10	NaClTracer
3-5	36.75	289.50	77.25	NA	-150.92	169.54	336	NA	-62.89	11/7 @ 10:20	1	NaClTracer
3-5	36.75	289.50	31.42	38.48	-90.67	95.96	336	297.52	-70.89	11/7 @ 8:30	5	NaClTracer
3-6	40.00	288.51	906.94	NA	0.00	906.94	336	NA	0.00	11/7 @ 13:43	1	NaClTracer
3-6	40.00	288.51	1269.74	NA	0.00	1269.74	336	Na	0.00	11/7 @ 12:20	5	NaClTracer
3-7	45.75	286.76	115.08	NA	86.14997	143.75	336	NA	36.82	11/7 @ 13:43	1	NaClTracer
3-7	45.75	286.76	177.28	120.69	0.00	177.28	336	215.31	0.00	11/7 @ 12:20	5	NaClTracer
4-1	22.00	293.99	0.00	NA	1143.60	1143.60	336	NA	90.00	11/7 @ 1550	1	NaClTracer
4-1	22.00	293.99	2318.72	NA	694.76	2420.57	325	NA	16.68	11/8 @ 9:40	3	NaClTracer
4-1	22.00	293.99	1254.09	NA	66.23	1255.83	325	NA	3.02	11/8 @ 14:00	5	NaClTracer
4-1	22.00	293.99	2352.41	NA	635.21	2436.67	325	NA	15.11	11/7 @ 1520	5	NaClTracer
4-1	22.00	293.99	0.00	NA	845.25	845.25	325	NA	90.00	11/8 @ 8:46	5	NaClTracer
4-2	30.80	291.31	503.62	81.91	0.00	503.62	325	243.09	0.00	11/8 @ 9:40	3	NaClTracer
4-2	30.80	291.31	3078.63	136.56	0.00	3078.63	325	188.44	0.00	11/8 @ 14:00	5	NaClTracer

PVP	Probe Depth (ft)	Estimated Probe Elevation (masl)	Horizontal Velocity (cm/d)	Alpha	Vertical Velocity (cm/d)- negative value is downward flow and positive is upward flow	Resultant Flow Magnitude (cm/d)	Measured Injection Port Orientation (Degrees from N)	Flow Direction (Degrees from N)	Vertical flow angle from horizontal	Launch time	mL Injected	Type of Tracer
4-2	30.80	291.31	1345.65	124.91	2352.41	2710.10	325	200.09	60.23	11/7 @ 1520	5	NaClTracer
4-2	30.80	291.31	1440.15	122.89	3394.14	3687.03	325	202.11	67.01	11/8 @ 8:46	5	NaClTracer
4-3	35.10	290.00	521.96	15.80	1049.12	1171.79	325	309.20	63.55	11/8 @ 9:40	3	NaClTracer
4-3	35.10	290.00	976.23	NA	0.00	976.23	325	NA	0.00	11/8 @ 14:00	5	NaClTracer
4-3	35.10	290.00	1403.55	1.15	0.00	1403.55	325	323.85	0.00	11/7 @ 1520	5	NaClTracer
4-3	35.10	290.00	601.04	NA	-930.57	1107.79	325	NA	-57.14	11/8 @ 8:46	5	NaClTracer
4-4	36.00	289.73	1864.87	91.67	-1610.59	2464.09	325	233.33	-40.82	11/7 @ 1550	1	NaClTracer
4-4	36.00	289.73	3367.40	123.83	-1144.42	3556.55	325	201.17	-18.77	11/8 @ 9:40	3	NaClTracer
4-4	36.00	289.73	2369.50	126.28	0.00	2369.50	325	198.72	0.00	11/8 @ 14:00	5	NaClTracer
4-4	36.00	289.73	4015.73	128.74	-1425.51	4261.24	325	196.26	-19.54	11/7 @ 1520	5	NaClTracer
4-4	36.00	289.73	2013.23	NA	-1422.37	2465.00	325	NA	-35.24	11/8 @ 8:46	5	NaClTracer
4-5	36.75	289.50	1942.53	4.10	0.00	1942.53	325	320.90	0.00	11/8 @ 9:40	3	NaClTracer
4-5	36.75	289.50	1832.21	11.40	0.00	1832.21	325	313.60	0.00	11/8 @ 8:40	5	NaClTracer
4-6	40.00	288.51	631.52	11.94	1589.45	1710.31	325	313.06	68.33	11/8 @ 9:40	3	NaClTracer
4-7	45.75	286.76	0.00	NA	-266.98	266.98	325	NA	-90.00	11/8 @ 8:40	5	NaClTracer
5-1	22.00	293.99	174.77	12.32	0.00	174.77	325	312.68	0.00	11/8 @ 12:30	1	NaClTracer
5-1	22.00	293.99	215.11	NA	-464.22	511.64	325	NA	-65.14	11/8 @ 13:40	3	NaClTracer
5-1	22.00	293.99	138.18	2.19	-235.73	273.24	325	322.81	-59.62	11/8 @ 11:00	5	NaClTracer
5-2	30.80	291.31	692.36	NA	0.00	692.36	325	NA	0.00	11/8 @ 12:30	1	NaClTracer
5-2	30.80	291.31	467.78	NA	-121.78	483.38	325	NA	-14.59	11/8 @ 13:40	3	NaClTracer
5-2	30.80	291.31	491.34	NA	0.00	491.34	325	NA	0.00	11/8 @ 11:00	5	NaClTracer
5-3	35.10	290.00	285.53	NA	0.00	285.53	325	NA	0.00	11/8 @ 12:30	1	NaClTracer
5-3	35.10	290.00	177.33	15.68	0.00	177.33	325	309.32	0.00	11/8 @ 13:40	3	NaClTracer
5-3	35.10	290.00	247.93	NA	0.00	247.93	325	NA	0.00	11/8 @ 11:00	5	NaClTracer
5-4	36.00	289.73	0.00	NA	-180.47	180.47	325	NA	-90.00	11/8 @ 13:40	3	NaClTracer
5-4	36.00	289.73	0.00	NA	-170.12	170.12	325	NA	90.00	11/8 @ 11:00	5	NaClTracer
5-5	36.75	289.50	81.63	37.75	-286.91	298.30	325	287.25	-74.12	11/8 @ 13:40	3	NaClTracer
5-5	36.75	289.50	211.24	NA	-3273.69	3280.50	325	NA	-86.31	11/8 @ 11:00	5	NaClTracer
5-6	40.00	288.51	0.00	NA	335.52	335.52	325	NA	90.00	11/8 @ 12:30	1	NaClTracer

PVP	Probe Depth (ft)	Estimated Probe Elevation (masl)	Horizontal Velocity (cm/d)	Alpha	Vertical Velocity (cm/d)- negative value is downward flow and positive is upward flow	Resultant Flow Magnitude (cm/d)	Measured Injection Port Orientation (Degrees from N)	Flow Direction (Degrees from N)	Vertical flow angle from horizontal	Launch time	mL Injected	Type of Tracer
5-6	40.00	288.51	0.00	NA	169.83	169.83	325	NA	90.00	11/8 @ 13:40	3	NaClTracer
5-6	40.00	288.51	0.00	NA	140.48	140.48	325	NA	90.00	11/8 @ 11:00	5	NaClTracer
5-7	45.75	286.76	580.36	NA	-165.88	603.60	325	NA	-15.95	11/8 @ 12:30	1	NaClTracer
5-7	45.75	286.76	449.74	141.19	-98.36	460.37	325	183.81	-12.34	11/8 @ 13:40	3	NaClTracer
5-7	45.75	286.76	286.71	132.54	-221.07	362.04	325	192.46	-37.63	11/8 @ 11:00	5	NaClTracer

Appendix 12: Slug Testing Results

Slug Testing Results

Well	Screen top elevation (masl)	Screen bottom elevation (masl)	Screen elevation midpoint (masl)	Average K (m/s)	Standard Deviation	min K (m/s)	max K (m/s)	error bar low K (m/s)	error bar high K (m/s)
WO74 S	291.61	290.39	291.00	8.70E-04	3.50E-04	5.30E-04	1.70E-03	3.40E-04	8.30E-04
WO74 M	288.24	287.02	287.63	1.10E-03	4.50E-04	7.00E-04	2.00E-03	4.00E-04	9.00E-04
WO74 D	285.81	282.77	284.29	9.60E-04	4.30E-04	4.80E-04	1.50E-03	4.80E-04	5.40E-04
WO75 S	293.84	292.32	293.08	8.20E-04	1.00E-04	6.00E-04	9.40E-04	2.20E-04	1.20E-04

Appendix 13: Pre and Post Biostimulation PVP Data

Probe	Date	Elapsed Days from injection	Vertical V (cm/d) Negative = downard flow	Horizontal Velocity (cm/d)	Resultant Velocity (cm/d)	Horizontal Flow Direction (azimuth)	Verical Flow direction (degrees)
3_1	6/21/2011	-33	0	574	574	315	0
3_1	7/1/2011	-23	623	480	787	329	52
3_1	7/4/2011	-20	525	313	611	328	59
3_1	7/23/2011	-1	729	308	792	315	67
3_1	8/3/2011	10	426	975	1064	315	24
3_1	8/19/2011	26	303	494	579	314	31
3_1	8/24/2011	31	384	460	599	315	40
3_1	8/31/2011	38	174	0	174		90
3_1	9/8/2011	46	183	190	263	315	44
3_2	6/21/2011	-33	0	146	146	315	0
3_2	7/1/2011	-23	241	224	329	328	47
3_2	7/4/2011	-20	230	122	261	302	62
3_2	7/23/2011	-1	1137	166	1149	315	82
3_2	8/3/2011	10	0	147	147	315	0
3_2	8/19/2011	26	0	157	157	315	0
3_3	6/24/2011	-30	-1335	212	1352	315	-81
3_3	6/28/2011	-26	-730	203	757	311	-74
3_3	7/1/2011	-23	-933	706	1170	330	-53
3_3	7/4/2011	-20	0	89	89	322	0
3_3	8/3/2011	10	1624	306	1653	315	79
3_3	8/19/2011	26	370	0	370		90
3_4	6/24/2011	-30	550	215	590	315	69
3_4	6/28/2011	-26	73	154	171	330	25
3_4	7/4/2011	-20	0	313	313	328	0
3_4	7/23/2011	-1	1895	0	1895		90
3_4	8/3/2011	10	602	1058	1217	315	30
3_4	8/19/2011	26	1348	0	1348		90
3_4	8/24/2011	31	2228	0	2228		90
3_4	8/31/2011	38	934	0	934		90
3_4	9/8/2011	46	608	130	622	315	78
3_5	6/24/2011	-30	0	160	160	315	0
3_5	7/23/2011	-1	0	205	205	315	0
3_5	7/27/2011	3	557	161	580	315	74
3_5	8/3/2011	10	611	667	905	315	43
3_5	8/20/2011	27	294	256	390	315	49
3_5	8/25/2011	32	270	72	280	303	75
3_5	9/1/2011	39	289	156	328	315	62
3_5	9/10/2011	48	232	146	274	321	58
3_6	6/24/2011	-30	0	498	498	315	0
3_6	6/28/2011	-26	0	1633	1633	334	0
3_6	7/1/2011	-23	0	360	360	311	0
3_6	7/4/2011	-20	-212	298	366	333	-35

Probe	Date	Elapsed Days from injection	Vertical V (cm/d) Negative = downard flow	Horizontal Velocity (cm/d)	Resultant Velocity (cm/d)	Horizontal Flow Direction (azimuth)	Verical Flow direction (degrees)
3_6	7/23/2011	-1	0	454	454	327	0
3_6	7/27/2011	3	0	142	142	322	0
3_6	8/3/2011	10	0	505	505	233	0
3_6	8/20/2011	27	-205	175	270	230	-50
3_6	8/25/2011	32	-229	577	621	329	-22
3_6	9/1/2011	39	526	328	619	315	58
3_6	9/10/2011	48	206	0	206		90
3_7	6/24/2011	-30	-594	204	628	315	-71
3_7	6/28/2011	-26	0	199	199	314	0
3_7	7/1/2011	-23	0	264	264	331	0
3_7	7/4/2011	-20	0	404	404	335	0
3_7	7/23/2011	-1	307	947	996	333	18
3_7	7/27/2011	3	176	150	231	250	49
3_7	8/3/2011	10	0	148	148	315	0
3_7	8/20/2011	27	211	135	251	315	57
3_7	8/25/2011	32	203	339	395	332	31
3_7	9/1/2011	39	203	225	303	315	42
3_7	9/10/2011	48	224	272	352	315	39
4_1	6/24/2011	-30	652	817	1045	317	39
4_2	6/22/2011	-32	0	1131	1131	315	0
4_2	6/27/2011	-27	819	999	1292	322	39
4_2	7/9/2011	-15	490	600	774	322	39
4_2	7/25/2011	1	1207	934	1527	322	52
4_2	7/28/2011	4	0	288	288	312	0
4_2	9/2/2011	40	1327	360	1375	317	75
4_2	9/9/2011	47	1106	648	1282	321	60
4_3	6/24/2011	-30	-1092	0	1092		-90
4_3	9/2/2011	40	0	222	222	315	0
4_4	6/24/2011	-30	-1679	2013	2622	315	-40
4_4	7/25/2011	1	0	744	744	287	0
4_4	7/28/2011	4	-695	573	901	247	-50
4_4	9/2/2011	40	519	1268	1370	315	22
4_4	9/9/2011	47	1849	1051	2127	322	60
4_5	6/24/2011	-30		632	632	292	0
4_5	6/27/2011	-27	0	387	387	284	0
4_5	7/4/2011	-20	0	406	406	320	0
4_5	7/25/2011	1	0	192	192	304	0
4_5	7/28/2011	4	0	94	94	298	0
4_5	8/1/2011	8	563	272	626	316	64
4_5	8/13/2011	20	0	428	428	324	0
4_5	8/27/2011	34	0	425	425	318	0
4_5	9/3/2011	41	0	477	477	320	0

Probe	Date	Elapsed Days from injection	Vertical V (cm/d) Negative = downard flow	Horizontal Velocity (cm/d)	Resultant Velocity (cm/d)	Horizontal Flow Direction (azimuth)	Verical Flow direction (degrees)
4_5	9/11/2011	49	0	451	451	323	0
4_6	6/24/2011	-30	-508	1448	1534	315	-19
4_6	7/25/2011	1	0	321	321	315	0
4_6	7/28/2011	4	-128	0	128		-90
4_6	8/1/2011	8	-553	524	762	323	-47
4_7	6/24/2011	-30	-1014	275	1050	310	-75
4_7	6/28/2011	-26	-4743	245	4750	234	-87
4_7	7/4/2011	-20	-4928	801	4993	315	-81
4_7	7/25/2011	1	-634	0	634		-90
4_7	7/28/2011	4	-611	362	710	322	-59
4_7	8/1/2011	8	1221	207	1239	315	80
4_7	8/13/2011	20	-1295	157	1304	317	-83
4_7	8/27/2011	34	-1238	213	1256	221	-80
4_7	9/3/2011	41	-1539	961	1814	315	-58
4_7	9/11/2011	49	7432	914	7488	323	83
5_1	6/25/2011	-29	143	180	230	315	38
5_1	7/1/2011	-23	0	223	223	323	0
5_1	7/4/2011	-20	-161	197	254	313	-39
5_1	8/22/2011	29	0	248	248	313	0
5_2	6/25/2011	-29	-1334	1399	1933	315	-44
5_2	7/4/2011	-20	-169	0	169		-90
5_2	7/26/2011	2	-362	296	468	305	-51
5_2	8/22/2011	29	279	1102	1137	305	14
5_3	6/22/2011	-32	0	421	421	291	0
5_3	7/4/2011	-20	0	103	103	283	0
5_3	7/26/2011	2	0	197	197	318	0
5_3	8/2/2011	9	155	119	195	305	52
5_3	8/22/2011	29	533	529	751	325	45
5_4	6/22/2011	-32	-825	596	1018	318	-54
5_4	7/4/2011	-20	-289	0	289		-90
5_4	7/26/2011	2	-4353	0	4353		-90
5_4	8/2/2011	9	-4400	0	4400		-90
5_4	8/22/2011	29	1445	654	1586	223	66
5_5	6/25/2011	-29	458	257	525	315	61
5_5	7/1/2011	-23	-291	191	348	315	-57
5_5	7/26/2011	2	-626	393	739	318	-58
5_5	8/5/2011	12	0	473	473	315	0
5_5	8/16/2011	23	0	204	204	315	0
5_5	8/23/2011	30	423	203	469	315	64
5_5	8/30/2011	37	1093	200	1112	315	80
5_5	9/6/2011	44	744	192	768	315	76
5_6	6/25/2011	-29	801	1015	1293	284	38

Probe	Date	Elapsed Days from injection	Vertical V (cm/d) Negative = downard flow	Horizontal Velocity (cm/d)	Resultant Velocity (cm/d)	Horizontal Flow Direction (azimuth)	Verical Flow direction (degrees)
5_6	7/1/2011	-23	-238	145	279	321	-59
5_6	7/26/2011	2	-835	576	1014	315	-55
5_6	8/5/2011	12	-1094	666	1281	322	-59
5_6	8/16/2011	23	590	1930	2018	315	17
5_6	8/30/2011	37	123	0	123		90
5_6	9/6/2011	44	300	133	328	315	66
5_7	6/25/2011	-29	250	261	361	313	44
5_7	7/1/2011	-23	223	163	276	308	54
5_7	7/26/2011	2	0	382	382	315	0
5_7	8/5/2011	12	694	671	965	324	46
5_7	8/16/2011	23	0	140	140	315	0
5_7	8/30/2011	37	-784	121	794	315	-81
5_7	9/6/2011	44	0	319	319	302	0

Less than ideal observed or calculated data

Fixed flow direction to 315° Azimuth needed to obtain velocity due to poor data on one horizontal detector

Appendix 14: Pre and Post Biostimulation Flow Direction Rose Diagrams

	Background	Biostimulated
WO 77, WO75s, WO74S	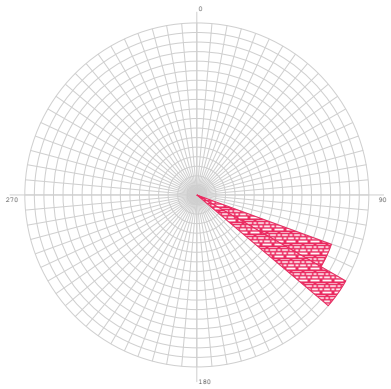	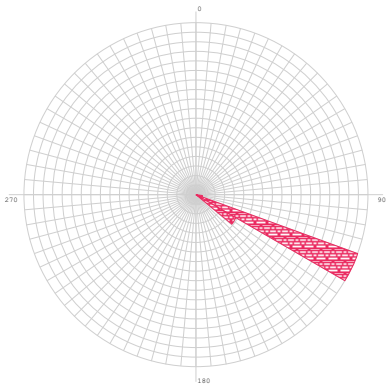
WO 77, WO80, WO74S	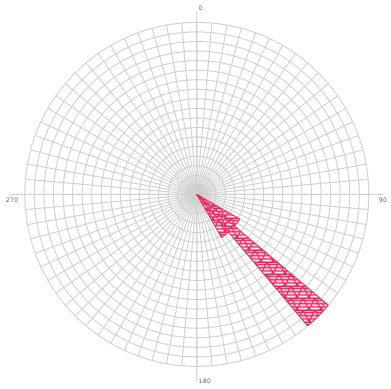	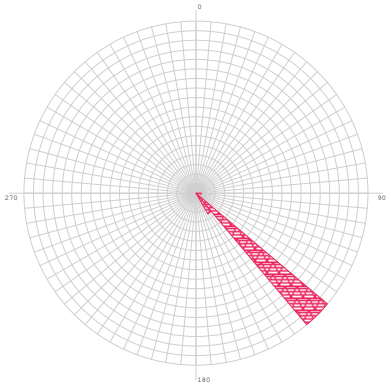
WO78, WO79, WO74WT	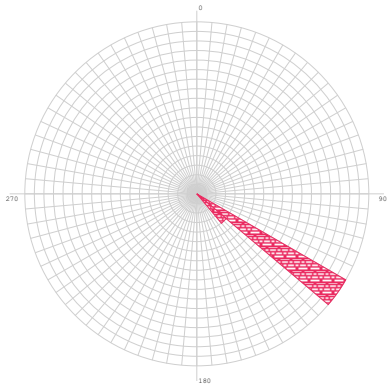	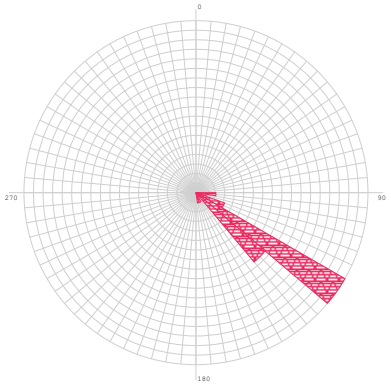
WO78, WO79, WO74S	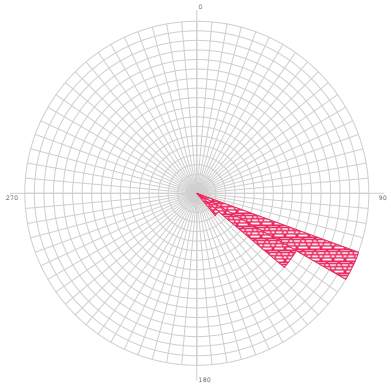	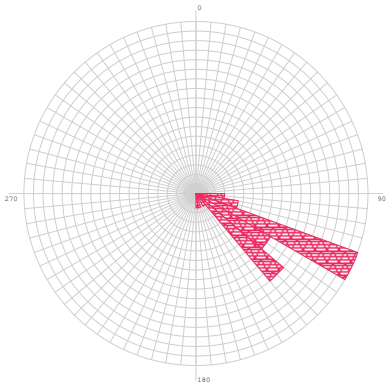

	Prior to biostimulation	After biostimulation	pre μ / post μ p value	pre σ^2 / post σ^2 p value
PVP 3	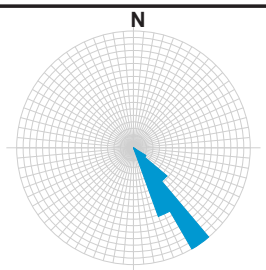	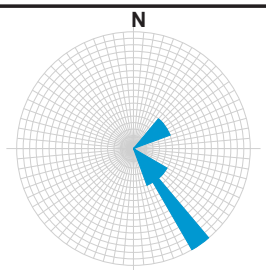	145/112	94/1804
			0.03	1.61 X 10^{-6}
PVP 4	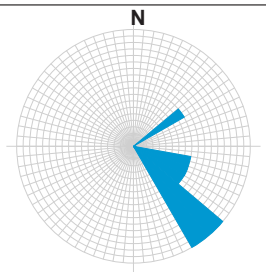	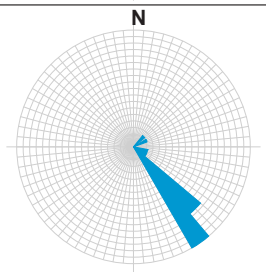	120/127	910/784
			0.29	0.74
PVP 5	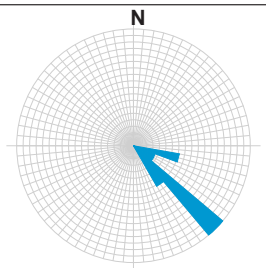	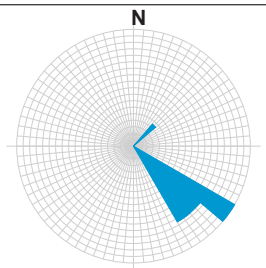	128/126	212/816
			0.13	0.04
Well-Sorted	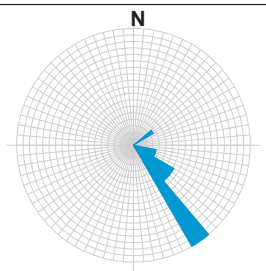	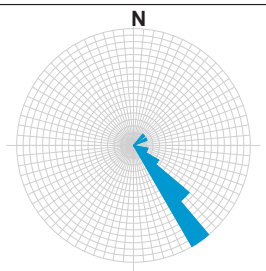	108/129	784/807
			0.13	0.99
Poorly-Sorted	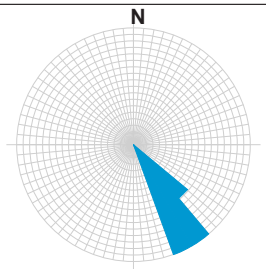	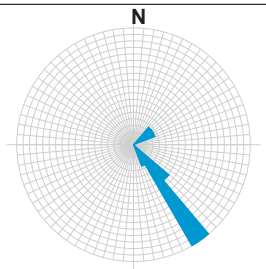	146/138	77/1613
			0.05	8.94 X 10^{-6}

	Prior to biostimulation	After biostimulation	pre μ / post μ p value	pre σ^2 / post σ^2 p value
PVP 3	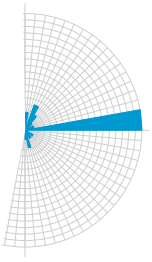	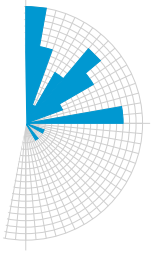	9/45	2079/1341
			8.79×10^{-4}	0.24
PVP 4		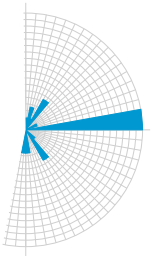	-21/-2	2378/2981
			0.14	0.70
PVP 5	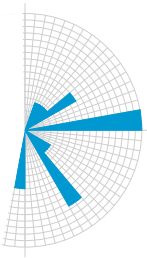	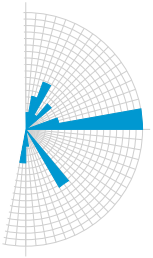	-12/5	2550/3120
			0.15	0.69
Well-Sorted	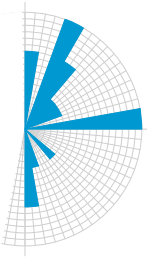	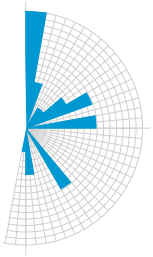	18/19	3381/3851
			0.49	0.80
Poorly-Sorted	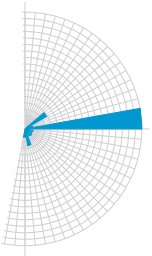	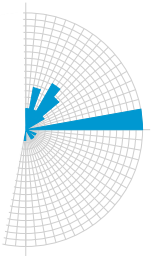	-12/27	1302/1865
			1.85×10^{-4}	0.36

Appendix 15: CLOUDPE Output Files from Biostimulation CIS Tracer Testing

ML5-2 July 2011

S I M P L E X O P T I M I Z A T I O N

C L O U D P E

INPUT SETTINGS

---

1) THE NUMBER OF OBSERVATIONS (MAX 60) : 13
2) THE NUMBER OF PARAMETERS TO DETERMINE : 6
3) THE NUMBER OF VARIABLES (X,Y,Z,. . .) : 2
4) THE DIFFUSION COEFFICIENT (M^2/SEC) : 0.1000E-09
5) THE DISTANCE FROM SOURCE (M) : 2.690

INITIAL GUESSES OF PARAMETERS

---

6) THE EFFECTIVE POROSITY (DIM) : -0.3300
7) THE FLOW VELOCITY (M/SEC) : 0.4340E-04
8) THE RETARDATION FACTOR : -1.000
9) THE DISPERSIVITY (M) : 1.500
10) THE CONTAMINANT MASS INJECTED (MG) : 0.1000E+09
11) THE FIRST ORDER DECAY CONST (/SEC) : 0.0000E+00
12) TYPE OF WEIGHTING : N

OPTIMIZED PARAMETER ESTIMATES:

VEL= 0.5784E-04
DISPERSIVITY= 0.9795
MASS= 0.1475E+06
POROSITY= 0.3300
LAMBDA= 0.0000E+00
Rf= 1.000

RESIDUAL SUM OF SQUARES = 1611.

THE F STATISTIC FOR NP= 3 NOBS= 13 IS: 3.71
THE CRITICAL RSS IS: 3403.

THE 95% CONFIDENCE INTERVALS ARE:

PARAMETER	BEST FIT	FROM (-VE=<95% CONF)	TO
X(1)	0.5784E-04	0.440E-04	0.752E-04
X(2)	0.9795	0.980	0.980
X(3)	0.1475E+06	0.133E+06	0.147E+06

TIME (HOURS)	OBS. CONC.	CALC. CONC.	RESIDUALS
0.1000E-53	20.73	0.0000E+00	20.73
0.3667	13.88	0.5577E-07	13.88
0.6500	15.56	0.1564E-02	15.56
1.100	12.12	0.3119	11.81
1.600	13.57	3.130	10.44
3.600	36.70	40.82	-4.121
4.167	50.70	51.48	-0.7804
4.650	47.46	59.25	-11.79
5.150	80.57	65.98	14.59
10.48	89.15	83.67	5.482
12.32	70.83	79.41	-8.579
14.85	69.45	71.48	-2.031
17.23	68.03	63.51	4.523
0.7832		0.1440E-01	
1.566		2.813	
2.350		14.55	
3.133		31.06	
3.916		46.95	
4.699		59.97	
5.482		69.74	
6.265		76.61	
7.049		81.08	
7.832		83.68	
8.615		84.84	
9.398		84.89	
10.18		84.13	
10.96		82.76	
11.75		80.94	
12.53		78.81	
13.31		76.46	
14.10		73.96	
14.88		71.38	
15.66		68.76	

ML5-2 Sept 2011

S I M P L E X O P T I M I Z A T I O N

C L O U D P E

INPUT SETTINGS

---

1) THE NUMBER OF OBSERVATIONS (MAX 60) : 26
2) THE NUMBER OF PARAMETERS TO DETERMINE : 6
3) THE NUMBER OF VARIABLES (X,Y,Z,. . .) : 2
4) THE DIFFUSION COEFFICIENT (M^2/SEC) : 0.1000E-09
5) THE DISTANCE FROM SOURCE (M) : 2.690

INITIAL GUESSES OF PARAMETERS

---

6) THE EFFECTIVE POROSITY (DIM) : -0.3300
7) THE FLOW VELOCITY (M/SEC) : 0.5200E-04
8) THE RETARDATION FACTOR : -1.000
9) THE DISPERSIVITY (M) : -0.3800
10) THE CONTAMINANT MASS INJECTED (MG) : 0.1000E+06
11) THE FIRST ORDER DECAY CONST (/SEC) : 0.0000E+00
12) TYPE OF WEIGHTING : N

OPTIMIZED PARAMETER ESTIMATES:

VEL= 0.5715E-04
DISPERSIVITY= 0.3800
MASS= 0.1982E+05
POROSITY= 0.3300
LAMBDA= 0.0000E+00
Rf= 1.000

RESIDUAL SUM OF SQUARES = 206.9

THE F STATISTIC FOR NP= 2 NOBS= 26 IS: 3.40
THE CRITICAL RSS IS: 265.5

THE 95% CONFIDENCE INTERVALS ARE:

PARAMETER	BEST FIT	FROM (-VE=<95% CONF)	TO
X(1)	0.5715E-04	0.509E-04	0.640E-04
X(3)	0.1982E+05	0.178E+05	0.202E+05

TIME (HOURS)	OBS. CONC.	CALC. CONC.	RESIDUALS
0.1000E-12	0.0000E+00	0.0000E+00	0.0000E+00
0.6333	0.0000E+00	0.3258E-12	-0.3258E-12
1.083	3.123	0.9105E-06	3.123
1.617	0.0000E+00	0.8041E-03	-0.8041E-03
2.100	4.600	0.1777E-01	4.582
2.617	0.0000E+00	0.1309	-0.1309
3.117	0.0000E+00	0.4629	-0.4629
3.600	3.529	1.092	2.437
4.083	0.0000E+00	2.055	-2.055
4.600	0.0000E+00	3.414	-3.414
5.100	3.499	4.961	-1.462
5.600	2.888	6.635	-3.747
6.083	14.01	8.279	5.731
6.600	15.27	9.984	5.286
7.100	11.50	11.52	-0.1509E-01
7.883	13.80	13.59	0.2132
8.950	15.39	15.66	-0.2710
10.68	16.47	17.24	-0.7742
12.05	15.10	17.25	-2.154
13.05	17.20	16.78	0.4234
14.07	14.77	16.00	-1.234
14.98	13.60	15.15	-1.554
18.20	10.57	11.69	-1.116
21.17	8.735	8.664	0.7081E-01
25.20	7.576	5.482	2.094
27.95	11.80	3.927	7.873

ML5-3 July 2011

S I M P L E X O P T I M I Z A T I O N

C L O U D P E

INPUT SETTINGS

---

1) THE NUMBER OF OBSERVATIONS (MAX 60) : 12
2) THE NUMBER OF PARAMETERS TO DETERMINE : 6
3) THE NUMBER OF VARIABLES (X,Y,Z,. . .) : 2
4) THE DIFFUSION COEFFICIENT (M^2/SEC) : 0.1000E-09
5) THE DISTANCE FROM SOURCE (M) : 2.690

INITIAL GUESSES OF PARAMETERS

---

6) THE EFFECTIVE POROSITY (DIM) : -0.3300
7) THE FLOW VELOCITY (M/SEC) : 0.5200E-04
8) THE RETARDATION FACTOR : -1.000
9) THE DISPERSIVITY (M) : -0.8500
10) THE CONTAMINANT MASS INJECTED (MG) : 0.1000E+06
11) THE FIRST ORDER DECAY CONST (/SEC) : 0.0000E+00
12) TYPE OF WEIGHTING : N

OPTIMIZED PARAMETER ESTIMATES:

VEL= 0.6065E-04
DISPERSIVITY= 0.8500
MASS= 0.4359E+06
POROSITY= 0.3300
LAMBDA= 0.0000E+00
Rf= 1.000

RESIDUAL SUM OF SQUARES = 6702.

THE F STATISTIC FOR NP= 2 NOBS= 12 IS: 4.10
THE CRITICAL RSS IS: 0.1220E+05

THE 95% CONFIDENCE INTERVALS ARE:

PARAMETER	BEST FIT	FROM (-VE=<95% CONF)	TO
X(1)	0.6065E-04	0.522E-04	0.704E-04
X(3)	0.4359E+06	0.392E+06	0.436E+06

TIME (HOURS)	OBS. CONC.	CALC. CONC.	RESIDUALS
0.1000E-08	14.95	0.0000E+00	14.95
0.3833	14.84	0.5996E-07	14.84
0.7000	16.87	0.4313E-02	16.87
1.150	25.43	0.7600	24.67
1.633	36.42	7.585	28.84
3.650	166.6	120.6	45.96
4.217	131.1	155.0	-23.88
4.667	170.8	178.9	-8.052
5.183	192.1	202.1	-10.03
10.50	267.4	261.6	5.814
12.33	219.7	246.3	-26.63
14.87	248.8	218.1	30.70
0.6759		0.2676E-02	
1.352		2.453	
2.028		21.21	
2.704		58.49	
3.380		103.0	
4.055		145.6	
4.731		182.0	
5.407		210.9	
6.083		232.6	
6.759		248.0	
7.435		258.1	
8.111		264.0	
8.787		266.4	
9.463		266.0	
10.14		263.6	
10.81		259.5	
11.49		254.2	
12.17		248.0	
12.84		241.0	
13.52		233.7	

ML5-3 Sept 2011

S I M P L E X O P T I M I Z A T I O N

C L O U D P E

INPUT SETTINGS

---

1) THE NUMBER OF OBSERVATIONS (MAX 60) : 25
2) THE NUMBER OF PARAMETERS TO DETERMINE : 6
3) THE NUMBER OF VARIABLES (X,Y,Z,. . .) : 2
4) THE DIFFUSION COEFFICIENT (M^2/SEC) : 0.1000E-09
5) THE DISTANCE FROM SOURCE (M) : 2.690

INITIAL GUESSES OF PARAMETERS

---

6) THE EFFECTIVE POROSITY (DIM) : -0.3300
7) THE FLOW VELOCITY (M/SEC) : 0.1290E-03
8) THE RETARDATION FACTOR : -1.000
9) THE DISPERSIVITY (M) : -0.5000
10) THE CONTAMINANT MASS INJECTED (MG) : 0.1000E+06
11) THE FIRST ORDER DECAY CONST (/SEC) : 0.0000E+00
12) TYPE OF WEIGHTING : N

OPTIMIZED PARAMETER ESTIMATES:

VEL= 0.1389E-03
DISPERSIVITY= 0.5000
MASS= 0.3894E+06
POROSITY= 0.3300
LAMBDA= 0.0000E+00
Rf= 1.000

RESIDUAL SUM OF SQUARES = 0.3783E+05

THE F STATISTIC FOR NP= 2 NOBS= 25 IS: 3.42
THE CRITICAL RSS IS: 0.4908E+05

THE 95% CONFIDENCE INTERVALS ARE:

PARAMETER	BEST FIT	FROM (-VE=<95% CONF)	TO
X(1)	0.1389E-03	0.125E-03	0.156E-03
X(3)	0.3894E+06	0.350E+06	0.409E+06

TIME (HOURS)	OBS. CONC.	CALC. CONC.	RESIDUALS
0.7000	27.40	0.3181	27.08
1.150	104.8	12.68	92.12
1.667	140.6	65.17	75.43
2.150	165.2	134.9	30.31
2.667	207.2	204.4	2.803
3.167	203.2	254.1	-50.88
3.650	246.0	283.8	-37.83
4.133	274.4	298.0	-23.65
4.650	334.4	300.0	34.39
5.150	334.4	292.6	41.77
5.633	230.0	279.7	-49.74
6.150	268.8	262.1	6.692
6.650	188.4	243.0	-54.63
7.233	244.8	219.9	24.90
7.933	263.6	192.5	71.05
9.000	197.2	154.3	42.93
10.73	108.0	104.4	3.614
12.10	49.90	75.34	-25.44
13.08	35.59	59.32	-23.73
14.13	35.58	45.74	-10.16
15.03	25.70	36.52	-10.82
18.25	11.18	16.13	-4.954
21.22	8.045	7.529	0.5160
25.27	3.301	2.648	0.6529
28.00	2.875	1.308	1.567

ML5-4 July 2011

S I M P L E X O P T I M I Z A T I O N

C L O U D P E

INPUT SETTINGS

---

1) THE NUMBER OF OBSERVATIONS (MAX 60) : 13
2) THE NUMBER OF PARAMETERS TO DETERMINE : 6
3) THE NUMBER OF VARIABLES (X,Y,Z,. . .) : 2
4) THE DIFFUSION COEFFICIENT (M^2/SEC) : 0.1000E-09
5) THE DISTANCE FROM SOURCE (M) : 2.690

INITIAL GUESSES OF PARAMETERS

---

6) THE EFFECTIVE POROSITY (DIM) : -0.3300
7) THE FLOW VELOCITY (M/SEC) : 0.2200E-03
8) THE RETARDATION FACTOR : -1.000
9) THE DISPERSIVITY (M) : -0.3800
10) THE CONTAMINANT MASS INJECTED (MG) : 0.1000E+06
11) THE FIRST ORDER DECAY CONST (/SEC) : 0.0000E+00
12) TYPE OF WEIGHTING : N

OPTIMIZED PARAMETER ESTIMATES:

VEL= 0.1704E-03
DISPERSIVITY= 0.3800
MASS= 0.4797E+06
POROSITY= 0.3300
LAMBDA= 0.0000E+00
Rf= 1.000

RESIDUAL SUM OF SQUARES = 0.4880E+05

THE F STATISTIC FOR NP= 2 NOBS= 13 IS: 3.98
THE CRITICAL RSS IS: 0.8412E+05

THE 95% CONFIDENCE INTERVALS ARE:

PARAMETER	BEST FIT	FROM (-VE=<95% CONF)	TO
X(1)	0.1704E-03	0.123E-03	0.218E-03
X(3)	0.4797E+06	0.432E+06	0.628E+06

TIME (HOURS)	OBS. CONC.	CALC. CONC.	RESIDUALS
0.1000E-08	21.02	0.0000E+00	21.02
0.4333	25.62	0.6231E-03	25.62
0.7667	68.75	0.9867	67.76
1.183	134.6	23.65	111.0
1.667	175.5	110.0	65.47
3.700	304.5	419.5	-115.0
4.250	405.2	411.3	-6.067
4.683	403.1	389.5	13.63
5.200	461.8	353.7	108.1
10.52	26.61	61.77	-35.16
12.37	18.96	30.15	-11.19
14.90	11.22	11.01	0.2145
17.28	0.0000E+00	4.201	-4.201
0.7855		1.232	
1.571		88.63	
2.356		273.5	
3.142		392.9	
3.927		419.5	
4.713		387.6	
5.498		330.7	
6.284		268.8	
7.069		211.7	
7.855		163.2	
8.640		124.0	
9.425		93.18	
10.21		69.47	
11.00		51.47	
11.78		37.96	
12.57		27.89	
13.35		20.44	
14.14		14.94	
14.92		10.90	
15.71		7.942	

ML5-4 Sept 2011

S I M P L E X O P T I M I Z A T I O N

C L O U D P E

INPUT SETTINGS

---

1) THE NUMBER OF OBSERVATIONS (MAX 60) : 25
2) THE NUMBER OF PARAMETERS TO DETERMINE : 6
3) THE NUMBER OF VARIABLES (X,Y,Z,. . .) : 2
4) THE DIFFUSION COEFFICIENT (M^2/SEC) : 0.1000E-09
5) THE DISTANCE FROM SOURCE (M) : 2.690

INITIAL GUESSES OF PARAMETERS

---

6) THE EFFECTIVE POROSITY (DIM) : -0.3300
7) THE FLOW VELOCITY (M/SEC) : 0.1290E-03
8) THE RETARDATION FACTOR : -1.000
9) THE DISPERSIVITY (M) : -0.5000
10) THE CONTAMINANT MASS INJECTED (MG) : 0.1000E+06
11) THE FIRST ORDER DECAY CONST (/SEC) : 0.0000E+00
12) TYPE OF WEIGHTING : N

OPTIMIZED PARAMETER ESTIMATES:

VEL= 0.1389E-03
DISPERSIVITY= 0.5000
MASS= 0.3894E+06
POROSITY= 0.3300
LAMBDA= 0.0000E+00
Rf= 1.000

RESIDUAL SUM OF SQUARES = 0.3783E+05

THE F STATISTIC FOR NP= 2 NOBS= 25 IS: 3.42
THE CRITICAL RSS IS: 0.4908E+05

THE 95% CONFIDENCE INTERVALS ARE:

PARAMETER	BEST FIT	FROM (-VE=<95% CONF)	TO
X(1)	0.1389E-03	0.125E-03	0.156E-03
X(3)	0.3894E+06	0.350E+06	0.409E+06

TIME (HOURS)	OBS. CONC.	CALC. CONC.	RESIDUALS
0.7000	27.40	0.3181	27.08
1.150	104.8	12.68	92.12
1.667	140.6	65.17	75.43
2.150	165.2	134.9	30.31
2.667	207.2	204.4	2.803
3.167	203.2	254.1	-50.88
3.650	246.0	283.8	-37.83
4.133	274.4	298.0	-23.65
4.650	334.4	300.0	34.39
5.150	334.4	292.6	41.77
5.633	230.0	279.7	-49.74
6.150	268.8	262.1	6.692
6.650	188.4	243.0	-54.63
7.233	244.8	219.9	24.90
7.933	263.6	192.5	71.05
9.000	197.2	154.3	42.93
10.73	108.0	104.4	3.614
12.10	49.90	75.34	-25.44
13.08	35.59	59.32	-23.73
14.13	35.58	45.74	-10.16
15.03	25.70	36.52	-10.82
18.25	11.18	16.13	-4.954
21.22	8.045	7.529	0.5160
25.27	3.301	2.648	0.6529
28.00	2.875	1.308	1.567

ML5-5 July 2011

S I M P L E X O P T I M I Z A T I O N

C L O U D P E

INPUT SETTINGS

---

1) THE NUMBER OF OBSERVATIONS (MAX 60) : 13
2) THE NUMBER OF PARAMETERS TO DETERMINE : 6
3) THE NUMBER OF VARIABLES (X,Y,Z,. . .) : 2
4) THE DIFFUSION COEFFICIENT (M^2/SEC) : 0.1000E-09
5) THE DISTANCE FROM SOURCE (M) : 2.690

INITIAL GUESSES OF PARAMETERS

---

6) THE EFFECTIVE POROSITY (DIM) : -0.3300
7) THE FLOW VELOCITY (M/SEC) : 0.1700E-03
8) THE RETARDATION FACTOR : -1.000
9) THE DISPERSIVITY (M) : -0.6000
10) THE CONTAMINANT MASS INJECTED (MG) : 0.1000E+06
11) THE FIRST ORDER DECAY CONST (/SEC) : 0.0000E+00
12) TYPE OF WEIGHTING : N

OPTIMIZED PARAMETER ESTIMATES:

VEL= 0.2071E-03
DISPERSIVITY= 0.6000
MASS= 0.5387E+06
POROSITY= 0.3300
LAMBDA= 0.0000E+00
Rf= 1.000

RESIDUAL SUM OF SQUARES = 0.3410E+05

THE F STATISTIC FOR NP= 2 NOBS= 13 IS: 3.98
THE CRITICAL RSS IS: 0.5877E+05

THE 95% CONFIDENCE INTERVALS ARE:

PARAMETER	BEST FIT	FROM (-VE=<95% CONF	TO
X(1)	0.2071E-03	0.168E-03	0.251E-03
X(3)	0.5387E+06	0.485E+06	0.609E+06

TIME (HOURS)	OBS. CONC.	CALC. CONC.	RESIDUALS
0.1000E-12	19.87	0.0000E+00	19.87
0.3333	56.97	0.5435E-01	56.92
0.8000	168.9	36.01	132.9
1.233	180.0	149.7	30.33
1.717	222.1	275.1	-53.01
3.750	293.2	355.0	-61.80
4.283	357.4	321.9	35.48
4.700	352.5	293.6	58.93
5.217	259.0	258.4	0.5698
10.53	29.95	51.64	-21.69
12.38	21.32	28.39	-7.073
14.92	12.58	12.42	0.1576
17.30	4.634	5.717	-1.083
0.7864		33.42	
1.573		242.2	
2.359		365.0	
3.145		380.1	
3.932		344.4	
4.718		292.3	
5.505		239.6	
6.291		192.4	
7.077		152.6	
7.864		120.1	
8.650		93.99	
9.436		73.28	
10.22		57.00	
11.01		44.26	
11.80		34.32	
12.58		26.59	
13.37		20.59	
14.15		15.94	
14.94		12.34	
15.73		9.548	

ML5-5 Sept 2011

S I M P L E X O P T I M I Z A T I O N

C L O U D P E

INPUT SETTINGS

---

1) THE NUMBER OF OBSERVATIONS (MAX 60) : 26
2) THE NUMBER OF PARAMETERS TO DETERMINE : 6
3) THE NUMBER OF VARIABLES (X,Y,Z,. . .) : 2
4) THE DIFFUSION COEFFICIENT (M^2/SEC) : 0.1000E-09
5) THE DISTANCE FROM SOURCE (M) : 2.690

INITIAL GUESSES OF PARAMETERS

---

6) THE EFFECTIVE POROSITY (DIM) : -0.3300
7) THE FLOW VELOCITY (M/SEC) : 0.2150E-03
8) THE RETARDATION FACTOR : -1.000
9) THE DISPERSIVITY (M) : -1.000
10) THE CONTAMINANT MASS INJECTED (MG) : 0.1000E+06
11) THE FIRST ORDER DECAY CONST (/SEC) : 0.0000E+00
12) TYPE OF WEIGHTING : N

OPTIMIZED PARAMETER ESTIMATES:

VEL= 0.2056E-03
DISPERSIVITY= 1.000
MASS= 0.5171E+06
POROSITY= 0.3300
LAMBDA= 0.0000E+00
Rf= 1.000

RESIDUAL SUM OF SQUARES = 0.7439E+05

THE F STATISTIC FOR NP= 2 NOBS= 26 IS: 3.40
THE CRITICAL RSS IS: 0.9547E+05

THE 95% CONFIDENCE INTERVALS ARE:

PARAMETER	BEST FIT	FROM (-VE=<95% CONF	TO
X(1)	0.2056E-03	0.173E-03	0.249E-03
X(3)	0.5171E+06	0.465E+06	0.589E+06

TIME (HOURS)	OBS. CONC.	CALC. CONC.	RESIDUALS
0.1000E-12	0.0000E+00	0.0000E+00	0.0000E+00
0.7333	150.4	71.77	78.63
1.167	168.8	181.2	-12.37
1.700	206.0	262.2	-56.23
2.167	257.6	290.4	-32.80
2.683	251.2	294.7	-43.47
3.183	311.2	284.6	26.64
3.667	330.8	268.3	62.55
4.183	324.8	247.8	76.95
4.683	318.8	227.3	91.51
5.167	45.00	207.8	-162.8
5.667	290.4	188.5	101.9
6.167	151.2	170.6	-19.43
6.667	112.4	154.1	-41.72
7.200	160.2	138.1	22.13
7.950	103.3	118.1	-14.79
9.017	73.50	94.38	-20.88
10.75	39.32	65.53	-26.21
12.12	19.12	49.14	-30.02
13.13	18.54	39.77	-21.23
14.15	13.54	32.15	-18.61
15.05	6.569	26.67	-20.10
18.27	4.884	13.72	-8.840
21.25	2.881	7.470	-4.589
25.28	3.020	3.309	-0.2888
28.02	1.027	1.911	-0.8837

ML5-6 July 2011

S I M P L E X O P T I M I Z A T I O N

C L O U D P E

INPUT SETTINGS

---

1) THE NUMBER OF OBSERVATIONS (MAX 60) : 13
2) THE NUMBER OF PARAMETERS TO DETERMINE : 6
3) THE NUMBER OF VARIABLES (X,Y,Z,. . .) : 2
4) THE DIFFUSION COEFFICIENT (M^2/SEC) : 0.1000E-09
5) THE DISTANCE FROM SOURCE (M) : 2.690

INITIAL GUESSES OF PARAMETERS

---

6) THE EFFECTIVE POROSITY (DIM) : -0.3300
7) THE FLOW VELOCITY (M/SEC) : 0.3880E-04
8) THE RETARDATION FACTOR : -1.000
9) THE DISPERSIVITY (M) : -1.580
10) THE CONTAMINANT MASS INJECTED (MG) : 0.1000E+06
11) THE FIRST ORDER DECAY CONST (/SEC) : 0.0000E+00
12) TYPE OF WEIGHTING : N

OPTIMIZED PARAMETER ESTIMATES:

VEL= 0.3732E-04
DISPERSIVITY= 1.580
MASS= 0.1931E+06
POROSITY= 0.3300
LAMBDA= 0.0000E+00
Rf= 1.000

RESIDUAL SUM OF SQUARES = 1613.

THE F STATISTIC FOR NP= 2 NOBS= 13 IS: 3.98
THE CRITICAL RSS IS: 2780.

THE 95% CONFIDENCE INTERVALS ARE:

PARAMETER	BEST FIT	FROM (-VE=<95% CONF)	TO
X(1)	0.3732E-04	0.295E-04	0.474E-04
X(3)	0.1931E+06	0.174E+06	0.193E+06

TIME (HOURS)	OBS. CONC.	CALC. CONC.	RESIDUALS
0.1000E-12	18.64	0.0000E+00	18.64
0.5333	13.92	0.1306E-03	13.92
0.8500	15.44	0.3958E-01	15.40
1.267	12.08	0.8708	11.21
1.750	17.27	4.694	12.58
3.783	35.24	41.86	-6.621
4.317	51.20	51.19	0.6223E-02
4.717	45.78	57.41	-11.63
5.250	72.45	64.63	7.816
10.55	102.6	92.07	10.53
12.42	97.31	92.09	5.218
14.95	89.69	89.34	0.3534
17.32	72.21	85.32	-13.11
0.7873		0.1853E-01	
1.575		2.887	
2.362		14.08	
3.149		29.55	
3.936		44.66	
4.724		57.51	
5.511		67.75	
6.298		75.61	
7.085		81.47	
7.873		85.72	
8.660		88.69	
9.447		90.64	
10.23		91.79	
11.02		92.31	
11.81		92.34	
12.60		91.98	
13.38		91.32	
14.17		90.41	
14.96		89.32	
15.75		88.09	

ML5-6 Sept 2011

S I M P L E X O P T I M I Z A T I O N

C L O U D P E

INPUT SETTINGS

---

1) THE NUMBER OF OBSERVATIONS (MAX 60) : 26
2) THE NUMBER OF PARAMETERS TO DETERMINE : 6
3) THE NUMBER OF VARIABLES (X,Y,Z,. . .) : 2
4) THE DIFFUSION COEFFICIENT (M^2/SEC) : 0.1000E-09
5) THE DISTANCE FROM SOURCE (M) : 2.690

INITIAL GUESSES OF PARAMETERS

---

6) THE EFFECTIVE POROSITY (DIM) : -0.3300
7) THE FLOW VELOCITY (M/SEC) : 0.4700E-04
8) THE RETARDATION FACTOR : -1.000
9) THE DISPERSIVITY (M) : -0.9300
10) THE CONTAMINANT MASS INJECTED (MG) : 0.1000E+06
11) THE FIRST ORDER DECAY CONST (/SEC) : 0.0000E+00
12) TYPE OF WEIGHTING : N

OPTIMIZED PARAMETER ESTIMATES:

VEL= 0.5179E-04
DISPERSIVITY= 0.9300
MASS= 0.2491E+06
POROSITY= 0.3300
LAMBDA= 0.0000E+00
Rf= 1.000

RESIDUAL SUM OF SQUARES = 9083.

THE F STATISTIC FOR NP= 2 NOBS= 26 IS: 3.40
THE CRITICAL RSS IS: 0.1166E+05

THE 95% CONFIDENCE INTERVALS ARE:

PARAMETER	BEST FIT	FROM (-VE=<95% CONF)	TO
X(1)	0.5179E-04	0.466E-04	0.580E-04
X(3)	0.2491E+06	0.224E+06	0.249E+06

TIME (HOURS)	OBS. CONC.	CALC. CONC.	RESIDUALS
0.1000E-12	0.0000E+00	0.0000E+00	0.0000E+00
0.7500	0.0000E+00	0.2198E-02	-0.2198E-02
1.200	0.0000E+00	0.3130	-0.3130
1.717	2.277	3.494	-1.217
2.200	3.900	11.44	-7.536
2.700	12.00	24.23	-12.23
3.200	19.60	39.69	-20.09
3.700	41.82	55.93	-14.11
4.200	56.34	71.61	-15.27
4.700	75.83	85.99	-10.16
5.200	67.89	98.70	-30.81
5.683	85.46	109.3	-23.82
6.183	119.8	118.5	1.273
6.700	183.6	126.4	57.22
7.217	174.4	132.7	41.75
7.983	158.3	139.4	18.86
9.050	156.8	144.8	11.98
10.77	151.3	146.4	4.900
12.15	137.9	143.6	-5.682
13.15	130.2	140.1	-9.925
14.17	123.2	135.8	-12.60
15.07	111.4	131.5	-20.13
18.28	102.0	114.8	-12.82
21.27	96.61	99.28	-2.670
25.30	78.32	80.42	-2.105
28.05	66.83	69.29	-2.461

ML5-7 July 2011

S I M P L E X O P T I M I Z A T I O N

C L O U D P E

INPUT SETTINGS

---

1) THE NUMBER OF OBSERVATIONS (MAX 60) : 13
2) THE NUMBER OF PARAMETERS TO DETERMINE : 6
3) THE NUMBER OF VARIABLES (X,Y,Z,. . .) : 2
4) THE DIFFUSION COEFFICIENT (M^2/SEC) : 0.1000E-09
5) THE DISTANCE FROM SOURCE (M) : 2.690

INITIAL GUESSES OF PARAMETERS

---

6) THE EFFECTIVE POROSITY (DIM) : -0.3300
7) THE FLOW VELOCITY (M/SEC) : 0.4000E-04
8) THE RETARDATION FACTOR : -1.000
9) THE DISPERSIVITY (M) : -1.620
10) THE CONTAMINANT MASS INJECTED (MG) : 0.1000E+06
11) THE FIRST ORDER DECAY CONST (/SEC) : 0.0000E+00
12) TYPE OF WEIGHTING : N

OPTIMIZED PARAMETER ESTIMATES:

VEL= 0.5470E-04
DISPERSIVITY= 1.620
MASS= 0.2200E+06
POROSITY= 0.3300
LAMBDA= 0.0000E+00
Rf= 1.000

RESIDUAL SUM OF SQUARES = 4712.

THE F STATISTIC FOR NP= 2 NOBS= 13 IS: 3.98
THE CRITICAL RSS IS: 8122.

THE 95% CONFIDENCE INTERVALS ARE:

PARAMETER	BEST FIT	FROM (-VE=<95% CONF	TO
X(1)	0.5470E-04	0.377E-04	0.815E-04
X(3)	0.2200E+06	0.198E+06	0.220E+06

TIME (HOURS)	OBS. CONC.	CALC. CONC.	RESIDUALS
0.1000E-12	14.40	0.0000E+00	14.40
0.5667	14.10	0.4500E-01	14.05
0.8833	13.85	1.289	12.56
1.333	21.41	9.027	12.38
1.800	31.77	23.09	8.677
3.850	60.32	79.40	-19.08
4.350	78.50	87.15	-8.646
4.733	62.87	91.77	-28.90
5.283	146.3	96.77	49.53
10.58	109.2	99.63	9.570
12.43	90.24	94.11	-3.868
14.97	76.48	85.77	-9.292
17.33	78.76	78.13	0.6313
0.7877		0.6283	
1.575		15.86	
2.363		41.98	
3.151		64.66	
3.939		80.93	
4.726		91.69	
5.514		98.38	
6.302		102.2	
7.090		103.9	
7.877		104.3	
8.665		103.7	
9.453		102.3	
10.24		100.5	
11.03		98.38	
11.82		96.04	
12.60		93.55	
13.39		90.99	
14.18		88.39	
14.97		85.78	
15.75		83.19	

ML5-7 Sept 2011

S I M P L E X O P T I M I Z A T I O N

C L O U D P E

INPUT SETTINGS

---

1) THE NUMBER OF OBSERVATIONS (MAX 60) : 26
2) THE NUMBER OF PARAMETERS TO DETERMINE : 6
3) THE NUMBER OF VARIABLES (X,Y,Z,. . .) : 2
4) THE DIFFUSION COEFFICIENT (M^2/SEC) : 0.1000E-09
5) THE DISTANCE FROM SOURCE (M) : 2.690

INITIAL GUESSES OF PARAMETERS

---

6) THE EFFECTIVE POROSITY (DIM) : -0.3300
7) THE FLOW VELOCITY (M/SEC) : 0.6030E-04
8) THE RETARDATION FACTOR : -1.000
9) THE DISPERSIVITY (M) : -1.350
10) THE CONTAMINANT MASS INJECTED (MG) : 0.1000E+06
11) THE FIRST ORDER DECAY CONST (/SEC) : 0.0000E+00
12) TYPE OF WEIGHTING : N

OPTIMIZED PARAMETER ESTIMATES:

VEL= 0.5654E-04
DISPERSIVITY= 1.350
MASS= 0.3115E+06
POROSITY= 0.3300
LAMBDA= 0.0000E+00
Rf= 1.000

RESIDUAL SUM OF SQUARES = 0.2056E+05

THE F STATISTIC FOR NP= 2 NOBS= 26 IS: 3.40
THE CRITICAL RSS IS: 0.2638E+05

THE 95% CONFIDENCE INTERVALS ARE:

PARAMETER	BEST FIT	FROM (-VE=<95% CONF	TO
X(1)	0.5654E-04	0.469E-04	0.684E-04
X(3)	0.3115E+06	0.280E+06	0.318E+06

TIME (HOURS)	OBS. CONC.	CALC. CONC.	RESIDUALS
0.1000E-12	0.0000E+00	0.0000E+00	0.0000E+00
0.7667	4.314	0.2849	4.029
1.217	12.85	5.331	7.519
1.733	34.00	21.93	12.07
2.217	43.50	43.63	-0.1325
2.733	60.60	67.52	-6.915
3.217	90.20	87.79	2.407
3.717	90.71	105.5	-14.84
4.217	128.6	120.0	8.634
4.717	132.8	131.3	1.458
5.217	149.8	140.1	9.702
5.700	192.8	146.5	46.34
6.200	151.6	151.3	0.3347
6.717	108.7	154.7	-45.96
7.250	219.6	156.8	62.79
8.000	168.3	158.0	10.29
9.067	58.64	157.1	-98.42
10.78	160.4	151.6	8.848
12.17	143.8	145.1	-1.332
13.17	132.0	140.0	-7.985
14.18	130.5	134.6	-4.075
15.08	115.6	129.7	-14.09
18.30	119.8	112.6	7.205
21.28	110.6	98.14	12.46
25.32	106.2	81.17	25.03
28.07	97.86	71.29	26.57

ML7-1 July 2011

S I M P L E X O P T I M I Z A T I O N

C L O U D P E

INPUT SETTINGS

---

1) THE NUMBER OF OBSERVATIONS (MAX 60) : 13
2) THE NUMBER OF PARAMETERS TO DETERMINE : 6
3) THE NUMBER OF VARIABLES (X,Y,Z,. . .) : 2
4) THE DIFFUSION COEFFICIENT (M^2/SEC) : 0.1000E-09
5) THE DISTANCE FROM SOURCE (M) : 5.590

INITIAL GUESSES OF PARAMETERS

---

6) THE EFFECTIVE POROSITY (DIM) : -0.3300
7) THE FLOW VELOCITY (M/SEC) : 0.4370E-04
8) THE RETARDATION FACTOR : -1.000
9) THE DISPERSIVITY (M) : -1.000
10) THE CONTAMINANT MASS INJECTED (MG) : 0.1000E+06
11) THE FIRST ORDER DECAY CONST (/SEC) : 0.0000E+00
12) TYPE OF WEIGHTING : N

OPTIMIZED PARAMETER ESTIMATES:

VEL= 0.4191E-04
DISPERSIVITY= 1.000
MASS= 0.2077E+06
POROSITY= 0.3300
LAMBDA= 0.0000E+00
Rf= 1.000

RESIDUAL SUM OF SQUARES = 2924.

THE F STATISTIC FOR NP= 2 NOBS= 13 IS: 3.98
THE CRITICAL RSS IS: 5040.

THE 95% CONFIDENCE INTERVALS ARE:

PARAMETER	BEST FIT	FROM (-VE=<95% CONF	TO
X(1)	0.4191E-04	0.272E-04	0.566E-04
X(3)	0.2077E+06	0.187E+06	0.210E+06

TIME (HOURS)	OBS. CONC.	CALC. CONC.	RESIDUALS
0.1000E-12	19.89	0.0000E+00	19.89
0.3333	14.67	0.4410E-63	14.67
0.6167	20.56	0.3222E-32	20.56
1.067	16.48	0.5874E-17	16.48
1.567	13.13	0.2520E-10	13.13
3.567	19.15	0.1720E-02	19.15
4.133	21.08	0.1142E-01	21.07
4.633	16.29	0.4090E-01	16.25
5.383	17.84	0.1750	17.67
10.23	10.17	10.08	0.9333E-01
12.10	13.78	18.88	-5.096
14.82	39.12	33.76	5.361
17.22	44.25	46.55	-2.302
0.7827		0.1540E-24	
1.565		0.2440E-10	
2.348		0.1187E-05	
3.131		0.2472E-03	
3.914		0.5862E-02	
4.696		0.4712E-01	
5.479		0.2046	
6.262		0.6054	
7.045		1.389	
7.827		2.667	
8.610		4.505	
9.393		6.913	
10.18		9.853	
10.96		13.26	
11.74		17.04	
12.52		21.10	
13.31		25.35	
14.09		29.69	
14.87		34.05	
15.65		38.34	

ML7-1 Sept 2011

S I M P L E X O P T I M I Z A T I O N

C L O U D P E

INPUT SETTINGS

---

1) THE NUMBER OF OBSERVATIONS (MAX 60) : 26
2) THE NUMBER OF PARAMETERS TO DETERMINE : 6
3) THE NUMBER OF VARIABLES (X,Y,Z,. . .) : 2
4) THE DIFFUSION COEFFICIENT (M^2/SEC) : 0.1000E-09
5) THE DISTANCE FROM SOURCE (M) : 5.590

INITIAL GUESSES OF PARAMETERS

---

6) THE EFFECTIVE POROSITY (DIM) : -0.3300
7) THE FLOW VELOCITY (M/SEC) : -0.2170E-04
8) THE RETARDATION FACTOR : -1.000
9) THE DISPERSIVITY (M) : -1.000
10) THE CONTAMINANT MASS INJECTED (MG) : 0.1000E+06
11) THE FIRST ORDER DECAY CONST (/SEC) : 0.0000E+00
12) TYPE OF WEIGHTING : N

OPTIMIZED PARAMETER ESTIMATES:

VEL= 0.2170E-04
DISPERSIVITY= 1.000
MASS= 0.2459E+06
POROSITY= 0.3300
LAMBDA= 0.0000E+00
Rf= 1.000

RESIDUAL SUM OF SQUARES = 603.6

THE F STATISTIC FOR NP= 1 NOBS= 26 IS: 4.24
THE CRITICAL RSS IS: 706.0

THE 95% CONFIDENCE INTERVALS ARE:

PARAMETER	BEST FIT	FROM (-VE=<95% CONF	TO
X(3)	0.2459E+06	0.221E+06	0.293E+06

TIME (HOURS)	OBS. CONC.	CALC. CONC.	RESIDUALS
0.1000E-12	0.0000E+00	0.0000E+00	0.0000E+00
0.6833	0.0000E+00	0.4062E-59	-0.4062E-59
1.117	0.0000E+00	0.1501E-34	-0.1501E-34
1.633	0.0000E+00	0.2371E-22	-0.2371E-22
2.117	2.000	0.2482E-16	2.000
2.633	2.100	0.2308E-12	2.100
3.133	0.0000E+00	0.8988E-10	-0.8988E-10
3.617	2.826	0.5933E-08	2.826
4.100	2.838	0.1434E-06	2.838
4.600	4.398	0.1899E-05	4.398
5.117	3.452	0.1603E-04	3.452
5.600	3.128	0.8190E-04	3.128
6.117	3.400	0.3509E-03	3.400
6.600	5.485	0.1107E-02	5.484
7.317	11.57	0.4576E-02	11.57
8.083	0.0000E+00	0.1566E-01	-0.1566E-01
9.150	8.897	0.6101E-01	8.836
11.00	6.900	0.3373	6.563
12.07	15.70	0.7059	14.99
13.08	1.500	1.261	0.2394
14.17	2.416	2.135	0.2812
15.02	6.940	3.040	3.900
18.22	8.300	8.350	-0.5003E-01
21.22	16.09	15.85	0.2363
25.23	28.71	28.43	0.2773
27.97	36.60	37.74	-1.141

ML7-2 July 2011

S I M P L E X O P T I M I Z A T I O N

C L O U D P E

INPUT SETTINGS

---

1) THE NUMBER OF OBSERVATIONS (MAX 60) : 13
2) THE NUMBER OF PARAMETERS TO DETERMINE : 6
3) THE NUMBER OF VARIABLES (X,Y,Z,. . .) : 2
4) THE DIFFUSION COEFFICIENT (M^2/SEC) : 0.1000E-09
5) THE DISTANCE FROM SOURCE (M) : 5.590

INITIAL GUESSES OF PARAMETERS

---

6) THE EFFECTIVE POROSITY (DIM) : -0.3300
7) THE FLOW VELOCITY (M/SEC) : 0.8960E-04
8) THE RETARDATION FACTOR : -1.000
9) THE DISPERSIVITY (M) : -1.640
10) THE CONTAMINANT MASS INJECTED (MG) : 0.1000E+06
11) THE FIRST ORDER DECAY CONST (/SEC) : 0.0000E+00
12) TYPE OF WEIGHTING : N

OPTIMIZED PARAMETER ESTIMATES:

VEL= 0.8703E-04
DISPERSIVITY= 1.640
MASS= 0.6318E+06
POROSITY= 0.3300
LAMBDA= 0.0000E+00
Rf= 1.000

RESIDUAL SUM OF SQUARES = 2173.

THE F STATISTIC FOR NP= 2 NOBS= 13 IS: 3.98
THE CRITICAL RSS IS: 3746.

THE 95% CONFIDENCE INTERVALS ARE:

PARAMETER	BEST FIT	FROM (-VE=<95% CONF	TO
X(1)	0.8703E-04	0.757E-04	0.983E-04
X(3)	0.6318E+06	0.569E+06	0.638E+06

TIME (HOURS)	OBS. CONC.	CALC. CONC.	RESIDUALS
0.1000E-12	15.95	0.0000E+00	15.95
0.3667	14.80	0.6620E-14	14.80
0.6500	13.17	0.3457E-06	13.17
1.100	15.75	0.3723E-02	15.75
1.600	14.63	0.2265	14.40
3.600	53.14	26.93	26.21
4.167	46.92	43.28	3.645
4.650	43.71	58.48	-14.77
5.400	81.23	82.45	-1.221
10.25	172.6	179.9	-7.296
12.12	198.4	190.2	8.188
14.83	185.9	190.0	-4.105
17.23	185.0	181.3	3.685
0.7832		0.1671E-04	
1.566		0.1870	
2.350		3.738	
3.133		15.72	
3.916		35.76	
4.699		60.05	
5.482		85.03	
6.265		108.4	
7.049		128.9	
7.832		146.1	
8.615		160.1	
9.398		171.1	
10.18		179.3	
10.96		185.2	
11.75		189.0	
12.53		191.1	
13.31		191.8	
14.10		191.3	
14.88		189.9	
15.66		187.6	

ML7-2 Sept 2011

S I M P L E X O P T I M I Z A T I O N

C L O U D P E

INPUT SETTINGS

---

1) THE NUMBER OF OBSERVATIONS (MAX 60) : 26
2) THE NUMBER OF PARAMETERS TO DETERMINE : 6
3) THE NUMBER OF VARIABLES (X,Y,Z,. . .) : 2
4) THE DIFFUSION COEFFICIENT (M^2/SEC) : 0.1000E-09
5) THE DISTANCE FROM SOURCE (M) : 5.590

INITIAL GUESSES OF PARAMETERS

---

6) THE EFFECTIVE POROSITY (DIM) : -0.3300
7) THE FLOW VELOCITY (M/SEC) : 0.8960E-04
8) THE RETARDATION FACTOR : -0.8600E-01
9) THE DISPERSIVITY (M) : -1.640
10) THE CONTAMINANT MASS INJECTED (MG) : 0.1000E+06
11) THE FIRST ORDER DECAY CONST (/SEC) : 0.0000E+00
12) TYPE OF WEIGHTING : N

OPTIMIZED PARAMETER ESTIMATES:

VEL= 0.6713E-05
DISPERSIVITY= 1.640
MASS= 0.6789E+05
POROSITY= 0.3300
LAMBDA= 0.0000E+00
Rf= 0.8600E-01

RESIDUAL SUM OF SQUARES = 5700.

THE F STATISTIC FOR NP= 2 NOBS= 26 IS: 3.40
THE CRITICAL RSS IS: 7315.

THE 95% CONFIDENCE INTERVALS ARE:

PARAMETER	BEST FIT	FROM (-VE=<95% CONF	TO
X(1)	0.6713E-05	0.638E-05	0.705E-05
X(3)	0.6789E+05	0.611E+05	0.686E+05

TIME (HOURS)	OBS. CONC.	CALC. CONC.	RESIDUALS
0.1000E-12	0.0000E+00	0.0000E+00	0.0000E+00
0.7333	0.0000E+00	0.5648E-06	-0.5648E-06
1.150	0.0000E+00	0.1924E-02	-0.1924E-02
1.667	1.800	0.1511	1.649
2.167	2.400	1.355	1.045
2.667	2.000	5.183	-3.183
3.183	12.40	13.00	-0.6027
3.650	27.89	23.53	4.364
4.150	30.31	37.79	-7.479
4.633	43.49	53.63	-10.14
5.167	52.27	72.45	-20.18
5.650	85.15	89.83	-4.680
6.167	67.86	108.1	-40.29
6.650	142.2	124.6	17.64
7.350	170.2	146.6	23.63
8.117	199.4	167.8	31.57
9.167	188.2	191.8	-3.580
11.03	206.0	220.6	-14.60
12.12	241.6	230.6	10.98
13.12	243.2	236.3	6.947
14.18	250.8	239.2	11.62
15.03	227.2	239.7	-12.48
18.27	222.8	231.1	-8.319
21.27	188.8	214.7	-25.91
25.27	197.6	188.3	9.323
28.00	178.6	169.9	8.722

ML7-3 July 2011

S I M P L E X O P T I M I Z A T I O N

C L O U D P E

INPUT SETTINGS

---

1) THE NUMBER OF OBSERVATIONS (MAX 60) : 13
2) THE NUMBER OF PARAMETERS TO DETERMINE : 6
3) THE NUMBER OF VARIABLES (X,Y,Z,. . .) : 2
4) THE DIFFUSION COEFFICIENT (M^2/SEC) : 0.1000E-09
5) THE DISTANCE FROM SOURCE (M) : 5.590

INITIAL GUESSES OF PARAMETERS

---

6) THE EFFECTIVE POROSITY (DIM) : -0.3300
7) THE FLOW VELOCITY (M/SEC) : 0.1710E-03
8) THE RETARDATION FACTOR : -1.000
9) THE DISPERSIVITY (M) : -0.7800
10) THE CONTAMINANT MASS INJECTED (MG) : 0.1000E+06
11) THE FIRST ORDER DECAY CONST (/SEC) : 0.0000E+00
12) TYPE OF WEIGHTING : N

OPTIMIZED PARAMETER ESTIMATES:

VEL= 0.1777E-03
DISPERSIVITY= 0.7800
MASS= 0.4998E+06
POROSITY= 0.3300
LAMBDA= 0.0000E+00
Rf= 1.000

RESIDUAL SUM OF SQUARES = 3806.

THE F STATISTIC FOR NP= 2 NOBS= 13 IS: 3.98
THE CRITICAL RSS IS: 6560.

THE 95% CONFIDENCE INTERVALS ARE:

PARAMETER	BEST FIT	FROM (-VE=<95% CONF	TO
X(1)	0.1777E-03	0.165E-03	0.192E-03
X(3)	0.4998E+06	0.450E+06	0.510E+06

TIME (HOURS)	OBS. CONC.	CALC. CONC.	RESIDUALS
0.1000E-12	11.49	0.0000E+00	11.49
0.3833	12.61	0.5885E-13	12.61
0.7000	13.28	0.4344E-05	13.28
1.150	14.43	0.1957E-01	14.41
1.633	20.53	0.8347	19.70
3.650	83.99	73.90	10.09
4.217	102.2	109.0	-6.769
4.667	99.20	135.1	-35.92
5.417	197.7	171.1	26.57
10.27	193.4	180.1	13.26
12.13	141.9	143.0	-1.123
14.85	73.30	93.76	-20.46
17.25	59.66	61.59	-1.931
0.7841		0.4443E-04	
1.568		0.5807	
2.352		11.26	
3.136		43.87	
3.920		90.69	
4.705		137.2	
5.489		174.0	
6.273		198.0	
7.057		209.7	
7.841		211.5	
8.625		205.9	
9.409		195.3	
10.19		181.6	
10.98		166.3	
11.76		150.4	
12.55		134.8	
13.33		119.8	
14.11		105.9	
14.90		93.01	
15.68		81.36	

ML7-3 Sept 2011

S I M P L E X O P T I M I Z A T I O N

C L O U D P E

INPUT SETTINGS

---

1) THE NUMBER OF OBSERVATIONS (MAX 60) : 26
2) THE NUMBER OF PARAMETERS TO DETERMINE : 6
3) THE NUMBER OF VARIABLES (X,Y,Z,. . .) : 2
4) THE DIFFUSION COEFFICIENT (M^2/SEC) : 0.1000E-09
5) THE DISTANCE FROM SOURCE (M) : 5.590

INITIAL GUESSES OF PARAMETERS

---

6) THE EFFECTIVE POROSITY (DIM) : -0.3300
7) THE FLOW VELOCITY (M/SEC) : -0.1070E-03
8) THE RETARDATION FACTOR : -1.000
9) THE DISPERSIVITY (M) : -0.6800
10) THE CONTAMINANT MASS INJECTED (MG) : 0.1000E+06
11) THE FIRST ORDER DECAY CONST (/SEC) : 0.0000E+00
12) TYPE OF WEIGHTING : N

OPTIMIZED PARAMETER ESTIMATES:

VEL= 0.1070E-03
DISPERSIVITY= 0.6800
MASS= 0.4303E+06
POROSITY= 0.3300
LAMBDA= 0.0000E+00
Rf= 1.000

RESIDUAL SUM OF SQUARES = 6648.

THE F STATISTIC FOR NP= 1 NOBS= 26 IS: 4.24
THE CRITICAL RSS IS: 7776.

THE 95% CONFIDENCE INTERVALS ARE:

PARAMETER	BEST FIT	FROM (-VE=<95% CONF	TO
X(3)	0.4303E+06	0.387E+06	0.456E+06

TIME (HOURS)	OBS. CONC.	CALC. CONC.	RESIDUALS
0.1000E-12	0.0000E+00	0.0000E+00	0.0000E+00
0.7500	0.0000E+00	0.2444E-12	-0.2444E-12
1.167	0.0000E+00	0.2738E-06	-0.2738E-06
1.700	0.0000E+00	0.6349E-03	-0.6349E-03
2.183	1.800	0.2538E-01	1.775
2.683	2.700	0.2721	2.428
3.200	4.000	1.395	2.605
3.667	8.685	3.997	4.688
4.167	10.54	9.269	1.271
4.667	17.90	17.57	0.3329
5.183	35.16	29.27	5.885
5.667	32.20	42.73	-10.53
6.200	35.13	59.56	-24.43
6.667	76.71	75.30	1.409
7.367	98.55	99.24	-0.6855
8.150	130.8	124.6	6.208
9.233	153.6	154.2	-0.6421
11.07	205.6	185.6	19.99
12.13	190.4	193.1	-2.711
13.15	188.9	194.3	-5.353
14.20	178.6	190.5	-11.92
15.07	238.9	184.6	54.32
18.28	129.1	150.6	-21.47
21.28	89.29	114.8	-25.56
25.28	47.69	74.65	-26.96
28.03	32.58	53.92	-21.34

ML7-4 July 2011

S I M P L E X O P T I M I Z A T I O N

C L O U D P E

INPUT SETTINGS

---

1) THE NUMBER OF OBSERVATIONS (MAX 60) : 13
2) THE NUMBER OF PARAMETERS TO DETERMINE : 6
3) THE NUMBER OF VARIABLES (X,Y,Z,. . .) : 2
4) THE DIFFUSION COEFFICIENT (M^2/SEC) : 0.1000E-09
5) THE DISTANCE FROM SOURCE (M) : 5.590

INITIAL GUESSES OF PARAMETERS

---

6) THE EFFECTIVE POROSITY (DIM) : -0.3300
7) THE FLOW VELOCITY (M/SEC) : 0.2050E-03
8) THE RETARDATION FACTOR : -1.000
9) THE DISPERSIVITY (M) : -1.270
10) THE CONTAMINANT MASS INJECTED (MG) : 0.1000E+06
11) THE FIRST ORDER DECAY CONST (/SEC) : 0.0000E+00
12) TYPE OF WEIGHTING : N

OPTIMIZED PARAMETER ESTIMATES:

VEL= 0.2150E-03
DISPERSIVITY= 1.270
MASS= 0.6107E+06
POROSITY= 0.3300
LAMBDA= 0.0000E+00
Rf= 1.000

RESIDUAL SUM OF SQUARES = 0.1966E+05

THE F STATISTIC FOR NP= 2 NOBS= 13 IS: 3.98
THE CRITICAL RSS IS: 0.3389E+05

THE 95% CONFIDENCE INTERVALS ARE:

PARAMETER	BEST FIT	FROM (-VE=<95% CONF)	TO
X(1)	0.2150E-03	0.168E-03	0.297E-03
X(3)	0.6107E+06	0.550E+06	0.623E+06

TIME (HOURS)	OBS. CONC.	CALC. CONC.	RESIDUALS
0.1000E-12	13.03	0.0000E+00	13.03
0.4333	12.29	0.7317E-04	12.29
0.7667	16.13	0.1522	15.98
1.183	26.50	4.414	22.09
1.667	44.43	24.29	20.14
3.700	146.8	164.2	-17.44
4.250	199.5	186.1	13.42
4.683	109.6	197.3	-87.68
5.433	304.5	206.5	97.99
10.28	136.8	143.0	-6.188
12.13	92.44	111.7	-19.29
14.87	75.84	75.00	0.8373
17.28	54.19	51.92	2.266
0.7855		0.1920	
1.571		18.97	
2.356		74.20	
3.142		132.5	
3.927		174.4	
4.713		197.9	
5.498		206.8	
6.284		205.6	
7.069		198.0	
7.855		186.4	
8.640		172.9	
9.425		158.6	
10.21		144.2	
11.00		130.4	
11.78		117.3	
12.57		105.1	
13.35		93.86	
14.14		83.65	
14.92		74.40	
15.71		66.07	

ML7-4 Sept 2011

S I M P L E X O P T I M I Z A T I O N

C L O U D P E

INPUT SETTINGS

---

1) THE NUMBER OF OBSERVATIONS (MAX 60) : 26
2) THE NUMBER OF PARAMETERS TO DETERMINE : 6
3) THE NUMBER OF VARIABLES (X,Y,Z,. . .) : 2
4) THE DIFFUSION COEFFICIENT (M^2/SEC) : 0.1000E-09
5) THE DISTANCE FROM SOURCE (M) : 5.590

INITIAL GUESSES OF PARAMETERS

---

6) THE EFFECTIVE POROSITY (DIM) : -0.3300
7) THE FLOW VELOCITY (M/SEC) : -0.1300E-03
8) THE RETARDATION FACTOR : -1.000
9) THE DISPERSIVITY (M) : -1.200
10) THE CONTAMINANT MASS INJECTED (MG) : 0.1000E+06
11) THE FIRST ORDER DECAY CONST (/SEC) : 0.0000E+00
12) TYPE OF WEIGHTING : N

OPTIMIZED PARAMETER ESTIMATES:

VEL= 0.1300E-03
DISPERSIVITY= 1.200
MASS= 0.5905E+06
POROSITY= 0.3300
LAMBDA= 0.0000E+00
Rf= 1.000

RESIDUAL SUM OF SQUARES = 0.2604E+05

THE F STATISTIC FOR NP= 1 NOBS= 26 IS: 4.24
THE CRITICAL RSS IS: 0.3046E+05

THE 95% CONFIDENCE INTERVALS ARE:

PARAMETER	BEST FIT	FROM (-VE=<95% CONF)	TO
X(3)	0.5905E+06	0.531E+06	0.644E+06

TIME (HOURS)	OBS. CONC.	CALC. CONC.	RESIDUALS
0.1000E-12	0.0000E+00	0.0000E+00	0.0000E+00
0.7667	2.039	0.9678E-04	2.039
1.200	5.966	0.5191E-01	5.914
1.717	34.50	1.353	33.15
2.217	50.65	7.051	43.60
2.717	46.70	19.25	27.45
3.217	77.20	37.34	39.86
3.700	108.8	58.40	50.40
4.200	126.0	81.68	44.32
4.683	97.88	103.8	-5.963
5.217	135.6	126.6	9.021
5.683	116.4	144.2	-27.81
6.217	133.2	161.5	-28.31
6.700	127.1	174.4	-47.30
7.400	262.8	188.6	74.17
8.167	258.0	198.8	59.21
9.283	204.4	205.2	-0.8370
11.08	200.0	201.0	-1.041
12.17	186.7	193.0	-6.313
13.17	175.8	183.6	-7.764
14.23	138.6	172.3	-33.69
15.10	138.4	162.6	-24.15
18.32	98.49	126.8	-28.27
21.32	86.87	97.60	-10.73
25.32	48.13	67.22	-19.09
28.07	40.63	51.53	-10.90

ML7-5 July 2011

S I M P L E X O P T I M I Z A T I O N

C L O U D P E

INPUT SETTINGS

---

1) THE NUMBER OF OBSERVATIONS (MAX 60) : 13
2) THE NUMBER OF PARAMETERS TO DETERMINE : 6
3) THE NUMBER OF VARIABLES (X,Y,Z,. . .) : 2
4) THE DIFFUSION COEFFICIENT (M^2/SEC) : 0.1000E-09
5) THE DISTANCE FROM SOURCE (M) : 5.590

INITIAL GUESSES OF PARAMETERS

---

6) THE EFFECTIVE POROSITY (DIM) : -0.3300
7) THE FLOW VELOCITY (M/SEC) : 0.1350E-03
8) THE RETARDATION FACTOR : -1.000
9) THE DISPERSIVITY (M) : -1.460
10) THE CONTAMINANT MASS INJECTED (MG) : 0.1000E+06
11) THE FIRST ORDER DECAY CONST (/SEC) : 0.0000E+00
12) TYPE OF WEIGHTING : N

OPTIMIZED PARAMETER ESTIMATES:

VEL= 0.1388E-03
DISPERSIVITY= 1.460
MASS= 0.3737E+06
POROSITY= 0.3300
LAMBDA= 0.0000E+00
Rf= 1.000

RESIDUAL SUM OF SQUARES = 2960.

THE F STATISTIC FOR NP= 2 NOBS= 13 IS: 3.98
THE CRITICAL RSS IS: 5102.

THE 95% CONFIDENCE INTERVALS ARE:

PARAMETER	BEST FIT	FROM (-VE=<95% CONF)	TO
X(1)	0.1388E-03	0.117E-03	0.164E-03
X(3)	0.3737E+06	0.336E+06	0.377E+06

TIME (HOURS)	OBS. CONC.	CALC. CONC.	RESIDUALS
0.1000E-12	11.25	0.0000E+00	11.25
0.3333	14.46	0.4788E-10	14.46
0.8000	14.97	0.4082E-02	14.97
1.233	12.63	0.3483	12.28
1.717	18.43	3.274	15.16
3.750	58.68	54.70	3.985
4.283	68.27	69.76	-1.486
4.700	51.17	80.21	-29.04
5.450	107.3	95.57	11.73
10.30	142.3	115.8	26.53
12.15	105.6	106.6	-0.9862
14.88	79.32	89.63	-10.31
17.30	60.25	74.73	-14.48
0.7864		0.3269E-02	
1.573		1.955	
2.359		14.43	
3.145		36.33	
3.932		60.01	
4.718		80.64	
5.505		96.52	
6.291		107.6	
7.077		114.6	
7.864		118.3	
8.650		119.3	
9.436		118.4	
10.22		116.1	
11.01		112.7	
11.80		108.6	
12.58		104.0	
13.37		99.21	
14.15		94.24	
14.94		89.24	
15.73		84.29	

ML7-5 Sept 2011

S I M P L E X O P T I M I Z A T I O N

C L O U D P E

INPUT SETTINGS

---

1) THE NUMBER OF OBSERVATIONS (MAX 60) : 26
2) THE NUMBER OF PARAMETERS TO DETERMINE : 6
3) THE NUMBER OF VARIABLES (X,Y,Z,. . .) : 2
4) THE DIFFUSION COEFFICIENT (M^2/SEC) : 0.1000E-09
5) THE DISTANCE FROM SOURCE (M) : 5.590

INITIAL GUESSES OF PARAMETERS

---

6) THE EFFECTIVE POROSITY (DIM) : -0.3300
7) THE FLOW VELOCITY (M/SEC) : 0.1000E-03
8) THE RETARDATION FACTOR : -1.000
9) THE DISPERSIVITY (M) : -0.8000
10) THE CONTAMINANT MASS INJECTED (MG) : 0.1000E+06
11) THE FIRST ORDER DECAY CONST (/SEC) : 0.0000E+00
12) TYPE OF WEIGHTING : N

OPTIMIZED PARAMETER ESTIMATES:

VEL= 0.9710E-04
DISPERSIVITY= 0.8000
MASS= 0.1410E+06
POROSITY= 0.3300
LAMBDA= 0.0000E+00
Rf= 1.000

RESIDUAL SUM OF SQUARES = 3044.

THE F STATISTIC FOR NP= 2 NOBS= 26 IS: 3.40
THE CRITICAL RSS IS: 3907.

THE 95% CONFIDENCE INTERVALS ARE:

PARAMETER	BEST FIT	FROM (-VE=<95% CONF)	TO
X(1)	0.9710E-04	0.835E-04	0.111E-03
X(3)	0.1410E+06	0.127E+06	0.145E+06

TIME (HOURS)	OBS. CONC.	CALC. CONC.	RESIDUALS
0.1000E-12	0.0000E+00	0.0000E+00	0.0000E+00
0.8000	0.0000E+00	0.5248E-11	-0.5248E-11
1.233	0.0000E+00	0.8538E-06	-0.8538E-06
1.767	0.0000E+00	0.6333E-03	-0.6333E-03
2.250	0.0000E+00	0.1585E-01	-0.1585E-01
2.750	1.900	0.1298	1.770
3.267	2.100	0.5617	1.538
3.733	2.319	1.452	0.8667
4.233	4.550	3.126	1.424
4.733	2.770	5.620	-2.850
5.250	4.621	9.019	-4.398
5.733	9.101	12.82	-3.717
6.267	16.25	17.52	-1.268
6.733	15.29	21.87	-6.577
7.450	24.98	28.66	-3.677
8.217	35.60	35.61	-0.1039E-01
9.317	77.79	44.30	33.49
11.13	77.30	54.19	23.11
12.20	38.50	57.39	-18.89
13.22	42.20	58.85	-16.65
14.27	52.14	59.00	-6.864
15.15	49.00	58.28	-9.281
18.37	52.71	51.44	1.270
21.35	38.09	42.61	-4.516
25.35	40.27	31.05	9.218
28.10	44.49	24.33	20.16

ML7-6 July 2011

S I M P L E X O P T I M I Z A T I O N

C L O U D P E

INPUT SETTINGS

---

1) THE NUMBER OF OBSERVATIONS (MAX 60) : 13
2) THE NUMBER OF PARAMETERS TO DETERMINE : 6
3) THE NUMBER OF VARIABLES (X,Y,Z,. . .) : 2
4) THE DIFFUSION COEFFICIENT (M^2/SEC) : 0.1000E-09
5) THE DISTANCE FROM SOURCE (M) : 5.590

INITIAL GUESSES OF PARAMETERS

---

6) THE EFFECTIVE POROSITY (DIM) : -0.3300
7) THE FLOW VELOCITY (M/SEC) : 0.1310E-03
8) THE RETARDATION FACTOR : -1.000
9) THE DISPERSIVITY (M) : -1.580
10) THE CONTAMINANT MASS INJECTED (MG) : 0.1000E+06
11) THE FIRST ORDER DECAY CONST (/SEC) : 0.0000E+00
12) TYPE OF WEIGHTING : N

OPTIMIZED PARAMETER ESTIMATES:

VEL= 0.1229E-03
DISPERSIVITY= 1.580
MASS= 0.2418E+06
POROSITY= 0.3300
LAMBDA= 0.0000E+00
Rf= 1.000

RESIDUAL SUM OF SQUARES = 1351.

THE F STATISTIC FOR NP= 2 NOBS= 13 IS: 3.98
THE CRITICAL RSS IS: 2328.

THE 95% CONFIDENCE INTERVALS ARE:

PARAMETER	BEST FIT	FROM (-VE=<95% CONF	TO
X(1)	0.1229E-03	0.995E-04	0.149E-03
X(3)	0.2418E+06	0.218E+06	0.247E+06

TIME (HOURS)	OBS. CONC.	CALC. CONC.	RESIDUALS
0.1000E-12	11.06	0.0000E+00	11.06
0.5333	13.96	0.1511E-05	13.96
0.8500	14.15	0.2884E-02	14.15
1.267	12.77	0.1739	12.60
1.750	15.14	1.632	13.51
3.783	30.71	29.81	0.9017
4.317	40.66	38.74	1.920
4.717	40.17	44.89	-4.716
5.467	51.86	54.76	-2.899
10.32	89.36	74.22	15.14
12.17	55.98	70.79	-14.81
14.92	65.30	62.47	2.830
17.32	53.63	54.38	-0.7472
0.7873		0.1056E-02	
1.575		0.8551	
2.362		7.042	
3.149		18.84	
3.936		32.44	
4.724		44.98	
5.511		55.27	
6.298		63.04	
7.085		68.51	
7.873		72.02	
8.660		73.94	
9.447		74.61	
10.23		74.30	
11.02		73.26	
11.81		71.66	
12.60		69.67	
13.38		67.39	
14.17		64.93	
14.96		62.34	
15.75		59.70	

ML7-6 Sept 2011

S I M P L E X O P T I M I Z A T I O N

C L O U D P E

INPUT SETTINGS

---

1) THE NUMBER OF OBSERVATIONS (MAX 60) : 26
2) THE NUMBER OF PARAMETERS TO DETERMINE : 6
3) THE NUMBER OF VARIABLES (X,Y,Z,. . .) : 2
4) THE DIFFUSION COEFFICIENT (M^2/SEC) : 0.1000E-09
5) THE DISTANCE FROM SOURCE (M) : 5.590

INITIAL GUESSES OF PARAMETERS

---

6) THE EFFECTIVE POROSITY (DIM) : -0.3300
7) THE FLOW VELOCITY (M/SEC) : 0.7410E-04
8) THE RETARDATION FACTOR : -1.000
9) THE DISPERSIVITY (M) : -1.600
10) THE CONTAMINANT MASS INJECTED (MG) : 0.1000E+06
11) THE FIRST ORDER DECAY CONST (/SEC) : 0.0000E+00
12) TYPE OF WEIGHTING : N

OPTIMIZED PARAMETER ESTIMATES:

VEL= 0.8183E-04
DISPERSIVITY= 1.600
MASS= 0.3312E+06
POROSITY= 0.3300
LAMBDA= 0.0000E+00
Rf= 1.000

RESIDUAL SUM OF SQUARES = 2168.

THE F STATISTIC FOR NP= 2 NOBS= 26 IS: 3.40
THE CRITICAL RSS IS: 2782.

THE 95% CONFIDENCE INTERVALS ARE:

PARAMETER	BEST FIT	FROM (-VE=<95% CONF	TO
X(1)	0.8183E-04	0.753E-04	0.892E-04
X(3)	0.3312E+06	0.298E+06	0.331E+06

TIME (HOURS)	OBS. CONC.	CALC. CONC.	RESIDUALS
0.1000E-12	0.0000E+00	0.0000E+00	0.0000E+00
0.8333	0.0000E+00	0.5737E-05	-0.5737E-05
1.267	0.0000E+00	0.4130E-02	-0.4130E-02
1.783	2.000	0.1498	1.850
2.283	4.200	0.9911	3.209
2.783	5.200	3.233	1.967
3.300	11.10	7.370	3.730
3.750	23.62	12.37	11.25
4.250	32.49	19.10	13.39
4.750	41.63	26.62	15.01
5.283	35.76	35.03	0.7327
5.750	58.23	42.40	15.83
6.283	52.03	50.54	1.490
6.750	34.79	57.28	-22.49
7.467	67.40	66.70	0.6978
8.233	78.16	75.39	2.770
9.350	64.70	85.47	-20.77
11.15	105.5	95.91	9.586
12.22	94.60	99.34	-4.739
13.23	98.90	101.1	-2.178
14.30	96.27	101.6	-5.376
15.17	100.6	101.3	-0.7317
18.38	102.5	96.11	6.390
21.37	92.30	88.12	4.181
25.37	71.00	76.03	-5.026
28.12	81.04	67.82	13.22

ML7-7 July 2011

S I M P L E X O P T I M I Z A T I O N

C L O U D P E

INPUT SETTINGS

---

1) THE NUMBER OF OBSERVATIONS (MAX 60) : 13
2) THE NUMBER OF PARAMETERS TO DETERMINE : 6
3) THE NUMBER OF VARIABLES (X,Y,Z,. . .) : 2
4) THE DIFFUSION COEFFICIENT (M^2/SEC) : 0.1000E-05
5) THE DISTANCE FROM SOURCE (M) : 5.590

INITIAL GUESSES OF PARAMETERS

---

6) THE EFFECTIVE POROSITY (DIM) : -0.3300
7) THE FLOW VELOCITY (M/SEC) : 0.1900E-03
8) THE RETARDATION FACTOR : -1.000
9) THE DISPERSIVITY (M) : -1.200
10) THE CONTAMINANT MASS INJECTED (MG) : 0.1000E+06
11) THE FIRST ORDER DECAY CONST (/SEC) : 0.0000E+00
12) TYPE OF WEIGHTING : N

OPTIMIZED PARAMETER ESTIMATES:

VEL= 0.2161E-03
DISPERSIVITY= 1.200
MASS= 0.3615E+06
POROSITY= 0.3300
LAMBDA= 0.0000E+00
Rf= 1.000

RESIDUAL SUM OF SQUARES = 1986.

THE F STATISTIC FOR NP= 2 NOBS= 13 IS: 3.98
THE CRITICAL RSS IS: 3423.

THE 95% CONFIDENCE INTERVALS ARE:

PARAMETER	BEST FIT	FROM (-VE=<95% CONF	TC
X(1)	0.2161E-03	0.188E-03	0.255E-03
X(3)	0.3615E+06	0.325E+06	0.369E+06

TIME (HOURS)	OBS. CONC.	CALC. CONC.	RESIDUALS
0.1000E-12	10.30	0.0000E+00	10.30
0.5667	13.32	0.1536E-02	13.32
0.8833	15.66	0.2325	15.43
1.333	25.72	4.302	21.42
1.800	46.02	17.50	28.52
3.850	91.76	102.0	-10.28
4.350	110.6	113.7	-3.052
4.733	123.1	119.6	3.450
5.483	123.8	125.4	-1.580
10.33	84.42	85.23	-0.8098
12.18	70.10	65.77	4.326
14.93	47.23	43.18	4.051
17.33	34.57	29.36	5.214
0.7877		0.7922E-01	
1.575		9.998	
2.363		42.21	
3.151		77.99	
3.939		104.4	
4.726		119.6	
5.514		125.5	
6.302		124.9	
7.090		120.1	
7.877		112.9	
8.665		104.3	
9.453		95.27	
10.24		86.24	
11.03		77.54	
11.82		69.35	
12.60		61.78	
13.39		54.85	
14.18		48.58	
14.97		42.93	
15.75		37.87	

ML7-7 Sept 2011

S I M P L E X O P T I M I Z A T I O N

C L O U D P E

INPUT SETTINGS

---

1) THE NUMBER OF OBSERVATIONS (MAX 60) : 26
2) THE NUMBER OF PARAMETERS TO DETERMINE : 6
3) THE NUMBER OF VARIABLES (X,Y,Z,. . .) : 2
4) THE DIFFUSION COEFFICIENT (M^2/SEC) : 0.1000E-05
5) THE DISTANCE FROM SOURCE (M) : 5.590

INITIAL GUESSES OF PARAMETERS

---

6) THE EFFECTIVE POROSITY (DIM) : -0.3300
7) THE FLOW VELOCITY (M/SEC) : 0.1080E-03
8) THE RETARDATION FACTOR : -1.000
9) THE DISPERSIVITY (M) : -1.140
10) THE CONTAMINANT MASS INJECTED (MG) : 0.1000E+06
11) THE FIRST ORDER DECAY CONST (/SEC) : 0.0000E+00
12) TYPE OF WEIGHTING : N

OPTIMIZED PARAMETER ESTIMATES:

VEL= 0.1157E-03
DISPERSIVITY= 1.140
MASS= 0.3098E+06
POROSITY= 0.3300
LAMBDA= 0.0000E+00
Rf= 1.000

RESIDUAL SUM OF SQUARES = 3343.

THE F STATISTIC FOR NP= 2 NOBS= 26 IS: 3.40
THE CRITICAL RSS IS: 4290.

THE 95% CONFIDENCE INTERVALS ARE:

PARAMETER	BEST FIT	FROM (-VE=<95% CONF	TC
X(1)	0.1157E-03	0.108E-03	0.125E-03
X(3)	0.3098E+06	0.279E+06	0.310E+06

TIME (HOURS)	OBS. CONC.	CALC. CONC.	RESIDUALS
0.1000E-12	0.0000E+00	0.0000E+00	0.0000E+00
0.8500	0.0000E+00	0.1757E-04	-0.1757E-04
1.283	1.382	0.9447E-02	1.373
1.800	2.400	0.3026	2.097
2.317	5.300	1.956	3.344
2.800	11.80	5.794	6.006
3.317	18.74	12.69	6.052
3.767	28.95	20.67	8.285
4.283	38.50	31.29	7.209
4.767	30.95	41.91	-10.96
5.300	31.51	53.57	-22.06
5.767	56.29	63.28	-6.986
6.317	72.96	73.71	-0.7479
6.783	70.17	81.52	-11.35
7.483	103.4	91.35	12.05
8.250	76.60	99.51	-22.91
9.383	127.9	107.0	20.85
11.18	135.0	110.3	24.68
12.23	114.1	108.7	5.365
13.27	105.5	105.5	0.1737E-01
14.32	106.8	101.0	5.764
15.20	100.1	96.72	3.383
18.40	65.52	79.22	-13.70
21.40	50.28	63.31	-13.03
25.40	34.24	45.52	-11.28
28.13	27.26	35.89	-8.632

Appendix 16: PULSEPE Results from Biostimulation CIS Tracer Testing

Observed Time (Hours)	Observed Br- Conc (mg/L)	Calculated Br- Conc (mg/L)	Residuals
0	20.7311	0	20.7311
0.36666667	13.8759	5.7228E-05	13.8758428
0.65	15.5597	0.03071014	15.5289899
1.1	12.1162	0.94666218	11.1695378
1.6	13.5669	4.72049898	8.84640102
3.6	36.6956	38.7609354	-2.0653354
4.16666667	50.7041	49.8120459	0.89205413
4.65	47.4576	59.060961	-11.603361
5.15	80.5659	68.350817	12.215083
10.4833333	89.1539	92.7589669	-3.6050669
12.3166667	70.8304	79.4657828	-8.6353828
14.85	69.4458	64.6415912	4.8042088
17.2333333	68.0339	54.1475242	13.8863758

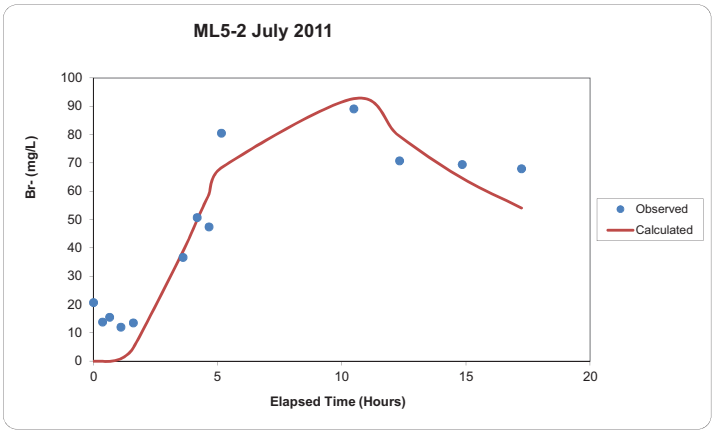

OPTIMIZED PARAMETER ESTIMATES

VELOCITY(cm/d)	375.3285	4.34408E-05
DISPERSIVITY (cm)	153.2187	
PULSE WIDTH (cm)	94.14602	
RF	1	
Co (mg/L)	372	
FODC (/sec)	0	

RESDIUAL SUM OF SQUARES = 1658.851

INITIAL GUESSES AND INPUT OF PARAMETERS

		FIX
VELOCITY(cm/d)	1100	
DISPERSIVITY (cm)	46	
PULSE WIDTH (cm)	167	
RF	1	Y
Co (mg/L)	372	Y
FODC (1/sec)	0	Y
DISTANCE FROM SOURCE (cm)	269	Y
DIFFUSION COEFF (cm^2/sec)	0.000001	Y

95% CONFIDENCE INTERVALS FOR ESTIMATED PARAMETERS

Parameter	Low	Optimized	High
VELOCITY(cm/d)	304.0161	375.3285	454.1475
DISPERSIVITY(cm)	98.05994	153.2187	237.4889
PULSE WIDTH (cm)	70.60951	94.14602	114.8581

Observed Time (Hours)	Observed Br- Conc (mg/L)	Calculated Br- Conc (mg/L)	Residuals
0	14.9538	0	14.9538
0.38333333	14.8437	0.41860498	14.425095
0.7	16.8724	6.42403781	10.4483622
1.15	25.4312	25.5284742	-0.0972742
1.63333333	36.4196	50.461054	-14.041454
3.65	166.6208	138.482161	28.1386394
4.21666667	131.0453	157.099956	-26.054656
4.66666667	170.7494	170.390173	0.35922693
5.18333333	192.1119	184.243669	7.86823108
10.5	267.4023	273.539342	-6.1370417
12.3333333	219.6538	219.644824	0.00897598
14.8666667	248.7525	142.010681	106.741819

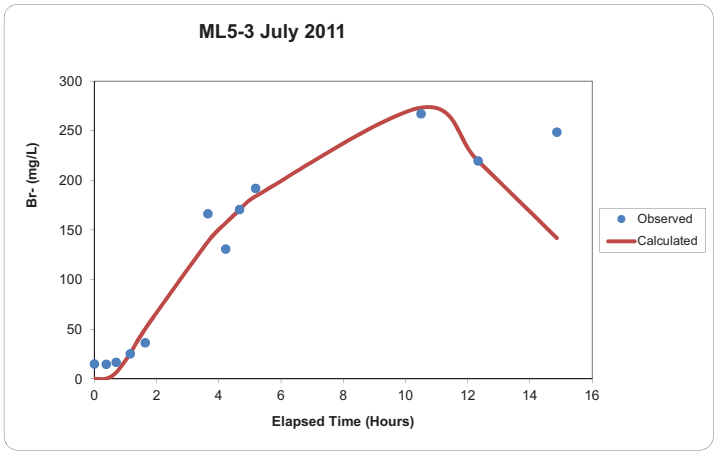

OPTIMIZED PARAMETER ESTIMATES

VELOCITY(cm/d)	621.3031	7.19E-05
DISPERSIVITY (cm)	85.62154	
PULSE WIDTH (cm)	266.0745	
RF	1	
Co (mg/L)	372	
FODC (/sec)	0	

RESDIUAL SUM OF SQUARES = 2326.344

INITIAL GUESSES AND INPUT OF PARAMETERS

		FIX
VELOCITY(cm/d)	1100	
DISPERSIVITY (cm)	46	
PULSE WIDTH (cm)	167	
RF	1	Y
Co (mg/L)	372	Y
FODC (1/sec)	0	Y
DISTANCE FROM SOURCE (cm)	269	Y
DIFFUSION COEFF (cm^2/sec)	0.000001	Y

95% CONFIDENCE INTERVALS FOR ESTIMATED PARAMETERS

Parameter	Low	Optimized	High
VELOCITY(cm/d)	584.0249	621.3031	671.0073
DISPERSIVITY(cm)	62.50372	85.62154	128.4323
PULSE WIDTH (cm)	247.4493	266.0745	282.039

Observed Time (Hours)	Observed Br- Conc (mg/L)	Calculated Br- Conc (mg/L)	Residuals
0	21.0156	0	21.0156
0.43333333	25.6217	17.2935974	8.32810262
0.76666667	68.7531	68.7709097	-0.0178097
1.18333333	134.6309	134.577923	0.0529766
1.66666667	175.5042	195.176653	-19.672453
3.7	304.5279	318.032932	-13.505032
4.25	405.198	332.253239	72.9447607
4.68333333	403.0524	339.195303	63.8570972
5.2	461.77	281.673742	180.096258
10.5166667	26.6056	13.3704902	13.2351098
12.3666667	18.9616	5.06053444	13.9010656
14.9	11.2214	1.38366654	9.83773346
17.2833333	0	0.41807276	-0.4180728

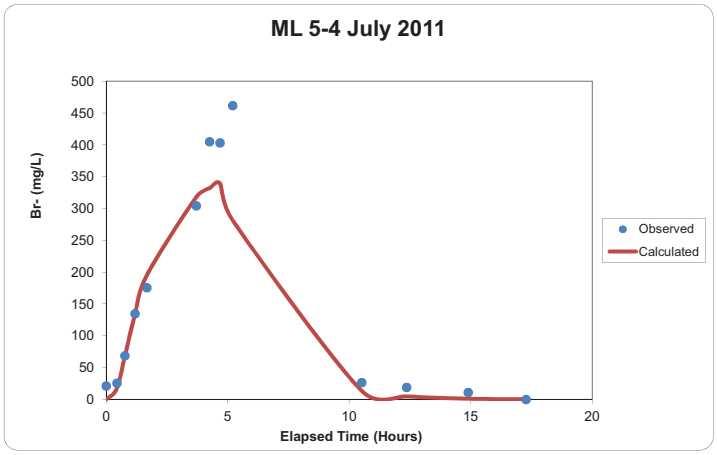

OPTIMIZED PARAMETER ESTIMATES

VELOCITY(cm/d)	1696.605	0.000196
DISPERSIVITY (cm)	38.14528	
PULSE WIDTH (cm)	314.2109	
RF	1	
Co (mg/L)	372	
FODC (/sec)	0	

RESDIUAL SUM OF SQUARES = 9148.198

INITIAL GUESSES AND INPUT OF PARAMETERS

		FIX
VELOCITY(cm/d)	1100	
DISPERSIVITY (cm)	46	
PULSE WIDTH (cm)	167	
RF	1	Y
Co (mg/L)	372	Y
FODC (1/sec)	0	Y
DISTANCE FROM SOURCE (cm)	269	Y
DIFFUSION COEFF (cm^2/sec)	0.000001	Y

95% CONFIDENCE INTERVALS FOR ESTIMATED PARAMETERS

Parameter	Low	Optimized	High
VELOCITY(cm/d)	1374.25	1696.605	1883.232
DISPERSIVITY(cm)	7.629055	38.14528	77.81636
PULSE WIDTH (cm)	276.5056	314.2109	361.3425

Observed Time (Hours)	Observed Br- Conc (mg/L)	Calculated Br- Conc (mg/L)	Residuals
0	19.8732	0	19.8732
0.33333333	56.9682	58.2802344	-1.3120344
0.8	168.8684	140.71101	28.1573897
1.23333333	179.9549	186.759036	-6.8041363
1.71666667	222.0534	222.036872	0.01652799
3.75	293.2018	298.645981	-5.4441812
4.28333333	357.3545	309.795432	47.5590681
4.7	352.521	317.108728	35.4122715
5.21666667	258.992	258.990435	0.00156494
10.5333333	29.9466	29.9288657	0.01773434
12.3833333	21.3166	17.6659103	3.65068972
14.9166667	12.5773	8.95850301	3.61879699
17.3	4.6335	4.86200477	-0.2285048

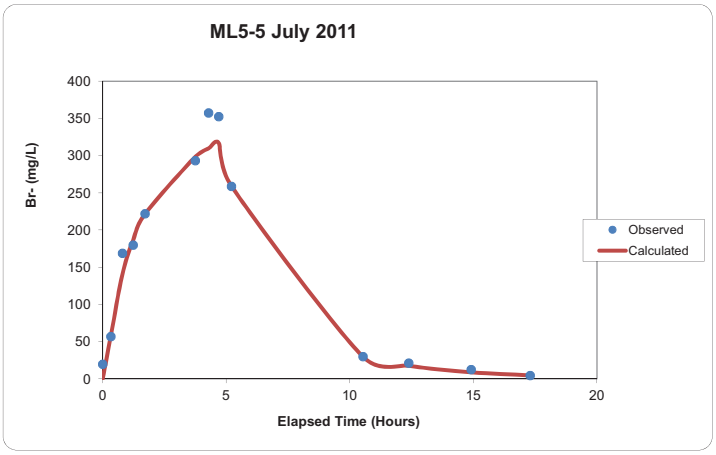

OPTIMIZED PARAMETER ESTIMATES

VELOCITY(cm/d)	1769.029	0.000205
DISPERSIVITY (cm)	86.49354	
PULSE WIDTH (cm)	357.6094	
RF	1	
Co (mg/L)	372	
FODC (/sec)	0	

RESDIUAL SUM OF SQUARES = 2353.97

INITIAL GUESSES AND INPUT OF PARAMETERS

		FIX
VELOCITY(cm/d)	1100	
DISPERSIVITY (cm)	46	
PULSE WIDTH (cm)	167	
RF	1	Y
Co (mg/L)	372	Y
FODC (1/sec)	0	Y
DISTANCE FROM SOURCE (cm)	269	Y
DIFFUSION COEFF (cm^2/sec)	0.000001	Y

95% CONFIDENCE INTERVALS FOR ESTIMATED PARAMETERS

Parameter	Low	Optimized	High
VELOCITY(cm/d)	1698.268	1769.029	1857.48
DISPERSIVITY(cm)	52.76106	86.49354	121.091
PULSE WIDTH (cm)	343.305	357.6094	375.4899

Observed Time (Hours)	Observed Br- Conc (mg/L)	Calculated Br- Conc (mg/L)	Residuals
0	18.6436	0	18.6436
0.53333333	13.922	0.00319337	13.9188066
0.85	15.4371	0.158629	15.278471
1.26666667	12.0844	1.46937842	10.6150216
1.75	17.2695	5.37050022	11.8989998
3.78333333	35.2376	37.7996471	-2.5620471
4.31666667	51.2025	47.3955857	3.80691433
4.71666667	45.7756	54.4851249	-8.7095249
5.25	72.4497	63.702358	8.74734199
10.55	102.5824	112.502113	-9.9197133
12.4166667	97.3089	98.4871162	-1.1782162
14.95	89.6851	80.6851826	8.99991742
17.3166667	72.2108	67.8095463	4.4012537

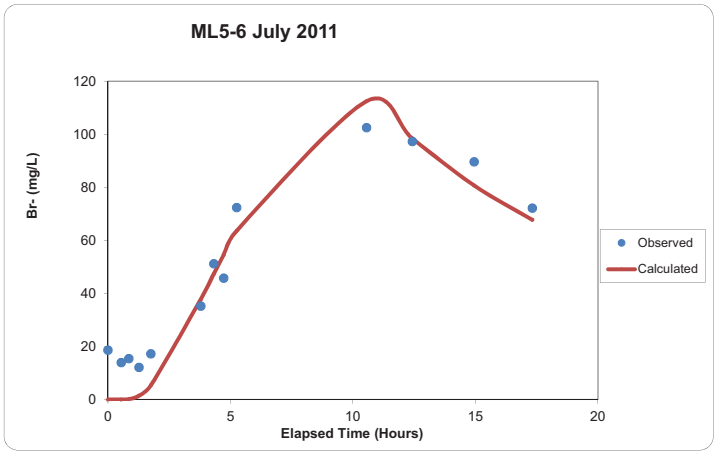

OPTIMIZED PARAMETER ESTIMATES

VELOCITY(cm/d)	335.433	3.88E-05
DISPERSIVITY (cm)	158.4665	
PULSE WIDTH (cm)	103.3099	
RF	1	
Co (mg/L)	372	
FODC (/sec)	0	

RESDIUAL SUM OF SQUARES = 1402.468

INITIAL GUESSES AND INPUT OF PARAMETERS

		FIX
VELOCITY(cm/d)	1100	
DISPERSIVITY (cm)	46	
PULSE WIDTH (cm)	167	
RF	1	Y
Co (mg/L)	372	Y
FODC (1/sec)	0	Y
DISTANCE FROM SOURCE (cm)	269	Y
DIFFUSION COEFF (cm^2/sec)	0.000001	Y

95% CONFIDENCE INTERVALS FOR ESTIMATED PARAMETERS

Parameter	Low	Optimized	High
VELOCITY(cm/d)	271.7008	335.433	399.1653
DISPERSIVITY(cm)	104.5879	158.4665	236.1151
PULSE WIDTH (cm)	84.71415	103.3099	120.8726

Observed Time (Hours)	Observed Br- Conc (mg/L)	Calculated Br- Conc (mg/L)	Residuals
0	14.3959	0	14.3959
0.56666667	14.0965	0.19058802	13.905912
0.88333333	13.8532	2.01274798	11.840452
1.33333333	21.4106	8.87610389	12.5344961
1.8	31.7683	19.5850557	12.1832443
3.85	60.3189	73.0803453	-12.761445
4.35	78.4997	84.7903166	-6.2906166
4.73333333	62.8741	93.2760205	-30.401921
5.28333333	146.2786	104.737607	41.5409934
10.5833333	109.2334	116.336777	-7.1033771
12.4333333	90.2429	94.3600834	-4.1171834
14.9666667	76.476	73.300394	3.17560598
17.3333333	78.7568	59.7238501	19.0329499

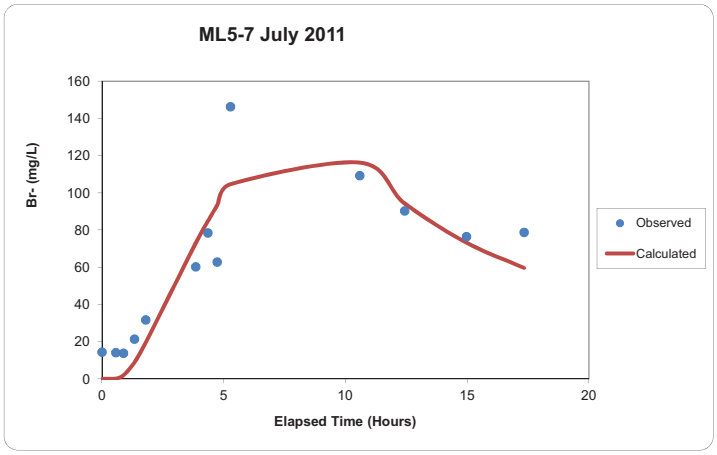

OPTIMIZED PARAMETER ESTIMATES

VELOCITY(cm/d)	453.1342	5.24E-05
DISPERSIVITY (cm)	160.8176	
PULSE WIDTH (cm)	131.3483	
RF	1	
Co (mg/L)	372	
FODC (/sec)	0	

RESDIUAL SUM OF SQUARES = 4137.86

INITIAL GUESSES AND INPUT OF PARAMETERS

		FIX
VELOCITY(cm/d)	1100	
DISPERSIVITY (cm)	46	
PULSE WIDTH (cm)	167	
RF	1	Y
Co (mg/L)	372	Y
FODC (1/sec)	0	Y
DISTANCE FROM SOURCE (cm)	269	Y
DIFFUSION COEFF (cm^2/sec)	0.000001	Y

95% CONFIDENCE INTERVALS FOR ESTIMATED PARAMETERS

Parameter	Low	Optimized	High
VELOCITY(cm/d)	357.976	453.1342	575.4804
DISPERSIVITY(cm)	88.44967	160.8176	315.2024
PULSE WIDTH (cm)	90.63035	131.3483	164.1854

Observed Time (Hours)	Observed Br- Conc (mg/L)	Calculated Br- Conc (mg/L)	Residuals
0	19.8865	0	19.8865
0.33333333	14.6688	1.8363E-52	14.6688
0.61666667	20.5549	1.3254E-27	20.5549
1.06666667	16.4803	3.2292E-15	16.4803
1.56666667	13.1342	9.0213E-10	13.1342
3.56666667	19.1532	0.00344861	19.1497514
4.13333333	21.082	0.01796604	21.064034
4.63333333	16.2898	0.05538717	16.2344128
5.38333333	17.8345	0.20375454	17.6307455
10.2333333	10.166	9.71819208	0.44780792
12.1	13.7787	18.834642	-5.055942
14.8166667	39.119	34.426512	4.69248802
17.2166667	44.248	46.3501953	-2.1021953

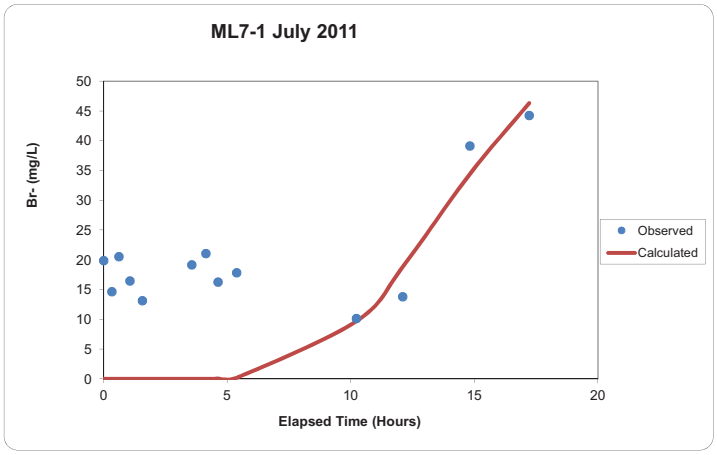

OPTIMIZED PARAMETER ESTIMATES

VELOCITY(cm/d)	377.4348	4.37E-05
DISPERSIVITY (cm)	98.69748	
PULSE WIDTH (cm)	103.6639	
RF	1	
Co (mg/L)	372	
FODC (/sec)	0	

RESDIUAL SUM OF SQUARES = 2914.261

INITIAL GUESSES AND INPUT OF PARAMETERS

		FIX
VELOCITY(cm/d)	1100	
DISPERSIVITY (cm)	38	
PULSE WIDTH (cm)	167	
RF	1	Y
Co (mg/L)	372	Y
FODC (1/sec)	0	Y
DISTANCE FROM SOURCE (cm)	559	Y
DIFFUSION COEFF (cm^2/sec)	0.000001	Y

95% CONFIDENCE INTERVALS FOR ESTIMATED PARAMETERS

Parameter	Low	Optimized	High
VELOCITY(cm/d)	135.8765	377.4348	698.2545
DISPERSIVITY(cm)	12.83067	98.69748	538.8883
PULSE WIDTH (cm)	1.036639	103.6639	256.0499

Observed Time (Hours)	Observed Br- Conc (mg/L)	Calculated Br- Conc (mg/L)	Residuals
0	15.9475	0	15.9475
0.36666667	14.7965	1.7836E-06	14.7964982
0.65	13.1648	0.00497677	13.1598232
1.1	15.7504	0.3678361	15.3825639
1.6	14.6333	2.72414558	11.9091544
3.6	53.1365	36.2314443	16.9050557
4.16666667	46.9186	49.0217096	-2.1031096
4.65	43.7071	60.1082555	-16.401155
5.4	81.2289	77.1485504	4.08034964
10.25	172.6035	168.750021	3.85347866
12.1166667	198.3953	195.069406	3.32589407
14.8333333	185.8926	202.066423	-16.173823
17.2333333	185.0195	170.755243	14.2642572

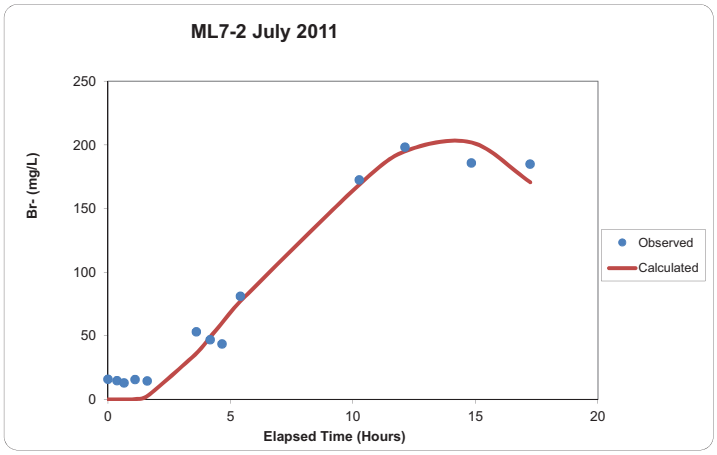

OPTIMIZED PARAMETER ESTIMATES

VELOCITY(cm/d)	774.1164	8.96E-05
DISPERSIVITY (cm)	163.7399	
PULSE WIDTH (cm)	380.1103	
RF	1	
Co (mg/L)	372	
FODC (/sec)	0	

RESDIUAL SUM OF SQUARES = 2091.484

INITIAL GUESSES AND INPUT OF PARAMETERS

		FIX
VELOCITY(cm/d)	1100	
DISPERSIVITY (cm)	46	
PULSE WIDTH (cm)	167	
RF	1	Y
Co (mg/L)	372	Y
FODC (1/sec)	0	Y
DISTANCE FROM SOURCE (cm)	559	Y
DIFFUSION COEFF (cm^2/sec)	0.000001	Y

95% CONFIDENCE INTERVALS FOR ESTIMATED PARAMETERS

Parameter	Low	Optimized	High
VELOCITY(cm/d)	665.7401	774.1164	874.7516
DISPERSIVITY(cm)	108.0683	163.7399	250.522
PULSE WIDTH (cm)	330.696	380.1103	429.5247

Observed Time (Hours)	Observed Br- Conc (mg/L)	Calculated Br- Conc (mg/L)	Residuals
0	11.4873	0	11.4873
0.38333333	12.6136	2.6882E-06	12.6135973
0.7	13.2804	0.0140403	13.2663597
1.15	14.4254	0.87582716	13.5495728
1.63333333	20.5265	6.08686404	14.439636
3.65	83.9855	82.140216	1.84528398
4.21666667	102.2033	109.127538	-6.9242376
4.66666667	99.2005	130.011891	-30.811391
5.41666667	197.7026	162.688838	35.0137623
10.2666667	193.3748	196.050694	-2.6758937
12.1333333	141.871	139.446782	2.424218
14.85	73.2947	79.3907168	-6.0960168
17.25	59.6595	47.4198122	12.2396878

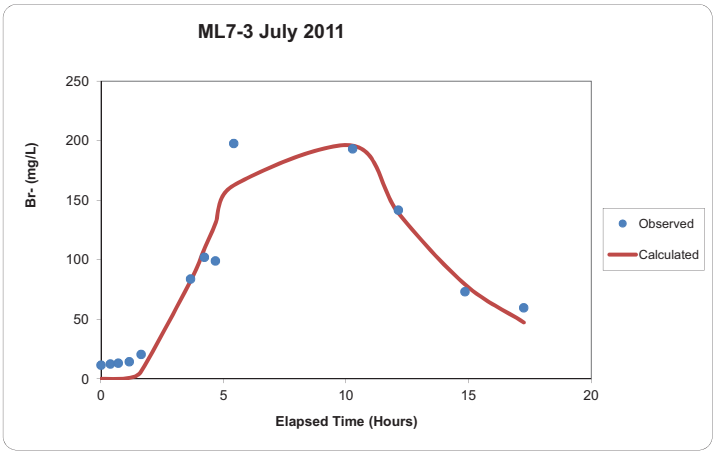

OPTIMIZED PARAMETER ESTIMATES

VELOCITY(cm/d)	1473.832	0.000171
DISPERSIVITY (cm)	77.96214	
PULSE WIDTH (cm)	382.4623	
RF	1	
Co (mg/L)	372	
FODC (/sec)	0	

RESDIUAL SUM OF SQUARES = 3285.77

INITIAL GUESSES AND INPUT OF PARAMETERS

		FIX
VELOCITY(cm/d)	1100	
DISPERSIVITY (cm)	46	
PULSE WIDTH (cm)	167	
RF	1	Y
Co (mg/L)	372	Y
FODC (1/sec)	0	Y
DISTANCE FROM SOURCE (cm)	559	Y
DIFFUSION COEFF (cm^2/sec)	0.000001	Y

95% CONFIDENCE INTERVALS FOR ESTIMATED PARAMETERS

Parameter	Low	Optimized	High
VELOCITY(cm/d)	1341.187	1473.832	1606.477
DISPERSIVITY(cm)	45.21804	77.96214	143.4503
PULSE WIDTH (cm)	317.4437	382.4623	439.8316

Observed Time (Hours)	Observed Br- Conc (mg/L)	Calculated Br- Conc (mg/L)	Residuals
0	13.028	0	13.028
0.43333333	12.2901	0.20683676	12.0832632
0.76666667	16.1304	4.58954569	11.5408543
1.18333333	26.5041	20.2999817	6.20411833
1.66666667	44.4274	46.6455081	-2.2181081
3.7	146.8059	156.236223	-9.4303234
4.25	199.518	179.349404	20.1685965
4.68333333	109.6129	195.647695	-86.034795
5.43333333	304.4503	220.348112	84.1021876
10.2833333	136.754	143.897291	-7.1432909
12.1333333	92.4401	97.2413515	-4.8012515
14.8666667	75.8361	56.3358879	19.5002121
17.2833333	54.1939	35.6787868	18.5151132

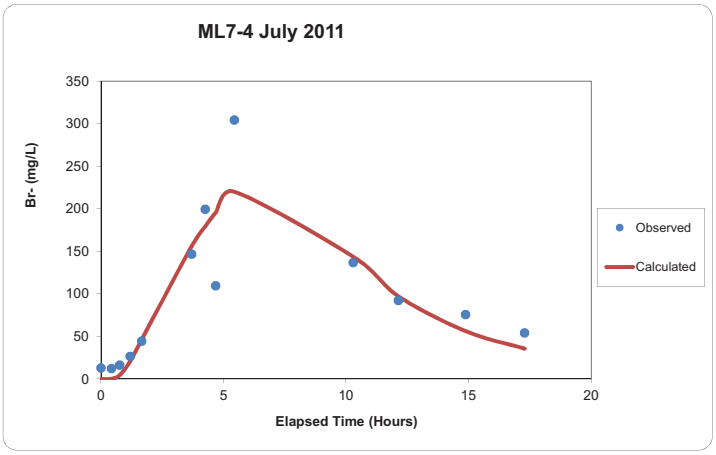

OPTIMIZED PARAMETER ESTIMATES

VELOCITY(cm/d)	1769.365	0.000205
DISPERSIVITY (cm)	127.2812	
PULSE WIDTH (cm)	466.0293	
RF	1	
Co (mg/L)	372	
FODC (/sec)	0	

RESDIUAL SUM OF SQUARES = 16258.3

INITIAL GUESSES AND INPUT OF PARAMETERS

		FIX
VELOCITY(cm/d)	1100	
DISPERSIVITY (cm)	46	
PULSE WIDTH (cm)	167	
RF	1	Y
Co (mg/L)	372	Y
FODC (1/sec)	0	Y
DISTANCE FROM SOURCE (cm)	559	Y
DIFFUSION COEFF (cm^2/sec)	0.000001	Y

95% CONFIDENCE INTERVALS FOR ESTIMATED PARAMETERS

Parameter	Low	Optimized	High
VELOCITY(cm/d)	1415.492	1769.365	2335.561
DISPERSIVITY(cm)	15.27374	127.2812	654.2253
PULSE WIDTH (cm)	284.2779	466.0293	629.1396

Observed Time (Hours)	Observed Br- Conc (mg/L)	Calculated Br- Conc (mg/L)	Residuals
0	11.2493	0	11.2493
0.33333333	14.458	7.8126E-07	14.4579992
0.8	14.9718	0.06389149	14.9079085
1.23333333	12.6262	1.19993582	11.4262642
1.71666667	18.4313	5.75157569	12.6797243
3.75	58.6821	56.2717693	2.41033067
4.28333333	68.272	72.5651086	-4.2931086
4.7	51.1722	85.2212533	-34.049053
5.45	107.3085	107.341382	-0.032882
10.3	142.3194	133.692662	8.62673815
12.15	105.6197	109.446148	-3.8264478
14.8833333	79.3238	79.6933918	-0.3695918
17.3	60.2508	60.2677826	-0.0169826

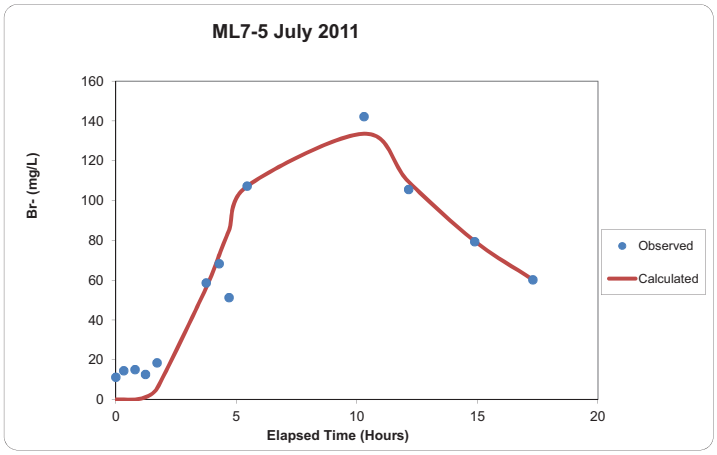

OPTIMIZED PARAMETER ESTIMATES

VELOCITY(cm/d)	1170.33	0.000135
DISPERSIVITY (cm)	146.0518	
PULSE WIDTH (cm)	275.6645	
RF	1	
Co (mg/L)	372	
FODC (/sec)	0	

RESDIUAL SUM OF SQUARES = 1293.181

INITIAL GUESSES AND INPUT OF PARAMETERS

		FIX
VELOCITY(cm/d)	1100	
DISPERSIVITY (cm)	46	
PULSE WIDTH (cm)	167	
RF	1	Y
Co (mg/L)	372	Y
FODC (1/sec)	0	Y
DISTANCE FROM SOURCE (cm)	559	Y
DIFFUSION COEFF (cm^2/sec)	0.000001	Y

95% CONFIDENCE INTERVALS FOR ESTIMATED PARAMETERS

Parameter	Low	Optimized	High
VELOCITY(cm/d)	1029.89	1170.33	1263.956
DISPERSIVITY(cm)	99.31519	146.0518	194.2488
PULSE WIDTH (cm)	234.3148	275.6645	311.5009

Observed Time (Hours)	Observed Br- Conc (mg/L)	Calculated Br- Conc (mg/L)	Residuals
0	11.0576	0	11.0576
0.53333333	13.9551	2.4795E-08	13.9551
0.85	14.1473	0.00015945	14.1471405
1.26666667	12.7708	0.02173978	12.7490602
1.75	15.1444	0.3591888	14.7852112
3.78333333	30.707	20.2982657	10.4087343
4.31666667	40.6607	31.4311847	9.22951528
4.71666667	40.1707	40.8769899	-0.7062899
5.46666667	51.8585	59.2569516	-7.3984516
10.3166667	89.3614	86.3731172	2.98828282
12.1666667	55.9793	73.8350807	-17.855781
14.9166667	65.3037	54.7004153	10.6032847
17.3166667	53.6246	40.9070552	12.7175448

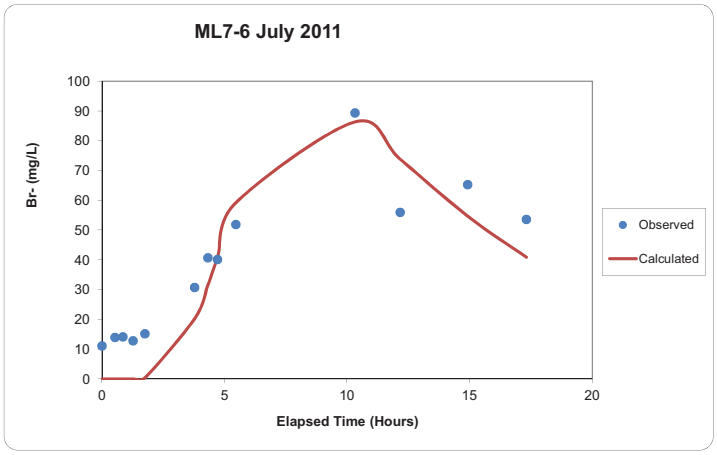

OPTIMIZED PARAMETER ESTIMATES

VELOCITY(cm/d)	1127.627	0.000131
DISPERSIVITY (cm)	100	
PULSE WIDTH (cm)	158.3228	
RF	1	
Co (mg/L)	372	
FODC (/sec)	0	

RESDIUAL SUM OF SQUARES = 1748.773

INITIAL GUESSES AND INPUT OF PARAMETERS

		FIX
VELOCITY(cm/d)	1100	
DISPERSIVITY (cm)	100	Y
PULSE WIDTH (cm)	163	
RF	1	Y
Co (mg/L)	372	Y
FODC (1/sec)	0	Y
DISTANCE FROM SOURCE (cm)	559	Y
DIFFUSION COEFF (cm^2/sec)	0.000001	Y

95% CONFIDENCE INTERVALS FOR ESTIMATED PARAMETERS

Parameter	Low	Optimized	High
VELOCITY(cm/d)	969.7594	1127.627	1285.495
PULSE WIDTH (cm)	121.9086	158.3228	196.3203

Observed Time (Hours)	Observed Br- Conc (mg/L)	Calculated Br- Conc (mg/L)	Residuals
0	10.2957	0	10.2957
0.56666667	13.3193	0.00268533	13.3166147
0.88333333	15.6601	0.18779176	15.4723082
1.33333333	25.7201	2.57748331	23.1426167
1.8	46.0239	10.0639624	35.9599376
3.85	91.7586	85.4279176	6.33068237
4.35	110.5817	106.544882	4.03681774
4.73333333	123.1092	121.77031	1.33888985
5.48333333	123.8026	141.928561	-18.125961
10.3333333	84.419	86.8831464	-2.4641464
12.1833333	70.101	62.9006262	7.20037384
14.9333333	47.2306	38.5187131	8.71188691
17.3333333	34.5708	25.1304009	9.44039905

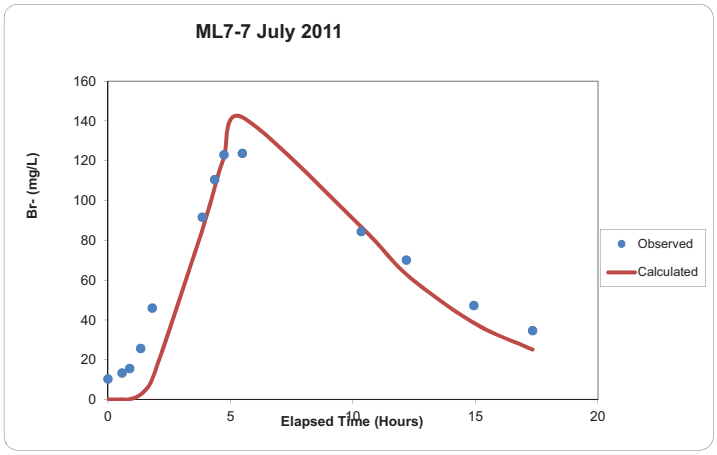

OPTIMIZED PARAMETER ESTIMATES

VELOCITY(cm/d)	1611.807
DISPERSIVITY (cm)	110
PULSE WIDTH (cm)	249.4063
RF	1
Co (mg/L)	372
FODC (/sec)	0

RESDIUAL SUM OF SQUARES = 2961.053

INITIAL GUESSES AND INPUT OF PARAMETERS

		FIX
VELOCITY(cm/d)	1800	
DISPERSIVITY (cm)	110	Y
PULSE WIDTH (cm)	160	
RF	1	Y
Co (mg/L)	372	Y
FODC (1/sec)	0	Y
DISTANCE FROM SOURCE (cm)	559	Y
DIFFUSION COEFF (cm^2/sec)	0.000001	Y

95% CONFIDENCE INTERVALS FOR ESTIMATED PARAMETERS

Parameter	Low	Optimized	High
VELOCITY(cm/d)	1434.509	1611.807	1853.578
PULSE WIDTH (cm)	197.031	249.4063	311.7579

Observed Time (Hours)	Observed Br- Conc (mg/L)
0.00	0
0.62	0
1.07	3.082
1.60	2.744
2.08	0
2.60	3.7
3.10	3.6
3.58	4.365
4.07	0
4.58	4.402
5.08	6.198
5.58	0
6.07	0
6.58	5.444
7.08	0.318
7.87	1.4
8.95	1.8
10.67	0.544
12.03	0.76
13.03	0.6815
14.05	0
14.97	0.3
18.18	0
21.15	0
25.18	0
27.93	0

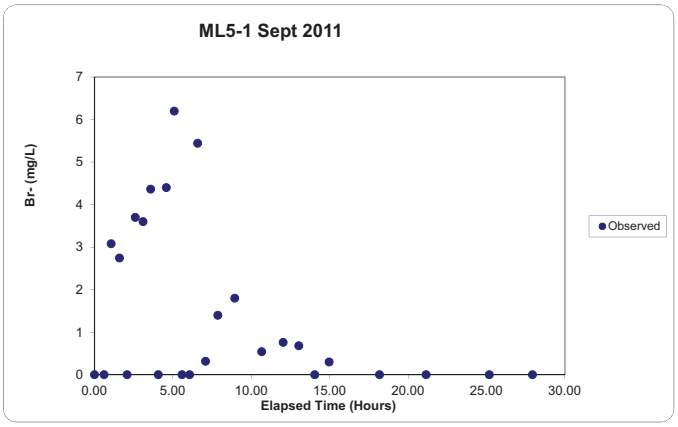

Observed Time (Hours)	Observed Br- Conc (mg/L)	Calculated Br- Conc (mg/L)	Residuals
0	0	0	0
0.63333333	0	6.5661E-12	-6.566E-12
1.08333333	3.123	3.1208E-06	3.12299688
1.61666667	0	0.00144216	-0.0014422
2.1	4.6	0.02618528	4.57381472
2.61666667	0	0.17971527	-0.1797153
3.11666667	0	0.61970045	-0.6197004
3.6	3.529	1.4269474	2.1020526
4.08333333	0	2.59990943	-2.5999094
4.6	0	4.14834474	-4.1483447
5.1	3.499	5.79513324	-2.2961332
5.6	2.888	7.46058058	-4.5725806
6.08333333	14.006	8.99976889	5.00623111
6.6	15.273	10.5051685	4.76783149
7.1	11.5	11.7901475	-0.2901475
7.88333333	13.8	13.4355098	0.36449015
8.95	15.389	14.9825863	0.40641371
10.6833333	16.472	16.1110349	0.36096509
12.05	15.1	16.152045	-1.052045
13.05	17.2	15.8742065	1.3257935
14.0666667	14.772	15.4137215	-0.6417215
14.9833333	13.6	14.8943756	-1.2943756
18.2	10.565	12.7169816	-2.1519816
21.1666667	8.735	10.6652378	-1.9302378
25.2	7.576	8.2134171	-0.6374171
27.95	11.8	6.82302784	4.97697216

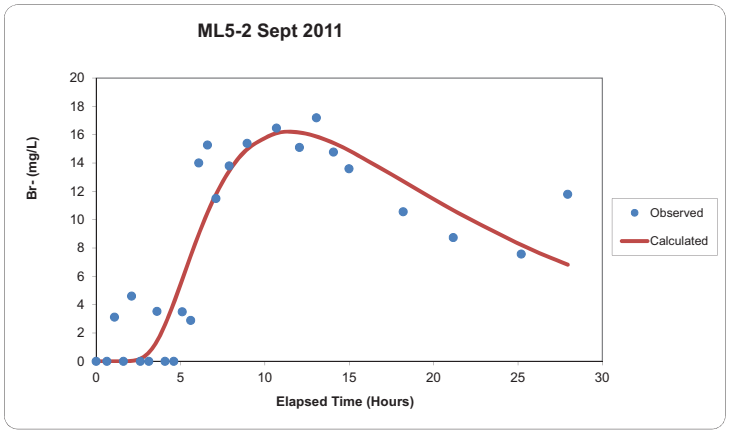

OPTIMIZED PARAMETER ESTIMATES

VELOCITY(cm/d)	348.049	4.02835E-05
DISPERSIVITY (cm)	60.68559	
PULSE WIDTH (cm)	15.04394	
RF	1	
Co (mg/L)	372	
FODC (/sec)	0	

RESDIUAL SUM OF SQUARES = 172.4451

INITIAL GUESSES AND INPUT OF PARAMETERS

		FIX
VELOCITY(cm/d)	1100	
DISPERSIVITY (cm)	38	
PULSE WIDTH (cm)	167	
RF	1	Y
Co (mg/L)	372	Y
FODC (1/sec)	0	Y
DISTANCE FROM SOURCE (cm)	269	Y
DIFFUSION COEFF (cm^2/sec)	0.000001	Y

95% CONFIDENCE INTERVALS FOR ESTIMATED PARAMETERS

Parameter	Low	Optimized	High
VELOCITY(cm/d)	295.8417	348.049	407.2174
DISPERSIVITY(cm)	45.51419	60.68559	80.10498
PULSE WIDTH (cm)	12.33603	15.04394	17.75185

Observed Time (Hours)	Observed Br- Conc (mg/L)	Calculated Br- Conc (mg/L)	Residuals
0	0	0	0
0.65	3.564	5.75047589	-2.1864759
1.1	25.706	30.2427611	-4.5367611
1.63333333	69.484	69.4087009	0.07529911
2.11666667	98.3	104.643255	-6.343255
2.63333333	144.2	138.711296	5.48870409
3.13333333	157.6	167.58963	-9.9896296
3.61666667	219.2	191.901379	27.2986211
4.1	182.8	213.072074	-30.272074
4.61666667	244.8	232.696788	12.1032121
5.11666667	27.205	249.153855	-221.94886
5.61666667	270	263.48212	6.5178798
6.11666667	322.4	275.987222	46.4127779
6.61666667	345.6	286.927107	58.6728927
7.13333333	296.8	296.818017	-0.0180168
7.9	302.4	309.266693	-6.8666926
8.96666667	294.8	323.030855	-28.230855
10.7	290.3	338.977556	-48.677556
12.0666667	274.8	307.941932	-33.141932
13.0666667	254	239.677264	14.3227364
14.0833333	174.6	182.517654	-7.9176539
15	227.2	143.346608	83.8533921
18.2166667	270.4	64.3674235	206.032577
21.2	236	32.128245	203.871755
25.2333333	7.722	13.1079264	-5.3859264
27.9666667	253.598	7.27037517	246.327625

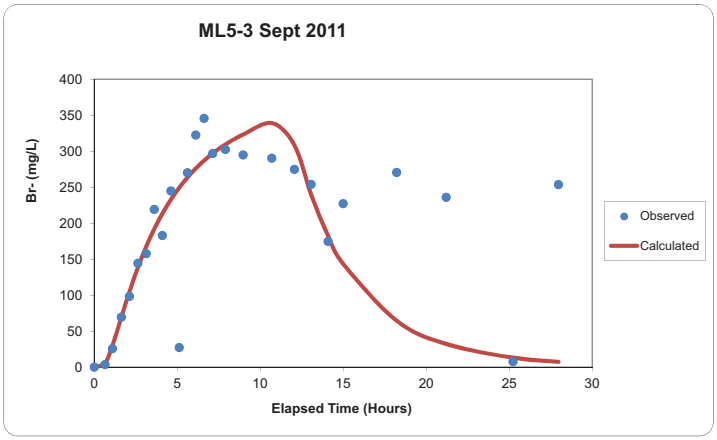

OPTIMIZED PARAMETER ESTIMATES

VELOCITY(cm/d)	724.8211	8.39E-05
DISPERSIVITY (cm)	40.35751	
PULSE WIDTH (cm)	327.0937	
RF	1	
Co (mg/L)	372	
FODC (/sec)	0	

RESDIUAL SUM OF SQUARES = 60478.74

INITIAL GUESSES AND INPUT OF PARAMETERS

		FIX
VELOCITY(cm/d)	1100	
DISPERSIVITY (cm)	38	
PULSE WIDTH (cm)	167	
RF	1	Y
Co (mg/L)	372	Y
FODC (1/sec)	0	Y
DISTANCE FROM SOURCE (cm)	269	Y
DIFFUSION COEFF (cm^2/sec)	0.000001	Y

95% CONFIDENCE INTERVALS FOR ESTIMATED PARAMETERS

Parameter	Low	Optimized	High
VELOCITY(cm/d)	659.5872	724.8211	775.5586
DISPERSIVITY(cm)	23.81093	40.35751	70.22206
PULSE WIDTH (cm)	300.9262	327.0937	353.2612

Observed Time (Hours)	Observed Br- Conc (mg/L)	Calculated Br- Conc (mg/L)	Residuals
0.7	27.397	36.3123565	-8.9153565
1.15	104.763	86.282091	18.480909
1.66666667	140.6	136.046924	4.55307617
2.15	165.2	173.586832	-8.3868318
2.66666667	207.2	205.897822	1.30217781
3.16666667	203.2	231.224451	-28.024451
3.65	246	251.404489	-5.4044887
4.13333333	274.4	268.24681	6.15319024
4.65	334.4	283.303295	51.0967046
5.15	334.4	295.534601	38.8653992
5.63333333	230	305.574239	-75.574239
6.15	268.8	314.708597	-45.908597
6.65	188.4	322.242643	-133.84264
7.23333333	244.8	326.198971	-81.398971
7.93333333	263.6	264.634034	-1.034034
9	197.2	176.511728	20.6882718
10.7333333	108	97.6266449	10.3733551
12.1	49.9	63.9081698	-14.00817
13.0833333	35.59	47.829486	-12.239486
14.1333333	35.58	35.4551285	0.12487152
15.0333333	25.7	27.6094883	-1.9094883
18.25	11.176	11.6898111	-0.5138111
21.2166667	8.045	5.46215077	2.58284923
25.2666667	3.301	1.99224871	1.30875129
28	2.875	1.0222473	1.8527527

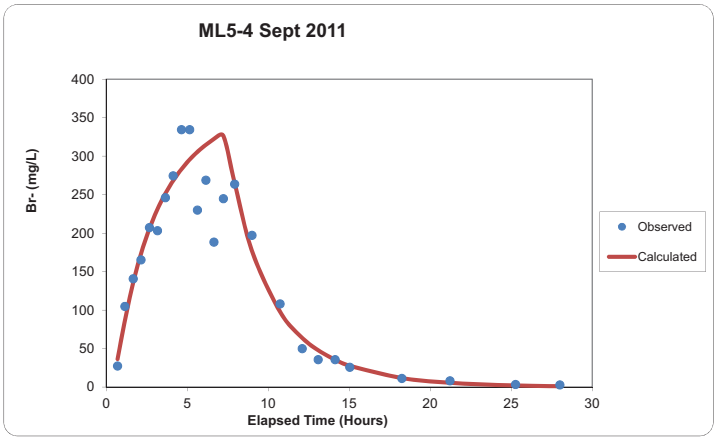

OPTIMIZED PARAMETER ESTIMATES

VELOCITY(cm/d)	1115.529	0.000129
DISPERSIVITY (cm)	52.70039	
PULSE WIDTH (cm)	320.5495	
RF	1	
Co (mg/L)	372	
FODC (/sec)	0	

RESDIUAL SUM OF SQUARES = 12717.99

INITIAL GUESSES AND INPUT OF PARAMETERS

		FIX
VELOCITY(cm/d)	1100	
DISPERSIVITY (cm)	38	
PULSE WIDTH (cm)	167	
RF	1	Y
Co (mg/L)	372	Y
FODC (1/sec)	0	Y
DISTANCE FROM SOURCE (cm)	269	Y
DIFFUSION COEFF (cm^2/sec)	0.000001	Y

95% CONFIDENCE INTERVALS FOR ESTIMATED PARAMETERS

Parameter	Low	Optimized	High
VELOCITY(cm/d)	1059.753	1115.529	1193.616
DISPERSIVITY(cm)	33.72825	52.70039	84.32062
PULSE WIDTH (cm)	291.7	320.5495	342.9879

Observed Time (Hours)	Observed Br- Conc (mg/L)	Calculated Br- Conc (mg/L)	Residuals
0	0	0	0
0.73333333	150.4	140.145599	10.2544014
1.16666667	168.8	186.039525	-17.239525
1.7	206	223.346902	-17.346902
2.16666667	257.6	246.857776	10.7422238
2.68333333	251.2	266.911059	-15.711059
3.18333333	311.2	282.27226	28.9277396
3.66666667	330.8	294.40548	36.3945205
4.18333333	324.8	305.153662	19.6463377
4.68333333	318.8	312.695462	6.10453839
5.16666667	44.999	208.999893	-164.00089
5.66666667	290.4	152.146784	138.253216
6.16666667	151.2	118.766822	32.4331776
6.66666667	112.4	96.1003939	16.2996061
7.2	160.2	78.5266093	81.6733907
7.95	103.3	60.7119399	42.5880601
9.01666667	73.5	43.5616081	29.9383919
10.75	39.32	26.7038044	12.6161956
12.1166667	19.12	18.6442803	0.47571972
13.1333333	18.54	14.4171778	4.12282224
14.15	13.54	11.2218762	2.3181238
15.05	6.569	9.02958534	-2.4605853
18.2666667	4.884	4.25792694	0.62607306
21.25	2.881	2.17286029	0.70813971
25.2833333	3.02	0.89639371	2.12360629
28.0166667	1.027	0.4974297	0.5295703

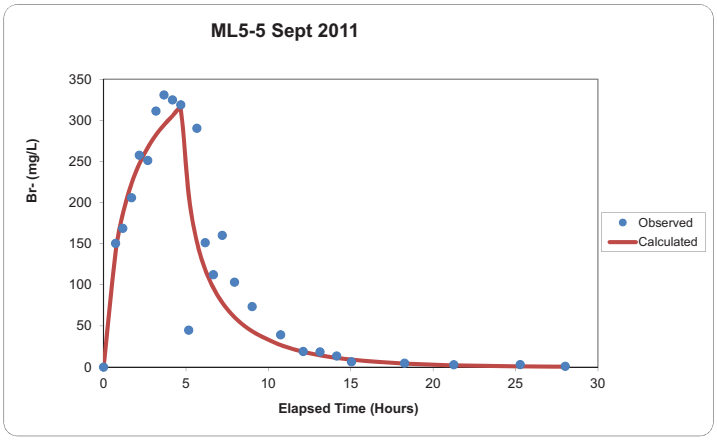

OPTIMIZED PARAMETER ESTIMATES

VELOCITY(cm/d)	1861.435	0.000215
DISPERSIVITY (cm)	100.3631	
PULSE WIDTH (cm)	358.5327	
RF	1	
Co (mg/L)	372	
FODC (/sec)	0	

RESDIUAL SUM OF SQUARES = 12197.21

INITIAL GUESSES AND INPUT OF PARAMETERS

		FIX
VELOCITY(cm/d)	1100	
DISPERSIVITY (cm)	38	
PULSE WIDTH (cm)	167	
RF	1	Y
Co (mg/L)	372	Y
FODC (1/sec)	0	Y
DISTANCE FROM SOURCE (cm)	269	Y
DIFFUSION COEFF (cm^2/sec)	0.000001	Y

95% CONFIDENCE INTERVALS FOR ESTIMATED PARAMETERS

Parameter	Low	Optimized	High
VELOCITY(cm/d)	1824.206	1861.435	1917.278
DISPERSIVITY(cm)	72.2614	100.3631	141.5119
PULSE WIDTH (cm)	344.1914	358.5327	369.2887

Observed Time (Hours)	Observed Br- Conc (mg/L)	Calculated Br- Conc (mg/L)	Residuals
0	0	0	0
0.75	0	0.03277742	-0.0327774
1.2	0	0.84341947	-0.8434195
1.71666667	2.277	4.53349943	-2.2564994
2.2	3.9	10.9830528	-7.0830528
2.7	12	19.9756496	-7.9756496
3.2	19.6	30.4631837	-10.863184
3.7	41.822	41.7603387	0.06166131
4.2	56.339	53.3941149	2.94488508
4.7	75.833	65.0552037	10.7777963
5.2	67.885	76.5477834	-8.6627834
5.68333333	85.464	87.3837417	-1.9197417
6.18333333	119.8	98.2412898	21.5587102
6.7	183.6	109.044231	74.555769
7.21666667	174.42	119.405111	55.0148892
7.98333333	158.3	133.959663	24.340337
9.05	156.8	152.193056	4.60694358
10.7666667	151.3	157.40555	-6.1055497
12.15	137.9	145.012112	-7.1121124
13.15	130.2	133.9465	-3.7465001
14.1666667	123.2	122.789163	0.41083739
15.0666667	111.4	113.480208	-2.0802083
18.2833333	101.945	85.8603199	16.0846801
21.2666667	96.612	67.1505227	29.4614773
25.3	78.315	49.1565696	29.1584304
28.05	66.833	40.1841843	26.6488157

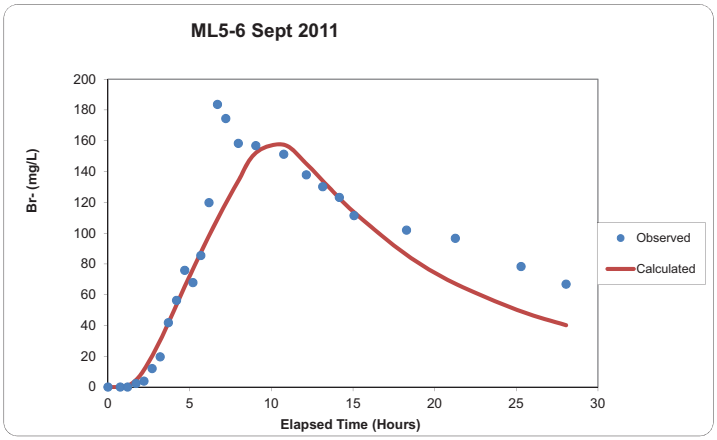

OPTIMIZED PARAMETER ESTIMATES

VELOCITY(cm/d)	420.8206	4.87E-05
DISPERSIVITY (cm)	93.64806	
PULSE WIDTH (cm)	140.6177	
RF	1	
Co (mg/L)	372	
FODC (/sec)	0	

RESDIUAL SUM OF SQUARES = 4625.501

INITIAL GUESSES AND INPUT OF PARAMETERS

		FIX
VELOCITY(cm/d)	1100	
DISPERSIVITY (cm)	38	
PULSE WIDTH (cm)	167	
RF	1	Y
Co (mg/L)	372	Y
FODC (1/sec)	0	Y
DISTANCE FROM SOURCE (cm)	269	Y
DIFFUSION COEFF (cm^2/sec)	0.000001	Y

95% CONFIDENCE INTERVALS FOR ESTIMATED PARAMETERS

Parameter	Low	Optimized	High
VELOCITY(cm/d)	387.1549	420.8206	454.4862
DISPERSIVITY(cm)	75.85493	93.64806	113.3142
PULSE WIDTH (cm)	132.1806	140.6177	153.2733

Observed Time (Hours)	Observed Br- Conc (mg/L)	Calculated Br- Conc (mg/L)	Residuals
0	0	0	0
0.76666667	4.314	3.74404256	0.56995744
1.21666667	12.851	15.6181496	-2.7671496
1.73333333	34	33.7917006	0.20829936
2.21666667	43.5	51.4274726	-7.9274726
2.73333333	60.6	69.4004546	-8.8004546
3.21666667	90.2	84.9846032	5.21539681
3.71666667	90.712	99.809916	-9.097916
4.21666667	128.6	113.40079	15.1992104
4.71666667	132.8	125.878408	6.92159201
5.21666667	149.8	137.366099	12.4339014
5.7	192.8	147.636419	45.1635807
6.2	151.6	157.494939	-5.8949394
6.71666667	108.7	166.954857	-58.254857
7.25	219.6	176.030876	43.569124
8	168.3	187.754701	-19.454701
9.06666667	58.641	202.645541	-144.00454
10.7833333	160.4	186.886135	-26.486135
12.1666667	143.8	153.145025	-9.3450254
13.1666667	132	133.547037	-1.5470375
14.1833333	130.5	117.39821	13.10179
15.0833333	115.6	105.577204	10.0227958
18.3	119.8	75.699177	44.100823
21.2833333	110.588	58.1407481	52.4472519
25.3166667	106.201	42.4354175	63.7655825
28.0666667	97.86	34.8797203	62.9802797

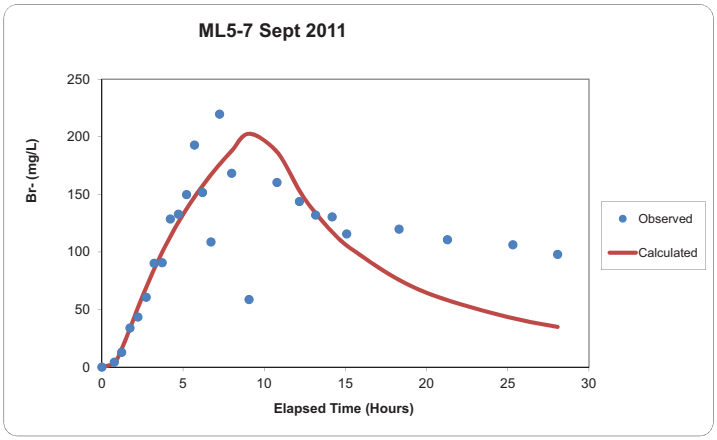

OPTIMIZED PARAMETER ESTIMATES

VELOCITY(cm/d)	520.6989	6.03E-05
DISPERSIVITY (cm)	134.5395	
PULSE WIDTH (cm)	195.5362	
RF	1	
Co (mg/L)	372	
FODC (/sec)	0	

RESDIUAL SUM OF SQUARES = 17616.46

INITIAL GUESSES AND INPUT OF PARAMETERS

		FIX
VELOCITY(cm/d)	1100	
DISPERSIVITY (cm)	160	
PULSE WIDTH (cm)	50	
RF	1	Y
Co (mg/L)	372	Y
FODC (1/sec)	0	Y
DISTANCE FROM SOURCE (cm)	269	Y
DIFFUSION COEFF (cm^2/sec)	0.000001	Y

95% CONFIDENCE INTERVALS FOR ESTIMATED PARAMETERS

Parameter	Low	Optimized	High
VELOCITY(cm/d)	453.008	520.6989	577.9758
DISPERSIVITY(cm)	88.79604	134.5395	196.4276
PULSE WIDTH (cm)	172.0718	195.5362	222.9112

Observed Time (Hours)	Observed Br- Conc (mg/L)	Calculated Br- Conc (mg/L)	Residuals
0	0	0	0
0.68333333	0	1.0005E-45	-1E-45
1.11666667	0	2.2884E-27	-2.288E-27
1.63333333	0	3.5083E-18	-3.508E-18
2.11666667	2	1.2385E-13	2
2.63333333	2.1	1.3109E-10	2.1
3.13333333	0	1.2619E-08	-1.262E-08
3.61666667	2.826	3.1707E-07	2.82599968
4.1	2.838	3.7511E-06	2.83799625
4.6	4.398	2.8138E-05	4.39797186
5.11666667	3.452	0.00014994	3.45185006
5.6	3.128	0.00054426	3.12745574
6.11666667	3.4	0.0017288	3.3982712
6.6	5.485	0.0043368	5.4806632
7.31666667	11.572	0.01360592	11.5583941
8.08333333	0	0.0370659	-0.0370659
9.15	8.897	0.11355001	8.78344999
11	6.9	0.47707517	6.42292483
12.0666667	15.7	0.89687584	14.8031242
13.0833333	1.5	1.4901827	0.0098173
14.1666667	2.416	2.3663314	0.0496686
15.0166667	6.94	3.24924619	3.69075381
18.2166667	8.3	8.26224151	0.03775849
21.2166667	16.092	15.4157819	0.67621815
25.2333333	28.71	28.2659835	0.44401647
27.9666667	36.6	38.6787778	-2.0787778

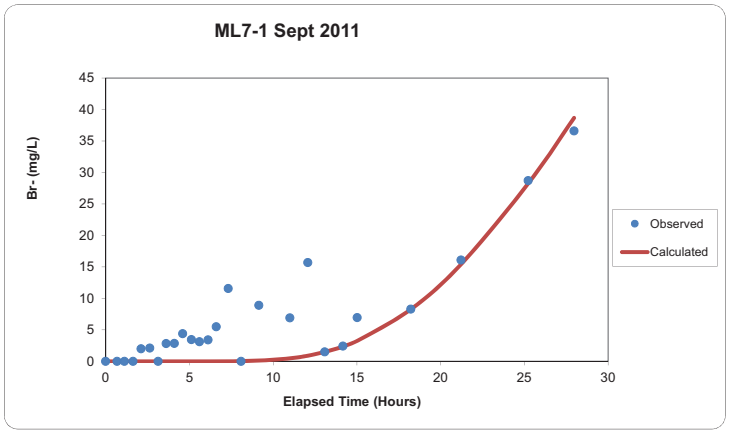

OPTIMIZED PARAMETER ESTIMATES

VELOCITY(cm/d)	187.2045	2.16672E-05
DISPERSIVITY (cm)	100	
PULSE WIDTH (cm)	158.9367	
RF	1	
Co (mg/L)	372	
FODC (/sec)	0	

RESDIUAL SUM OF SQUARES = 596.8031

INITIAL GUESSES AND INPUT OF PARAMETERS

		FIX
VELOCITY(cm/d)	300	
DISPERSIVITY (cm)	100	Y
PULSE WIDTH (cm)	162	
RF	1	Y
Co (mg/L)	372	Y
FODC (1/sec)	0	Y
DISTANCE FROM SOURCE (cm)	559	Y
DIFFUSION COEFF (cm^2/sec)	0.000001	Y

95% CONFIDENCE INTERVALS FOR ESTIMATED PARAMETERS

Parameter	Low	Optimized	High
VELOCITY(cm/d)	170.3561	187.2045	200.3088
PULSE WIDTH (cm)	100.1301	158.9367	209.7965

Observed Time (Hours)	Observed Br- Conc (mg/L)	Calculated Br- Conc (mg/L)	Residuals
0	0	0	0
0.73333333	0	0.00035832	-0.0003583
1.15	0	0.05313171	-0.0531317
1.66666667	1.8	0.8539834	0.9460166
2.16666667	2.4	3.64702246	-1.2470225
2.66666667	2	9.1592842	-7.1592842
3.18333333	12.4	17.6507939	-5.2507939
3.65	27.894	27.3383728	0.55562722
4.15	30.31	39.2905131	-8.9805131
4.63333333	43.487	51.8931689	-8.4061689
5.16666667	52.27	66.5010659	-14.231066
5.65	85.153	80.0273148	5.12568525
6.16666667	67.865	94.5075596	-26.64256
6.65	142.2	107.8872	34.3127997
7.35	170.2	126.725983	43.4740165
8.11666667	199.4	146.37768	53.0223204
9.16666667	188.2	171.340648	16.8593522
11.0333333	206	209.871704	-3.8717039
12.1166667	241.6	228.950577	12.6494226
13.1166667	243.2	244.617074	-1.4170744
14.1833333	250.8	258.966733	-8.1667331
15.0333333	227.2	264.360271	-37.160271
18.2666667	222.8	222.830243	-0.0302426
21.2666667	188.8	163.828184	24.9718157
25.2666667	197.6	103.55618	94.0438197
28	178.6	75.1972319	103.402768

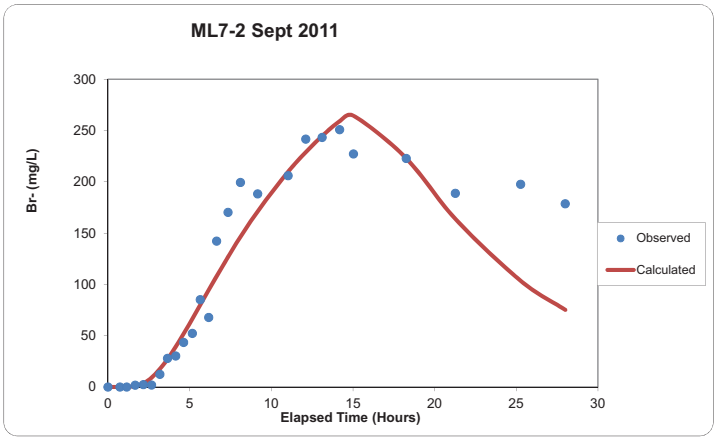

OPTIMIZED PARAMETER ESTIMATES

VELOCITY(cm/d)	831.9146	9.63E-05
DISPERSIVITY (cm)	85.69714	
PULSE WIDTH (cm)	437.8565	
RF	1	
Co (mg/L)	372	
FODC (/sec)	0	

RESDIUAL SUM OF SQUARES = 9261.235

INITIAL GUESSES AND INPUT OF PARAMETERS

		FIX
VELOCITY(cm/d)	1100	
DISPERSIVITY (cm)	38	
PULSE WIDTH (cm)	167	
RF	1	Y
Co (mg/L)	372	Y
FODC (1/sec)	0	Y
DISTANCE FROM SOURCE (cm)	559	Y
DIFFUSION COEFF (cm^2/sec)	0.000001	Y

95% CONFIDENCE INTERVALS FOR ESTIMATED PARAMETERS

Parameter	Low	Optimized	High
VELOCITY(cm/d)	773.6805	831.9146	898.4677
DISPERSIVITY(cm)	62.55891	85.69714	112.2633
PULSE WIDTH (cm)	402.828	437.8565	486.0207

Observed Time (Hours)	Observed Br- Conc (mg/L)	Calculated Br- Conc (mg/L)	Residuals
0	0	0	0
0.75	0	2.3027E-07	-2.303E-07
1.16666667	0	0.00056958	-0.0005696
1.7	0	0.04897255	-0.0489725
2.18333333	1.8	0.43088909	1.36911091
2.68333333	2.7	1.80632494	0.89367506
3.2	4	4.98063365	-0.9806336
3.66666667	8.685	9.74944426	-1.0644443
4.16666667	10.543	16.9445038	-6.4015038
4.66666667	17.903	26.1428556	-8.2398556
5.18333333	35.156	37.4361256	-2.2801256
5.66666667	32.202	49.3025414	-17.100541
6.2	35.127	63.4601062	-28.333106
6.66666667	76.713	76.4592194	0.25378062
7.36666667	98.552	96.5042916	2.04770839
8.15	130.8	119.032556	11.7674436
9.23333333	153.6	149.217708	4.38229218
11.0666667	205.6	188.606566	16.9934343
12.1333333	190.4	196.524574	-6.1245738
13.15	188.9	193.93134	-5.0313405
14.2	178.6	184.020923	-5.4209233
15.0666667	238.914	172.513883	66.4001174
18.2833333	129.11	122.965975	6.14402491
21.2833333	89.293	83.4735971	5.81940291
25.2833333	47.694	47.6714344	0.02256555
28.0333333	32.583	32.0049919	0.57800815

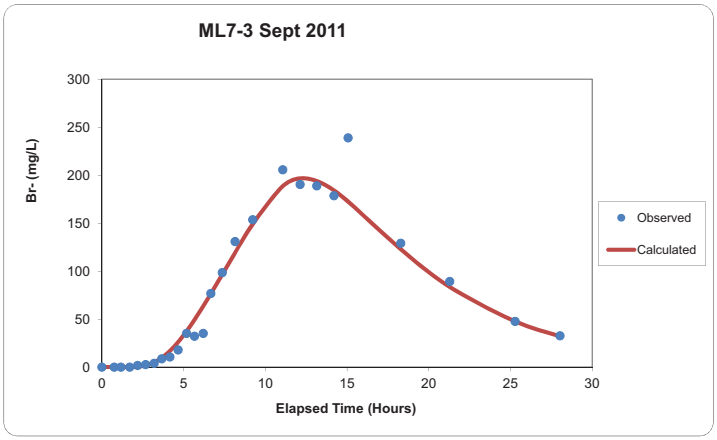

OPTIMIZED PARAMETER ESTIMATES

VELOCITY(cm/d)	925.1696	0.000107
DISPERSIVITY (cm)	68.41306	
PULSE WIDTH (cm)	295.3599	
RF	1	
Co (mg/L)	372	
FODC (/sec)	0	

RESDIUAL SUM OF SQUARES = 1148.68

INITIAL GUESSES AND INPUT OF PARAMETERS

		FIX
VELOCITY(cm/d)	1100	
DISPERSIVITY (cm)	38	
PULSE WIDTH (cm)	167	
RF	1	Y
Co (mg/L)	372	Y
FODC (1/sec)	0	Y
DISTANCE FROM SOURCE (cm)	559	Y
DIFFUSION COEFF (cm^2/sec)	0.000001	Y

95% CONFIDENCE INTERVALS FOR ESTIMATED PARAMETERS

Parameter	Low	Optimized	High
VELOCITY(cm/d)	897.4146	925.1696	952.9247
DISPERSIVITY(cm)	57.46697	68.41306	77.30676
PULSE WIDTH (cm)	280.5919	295.3599	310.1279

Observed Time (Hours)	Observed Br- Conc (mg/L)	Calculated Br- Conc (mg/L)	Residuals
0	0	0	0
0.76666667	2.039	0.07596327	1.96303673
1.2	5.966	1.49472328	4.47127672
1.71666667	34.5	7.65584156	26.8441584
2.21666667	50.65	18.4567401	32.1932599
2.71666667	46.7	32.6158605	14.0841395
3.21666667	77.2	48.6827102	28.5172898
3.7	108.8	65.0169999	43.7830001
4.2	126	82.0535675	43.9464325
4.68333333	97.881	98.2415115	-0.3605115
5.21666667	135.6	115.491859	20.1081407
5.68333333	116.4	129.92088	-13.52088
6.21666667	133.2	145.570225	-12.370225
6.7	127.057	158.951776	-31.894776
7.4	262.8	176.990621	85.8093788
8.16666667	258	194.99748	63.0025198
9.28333333	204.359	217.838423	-13.479423
11.0833333	200	215.461504	-15.461504
12.1666667	186.7	194.891078	-8.1910779
13.1666667	175.8	173.660523	2.13947739
14.2333333	138.6	151.979284	-13.379284
15.1	138.434	135.910543	2.52345676
18.3166667	98.491	89.4301515	9.06084846
21.3166667	86.866	60.9996615	25.8663385
25.3166667	48.134	37.2087344	10.9252656
28.0666667	40.629	26.7317388	13.8972612

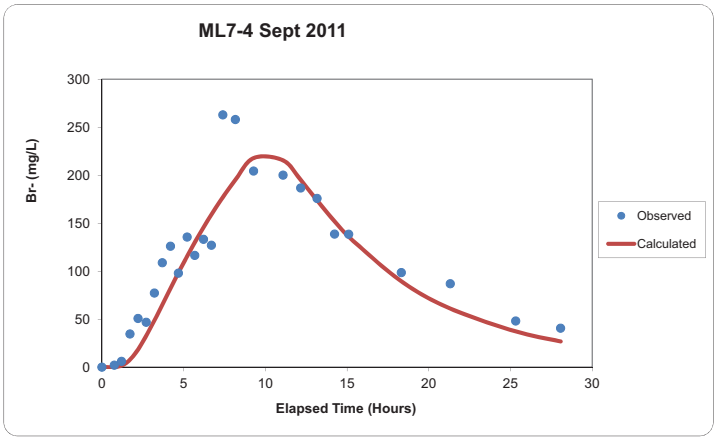

OPTIMIZED PARAMETER ESTIMATES

VELOCITY(cm/d)	1119.267	0.00013
DISPERSIVITY (cm)	120	
PULSE WIDTH (cm)	388.7272	
RF	1	
Co (mg/L)	372	
FODC (/sec)	0	

RESDIUAL SUM OF SQUARES = 12902.43

INITIAL GUESSES AND INPUT OF PARAMETERS

		FIX
VELOCITY(cm/d)	1100	
DISPERSIVITY (cm)	120	Y
PULSE WIDTH (cm)	162	
RF	1	Y
Co (mg/L)	372	Y
FODC (1/sec)	0	Y
DISTANCE FROM SOURCE (cm)	559	Y
DIFFUSION COEFF (cm^2/sec)	0.000001	Y

95% CONFIDENCE INTERVALS FOR ESTIMATED PARAMETERS

Parameter	Low	Optimized	High
VELOCITY(cm/d)	1052.111	1119.267	1242.387
PULSE WIDTH (cm)	357.629	388.7272	427.5999

Observed Time (Hours)	Observed Br- Conc (mg/L)	Calculated Br- Conc (mg/L)	Residuals
0	0	0	0
0.8	0	7.3798E-07	-7.38E-07
1.23333333	0	0.00060867	-0.0006087
1.76666667	0	0.02714331	-0.0271433
2.25	0	0.18424471	-0.1842447
2.75	1.9	0.66951183	1.23048817
3.26666667	2.1	1.69834073	0.40165927
3.73333333	2.319	3.1799185	-0.8609185
4.23333333	4.55	5.37411606	-0.8241161
4.73333333	2.77	8.1694704	-5.3994704
5.25	4.621	11.6281874	-7.0071874
5.73333333	9.101	15.319094	-6.218094
6.26666667	16.246	19.8198238	-3.5738238
6.73333333	15.293	24.0551577	-8.7621577
7.45	24.98	30.835473	-5.855473
8.21666667	35.6	37.7792371	-2.1792371
9.31666667	77.788	45.8642195	31.9237805
11.1333333	77.3	53.4255665	23.8744335
12.2	38.5	55.19402	-16.69402
13.2166667	42.2	55.6429286	-13.442929
14.2666667	52.136	55.2327616	-3.0967616
15.15	49	54.4169833	-5.4169833
18.3666667	52.708	49.6132318	3.0947682
21.35	38.092	44.3850373	-6.2930373
25.35	40.27	37.7608736	2.50912636
28.1	44.492	33.7289861	10.7630139

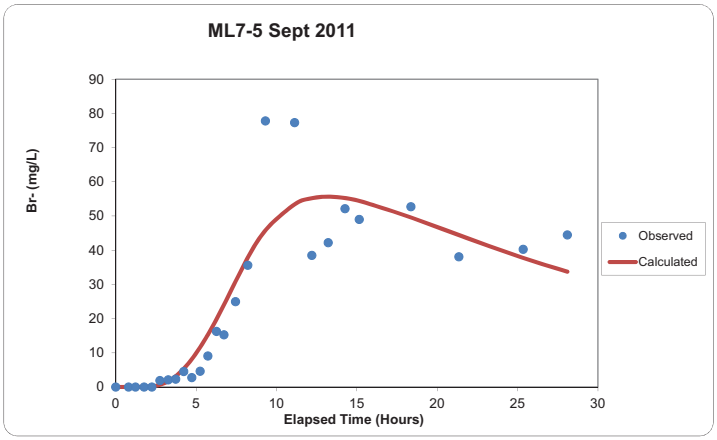

OPTIMIZED PARAMETER ESTIMATES

VELOCITY(cm/d)	498.363	5.77E-05
DISPERSIVITY (cm)	206.8818	
PULSE WIDTH (cm)	108.7867	
RF	1	
Co (mg/L)	372	
FODC (/sec)	0	

RESDIUAL SUM OF SQUARES = 2507.112

INITIAL GUESSES AND INPUT OF PARAMETERS

		FIX
VELOCITY(cm/d)	1100	
DISPERSIVITY (cm)	120	
PULSE WIDTH (cm)	162	
RF	1	Y
Co (mg/L)	372	Y
FODC (1/sec)	0	Y
DISTANCE FROM SOURCE (cm)	559	Y
DIFFUSION COEFF (cm^2/sec)	0.000001	Y

95% CONFIDENCE INTERVALS FOR ESTIMATED PARAMETERS

Parameter	Low	Optimized	High
VELOCITY(cm/d)	413.6412	498.363	593.0519
DISPERSIVITY(cm)	146.8861	206.8818	281.3593
PULSE WIDTH (cm)	87.02936	108.7867	131.6319

Observed Time (Hours)	Observed Br- Conc (mg/L)	Calculated Br- Conc (mg/L)	Residuals
0	0	0	0
0.83333333	0	4.7208E-05	-4.721E-05
1.26666667	0	0.00873334	-0.0087333
1.78333333	2	0.16810333	1.83189667
2.28333333	4.2	0.84519379	3.35480621
2.78333333	5.2	2.41778454	2.78221546
3.3	11.1	5.18413881	5.91586119
3.75	23.624	8.54521596	15.078784
4.25	32.489	13.2223492	19.2666508
4.75	41.625	18.7432272	22.8817728
5.28333333	35.759	25.377118	10.381882
5.75	58.23	31.6681477	26.5618523
6.28333333	52.026	39.2654309	12.7605691
6.75	34.789	46.1644389	-11.375439
7.46666667	67.402	57.0342098	10.3677902
8.23333333	78.159	68.8164234	9.34257661
9.35	64.696	85.7979385	-21.101939
11.15	105.5	106.263378	-0.7633784
12.2166667	94.6	111.27494	-16.67494
13.2333333	98.9	112.114773	-13.214773
14.3	96.274	110.252988	-13.978988
15.1666667	100.592	107.43706	-6.8450596
18.3833333	102.518	92.8113647	9.70663532
21.3666667	92.298	78.6261851	13.6718149
25.3666667	70.997	62.2295733	8.76742673
28.1166667	81.035	52.9563122	28.0786878

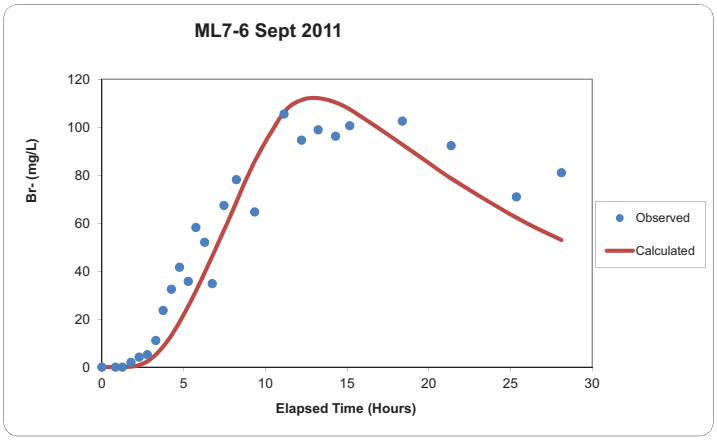

OPTIMIZED PARAMETER ESTIMATES

VELOCITY(cm/d)	640.0892	7.41E-05
DISPERSIVITY (cm)	160	
PULSE WIDTH (cm)	205.9083	
RF	1	
Co (mg/L)	372	
FODC (/sec)	0	

RESDIUAL SUM OF SQUARES = 4767.043

INITIAL GUESSES AND INPUT OF PARAMETERS

		FIX
VELOCITY(cm/d)	1100	
DISPERSIVITY (cm)	160	Y
PULSE WIDTH (cm)	162	
RF	1	Y
Co (mg/L)	372	Y
FODC (1/sec)	0	Y
DISTANCE FROM SOURCE (cm)	559	Y
DIFFUSION COEFF (cm^2/sec)	0.000001	Y

95% CONFIDENCE INTERVALS FOR ESTIMATED PARAMETERS

Parameter	Low	Optimized	High
VELOCITY(cm/d)	563.2785	640.0892	723.3008
PULSE WIDTH (cm)	181.1993	205.9083	230.6173

Observed Time (Hours)	Observed Br- Conc (mg/L)	Calculated Br- Conc (mg/L)	Residuals
0	0	0	0
0.85	0	0.00030775	-0.0003078
1.28333333	1.382	0.03402422	1.34797578
1.8	2.4	0.5022244	1.8977756
2.31666667	5.3	2.28434908	3.01565092
2.8	11.8	5.75077128	6.04922872
3.31666667	18.738	11.5511115	7.1868885
3.76666667	28.953	18.2265745	10.7264255
4.28333333	38.5	27.4361436	11.0638564
4.76666667	30.953	37.2082634	-6.2552634
5.3	31.51	48.9114713	-17.401471
5.76666667	56.29	59.6725474	-3.3825474
6.31666667	72.958	72.70138	0.25662005
6.78333333	70.167	83.8623498	-13.69535
7.48333333	103.4	100.01841	3.38159019
8.25	76.6	114.46238	-37.86238
9.38333333	127.9	126.169358	1.73064167
11.1833333	135	125.794904	9.20509556
12.2333333	114.1	119.66825	-5.5682499
13.2666667	105.5	111.796162	-6.2961618
14.3166667	106.8	103.049816	3.75018437
15.2	100.091	95.6066494	4.48435063
18.4	65.518	70.9545629	-5.4365629
21.4	50.276	52.7702568	-2.4942568
25.4	34.242	35.3429109	-1.1009109
28.1333333	27.259	26.8786868	0.3803132

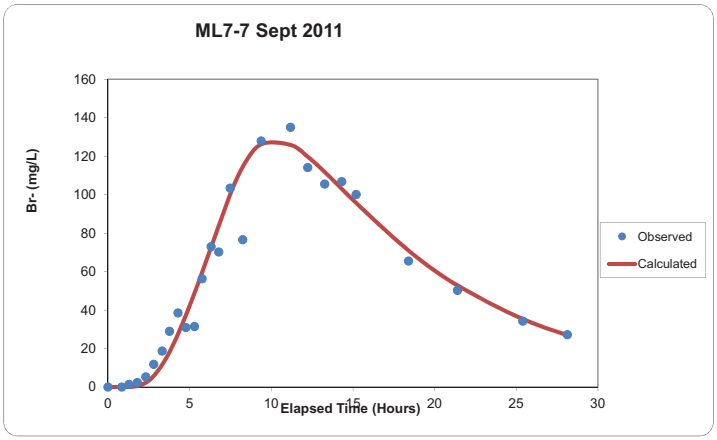

OPTIMIZED PARAMETER ESTIMATES

VELOCITY(cm/d)	934.0263	0.000108
DISPERSIVITY (cm)	113.7176	
PULSE WIDTH (cm)	220.5624	
RF	1	
Co (mg/L)	372	
FODC (/sec)	0	

RESDIUAL SUM OF SQUARES = 900.5101

INITIAL GUESSES AND INPUT OF PARAMETERS

		FIX
VELOCITY(cm/d)	1100	
DISPERSIVITY (cm)	38	
PULSE WIDTH (cm)	167	
RF	1	Y
Co (mg/L)	372	Y
FODC (1/sec)	0	Y
DISTANCE FROM SOURCE (cm)	559	Y
DIFFUSION COEFF (cm^2/sec)	0.000001	Y

95% CONFIDENCE INTERVALS FOR ESTIMATED PARAMETERS

Parameter	Low	Optimized	High
VELOCITY(cm/d)	896.6653	934.0263	971.3874
DISPERSIVITY(cm)	98.9343	113.7176	133.0496
PULSE WIDTH (cm)	209.5343	220.5624	233.7962

Appendix 17: Summary Table of CIS Biostimulation Tracer Testing

Prebiostimulation							
Multilevel	Elevation (masl)	PULSEPE Velocity (m/d)	PULSEPE Dispersivity (m)	PULSEPE Pulse Width (m)	CLOUDPE Velocity (m/d)	CLOUDPE Dispersivity (m)	CLOUDPE Mass (mg)
ML5-2	295.54	3.75	1.53	0.94	4.99	9.79E-01	1.48E+05
ML5-3	293.84	6.21	0.86	2.66	5.24	8.50E-01	4.36E+05
ML5-4	292.14	16.93	0.38	3.14	14.69	3.80E-01	4.80E+05
ML5-5	290.44	17.71	0.86	3.58	17.88	6.00E-01	5.39E+05
ML5-6	288.74	3.35	1.58	1.03	3.22	1.58E+00	1.93E+05
ML5-7	287.04	4.53	1.61	1.31	4.73	1.62E+00	2.20E+05
ML7-1	295.17	3.78	0.99	1.04	3.62	1.00E+00	2.08E+05
ML7-2	293.47	7.74	1.64	3.80	7.52	1.64E+00	6.32E+05
ML7-3	291.77	14.77	0.78	3.82	15.38	7.80E-01	5.00E+05
ML7-4	290.07	17.71	1.27	4.66	18.58	1.27E+00	6.11E+05
ML7-5	288.37	11.66	1.46	2.76	12.01	1.46E+00	3.74E+05
ML7-6	286.67	11.32	1.00	1.58	10.63	1.58E+00	2.42E+05
ML7-7	284.97	16.16	1.10	2.49	18.66	1.20E+00	3.62E+05

Post biostimulation							
Multilevel	Elevation (masl)	PULSEPE Velocity (m/d)	PULSEPE Dispersivity (m)	PULSEPE Pulse Width (m)	CLOUDPE Velocity (m/d)	CLOUDPE Dispersivity (m)	CLOUDPE Mass (mg)
ML5-2	295.54	3.48	6.07E-01	1.50E-01	4.94	3.80E-01	1.98E+04
ML5-3	293.84	7.25	4.04E-01	3.27E+00	6.20	5.00E-01	4.34E+05
ML5-4	292.14	11.15	5.27E-01	3.21E+00	11.58	5.00E-01	3.89E+05
ML5-5	290.44	18.58	1.00E+00	3.59E+00	17.80	1.00E+00	5.17E+05
ML5-6	288.74	4.21	9.36E-01	1.41E+00	4.48	9.30E-01	2.49E+05
ML5-7	287.04	5.21	1.35E+00	1.96E+00	4.88	1.35E+00	3.12E+05
ML7-1	295.17	1.87	1.00E+00	1.59E+00	2.37	1.00E+00	1.39E+05
ML7-2	293.47	8.32	8.57E-01	4.38E+00	0.58	8.60E-01	6.79E+04
ML7-3	291.77	9.24	6.84E-01	2.95E+00	9.42	6.80E-01	4.29E+05
ML7-4	290.07	11.23	1.20E+00	3.89E+00	12.36	1.20E+00	5.88E+05
ML7-5	288.37	4.99	2.07E+00	1.09E+00	8.39	8.00E-01	1.41E+05
ML7-6	286.67	6.40	1.60E+00	2.06E+00	7.07	1.60E+00	3.31E+05
ML7-7	284.97	9.33	1.11E+00	2.21E+00	10.02	1.14E+00	3.10E+05

Percent Difference							
Multilevel	**Elevation (masl)**	**PULSEPE Velocity**	**PULSEPE Dispersivity**	**PULSEPE Pulse Width**	**CLOUDPE Velocity**	**CLOUDPE Dispersivity**	**CLOUDPE Mass**
ML5-2	295.54	-7.54	-86.41	-144.90	-1.04	-88.15	-152.80
ML5-3	293.84	15.40	-71.86	20.57	16.75	-51.85	-0.46
ML5-4	292.14	-41.23	32.03	2.05	-23.68	27.27	-20.94
ML5-5	290.44	4.76	14.49	0.25	-0.48	50.00	-4.17
ML5-6	288.74	22.63	-51.42	30.59	32.55	-51.79	25.34
ML5-7	287.04	14.02	-17.81	39.29	3.24	-18.18	34.59
ML7-1	295.17	-67.41	1.32	42.08	-41.85	0.00	-39.77
ML7-2	293.47	7.21	-62.56	14.11	-171.36	-62.40	-161.19
ML7-3	291.77	-46.04	-13.06	-25.60	-48.08	-13.70	-15.29
ML7-4	290.07	-44.78	-5.90	-18.09	-40.22	-5.67	-3.84
ML7-5	288.37	-80.23	34.43	-86.78	-35.49	-58.41	-90.49
ML7-6	286.67	-55.49	46.15	26.14	-40.23	1.26	31.06
ML7-7	284.97	-53.56	1.24	-12.30	-60.24	-5.13	-15.48

Probe	Elevation (masl)	Prebiostimulation Average Velocity (m/d)	Post Biostimulation Aveage Velocity (m/d)	Percent Difference	Standard Error
PVP3-1	293.99	7.54	6.43	-15.87	5.46
PVP3-2	291.31	4.91	2.20	-76.22	37.44
PVP3-3	290.00	8.45	10.27	19.42	28.90
PVP3-4	289.73	7.52	13.58	57.41	41.24
PVP3-5	289.50	2.64	5.17	64.80	42.77
PVP3-6	288.51	7.07	4.04	-54.42	23.33
PVP3-7	286.76	5.05	3.19	-45.18	19.63
PVP4-1	293.99	10.45	NA	NA	
PVP4-2	291.31	10.66	11.18	4.78	9.44
PVP4-3	290.00	10.92	2.22	-132.48	
PVP4-4	289.73	26.22	12.86	-68.38	
PVP4-5	289.50	4.75	3.85	-21.00	9.36
PVP4-6	288.51	15.34	4.04	-116.67	
PVP4-7	286.76	35.97	20.64	-54.19	21.44
PVP5-1	293.99	2.36	2.48	5.14	
PVP5-2	291.31	10.51	8.02	-26.84	59.57
PVP5-3	290.00	2.62	3.81	37.12	45.76
PVP5-4	289.73	6.54	34.46	136.24	
PVP5-5	289.50	4.37	6.27	35.85	15.03
PVP5-6	288.51	7.86	9.53	19.23	35.37
PVP5-7	286.76	3.19	5.20	47.93	26.77

Appendix 18: Co-Authored Manuscript in Preparation Regarding Woodstock Site Characterization

Stimulating *In situ* Denitrification in an Aerobic, Highly Conductive Municipal Drinking Water Aquifer

by

K. Critchley[1], D. Rudolph[2], J.F. Devlin[3], P.C. Schillig[4]

February, 2012

[1]Golder Associates Ltd., London, Ontario, (t) 519-652-0099, email: kcritchley@golder.com
[2] Corresponding author, Dept. of Earth and Environmental Sciences, University of Waterloo, Waterloo, Ontario, Canada
[3]Dept. of Geology, University of Kansas, (t) 785-864-4994, email: jfrickdevlin@gmail.com
[4]Dept. of Geology, University of Kansas, (t) 785-864-4994, email: schillig@ku.edu

Abstract

A preliminary trial of a cross-injection system (CIS) was designed to stimulate *in situ* denitrification in an aquifer servicing an urban community in southern Ontario. It was hypothesized that this remedial strategy could be used to reduce groundwater nitrate in the aquifer such that it could remain in use as a municipal supply while the time lagged impacts of local reduced nutrient loadings migrated through the system. The CIS application involved injecting a carbon source (acetate) into the subsurface using an injection-extraction well pair positioned perpendicular to the regional flow direction, up-gradient of the water supply wells, with the objective of stimulating native denitrifying bacteria. Acetate injections were performed at intervals ranging from daily to bi-daily. The carbon additions led to general declines in dissolved oxygen concentrations, with localized nitrate declines observed in aquifer layers with velocities estimated to be less than 0.5 m/day. NO_3-^{15}N and NO_3-^{18}O isotope data indicated the nitrate losses were due to denitrification. Relatively little nitrate was removed from groundwater in the more permeable strata, where velocities were estimated to be on the order of 18 m/day. Overall, about 11 percent of the nitrate mass passing through the treatment zone was removed. This work demonstrates that stimulating *in situ* denitrification in an aerobic, highly conductive aquifer is challenging but achievable. Further work is needed to increase rates of denitrification in the most permeable units of the aquifer.

1. Introduction

The accumulation of nitrate in the subsurface from agricultural operations has drawn international attention. Concern regarding this contaminant is driven by its high mobility in groundwater, and widely accepted links to various health conditions, such as methemoglobinemia (Johnson *et al.*, 1987; Gelberg *et al.*, 1999; Knobeloch *et al.*, 2000) and an assortment of gastrointestinal cancers (Ward *et al.*, 1996; Yang *et al.*, 1998). As a result, various mandatory and voluntary standards for agricultural practice have been established in some jurisdictions to limit loadings to the subsurface. These or beneficialmanagement practices (BMPs) include any action that considers the balance of nutrients in agriculture, with an overall goal of protecting environmental resources without sacrificing crop production (Crop Nutrients Council, 2009). Examples of such efforts include crop rotation, reduction of nutrient application rates, synchronisation of nitrogen supply and plant demand, the use of buffer strips and riparian zones, and the use of cover crops (Di and Cameron, 2002; Dinnes *et al.*, 2002; Mckague *et al.*, 2005). These strategies have been demonstrated to reduce the environmental impact of agriculture on groundwater systems. However, the time interval, or lag, between BMP implementation and a noticeable improvement in groundwater quality can range from years to decades (Honisch *et al.*, 2002; Meissner *et al.*, 2002; Tomer and Burkart, 2003; Wassenaar *et al.*, 2006; Cole, 2008). A possible alternative approach of mitigating the risk during the lag period is to adopt groundwater remediation strategies based on biostimulation as part of an integrated water quality management plan.

The objectives of this research focused on a field application of the integrated approach, with emphasis on evaluating the biostimulation phase. It was hypothesized that *in situ* denitrification

can be initiated in highly conductive, heterogeneous, and aerobic aquifers through the introduction of a carbon source (i.e., an electron donor) using an appropriate injection system. The reduction in groundwater nitrogen through this remedial approach may provide an interim improvement in groundwater quality while regional BMPs gradually become fully effective. The field experiments were located at a site where elevated nitrate concentrations had been documented in municipal water wells.

2. Background

2.1 Site History

The City of Woodstock, Ontario, Canada relies on groundwater to meet all domestic and industrial water demands. The Thornton Well Field, located adjacent to the study site in a rural setting southwest of the city (Figure 1), provides the majority of the water supply.

Here I suggest we provide the reader with the briefest of summaries of the geologic setting.

- Glacial moraine
- Aquifers are sand and gravel with intermingled silt till aquitards
- Wells are on average 30 m deep.
- Terrain is gently rolling
- Agriculture in the region includes crop farming with corn, soya bean rotations dominating and some livestock operations.

Kate you have a nice short discussion in the thesis and an even short form would fit well here.

Over the last 3 decades, nitrate concentrations at this well field have progressively increased, finally surpassing World Health Organization and Canadian water quality guidelines in several of the wells in the mid-1990s. The rising nitrate concentrations are thought to originate from excess fertilizer applications to the surrounding agricultural land. To address this problem, the municipal government (Oxford County) purchased 111 hectares of land within the capture zone of the Thornton Well Field in 2003. Presently, the land is rented back to farmers with the understanding that they follow strict BMPs designed to minimize over-application of nutrients. It was predicted that nitrate concentrations would gradually decline in the supply wells, but a decade or more would be required before significant reductions would be observed in the municipal wells. Consequently, the municipal government began to consider an integrated approach, including *in situ* remediation through stimulated denitrification, shown to be feasible in a neighbouring aquifer near the town of Baden, Ontario (Devlin *et al.,* 2000; Gierczak *et al.*, 2006, 2007), to maintain the serviceability of the wells. Unanticipated challenges were encountered at the Woodstock site when the detailed field characterization program revealed strata conducting groundwater at extremely high velocities (Devlin *et al.*, in press) and aerobic groundwater conditions .

Geochemically, the aquifer was fairly uniform. There were generally no variations with depth in concentrations of oxygen, nitrate or sulphate across the test area (Table 1). Prior to treatment, the aquifer was found to be aerobic, with an average dissolved oxygen concentration of 8.7 mg/L. Nitrate was also elevated, with an average concentration of 13.0 mg-N/L. Additionally,

sulfate was detected at approximately 32.9 mg-SO_4/L, which is typical of the region (Haslauer, 2005).

2.2 Stimulated In situ Denitrification

Under proper conditions, nitrate is readily transformed to innocuous nitrogen gas by a wide range of facultative anaerobic organisms (Foth, 1984). Following the consumption of oxygen, these organisms rely on nitrate to generate energy via cellular respiration (Foth, 1984). The denitrification process involves the formation of several intermediate products, culminating in the formation of dinitrogen gas (Soares, 2000):

$$NO_3^- \longrightarrow NO_2^- \longrightarrow NO \longrightarrow N_2O \longrightarrow N_2 \quad (1)$$

Microbial denitrification results in the enrichment of both $\delta^{15}N$ and $\delta^{18}O$ in residual nitrate due to the preferential reduction of the lighter ^{14}N and ^{16}O isotopes by the denitrifying bacteria (Bottcher *et al.*, 1990; Aravena and Robertson, 1998; Lund *et al.*, 2000; Cole, 2008). The result is linear isotopic enrichment of the heavier isotopes in the residual nitrate, typically by a factor of 2.1:1 on a plot of $\delta^{15}N$ and $\delta^{18}O$ in nitrate (Bottcher *et al.*, 1990; Aravena and Robertson, 1998), making isotopic data a tool to verify that declines in nitrate concentrations are due to denitrification.

Although denitrifying bacteria are very common in soil and aquifers, nitrate remains one of the most common groundwater contaminants because many aquifers lack the appropriate electron donors, such as organic carbon, and redox conditions to support denitrification (Starr and Gillham, 1986). This recognition has led to the development of *in situ* denitrification

technologies based on the addition of electron donors to the subsurface. Other substances, such as phosporus and trace metals, are sometimes added to the amendments so the injectate is sometimes called a nutrient amendment. Of particular interest for delivering such solutions to aquifers are semi-passive injection-withdrawal systems, as reviewed by Gierczak *et al.* (2007).

It has been demonstrated that in typical aquifers injection-withdrawal systems perform optimally when the electron donor is introduced in a series of discrete pulses, as opposed to a continuous injection (Devlin and Barker, 1996; Peyton, 1996; Khan and Spalding, 2003). The pulses help limit the formation of biofilms, which can lead to aquifer and screen clogging (Devlin and Barker, 1994). Challenges associated with these treatment systems include the possible accumulation of undesirable intermediate products, such as nitrite, and achieving a uniform distribution of the injected solution throughout the aquifer (Soares, 2000; Gierczak *et al.*, 2007). In addition, passive or semi-passive *in situ* treatment methods should be preceded with site characterization efforts that are significantly more detailed than conventionally undertaken (Soares, 2000).

2.3 Selection of the Cross-Injection Scheme and Electron Donor

Gierczak *et al.* (2006, 2007) demonstrated the cross-injection scheme (CIS) in a pilot-scale study near Baden, Ontario, approximately 45 kilometres northeast of the Woodstock site. The CIS is an adaptation of the solute pulse generation technique that utilized a nutrient injection wall (NIW) to facilitate the cross (ambient) gradient injection (Devlin and Barker, 1994). In both the CIS and the NIW methods, the injection phase is followed by a passive phase in which the wells

are turned off and the nutrient pulse migrates into the aquifer under natural gradient conditions (Devlin and Barker, 1994; Gierczak *et al.,* 2007). This active-passive pattern is repeated throughout the treatment time, with dispersion acting to mix the contaminated groundwater with the injected pulses down-gradient. The CIS combines the design flexibility of a daisy-well system (Kahn and Spalding, 2003) with the predominantly passive operation of a permeable reactive barrier (PRB) (O'Hannesin and Gillham, 1992). In addition, previous studies have clearly demonstrated the success of this technology for stimulating *in situ* denitrification (Dybas *et al.*, 2002; Gierczak *et al.*, 2007). (All, I still wonder if it would be useful to the reder if we provided a cartoon depiction of the CIS method at this stage. I know i have brought this up several times and it is only because people with little experience with these technologies and lots of potential applications (me for instance) might benefit from a visual reference.)

Several electron donor choices were considered for the current project, including organic compounds, such as simple organic acid anions, and inorganic compounds, such as ferrous iron, hydrogen, and reduced sulphur (Devlin *et al.,* 2000). Acetate was identified as the preferred electron donor based on its proven success at stimulating complete denitrification (Kahn and Spalding, 2003; Kahn and Spalding, 2004; Gierczak *et al.,* 2007), and reports that it is generally less readily utilized by microorganisms than other carbon sources, increasing denitrification efficiency and decreasing the likelihood of biofouling the treatment zone and well screens (Mateju *et al.,* 1992; Constantin and Fick, 1997; Devlin *et al.,* 2000).

3. Methods

3.1 Site Instrumentation

A total of four injection-extraction wells, WO77, WO78, WO79, and WO80, were installed perpendicular to the regional flow direction, with separation distances of 5 m (Figure 1 (b)) (regional flow direction should be shown on Figure 1b). Each well was constructed from 50.8-mm (2-inch) diameter, 10-slot PVC screens and schedule 40 PVC riser pipe. The total depths of the wells and the screen lengths varied with local elevation changes of an underlying clay layer. WO77, WO78, and WO80 included 7.62-m (25-foot) long screens and reached a depth of approximately 17 metres below ground surface (mbgs), while WO79 had a 6.10-m (20-foot) long screen and reached a depth of approximately 15 mbgs.

Twelve bundle-type multi-level monitoring wells, ML1 to ML12, were installed down gradient of the injection-extraction wells to monitor tracer progress during initial solute transport testing, to gather detailed background chemical data, and to track geochemical changes during the acetate injections (Figure 1 (b)). Each multi-level well was assembled with eight individual 10-cm long screens placed at vertical increments of 1.7 m. The bundles were constructed by securing seven 9.5-mm inner diameter polyethylene tubes around a central 12.7-mm inner diameter PVC pipe. The screen tips were made from slotted 9.5-mm inner diameter polyethylene tubing wrapped in fine Nitex™ screen. For all multi-level bundles, the sampling ports were labelled 1 (shallowest) to 8 (deepest).

Two additional well groupings, the WO74 and WO75 series wells, were relied upon for geochemical and water level datasets (Figure 1 (b)). These wells, installed during previous research activites by Koch (2009), consisted of two Solinst® CMT Multi-level Systems (WO74-

ML, WL075-ML, with six multi-level ports each) and six conventional wells (WO74-WT, WO74-S, WO74-M, WO74-D, WO75-S and WO75-D, with 50.8-mm (2-inch) diameter, 10-slot PVC screens and schedule 40 PVC riser pipe). Additional well installation details, including well depths, are provided in Koch (2009) and Critchley (2010). (There is a lot of detail here and many wells in the field. One suggestion might be to split Figure 1 into figure 1 and 2 and expand Figure 1b so that the detail is not lost when it is compacted for the journal. It is already a bit challenging to follow and we have space for an additional figure or 3.)

3.2 Physical Characterization

Core logging, grain size analysis, slug testing, borehole flowmeter testing, tracer testing, and three-dimensional groundwater modelling were used to quantify the physical properties of the target aquifer and to develop a hydrogeologic conceptual model of the site. Point velocity probes (PVPs) were also used in the site characterization. The preliminary results of the PVP tests are given by Devlin *et al.* (in press) and will be referred to in subsequent sections.

3.2.1 Core Logging and Grain Size Analysis

Four continuous cores were collected at the study site with total depths ranging from 5.8 to 15.2 mbgs using a Geoprobe® direct push method with 5.7 cm (2.25 in.) outer-diameter core barrels. The boreholes were immediately backfilled with bentonite chips after the core was retrieved. The core were split open, logged according to the Unified Soil Classification System, and sub-sampled for grain size analysis. Approximately 102 individual grain size analyses were performed on sub-samples taken at intervals of 20 to 30 cm. Due to the coarse nature of material, the method

developed by Terzaghi (1925) was used to estimate hydraulic conductivity from the grain size data.

3.2.2 Slug Tests

A total of 47 individual slug tests were performed at various depths within the target aquifer on the WO74 and WO75 series wells (Figure 1b) using solid PVC slugs. A minimum of 4 rising and 4 falling head tests were completed for each of the seven wells. The initial head displacement was altered for each test by using a variety of slugs with different volumes. The wells were all thoroughly developed via extended pumping prior to the slug testing. The water level displacement datasets were analyzed using a mathematical solution developed by Springer and Gelhar (1991) designed for unconfined aquifers and accommodating oscillatory water level responses.

3.2.3 Borehole Flowmeter Tests

A series of borehole flowmeter tests were performed on the injection-extraction wells WO77, WO78, WO79, and WO80 using a Mount Sopris FLP2492 Impeller Flowmeter, a Mount Sopris 4MXA-1000 winch, and a Honda WH15XK1C1 high-pressure pump. The pump extracted water at 230 L/min from just above the well screen. Flowmeter measurements were collected along the entire screen length at an interval of 10 cm. Conversion of the raw flowmeter output in rotations per second to hydraulic conductivity was accomplished using the method described by Moltz *et al.* (1989).

3.2.4 Tracer Testing with the CIS Well Pair

To better characterize the flow system, and confirm that the carbon amendments could be emplaced as required, two tracer tests were performed prior to the carbon additions to the aquifer. In both cases a potassium bromide tracer was introduced into one of the injection-extraction wells while a second well 5 m away was pumped. Pumping continued until the tracer broke through at the pumping well, creating a slug that was elongated perpendicular to the ambient flow direction.

In the first tracer test, groundwater was extracted from WO77 at an average rate of about 200 L/min, amended with a 250,000 mg/L bromide solution at the surface, and re-injected into WO78. The bromide solution was mixed with the groundwater in-line at a rate of 0.19-0.20 L/min for a period of 4 hours, yielding an injection concentration of approximately 242 mg/L. Following the 4 hour injection, the pumps continued to operate for an additional 11 hours, to facilitate complete tracer transport from the injection well (WO78) to the extraction well (WO77). Throughout this test, ML12, located between the injection and extraction wells approximately 1 metre from WO77, was sampled for anions at an interval of 0.5 hours to track the tracer progress and confirm the time to breakthrough at WO77.

In the second tracer test, groundwater was extracted from WO78 at an average rate of approximately 190 L/min, amended with a 250,000 mg/L bromide solution, and reinjected into WO79. The solution was mixed in-line at a rate of 0.20 L/min for a period of just under 4 hours, yielding an injection concentration of approximately 263 mg/L. Following the injection period, the circulation cycle was operated for an additional 2.5 hours. Anion samples were

subsequently collected over a 17 hour period after the injection and extraction cycle ceased from multi-level bundles ML5, ML6, ML7, and ML8, located between the injection-extraction well pair at downgradient distances of 1, 3, 5, and 7 metres, respectively (Figure 1b)(We need this figure to be loud and clear).

3.2.5 Parameter Estimation and Groundwater Modelling

Based on the information derived from the initial tracer tests, estimates of the average linear groundwater velocity and subsurface dispersivity at each multi-level sampling depth were generated by fitting the bromide breakthrough data with one-dimensional solutions of the advection-dispersion equation, as described by Devlin and Barker (1996) and Gierczak *et al.* (2006).

A 3D finite difference model was prepared using MODFLOW and MT3D to demonstrate the effects of substrate injection and circulation, to test the various design parameters of the Woodstock injection experiment, and to refine the site hydrostratigraphy. More specifically, the goal of the modelling was to assist with the design of the CIS (e.g., to determine the pumping rate and duration required to draw the solute perpendicular to the ambient flow direction between the injection-extraction well pair). The model was also useful to validate the conceptual model of aquifer layering at the site.

3.3 Geochemical Characterization

Most groundwater samples were analyzed for nitrate, nitrite, acetate, bromide, sulfate, oxygen and chloride. Some samples were collected for environmental isotopic analysis as well. All anion samples were collected in 25 mL scintillation vials and frozen as soon as possible to

prevent biological activity. Sample analysis was performed on a Dionex ICS 3000 ion chromatograph featuring a Dionex IonPac AS18 analytical column. Prior to analysis, samples were thawed completely in the refrigerator and agitated to homogenize the samples. Duplicate samples were collected and analyzed approximately every ten samples.

In addition, selected samples were analyzed for cations including calcium, aluminum, silicon, iron, and manganese. These were filtered at the time of collection with a 0.45 µm membrane and stored in pre-acidified 60 mL high density polyethylene bottles. Duplicate samples were collected approximately every eight samples. All samples were stored on ice or in a refrigerator until analyzed by inductively coupled plasma atomic emission spectrometry (ICPAES) at the Plasma Analytical Laboratory (KU-PAL), University of Kansas.

CHEMetrics dissolved oxygen vacu-vials, and a CHEMetrics Model V-2000 Photometer were used to determine dissolved oxygen concentrations. All analyses were performed on site using 25 mL groundwater samples.

Isotope samples were collected in 500 mL to 1.5 L plastic bottles and frozen within a few hours of collection. Measurement of the $^{15}N/^{14}N$ and $^{18}O/^{16}O$ ratios was performed at the Environmental Isotope Laboratory at the University of Waterloo. This is a bit out of the blue. I wonder if we should explain earlier in the text why we are analyzing the isotopic species and how many and where these samples will be collected from.

3.4 Carbon Injection Experiments

3.4.1 The C:N Ratio

The ratio of carbon consumed to nitrogen reduced, also known as the C:N ratio, has been identified as one of the primary factors affecting *in situ* denitrification (Sobieszuk and Szewczyk, 2006). Insufficient carbon can result in partial denitrification, potentially leading to an accumulation of nitrite in the subsurface (Hamon and Fustec, 1991).

The biologically-mediated denitrification reaction with acetate as the electron donor is summarized as follows (Devlin *et al.*, 2000):

$$5CH_3COO^-_{(aq)} + 8NO_3^-_{(aq)} + 3H^+_{(aq)} \longrightarrow 10HCO_3^-_{(aq)} + 4N_{2(g)} + 4H_2O_{(l)} \quad (2)$$

This equation, which assumes complete denitrification, states that 5 moles of acetate are required to reduce 8 moles of nitrate. The average background nitrate concentration at the Woodstock site is approximately 13.0 mg-N/L (57.6 mg-NO_3/L), or 0.93 mmoles/L. Applying the stoichiometric balance of the above equation generates a required acetate concentration of approximately 0.58 mmoles/L or 34.3 mg/L, corresponding to an elemental C:N of 1.25:1. If C is reported as acetate (C_{ac}:N), for convenience, the molar ratio is 0.62:1. This ratio applies to the minimum carbon necessary, as it assumes perfect efficiency (i.e., all of the carbon is consumed in denitrification). It was anticipated that a greater than ideal acetate concentration would be required to achieve complete denitrification at Woodstock due to the carbon demand imposed by the ambient dissolved oxygen in the groundwater, and other less well defined inefficiencies. Further, carbon would be utilized for cell growth as well as denitrification. The results presented in Gierczak *et al.* (2007), which appeared as C:N in that publication but correspond to

C_{Ac}:N as defined here, demonstrated complete denitrification with C_{Ac}:N ratios of up to 1.8. The aquifer examined in their work exerted a lower carbon demand from dissolved oxygen consumption than anticipated at the Woodstock site aquifer. Based on this information, an elemental C:N ratio range of 3.8 to 5.5 (C_{AC}:N = 1.9 to 2.8), representing approximately 3 to 4.5 times the theoretical requirement, was selected for the pilot injections.

3.4.2 Acetate Injection Tests

Following a single CIS injection to field-test procedures (injection 1), a larger experiment was performed to demonstrate the CIS operating over several injection cycles. There were three phases to this experiment, including: (I) a daily injection phase (injections 2 to 12) to establish microbial consumption of dissolved oxygen and support the growth and development of denitrifying populations within the treatment zone; (II) injection 13, which was followed by detailed groundwater sampling to characterize the extent of the redox change and nitrate attenuation; and (III) a bi-daily injection phase (injections 14 to 20), to determine whether a 2-day injection interval could sustain stimulated *in situ* denitrification following the establishment of denitrifying populations in phase 1 (Table 2).

The sampling program involved daily sampling for dissolved oxygen, nitrate, and acetate from the ports of ML7. Sample collection was performed immediately prior to and following operation of the circulation cycle. Multi-level bundle ML7 was selected for detailed monitoring based on its location, 5 metres downgradient of the injection-extraction plane, which was considered a sufficient distance from the injection system for changes to be evident (based on

previous experience and preliminary modelling). Following injection 13, a detailed sampling was conducted on wells ML5, ML6, ML7, and ML8. (Was the isotope sampling related to the injection schedule as well?

4. Results and Discussion

4.1 Physical Characterization, Hydrostratigraphy, and Flow Modelling

Relative hydraulic conductivity profiles, plotted as (K_i/K), where K_i is a depth-specific hydraulic conductivity and K is the average hydraulic conductivity for the dataset from which K_i originated (Moltz *et al.*, 1989), were compiled and plotted based on the data from the grain size analyses and borehole flowmeter testing. Similar profiles were compiled from (K_i/K) values estimated from tracer breakthrough times at the multi-level wells, and from the calibration of a 5-layer model in MODFLOW (Figure 2). Differences in the details of the (K_i/K) profiles between the various methods are attributed to the different locations represented, the different sampling intervals and the various scales under consideration.

Taken together, the (K_i/K) profiles indicate that the aquifer comprises a variably conductive multi-layered system, with K values ranging over nearly four orders of magnitude. Since the CIS injections are most closely represented by the tracer test results, the tracer studies were regarded as the best indicators of permeability distribution in the aquifer for the purposes of this work. (so as the reader glances back at the data from the tracer tests, they would see very little detail and lots of variability (Figure 2). The tracer test data suggested that the aquifer

could be reasonably described with 5 to 6 layers (really... based on the data provided in Figure 2? Very hard to see this.) of varying K, leading to the development of a 3D finite difference model (Figure 3). The model was subsequently calibrated with data from the tracer testing (Critchley, 2010). Hydraulic conductivity values ranging from $1.9x10^{-2}$ m/s, typical of sand to gravel units, to $4.8x10^{-4}$ m/s, typical of sand units, were found to produce the best agreement between modelled and measured breakthrough curves. Two layers with potentially high relative permeabilities, at depths of approximately 290 metres above sea level (masl) (based on grain size analysis, flowmeter test, tracer test, and model calibration) and 294 masl (based on grain size analysis and flowmeter test results), were of particular interest to this study since they were likely to be responsible for large nitrate and acetate fluxes. (OK but how do these K values (numerically) compare to the measured ones from the slug tests and the grain size analysis? Does the model provide some reasonable values?

Flow across the site was modelled assuming the water table acted as the upper limit of the aquifer. The water table (average annual at one place or at the injection site?)was estimated to occur at approximately 297.6 masl, based on monthly manual water level measurements taken at well WO74-WT over a one-year period. (OK but you stated earlier that you monitored the water table in a series of wells to get a regional flow gradient. How were those data uses in the model? I recall that the flow system was controlled by the differences in water levels in the wells to be able to set up a steady state flow field. One well would not provide the data required for that. I see you have some of this below. You should move it up and be clear on how the regional gradient was estimated.) The bottom of the aquifer was assumed to be the top of the underlying clay aquitard at approximately 283.0 masl, based on core logs and

unresponsive multi-level sampling ports at this depth. With a mean site hydraulic gradient of 3.3 X 10^{-3} to the southeast, and an assumed porosity of 0.3, a range of groundwater velocities between 0.5 and 18 m/day were calculated within the stratified aquifer unit, suggesting rapid groundwater flow across the site. Velocities of this magnitude were later confirmed with direct velocity measurements using point velocity probes and the natural gradient tracer test (Devlin *et al.*, in press).

4.2 Acetate Injections

Oxygen concentrations began to decline during the first phase of acetate injections, i.e., between September 16 (injection 4) and September 18 (injection 6) (Figure 4). This, demonstrates that successive daily injections, sustained over several days, were sufficient to diminish the dissolved oxygen loading to the treatment zone in many locations, but insufficient to drive all layers to a fully anaerobic condition. Considering the oxygen and nitrate concentration data – the latter discussed in more detail below – these results were consistent with predictions from eq 3, which estimates a pulsing interval (Δt) of 1 day is required for mixing at a distance of 5 m from the injection point ($\bar{x}$, distance to ML7).

$$\Delta t = \sqrt{\frac{32 D_x \bar{x}}{v^3}} \qquad (3)$$

where D_x is the dispersion coefficient, estimated to be 0.82 m^2/day (Gierczak *et al*., 2007)(earlier you explained that the tracer tests at this site could be used to get at the dispersion coefficient but here we are using a value from a completely different site. This may raise a red flag or at least a question. We should at least explain this.), and v is groundwater velocity (up to 5 m/day) (Devlin and Barker, 1996). In general, the dissolved oxygen

concentrations at ML7 declined to between the detection limit (0.1 mg/L) and 4 mg/L, until injection 13 on September 25. At that time, the dissolved oxygen concentrations partially rebounded to between 4 and 6 mg/L. A similar rebound was observed on September 15 (injection 3), when concentrations reached peak values on the order of 9 to 12 mg/L. Both rebounds occurred immediately following injections containing both acetate and bromide, suggesting some microbial inhibition due to the presence of the bromide salt. This result was not expected, and further work is needed to establish causality. Nevertheless, following injection 13, the breakthrough curves for bromide and acetate at ML7 were very similar, except that the acetate relative peak concentrations were generally lower than those for bromide (Figure 5 (a) and (b)), suggesting continued consumption of acetate by subsurface microorganisms despite the rebounding oxygen values.

Later acetate injections (injections 14 to 20) re-established the diminished oxygen levels, which once again declined to between the detection limit and 4 mg/L, providing evidence that an injection interval of every other day was sufficient to maintain the altered redox environment. Once the injections were stopped (October 9, Figure 4), the dissolved oxygen concentrations increased toward background levels, demonstrating that the diminished oxygen levels were the result of biostimulation.

The oxygen concentrations corresponding to ports ML7-3, ML7-4, and ML7-7 tended to be higher than those observed at the other ports throughout the experiment (Figure 4). These

ports were installed in relatively high-K units, with groundwater velocities (estimated from tracer breakthrough curves at ML7) in excess of 20 m/day, while ports ML7-1, ML7-2, ML7-5, and ML7-6 were installed in lower-K units with velocities between about <5 to 12 m/day (Figure 6). (What about the PVP data? Are we not planning on using it here for velocity verification or back in the modelling section to justify the numbers estimated through Darcy's Law? If we do not use the data, we should not refer to the PVP's in the methods.)The data therefore show a correspondence between the velocity profile and the success of the redox manipulation. Paradoxically, the strata accepting the greatest acetate masses – and possessing the highest groundwater velocities – remained aerobic despite the increased oxygen demands associated with the carbon additions. It is hypothesized that these layers conducted the acetate pulses so quickly that sustained acetate concentrations were not achieved, and therefore bacteria were not continuously stimulated. As a result, oxygen concentrations in these strata did not decline to the extent observed elsewhere, averaging between 4.2 and 4.8 mg/L, throughout injections 2-12 (Figure 4).

In keeping with the persistence of aerobic conditions in the highly permeable layers, data from ML7-3, ML7-4, and ML7-7 indicated that denitrification was poorly established at those locations. Nitrate concentrations remained within the span of background values, ranging from 11.2 to 14.0 mg-N/L. Despite this, the appearance of nitrite at detectable concentrations (0.9 to 2.1 mg-N/L) above background suggested that some denitrification occurred in these high-K layers. Further work is required to establish that the nitrite was not simply transported into

these layers from surrounding units. Regardless, these results indicate that the high-K units must be more aggressively stimulated to achieve meaningful rates of denitrification.

At ML7-2, ML7-5, and ML7-6, situated in strata of intermediate permeability, dissolved oxygen concentrations were depressed to a notable degree, and there were unmistakeable indications of nitrate attenuation. Concentrations of nitrate at these ports ranged from 2.9 to 9.4 mg-N/L, with an average value of 7.0 mg-N/L, almost 50 percent lower than the mean background concentration of 13.0 mg-N/L. The appearance of nitrite at concentrations of 1.1 to 5.6 mg/L at these depths, however, demonstrated that denitrification did not proceed to completion. The nitrate concentrations measured during the 25-hour sampling period following injection 13 showed little evidence of rebounding. This was not surprising considering denitrifiers are not strict anaerobes, so increasing oxygen concentrations would not necessarily have created immediately detrimental conditions. By the end of the experiment, oxygen concentrations were declining (Figure 4). It is possible that denitrification rates would have eventually increased. Such a result was observed by Gierczak *et al.* (2007) who reported maximum nitrate removal only after about 80 days of acetate injections.

A decline in dissolved oxygen concentrations was most pronounced at ML7-1, indicating the onset of reducing conditions in that unit. Even after injection 13, when oxygen concentrations rebounded (Figure 4), nitrate concentrations at ML7-1 (Figure 5 (c)) remained below detection. In addition, little nitrite was produced at ML7-1, with concentrations limited to between 0.5

and 1.5 mg-N/L, averaging 0.9 mg-N/L. The relatively low groundwater velocity in this unit (<5 m/day) appears to have limited oxygen invasion to a manageable level, facilitating the achievement of redox conditions conducive to denitrification.

A profile overlay of the physical hydrogeology (from K and tracer velocity) and denitrification intensity during the extended injection phase reveals a pattern at ML7. The data suggest that with daily acetate injections, sediments conducting groundwater at velocities up to 10 to 20 m/day are capable of supporting at least partial denitrification under the conditions of this test (Figure 6). Eq 3 predicts the upper velocity limit to be about 5 m/day for *maximum* denitrification, which is generally consistent with what was observed at ML7-1 (Figure 6). Therefore, these data extend the work of Gierczak *et al.* (2007) by demonstrating, in the field, a groundwater velocity threshold past which pulse mixing, sufficient to sustain denitrification with daily acetate injections, is not achieved.

To further illustrate the concept of a velocity threshold, the acetate injections were reduced in frequency to bi-daily (injections 14-20, Figure 4). According to eq 3, this would have the effect of lowering the threshold from about 5 m/day to about 3 m/day. Samples were collected from ML7-1 and ML7-2 and analyzed for nitrate and nitrite concentrations throughout injections 14 to 20. These ports were selected as they yielded the lowest oxygen and nitrate concentrations throughout injections 2-12. Also, geochemical changes observed at ML7-2 were very similar to those observed at ML7-5 and ML7-6, suggesting that the ML7-2 results might be representative

of the other depths. It was observed that nitrate concentrations that had declined in response to daily acetate injections began to rise with the bi-daily injections, consistent with a declining threshold (Figure 7). At ML7-1, where v < 5 m/day, nitrate levels rose only a little and may have been declining again when the test stopped. At ML7-2, where v ≈ 8 m/day, nearly 3 times the new threshold of 3 m/day, nitrate levels rose to just below background levels.

Over the course of the experiment, an estimated 11 percent decline in nitrate mass crossing the 5-m wide treatment zone was achieved. To increase this mass removal rate, a strategy for increasing denitrification in the highest velocity layers is required. According to eq 3, the interval required to mix pulses in 20 m/day groundwater, assuming $\bar{x}$ and D_x values as before, is 3 hours, an unrealistically short time for the CIS. However, eq 3 assumes that the mixing distance, $\bar{x}$, is large compared to the source width, and the degree of mixing assumed in eq 3 was arbitrarily selected (Devlin and Barker, 1996). There is a possibility that eq 3 somewhat underestimates the pulsing interval required for mixing, and this possibility is supported by the declining oxygen levels at ML7-2, 5, and 6 during the bi-daily acetate injection phase. Additional work is needed in the form of a longer period of pulsed injections to more precisely define the limits placed on mixing by the high groundwater velocities at the site. (Higher concentrations of acetate? potential that the reaction is occurring further down gradient and we just missed it?)

4.4 Isotope Analysis

Isotope analysis was undertaken to verify that nitrate disappearances were due to denitrification (we need to explain this a bit earlier in the text.). A clear relationship between ^{15}N enrichment and decreasing nitrate concentrations was observed following injection 13, indicating denitrification and suggesting it occurred to varying degrees in all aquifer layers (Figure 8 (a)). The isotopic enrichment factor for denitrification (ε) was computed for ^{15}N in nitrate using a simplified Rayleigh equation (Mariotti *et al.*, 1981; Aravena and Robertson, 1998):

$$\delta^{15}N_r = \delta^{15}N_o + \varepsilon \ln f \quad (4)$$

where $\delta^{15}N_r$ and $\delta^{15}N_o$ represent the isotopic composition of the residual and initial nitrate, respectively, and f is the ratio of the initial nitrate concentration to the final nitrate concentration (Aravena and Robertson, 1998). The resultant enrichment factor was estimated to be -9.77‰, which falls within the range of enrichment factors previously reported for denitrification (Mariotti *et al.*, 1988; Bottcher *et al.*, 1990; Spalding and Parrot, 1994; Aravena and Robertson, 1998; Fukada *et al.*, 2003).

The $\delta^{18}O$ values collected following injection 13 also support the occurrence of denitrification. Figure 8 (b) displays a clear linear relationship between $\delta^{18}O$ values and $\delta^{15}N$ values, indicative of denitrification. The slope of the line denotes a ^{15}N:^{18}O fractionation ratio of approximately 2.1:1. This ratio is again consistent with literature values (Bottcher *et al.*, 1990; Aravena and Robertson, 1998). The enriched ^{15}N and ^{18}O isotope measurements observed provide additional evidence of *in situ* denitrification in all aquifer layers during the daily injection phase. The high-

K layers demonstrated limited enrichment, while the low-K layers experienced elevated enrichment, suggesting varying degrees of denitrification.

5. Implications

By showing a strong qualitative correspondence between physical hydrogeology and denitrification intensity, this experiment illustrates that the greatest challenges in achieving *in situ* denitrification – particularly in layers with high groundwater velocities – are primarily hydrogeological in nature. A simple equation (eq 3) provided reasonably good predictions concerning the relationship between pulse mixing and nitrate reduction, further supporting the importance of acetate delivery to the success of the treatment program. Although nitrate treatment was not fully realized throughout the aquifer in this test, mainly due to extremely high groundwater velocities, small indications that the pulsing interval predictions may have been underestimated by eq 3 mean that the stimulation of denitrification in all units may still be possible.

With different layers showing markedly different propensities for sustaining denitrification, future treatment system designs would be made more efficient with depth-selective acetate pulsing intervals, and possibly concentrations. Layers requiring more frequent injections could be treated from well sections packed off at the appropriate depths, while other layers could receive less frequent injections.

The mixing required for the CIS to function properly occurs by dispersion in the aquifer. Presently, dispersion at the field scale is understood at an empirical level. Future work to

understand the interplay between solute transport and microbial response is needed to fine tune delivery systems for bioremediation, like the CIS.

6. Conclusions

The water supply aquifer near Woodstock, Ontario, can be described by six hydrostratigraphic units, with hydraulic conductivity values between $4.8x10^{-2}$ m/s $1.9x10^{-2}$ m/s (typical of sand and coarser grained units) and local groundwater velocities exceeding 20 m/day. The aquifer was shown to be initially aerobic over its entire profile, explaining why denitrification was not naturally occurring at rates sufficient to keep nitrate concentrations below the regulatory limits.

It is further concluded that nitrate attenuation, most likely by denitrification, can be stimulated in the aquifer through multiple, consecutive injections of an electron donor such as acetate. Overall, the system achieved an 11 percent reduction in nitrate mass crossing the 5-m wide treatment zone. A conditioning period of six to eight injections was needed to initiate nitrate reduction at the site. The conditioning period is likely site specific, depending on several subsurface properties such as the rate of groundwater flow, native microbial populations, and the amount of dissolved oxygen in the groundwater.

The nitrite, nitrate and NO_3-^{15}N and NO_3-^{18}O isotope data demonstrated that the acetate injections were most successful in stimulating denitrification in the least conductive layers, where groundwater was moving at less than 5 m/day. To a lesser degree, denitrification was

stimulated in the layers with intermediate groundwater velocities up to about 12 m/day. In contrast, relatively little denitrification was observed in the layers with the fastest flowing groundwater (on the order of 20 m/day or greater). Similar trends were observed with respect to dissolved oxygen consumption. This result suggests a hydrogeological control on the observed nitrate and oxygen attenuation rates. Future work will need to address the problem of acetate delivery to high velocity zones.

This work provides one of the first examples of a technology applied in conjunction with BMPs to solve an agricultural nitrate problem in groundwater. Once the ideal injection scenario for the higher-K layers has been identified and a full-scale cross-injection scheme is established at the site, it is thought that the stimulation of *in situ* denitrification will accelerate nitrate remediation at the Thornton Well Field, bridging the gap between BMP implementation and the resulting decline in aquifer nitrate concentrations.

Acknowledgements

Funding for this project was provided by the Natural Sciences and Engineering Council of Canada, the County of Oxford, the Canadian Water Network, and the Ontario Ministry of the Environment and the National Science Foundation through Career Grant No. 0134545 to J.F. Devlin. Any opinions, findings, and conclusions or recommendations expressed in this material are those of the authors and do not necessarily reflect the views of the NSF.In addition, the people at Oxford County are gratefully acknowledged for financial assistance and providing access to the study site.

References

Appelo, C. A. J., and D. Postma. 2005. *Geochemistry, Groundwater and Pollution, Second Edition.* Amsterdam, Netherlands: A.A. Balkema Publishers.

Aravena, R., and W. D. Robertson. 1998. Use of Multiple Isotope Tracers to Evaluate Denitrification in Groundwater: Case Study of Nitrate from a Large-Flux Septic System Plume. *Ground Water* 36: 975- 982.

Bekeris, L. 2007. *Field-Scale Evaluation of Enhanced Agricultural Management Practices Using a Novel Unsaturated Zone Nitrate Mass Load Approach.* Master's thesis, University of Waterloo.

Blowes, D. W., C. J. Ptacek, S. G. Benner, C. W. T. McRae, T. A. Bennett, and R. W. Puls. 2000. Treatment of Inorganic Contaminants Using Permeable Reactive Barriers. *Journal of Contaminant Hydrology* 45: 123-137.

Bottcher, J., O. Strebel, S. Voerkelius, and H. L. Schmidt. 1990. Using Isotope Fractionation of Nitrate-Nitrogen and Nitrate-Oxygen for Evaluation of Microbial Denitrification in a Sandy Aquifer. *Journal of Hydrology* 114: 413-424.

Bradbury, K. R. and M. A. Muldoon. 1990. Hydraulic Conductivity Determinations in Unlithified Glacial and Fluvial Sediments. In *Groundwater and Vadose Zone Monitoring, ASTM Special Technical Publication 1053*. American Society for Testing Materials, Philidelphia, 138-151.

Cole, J. 2008. *Quantification of the Long-Term Effects from Nutrient Reductions on Groundwater Nitrate Concentrations in an Agricultural Setting.* Master's thesis, University of Waterloo.

Constantin, H., S. Raoult, W. Montigny, and M. Fick. 1996. Denitrification of Concentrated Industrial Wastewater: Microorganism Selection and Kinetic Studies. *Environmental Technology* 17: 831-840.

Constantin, H. and M. Fick. 1997. Influence of C-sources on the Denitrification Rate of a High-Nitrate Concentrated Industrial Wastewater. *Water Research* 31(3): 583–589.

Critchley, C. E. 2010. *Stimulating In situ Denitrification in an Aerobic, Highly Conductive Municipal Drinking Water Aquifer*. Master's Thesis, University of Waterloo.

Crop Nutrients Council. 2009. Beneficial Management Practices. Agriculture and Agri-Food Canada. http://www.cropnutrients.ca/Beneficial_Management_Practices/.

Devlin, J. F. and J. F. Barker. 1994. A Semipassive Nutrient Injection Scheme for Enhanced *In situ* Denitrification. *Groundwater* 32(3): 374-380.

Devlin, J. F., and J. F. Barker. 1996. Field Investigation of Nutrient Pulse Mixing in an *In situ* Biostimulation Experiment. *Water Resources Research* 32(9): 2869–2877.

Devlin, J. F., R. Eedy, and B. J. Butler. 2000. The Effects of Electron Donor and Granular Iron on Nitrate Transformation Rates in Sediments from a Municipal Water Supply Aquifer. *Journal of Contaminant Hydrology* 46: 81–97.

Devlin, J.F., Schillig, P.C., Bowen, I., Critchley, C.E., Rudolph, D.L., Thomson, N.R., Tsoflias,G.P., Roberts, J.A. (in review) Applications and Implications of Direct Groundwater Velocity Measurement at the Centimetre Scale. *Journal of Contaminant Hydrology*.

Di, H. J., and K. C. Cameron. 2002. Nitrate Leaching in Temperate Agroecosystems: Sources, Factors, and Mitigating Strategies. *Nutrient Cycling in Agroecosystems* 46: 237-256.

Dinnes, D. L., D. L. Karlen, D. B. Jaynes, T. C. Kaspar, J. L. Hatfield, T. S. Colvin, and C. A. Cambadella. 2002. Nitrogen Management Strategies to Reduce Nitrate Leaching in Tile-Drained Midwestern Soils. *Agronomy Journal* 94: 153-171.

Dybas, M.J., D. W. Hyndman, R. Heine, J. Tiedje, K. Linning, D. Wiggert, T. Voice, X. Zhao, L. Dybas, and C. S. Criddle. 2002. Development, Operation and Long-Term Performance of a Full-Scale Biocurtain Utilizing Bioaugmentation. *Environmental Science and Technology* 36(16): 3635–3644.

Foth, H. D. 1984. *Fundamentals of Soil Science.* New York: John Wiley & Sons.

Fukada, T., K. M. Hiscock, P. F. Dennis, T. Grishek. 2003. A Dual Isotope Approach to Identify Denitrification in Groundwater at a River-Bank Infiltration Site. *Water Research* 37: 3070-3078.

Gelberg, K.H., L. Church, G. Casey, M. London, D. S. Roerig, J. Boyd, and M. Hill. 1999. Nitrate Levels in Drinking Water in Rural New York State. *Environmental Research* 80(1): 34-40.

Gierczak, R., J. F. Devlin, and D. L. Rudolph. 2006. Combined Use of Field and Laboratory Testing to Predict Preferred Flow Paths in an Heterogeneous Aquifer. Journal of Contaminant Hydrology 82: 75-98.

Gierczak, R., J. F. Devlin, and D. L. Rudolph. 2007. Field Test of a Cross-Injection Scheme for Stimulating *In situ* Denitrification near a Municipal Water Supply Well. *Journal of Contaminant Hydrology* 89: 48-70.

Hamon, M. and E. Fustec. 1991. Laboratory and Field Study of an *In situ* Groundwater Denitrification Reactor. *Research Journal of the Water Pollution Control Federation* 63(7): 942-949.

Haslauer, C. P. 2005. *Hydrogeologic Analysis of a Complex Aquifer System and Impacts of Changes in Agricultural Practices on Nitrate Concentrations in a Municipal Well Field: Woodstock, Ontario.* Master's thesis, University of Waterloo.

Honisch, M., C. Hellmeier, and K. Weiss. 2002. Response of Surface and Subsurface Water Quality to Land Use Changes. *Geoderma* 105: 277-298.

Johnson, C. J., P. A. Bonrod, T. I. Dosch, A. W. Kilness, K. A. Senger, D. C. Busch, and M. R. Meyer. 1987. Fatal Outcome of Methemoglobinemia in an Infant. *Journal of the American Medical Association* 257: 2796–2797.

Khan, I. A. and R. F. Spalding. 2003. Development of a Procedure for Sustainable *In situ* Aquifer Denitrification. *Remediation* 13(2): 53-69.

Khan, I. A. and R. F. Spalding. 2004. Enhanced *In situ* Denitrificaiton for a Municipal Well. *Water Research* 38: 3382–3388.

Knobeloch, L., B. Salna, A. Hogan, J. Postle, and H. Anderson. 2000. Blue Babies and Nitrate-Contaminated Well Water. *Environmental Health Perspectives* 108(7): 675-678.

Koch, J. T. 2009. *Evaluating Regional Aquifer Vulnerability and BMP Performance in an Agricultural Environment Using A Multi-Scale Data Integration Approach.* Master's thesis, University of Waterloo.

Lund, L. J., A. J. Horne, and A. E. Williams. 2000. Estimating Denitrification in a Large Constructed Wetland using Stable Nitrogen Isotope Ratios. *Ecological Engineering* 14: 67-76.

Mariotti, A., J. C. Germon, P. Hubert, P. Kaiser, R. Letolle, A. Tardieux, and P. Tardieux. 1981. Experimental Determination of Nitrogen Kinetic Isotope Fractionation: Some Principles; Illustration for the Denitrification and Nitrification Processes. *Plant Soil* 62: 413-430.

Mariotti, A., A Landreau, and B. Simon. 1988. 15N Isotope Biogeochemistry and Natural Denitrification Process in Groundwater: Application to the Chalk Aquifer in Northern France. *Geochimica Cosmochimica Acta* 52(7): 1869-1878.

Mateju, V., S. Cizinsica, J. Krejci, and T. Janoch. 1992. Biological Water Denitrification. *Enzyme and Microbiological Technology* 14: 170–183.

McKague, K., K. Reid, and H. Simpson. 2005. Environmental Impacts of Nitrogen Use in Agriculture. Ontario Ministry of Agriculture, Food, and Rural Affairs. http://www.omafra.gov.on.ca/english/engineer/facts/05-073.htm.

Meissner, R., J. Seeger, and H. Rupp. 2002. Effects of Agricultural Land Use Changes on Diffuse Pollution of Water Resources. *Irrigation and Drainage* 51:119-127.

Moltz, F. J., R. H. Morin, A. E. Hess, J. G. Melville, and O. Güven. 1989. The Impeller Meter for Measuring Aquifer Permeability Variations: Evaluation and Comparison with other Tests. *Water Resources Research* 25(7): 1677-1683.

O'Hannesin, S.F., Gillham, R.W. 1992. A permeable reaction wall for *in situ* degradation of halogenated organic compounds. Presented at the 45th Canadian Geotechnical Society Conference, Toronto, Ontario, Oct. 25-28.

Peyton, B. 1996. Improved Biomass Distribution using Pulsed Injections of Electron Donor and Acceptor. *Water Research* 30(3): 756–758.

Robertson, W. D., D. W. Blowes, C. J. Ptacek, and J. A. Cherry. 2000. Long-Term Performance of *In situ* Reactive Barriers for Nitrate Remediation. *Ground Water* 38(5): 689-695.

Robertson, W. D. and J. A. Cherry. 1995. *In situ* Denitrification of Septic-System Nitrate Using Reactive Porous Media Barriers: Field Trials. *Ground Water* 33(1): 99-111.

Scherer, M. M., S. Richter, R. L. Valentine, and P. J. J. Alvarez. 2000. Chemistry and Microbiology of Permeable Reactive Barriers for *In situ* Groundwater Clean up. *Critical Reviews in Microbiology* 26(4): 221-264.

Soares, M. I. M. 2000. Biological Denitrification of Groundwater. *Water, Air, and Soil Pollution* 123: 183-193.

Sobieszuk, P. and K. W. Szewczyk. 2006. Estimation of (C/N) Ratio for Microbial Denitrification. *Environmental Technology* 27: 103-108.

Spalding, R. F. and J. D. Parrott. 1994. Shallow Groundwater Denitrification. *The Science of the Total Environment* 141: 17-25.

Springer, R. K. and L. W. Gelhar. 1991. Characterization of Large-Scale Aquifer Heterogeneity in Glacial Outwash by Analysis of Slug Tests with Oscillatory Response, Cape Cod, Massachusetts. U.S. Geological Survey Water Resources Investigation Report 91-4034: 36-40.

Spruill, T.B. 2000. Statistical Evaluation of Effects of Riparian Buffers on Nitrate and Ground Water Quality. *Journal of Environmental Quality* 29: 1523–1538.

Starr, R. C. and R. W. Gillham. 1986. The role of organic carbon in controlling the occurrence of denitrification in groundwater. Proceedings of the Technology Transfer Conference, Part B, Ontario Ministry of the Environment, Toronto, pg. 67-83.

Terzaghi, K. 1925. *Erdbaumechanik auf Bodenphysikalischer Grundlage*. Franz Deuticke, Leipzig.

Tomer, M. D. and M. R. Burkart. 2003. Long-Term Effects of Nitrogen Fertilizer Use on Groundwater Nitrate in Two Small Watersheds. *Journal of Environmental Quality* 32: 2158-2171.

Ward, M. H., S. D. Mark, K. P. Cantor, D. D. Weisenburger, A. Correa-Villasenor, and S. H. Zahm. 1996. Drinking Water Nitrate and the Risk of Non-Hodgkin's Lymphoma. *Epidemiology* 7(5): 465–471.

Wassenaar, L. I., M. J. Hendry, and N. Harrington. 2006. Decadal Geochemical and Isotopic Trends for Nitrate in a Transboundary Aquifer and Implications for Agricultural Beneficial Management Practices. *Environmental Science and Technology* 40: 4626-4632.

Yang, C. Y., M. F. Cheng, S. S. Tsai, and Y. L. Hsieh. 1998. Calcium, Magnesium, and Nitrate in Drinking Water and Gastric Cancer Mortality. *Japanese Journal of Cancer Research* 89: 124-130.

Table 1: Summary of background geochemistry

Parameter	Mean Value	Standard Deviation
Nitrate	13.0 mg-N/L	2.6 mg-N/L
Nitrite	All values < detection limit	-
Sulphate	32.9 mg-SO4/L	5.2 mg-SO4/L
Bromide	All values < detection limit	-
Acetate	All values < detection limit	-
Manganese	All values < detection limit	-
Iron	All values < detection limit	-
Dissolved Oxygen	8.7 mg/L	1.4 mg/L
pH	7.3	0.1
Conductivity	550.7 µS	36.3 µS
$\delta^{15}N$ – Nitrate	6.3 ‰	0.7 ‰
$\delta^{18}O$ – Nitrate	1.3 ‰	1.1 ‰

Table 2: Summary of acetate injections.

Inj. No.	Date	Total Injection Time (hours)	Total Pumping Time (hours)	Average Honda Pump Rate (L/min)	Average Injection Pump Rate (L/min)	Average Bromide Injection Concentraion (mg/L)	Average Acetate Injection Concentraion (mg/L)	C_{ac}:N Ratio[a] (moles/mole)
1	14-Jul-09	5.6	6.9	174	0.214	291	103	1.9
2	14-Sep-09	5.5	6.5	206	0.219	-	133	2.4
3	15-Sep-09	6	7	202	0.202	237	141	2.6
4	16-Sep-09	6.1	7.1	202	0.198	-	130	2.4
5	17-Sep-09	6	7	199	0.202	-	134	2.4
6	18-Sep-09	6.4	7.4	199	0.189	-	125	2.3
7	19-Sep-09	6.2	7.2	199	0.195	-	130	2.4
8	20-Sep-09	6	7	198	0.202	-	134	2.5
9	21-Sep-09	6.2	7.2	198	0.195	-	130	2.4
10	22-Sep-09	6	7.1	198	0.202	-	134	2.4
11	23-Sep-09	6.4	7.4	196	0.189	-	127	2.3
12	24-Sep-09	6.4	7.3	197	0.189	-	127	2.3
13	25-Sep-09	6.1	7.1	198	0.198	237	148	2.7
14	27-Sep-09	5.8	6.8	192	0.209	-	143	2.6
15	29-Sep-09	5.8	6.8	193	0.209	-	143	2.6
16	01-Oct-09	5.6	6.7	195	0.216	-	146	2.7
17	03-Oct-09	5.9	7.1	193	0.205	-	140	2.6
18	05-Oct-09	5.4	6.5	195	0.224	-	152	2.8
19	07-Oct-09	5.7	6.7	191	0.212	-	147	2.7
20	09-Oct-09	5.7	6.7	192	0.212	-	146	2.7

[a] Moles of acetate to moles of nitrogen; calculated assuming average nitrate concentration of 13 mg-N/L.

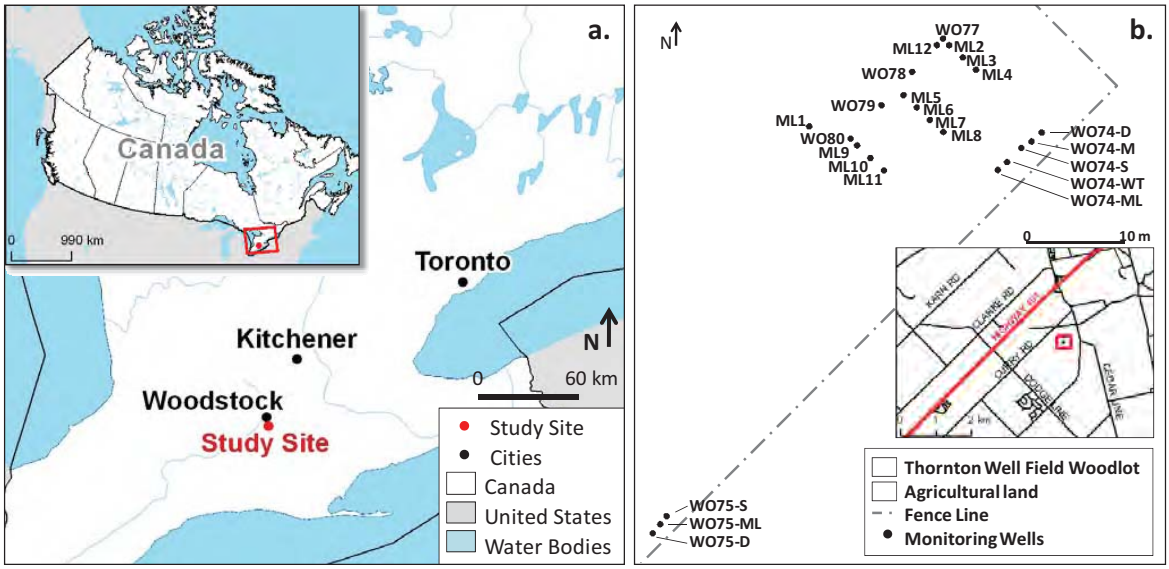

Figure 1: Maps depicting the study site (a) location and (b) layout.

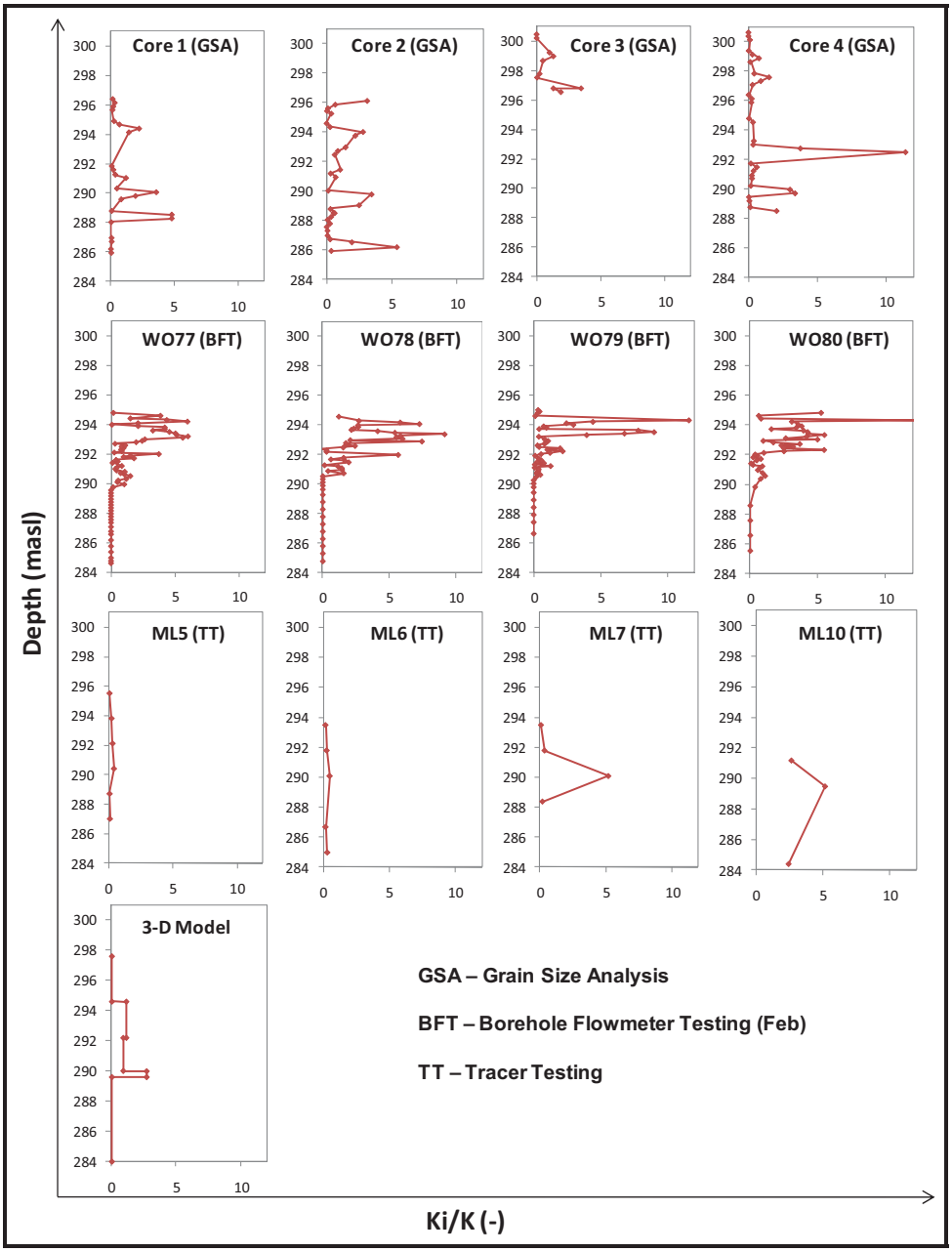

Figure 2: Graphical summary of relative hydraulic conductivity profile estimates. Normalized values (K_i/K) are plotted on the abscissa, where K_i is an individual hydraulic conductivity estimate in a particular dataset and K is the average hydraulic conductivity of that dataset.

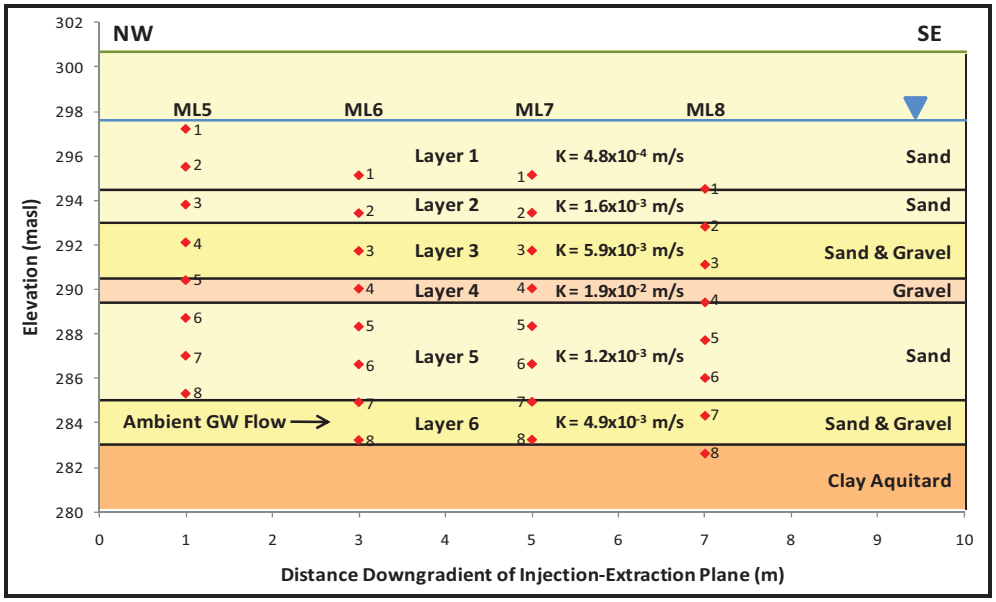

Figure 3: The hydrostratigraphic model for the study site.

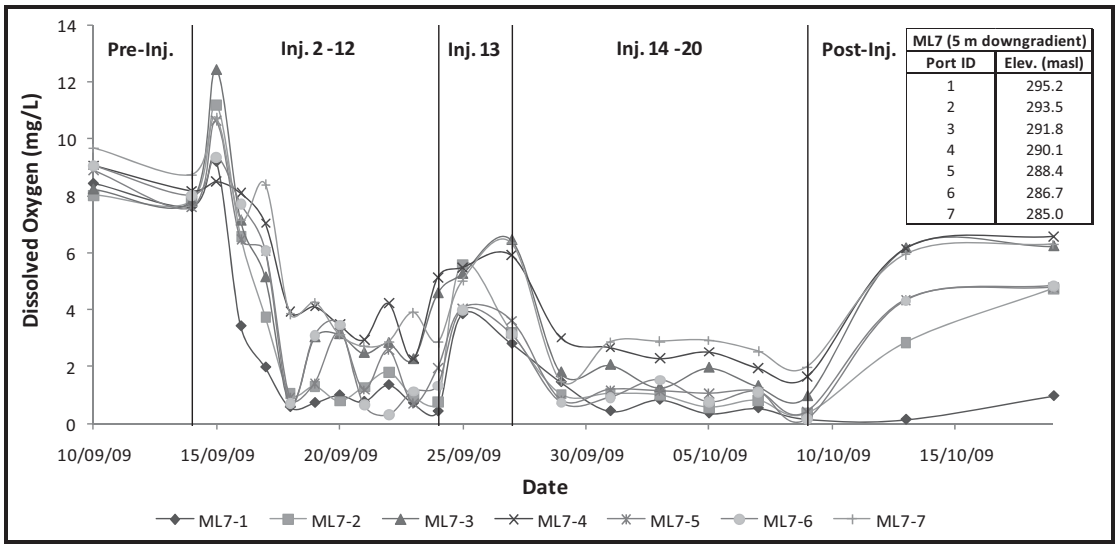

Figure 4: Dissolved oxygen results from ML7.

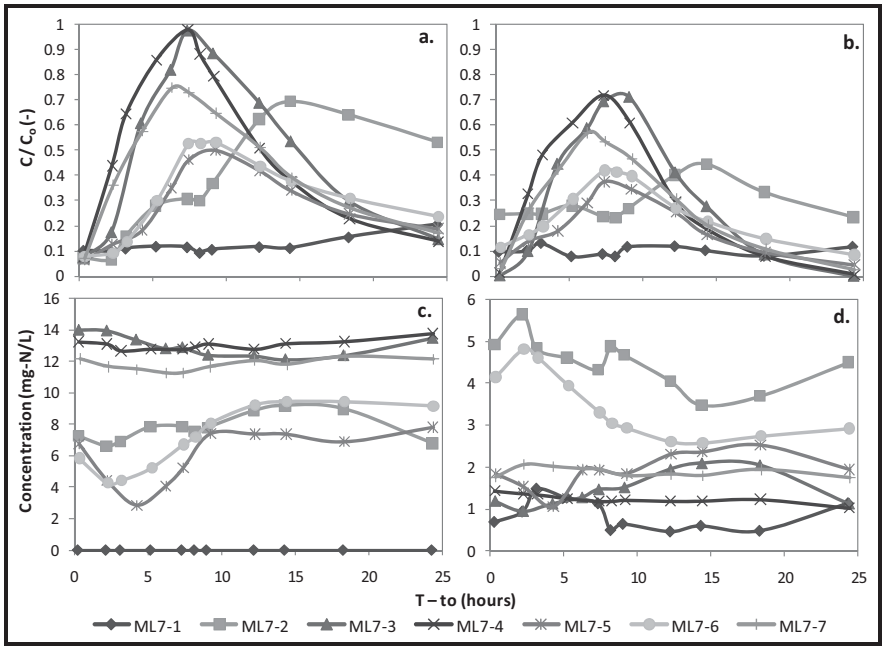

Figure 5: ML7 (a) bromide, (b) acetate, (c) nitrate, and (d) nitrite results following injection 13.

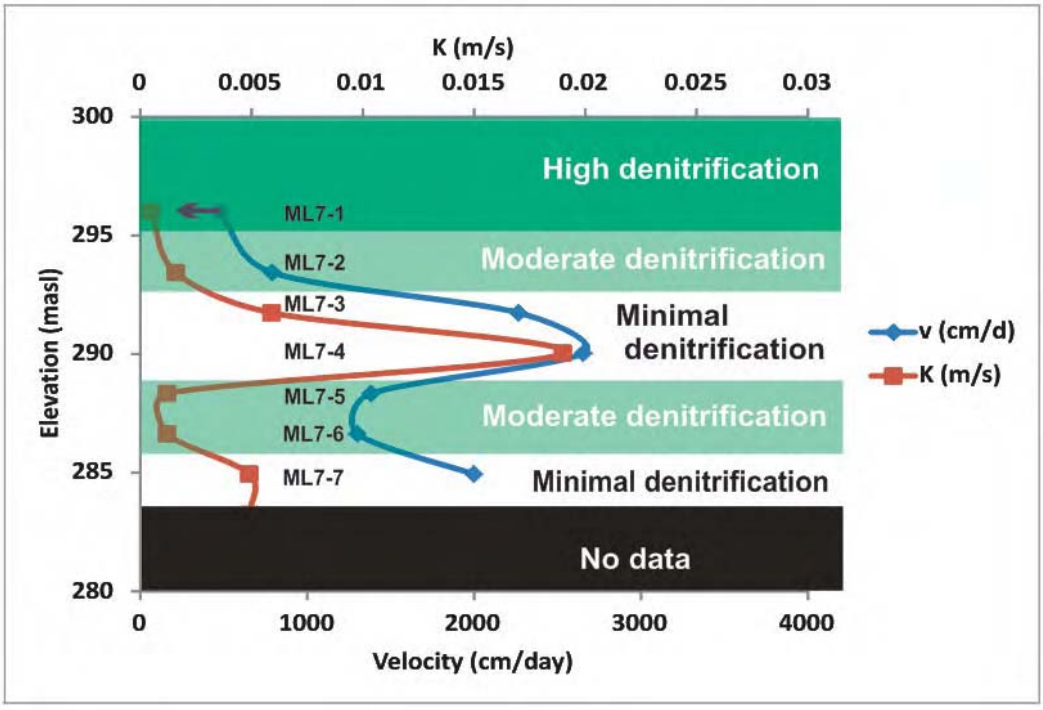

Figure 6: Correspondence between K (as shown in Figure 3), tracer velocity, and denitrification intensity at ML7 with daily acetate injections.

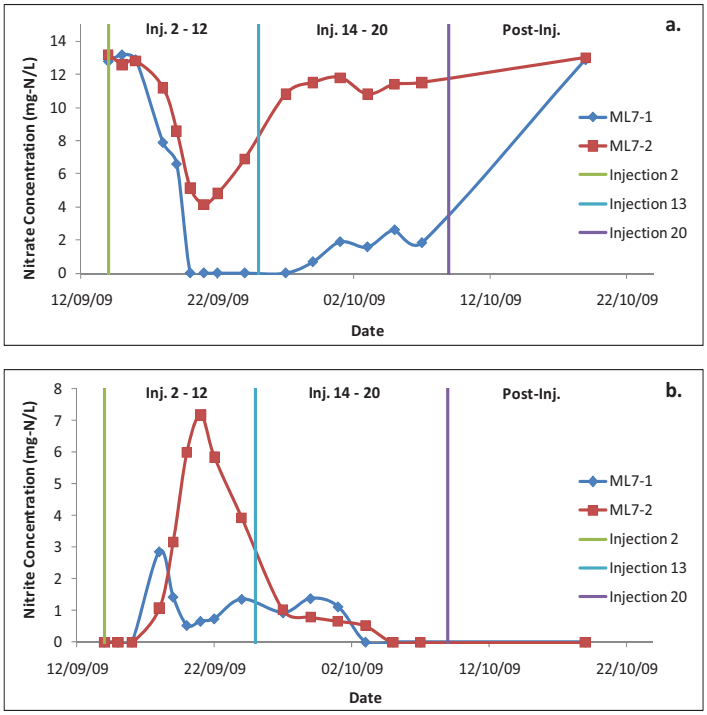

Figure 7: Additional (a) nitrate and (b) nitrite monitored at ML7-1 and ML7-2 throughout injections 2 to 20, and following system cessation.

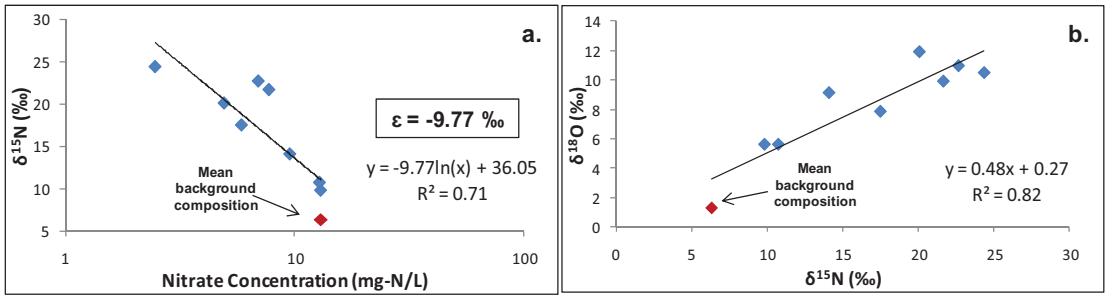

Figure 8: Nitrate isotope results from samples collected during injection 13. The plotted points represent the isotope compositions of samples from multi-level wells ML5, ML6 and ML7.

Appendix 19: Field Core Logs from PVP 3, 4, 5, Biomass and Acetylene Block Cores

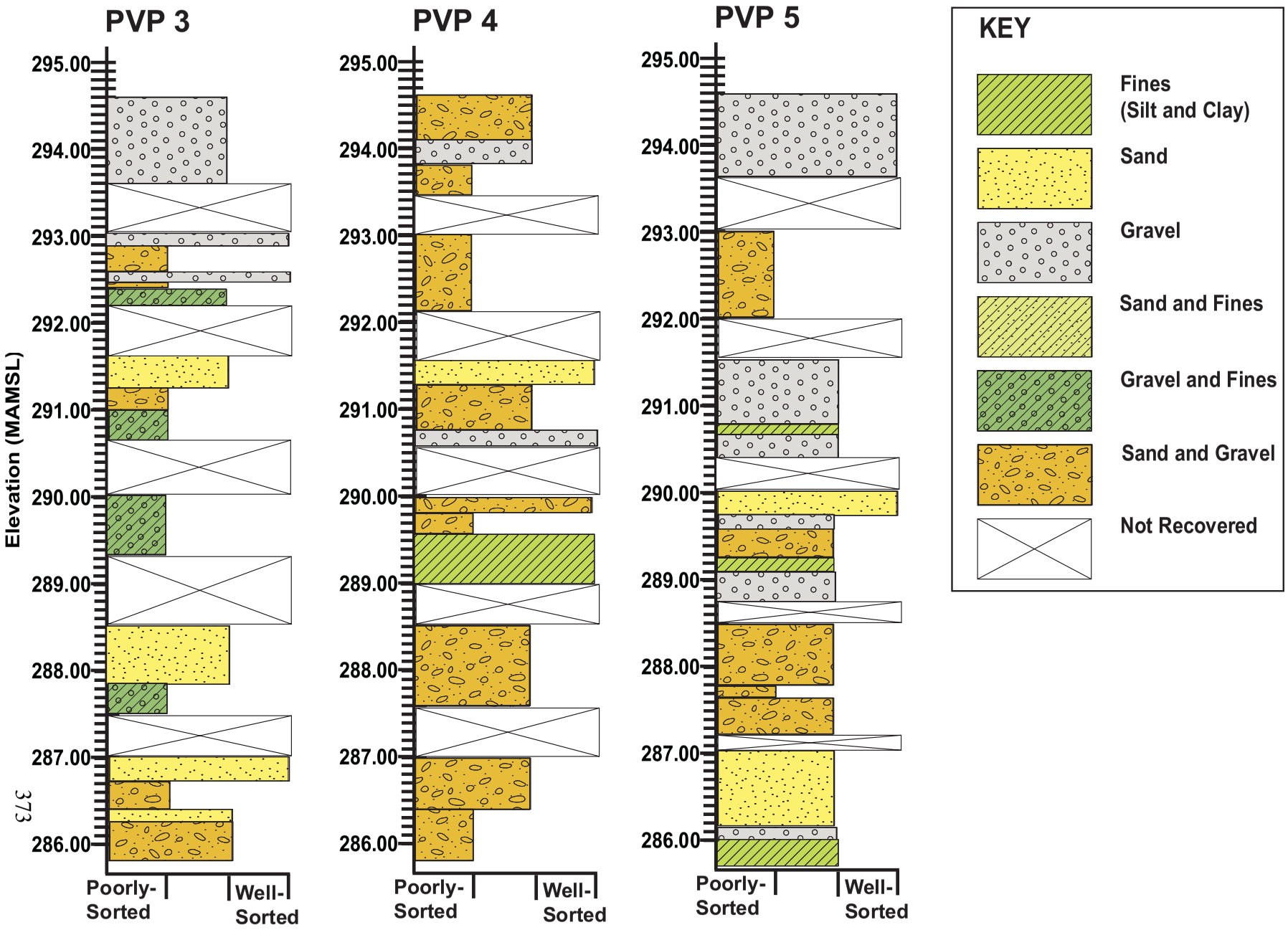
PVP 3
PVP 4
PVP 5
Elevation (MAMSL)
295.00
294.00
293.00
292.00
291.00
290.00
289.00
288.00
287.00
286.00
Poorly-Sorted
Well-Sorted
KEY
Fines (Silt and Clay)
Sand
Gravel
Sand and Fines
Gravel and Fines
Sand and Gravel
Not Recovered

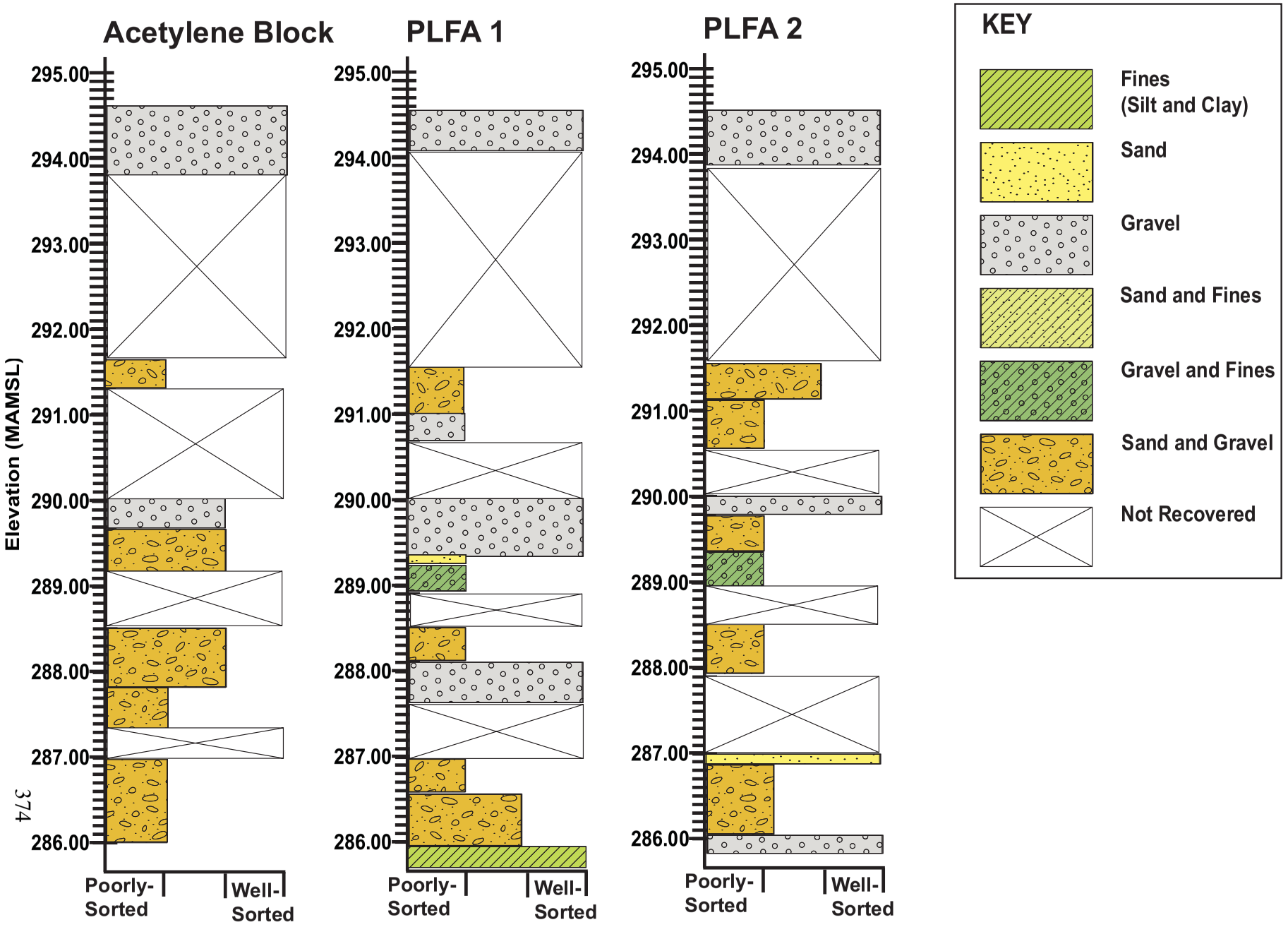
Acetylene Block
PLFA 1
PLFA 2
Elevation (MAMSL)
295.00
294.00
293.00
292.00
291.00
290.00
289.00
288.00
287.00
286.00
Poorly-Sorted
Well-Sorted
KEY
Fines (Silt and Clay)
Sand
Gravel
Sand and Fines
Gravel and Fines
Sand and Gravel
Not Recovered

Appendix 20: Hydraulic Conductivity From Grain-Size Analysis of PVP 3, 4, and 5 Cores

PVP	Elevation	D10 uM	K Rounded (m/s)	K Angular (m/s)	Average K (m/s)
3_1	293.99	720.7	5.01E-04	8.72E-04	6.87E-04
3_2	291.31	887.8	7.60E-04	1.32E-03	1.04E-03
3_3	290.00	564.1	3.07E-04	5.34E-04	4.21E-04
3_4	289.73	728.0	5.11E-04	8.90E-04	7.00E-04
3_5	289.50	477.2	2.20E-04	3.82E-04	3.01E-04
3_6	288.51	387.4	1.45E-04	2.52E-04	1.98E-04
3_7	286.76	516.8	2.58E-04	4.48E-04	3.53E-04
4_1	293.99	1102.9	1.17E-03	2.04E-03	1.61E-03
4_2	291.31	751.2	5.44E-04	9.47E-04	7.46E-04
4_3	290.00	407.0	1.60E-04	2.78E-04	2.19E-04
4_4	289.73	576.3	3.20E-04	5.58E-04	4.39E-04
4_5	289.50	384.1	1.42E-04	2.48E-04	1.95E-04
4_6	288.51	178.6	3.08E-05	5.35E-05	4.21E-05
4_7	286.76	1484.2	2.12E-03	3.70E-03	2.91E-03
5_1	293.99	682.9	4.50E-04	7.83E-04	6.16E-04
5_2	291.31	1989.4	3.82E-03	6.65E-03	5.23E-03
5_3	290.00	431.9	1.80E-04	3.13E-04	2.47E-04
5_4	289.73	741.7	5.31E-04	9.24E-04	7.27E-04
5_5	289.50	590.3	3.36E-04	5.85E-04	4.61E-04
5_6	288.51	326.0	1.03E-04	1.78E-04	1.40E-04
5_7	286.76	757.4	5.53E-04	9.63E-04	7.58E-04

Hydraulic Conductivity (K) Values after Terzaghi, 1925 (Chapter 4)

Appendix 21: Grain-Size Analysis Details from PVP 3, 4, and 5 Core

Aperture (microns)	Class Weight Retained (g or %) in Different Samples					
Sample Ide	**PVP 3-1**	**PVP 3-2**	**PVP 3-3**	**PVP 3-4**	**PVP 3-5**	**PVP 3-6**
Initial Sample Weight (g):	112.51	109.62	108.84	115.34	110.1	102.97
4000	54.87	63.55	17.72	81.95	68.95	0.49
2000	22.15	17.49	49.73	11.57	10.23	12.18
1000	19	15.9	25.39	7.23	9.86	42.1
500	10.44	7.02	5.54	4.55	9.25	33.98
297	2.64	2.32	2.04	2.35	4.92	7.55
177	1.15	1.19	1.67	1.72	2.91	3.15
125	0.51	0.48	1.9	0.98	1.88	1.21
63	0.69	0.53	2.56	1.35	1.24	1.32
pan	0.72	0.57	1.69	2.56	0.46	0.74

Aperture (microns) Sample Ide		PVP 3-7	PVP 4-1	PVP 4-2	PVP 4-3	PVP 4-4	PVP 4-5
Initial Sample Weight (g):		106.95	114.47	98.24	105.05	112.35	110.69
	4000	24.96	72.67	12.01	9.06	74.97	64.33
	2000	28.08	19.11	32.49	26.04	10.97	12.89
	1000	27.67	12.79	39.32	30.72	8.56	11.81
	500	16.24	5.97	10.7	26.1	7.38	7.51
	297	4.98	2.1	1.45	6.3	3.43	3.56
	177	2.21	0.69	0.78	2.48	2.63	2.38
	125	0.84	0.24	0.64	2.14	2.13	2.97
	63	0.89	0.38	0.58	1.32	0.77	2.28
	pan	0.99	0.23	0.07	0.74	0.68	1.54

Aperture (microns) Sample Ide		PVP 4-6	PVP 4-7	PVP 5-1	PVP 5-2	PVP 5-3	PVP 5-4
Initial Sample Weight (g):		114.11	109.1	113.69	120.97	109.34	112.94
	4000	0.4	80.97	45.53	100.09	2.86	82.16
	2000	4.26	13.45	25.14	7.61	15.03	8.94
	1000	31.07	7.15	25.47	7.46	46.87	7.68
	500	40.18	3.29	10.43	2.75	32.11	5.25
	297	14.66	1.5	3.21	0.71	5.27	1.99
	177	12.23	0.84	1.27	0.37	2.01	1.36
	125	5.24	0.39	0.61	0.28	0.94	1.14
	63	3.95	0.46	0.9	0.26	1.47	2.63
	pan	2	0.28	0.64	0.2	2.72	1.12

Aperture (microns) Sample Ide		PVP 5-5	PVP 5-6	PVP 5-7
Initial Sample Weight (g):		107.41	104.22	111.57
	4000	67.87	3.57	74.36
	2000	15.71	13.56	11.55
	1000	9.56	36.27	11.04
	500	4.44	31.46	8.3
	297	3.08	10.23	3.16
	177	1.48	4.84	1.74
	125	0.92	1.71	0.59
	63	1.53	1.29	0.59
	pan	2.65	0.69	0.09

SAMPLE STATISTICS

SIEVING ERROR: 0.3%

SAMPLE IDENTITY: **PVP 3-1**

ANALYST & DATE: Pete, 9/30/2011

SAMPLE TYPE: Unimodal, Very Well Sorted

TEXTURAL GROUP: Sandy Gravel

SEDIMENT NAME: Sandy Very Fine Gravel

	μm	ϕ
MODE 1:	3000.0	-1.500
MODE 2:		
MODE 3:		
D_{10}:	720.7	-4.538
MEDIAN or D_{50}:	3850.8	-1.945
D_{90}:	23238.7	0.473
(D_{90} / D_{10}):	32.24	-0.104
(D_{90} - D_{10}):	22518.0	5.011
(D_{75} / D_{25}):	1.316	0.612
(D_{75} - D_{25}):	487.7	0.396

GRAIN SIZE DISTRIBUTION

GRAVEL:	68.7%	COARSE SAND:	9.3%
SAND:	30.7%	MEDIUM SAND:	2.7%
MUD:	0.6%	FINE SAND:	1.1%
		V FINE SAND:	0.6%
V COARSE GRAVEL:	0.0%	V COARSE SILT:	0.1%
COARSE GRAVEL:	0.0%	COARSE SILT:	0.1%
MEDIUM GRAVEL:	0.0%	MEDIUM SILT:	0.1%
FINE GRAVEL:	0.0%	FINE SILT:	0.1%
V FINE GRAVEL:	68.7%	V FINE SILT:	0.1%
V COARSE SAND:	16.9%	CLAY:	0.1%

	METHOD OF MOMENTS			FOLK & WARD METHOD		
	Arithmetic	Geometric	Logarithmic	Geometric	Logarithmic	Description
	μm	μm	ϕ	μm	ϕ	
MEAN ($\bar{x}$):	929.6	39.18	-0.201	1863.4	-0.898	Very Coarse Sand
SORTING (σ):	1162.4	38.56	0.992	1.254	0.327	Very Well Sorted
SKEWNESS (Sk):	0.874	0.035	2.705	-4.718	4.718	Very Fine Skewed
KURTOSIS (K):	2.205	1.068	20.39	1.276	1.276	Leptokurtic

GRAIN SIZE DISTRIBUTION

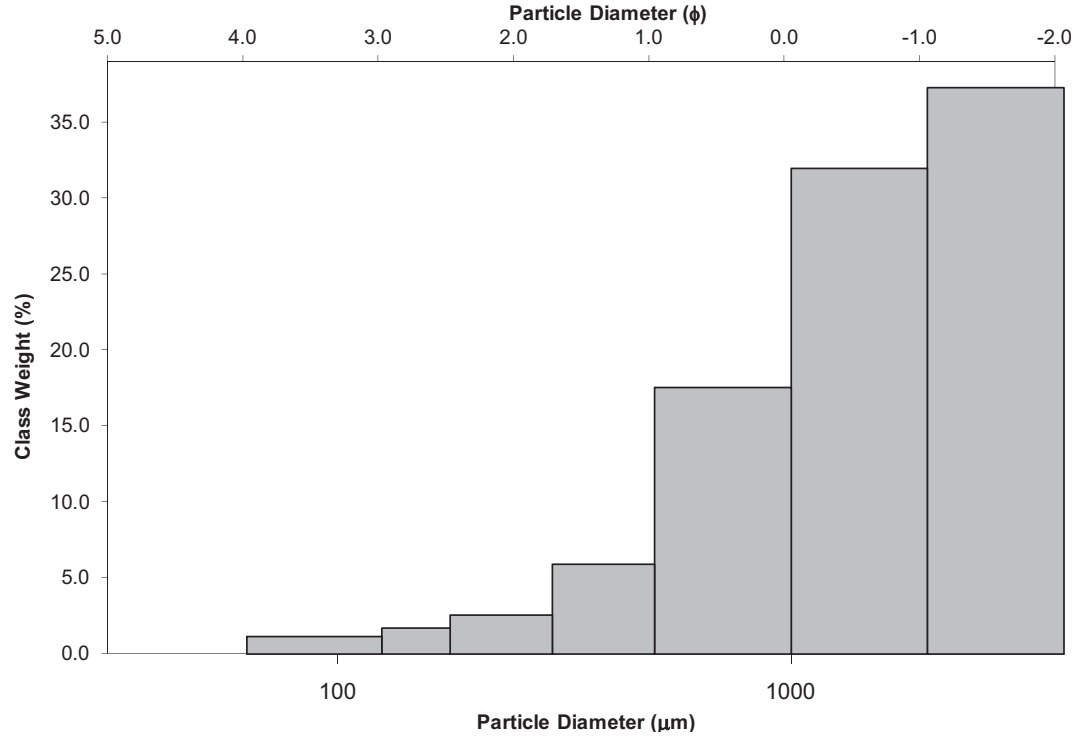

SAMPLE STATISTICS

SIEVING ERROR: 0.5%

SAMPLE IDENTITY: **PVP 3-2**

ANALYST & DATE: Pete, 9/30/2011

SAMPLE TYPE: Unimodal, Very Well Sorted

TEXTURAL GROUP: Sandy Gravel

SEDIMENT NAME: Sandy Very Fine Gravel

	μm	ϕ
MODE 1:	3000.0	-1.500
MODE 2:		
MODE 3:		
D_{10}:	887.8	-5.153
MEDIAN or D_{50}:	3285.2	-1.716
D_{90}:	35588.5	0.172
(D_{90} / D_{10}):	40.09	-0.033
(D_{90} - D_{10}):	34700.7	5.325
(D_{75} / D_{25}):	0.936	1.111
(D_{75} - D_{25}):	-123.371	-0.095

GRAIN SIZE DISTRIBUTION

GRAVEL:	74.3%	COARSE SAND:	6.4%
SAND:	25.2%	MEDIUM SAND:	2.5%
MUD:	0.5%	FINE SAND:	1.2%
		V FINE SAND:	0.5%
V COARSE GRAVEL:	0.0%	V COARSE SILT:	0.1%
COARSE GRAVEL:	0.0%	COARSE SILT:	0.1%
MEDIUM GRAVEL:	0.0%	MEDIUM SILT:	0.1%
FINE GRAVEL:	0.0%	FINE SILT:	0.1%
V FINE GRAVEL:	74.3%	V FINE SILT:	0.1%
V COARSE SAND:	14.6%	CLAY:	0.1%

	METHOD OF MOMENTS			FOLK & WARD METHOD		
	Arithmetic	Geometric	Logarithmic	Geometric	Logarithmic	Description
	μm	μm	ϕ	μm	ϕ	
MEAN ($\bar{x}$):	760.5	19.99	-0.163	1823.8	-0.867	Very Coarse Sand
SORTING (σ):	1110.6	36.34	0.908	1.167	0.223	Very Well Sorted
SKEWNESS (Sk):	1.166	0.404	2.810	-7.847	7.847	Very Fine Skewed
KURTOSIS (K):	2.811	1.223	23.31	-4.831	-4.831	Very Platykurtic

GRAIN SIZE DISTRIBUTION

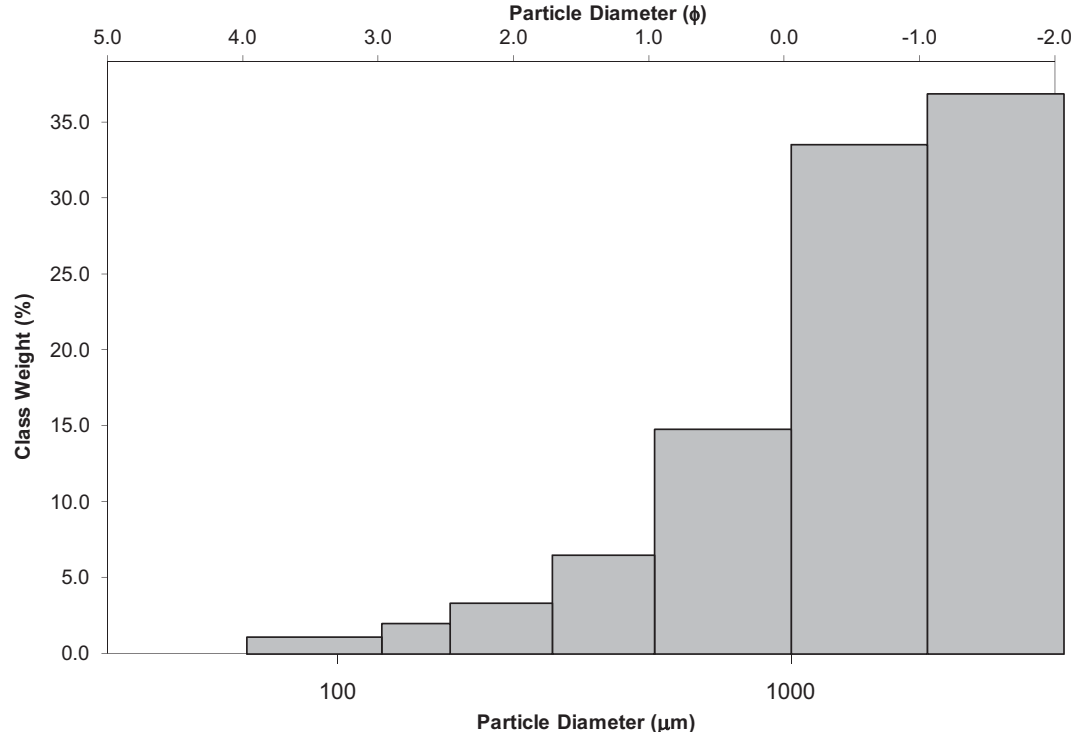

SAMPLE STATISTICS

SIEVING ERROR: 0.6%

SAMPLE IDENTITY: **PVP 3-3**

ANALYST & DATE: Pete, 9/30/2011

SAMPLE TYPE: Unimodal, Moderately Sorted

TEXTURAL GROUP: Sandy Gravel

SEDIMENT NAME: Sandy Very Fine Gravel

	μm	ϕ
MODE 1:	3000.0	-1.500
MODE 2:		
MODE 3:		
D_{10}:	564.1	-2.368
MEDIAN or D_{50}:	2408.4	-1.268
D_{90}:	5161.0	0.826
(D_{90} / D_{10}):	9.149	-0.349
(D_{90} - D_{10}):	4596.9	3.194
(D_{75} / D_{25}):	2.554	0.253
(D_{75} - D_{25}):	2136.9	1.353

GRAIN SIZE DISTRIBUTION

GRAVEL:	62.3%	COARSE SAND:	5.1%
SAND:	36.1%	MEDIUM SAND:	2.4%
MUD:	1.6%	FINE SAND:	2.8%
		V FINE SAND:	2.4%
V COARSE GRAVEL:	0.0%	V COARSE SILT:	0.3%
COARSE GRAVEL:	0.0%	COARSE SILT:	0.3%
MEDIUM GRAVEL:	0.0%	MEDIUM SILT:	0.3%
FINE GRAVEL:	0.0%	FINE SILT:	0.3%
V FINE GRAVEL:	62.3%	V FINE SILT:	0.3%
V COARSE SAND:	23.5%	CLAY:	0.3%

	METHOD OF MOMENTS			FOLK & WARD METHOD		
	Arithmetic	Geometric	Logarithmic	Geometric	Logarithmic	Description
	μm	μm	ϕ	μm	ϕ	
MEAN ($\bar{x}$):	1785.1	450.8	-0.482	2142.7	-1.099	Very Fine Gravel
SORTING (σ):	1228.6	17.92	1.471	1.959	0.970	Moderately Sorted
SKEWNESS (Sk):	-0.298	-1.470	2.696	-0.834	0.834	Very Fine Skewed
KURTOSIS (K):	1.469	3.436	12.41	1.001	1.001	Mesokurtic

GRAIN SIZE DISTRIBUTION

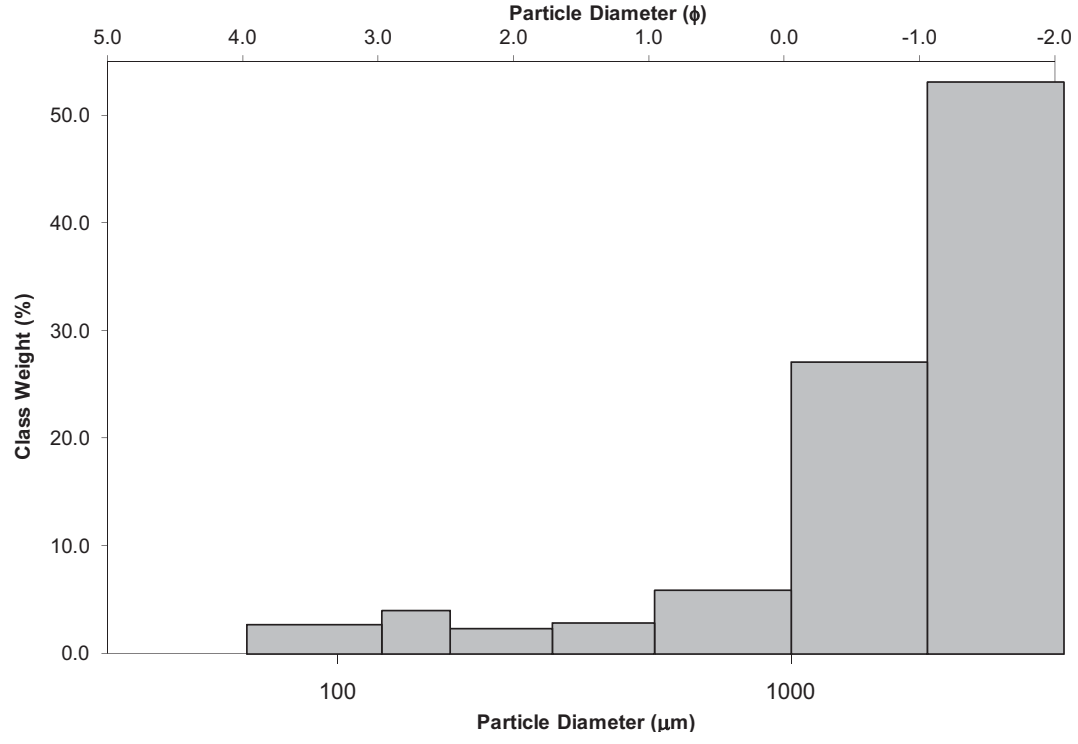

SAMPLE STATISTICS

SIEVING ERROR: 0.9%

SAMPLE IDENTITY: **PVP 3-4**

ANALYST & DATE: Pete, 9/30/2011

SAMPLE TYPE: Unimodal, Very Well Sorted

TEXTURAL GROUP: Gravel

SEDIMENT NAME: Very Fine Gravel

	μm	ϕ
MODE 1:	3000.0	-1.500
MODE 2:		
MODE 3:		
D_{10}:	728.0	-12.294
MEDIAN or D_{50}:	2628.5	-1.394
D_{90}:	5023536.1	0.458
(D_{90} / D_{10}):	6900.6	-0.037
(D_{90} - D_{10}):	5022808.1	12.75
(D_{75} / D_{25}):	0.507	2.405
(D_{75} - D_{25}):	-1574.833	-0.979

GRAIN SIZE DISTRIBUTION

GRAVEL:	81.8%	COARSE SAND:	4.0%
SAND:	15.9%	MEDIUM SAND:	2.6%
MUD:	2.2%	FINE SAND:	1.9%
		V FINE SAND:	1.2%
V COARSE GRAVEL:	0.0%	V COARSE SILT:	0.4%
COARSE GRAVEL:	0.0%	COARSE SILT:	0.4%
MEDIUM GRAVEL:	0.0%	MEDIUM SILT:	0.4%
FINE GRAVEL:	0.0%	FINE SILT:	0.4%
V FINE GRAVEL:	81.8%	V FINE SILT:	0.4%
V COARSE SAND:	6.3%	CLAY:	0.4%

	METHOD OF MOMENTS			FOLK & WARD METHOD		
	Arithmetic	Geometric	Logarithmic	Geometric	Logarithmic	Description
	μm	μm	ϕ	μm	ϕ	
MEAN ($\bar{x}$):	443.4	6.497	0.118	1782.0	-0.833	Very Coarse Sand
SORTING (σ):	940.2	22.37	1.285	1.224	0.292	Very Well Sorted
SKEWNESS (Sk):	2.049	1.151	3.587	2.884	-2.884	Very Coarse Skewed
KURTOSIS (K):	5.675	2.451	19.44	-0.954	-0.954	Very Platykurtic

GRAIN SIZE DISTRIBUTION

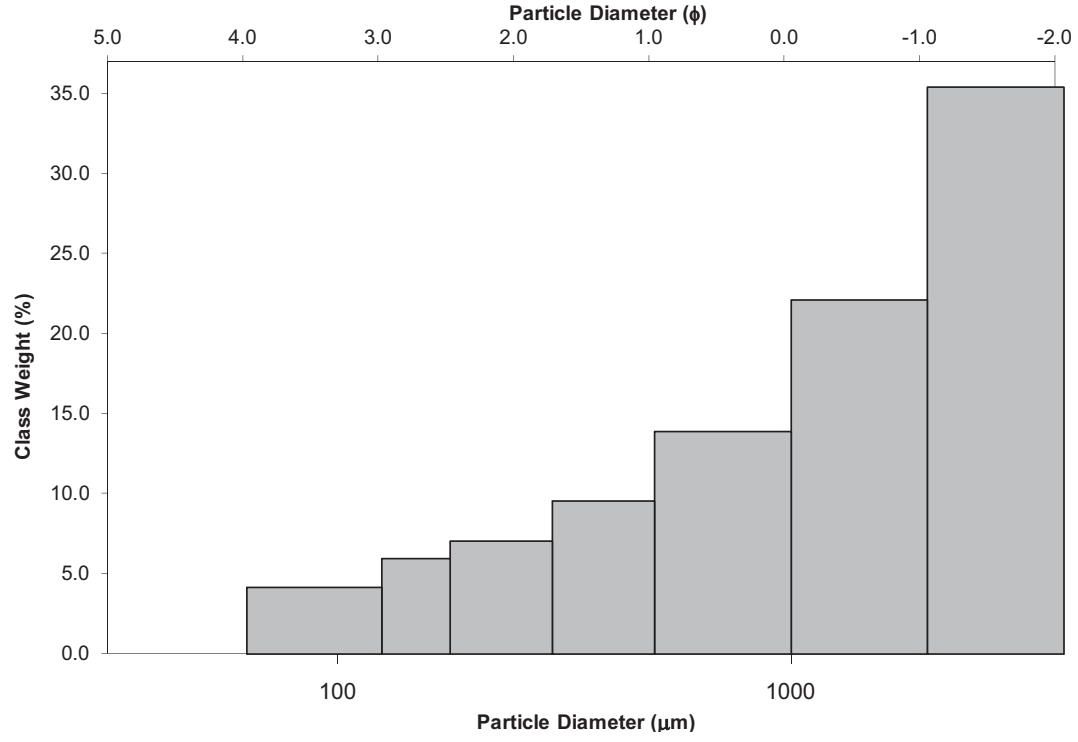

SAMPLE STATISTICS

SIEVING ERROR: 0.4%

SAMPLE IDENTITY: **PVP 3-5**

ANALYST & DATE: Pete, 9/30/2011

SAMPLE TYPE: Unimodal, Moderately Well Sorted

TEXTURAL GROUP: Sandy Gravel

SEDIMENT NAME: Sandy Very Fine Gravel

	μm	ϕ
MODE 1:	3000.0	-1.500
MODE 2:		
MODE 3:		
D_{10}:	477.2	-8.349
MEDIAN or D_{50}:	3012.6	-1.591
D_{90}:	326016.6	1.067
(D_{90} / D_{10}):	683.1	-0.128
(D_{90} - D_{10}):	325539.4	9.416
(D_{75} / D_{25}):	1.079	0.862
(D_{75} - D_{25}):	126.7	0.109

GRAIN SIZE DISTRIBUTION

GRAVEL:	72.2%	COARSE SAND:	8.4%
SAND:	27.4%	MEDIUM SAND:	5.4%
MUD:	0.4%	FINE SAND:	3.5%
		V FINE SAND:	1.1%
V COARSE GRAVEL:	0.0%	V COARSE SILT:	0.1%
COARSE GRAVEL:	0.0%	COARSE SILT:	0.1%
MEDIUM GRAVEL:	0.0%	MEDIUM SILT:	0.1%
FINE GRAVEL:	0.0%	FINE SILT:	0.1%
V FINE GRAVEL:	72.2%	V FINE SILT:	0.1%
V COARSE SAND:	9.0%	CLAY:	0.1%

	METHOD OF MOMENTS			FOLK & WARD METHOD		
	Arithmetic	Geometric	Logarithmic	Geometric	Logarithmic	Description
	μm	μm	ϕ	μm	ϕ	
MEAN ($\bar{x}$):	505.8	12.22	0.091	1503.2	-0.588	Very Coarse Sand
SORTING (σ):	917.7	27.71	0.960	1.454	0.540	Moderately Well Sorted
SKEWNESS (Sk):	1.879	0.637	2.343	-2.940	2.940	Very Fine Skewed
KURTOSIS (K):	5.271	1.515	15.37	8.124	8.124	Extremely Leptokurtic

GRAIN SIZE DISTRIBUTION

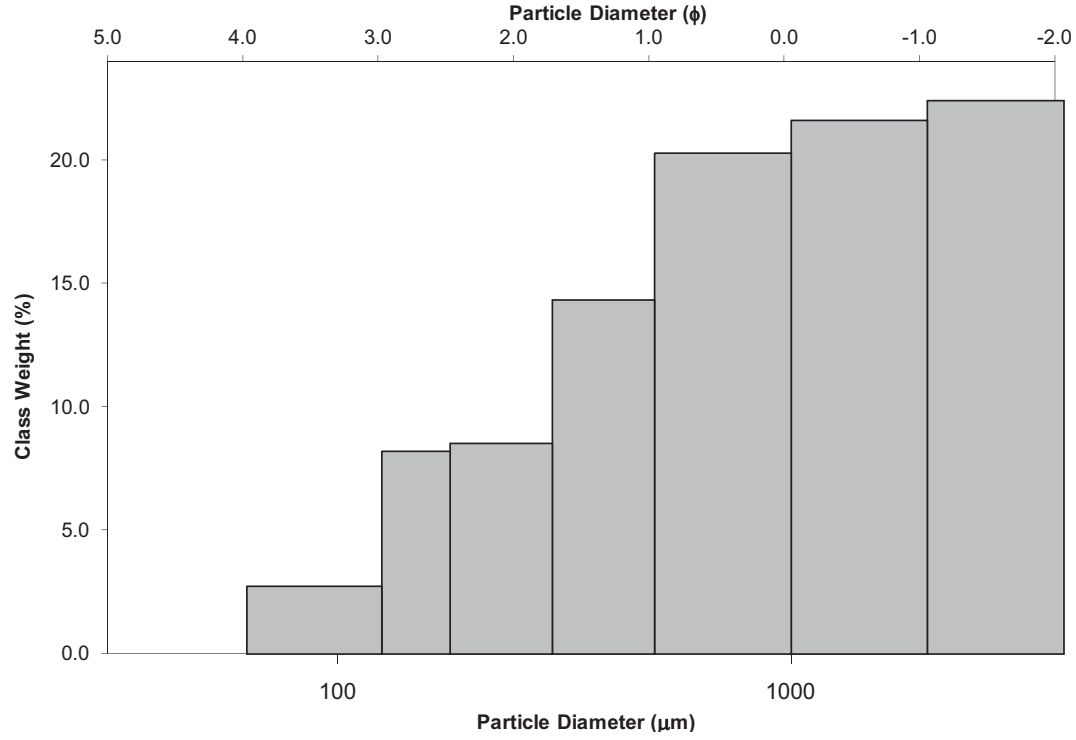

SAMPLE STATISTICS

SIEVING ERROR: 0.2%

SAMPLE IDENTITY: **PVP 3-6**

ANALYST & DATE: Pete, 9/30/2011

SAMPLE TYPE: Unimodal, Poorly Sorted

TEXTURAL GROUP: Gravelly Sand

SEDIMENT NAME: Very Fine Gravelly Very Coarse Sand

	μm	ϕ
MODE 1:	1500.0	-0.500
MODE 2:		
MODE 3:		
D_{10}:	387.4	-1.197
MEDIAN or D_{50}:	1057.7	-0.081
D_{90}:	2292.4	1.368
(D_{90} / D_{10}):	5.917	-1.143
(D_{90} - D_{10}):	1905.0	2.565
(D_{75} / D_{25}):	2.543	-0.948
(D_{75} - D_{25}):	979.5	1.346

GRAIN SIZE DISTRIBUTION

GRAVEL:	12.3%	COARSE SAND:	33.1%
SAND:	86.9%	MEDIUM SAND:	8.4%
MUD:	0.7%	FINE SAND:	3.2%
		V FINE SAND:	1.3%
V COARSE GRAVEL:	0.0%	V COARSE SILT:	0.1%
COARSE GRAVEL:	0.0%	COARSE SILT:	0.1%
MEDIUM GRAVEL:	0.0%	MEDIUM SILT:	0.1%
FINE GRAVEL:	0.0%	FINE SILT:	0.1%
V FINE GRAVEL:	12.3%	V FINE SILT:	0.1%
V COARSE SAND:	41.0%	CLAY:	0.1%

	METHOD OF MOMENTS			FOLK & WARD METHOD		
	Arithmetic	Geometric	Logarithmic	Geometric	Logarithmic	Description
	μm	μm	ϕ	μm	ϕ	
MEAN ($\bar{x}$):	1258.4	917.6	0.077	1014.9	-0.021	Very Coarse Sand
SORTING (σ):	778.3	2.525	1.150	2.023	1.016	Poorly Sorted
SKEWNESS (Sk):	0.955	-3.095	1.993	-0.130	0.130	Fine Skewed
KURTOSIS (K):	3.428	20.24	11.67	1.118	1.118	Leptokurtic

GRAIN SIZE DISTRIBUTION

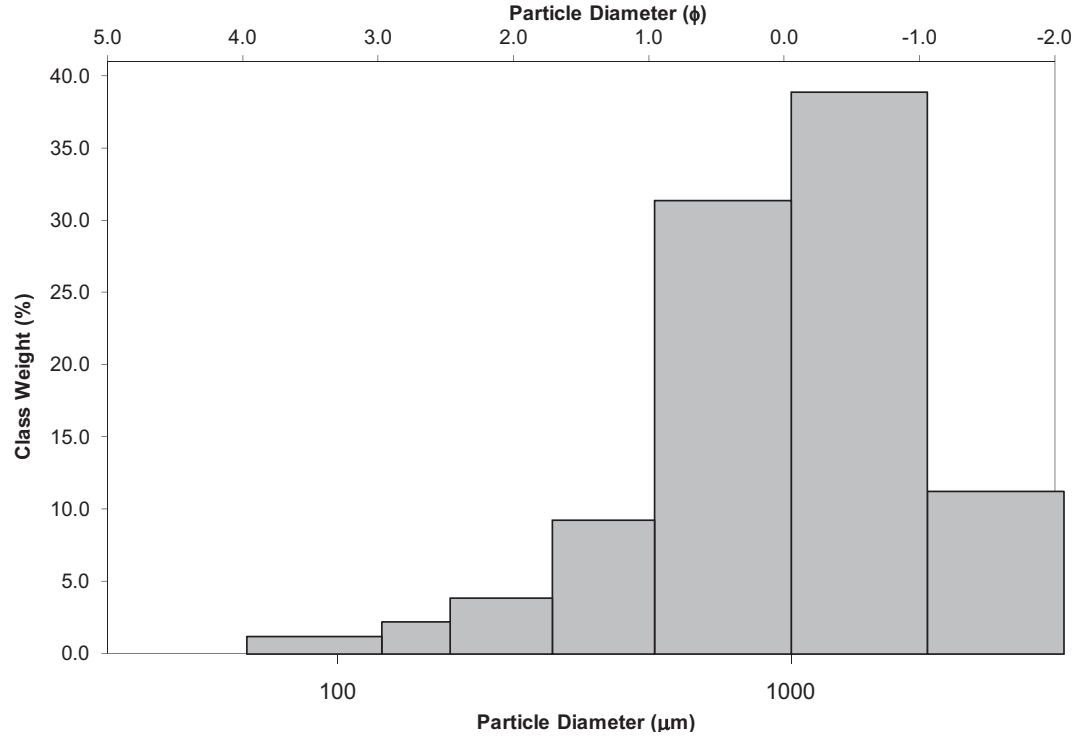

SAMPLE STATISTICS

SIEVING ERROR: 0.1%

SAMPLE IDENTITY: **PVP 3-7**

ANALYST & DATE: Pete, 9/30/2011

SAMPLE TYPE: Unimodal, Moderately Sorted

TEXTURAL GROUP: Sandy Gravel

SEDIMENT NAME: Sandy Very Fine Gravel

	μm	ϕ
MODE 1:	3000.0	-1.500
MODE 2:		
MODE 3:		
D_{10}:	516.8	-2.595
MEDIAN or D_{50}:	1980.6	-0.986
D_{90}:	6041.2	0.952
(D_{90} / D_{10}):	11.69	-0.367
(D_{90} - D_{10}):	5524.4	3.547
(D_{75} / D_{25}):	3.777	0.011
(D_{75} - D_{25}):	2816.2	1.917

GRAIN SIZE DISTRIBUTION

GRAVEL:	49.6%	COARSE SAND:	15.2%
SAND:	49.4%	MEDIUM SAND:	5.3%
MUD:	0.9%	FINE SAND:	2.2%
		V FINE SAND:	0.8%
V COARSE GRAVEL:	0.0%	V COARSE SILT:	0.2%
COARSE GRAVEL:	0.0%	COARSE SILT:	0.2%
MEDIUM GRAVEL:	0.0%	MEDIUM SILT:	0.2%
FINE GRAVEL:	0.0%	FINE SILT:	0.2%
V FINE GRAVEL:	49.6%	V FINE SILT:	0.2%
V COARSE SAND:	25.9%	CLAY:	0.2%

	METHOD OF MOMENTS			FOLK & WARD METHOD		
	Arithmetic	Geometric	Logarithmic	Geometric	Logarithmic	Description
	μm	μm	ϕ	μm	ϕ	
MEAN ($\bar{x}$):	1316.4	232.7	-0.224	1515.2	-0.599	Very Coarse Sand
SORTING (σ):	1144.1	22.65	1.200	1.744	0.803	Moderately Sorted
SKEWNESS (Sk):	0.391	-1.065	2.366	-1.064	1.064	Very Fine Skewed
KURTOSIS (K):	1.721	2.326	14.01	0.453	0.453	Very Platykurtic

GRAIN SIZE DISTRIBUTION

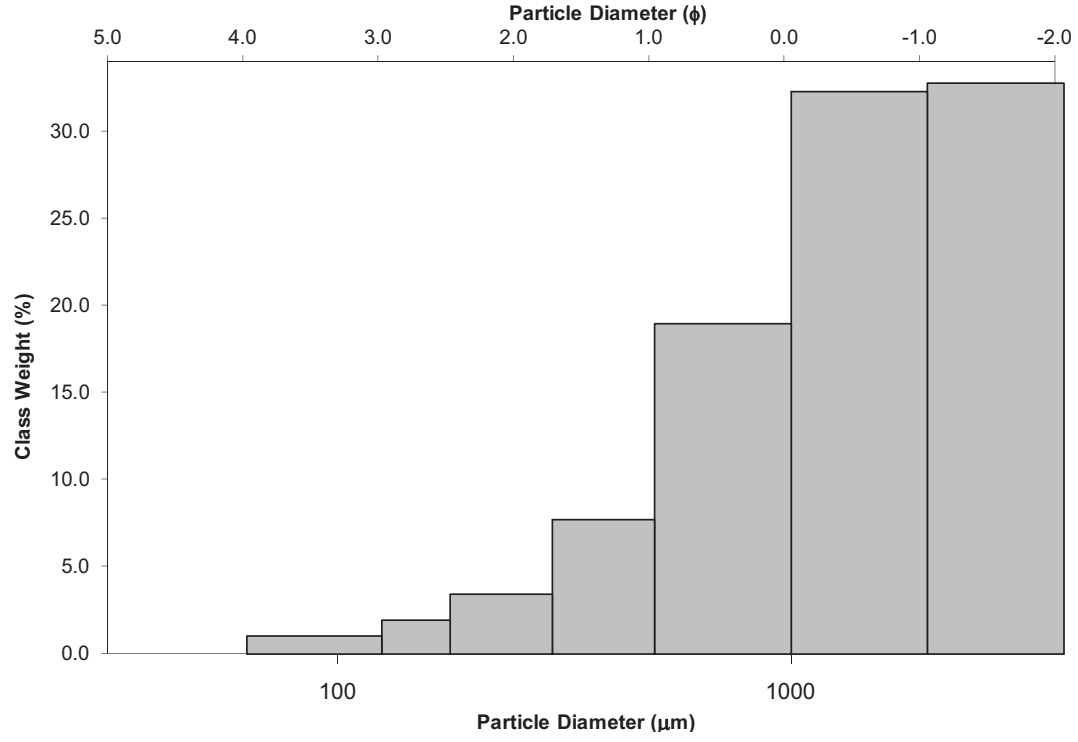

SAMPLE STATISTICS

SIEVING ERROR: 0.3%

SAMPLE IDENTITY: **PVP 4-1**

ANALYST & DATE: Pete, 9/30/2011

SAMPLE TYPE: Unimodal, Very Well Sorted

TEXTURAL GROUP: Gravel

SEDIMENT NAME: Very Fine Gravel

	μm	ϕ
MODE 1:	3000.0	-1.500
MODE 2:		
MODE 3:		
D_{10}:	1102.9	-5.840
MEDIAN or D_{50}:	2971.5	-1.571
D_{90}:	57291.6	-0.141
(D_{90} / D_{10}):	51.94	0.024
(D_{90} - D_{10}):	56188.6	5.699
(D_{75} / D_{25}):	0.690	1.682
(D_{75} - D_{25}):	-775.545	-0.536

GRAIN SIZE DISTRIBUTION

GRAVEL:	80.4%	COARSE SAND:	5.2%
SAND:	19.4%	MEDIUM SAND:	2.0%
MUD:	0.2%	FINE SAND:	0.6%
		V FINE SAND:	0.3%
V COARSE GRAVEL:	0.0%	V COARSE SILT:	0.0%
COARSE GRAVEL:	0.0%	COARSE SILT:	0.0%
MEDIUM GRAVEL:	0.0%	MEDIUM SILT:	0.0%
FINE GRAVEL:	0.0%	FINE SILT:	0.0%
V FINE GRAVEL:	80.4%	V FINE SILT:	0.0%
V COARSE SAND:	11.2%	CLAY:	0.0%

	METHOD OF MOMENTS			FOLK & WARD METHOD		
	Arithmetic	Geometric	Logarithmic	Geometric	Logarithmic	Description
	μm	μm	ϕ	μm	ϕ	
MEAN ($\bar{x}$):	718.8	14.26	-0.211	1888.2	-0.917	Very Coarse Sand
SORTING (σ):	1128.9	34.86	0.768	1.056	0.079	Very Well Sorted
SKEWNESS (Sk):	1.252	0.617	1.747	3.388	-3.388	Very Coarse Skewed
KURTOSIS (K):	2.922	1.431	20.08	-0.620	-0.620	Very Platykurtic

GRAIN SIZE DISTRIBUTION

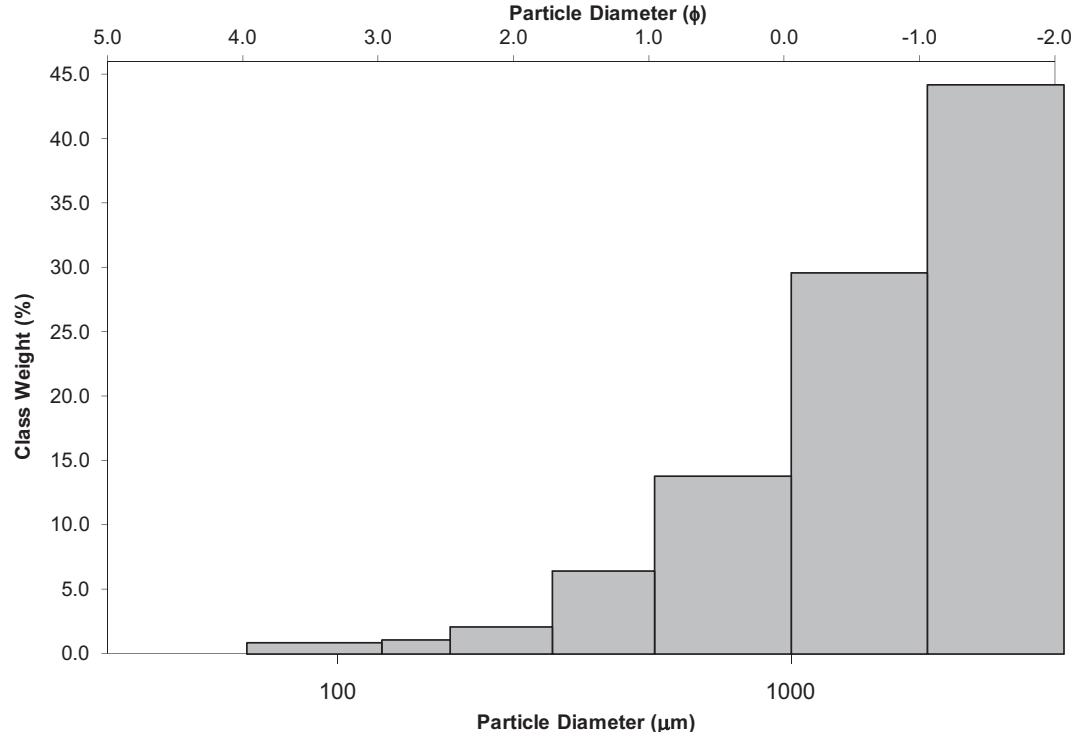

SAMPLE STATISTICS

SIEVING ERROR: 0.2%

SAMPLE IDENTITY: **PVP 4-2**

ANALYST & DATE: Pete, 9/30/2011

SAMPLE TYPE: Unimodal, Moderately Sorted

TEXTURAL GROUP: Sandy Gravel

SEDIMENT NAME: Sandy Very Fine Gravel

	μm	ϕ
MODE 1:	1500.0	-0.500
MODE 2:		
MODE 3:		
D_{10}:	751.2	-2.061
MEDIAN or D_{50}:	1846.8	-0.885
D_{90}:	4174.0	0.413
(D_{90} / D_{10}):	5.556	-0.200
(D_{90} - D_{10}):	3422.8	2.474
(D_{75} / D_{25}):	2.555	0.162
(D_{75} - D_{25}):	1864.8	1.354

GRAIN SIZE DISTRIBUTION

GRAVEL:	45.4%	COARSE SAND:	10.9%
SAND:	54.5%	MEDIUM SAND:	1.7%
MUD:	0.1%	FINE SAND:	1.2%
		V FINE SAND:	0.6%
V COARSE GRAVEL:	0.0%	V COARSE SILT:	0.0%
COARSE GRAVEL:	0.0%	COARSE SILT:	0.0%
MEDIUM GRAVEL:	0.0%	MEDIUM SILT:	0.0%
FINE GRAVEL:	0.0%	FINE SILT:	0.0%
V FINE GRAVEL:	45.4%	V FINE SILT:	0.0%
V COARSE SAND:	40.1%	CLAY:	0.0%

	METHOD OF MOMENTS			FOLK & WARD METHOD		
	Arithmetic	Geometric	Logarithmic	Geometric	Logarithmic	Description
	μm	μm	ϕ	μm	ϕ	
MEAN ($\bar{x}$):	1687.0	633.5	-0.562	1913.7	-0.936	Very Coarse Sand
SORTING (σ):	1050.5	11.97	0.882	1.645	0.718	Moderately Sorted
SKEWNESS (Sk):	-0.032	-2.073	1.577	-0.499	0.499	Very Fine Skewed
KURTOSIS (K):	1.821	5.646	9.503	0.511	0.511	Very Platykurtic

GRAIN SIZE DISTRIBUTION

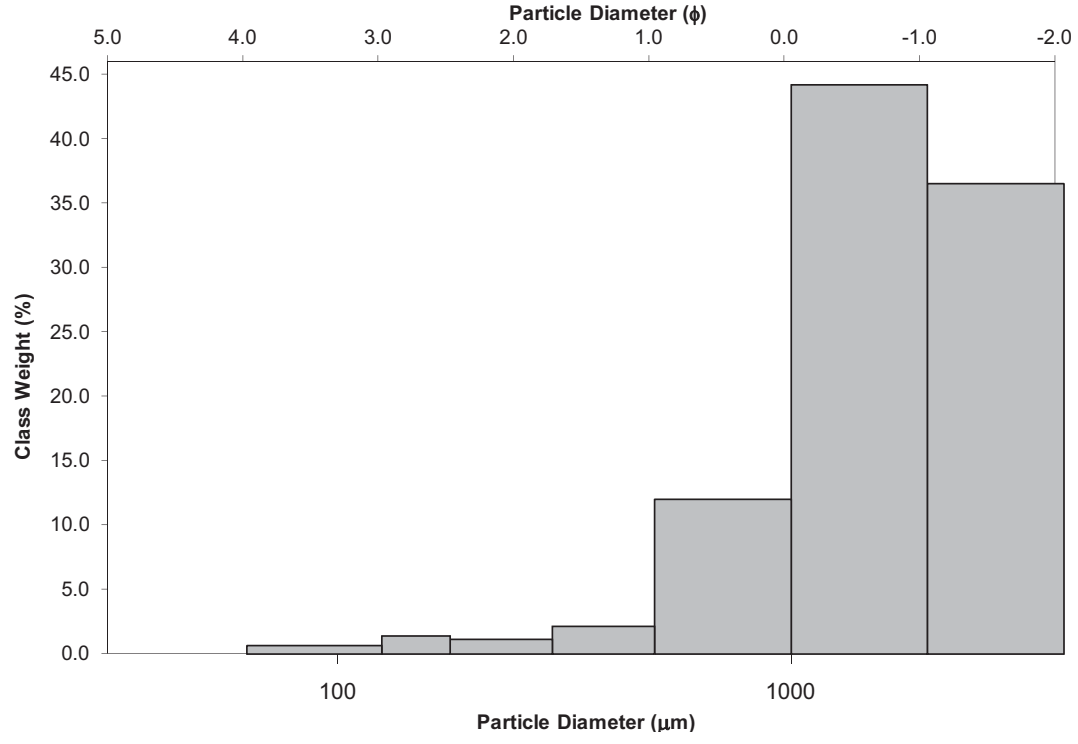

SAMPLE STATISTICS

SIEVING ERROR: 0.1%

SAMPLE IDENTITY: **PVP 4-3**

ANALYST & DATE: Pete, 9/30/2011

SAMPLE TYPE: Unimodal, Poorly Sorted

TEXTURAL GROUP: Sandy Gravel

SEDIMENT NAME: Sandy Very Fine Gravel

	μm	ϕ
MODE 1:	1500.0	-0.500
MODE 2:		
MODE 3:		
D_{10}:	407.0	-1.945
MEDIAN or D_{50}:	1352.1	-0.435
D_{90}:	3850.6	1.297
(D_{90} / D_{10}):	9.462	-0.667
(D_{90} - D_{10}):	3443.6	3.242
(D_{75} / D_{25}):	3.564	-0.367
(D_{75} - D_{25}):	1822.2	1.833

GRAIN SIZE DISTRIBUTION

GRAVEL:	33.5%	COARSE SAND:	24.9%
SAND:	65.8%	MEDIUM SAND:	6.8%
MUD:	0.7%	FINE SAND:	3.6%
		V FINE SAND:	1.3%
V COARSE GRAVEL:	0.0%	V COARSE SILT:	0.1%
COARSE GRAVEL:	0.0%	COARSE SILT:	0.1%
MEDIUM GRAVEL:	0.0%	MEDIUM SILT:	0.1%
FINE GRAVEL:	0.0%	FINE SILT:	0.1%
V FINE GRAVEL:	33.5%	V FINE SILT:	0.1%
V COARSE SAND:	29.3%	CLAY:	0.1%

	METHOD OF MOMENTS			FOLK & WARD METHOD		
	Arithmetic	Geometric	Logarithmic	Geometric	Logarithmic	Description
	μm	μm	ϕ	μm	ϕ	
MEAN ($\bar{x}$):	1404.6	595.2	-0.112	1345.5	-0.428	Very Coarse Sand
SORTING (σ):	1035.1	8.550	1.247	2.212	1.146	Poorly Sorted
SKEWNESS (Sk):	0.463	-2.240	1.774	-0.288	0.288	Fine Skewed
KURTOSIS (K):	1.923	6.992	9.654	0.747	0.747	Platykurtic

GRAIN SIZE DISTRIBUTION

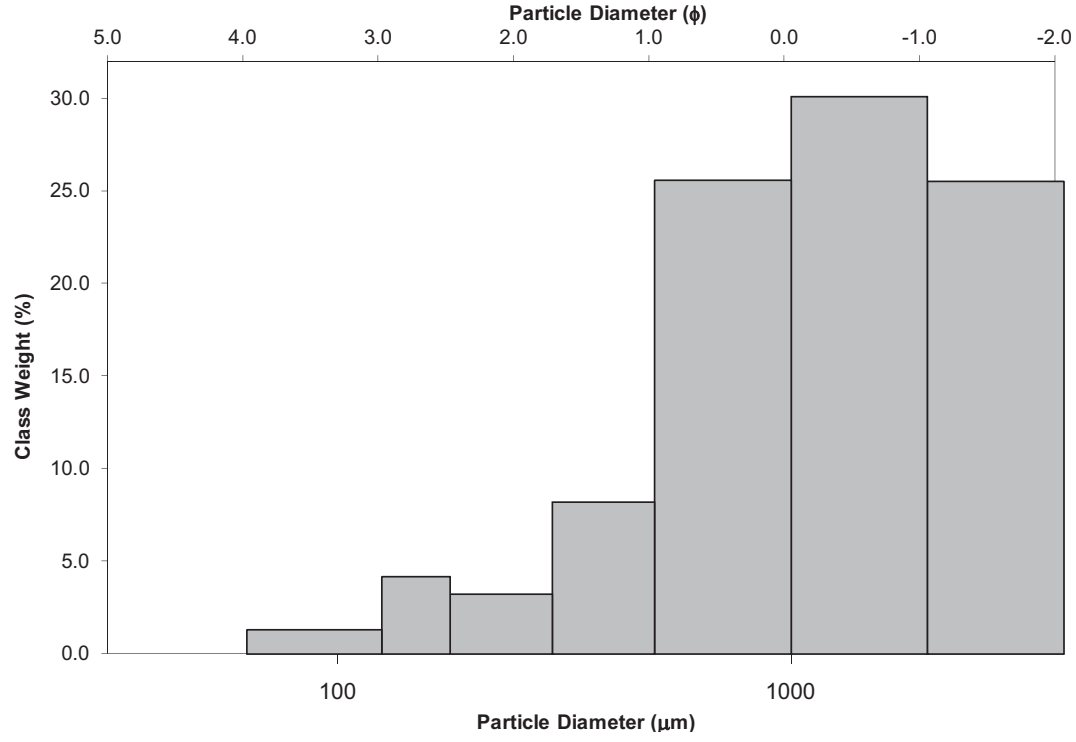

SAMPLE STATISTICS

SIEVING ERROR: 0.7%

SAMPLE IDENTITY: **PVP 4-4**

ANALYST & DATE: Pete, 9/30/2011

SAMPLE TYPE: Bimodal, Well Sorted

TEXTURAL GROUP: Sandy Gravel

SEDIMENT NAME: Sandy Very Fine Gravel

	μm	ϕ
MODE 1:	3000.0	-1.500
MODE 2:	151.0	2.749
MODE 3:		
D_{10}:	576.3	-9.891
MEDIAN or D_{50}:	2804.1	-1.488
D_{90}:	949442.1	0.795
(D_{90} / D_{10}):	1647.5	-0.080
(D_{90} - D_{10}):	948865.8	10.69
(D_{75} / D_{25}):	0.724	1.626
(D_{75} - D_{25}):	-638.296	-0.466

GRAIN SIZE DISTRIBUTION

GRAVEL:	77.1%	COARSE SAND:	6.6%
SAND:	22.3%	MEDIUM SAND:	3.9%
MUD:	0.6%	FINE SAND:	3.5%
		V FINE SAND:	0.7%
V COARSE GRAVEL:	0.0%	V COARSE SILT:	0.1%
COARSE GRAVEL:	0.0%	COARSE SILT:	0.1%
MEDIUM GRAVEL:	0.0%	MEDIUM SILT:	0.1%
FINE GRAVEL:	0.0%	FINE SILT:	0.1%
V FINE GRAVEL:	77.1%	V FINE SILT:	0.1%
V COARSE SAND:	7.7%	CLAY:	0.1%

	METHOD OF MOMENTS			FOLK & WARD METHOD		
	Arithmetic	Geometric	Logarithmic	Geometric	Logarithmic	Description
	μm	μm	ϕ	μm	ϕ	
MEAN ($\bar{x}$):	481.4	9.237	0.059	1609.5	-0.687	Very Coarse Sand
SORTING (σ):	932.8	25.89	0.972	1.329	0.410	Well Sorted
SKEWNESS (Sk):	1.943	0.845	2.811	-4.307	4.307	Very Fine Skewed
KURTOSIS (K):	5.385	1.823	19.23	-1.830	-1.830	Very Platykurtic

GRAIN SIZE DISTRIBUTION

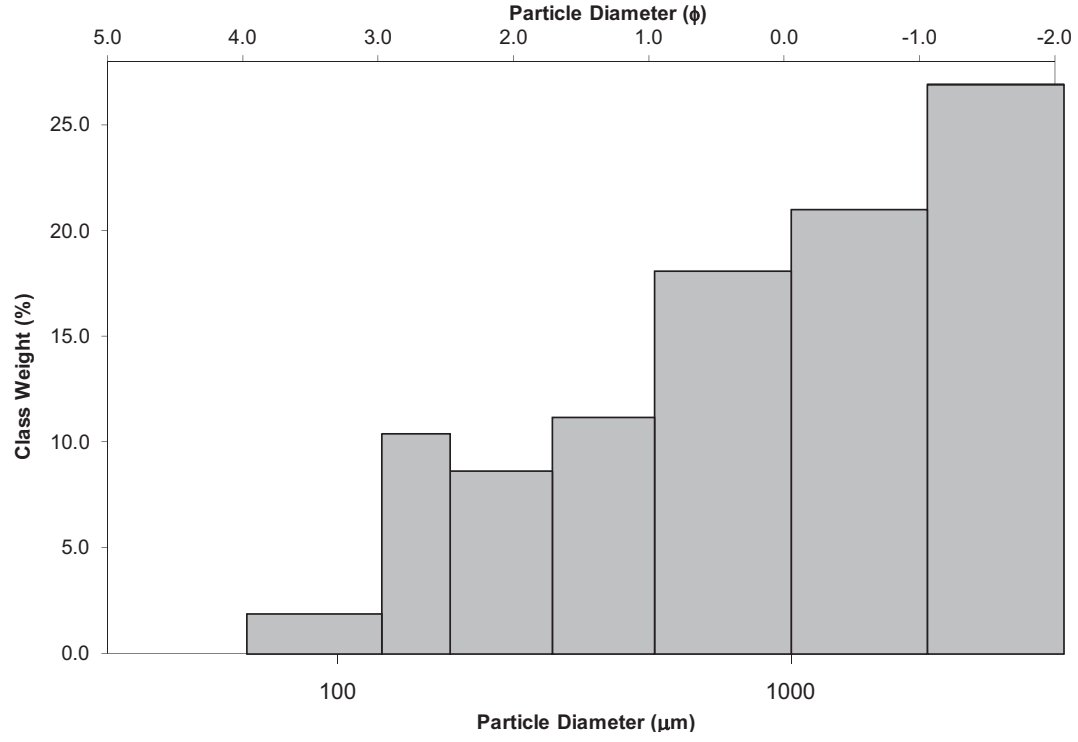

SAMPLE STATISTICS

SIEVING ERROR: 1.3%

SAMPLE IDENTITY: **PVP 4-5**

ANALYST & DATE: Pete, 9/30/2011

SAMPLE TYPE: Bimodal, Moderately Well Sorted

TEXTURAL GROUP: Sandy Gravel

SEDIMENT NAME: Sandy Very Fine Gravel

	μm	ϕ
MODE 1:	3000.0	-1.500
MODE 2:	151.0	2.749
MODE 3:		
D_{10}:	384.1	-8.297
MEDIAN or D_{50}:	3245.8	-1.699
D_{90}:	314436.5	1.381
(D_{90} / D_{10}):	818.7	-0.166
(D_{90} - D_{10}):	314052.4	9.677
(D_{75} / D_{25}):	1.189	0.706
(D_{75} - D_{25}):	286.7	0.250

GRAIN SIZE DISTRIBUTION

GRAVEL:	70.7%	COARSE SAND:	6.9%
SAND:	27.9%	MEDIUM SAND:	4.0%
MUD:	1.4%	FINE SAND:	4.2%
		V FINE SAND:	2.1%
V COARSE GRAVEL:	0.0%	V COARSE SILT:	0.2%
COARSE GRAVEL:	0.0%	COARSE SILT:	0.2%
MEDIUM GRAVEL:	0.0%	MEDIUM SILT:	0.2%
FINE GRAVEL:	0.0%	FINE SILT:	0.2%
V FINE GRAVEL:	70.7%	V FINE SILT:	0.2%
V COARSE SAND:	10.8%	CLAY:	0.2%

	METHOD OF MOMENTS			FOLK & WARD METHOD		
	Arithmetic	Geometric	Logarithmic	Geometric	Logarithmic	Description
	μm	μm	ϕ	μm	ϕ	
MEAN ($\bar{x}$):	592.2	15.54	0.141	1542.2	-0.625	Very Coarse Sand
SORTING (σ):	1000.0	29.83	1.265	1.587	0.666	Moderately Well Sorted
SKEWNESS (Sk):	1.597	0.514	2.714	-2.797	2.797	Very Fine Skewed
KURTOSIS (K):	4.115	1.390	14.18	4.741	4.741	Extremely Leptokurtic

GRAIN SIZE DISTRIBUTION

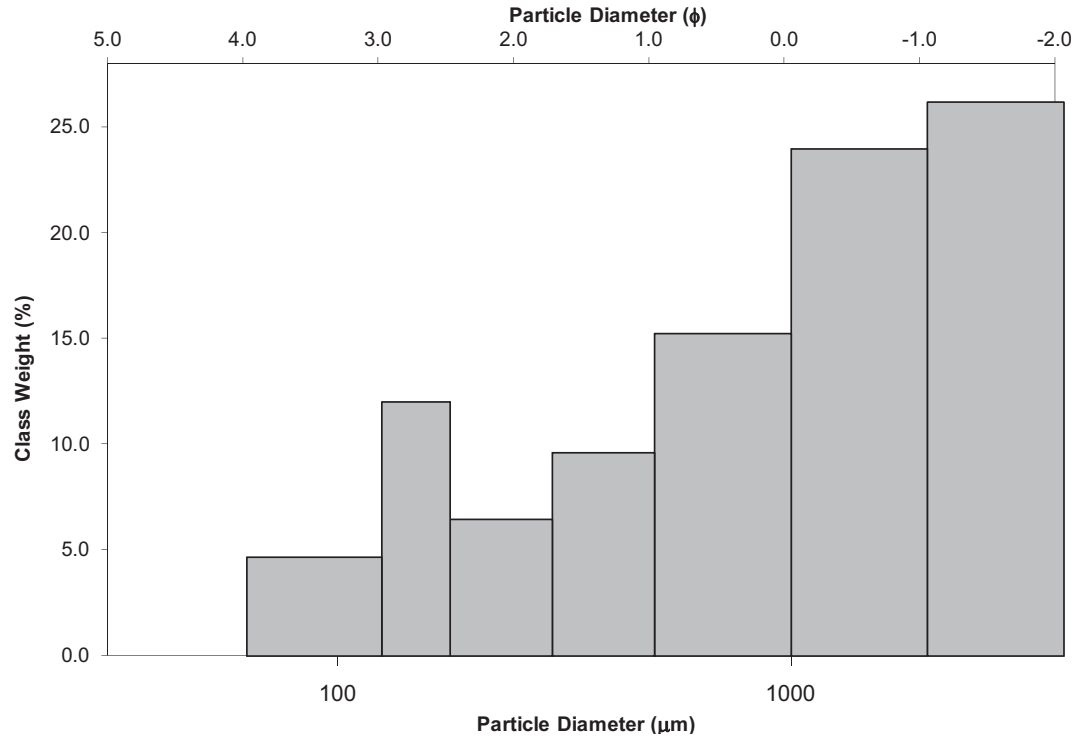

SAMPLE STATISTICS

SIEVING ERROR: 0.1%

SAMPLE IDENTITY: **PVP 4-6**

ANALYST & DATE: Pete, 9/30/2011

SAMPLE TYPE: Unimodal, Poorly Sorted

TEXTURAL GROUP: Slightly Gravelly Sand

SEDIMENT NAME: Slightly Very Fine Gravelly Coarse Sand

	μm	ϕ
MODE 1:	750.0	0.500
MODE 2:		
MODE 3:		
D_{10}:	178.6	-0.783
MEDIAN or D_{50}:	692.9	0.529
D_{90}:	1720.8	2.485
(D_{90} / D_{10}):	9.637	-3.174
(D_{90} - D_{10}):	1542.3	3.269
(D_{75} / D_{25}):	3.303	-6.406
(D_{75} - D_{25}):	819.4	1.724

GRAIN SIZE DISTRIBUTION

GRAVEL:	4.1%	COARSE SAND:	35.2%
SAND:	94.2%	MEDIUM SAND:	16.4%
MUD:	1.8%	FINE SAND:	11.8%
		V FINE SAND:	3.5%
V COARSE GRAVEL:	0.0%	V COARSE SILT:	0.3%
COARSE GRAVEL:	0.0%	COARSE SILT:	0.3%
MEDIUM GRAVEL:	0.0%	MEDIUM SILT:	0.3%
FINE GRAVEL:	0.0%	FINE SILT:	0.3%
V FINE GRAVEL:	4.1%	V FINE SILT:	0.3%
V COARSE SAND:	27.3%	CLAY:	0.3%

	METHOD OF MOMENTS			FOLK & WARD METHOD		
	Arithmetic	Geometric	Logarithmic	Geometric	Logarithmic	Description
	μm	μm	ϕ	μm	ϕ	
MEAN ($\bar{x}$):	872.8	576.8	0.759	625.0	0.678	Coarse Sand
SORTING (σ):	643.4	2.871	1.422	2.409	1.268	Poorly Sorted
SKEWNESS (Sk):	1.271	-2.028	1.617	-0.214	0.214	Fine Skewed
KURTOSIS (K):	5.062	10.34	7.648	0.958	0.958	Mesokurtic

GRAIN SIZE DISTRIBUTION

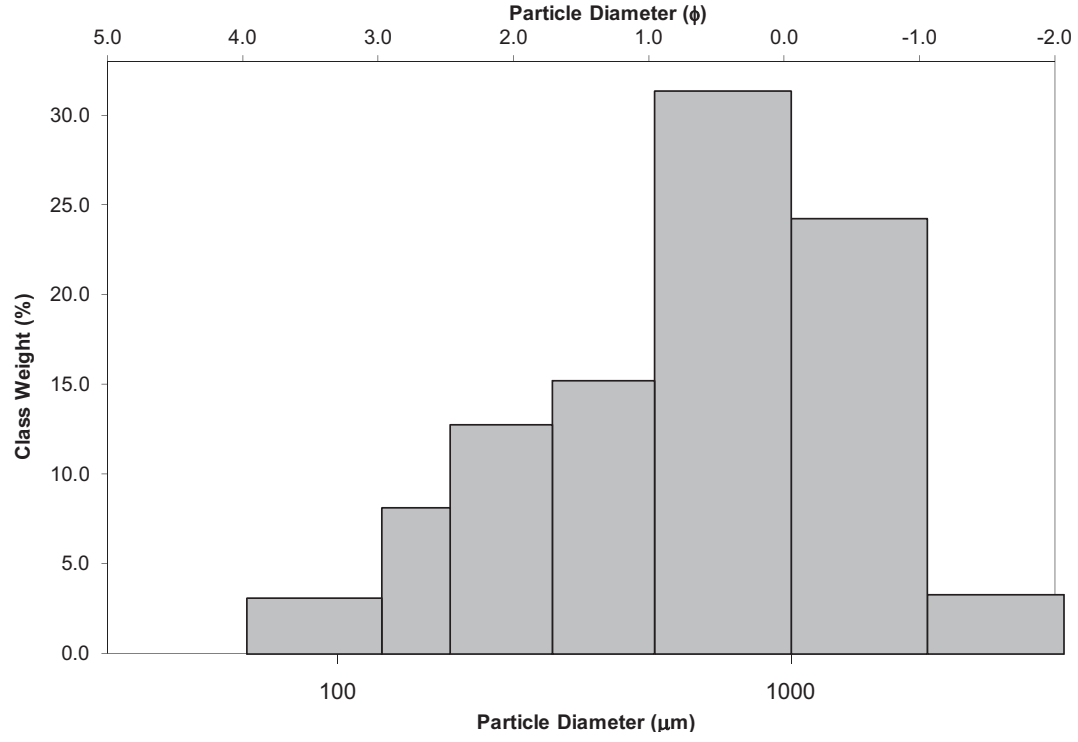

SAMPLE STATISTICS

SIEVING ERROR: 0.7%

SAMPLE IDENTITY: **PVP 4-7**

ANALYST & DATE: Pete, 9/30/2011

SAMPLE TYPE: Unimodal, Very Well Sorted

TEXTURAL GROUP: Gravel

SEDIMENT NAME: Very Fine Gravel

	μm	ϕ
MODE 1:	3000.0	-1.500
MODE 2:		
MODE 3:		
D_{10}:	1484.2	-8.809
MEDIAN or D_{50}:	2527.8	-1.338
D_{90}:	448640.9	-0.570
(D_{90} / D_{10}):	302.3	0.065
(D_{90} - D_{10}):	447156.8	8.240
(D_{75} / D_{25}):	0.403	2.959
(D_{75} - D_{25}):	-2353.286	-1.310

GRAIN SIZE DISTRIBUTION

GRAVEL:	87.2%	COARSE SAND:	3.0%
SAND:	12.6%	MEDIUM SAND:	1.6%
MUD:	0.3%	FINE SAND:	0.9%
		V FINE SAND:	0.4%
V COARSE GRAVEL:	0.0%	V COARSE SILT:	0.0%
COARSE GRAVEL:	0.0%	COARSE SILT:	0.0%
MEDIUM GRAVEL:	0.0%	MEDIUM SILT:	0.0%
FINE GRAVEL:	0.0%	FINE SILT:	0.0%
V FINE GRAVEL:	87.2%	V FINE SILT:	0.0%
V COARSE SAND:	6.6%	CLAY:	0.0%

	METHOD OF MOMENTS			FOLK & WARD METHOD		
	Arithmetic	Geometric	Logarithmic	Geometric	Logarithmic	Description
	μm	μm	ϕ	μm	ϕ	
MEAN ($\bar{x}$):	502.6	6.245	-0.126	2009.5	-1.007	Very Fine Gravel
SORTING (σ):	1016.4	24.28	0.745	0.917	-0.124	Very Well Sorted
SKEWNESS (Sk):	1.813	1.204	2.516	-2.120	2.120	Very Fine Skewed
KURTOSIS (K):	4.631	2.514	27.12	-0.170	-0.170	Very Platykurtic

GRAIN SIZE DISTRIBUTION

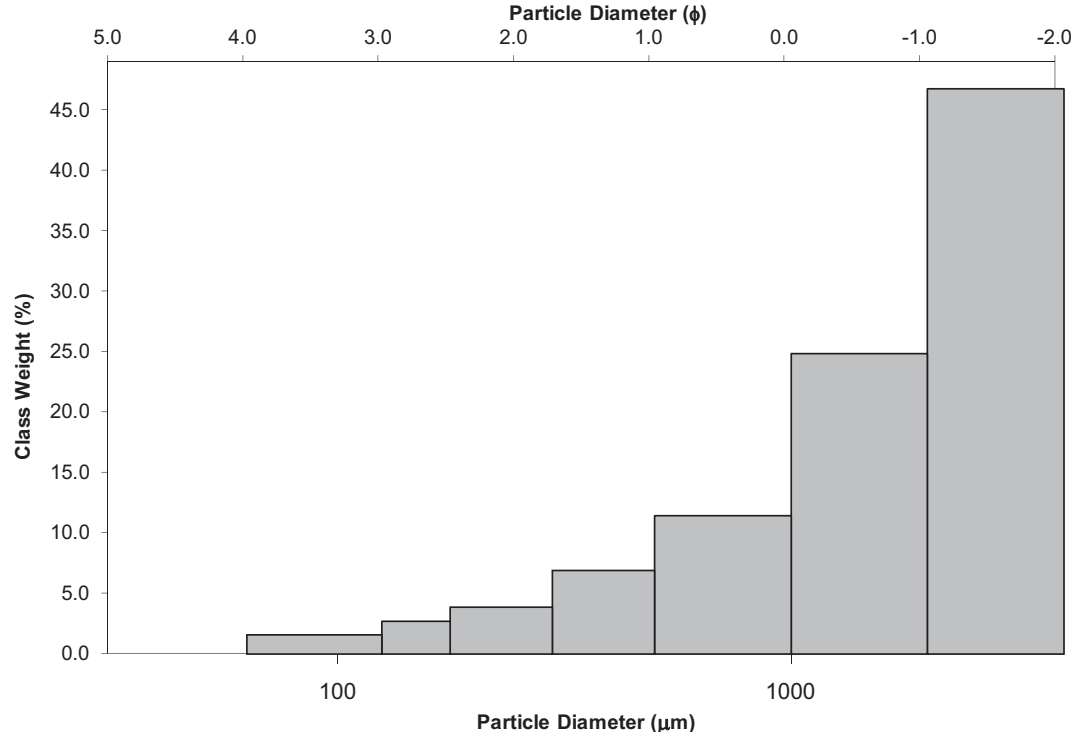

SAMPLE STATISTICS

SIEVING ERROR: 0.4%

SAMPLE IDENTITY: **PVP 5-1**

ANALYST & DATE: Pete, 9/30/2011

SAMPLE TYPE: Unimodal, Well Sorted

TEXTURAL GROUP: Sandy Gravel

SEDIMENT NAME: Sandy Very Fine Gravel

	μm	ϕ
MODE 1:	1500.0	-0.500
MODE 2:		
MODE 3:		
D_{10}:	682.9	-3.681
MEDIAN or D_{50}:	2947.9	-1.560
D_{90}:	12829.2	0.550
(D_{90} / D_{10}):	18.79	-0.149
(D_{90} - D_{10}):	12146.3	4.232
(D_{75} / D_{25}):	1.743	0.355
(D_{75} - D_{25}):	1009.3	0.802

GRAIN SIZE DISTRIBUTION

GRAVEL:	62.4%	COARSE SAND:	9.2%
SAND:	37.0%	MEDIUM SAND:	3.2%
MUD:	0.6%	FINE SAND:	1.3%
		V FINE SAND:	0.8%
V COARSE GRAVEL:	0.0%	V COARSE SILT:	0.1%
COARSE GRAVEL:	0.0%	COARSE SILT:	0.1%
MEDIUM GRAVEL:	0.0%	MEDIUM SILT:	0.1%
FINE GRAVEL:	0.0%	FINE SILT:	0.1%
V FINE GRAVEL:	62.4%	V FINE SILT:	0.1%
V COARSE SAND:	22.5%	CLAY:	0.1%

	METHOD OF MOMENTS			FOLK & WARD METHOD		
	Arithmetic	Geometric	Logarithmic	Geometric	Logarithmic	Description
	μm	μm	ϕ	μm	ϕ	
MEAN ($\bar{x}$):	1088.6	74.13	-0.255	1739.7	-0.799	Very Coarse Sand
SORTING (σ):	1173.5	36.55	1.016	1.331	0.412	Well Sorted
SKEWNESS (Sk):	0.624	-0.311	2.483	-2.901	2.901	Very Fine Skewed
KURTOSIS (K):	1.881	1.175	17.57	0.754	0.754	Platykurtic

GRAIN SIZE DISTRIBUTION

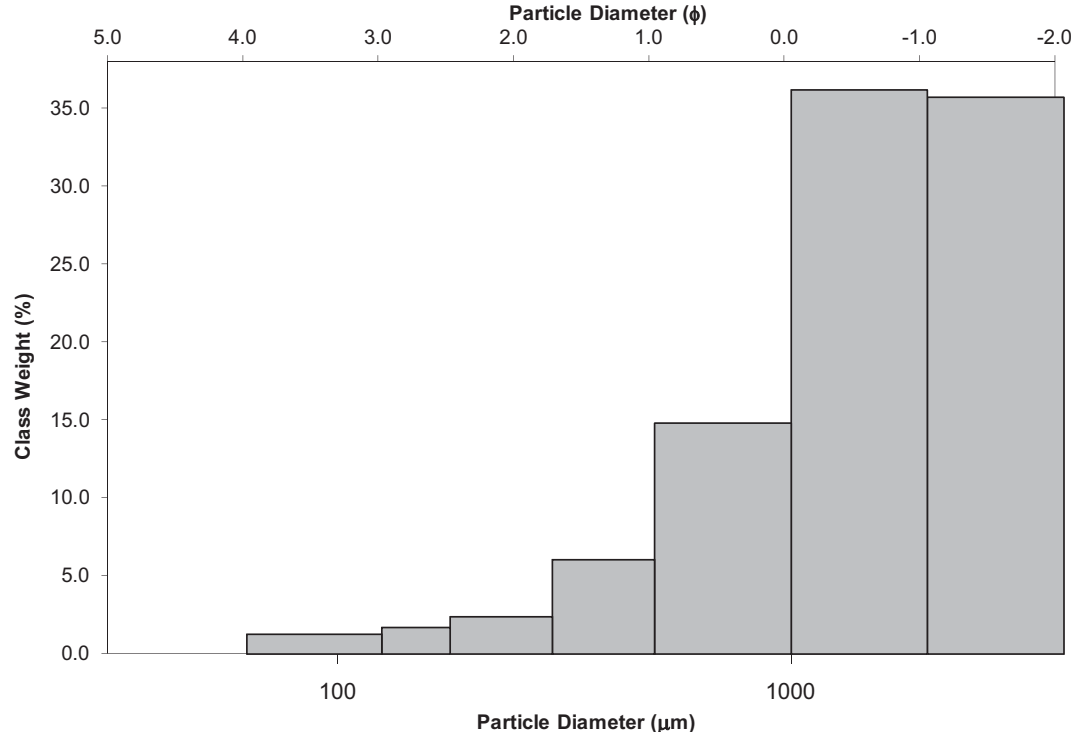

SAMPLE STATISTICS

SIEVING ERROR: 1.0%

SAMPLE IDENTITY: **PVP 5-2**

ANALYST & DATE: Pete, 9/30/2011

SAMPLE TYPE: Unimodal, Very Well Sorted

TEXTURAL GROUP: Gravel

SEDIMENT NAME: Very Fine Gravel

	μm	ϕ
MODE 1:	3000.0	-1.500
MODE 2:		
MODE 3:		
D_{10}:	1989.4	-13.579
MEDIAN or D_{50}:	2291.4	-1.196
D_{90}:	########	-0.992
(D_{90} / D_{10}):	6151.6	0.073
(D_{90} - D_{10}):	########	12.59
(D_{75} / D_{25}):	0.436	3.000
(D_{75} - D_{25}):	-1954.822	-1.196

GRAIN SIZE DISTRIBUTION

GRAVEL:	90.0%	COARSE SAND:	2.3%
SAND:	9.9%	MEDIUM SAND:	0.7%
MUD:	0.2%	FINE SAND:	0.4%
		V FINE SAND:	0.2%
V COARSE GRAVEL:	0.0%	V COARSE SILT:	0.0%
COARSE GRAVEL:	0.0%	COARSE SILT:	0.0%
MEDIUM GRAVEL:	0.0%	MEDIUM SILT:	0.0%
FINE GRAVEL:	0.0%	FINE SILT:	0.0%
V FINE GRAVEL:	90.0%	V FINE SILT:	0.0%
V COARSE SAND:	6.2%	CLAY:	0.0%

	METHOD OF MOMENTS			FOLK & WARD METHOD		
	Arithmetic	Geometric	Logarithmic	Geometric	Logarithmic	Description
	μm	μm	ϕ	μm	ϕ	
MEAN ($\bar{x}$):	305.1	3.270	-0.075	2253.0	-1.172	Very Fine Gravel
SORTING (σ):	795.8	14.88	0.557	0.758	-0.399	Very Well Sorted
SKEWNESS (Sk):	2.636	1.873	3.526	14.85	-14.847	Very Coarse Skewed
KURTOSIS (K):	8.697	4.576	52.47	0.024	0.024	Very Platykurtic

GRAIN SIZE DISTRIBUTION

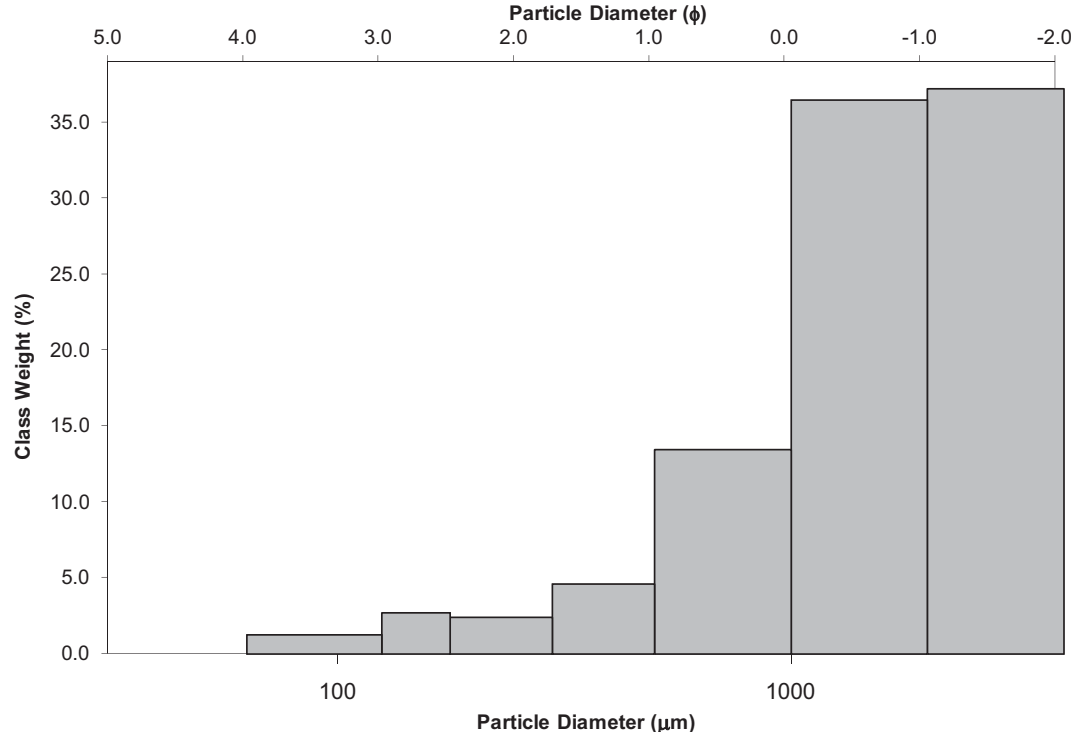

SAMPLE STATISTICS

SIEVING ERROR: 0.1%

SAMPLE IDENTITY: **PVP 5-3**

ANALYST & DATE: Pete, 9/30/2011

SAMPLE TYPE: Unimodal, Poorly Sorted

TEXTURAL GROUP: Gravelly Sand

SEDIMENT NAME: Very Fine Gravelly Very Coarse Sand

	μm	ϕ
MODE 1:	1500.0	-0.500
MODE 2:		
MODE 3:		
D_{10}:	431.9	-1.463
MEDIAN or D_{50}:	1161.4	-0.216
D_{90}:	2757.2	1.211
(D_{90} / D_{10}):	6.384	-0.828
(D_{90} - D_{10}):	2325.3	2.675
(D_{75} / D_{25}):	2.522	-0.671
(D_{75} - D_{25}):	1049.8	1.334

GRAIN SIZE DISTRIBUTION

GRAVEL:	16.4%	COARSE SAND:	29.4%
SAND:	81.1%	MEDIUM SAND:	5.4%
MUD:	2.5%	FINE SAND:	2.1%
		V FINE SAND:	1.3%
V COARSE GRAVEL:	0.0%	V COARSE SILT:	0.4%
COARSE GRAVEL:	0.0%	COARSE SILT:	0.4%
MEDIUM GRAVEL:	0.0%	MEDIUM SILT:	0.4%
FINE GRAVEL:	0.0%	FINE SILT:	0.4%
V FINE GRAVEL:	16.4%	V FINE SILT:	0.4%
V COARSE SAND:	42.9%	CLAY:	0.4%

	METHOD OF MOMENTS			FOLK & WARD METHOD		
	Arithmetic	Geometric	Logarithmic	Geometric	Logarithmic	Description
	μm	μm	ϕ	μm	ϕ	
MEAN ($\bar{x}$):	1303.3	791.6	0.076	1097.1	-0.134	Very Coarse Sand
SORTING (σ):	823.8	4.420	1.451	2.149	1.104	Poorly Sorted
SKEWNESS (Sk):	0.754	-3.075	2.817	-0.183	0.183	Fine Skewed
KURTOSIS (K):	3.058	13.13	13.68	1.290	1.290	Leptokurtic

GRAIN SIZE DISTRIBUTION

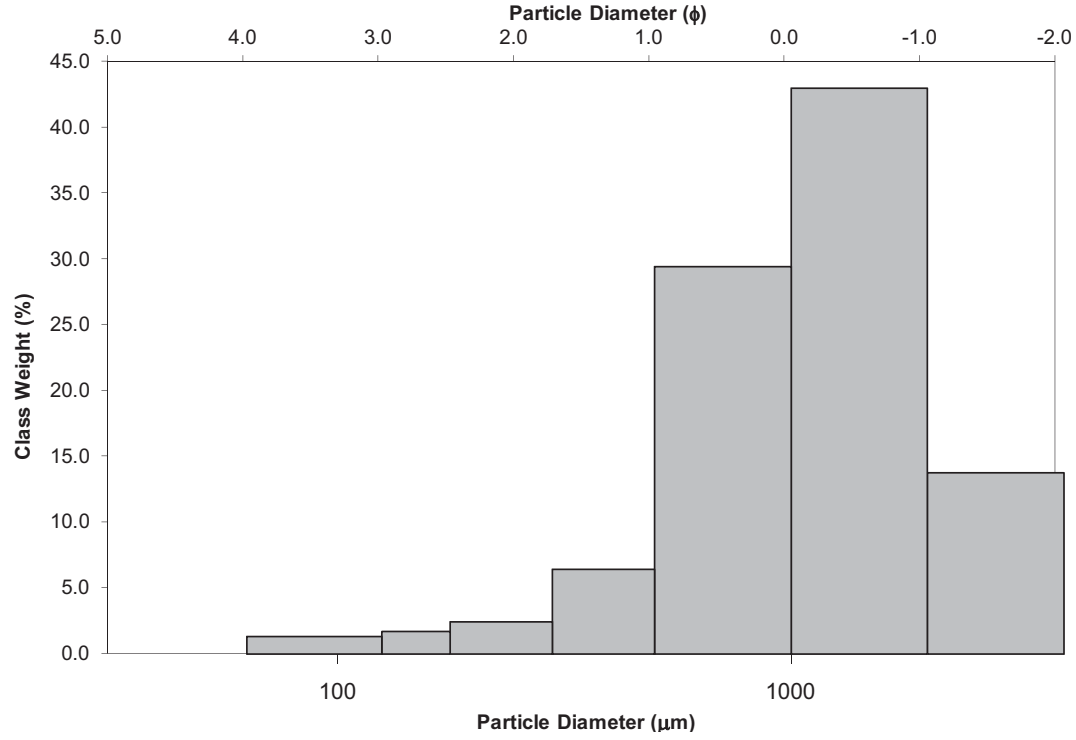

SAMPLE STATISTICS

SIEVING ERROR: 0.6%

SAMPLE IDENTITY: **PVP 5-4**

ANALYST & DATE: Pete, 9/30/2011

SAMPLE TYPE: Bimodal, Very Well Sorted

TEXTURAL GROUP: Gravel

SEDIMENT NAME: Very Fine Gravel

	μm	ϕ
MODE 1:	3000.0	-1.500
MODE 2:	94.00	3.494
MODE 3:		
D_{10}:	741.7	-13.153
MEDIAN or D_{50}:	2578.4	-1.366
D_{90}:	9106423.5	0.431
(D_{90} / D_{10}):	12277.4	-0.033
(D_{90} - D_{10}):	9105681.8	13.58
(D_{75} / D_{25}):	0.470	2.593
(D_{75} - D_{25}):	-1808.422	-1.088

GRAIN SIZE DISTRIBUTION

GRAVEL:	81.1%	COARSE SAND:	4.7%
SAND:	17.9%	MEDIUM SAND:	2.2%
MUD:	1.0%	FINE SAND:	1.8%
		V FINE SAND:	2.3%
V COARSE GRAVEL:	0.0%	V COARSE SILT:	0.2%
COARSE GRAVEL:	0.0%	COARSE SILT:	0.2%
MEDIUM GRAVEL:	0.0%	MEDIUM SILT:	0.2%
FINE GRAVEL:	0.0%	FINE SILT:	0.2%
V FINE GRAVEL:	81.1%	V FINE SILT:	0.2%
V COARSE SAND:	6.8%	CLAY:	0.2%

	METHOD OF MOMENTS			FOLK & WARD METHOD		
	Arithmetic	Geometric	Logarithmic	Geometric	Logarithmic	Description
	μm	μm	ϕ	μm	ϕ	
MEAN ($\bar{x}$):	390.6	5.952	0.099	1735.6	-0.795	Very Coarse Sand
SORTING (σ):	865.0	20.81	1.066	1.233	0.303	Very Well Sorted
SKEWNESS (Sk):	2.264	1.196	3.443	4.851	-4.851	Very Coarse Skewed
KURTOSIS (K):	6.811	2.565	20.83	-0.843	-0.843	Very Platykurtic

GRAIN SIZE DISTRIBUTION

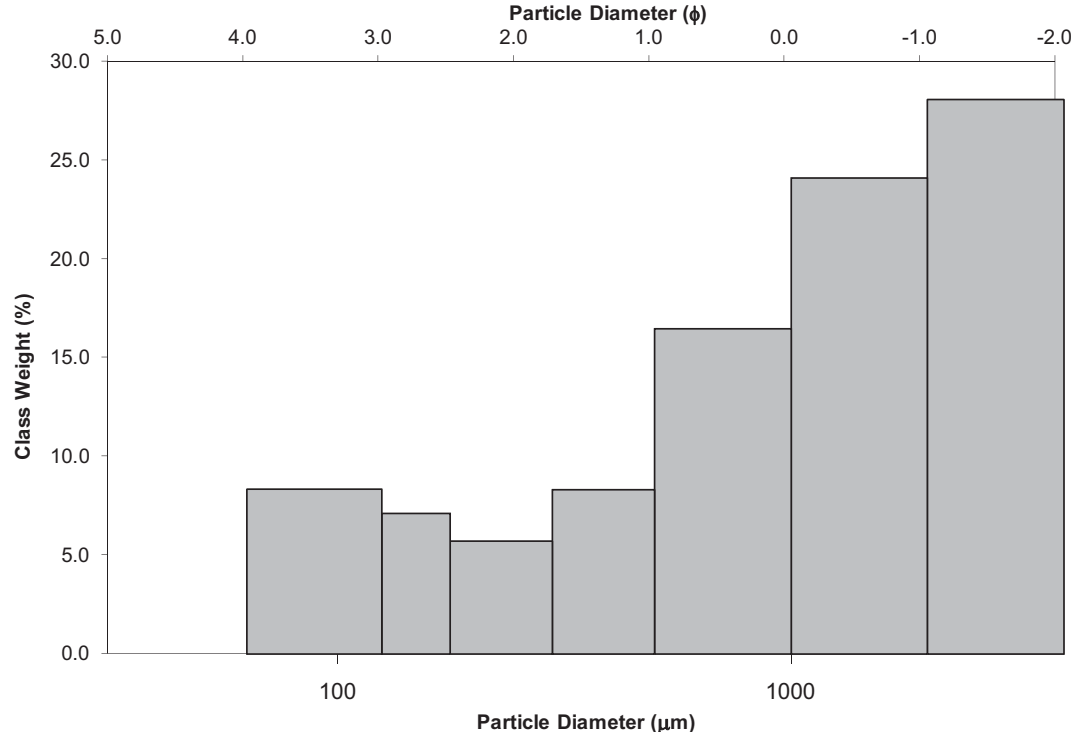

SAMPLE STATISTICS

SIEVING ERROR: 0.2%

SAMPLE IDENTITY: **PVP 5-5**

ANALYST & DATE: Pete, 9/30/2011

SAMPLE TYPE: Unimodal, Well Sorted

TEXTURAL GROUP: Muddy Sandy Gravel

SEDIMENT NAME: Very Coarse Silty Sandy Very Fine Gravel

	μm	ϕ
MODE 1:	3000.0	-1.500
MODE 2:		
MODE 3:		
D_{10}:	590.3	-8.538
MEDIAN or D_{50}:	2989.9	-1.580
D_{90}:	371703.0	0.760
(D_{90} / D_{10}):	629.6	-0.089
(D_{90} - D_{10}):	371112.6	9.298
(D_{75} / D_{25}):	0.752	1.520
(D_{75} - D_{25}):	-569.086	-0.410

GRAIN SIZE DISTRIBUTION

GRAVEL:	77.9%	COARSE SAND:	4.1%
SAND:	19.6%	MEDIUM SAND:	3.3%
MUD:	2.5%	FINE SAND:	1.8%
		V FINE SAND:	1.4%
V COARSE GRAVEL:	0.0%	V COARSE SILT:	0.4%
COARSE GRAVEL:	0.0%	COARSE SILT:	0.4%
MEDIUM GRAVEL:	0.0%	MEDIUM SILT:	0.4%
FINE GRAVEL:	0.0%	FINE SILT:	0.4%
V FINE GRAVEL:	77.9%	V FINE SILT:	0.4%
V COARSE SAND:	8.9%	CLAY:	0.4%

	METHOD OF MOMENTS			FOLK & WARD METHOD		
	Arithmetic	Geometric	Logarithmic	Geometric	Logarithmic	Description
	μm	μm	ϕ	μm	ϕ	
MEAN ($\bar{x}$):	622.4	12.02	0.071	1743.4	-0.802	Very Coarse Sand
SORTING (σ):	1077.3	30.04	1.386	1.346	0.429	Well Sorted
SKEWNESS (Sk):	1.494	0.721	3.204	-7.349	7.349	Very Fine Skewed
KURTOSIS (K):	3.589	1.625	16.35	-2.520	-2.520	Very Platykurtic

GRAIN SIZE DISTRIBUTION

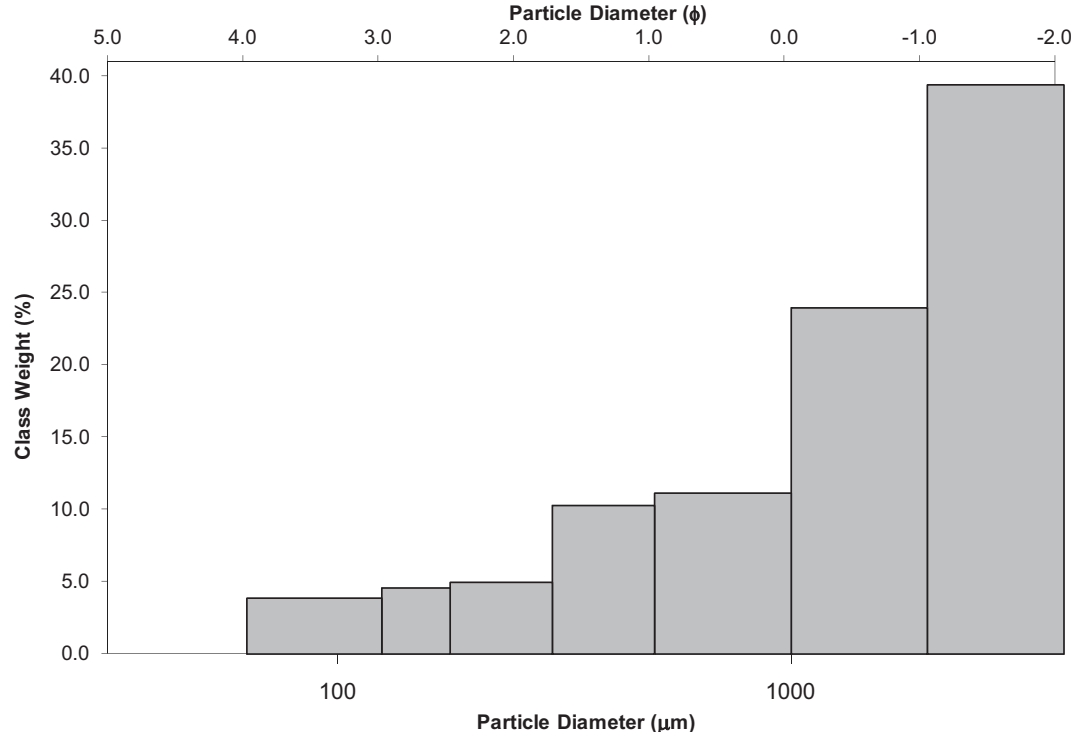

SAMPLE STATISTICS

SIEVING ERROR: 0.6%

SAMPLE IDENTITY: **PVP 5-6**

ANALYST & DATE: Pete, 9/30/2011

SAMPLE TYPE: Unimodal, Poorly Sorted

TEXTURAL GROUP: Gravelly Sand

SEDIMENT NAME: Very Fine Gravelly Very Coarse Sand

	μm	ϕ
MODE 1:	1500.0	-0.500
MODE 2:		
MODE 3:		
D_{10}:	326.0	-1.499
MEDIAN or D_{50}:	1030.9	-0.044
D_{90}:	2826.7	1.617
(D_{90} / D_{10}):	8.670	-1.079
(D_{90} - D_{10}):	2500.7	3.116
(D_{75} / D_{25}):	2.890	-1.020
(D_{75} - D_{25}):	1106.0	1.531

GRAIN SIZE DISTRIBUTION

GRAVEL:	16.5%	COARSE SAND:	30.4%
SAND:	82.8%	MEDIUM SAND:	11.4%
MUD:	0.7%	FINE SAND:	4.8%
		V FINE SAND:	1.2%
V COARSE GRAVEL:	0.0%	V COARSE SILT:	0.1%
COARSE GRAVEL:	0.0%	COARSE SILT:	0.1%
MEDIUM GRAVEL:	0.0%	MEDIUM SILT:	0.1%
FINE GRAVEL:	0.0%	FINE SILT:	0.1%
V FINE GRAVEL:	16.5%	V FINE SILT:	0.1%
V COARSE SAND:	35.0%	CLAY:	0.1%

	METHOD OF MOMENTS			FOLK & WARD METHOD		
	Arithmetic	Geometric	Logarithmic	Geometric	Logarithmic	Description
	μm	μm	ϕ	μm	ϕ	
MEAN ($\bar{x}$):	1199.6	709.9	0.151	982.7	0.025	Coarse Sand
SORTING (σ):	846.1	4.448	1.198	2.264	1.179	Poorly Sorted
SKEWNESS (Sk):	0.904	-3.058	1.603	-0.104	0.104	Fine Skewed
KURTOSIS (K):	3.109	13.65	9.166	1.111	1.111	Leptokurtic

GRAIN SIZE DISTRIBUTION

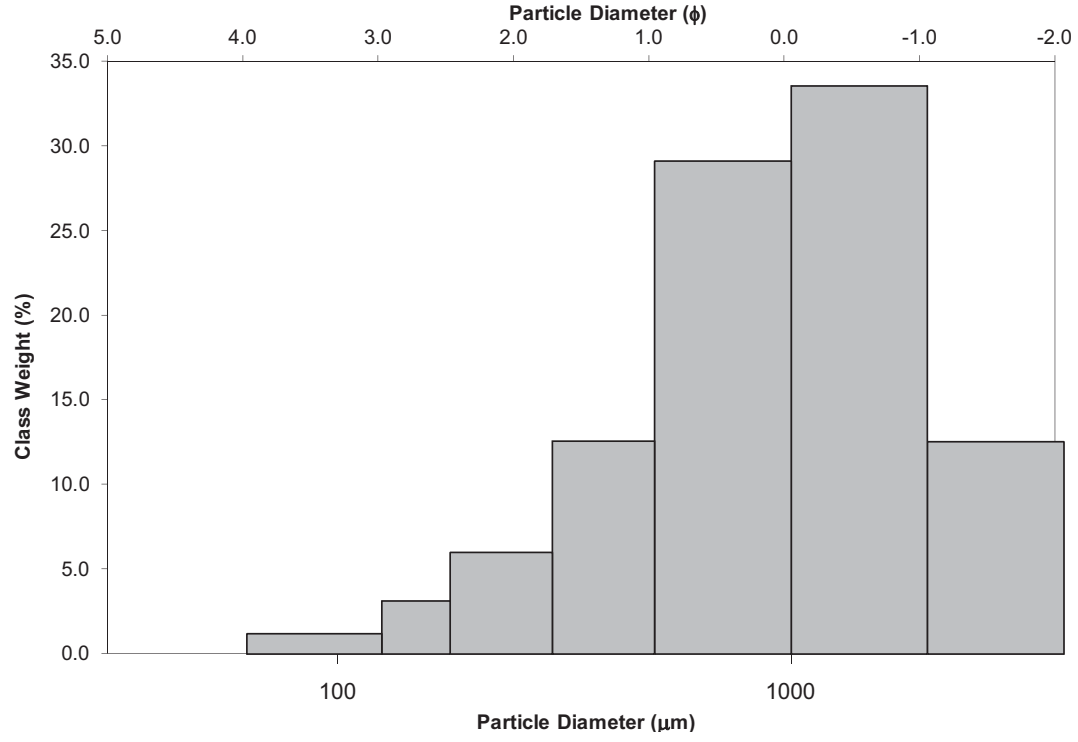

SAMPLE STATISTICS

SIEVING ERROR: 0.1%

SAMPLE IDENTITY: **PVP 5-7**

ANALYST & DATE: Pete, 9/30/2011

SAMPLE TYPE: Unimodal, Very Well Sorted

TEXTURAL GROUP: Sandy Gravel

SEDIMENT NAME: Sandy Very Fine Gravel

	μm	ϕ
MODE 1:	3000.0	-1.500
MODE 2:		
MODE 3:		
D_{10}:	757.4	-8.140
MEDIAN or D_{50}:	2825.3	-1.498
D_{90}:	282020.6	0.401
(D_{90} / D_{10}):	372.4	-0.049
(D_{90} - D_{10}):	281263.3	8.541
(D_{75} / D_{25}):	0.730	1.606
(D_{75} - D_{25}):	-621.375	-0.454

GRAIN SIZE DISTRIBUTION

GRAVEL:	77.1%	COARSE SAND:	7.4%
SAND:	22.8%	MEDIUM SAND:	3.4%
MUD:	0.1%	FINE SAND:	1.6%
		V FINE SAND:	0.5%
V COARSE GRAVEL:	0.0%	V COARSE SILT:	0.0%
COARSE GRAVEL:	0.0%	COARSE SILT:	0.0%
MEDIUM GRAVEL:	0.0%	MEDIUM SILT:	0.0%
FINE GRAVEL:	0.0%	FINE SILT:	0.0%
V FINE GRAVEL:	77.1%	V FINE SILT:	0.0%
V COARSE SAND:	9.9%	CLAY:	0.0%

	METHOD OF MOMENTS			FOLK & WARD METHOD		
	Arithmetic	Geometric	Logarithmic	Geometric	Logarithmic	Description
	μm	μm	ϕ	μm	ϕ	
MEAN ($\bar{x}$):	531.8	10.35	-0.057	1694.3	-0.761	Very Coarse Sand
SORTING (σ):	959.4	28.48	0.736	1.181	0.240	Very Well Sorted
SKEWNESS (Sk):	1.752	0.776	1.444	-7.853	7.853	Very Fine Skewed
KURTOSIS (K):	4.707	1.677	13.97	-1.167	-1.167	Very Platykurtic

GRAIN SIZE DISTRIBUTION

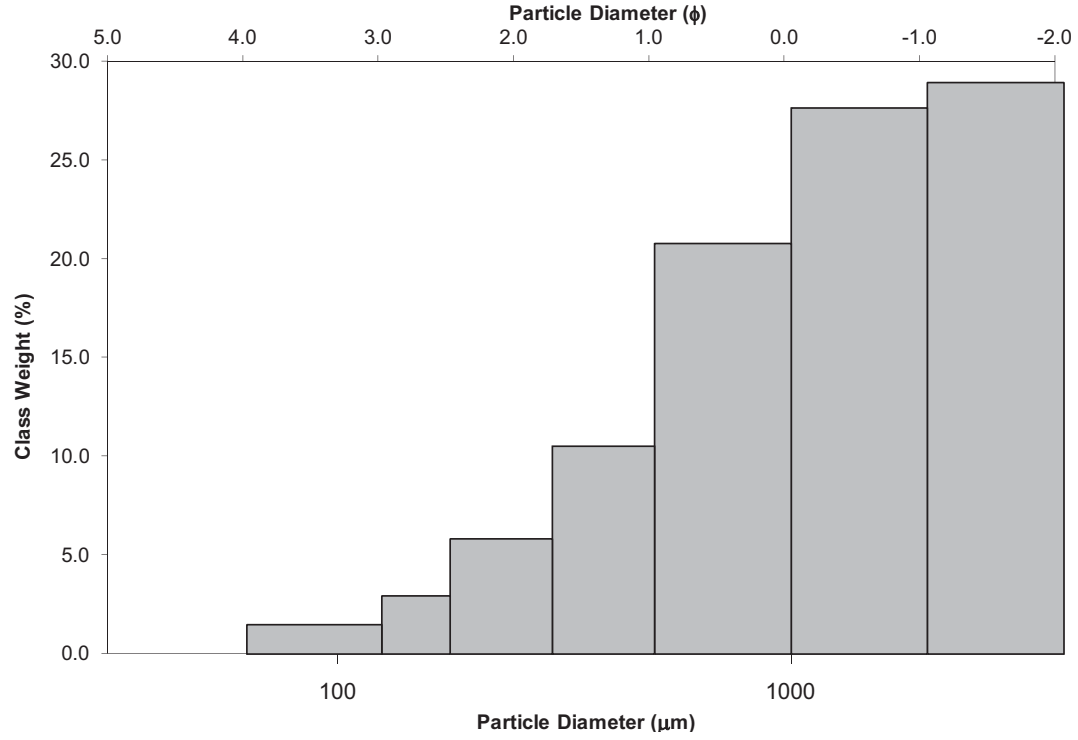

Triangular Diagram

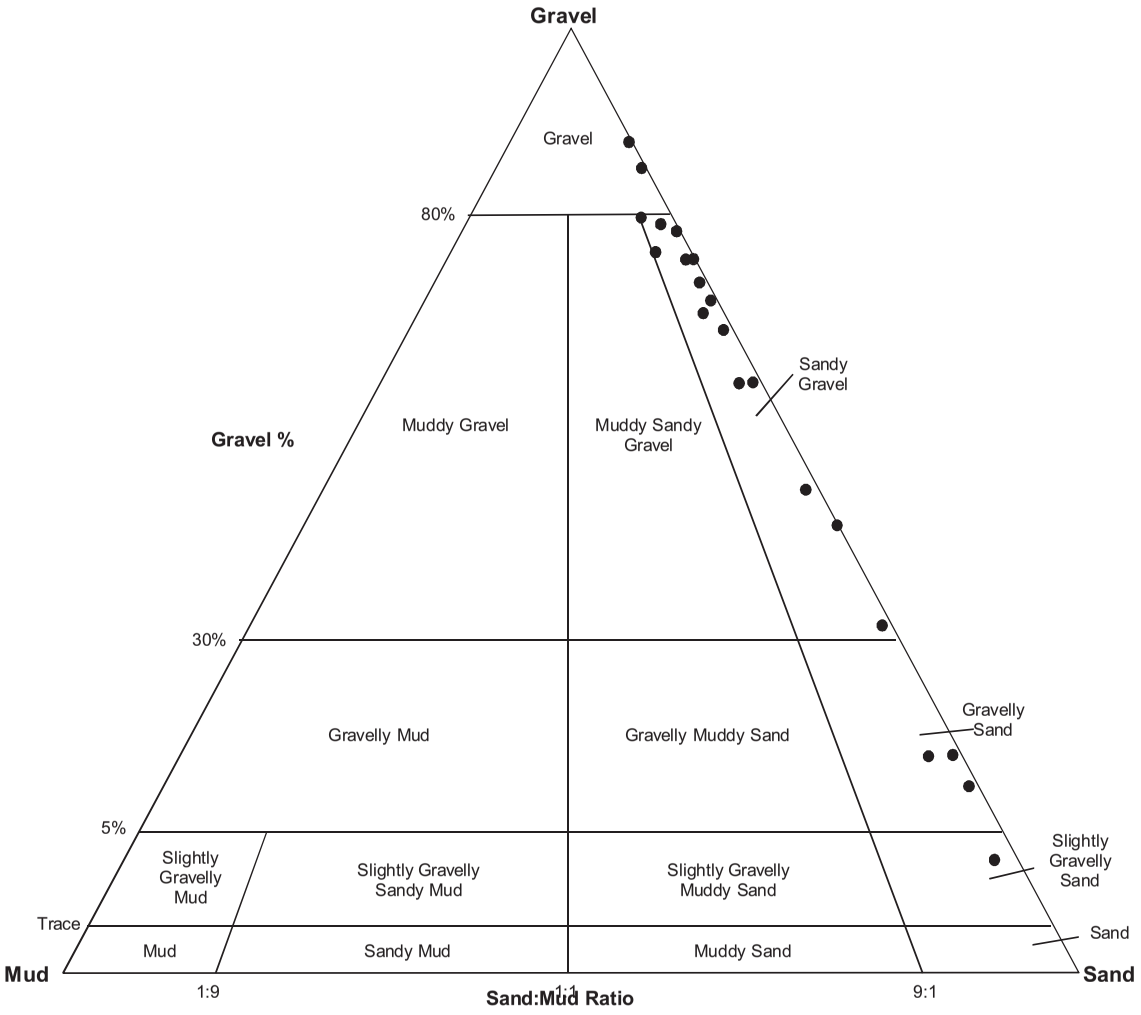

Appendix 22: Woodstock Biostimulation Aqueous Geochemistry

Sample	pH	Na^{+} (mg/L)	Na^{+} (mol/L)	Na^{+} (meq/L)	K^{+} (mg/L)	K^{+} (mol/L)	K^{+} (meq/L)	Ca^{+2} (mg/L)	Ca^{+2} (mol/L)	Ca^{+2} (meq/L)	Mg^{+2} (mg/L)
Day 0 Biostimulation											
ML5-1, t0	7.24	2.39	1.04E-04	0.10	0.74	1.89E-05	0.02	97.64	2.44E-03	4.87	18.63
ML5-2, t0	7.19	7.26	3.16E-04	0.32	2.02	5.17E-05	0.05	97.51	2.43E-03	4.87	26.57
ML5-3, t0	7.22	10.05	4.37E-04	0.44	1.72	4.40E-05	0.04	99.96	2.49E-03	4.99	28.23
ML5-4, t0	7.25	10.42	4.53E-04	0.45	1.56	3.99E-05	0.04	100.39	2.50E-03	5.01	27.21
ML5-5, t0	7.27	15.16	6.59E-04	0.66	1.38	3.52E-05	0.04	101.08	2.52E-03	5.04	27.99
ML5-6, t0	7.23	18.76	8.16E-04	0.82	1.36	3.48E-05	0.03	99.60	2.48E-03	4.97	27.23
ML5-7, t0	7.26	20.32	8.84E-04	0.88	1.33	3.41E-05	0.03	102.24	2.55E-03	5.10	28.21
ML7-1, t0	7.30	8.38	3.65E-04	0.36	2.11	5.40E-05	0.05	100.66	2.51E-03	5.02	27.77
ML7-2, t0	7.32	13.67	5.95E-04	0.59	1.45	3.70E-05	0.04	99.45	2.48E-03	4.96	27.67
ML7-3, t0	7.34	11.60	5.04E-04	0.50	1.58	4.04E-05	0.04	101.01	2.52E-03	5.04	28.62
ML7-4, t0	7.34	13.54	5.89E-04	0.59	1.56	4.00E-05	0.04	110.84	2.77E-03	5.53	32.05
ML7-5, t0	7.34	16.02	6.97E-04	0.70	1.50	3.83E-05	0.04	111.17	2.77E-03	5.55	30.95
ML7-6, t0	7.33	18.68	8.12E-04	0.81	1.51	3.86E-05	0.04	111.49	2.78E-03	5.56	30.58
ML7-7, t0	7.34	19.64	8.54E-04	0.85	1.47	3.77E-05	0.04	113.03	2.82E-03	5.64	31.60
ML5-1, t18	7.24	2.83	1.23E-04	0.12	0.87	2.23E-05	0.02	104.90	2.62E-03	5.23	21.26
ML5-2, t18	7.24	41.90	1.82E-03	1.82	2.82	7.21E-05	0.07	127.73	3.19E-03	6.37	33.93
ML5-3, t18	7.28	181.68	7.90E-03	7.90	3.24	8.30E-05	0.08	135.31	3.38E-03	6.75	36.89
ML5-4, t18	7.29	24.68	1.07E-03	1.07	1.78	4.55E-05	0.05	104.71	2.61E-03	5.23	29.73
ML5-5, t18	7.31	33.19	1.44E-03	1.44	1.68	4.29E-05	0.04	110.00	2.74E-03	5.49	30.87
ML5-6, t18	7.30	71.52	3.11E-03	3.11	2.13	5.45E-05	0.05	123.38	3.08E-03	6.16	34.65
ML5-7, t18	7.29	71.36	3.10E-03	3.10	2.00	5.12E-05	0.05	121.77	3.04E-03	6.08	33.54
ML7-1, t17	7.33	9.74	4.24E-04	0.42	2.30	5.88E-05	0.06	108.14	2.70E-03	5.40	30.43
ML7-2, t17	7.36	98.05	4.26E-03	4.26	2.49	6.37E-05	0.06	137.67	3.43E-03	6.87	38.77
ML7-3, t17	7.32	129.41	5.63E-03	5.63	2.54	6.51E-05	0.07	110.76	2.76E-03	5.53	31.30
ML7-4, t17	7.31	112.66	4.90E-03	4.90	2.30	5.89E-05	0.06	107.98	2.69E-03	5.39	30.62
ML7-5, t17	7.32	83.69	3.64E-03	3.64	2.10	5.38E-05	0.05	110.96	2.77E-03	5.54	31.10
ML7-6, t17	7.33	61.80	2.69E-03	2.69	1.92	4.90E-05	0.05	115.39	2.88E-03	5.76	32.18
ML7-7, t17	7.32	67.59	2.94E-03	2.94	1.90	4.85E-05	0.05	110.97	2.77E-03	5.54	30.87

Sample	Mg^{+2} (mol/L)	Mg^{+2} (meq/L)	Mn^{+2} (mg/L)	Mn^{+2} (mol/L)	Mn^{+2} (meq/L)	Fe^{+2} (mg/L)	Fe^{+2} (mol/L)	Fe^{+2} (meq/L)	Cl^{-} (mg/L)	Cl^{-} (mol/L)	Cl^{-} (meq/L)
Day 0 Biostimulation											
ML5-1, t0	7.66E-04	1.53	0.03	4.57E-07	0.00	0.69	1.24E-05	0.02	2.25	6.36E-05	0.06
ML5-2, t0	1.09E-03	2.19	0.00	1.08E-08	0.00	0.03	5.07E-07	0.00	30.34	8.56E-04	0.86
ML5-3, t0	1.16E-03	2.32	0.00	1.30E-08	0.00	0.03	4.55E-07	0.00	38.79	1.09E-03	1.09
ML5-4, t0	1.12E-03	2.24	0.00	1.54E-09	0.00	0.01	2.44E-07	0.00	38.80	1.09E-03	1.09
ML5-5, t0	1.15E-03	2.30	0.00	0.00E+00	0.00	0.01	2.40E-07	0.00	47.71	1.35E-03	1.35
ML5-6, t0	1.12E-03	2.24	0.00	1.57E-08	0.00	0.03	4.93E-07	0.00	62.43	1.76E-03	1.76
ML5-7, t0	1.16E-03	2.32	0.00	3.47E-08	0.00	0.07	1.20E-06	0.00	65.73	1.85E-03	1.85
ML7-1, t0	1.14E-03	2.29	0.01	2.57E-07	0.00	0.36	6.42E-06	0.01	31.60	8.91E-04	0.89
ML7-2, t0	1.14E-03	2.28	0.00	0.00E+00	0.00	0.01	1.01E-07	0.00	49.91	1.41E-03	1.41
ML7-3, t0	1.18E-03	2.35	0.00	0.00E+00	0.00	0.02	3.47E-07	0.00	41.61	1.17E-03	1.17
ML7-4, t0	1.32E-03	2.64	0.00	0.00E+00	0.00	0.01	1.12E-07	0.00	46.20	1.30E-03	1.30
ML7-5, t0	1.27E-03	2.55	0.00	7.07E-09	0.00	0.02	3.22E-07	0.00	54.32	1.53E-03	1.53
ML7-6, t0	1.26E-03	2.52	0.00	9.43E-10	0.00	0.03	5.39E-07	0.00	62.48	1.76E-03	1.76
ML7-7, t0	1.30E-03	2.60	0.00	0.00E+00	0.00	0.01	2.61E-07	0.00	59.45	1.68E-03	1.68
ML5-1, t18	8.75E-04	1.75	0.00	7.50E-09	0.00	0.01	1.62E-07	0.00	6.35	1.79E-04	0.18
ML5-2, t18	1.40E-03	2.79	0.00	9.43E-09	0.00	0.04	6.55E-07	0.00	35.82	1.01E-03	1.01
ML5-3, t18	1.52E-03	3.04	0.00	0.00E+00	0.00	0.01	1.70E-07	0.00	39.98	1.13E-03	1.13
ML5-4, t18	1.22E-03	2.45	0.00	1.10E-09	0.00	0.00	8.52E-08	0.00	38.06	1.07E-03	1.07
ML5-5, t18	1.27E-03	2.54	0.04	6.50E-07	0.00	0.00	0.00E+00	0.00	41.60	1.17E-03	1.17
ML5-6, t18	1.43E-03	2.85	0.03	6.18E-07	0.00	0.00	0.00E+00	0.00	50.77	1.43E-03	1.43
ML5-7, t18	1.38E-03	2.76	0.03	6.21E-07	0.00	0.00	0.00E+00	0.00	52.98	1.49E-03	1.49
ML7-1, t17	1.25E-03	2.50	0.03	6.27E-07	0.00	0.00	0.00E+00	0.00	36.63	1.03E-03	1.03
ML7-2, t17	1.60E-03	3.19	0.03	6.33E-07	0.00	0.00	0.00E+00	0.00	43.28	1.22E-03	1.22
ML7-3, t17	1.29E-03	2.58	0.03	6.29E-07	0.00	0.00	0.00E+00	0.00	39.43	1.11E-03	1.11
ML7-4, t17	1.26E-03	2.52	0.03	6.22E-07	0.00	0.00	0.00E+00	0.00	33.29	9.39E-04	0.94
ML7-5, t17	1.28E-03	2.56	0.03	6.18E-07	0.00	0.00	0.00E+00	0.00	49.33	1.39E-03	1.39
ML7-6, t17	1.32E-03	2.65	0.03	6.17E-07	0.00	0.00	0.00E+00	0.00	49.69	1.40E-03	1.40
ML7-7, t17	1.27E-03	2.54	0.03	6.27E-07	0.00	0.00	0.00E+00	0.00	45.92	1.30E-03	1.30

Sample	NO_2^- (mg/L)	NO_2^- (mol/L)	NO_2^- (meq/L)	Br^- (mg/L)	Br^- (mol/L)	Br^- (meq/L)	NO_3^- (mg/L)	NO_3^- (mol/L)	NO_3^- (meq/L)	SO_4^{-2} (mg/L)	SO_4^{-2} (mol/L)
Day 0 Biostimulation											
ML5-1, t0	0.03	5.43E-07	0.00	20.57	2.57E-04	0.26	6.22	1.00E-04	0.10	5.91	6.15E-05
ML5-2, t0	0.03	5.43E-07	0.00	18.49	2.31E-04	0.23	58.68	9.46E-04	0.95	27.80	2.89E-04
ML5-3, t0	0.03	5.43E-07	0.00	20.24	2.53E-04	0.25	66.57	1.07E-03	1.07	32.31	3.36E-04
ML5-4, t0	0.03	5.43E-07	0.00	19.61	2.45E-04	0.25	67.76	1.09E-03	1.09	33.59	3.50E-04
ML5-5, t0	0.21	4.64E-06	0.00	19.84	2.48E-04	0.25	66.71	1.08E-03	1.08	34.07	3.55E-04
ML5-6, t0	0.03	5.43E-07	0.00	18.41	2.30E-04	0.23	59.57	9.61E-04	0.96	34.15	3.56E-04
ML5-7, t0	0.03	5.43E-07	0.00	14.56	1.82E-04	0.18	55.01	8.87E-04	0.89	33.44	3.48E-04
ML7-1, t0	0.03	5.43E-07	0.00	16.22	2.03E-04	0.20	57.30	9.24E-04	0.92	27.57	2.87E-04
ML7-2, t0	0.03	5.43E-07	0.00	20.17	2.52E-04	0.25	63.81	1.03E-03	1.03	33.85	3.52E-04
ML7-3, t0	0.03	5.43E-07	0.00	17.40	2.18E-04	0.22	66.59	1.07E-03	1.07	32.39	3.37E-04
ML7-4, t0	0.03	5.43E-07	0.00	21.71	2.72E-04	0.27	63.39	1.02E-03	1.02	33.32	3.47E-04
ML7-5, t0	7.27	1.58E-04	0.16	21.35	2.67E-04	0.27	61.73	9.95E-04	1.00	34.11	3.55E-04
ML7-6, t0	0.03	5.43E-07	0.00	11.47	1.44E-04	0.14	57.33	9.24E-04	0.92	33.63	3.50E-04
ML7-7, t0	0.03	5.43E-07	0.00	11.38	1.42E-04	0.14	58.54	9.44E-04	0.94	33.41	3.48E-04
ML5-1, t18	0.00	0.00E+00	0.00	0.00	0.00E+00	0.00	15.69	2.53E-04	0.25	9.03	9.40E-05
ML5-2, t18	0.00	0.00E+00	0.00	89.15	1.12E-03	1.12	56.78	9.16E-04	0.92	32.11	3.34E-04
ML5-3, t18	0.00	0.00E+00	0.00	267.40	3.35E-03	3.35	58.88	9.50E-04	0.95	33.30	3.47E-04
ML5-4, t18	0.00	0.00E+00	0.00	26.61	3.33E-04	0.33	58.55	9.44E-04	0.94	34.17	3.56E-04
ML5-5, t18	0.00	0.00E+00	0.00	29.95	3.75E-04	0.37	55.84	9.01E-04	0.90	32.77	3.41E-04
ML5-6, t18	0.00	0.00E+00	0.00	102.58	1.28E-03	1.28	55.93	9.02E-04	0.90	34.46	3.59E-04
ML5-7, t18	0.00	0.00E+00	0.00	109.23	1.37E-03	1.37	55.47	8.95E-04	0.89	36.12	3.76E-04
ML7-1, t17	0.12	2.51E-06	0.00	10.17	1.27E-04	0.13	57.21	9.23E-04	0.92	33.81	3.52E-04
ML7-2, t17	0.58	1.27E-05	0.01	172.60	2.16E-03	2.16	59.77	9.64E-04	0.96	37.36	3.89E-04
ML7-3, t17	0.00	0.00E+00	0.00	193.37	2.42E-03	2.42	55.20	8.90E-04	0.89	34.24	3.56E-04
ML7-4, t17	0.13	2.77E-06	0.00	136.75	1.71E-03	1.71	46.79	7.55E-04	0.75	31.97	3.33E-04
ML7-5, t17	1.00	2.17E-05	0.02	142.32	1.78E-03	1.78	59.49	9.59E-04	0.96	35.58	3.70E-04
ML7-6, t17	0.00	0.00E+00	0.00	89.36	1.12E-03	1.12	52.85	8.52E-04	0.85	30.50	3.17E-04
ML7-7, t17	0.00	0.00E+00	0.00	84.42	1.06E-03	1.06	49.15	7.93E-04	0.79	32.37	3.37E-04

Sample	SO_4^{-2} (meq/L)	CH_3COO^- (mg/L)	CH_3COO^- (mol/L)	CH_3COO^- (meq/L)	HCO_3^- (mg/L)	HCO_3^- (meq/L)	HCO_3^- (mol/L)	CO_3^{-2} (mol/L)	Ionic Strength	Sum Cations
Day 0 Biostimulation										
ML5-1, t0	0.12	0.81	1.36E-05	0.01	448.96	7.36	7.36E-03	4.14E-06	5.28E-05	6.55
ML5-2, t0	0.58	0.93	1.57E-05	0.02	317.20	5.20	5.20E-03	2.61E-06	5.81E-05	7.42
ML5-3, t0	0.67	1.24	2.09E-05	0.02	305.00	5.00	5.00E-03	2.68E-06	6.33E-05	7.79
ML5-4, t0	0.70	1.07	1.81E-05	0.02	278.16	4.56	4.56E-03	2.62E-06	5.97E-05	7.74
ML5-5, t0	0.71	1.22	2.07E-05	0.02	314.76	5.16	5.16E-03	3.11E-06	6.90E-05	8.04
ML5-6, t0	0.71	1.01	1.71E-05	0.02	302.56	4.96	4.96E-03	2.73E-06	6.99E-05	8.06
ML5-7, t0	0.70	0.88	1.49E-05	0.01	308.66	5.06	5.06E-03	2.98E-06	7.27E-05	8.34
ML7-1, t0	0.57	3.02	5.11E-05	0.05		0.00	0.00E+00	0.00E+00	3.43E-05	7.74
ML7-2, t0	0.70	4.34	7.35E-05	0.07		0.00	0.00E+00	0.00E+00	3.73E-05	7.87
ML7-3, t0	0.67	1.62	2.75E-05	0.03		0.00	0.00E+00	0.00E+00	3.72E-05	7.94
ML7-4, t0	0.69	1.18	2.00E-05	0.02		0.00	0.00E+00	0.00E+00	4.45E-05	8.80
ML7-5, t0	0.71	2.19	3.70E-05	0.04		0.00	0.00E+00	0.00E+00	4.57E-05	8.83
ML7-6, t0	0.70	0.48	8.05E-06	0.01		0.00	0.00E+00	0.00E+00	4.54E-05	8.93
ML7-7, t0	0.70	0.88	1.48E-05	0.01		0.00	0.00E+00	0.00E+00	4.67E-05	9.13
ML5-1, t18	0.19	2.30	3.90E-05	0.04	363.56	5.96	5.96E-03	3.35E-06	4.73E-05	7.13
ML5-2, t18	0.67	108.23	1.83E-03	1.83	315.98	5.18	5.18E-03	2.91E-06	1.20E-04	11.06
ML5-3, t18	0.69	0.00	0.00E+00	0.00	356.24	5.84	5.84E-03	3.60E-06	2.40E-04	17.77
ML5-4, t18	0.71	31.17	5.28E-04	0.53	337.94	5.54	5.54E-03	3.49E-06	8.06E-05	8.79
ML5-5, t18	0.68	28.25	4.79E-04	0.48	328.18	5.38	5.38E-03	3.55E-06	8.59E-05	9.52
ML5-6, t18	0.72	127.77	2.16E-03	2.16	319.64	5.24	5.24E-03	3.38E-06	1.48E-04	12.17
ML5-7, t18	0.75	129.95	2.20E-03	2.20	326.96	5.36	5.36E-03	3.38E-06	1.51E-04	11.99
ML7-1, t17	0.70	3.52	5.97E-05	0.06	306.22	5.02	5.02E-03	3.47E-06	6.63E-05	8.38
ML7-2, t17	0.78	211.40	3.58E-03	3.58	298.90	4.90	4.90E-03	3.63E-06	2.06E-04	14.39
ML7-3, t17	0.71	227.37	3.85E-03	3.85	331.84	5.44	5.44E-03	3.68E-06	2.27E-04	13.80
ML7-4, t17	0.67	147.49	2.50E-03	2.50	305.00	5.00	5.00E-03	3.30E-06	1.63E-04	12.87
ML7-5, t17	0.74	69.94	1.19E-03	1.19	312.32	5.12	5.12E-03	3.46E-06	1.39E-04	11.79
ML7-6, t17	0.63	112.75	1.91E-03	1.91	313.54	5.14	5.14E-03	3.56E-06	1.27E-04	11.14
ML7-7, t17	0.67	101.44	1.72E-03	1.72	401.38	6.58	6.58E-03	4.45E-06	1.42E-04	11.07

Sample	Sum Anions	Charge Balance %	Synthetic HCO_3^- (mg/L)	Synthetic HCO_3^- (meq/L)	Synthetic HCO_3^- (mol/L)	Synthetic CO_3^{-2} (mol/L)	Sum Anions With Synthetic HCO_3^-	Charge Balance %	Ionic Strength
Day 0 Biostimulation									
ML5-1, t0	7.92	-9.42	365.50	5.99	5.99E-03	3.37E-06	6.55	0.03	4.29E-05
ML5-2, t0	7.83	-2.67	292.33	4.79	4.79E-03	2.40E-06	7.42	0.00	5.51E-05
ML5-3, t0	8.11	-2.02	284.83	4.67	4.67E-03	2.51E-06	7.78	0.06	6.07E-05
ML5-4, t0	7.71	0.21	280.01	4.59	4.59E-03	2.64E-06	7.74	0.01	6E-05
ML5-5, t0	8.56	-3.14	282.52	4.63	4.63E-03	2.79E-06	8.04	0.04	6.46E-05
ML5-6, t0	8.64	-3.46	267.43	4.38	4.38E-03	2.41E-06	8.06	-0.01	6.5E-05
ML5-7, t0	8.69	-2.06	287.64	4.71	4.71E-03	2.78E-06	8.35	-0.04	6.97E-05
ML7-1, t0	2.64	49.07	311.34	5.10	5.10E-03	3.29E-06	7.75	-0.05	6E-05
ML7-2, t0	3.47	38.83	268.71	4.40	4.40E-03	2.98E-06	7.87	-0.01	6.2E-05
ML7-3, t0	3.17	42.97	291.49	4.78	4.78E-03	3.38E-06	7.95	-0.03	6.31E-05
ML7-4, t0	3.31	45.30	334.35	5.48	5.48E-03	3.88E-06	8.79	0.03	7.73E-05
ML7-5, t0	3.70	40.94	312.56	5.12	5.12E-03	3.63E-06	8.82	0.04	7.79E-05
ML7-6, t0	3.54	43.24	329.40	5.40	5.40E-03	3.74E-06	8.94	-0.04	7.99E-05
ML7-7, t0	3.47	44.88	345.67	5.67	5.67E-03	4.01E-06	9.14	-0.04	8.35E-05
ML5-1, t18	6.62	3.73	394.80	6.47	6.47E-03	3.64E-06	7.13	0.00	5.08E-05
ML5-2, t18	10.72	1.55	335.29	5.50	5.50E-03	3.09E-06	11.04	0.10	0.000124
ML5-3, t18	11.96	19.57	712.09	11.67	1.17E-02	7.20E-06	17.79	-0.04	0.000369
ML5-4, t18	9.13	-1.89	317.55	5.20	5.20E-03	3.28E-06	8.80	-0.03	7.75E-05
ML5-5, t18	8.99	2.85	360.51	5.91	5.91E-03	3.90E-06	9.52	-0.02	9.12E-05
ML5-6, t18	11.74	1.82	345.39	5.66	5.66E-03	3.66E-06	12.16	0.05	0.000154
ML5-7, t18	12.07	-0.32	320.57	5.25	5.25E-03	3.32E-06	11.96	0.11	0.000149
ML7-1, t17	7.87	3.16	337.94	5.54	5.54E-03	3.83E-06	8.39	-0.03	7.04E-05
ML7-2, t17	13.62	2.76	348.78	5.72	5.72E-03	4.24E-06	14.43	-0.16	0.00022
ML7-3, t17	14.43	-2.23	284.54	4.66	4.66E-03	3.15E-06	13.65	0.53	0.000212
ML7-4, t17	11.57	5.30	383.04	6.28	6.28E-03	4.15E-06	12.85	0.07	0.000184
ML7-5, t17	11.20	2.57	350.68	5.75	5.75E-03	3.89E-06	11.83	-0.16	0.000148
ML7-6, t17	11.06	0.39	320.89	5.26	5.26E-03	3.64E-06	11.18	-0.15	0.000129
ML7-7, t17	12.12	-4.53	335.88	5.51	5.51E-03	3.72E-06	11.04	0.11	0.000127

Sample	SI with Observed HCO_3^-	SI with Synthetic HCO_3^-
Day 0 Biostimulation		
ML5-1, t0	0.41	0.32
ML5-2, t0	0.21	0.18
ML5-3, t0	0.24	0.21
ML5-4, t0	0.23	0.23
ML5-5, t0	0.30	0.26
ML5-6, t0	0.24	0.19
ML5-7, t0	0.29	0.26
ML7-1, t0		0.33
ML7-2, t0		0.28
ML7-3, t0		0.34
ML7-4, t0		0.44
ML7-5, t0		0.41
ML7-6, t0		0.43
ML7-7, t0		0.46
ML5-1, t18	0.35	0.39
ML5-2, t18	0.38	0.40
ML5-3, t18	0.49	0.80
ML5-4, t18	0.37	0.34
ML5-5, t18	0.40	0.44
ML5-6, t18	0.43	0.46
ML5-7, t18	0.42	0.41
ML7-1, t17	0.38	0.42
ML7-2, t17	0.51	0.57
ML7-3, t17	0.42	0.35
ML7-4, t17	0.36	0.46
ML7-5, t17	0.39	0.44
ML7-6, t17	0.42	0.43
ML7-7, t17	0.50	0.42

Sample	pH	Na^{+} (mg/L)	Na^{+} (mol/L)	Na^{+} (meq/L)	K^{+} (mg/L)	K^{+} (mol/L)	K^{+} (meq/L)	Ca^{+2} (mg/L)	Ca^{+2} (mol/L)	Ca^{+2} (meq/L)	Mg^{+2} (mg/L)
Day 55 Biostimulation											
ML5-1, t1	7.25	4.16	1.81E-04	0.18	1.99	5.08E-05	0.05	116.86	2.92E-03	5.83	25.08
ML5-2, t1	7.52	44.54	1.94E-03	1.94	3.86	9.86E-05	0.10	89.38	2.23E-03	4.46	30.02
ML5-3, t1	7.48	160.07	6.96E-03	6.96	5.11	1.31E-04	0.13	109.16	2.72E-03	5.45	31.39
ML5-4, t1	7.49	120.57	5.24E-03	5.24	4.90	1.25E-04	0.13	112.58	2.81E-03	5.62	31.78
ML5-5, t1	7.44	49.81	2.17E-03	2.17	3.40	8.70E-05	0.09	105.45	2.63E-03	5.26	30.74
ML5-6, t1	7.52	90.52	3.94E-03	3.94	3.96	1.01E-04	0.10	106.26	2.65E-03	5.30	34.18
ML5-7, t1	7.59	107.26	4.67E-03	4.67	4.26	1.09E-04	0.11	105.41	2.63E-03	5.26	32.16
ML7-1, t1	7.48	63.58	2.77E-03	2.77	3.36	8.58E-05	0.09	87.33	2.18E-03	4.36	29.99
ML7-2, t1	7.44	100.58	4.37E-03	4.37	4.29	1.10E-04	0.11	106.22	2.65E-03	5.30	33.29
ML7-3, t1	7.53	94.25	4.10E-03	4.10	4.20	1.07E-04	0.11	109.07	2.72E-03	5.44	33.59
ML7-4, t1	7.46	123.49	5.37E-03	5.37	4.27	1.09E-04	0.11	111.29	2.78E-03	5.55	32.37
ML7-5, t1	7.52	65.68	2.86E-03	2.86	3.65	9.34E-05	0.09	110.67	2.76E-03	5.52	34.41
ML7-6, t1	7.54	66.52	2.89E-03	2.89	3.32	8.50E-05	0.09	99.66	2.49E-03	4.97	30.36
ML7-7, t1	7.42	71.29	3.10E-03	3.10	3.45	8.82E-05	0.09	108.94	2.72E-03	5.44	30.45
ML5-1, t2	7.36	4.18	1.82E-04	0.18	1.84	4.69E-05	0.05	112.29	2.80E-03	5.60	24.27
ML5-2, t2	7.60	37.87	1.65E-03	1.65	3.58	9.17E-05	0.09	86.03	2.15E-03	4.29	29.17
ML5-3, t2	7.51	141.80	6.17E-03	6.17	4.44	1.14E-04	0.11	100.92	2.52E-03	5.04	29.39
ML5-4, t2	7.52	9.65	4.20E-04	0.42	3.13	8.01E-05	0.08	101.94	2.54E-03	5.09	30.13
ML5-5, t2	7.52	9.34	4.06E-04	0.41	2.52	6.45E-05	0.06	102.12	2.55E-03	5.10	30.22
ML5-6, t2	7.58	48.12	2.09E-03	2.09	3.24	8.27E-05	0.08	93.07	2.32E-03	4.64	29.98
ML5-7, t2	7.59	75.82	3.30E-03	3.30	3.64	9.31E-05	0.09	95.26	2.38E-03	4.75	30.60
ML7-1, t2	7.52	62.97	2.74E-03	2.74	3.26	8.33E-05	0.08	85.91	2.14E-03	4.29	28.62
ML7-2, t2	7.50	112.72	4.90E-03	4.90	4.32	1.10E-04	0.11	101.18	2.52E-03	5.05	30.89
ML7-3, t2	7.55	37.72	1.64E-03	1.64	2.93	7.49E-05	0.07	92.36	2.30E-03	4.61	27.66
ML7-4, t2	7.51	33.33	1.45E-03	1.45	2.85	7.30E-05	0.07	97.41	2.43E-03	4.86	29.14
ML7-5, t2	7.58	67.41	2.93E-03	2.93	3.17	8.10E-05	0.08	88.21	2.20E-03	4.40	28.89
ML7-6, t2	7.54	55.12	2.40E-03	2.40	3.28	8.38E-05	0.08	96.85	2.42E-03	4.83	29.34
ML7-7, t2	7.48	31.54	1.37E-03	1.37	2.94	7.52E-05	0.08	103.07	2.57E-03	5.14	29.79

Sample	Mg^{+2} (mol/L)	Mg^{+2} (meq/L)	Mn^{+2} (mg/L)	Mn^{+2} (mol/L)	Mn^{+2} (meq/L)	Fe^{+2} (mg/L)	Fe^{+2} (mol/L)	Fe^{+2} (meq/L)	Cl^{-} (mg/L)	Cl^{-} (mol/L)	Cl^{-} (meq/L)
Day 55 Biostimulation											
ML5-1, t1	1.03E-03	2.06	0.00	5.07E-08	0.00	0.01	1.74E-07	0.00	26.48	7.47E-04	0.75
ML5-2, t1	1.24E-03	2.47	0.39	7.08E-06	0.01	0.07	1.26E-06	0.00	34.57	9.75E-04	0.98
ML5-3, t1	1.29E-03	2.58	0.01	1.71E-07	0.00	0.03	5.22E-07	0.00	36.31	1.02E-03	1.02
ML5-4, t1	1.31E-03	2.61	0.00	0.00E+00	0.00	0.02	3.44E-07	0.00	35.84	1.01E-03	1.01
ML5-5, t1	1.26E-03	2.53	0.00	0.00E+00	0.00	0.02	3.55E-07	0.00	35.94	1.01E-03	1.01
ML5-6, t1	1.41E-03	2.81	0.22	3.95E-06	0.01	0.03	4.70E-07	0.00	36.82	1.04E-03	1.04
ML5-7, t1	1.32E-03	2.65	0.13	2.38E-06	0.00	0.01	2.42E-07	0.00	13.81	3.90E-04	0.39
ML7-1, t1	1.23E-03	2.47	0.89	1.62E-05	0.03	0.27	4.86E-06	0.01	31.50	8.89E-04	0.89
ML7-2, t1	1.37E-03	2.74	0.05	8.19E-07	0.00	0.02	2.83E-07	0.00	38.68	1.09E-03	1.09
ML7-3, t1	1.38E-03	2.76	0.01	2.41E-07	0.00	0.02	2.74E-07	0.00	39.10	1.10E-03	1.10
ML7-4, t1	1.33E-03	2.66	0.01	1.06E-07	0.00	0.04	6.49E-07	0.00	33.62	9.48E-04	0.95
ML7-5, t1	1.42E-03	2.83	0.87	1.59E-05	0.03	2.31	4.14E-05	0.08	40.27	1.14E-03	1.14
ML7-6, t1	1.25E-03	2.50	0.14	2.54E-06	0.01	0.02	2.97E-07	0.00	29.21	8.24E-04	0.82
ML7-7, t1	1.25E-03	2.51	0.01	2.03E-07	0.00	0.01	2.40E-07	0.00	40.46	1.14E-03	1.14
ML5-1, t2	9.99E-04	2.00	0.00	0.00E+00	0.00	0.01	2.19E-07	0.00	25.51	7.20E-04	0.72
ML5-2, t2	1.20E-03	2.40	0.45	8.23E-06	0.02	0.10	1.73E-06	0.00	34.97	9.86E-04	0.99
ML5-3, t2	1.21E-03	2.42	0.02	3.04E-07	0.00	0.02	3.08E-07	0.00	37.23	1.05E-03	1.05
ML5-4, t2	1.24E-03	2.48	0.00	1.42E-09	0.00	0.01	2.43E-07	0.00	32.44	9.15E-04	0.92
ML5-5, t2	1.24E-03	2.49	0.00	0.00E+00	0.00	0.01	2.57E-07	0.00	30.57	8.62E-04	0.86
ML5-6, t2	1.23E-03	2.47	0.17	3.15E-06	0.01	0.04	7.14E-07	0.00	41.85	1.18E-03	1.18
ML5-7, t2	1.26E-03	2.52	0.18	3.30E-06	0.01	0.02	3.50E-07	0.00	40.39	1.14E-03	1.14
ML7-1, t2	1.18E-03	2.36	0.91	1.65E-05	0.03	0.26	4.57E-06	0.01	36.60	1.03E-03	1.03
ML7-2, t2	1.27E-03	2.54	0.04	7.87E-07	0.00	0.02	3.59E-07	0.00	36.03	1.02E-03	1.02
ML7-3, t2	1.14E-03	2.28	0.01	1.16E-07	0.00	0.01	2.03E-07	0.00	33.66	9.49E-04	0.95
ML7-4, t2	1.20E-03	2.40	0.00	3.39E-08	0.00	0.01	2.41E-07	0.00	35.20	9.93E-04	0.99
ML7-5, t2	1.19E-03	2.38	0.69	1.25E-05	0.03	0.22	3.92E-06	0.01	37.10	1.05E-03	1.05
ML7-6, t2	1.21E-03	2.41	0.09	1.57E-06	0.00	0.02	2.71E-07	0.00	41.13	1.16E-03	1.16
ML7-7, t2	1.23E-03	2.45	0.02	3.01E-07	0.00	0.23	4.16E-06	0.01	41.65	1.18E-03	1.18

Sample	NO_2^- (mg/L)	NO_2^- (mol/L)	NO_2^- (meq/L)	Br^- (mg/L)	Br^- (mol/L)	Br^- (meq/L)	NO_3^- (mg/L)	NO_3^- (mol/L)	NO_3^- (meq/L)	SO_4^{-2} (mg/L)	SO_4^{-2} (mol/L)
Day 55 Biostimulation											
ML5-1, t1	0.00	0.00E+00	0.00	1.80	2.25E-05	0.02	54.60	8.81E-04	0.88	23.80	2.48E-04
ML5-2, t1	0.00	0.00E+00	0.00	15.39	1.93E-04	0.19	4.08	6.58E-05	0.07	34.05	3.54E-04
ML5-3, t1	0.93	2.02E-05	0.02	294.80	3.69E-03	3.69	32.20	5.19E-04	0.52	29.40	3.06E-04
ML5-4, t1	0.54	1.17E-05	0.01	197.20	2.47E-03	2.47	49.60	8.00E-04	0.80	30.82	3.21E-04
ML5-5, t1	0.00	0.00E+00	0.00	73.50	9.20E-04	0.92	62.60	1.01E-03	1.01	35.39	3.68E-04
ML5-6, t1	1.29	2.80E-05	0.03	156.80	1.96E-03	1.96	16.60	2.68E-04	0.27	27.22	2.83E-04
ML5-7, t1	0.00	0.00E+00	0.00	58.64	7.34E-04	0.73	5.62	9.07E-05	0.09	10.20	1.06E-04
ML7-1, t1	0.00	0.00E+00	0.00	8.90	1.11E-04	0.11	1.80	2.90E-05	0.03	28.47	2.96E-04
ML7-2, t1	0.00	0.00E+00	0.00	188.20	2.36E-03	2.36	25.60	4.13E-04	0.41	34.05	3.54E-04
ML7-3, t1	1.50	3.26E-05	0.03	153.60	1.92E-03	1.92	35.60	5.74E-04	0.57	33.20	3.46E-04
ML7-4, t1	1.30	2.82E-05	0.03	204.36	2.56E-03	2.56	40.32	6.50E-04	0.65	28.13	2.93E-04
ML7-5, t1	0.37	8.11E-06	0.01	77.79	9.73E-04	0.97	18.49	2.98E-04	0.30	33.03	3.44E-04
ML7-6, t1	1.26	2.73E-05	0.03	64.70	8.10E-04	0.81	12.70	2.05E-04	0.20	21.07	2.19E-04
ML7-7, t1	2.19	4.77E-05	0.05	127.90	1.60E-03	1.60	47.32	7.63E-04	0.76	31.74	3.30E-04
ML5-1, t2	0.00	0.00E+00	0.00	0.00	0.00E+00	0.00	53.26	8.59E-04	0.86	20.78	2.16E-04
ML5-2, t2	0.00	0.00E+00	0.00	11.80	1.48E-04	0.15	3.60	5.81E-05	0.06	30.41	3.17E-04
ML5-3, t2	0.00	0.00E+00	0.00	253.60	3.17E-03	3.17	0.00	0.00E+00	0.00	26.90	2.80E-04
ML5-4, t2	0.00	0.00E+00	0.00	2.88	3.60E-05	0.04	65.30	1.05E-03	1.05	29.37	3.06E-04
ML5-5, t2	0.00	0.00E+00	0.00	1.03	1.29E-05	0.01	55.07	8.88E-04	0.89	23.82	2.48E-04
ML5-6, t2	0.00	0.00E+00	0.00	66.83	8.36E-04	0.84	9.38	1.51E-04	0.15	32.19	3.35E-04
ML5-7, t2	0.00	0.00E+00	0.00	97.86	1.22E-03	1.22	6.28	1.01E-04	0.10	28.00	2.91E-04
ML7-1, t2	0.00	0.00E+00	0.00	36.60	4.58E-04	0.46	0.00	0.00E+00	0.00	32.50	3.38E-04
ML7-2, t2	0.00	0.00E+00	0.00	178.60	2.24E-03	2.24	8.72	1.41E-04	0.14	34.20	3.56E-04
ML7-3, t2	0.00	0.00E+00	0.00	32.58	4.08E-04	0.41	44.95	7.25E-04	0.72	32.64	3.40E-04
ML7-4, t2	0.97	2.12E-05	0.02	40.63	5.08E-04	0.51	43.22	6.97E-04	0.70	29.82	3.10E-04
ML7-5, t2	0.00	0.00E+00	0.00	44.49	5.57E-04	0.56	2.03	3.27E-05	0.03	24.64	2.57E-04
ML7-6, t2	3.68	8.00E-05	0.08	81.04	1.01E-03	1.01	11.62	1.87E-04	0.19	28.70	2.99E-04
ML7-7, t2	2.51	5.46E-05	0.05	27.26	3.41E-04	0.34	45.93	7.41E-04	0.74	29.54	3.07E-04

Sample	SO_4^{-2} (meq/L)	CH_3COO^- (mg/L)	CH_3COO^- (mol/L)	CH_3COO^- (meq/L)	HCO_3^- (mg/L)	HCO_3^- (meq/L)	HCO_3^- (mol/L)	CO_3^{-2} (mol/L)	Ionic Strength	Sum Cations
Day 55 Biostimulation										
ML5-1, t1	0.50	3.33	5.65E-05	0.06	347.30	5.69	5.69E-03	3.29E-06	6.43E-05	8.13
ML5-2, t1	0.71	34.80	5.90E-04	0.59	444.20	7.28	7.28E-03	7.77E-06	9.14E-05	8.98
ML5-3, t1	0.61	145.24	2.46E-03	2.46	578.50	9.48	9.48E-03	9.22E-06	3.32E-04	15.12
ML5-4, t1	0.64	121.64	2.06E-03	2.06	529.80	8.68	8.68E-03	8.74E-06	2.48E-04	13.60
ML5-5, t1	0.74	46.36	7.86E-04	0.79	408.10	6.69	6.69E-03	5.99E-06	1.17E-04	10.05
ML5-6, t1	0.57	101.65	1.72E-03	1.72	517.40	8.48	8.48E-03	9.15E-06	1.92E-04	12.16
ML5-7, t1	0.21	42.17	7.14E-04	0.71	517.50	8.48	8.48E-03	1.07E-05	1.48E-04	12.69
ML7-1, t1	0.59	84.05	1.42E-03	1.42	505.50	8.29	8.29E-03	8.04E-06	1.20E-04	9.72
ML7-2, t1	0.71	150.99	2.56E-03	2.56	529.80	8.68	8.68E-03	7.81E-06	2.30E-04	12.53
ML7-3, t1	0.69	117.27	1.99E-03	1.99	517.60	8.48	8.48E-03	9.37E-06	2.07E-04	12.41
ML7-4, t1	0.59	132.42	2.24E-03	2.24	505.60	8.29	8.29E-03	7.65E-06	2.43E-04	13.70
ML7-5, t1	0.69	83.61	1.42E-03	1.42	493.10	8.08	8.08E-03	8.68E-06	1.52E-04	11.42
ML7-6, t1	0.44	59.81	1.01E-03	1.01	486.90	7.98	7.98E-03	8.87E-06	1.27E-04	10.46
ML7-7, t1	0.66	83.12	1.41E-03	1.41	444.50	7.29	7.29E-03	6.26E-06	1.56E-04	11.13
ML5-1, t2	0.43	0.00	0.00E+00	0.00	347.30	5.69	5.69E-03	4.22E-06	6.04E-05	7.83
ML5-2, t2	0.63	19.81	3.36E-04	0.34	432.30	7.09	7.09E-03	9.17E-06	8.06E-05	8.45
ML5-3, t2	0.56	117.07	1.98E-03	1.98	541.90	8.88	8.88E-03	9.22E-06	2.60E-04	13.74
ML5-4, t2	0.61	1.90	3.22E-05	0.03	335.10	5.49	5.49E-03	5.93E-06	6.57E-05	8.07
ML5-5, t2	0.50	0.00	0.00E+00	0.00	335.10	5.49	5.49E-03	5.89E-06	6.25E-05	8.05
ML5-6, t2	0.67	27.63	4.68E-04	0.47	432.10	7.08	7.08E-03	8.63E-06	1.01E-04	9.30
ML5-7, t2	0.58	50.36	8.53E-04	0.85	468.70	7.68	7.68E-03	9.67E-06	1.34E-04	10.67
ML7-1, t2	0.68	90.60	1.54E-03	1.54	493.20	8.08	8.08E-03	8.68E-06	1.24E-04	9.51
ML7-2, t2	0.71	91.20	1.55E-03	1.55	517.60	8.48	8.48E-03	8.68E-06	2.04E-04	12.61
ML7-3, t2	0.68	3.65	6.18E-05	0.06	383.70	6.29	6.29E-03	7.19E-06	8.01E-05	8.60
ML7-4, t2	0.62	14.22	2.41E-04	0.24	383.80	6.29	6.29E-03	6.62E-06	8.38E-05	8.78
ML7-5, t2	0.51	50.01	8.47E-04	0.85	493.20	8.08	8.08E-03	9.92E-06	1.19E-04	9.82
ML7-6, t2	0.60	38.62	6.54E-04	0.65	432.30	7.09	7.09E-03	7.93E-06	1.11E-04	9.73
ML7-7, t2	0.61	11.01	1.87E-04	0.19	371.60	6.09	6.09E-03	5.92E-06	8.41E-05	9.05

Sample	Sum Anions	Charge Balance %	Synthetic HCO_3^- (mg/L)	Synthetic HCO_3^- (meq/L)	Synthetic HCO_3^- (mol/L)	Synthetic CO_3^{-2} (mol/L)	Sum Anions With Synthetic HCO_3^-	Charge Balance %	Ionic Strength
Day 55 Biostimulation									
ML5-1, t1	7.89	1.45	360.98	5.92	5.92E-03	3.42E-06	8.12	0.05	6.61E-05
ML5-2, t1	9.81	-4.41	392.71	6.44	6.44E-03	6.87E-06	8.97	0.08	8.23E-05
ML5-3, t1	17.81	-8.15	424.61	6.96	6.96E-03	6.77E-06	15.29	-0.53	0.000274
ML5-4, t1	15.68	-7.08	401.55	6.58	6.58E-03	6.63E-06	13.57	0.11	0.000207
ML5-5, t1	11.15	-5.23	340.34	5.58	5.58E-03	4.99E-06	10.04	0.01	0.000103
ML5-6, t1	14.07	-7.26	400.35	6.56	6.56E-03	7.08E-06	12.15	0.06	0.00016
ML5-7, t1	10.62	8.85	643.51	10.55	1.05E-02	1.32E-05	12.69	-0.01	0.000182
ML7-1, t1	11.33	-7.66	406.94	6.67	6.67E-03	6.47E-06	9.72	0.02	9.95E-05
ML7-2, t1	15.81	-11.59	329.51	5.40	5.40E-03	4.86E-06	12.53	0.00	0.000171
ML7-3, t1	14.79	-8.74	373.53	6.12	6.12E-03	6.76E-06	12.43	-0.07	0.000167
ML7-4, t1	15.30	-5.52	406.21	6.66	6.66E-03	6.14E-06	13.67	0.10	0.000211
ML7-5, t1	12.60	-4.92	422.47	6.92	6.92E-03	7.44E-06	11.44	-0.11	0.000136
ML7-6, t1	11.30	-3.87	435.17	7.13	7.13E-03	7.93E-06	10.45	0.02	0.000116
ML7-7, t1	12.91	-7.39	335.94	5.51	5.51E-03	4.73E-06	11.13	0.02	0.00013
ML5-1, t2	7.70	0.81	355.16	5.82	5.82E-03	4.32E-06	7.83	-0.02	6.14E-05
ML5-2, t2	9.25	-4.49	383.58	6.29	6.29E-03	8.14E-06	8.45	0.03	7.26E-05
ML5-3, t2	15.65	-6.51	423.18	6.94	6.94E-03	7.20E-06	13.70	0.12	0.000221
ML5-4, t2	8.14	-0.46	330.68	5.42	5.42E-03	5.85E-06	8.07	-0.01	6.51E-05
ML5-5, t2	7.75	1.91	353.59	5.80	5.80E-03	6.21E-06	8.05	-0.01	6.49E-05
ML5-6, t2	10.39	-5.56	365.51	5.99	5.99E-03	7.30E-06	9.30	-0.01	8.87E-05
ML5-7, t2	11.58	-4.10	413.01	6.77	6.77E-03	8.52E-06	10.67	0.00	0.000122
ML7-1, t2	11.79	-10.71	354.85	5.82	5.82E-03	6.25E-06	9.52	-0.06	9.51E-05
ML7-2, t2	14.13	-5.71	424.97	6.97	6.97E-03	7.13E-06	12.61	-0.03	0.000178
ML7-3, t2	9.11	-2.89	352.77	5.78	5.78E-03	6.61E-06	8.61	-0.03	7.51E-05
ML7-4, t2	9.37	-3.25	348.08	5.71	5.71E-03	6.00E-06	8.79	-0.03	7.8E-05
ML7-5, t2	11.08	-6.01	416.50	6.83	6.83E-03	8.38E-06	9.82	0.01	0.000103
ML7-6, t2	10.78	-5.10	369.79	6.06	6.06E-03	6.79E-06	9.75	-0.11	9.85E-05
ML7-7, t2	9.20	-0.84	362.30	5.94	5.94E-03	5.78E-06	9.05	0.00	8.26E-05

Sample	SI with Observed HCO_3^-	SI with Synthetic HCO_3^-
Day 55 Biostimulation		
ML5-1, t1	0.39	0.41
ML5-2, t1	0.65	0.60
ML5-3, t1	0.81	0.68
ML5-4, t1	0.80	0.68
ML5-5, t1	0.61	0.53
ML5-6, t1	0.79	0.68
ML5-7, t1	0.86	0.95
ML7-1, t1	0.65	0.56
ML7-2, t1	0.73	0.52
ML7-3, t1	0.82	0.67
ML7-4, t1	0.74	0.64
ML7-5, t1	0.79	0.72
ML7-6, t1	0.75	0.70
ML7-7, t1	0.64	0.52
ML5-1, t2	0.48	0.49
ML5-2, t2	0.70	0.65
ML5-3, t2	0.78	0.67
ML5-4, t2	0.59	0.58
ML5-5, t2	0.59	0.61
ML5-6, t2	0.71	0.64
ML5-7, t2	0.77	0.72
ML7-1, t2	0.68	0.54
ML7-2, t2	0.75	0.67
ML7-3, t2	0.63	0.59
ML7-4, t2	0.62	0.57
ML7-5, t2	0.75	0.68
ML7-6, t2	0.69	0.62
ML7-7, t2	0.59	0.58

Appendix 23: Acetate Delivery Rate Calculation for Woodstock CIS

Input	
Average NO_3 Concentration (mg/L-N)	15
Average D.O. Conc (mg/L)	10
Average Porosity	0.33
Molar Mass NO_3	62.0049
Molar Mass O_2	31.9988
Molar Mass CH_3COO^-	59.04421
Molar Mass $NaCH_3COO$	82.03401
Number of carbons in acetate molecule	2
C:N	1.25
C:O	0.5
Duration of pumping (d)	0.21
Total acetate solution to be injected (L)	60
Feed line Flow Rate (L/min)	0.2
Recirculation line flow Rate (L/min)	190

Output	
Total Moles NO_3 to be treated	2.81E+02
Total Moles O_2 to be treated	8.19E+01
Total Moles C needed for treatment	3.92E+02
Final C:N Based on Daily Flux	1.40
Total mass sodium acetate needed for 24 hrs (kg/ day)	16.07
Total mass sodium acetate (kg) if only treating duration of injection period	3.35
Total mass acetate (kg) needed to inject for 24 hrs	11.57
Concentration of Solution to inject (mg/L)	1.93E+05
Rate of mass flow in feed line (mg/min)	3.86E+04
Concentration of Solution recirculation line (mg/L)	202.95

Denotes calculated field, do not change value

Flux Calculation

Critchley 2010 Model Layer ID	Velocity estimated from April 2009 CIS Tracer Test (m/d)	Y_2 (mamsl)	Y_1 (mamsl)	ΔY (m) depth	ΔX (m) space between WO78 and WO79	Area (m^2)	Nitrate Conc (mg/L-NO_3)	Oxygen Conc (mg/L)	Nitrate mass flux (g-NO_3/Ld)	Nitrate flux (Moles-NO_3/Ld)	Oxygen Flux (g O_2/Ld)	Oxygen Flux (Moles-O_2/Ld)	Moles C need to treat both daily fluxes of NO_3 and O_2	Dosage of sodium acetate needed (g/d)
1	0.41	297.6	294.5	3.1	5	15.5	66.40204	10	1.38E+02	2.22E+00	2.08E+01	6.49E-01	3.11E+00	127.3602
2	7.41	294.5	292.5	2	5	10	66.40204	10	1.62E+03	2.62E+01	2.44E+02	7.64E+00	3.65E+01	1498.733
3	15.25	292.5	290.5	2	5	10	66.40204	10	3.34E+03	5.39E+01	5.03E+02	1.57E+01	7.53E+01	3086.539
4	32.15	290.5	289.4	1.1	5	5.5	66.40204	10	3.87E+03	6.25E+01	5.83E+02	1.82E+01	8.72E+01	3577.404
5	9.49	289.4	285	4.4	5	22	66.40204	10	4.57E+03	7.37E+01	6.89E+02	2.15E+01	1.03E+02	4222.405
6	17.60	285	283	2	5	10	66.40204	10	3.86E+03	6.22E+01	5.81E+02	1.81E+01	8.68E+01	3560.315
	No velocty data at this interval. Use Critchley's model velocity value instead													

April 2009 CIS tracer test results

Multilevel	Depth	Velocity (m/s)
ML6-2	293.46	1.16E-04
ML6-3	291.76	1.74E-04
ML6-4	290.06	3.15E-04
ML6-6	286.66	1.19E-04
ML6-7	284.96	2.04E-04
ML7-2	293.44	5.54E-05
ML7-3	291.74	1.80E-04
ML7-4	290.04	4.29E-04
ML7-5	288.34	1.01E-04

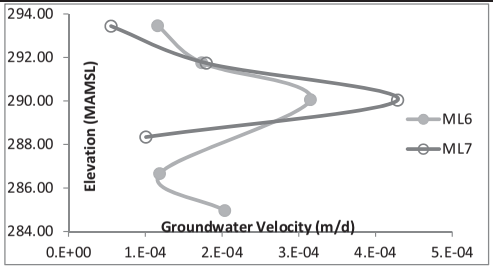

Appendix 24: Zero-Order Denitrification Rate Calculation

Multilevel	Mass Nitrate Day 0 (mg)	Mass Nitrate Day 55 (mg)	Residence Time on Day 55 (Days)	Zero-Order Removal Rate (mg/Day)
ML5-2	2.88E+05	1.77E+04	7.73E-01	3.50E+05
ML5-3	3.27E+05	0.00E+00	3.71E-01	8.81E+05
ML5-4	3.33E+05	3.21E+05	2.41E-01	5.00E+04
ML5-5	3.28E+05	2.71E+05	1.45E-01	3.95E+05
ML5-6	2.93E+05	4.61E+04	6.39E-01	3.86E+05
ML5-7	2.70E+05	3.08E+04	5.16E-01	4.64E+05
ML7-1	2.86E+05	0.00E+00	2.99E+00	9.57E+04
ML7-2	2.93E+05	6.62E+04	6.72E-01	3.37E+05
ML7-3	2.97E+05	1.92E+05	6.05E-01	1.74E+05
ML7-4	2.93E+05	1.96E+05	4.98E-01	1.94E+05
ML7-5	2.91E+05	0.00E+00	1.14E+00	2.55E+05
ML7-6	2.77E+05	4.53E+04	8.73E-01	2.65E+05
ML7-7	2.91E+05	2.20E+05	5.99E-01	1.18E+05

Appendix 25: Relevant Acetylene Block Results

2010 Acetylene Block Experiment

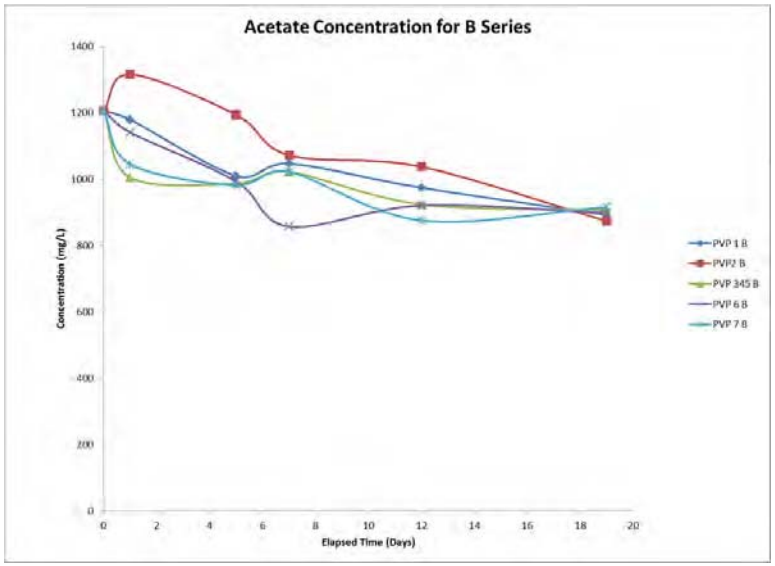

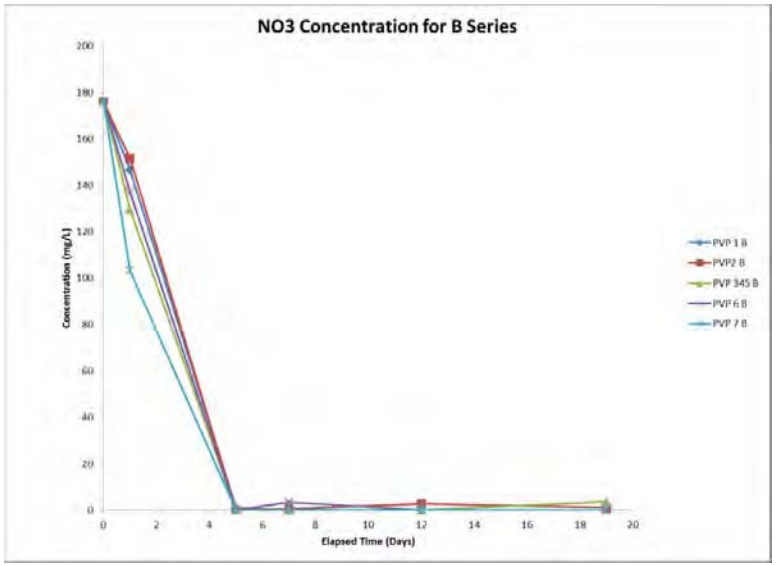

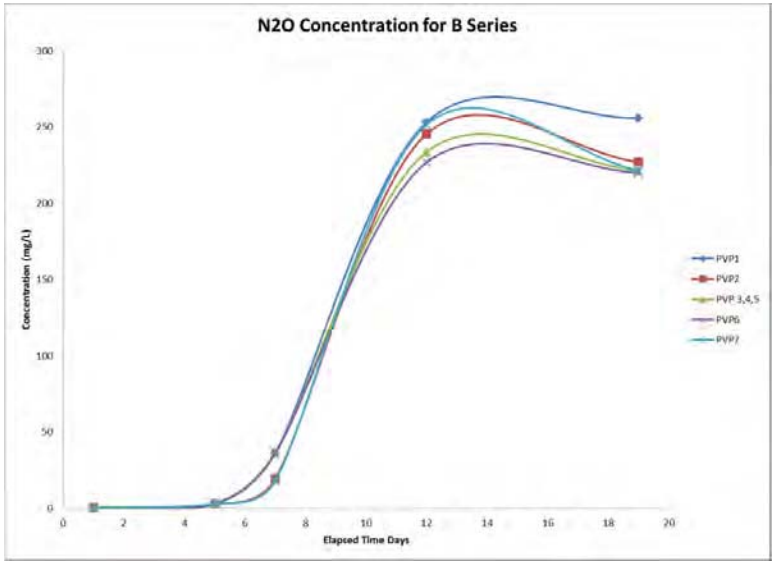

2011 Acetylene Block Experiment

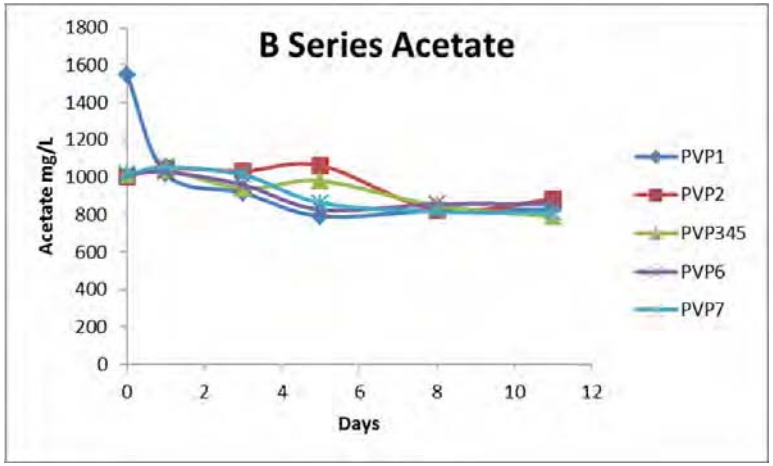

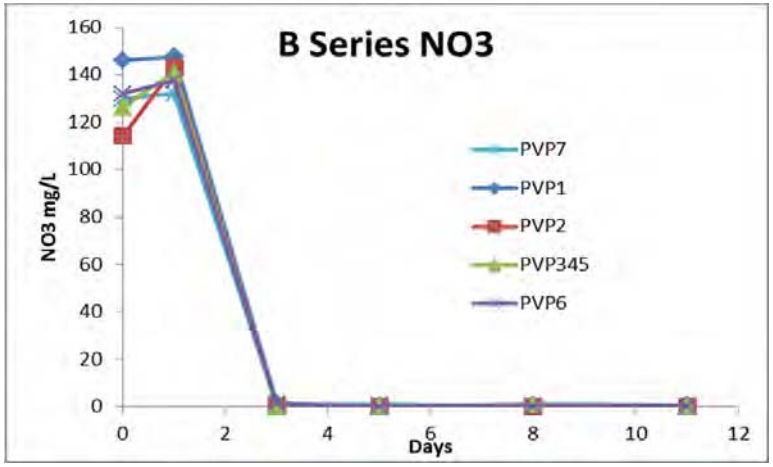

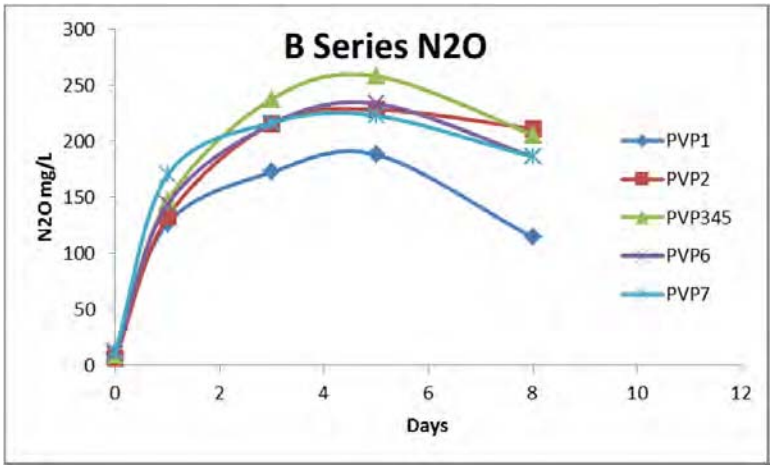

Appendix 26: Total Lipid Biomass Data for Woodstock

Location: Near PVPs 3 and 4 in 2010

Standards	Conc	Abs	Conc	Abs
	0	0.037	0	0.043
	1.5	0.057	1.5	0.051
	3	0.079	3	0.078
	6	0.128	6	0.133
	10	0.237	10	0.2
	15	0.292	15	0.281

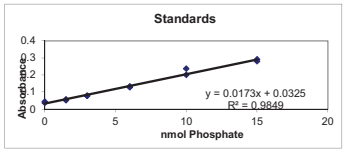

Sample	Mass weighed (g dry sediment)	Lab notes	Absorbance	Amount of Phosphate nmol	Biomass (cells/g dry weight sed) (Dobbs&Findlay 1993)	High Value (cells/g dry weight sed)	Average (cells/g dry weight sed)
2_1_1	12.08		0.033	0.0289017	8.13E+04	4.79E+06	2.43E+06
2_1_2	12.34		0.033	0.0289017	7.96E+04	4.68E+06	2.38E+06
2_2_1	12.09		0.032	-0.0289017	-8.13E+04	-4.78E+06	-2.43E+06
2_2_2	12.34		0.038	0.3179191	8.76E+05	5.15E+07	2.62E+07
2_3_1	12.06		0.038	0.3179191	8.96E+05	5.27E+07	2.68E+07
2_3_2	12.09		0.041	0.4913295	1.38E+06	8.13E+07	4.13E+07
2_3_3	12.02		0.031	-0.0867052	-2.45E+05	-1.44E+07	-7.34E+06
2_3_4	11.95		0.031	-0.0867052	-2.47E+05	-1.45E+07	-7.38E+06
2_3_5	12.35		0.042	0.5491329	1.51E+06	8.89E+07	4.52E+07
2_3_6	12.13		0.04	0.433526	1.22E+06	7.15E+07	3.63E+07
2_4_1	12.43		0.028	-0.2601156	-7.11E+05	-4.19E+07	-2.13E+07
2_4_2	12.34		0.026	-0.3757225	-1.04E+06	-6.09E+07	-3.10E+07
2_5_1	12.07		0.028	-0.2601156	-7.33E+05	-4.31E+07	-2.19E+07
2_5_2	12.19		0.032	-0.0289017	-8.06E+04	-4.74E+06	-2.41E+06
1_1_1	12.02		0.053	1.1849711	3.35E+06	1.97E+08	1.00E+08
1_1_2	12.20		0.043	0.6069364	1.69E+06	9.95E+07	5.06E+07
1_2_1	12.24		0.043	0.6069364	1.69E+06	9.92E+07	5.04E+07
1_2_2	13.72		0.042	0.5491329	1.36E+06	8.00E+07	4.07E+07
1_3_1	12.26		0.037	0.2601156	7.21E+05	4.24E+07	2.16E+07
1_3_2	12.80		0.045	0.7225434	1.92E+06	1.13E+08	5.74E+07
1_3_3	12.00		0.048	0.8959538	2.54E+06	1.49E+08	7.59E+07
1_3_4	12.01		0.054	1.2427746	3.52E+06	2.07E+08	1.05E+08
1_3_5	12.06		0.056	1.3583815	3.83E+06	2.25E+08	1.15E+08
1_3_6	12.07		0.047	0.8381503	2.36E+06	1.39E+08	7.06E+07
1_4_1	12.47		0.043	0.6069364	1.65E+06	9.73E+07	4.95E+07
1_4_2	12.62		0.067	1.9942197	5.37E+06	3.16E+08	1.61E+08
1_5_1	12.01		0.047	0.8381503	2.37E+06	1.40E+08	7.10E+07
1_5_2	12.15		0.041	0.4913295	1.37E+06	8.09E+07	4.11E+07

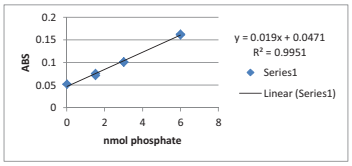

Standards	Conc	Abs	Conc	Abs
	0	0.094	0	0.052
	1.5	0.072	1.5	0.076
	3	0.101	3	0.102
	6	0.162	6	0.163

DATA NOT USED FOR FIRST 0

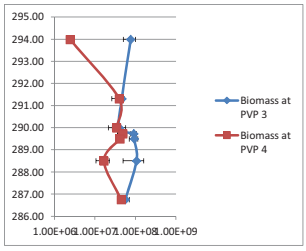

Sample	Mass weighed (g dry sediment)	Volume of sample (uL)	Absorbance	Amount of Phosphate nmol	Biomass (cells/g dry weight sed) (Dobbs&Findlay 1993)	High Value (cells/g dry weight sed)	Average (cells/g dry weight sed)
2_2_1	12.09	715	0.081	1.7842105	1.75E+06	1.03E+08	5.25E+07
2_4_1	12.43	705	0.054	0.3631579	3.52E+05	2.07E+07	1.05E+07
2_5_2	12.19	695	0.078	1.6263158	1.63E+06	9.60E+07	4.88E+07
2_3_4	11.95	715	0.086	2.0473684	2.04E+06	1.20E+08	6.09E+07
2_4_2	12.34	720	0.062	0.7842105	7.50E+05	4.41E+07	2.24E+07
2_3_3	12.02	710	0.07	1.2052632	1.20E+06	7.06E+07	3.59E+07
2_5_1	12.07	600	0.068	1.1	1.29E+06	7.59E+07	3.86E+07

PVP location	Sample 1	Sample 2	Depth (ft)	Elevation (MAMSL)	Average Biomass 1	Average Biomass 2	Average Biomass	Error High	Error Low
3_1	1_1_1	1_1_2	22	293.99	1.00E+08	5.06E+07	7.54E+07	2.48E+07	2.48E+07
3_2	1_2_1	1_2_2	30.8	291.31	5.04E+07	4.07E+07	4.56E+07	4.86E+06	4.86E+06
3_3	1_3_1	1_3_2	35.1	290.00	2.16E+07	5.74E+07	3.95E+07	1.79E+07	1.79E+07
3_4	1_3_3	1_3_4	36	289.73	7.59E+07	1.05E+08	9.06E+07	1.47E+07	1.47E+07
3_5	1_3_5	1_3_6	36.75	289.50	1.15E+08	7.06E+07	9.26E+07	2.20E+07	2.20E+07
3_6	1_4_1	1_4_2	40	288.51	4.95E+07	1.61E+08	1.05E+08	5.56E+07	5.56E+07
3_7	1_5_1	1_5_2	45.75	286.76	7.10E+07	4.11E+07	5.61E+07	1.49E+07	1.49E+07
4_1	2_1_1	2_1_2	22	293.99	2.43E+06	2.38E+06	2.41E+06	2.56E+04	2.56E+04
4_2	2_2_1	2_2_2	30.8	291.31	5.25E+07	2.62E+07	3.93E+07	1.31E+07	1.31E+07
4_3	2_3_1	2_3_2	35.1	290.00	2.68E+07	4.13E+07	3.41E+07	7.26E+06	7.26E+06
4_4	2_3_3	2_3_4	36	289.73	3.59E+07	6.09E+07	4.84E+07	1.25E+07	1.25E+07
4_5	2_3_5	2_3_6	36.75	289.50	4.52E+07	3.63E+07	4.08E+07	4.44E+06	4.44E+06
4_6	2_4_1	2_4_2	40	288.51	1.05E+07	2.24E+07	1.65E+07	5.95E+06	5.95E+06
4_7	2_5_1	2_5_2	45.75	286.76	3.86E+07	4.88E+07	4.37E+07	5.09E+06	5.09E+06

PVP 3 and 4 2011
Post Biostimulation

Standards	Conc	Abs	Conc	Abs
	0	0.01	0	0.022
	1.5	0.035	1.5	0.038
	3	0.062	3	0.058
	6	0.094	6	0.109
	10	0.152	10	0.148
	15	0.213	15	0.205

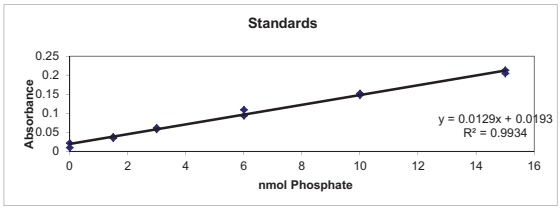

Sample	Mass weighed (g dry sediment)	Absorbance	Amount of Phosphate nmol	Biomass (cells/g dry weight sed) (Dobbs&Findlay 1993)	High Value (cells/g dry weight sed)	Average (cells/g dry weight sed)
PVP3 22_1	12.24	0.042	1.7596899	4.89E+06	2.88E+08	1.46E+08
PVP3 22_2	12.19	0.049	2.3023256	6.42E+06	3.78E+08	1.92E+08
PVP3_30.8_1	12.16	0.061	3.2325581	9.04E+06	5.32E+08	2.70E+08
PVP3_30.8_2	12.23	0.022	0.2093023	5.82E+05	3.42E+07	1.74E+07
PVP3_35.1_1	12.11	0.078	4.5503876	1.28E+07	7.52E+08	3.82E+08
PVP3_35.1_2	12.18	0.054	2.6899225	7.51E+06	4.42E+08	2.25E+08
PVP3_36.00_1	12.29	0.068	3.7751938	1.04E+07	6.14E+08	3.12E+08
PVP3_36.00_2	12.2	0.062	3.3100775	9.22E+06	5.43E+08	2.76E+08
PVP3_36.75_1	13.48	0.06	3.1550388	7.96E+06	4.68E+08	2.38E+08
PVP3_36.75_2	13.59	0.062	3.3100775	8.28E+06	4.87E+08	2.48E+08
PVP3_40.00_1	12.26	0.022	0.2093023	5.80E+05	3.41E+07	1.74E+07
PVP3_40.00_2	12.36	0.02	0.0542636	1.49E+05	8.78E+06	4.46E+06
PVP3_45.75_1	12.15	0.035	1.2170543	3.41E+06	2.00E+08	1.02E+08
PVP3_45.75_2	12.55	0.052	2.5348837	6.87E+06	4.04E+08	2.05E+08
PVP3_45-50Gravel1	12.86	0.034	1.1395349	3.01E+06	1.77E+08	9.01E+07
PVP3 45-50Gravel2	12.92	0.038	1.4496124	3.81E+06	2.24E+08	1.14E+08
PVP4 22_sand1	12.16	0.025	0.4418605	1.24E+06	7.27E+07	3.70E+07
PVP4 22_sand2	12.17	0.076	4.3953488	1.23E+07	7.22E+08	3.67E+08
PVP4 22_gravel1	12.57	0.021	0.1317829	3.56E+05	2.10E+07	1.07E+07
PVP4 22_gravel2	12.45	0.023	0.2868217	7.83E+05	4.61E+07	2.34E+07
PVP4_30.8_1	12.41	0.035	1.2170543	3.33E+06	1.96E+08	9.97E+07
PVP4_30.8_2	12.85	0.041	1.6821705	4.45E+06	2.62E+08	1.33E+08
PVP4_35.1_1	12.43	0.057	2.9224806	7.99E+06	4.70E+08	2.39E+08
PVP4_35.1_2	12.82	0.052	2.5348837	6.72E+06	3.95E+08	2.01E+08
PVP4_36.00_1	12.27	0.05	2.379845	6.59E+06	3.88E+08	1.97E+08
PVP4_36.00_2	12.36	0.078	4.5503876	1.25E+07	7.36E+08	3.74E+08
PVP4_36.75_1	12.87	0.039	1.5271318	4.03E+06	2.37E+08	1.21E+08
PVP4_36.75_2	13.38	0.041	1.6821705	4.27E+06	2.51E+08	1.28E+08
PVP4_40.00_1	12.65	0.03	0.8294574	2.23E+06	1.31E+08	6.67E+07
PVP4_40.00_2	12.79	0.041	1.6821705	4.47E+06	2.63E+08	1.34E+08
PVP4_45.75_1	12.79	0.021	0.1317829	3.50E+05	2.06E+07	1.05E+07
PVP4_45.75_2	13.12	0.021	0.1317829	3.42E+05	2.01E+07	1.02E+07
PVP4_45-50Gravel1	13.53	0.018	-0.1007752	-2.53E+05	-1.49E+07	-7.57E+06
PVP4 45-50Gravel2	13.38	0.014	-0.4108527	-1.04E+06	-6.14E+07	-3.12E+07

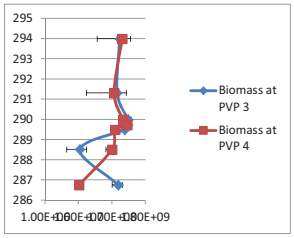

PVP location	Sample 1	Sample 2	Depth (ft)	Elevation (M.	Average Biom	Average Biomass 2	Average Bi	Error High	Error Low
3_1			22	293.9944	1.46E+08	1.92E+08	1.69E+08	2.29E+07	2.29E+07
3_2			30.8	291.31216	2.70E+08	1.74E+07	1.44E+08	1.26E+08	1.26E+08
3_3			35.1	290.00152	3.82E+08	2.25E+08	3.03E+08	7.88E+07	7.88E+07
3_4			36	289.7272	3.12E+08	2.76E+08	2.94E+08	1.82E+07	1.82E+07
3_5			36.75	289.4986	2.38E+08	2.48E+08	2.43E+08	4.84E+06	4.84E+06
3_6			40	288.508	1.74E+07	4.46E+06	1.09E+07	6.45E+06	6.45E+06
3_7			45.75	286.7554	1.02E+08	2.05E+08	1.54E+08	5.18E+07	5.18E+07
4_1			22	293.9944	3.70E+07	3.67E+08	2.02E+08	1.65E+08	1.65E+08
4_2			30.8	291.31216	9.97E+07	1.33E+08	1.16E+08	1.67E+07	1.67E+07
4_3			35.1	290.00152	2.39E+08	2.01E+08	2.20E+08	1.90E+07	1.90E+07
4_4			36	289.7272	1.97E+08	3.74E+08	2.86E+08	8.86E+07	8.86E+07
4_5			36.75	289.4986	1.21E+08	1.28E+08	1.24E+08	3.59E+06	3.59E+06
4_6			40	288.508	6.67E+07	1.34E+08	1.00E+08	3.35E+07	3.35E+07
4_7			45.75	286.7554	1.05E+07	1.02E+07	1.03E+07	1.32E+05	1.32E+05

Location: Near PVP 1 and 2
Date of Core Extractio 10/6/2008
Date of PLFA Extractic 2/5/2009
Date of PLFA Absorba 2/10/2009 and 2/16/09 (for samples that were BDL on 2/10)

Standards	Conc	Abs	Conc	Abs
	0	0.093	0	0.085
	1.5	0.118	1.5	0.119
	3	0.145	3	0.146
	6	0.203	6	0.211
	10	0.29	10	0.296
	15	0.355	15	0.441

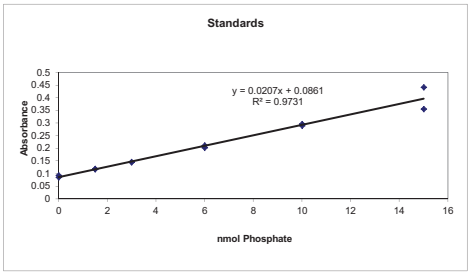

Sample	Mass weighed (g dry sediment)	Lab notes	Absorbance	Amount of Phosphate nmol	Biomass (cells/g dry weight sed) (Dobbs&Findlay 1993)	High Value (cells/g dry weight sed)	Average (cells/g dry weight sed)
George's Column Close	10.03		0.244	7.6280193	2.59E+07	1.52E+09	7.73E+08
George's Column Middle	10.03		0.229	6.9033816	2.34E+07	1.38E+09	7.00E+08
George's Column Far	10.03	Spilled_may not be representative	0.103	0.8164251	2.77E+06	1.63E+08	8.28E+07
1-3_1A	12.35		0.099	0.6231884	1.72E+06	1.01E+08	5.13E+07
1-3_1B	10.87		0.102	0.7681159	2.40E+06	1.41E+08	7.19E+07
1-3_2A	10.65		0.091	0.236715	7.56E+05	4.45E+07	2.26E+07
1-3_2B	13.19		0.06	-1.2608696	-3.25E+06	-1.91E+08	-9.72E+07
1-4_3A	14.62		0.093	0.3333333	7.75E+05	4.56E+07	2.32E+07
1-4_3B	11.13		0.081	-0.2463768	-7.53E+05	-4.43E+07	-2.25E+07
1-5_4A	10.04		0.075	-0.5362319	-1.82E+06	-1.07E+08	-5.43E+07
1-5_4B	10.1		0.121	1.6859903	5.68E+06	3.34E+08	1.70E+08
1-5_5A	13.66		0.072	-0.6811594	-1.70E+06	-9.97E+07	-5.07E+07
1-5_5B	12.7		0.046	-1.9371981	-5.19E+06	-3.05E+08	-1.55E+08
1-6_6A	10.31		0.073	-0.6328502	-2.09E+06	-1.23E+08	-6.24E+07
1-6_6B	10.78		0.069	-0.826087	-2.61E+06	-1.53E+08	-7.79E+07

250 ul of suspended sample used
Added 2mls of MeOH to all samples except M and C

Standards	Conc	Abs	Conc	Abs	
	0	0.093	0	0.078	
	1.5	0.113	1.5	0.184	not used for equation
	3	0.14	3	0.141	
	6	0.201	6	0.217	
	10	0.273	10	0.244	
	15	0.342	15	0.347	

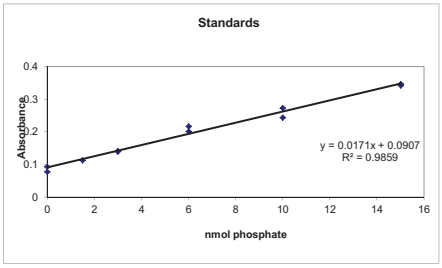

Sample	Mass weighed (g dry sediment)	Lab notes	Absorbance	Amount of Phosphate nmol*	Biomass (cells/g dry weight sed) (Dobbs&Findlay 1993)	High Value (cells/g dry weight sed)	Average (cells/g dry weight sed)
1-3_2B	10.87		0.175	1.6432749	5.14E+06	3.02E+08	1.54E+08
1-4_3B	11.13		0.139	0.9415205	2.88E+06	1.69E+08	8.60E+07
1-5_4A	10.04		0.096	0.1033138	3.50E+05	2.06E+07	1.05E+07
1-5_5A	13.66		0.092	0.0253411	6.31E+04	3.71E+06	1.89E+06
1-5_5B	12.7		0.093	0.0448343	1.20E+05	7.06E+06	3.59E+06
1-6_6A	10.31		0.093	0.0448343	1.48E+05	8.70E+06	4.42E+06
1-6_6B	10.78		0.091	0.005848	1.84E+04	1.08E+06	5.52E+05

750 ul of suspended sample used
* NOTE: Since 750 ul of sample was used, compared to 250 ul above, phosphate concentration is divided by 3.

Standards	Conc	Abs	Conc	Abs
	0	0.054	0	0.066
	1.5	0.076	1.5	0.078
	3	0.117	3	0.112
	6	0.168	6	0.161
	10	0.236	10	0.236
	15	0.334	15	0.317

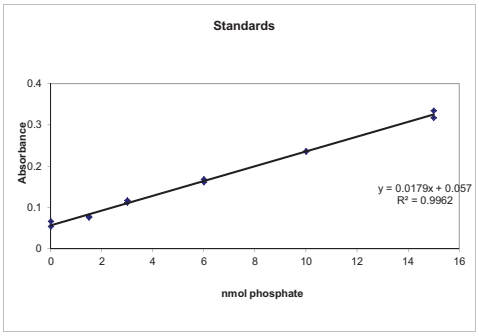

Sample	Mass weighed (g dry sediment)	Lab notes	Absorbance	Amount of Phosphate nmol*	Biomass (cells/g dry weight sed) (Dobbs&Findlay 1993)	High Value (cells/g dry weight sed)	Average (cells/g dry weight sed)
1-7_7A	12.48		0.129	1.0055866	2.74E+06	1.61E+08	8.19E+07
1-7_7B	12.64		0.157	1.396648	3.76E+06	2.21E+08	1.12E+08
2-2_0A	17.45		0.184	1.773743	3.46E+06	2.03E+08	1.03E+08
2-2_0B	17.02		0.171	1.5921788	3.18E+06	1.87E+08	9.51E+07
2-3_1A	12.23		0.18	1.7178771	4.78E+06	2.81E+08	1.43E+08
2-3-1B	12.25		0.063	0.0837989	2.33E+05	1.37E+07	6.96E+06
2-3_2A	10.95		0.051	-0.0837989	-2.60E+05	-1.53E+07	-7.78E+06
2-3_2B	10.37		0.15	1.2988827	4.26E+06	2.51E+08	1.27E+08
2-4_3A	14.31		0.049	-0.1117318	-2.65E+05	-1.56E+07	-7.94E+06
2-4_3B	16.69		0.058	0.0139665	2.85E+04	1.67E+06	8.51E+05
2-5_4A	16.99		0.067	0.1396648	2.79E+05	1.64E+07	8.36E+06
2-5_4B	16.8		0.073	0.2234637	4.52E+05	2.66E+07	1.35E+07
2-6_5A	16.99		0.064	0.0977654	1.96E+05	1.15E+07	5.85E+06
2-6_5B	16.1		0.062	0.0698324	1.47E+05	8.67E+06	4.41E+06
2-6_6A	14.08		0.074	0.2374302	5.73E+05	3.37E+07	1.71E+07
2-6_6B	16.26		0.069	0.1675978	3.50E+05	2.06E+07	1.05E+07
2-7_7A	17.4		0.08	0.3212291	6.28E+05	3.69E+07	1.88E+07
2-7_7B	17.48		0.065	0.1117318	2.17E+05	1.28E+07	6.50E+06
1-3_1R	16.05		0.051	-0.0837989	-1.78E+05	-1.04E+07	-5.31E+06
1-3_2R	17.5		0.065	0.1117318	2.17E+05	1.28E+07	6.49E+06
1-5_5R	16.64		0.101	0.6145251	1.26E+06	7.39E+07	3.76E+07
2-3_1R	15.68		0.142	1.1871508	2.57E+06	1.51E+08	7.70E+07
2-6_6R	15.86		0.089	0.4469274	9.58E+05	5.64E+07	2.87E+07
2-7_7R	15.04		0.152	1.3268156	3.00E+06	1.76E+08	8.97E+07

sampled larger rocks that wouldn't fit into test tubes

1000 ul of suspended sample used
* NOTE: Since 1000 ul of sample was used, compared to 250 ul above, phosphate concentration is divided by 4.

Depth	Elevation	Core 1 Dep	Biomass1	Biomass2	AverageBiom	Error high	Error Low
1-3_1	292.38	7.62	5.13E+07	7.19E+07	6.16E+07	1.03E+07	1.03E+07
1-3_2	291.8149	8.18515	2.26E+07	5.14E+06	1.39E+07	8.73E+06	8.73E+06
1-4_3	290.4369	9.5631	8.60E+07	1.54E+08	1.20E+08	3.39E+07	3.39E+07
1-5_4	289.332	10.668	1.05E+07	1.70E+08	9.01E+07	7.97E+07	7.97E+07
1-5_5	288.18	11.82	1.89E+06	3.59E+06	2.74E+06	8.52E+05	8.52E+05
1-6_6	286.9317	13.0683	4.42E+06	5.52E+05	2.49E+06	1.94E+06	1.94E+06
1-7_7	286.284	13.716	8.19E+07	1.12E+08	9.72E+07	1.52E+07	1.52E+07

Depth	Elevation	Core 2 Dep	Biomass1	Biomass2	AverageBiom	Error high	Error Low
2-2_0	293.4849	6.5151	1.03E+08	9.51E+07	9.93E+07	4.12E+06	4.12E+06
2-3_1	292.38	7.62	1.43E+08	6.96E+06	7.49E+07	6.79E+07	6.79E+07
2-3_2	291.97	8.03E+00	BDL	1.27E+08	1.27E+08	0.00E+00	#VALUE!
2-4_3	290.856	9.144	BDL	8.51E+05	8.51E+05	0.00E+00	#VALUE!
2-5_4	289.0145	10.9855	8.36E+06	1.35E+07	1.09E+07	2.58E+06	2.58E+06
2-6_5	287.808	12.192	5.85E+06	4.41E+06	5.13E+06	7.20E+05	7.20E+05
2-6_6	287.1298	12.87018	1.71E+07	1.88E+07	1.80E+07	8.13E+05	8.13E+05
2-7_7	285.7506	14.2494	1.88E+07	6.50E+06	1.26E+07	6.14E+06	6.14E+06

Appendix 27: Headspace Gas Analysis for Woodstock

Specie	Temperature °C	Henry's Law Constant	Reference
CO_2	10	5.33E-02	Eby 2004
CO_2	25	3.39E-02	Stumm and Morgan 1996
N_2O	25	2.57E-02	Stumm and Morgan 1996

Stumm, W. and Morgan, J.J. 1996. *Aquatic Chemistry, Chemical Equilibria and Rates in Natural Waters* , 3rd ed. New York: John Wiley & Sons, Inc.

Eby, G.N. 2004. Principles of environmental geochemistry. Pacific Grove, CA: Thomson-Brooks/Cole.

ML5 and ML7

Ambient Temp (°C) assuming 22.4

TCD 160C, ref flow 30.0 ml/min,inlet 120C, Haysep Q He gas, column flow = 20mL/min, oven temp = 90

Counter	Bottle ID	Sample	Date	Depth (m bgs)	pressure depth (Bar)	Inject (uL)	RT CO2 (min)	RT N2O (min)	Area CO2	Area N2O	% CO2	N2O (ppm)	Mass pre-filled Bottle (g)	Mass post-filled bottle (g)	Mass H2O (g)	H2O (mL)	Hdspace (mL)	Hdspace CO2 (ppm)	Aqueous CO2 (mg/L)	Headspace N2O (ppm)	Aqueous N2O (mg/L)	N2O (% Saturated)	Concentration CO2 (mol/L)	pCO2 (atm)	CO2 Solubility	CO2 (% Saturated)
New Curve 1% CO2, 1% N2O stds					July Std	100	0.883	1.051	96.05	109.6784																
						175	NA	1.052	NA	187.045																
						250	0.879	1.05	243.9421	222.35																
						500	0.862	1.109	559.6062	420.4																
					Sept Std	100	NA	1.055	NA	137.9509																
						175	NA	NA	NA	NA																
						250	0.889	1.053	215.8728	289.401																
						500	0.873	1.042	605.6828	687.8955																
						750	0.856	NA	1309.884	NA																
						1000	0.849	NA	1527.999	NA																

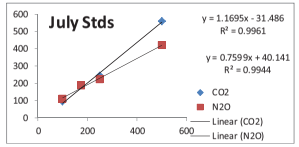

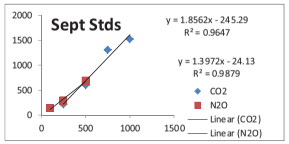

1	ML5-1	7/20/2011	3.40	1.33	250	0.869	NA	456.44	0.00	1.87	0.00	68.25	119.65	51.40	51.40	19.60	18710.82	605.70	0.00	0.00	0.00	0.014	0.26	2130.08	28.44
2	ML5-2	7/20/2011	5.10	1.49	250	0.879	NA	332.01	0.00	1.36	0.00	70.43	119.60	49.17	49.17	21.83	13610.00	442.26	0.00	0.00	0.00	0.010	0.19	2130.08	20.76
3	ML5-3	7/20/2011	6.80	1.66	250	0.877	NA	364.62	0.00	1.49	0.00	69.61	119.54	49.93	49.93	21.07	14947.13	485.06	0.00	0.00	0.00	0.011	0.21	2130.08	22.77
4	ML5-4	7/20/2011	8.50	1.82	250	0.88	NA	326.40	0.00	1.34	0.00	70.34	120.56	50.22	50.22	20.78	13380.32	434.00	0.00	0.00	0.00	0.010	0.19	2130.08	20.37
5	ML5-5	7/20/2011	10.20	1.99	250	0.873	NA	364.73	0.00	1.50	0.00	69.47	124.28	54.81	54.81	16.19	14951.57	481.49	0.00	0.00	0.00	0.011	0.21	2130.08	22.60
6	ML5-6	7/20/2011	11.90	2.15	250	0.876	NA	383.84	0.00	1.57	0.00	70.08	124.42	54.34	54.34	16.66	15734.81	507.05	0.00	0.00	0.00	0.012	0.22	2130.08	23.80
7	ML5-7	7/20/2011	13.60	2.32	250	0.878	NA	332.81	0.00	1.36	0.00	70.67	119.23	48.56	48.56	22.44	13642.94	443.81	0.00	0.00	0.00	0.010	0.19	2130.08	20.84
8	ML7-1	7/20/2011	5.52	1.53	250	0.878	NA	435.83	0.00	1.79	0.00	70.08	128.74	58.66	58.66	12.34	17866.14	572.36	0.00	0.00	0.00	0.013	0.24	2130.08	26.87
9	ML7-2	7/20/2011	7.22	1.70	250	0.875	NA	354.62	0.00	1.45	0.00	70.31	119.47	49.16	49.16	21.84	14536.98	472.39	0.00	0.00	0.00	0.011	0.20	2130.08	22.18
10	ML7-3	7/20/2011	8.92	1.86	250	0.878	NA	313.28	0.00	1.28	0.00	70.23	120.39	50.16	50.16	20.84	12842.52	416.60	0.00	0.00	0.00	0.009	0.18	2130.08	19.56
11	ML7-4	7/20/2011	10.62	2.03	250	0.874	NA	356.72	0.00	1.46	0.00	68.29	126.77	58.48	58.48	12.52	14623.33	468.58	0.00	0.00	0.00	0.011	0.20	2130.08	22.00
12	ML7-5	7/20/2011	12.32	2.19	250	0.878	NA	279.50	0.00	1.15	0.00	70.15	118.53	48.38	48.38	22.62	11457.70	372.85	0.00	0.00	0.00	0.008	0.16	2130.08	17.50
13	ML7-6	7/20/2011	14.02	2.36	250	0.877	NA	270.24	0.00	1.11	0.00	68.00	117.52	49.52	49.52	21.48	11078.23	359.76	0.00	0.00	0.00	0.008	0.15	2130.08	16.89
14	ML7-7	7/20/2011	15.72	2.52	250	0.877	NA	237.44	0.00	0.97	0.00	68.16	118.16	50.00	50.00	21.00	9733.59	315.84	0.00	0.00	0.00	0.007	0.13	2130.08	14.83
15	ML7-7 DUP	7/20/2011	15.72	2.52	250	0.877	NA	214.76	0.00	0.88	0.00	70.40	120.48	50.08	50.08	20.92	8803.65	285.62	0.00	0.00	0.00	0.006	0.12	2130.08	13.41
16	DI Blank	NA			250	0.873	NA	71.11	0.00	0.29	0.00	70.17	127.56	57.39	57.39	13.61	2915.12	93.54	0.00	0.00	0.00	0.002	0.04	2130.08	4.39
46	ML5-1	9/12/2011	3.40	1.33	250	0.88	NA	390.36	0.00	1.81	0.00	70.05	119.00	48.95	48.95	22.05	18083.09	587.84	0.00	0.00	0.00	0.013	0.25	2130.08	27.60
47	ML5-2	9/12/2011	5.10	1.49	250	0.88	NA	277.90	0.00	1.29	0.00	69.85	120.68	50.83	50.83	20.17	12873.12	417.12	0.00	0.00	0.00	0.009	0.18	2130.08	19.58
48	ML5-3	9/12/2011	6.80	1.66	250	0.88	1.05	326.04	6.52	1.51	225.25	70.83	119.35	48.52	48.52	22.48	15103.48	491.36	225.25	5.86	0.39	0.011	0.21	2130.08	23.07
49	ML5-4	9/12/2011	8.50	1.82	250	0.88	1.05	290.12	3.27	1.34	113.11	68.05	118.18	50.13	50.13	20.87	13439.42	435.98	113.11	2.93	0.20	0.010	0.19	2130.08	20.47
50	ML5-5	9/12/2011	10.20	1.99	250	0.88	1.05	328.10	1.93	1.52	66.60	69.63	119.25	49.62	49.62	21.38	15198.78	493.49	66.60	1.73	0.12	0.011	0.21	2130.08	23.17
51	ML5-6	9/12/2011	11.90	2.15	250	0.88	NA	271.33	0.00	1.26	0.00	70.28	119.50	49.22	49.22	21.78	12569.14	408.40	0.00	0.00	0.00	0.009	0.17	2130.08	19.17
52	ML5-7	9/12/2011	13.60	2.32	250	0.88	NA	243.80	0.00	1.13	0.00	70.16	121.15	50.99	50.99	20.01	11293.82	365.85	0.00	0.00	0.00	0.008	0.16	2130.08	17.18
53	ML7-1	9/12/2011	5.52	1.53	250	0.87	NA	422.92	0.00	1.96	0.00	69.49	119.62	50.13	50.13	20.87	19591.12	635.55	0.00	0.00	0.00	0.014	0.27	2130.08	29.84
60	ML7-2	9/12/2011	7.22	1.70	250	0.88	NA	323.71	0.00	1.50	0.00	69.85	119.36	49.51	49.51	21.49	14995.56	486.99	0.00	0.00	0.00	0.011	0.21	2130.08	22.86
19	ML7-3	9/12/2011	8.92	1.86	250	0.88	1.05	249.54	5.48	1.16	189.26	69.67	118.36	48.69	48.69	22.31	11559.66	375.95	189.26	4.92	0.33	0.009	0.16	2130.08	17.65
20	ML7-4	9/12/2011	10.62	2.03	250	0.88	NA	280.41	0.00	1.30	0.00	69.47	118.58	49.11	49.11	21.89	12989.42	422.13	0.00	0.00	0.00	0.010	0.18	2130.08	19.82
21	ML7-4 Dup	9/12/2011	10.62	2.03	250	0.87	1.05	300.07	4.21	1.39	145.54	70.43	119.95	49.52	49.52	21.48	13900.47	451.41	145.54	3.78	0.25	0.010	0.19	2130.08	21.19
22	ML7-5	9/12/2011	12.32	2.19	250	0.88	NA	304.57	0.00	1.41	0.00	70.18	119.19	49.00	49.00	22.00	14108.72	458.60	0.00	0.00	0.00	0.010	0.20	2130.08	21.53
23	ML7-6	9/12/2011	14.02	2.36	250	0.88	NA	221.10	0.00	1.02	0.00	70.27	119.33	49.07	49.07	21.93	10242.05	332.88	0.00	0.00	0.00	0.008	0.14	2130.08	15.63
24	ML7-7	9/12/2011	15.72	2.52	250	0.88	NA	246.89	0.00	1.14	0.00	70.48	120.99	50.51	50.51	20.49	11436.77	370.78	0.00	0.00	0.00	0.008	0.16	2130.08	17.41

Appendix 28: Tracer Breakthrough Curves for Column Experiments

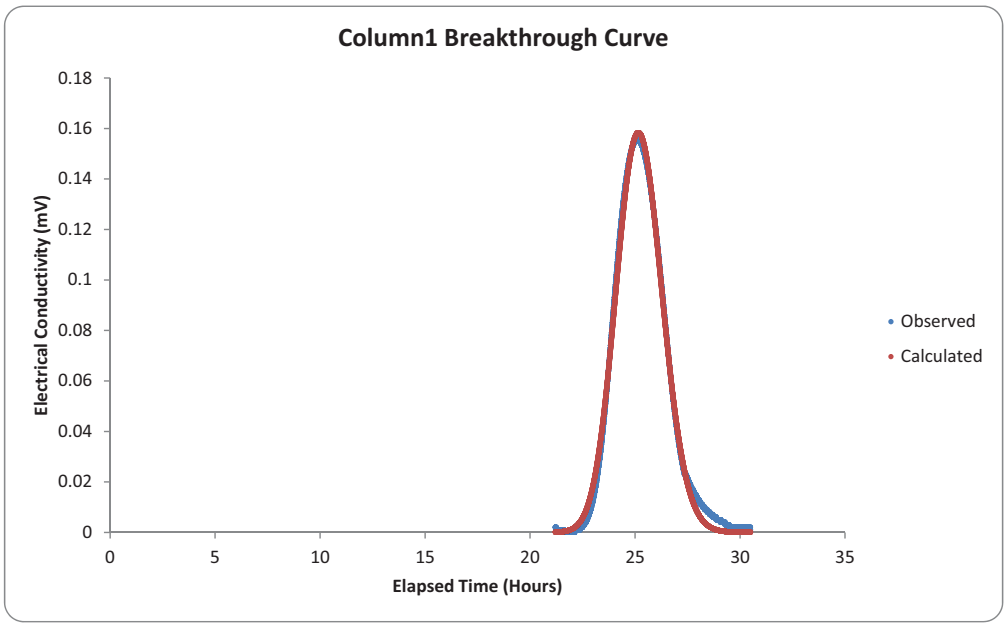

OPTIMIZED PARAMETER ESTIMATES

VELOCITY(cm/d)	37.13227
DISPERSIVITY (cm)	0.034203
PULSE WIDTH (cm)	0.013741
RF	1
Co (mV)	48.72846

RESDIUAL SUM OF SQUARES = 0.068164

INITIAL GUESSES AND INPUT OF PARAMETERS

		FIX
VELOCITY(cm/d)	50	
DISPERSIVITY (cm)	0.38	
PULSE WIDTH (cm)	0.01	
RF	1	Y
Co (mV)	2	
DISTANCE FROM SOURCE (cm)	39	Y
DIFFUSION COEFF (cm^2/sec)	0.000001	Y

95% CONFIDENCE INTERVALS FOR ESTIMATED PARAMETERS

Parameter	Low	Optimized	High
VELOCITY(cm/d)	37.13227	37.13227	37.13227
DISPERSIVITY(cm)	0.034203	0.034203	0.034203
PULSE WIDTH (cm)	0.013741	0.013741	0.013741
Co(mV)	48.72846	48.72846	48.72846

CRITICAL RSS VALUE = 0.068326

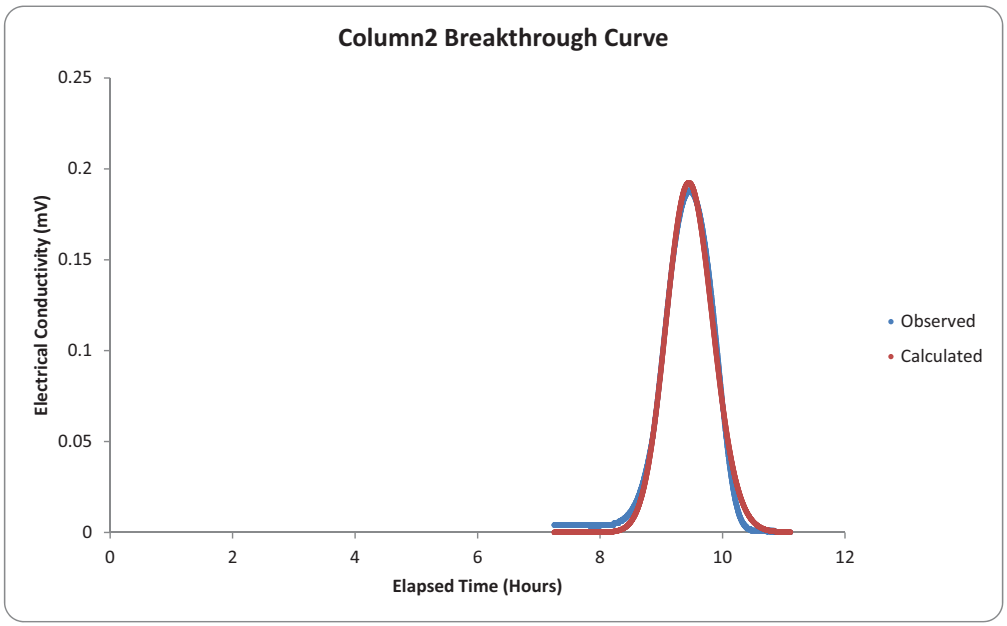

OPTIMIZED PARAMETER ESTIMATES

VELOCITY(cm/d)	100.1493
DISPERSIVITY (cm)	0.03058
PULSE WIDTH (cm)	0.074054
RF	1
Co (mV)	10.24813

RESDIUAL SUM OF SQUARES = 0.067274

INITIAL GUESSES AND INPUT OF PARAMETERS

		FIX
VELOCITY(cm/d)	100	
DISPERSIVITY (cm)	0.38	
PULSE WIDTH (cm)	0.01	
RF	1	Y
Co (mV)	2	
DISTANCE FROM SOURCE (cm)	39.5	Y
DIFFUSION COEFF (cm^2/sec)	0.000001	Y

95% CONFIDENCE INTERVALS FOR ESTIMATED PARAMETERS

Parameter	Low	Optimized	High
VELOCITY(cm/d)	100.1493	100.1493	100.1493
DISPERSIVITY(cm)	0.030274	0.03058	0.03058
PULSE WIDTH (cm)	0.074054	0.074054	0.074054
Co(mV)	10.24813	10.24813	10.24813

CRITICAL RSS VALUE = 0.067638

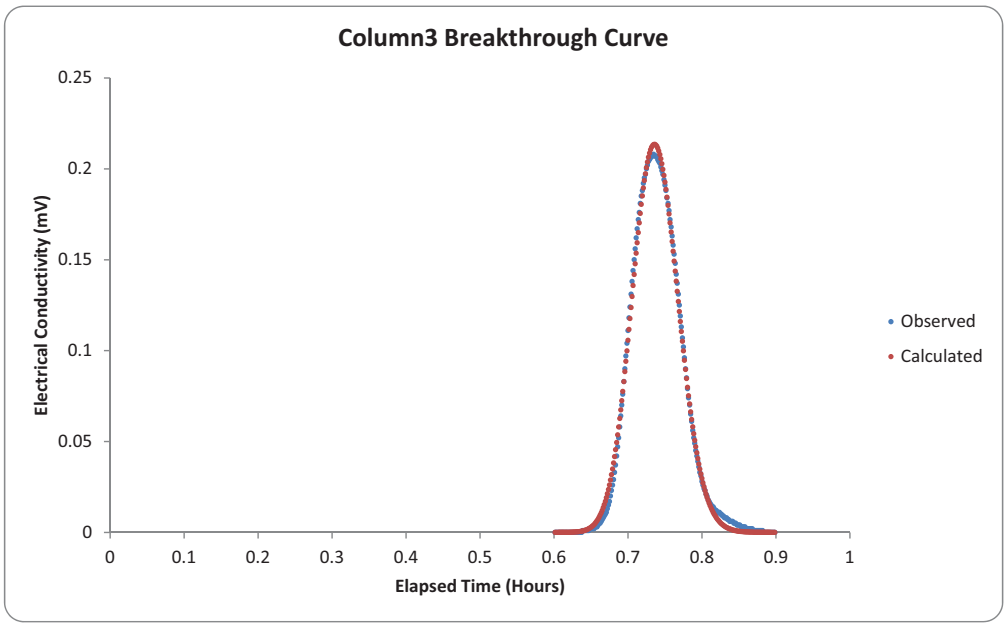

OPTIMIZED PARAMETER ESTIMATES

VELOCITY(cm/d)	1294.226
DISPERSIVITY (cm)	0.03513
PULSE WIDTH (cm)	0.065412
RF	1
Co (mV)	13.66983

RESDIUAL SUM OF SQUARES = 0.003072

INITIAL GUESSES AND INPUT OF PARAMETERS

		FIX
VELOCITY(cm/d)	1200	
DISPERSIVITY (cm)	0.38	
PULSE WIDTH (cm)	0.01	
RF	1	Y
Co (mV)	2	
DISTANCE FROM SOURCE (cm)	39.75	Y
DIFFUSION COEFF (cm^2/sec)	0.000001	Y

95% CONFIDENCE INTERVALS FOR ESTIMATED PARAMETERS

Parameter	Low	Optimized	High
VELOCITY(cm/d)	1294.226	1294.226	1294.226
DISPERSIVITY(cm)	0.034427	0.03513	0.035833
PULSE WIDTH (cm)	0.064758	0.065412	0.066066
Co(mV)	13.53313	13.66983	13.80653

CRITICAL RSS VALUE = 0.003287

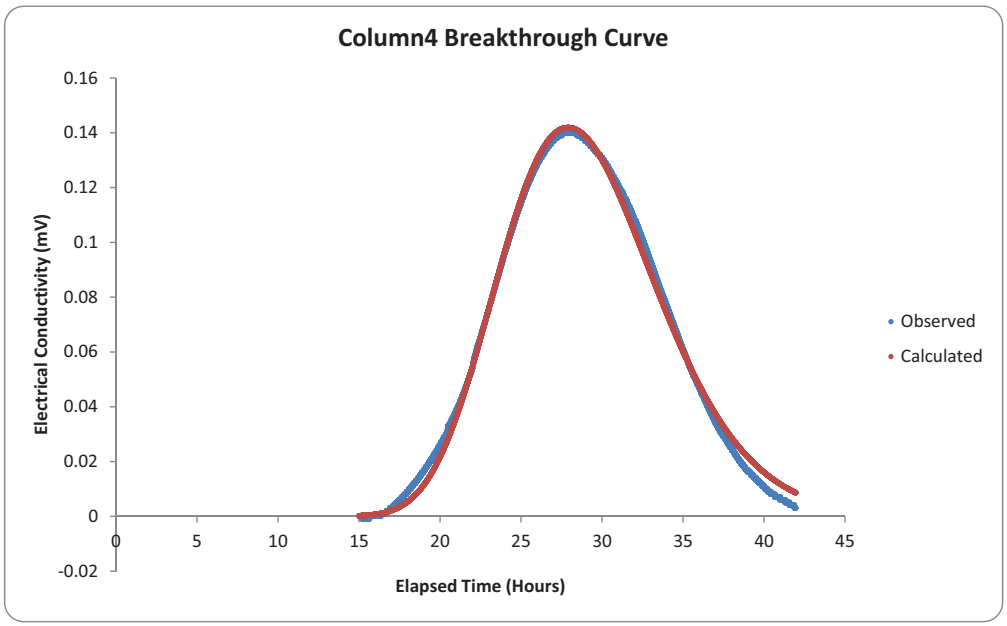

OPTIMIZED PARAMETER ESTIMATES

VELOCITY(cm/d)	32.12615
DISPERSIVITY (cm)	0.570264
PULSE WIDTH (cm)	0.271014
RF	1
Co (mV)	8.572143

RESDIUAL SUM OF SQUARES = 0.191752

INITIAL GUESSES AND INPUT OF PARAMETERS

		FIX
VELOCITY(cm/d)	50	
DISPERSIVITY (cm)	0.38	
PULSE WIDTH (cm)	0.01	
RF	1	Y
Co (mV)	2	
DISTANCE FROM SOURCE (cm)	38.5	Y
DIFFUSION COEFF (cm^2/sec)	0.000001	Y

95% CONFIDENCE INTERVALS FOR ESTIMATED PARAMETERS

Parameter	Low	Optimized	High
VELOCITY(cm/d)	32.12615	32.12615	32.12615
DISPERSIVITY(cm)	0.570264	0.570264	0.570264
PULSE WIDTH (cm)	0.271014	0.271014	0.271014
Co(mV)	8.572143	8.572143	8.572143

CRITICAL RSS VALUE = 0.191916

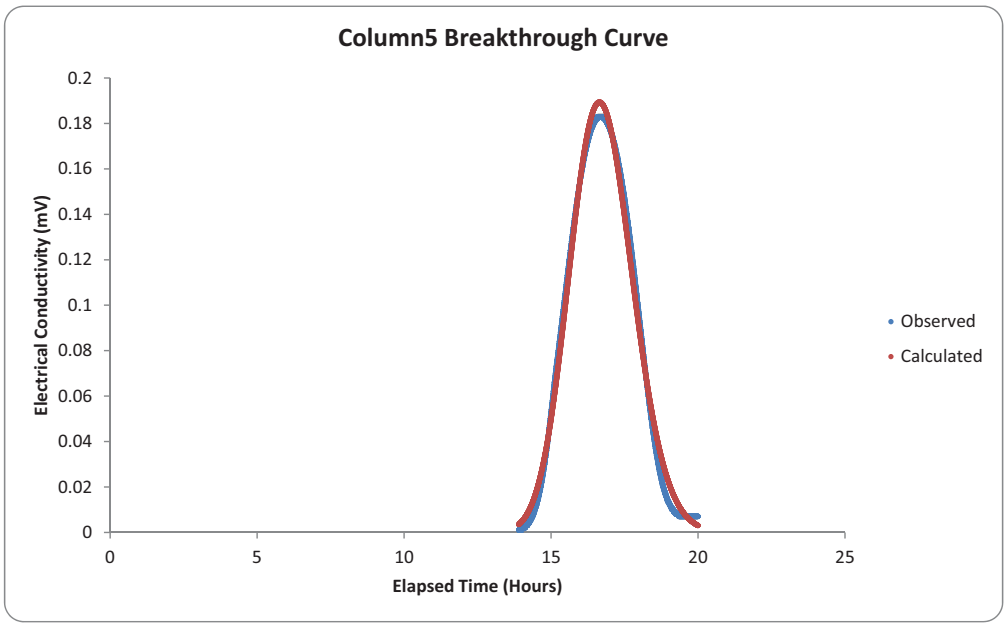

OPTIMIZED PARAMETER ESTIMATES

VELOCITY(cm/d)	54.20238
DISPERSIVITY (cm)	0.075206
PULSE WIDTH (cm)	0.096285
RF	1
Co (mV)	11.83568

RESDIUAL SUM OF SQUARES = 0.126299

INITIAL GUESSES AND INPUT OF PARAMETERS

		FIX
VELOCITY(cm/d)	50	
DISPERSIVITY (cm)	0.38	
PULSE WIDTH (cm)	0.01	
RF	1	Y
Co (mV)	2	
DISTANCE FROM SOURCE (cm)	37.75	Y
DIFFUSION COEFF (cm^2/sec)	0.000001	Y

95% CONFIDENCE INTERVALS FOR ESTIMATED PARAMETERS

Parameter	Low	Optimized	High
VELOCITY(cm/d)	54.20238	54.20238	54.20238
DISPERSIVITY(cm)	0.075206	0.075206	0.075206
PULSE WIDTH (cm)	0.096285	0.096285	0.096285
Co(mV)	11.83568	11.83568	11.83568

CRITICAL RSS VALUE = 0.126737

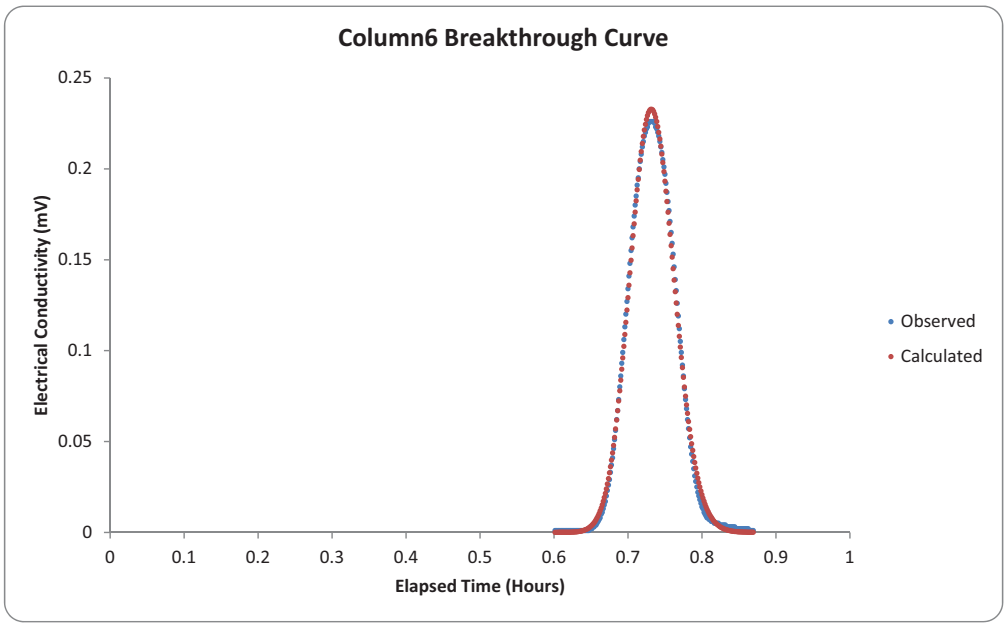

OPTIMIZED PARAMETER ESTIMATES

VELOCITY(cm/d)	1252.717
DISPERSIVITY (cm)	0.031547
PULSE WIDTH (cm)	0.071261
RF	1
Co (mV)	12.72018

RESDIUAL SUM OF SQUARES = 0.002551

INITIAL GUESSES AND INPUT OF PARAMETERS

		FIX
VELOCITY(cm/d)	1200	
DISPERSIVITY (cm)	0.38	
PULSE WIDTH (cm)	0.01	
RF	1	Y
Co (mV)	2	
DISTANCE FROM SOURCE (cm)	38.25	Y
DIFFUSION COEFF (cm^2/sec)	0.000001	Y

95% CONFIDENCE INTERVALS FOR ESTIMATED PARAMETERS

Parameter	Low	Optimized	High
VELOCITY(cm/d)	1252.717	1252.717	1252.717
DISPERSIVITY(cm)	0.030917	0.031547	0.032178
PULSE WIDTH (cm)	0.071261	0.071261	0.071973
Co(mV)	12.72018	12.72018	12.84738

CRITICAL RSS VALUE = 0.00275

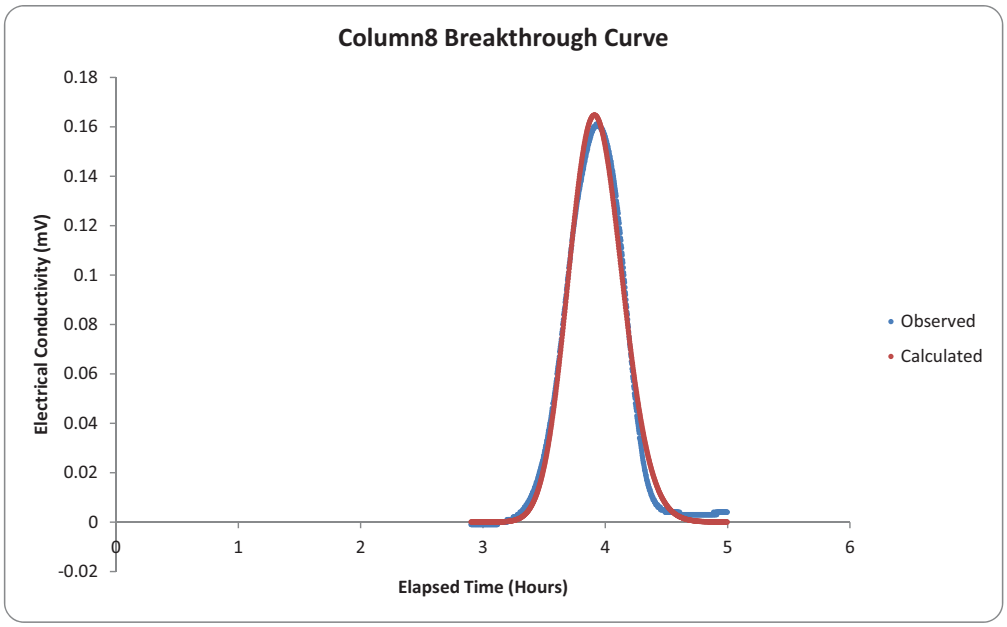

OPTIMIZED PARAMETER ESTIMATES

VELOCITY(cm/d)	237.9296
DISPERSIVITY (cm)	0.05991
PULSE WIDTH (cm)	0.065058
RF	1
Co (mV)	13.7179

RESDIUAL SUM OF SQUARES = 0.018802

INITIAL GUESSES AND INPUT OF PARAMETERS

		FIX
VELOCITY(cm/d)	200	
DISPERSIVITY (cm)	0.38	
PULSE WIDTH (cm)	0.01	
RF	1	Y
Co (mV)	2	
DISTANCE FROM SOURCE (cm)	38.9	Y
DIFFUSION COEFF (cm^2/sec)	0.000001	Y

95% CONFIDENCE INTERVALS FOR ESTIMATED PARAMETERS

Parameter	Low	Optimized	High
VELOCITY(cm/d)	237.9296	237.9296	237.9296
DISPERSIVITY(cm)	0.058712	0.05991	0.061108
PULSE WIDTH (cm)	0.064407	0.065058	0.065058
Co(mV)	13.58072	13.7179	13.7179

CRITICAL RSS VALUE = 0.019172

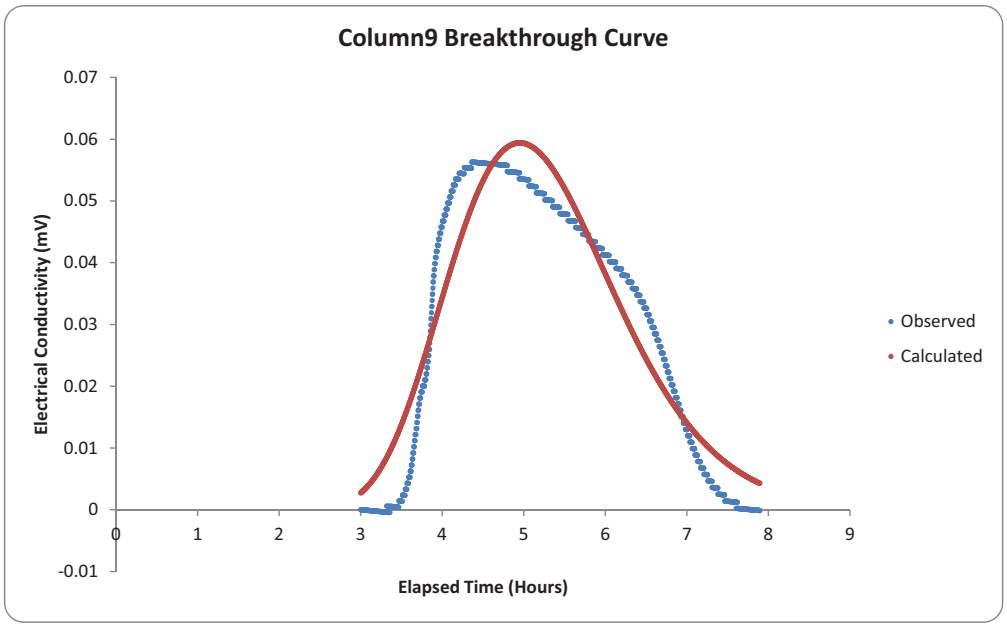

OPTIMIZED PARAMETER ESTIMATES

VELOCITY(cm/d)	180.8141
DISPERSIVITY (cm)	0.805347
PULSE WIDTH (cm)	0.076178
RF	1
Co (mV)	15.14844

RESDIUAL SUM OF SQUARES = 0.070765

INITIAL GUESSES AND INPUT OF PARAMETERS

		FIX
VELOCITY(cm/d)	200	
DISPERSIVITY (cm)	0.38	
PULSE WIDTH (cm)	0.01	
RF	1	Y
Co (mV)	2	
DISTANCE FROM SOURCE (cm)	38.9	Y
DIFFUSION COEFF (cm^2/sec)	0.000001	Y

95% CONFIDENCE INTERVALS FOR ESTIMATED PARAMETERS

Parameter	Low	Optimized	High
VELOCITY(cm/d)	180.8141	180.8141	180.8141
DISPERSIVITY(cm)	0.781186	0.805347	0.829507
PULSE WIDTH (cm)	0.075416	0.076178	0.07694
Co(mV)	14.99695	15.14844	15.29992

CRITICAL RSS VALUE = 0.071364

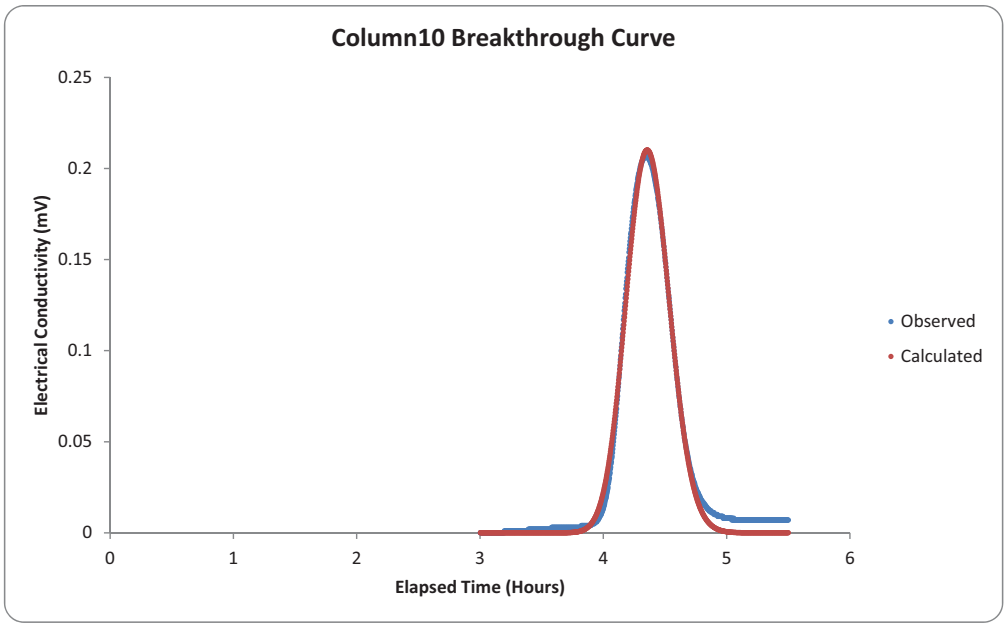

OPTIMIZED PARAMETER ESTIMATES

VELOCITY(cm/d)	207.9197
DISPERSIVITY (cm)	0.030122
PULSE WIDTH (cm)	0.056327
RF	1
Co (mV)	14.20303

RESDIUAL SUM OF SQUARES = 0.021451

INITIAL GUESSES AND INPUT OF PARAMETERS

		FIX
VELOCITY(cm/d)	200	
DISPERSIVITY (cm)	0.38	
PULSE WIDTH (cm)	0.01	
RF	1	Y
Co (mV)	2	
DISTANCE FROM SOURCE (cm)	37.8	Y
DIFFUSION COEFF (cm^2/sec)	0.000001	Y

95% CONFIDENCE INTERVALS FOR ESTIMATED PARAMETERS

Parameter	Low	Optimized	High
VELOCITY(cm/d)	207.9197	207.9197	207.9197
DISPERSIVITY(cm)	0.029821	0.030122	0.030725
PULSE WIDTH (cm)	0.056327	0.056327	0.056327
Co(mV)	14.20303	14.20303	14.20303

CRITICAL RSS VALUE = 0.021805

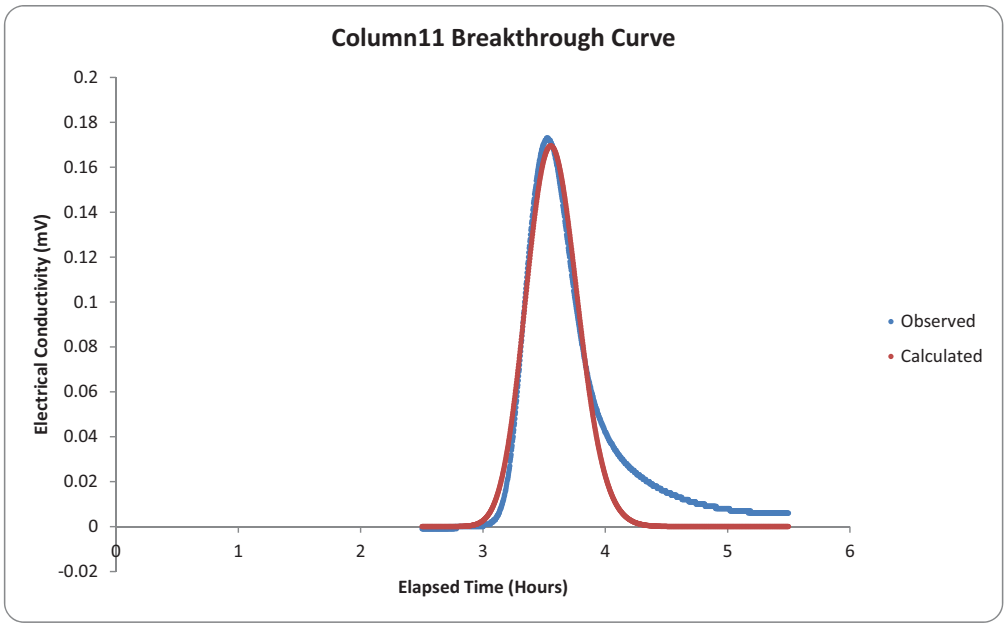

OPTIMIZED PARAMETER ESTIMATES

VELOCITY(cm/d)	255.0037
DISPERSIVITY (cm)	0.065347
PULSE WIDTH (cm)	0.060055
RF	1
Co (mV)	15.75414

RESDIUAL SUM OF SQUARES = 0.109966

INITIAL GUESSES AND INPUT OF PARAMETERS

		FIX
VELOCITY(cm/d)	200	
DISPERSIVITY (cm)	0.38	
PULSE WIDTH (cm)	0.01	
RF	1	Y
Co (mV)	2	
DISTANCE FROM SOURCE (cm)	37.9	Y
DIFFUSION COEFF (cm^2/sec)	0.000001	Y

95% CONFIDENCE INTERVALS FOR ESTIMATED PARAMETERS

Parameter	Low	Optimized	High
VELOCITY(cm/d)	255.0037	255.0037	255.0037
DISPERSIVITY(cm)	0.062734	0.065347	0.068615
PULSE WIDTH (cm)	0.058854	0.060055	0.060656
Co(mV)	15.43906	15.75414	15.91168

CRITICAL RSS VALUE = 0.111482

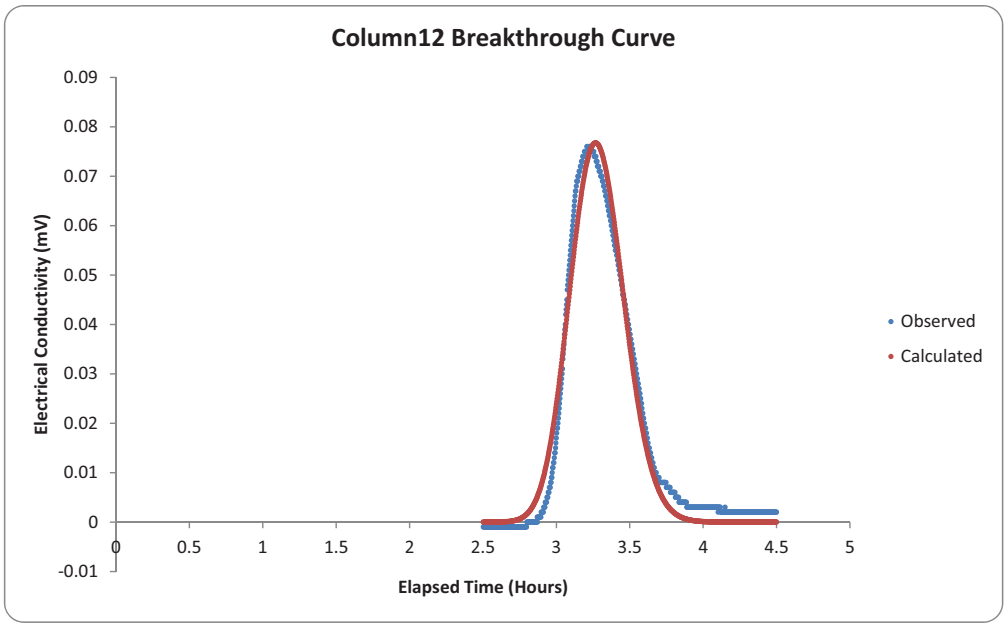

OPTIMIZED PARAMETER ESTIMATES

VELOCITY(cm/d)	281.1925
DISPERSIVITY (cm)	0.059334
PULSE WIDTH (cm)	0.037235
RF	1
Co (mV)	11.03855

RESDIUAL SUM OF SQUARES = 0.009443

INITIAL GUESSES AND INPUT OF PARAMETERS

		FIX
VELOCITY(cm/d)	200	
DISPERSIVITY (cm)	0.38	
PULSE WIDTH (cm)	0.01	
RF	1	Y
Co (mV)	2	
DISTANCE FROM SOURCE (cm)	38.4	Y
DIFFUSION COEFF (cm^2/sec)	0.000001	Y

95% CONFIDENCE INTERVALS FOR ESTIMATED PARAMETERS

Parameter	Low	Optimized	High
VELOCITY(cm/d)	281.1925	281.1925	281.1925
DISPERSIVITY(cm)	0.057554	0.059334	0.061708
PULSE WIDTH (cm)	0.036862	0.037235	0.037607
Co(mV)	10.92816	11.03855	11.14893

CRITICAL RSS VALUE = 0.009641

Appendix 29: Transducer Calibration for Column Experiments

V (cm/d)	5.320918	267.3761	542.7336	1436.648	2902.029	#DIV/0!
K (cm/min)	0.036086	1.215902	1.443922	1.503628	1.598519	#DIV/0!
Q (mL/min)	0.005556	0.279167	0.566667	1.5	3.03	0
q (cm/min)	0.001145	0.05756	0.116838	0.309278	0.624742	0
Head Drop	1.73	2.58	4.41	11.21	21.3	0
i	0.031743	0.047339	0.080917	0.205688	0.390826	0
Average mV	0.206549	1.175841	1.784739	3.691188	6.82546	0.457249
	mV Response	mV Response	mV Response	mV Response	mV Response	mV Response
	0.115	1.317	1.815	3.637	6.821	0.464
	0.122	1.26	1.914	3.678	6.784	0.467
	0.122	1.212	1.768	3.719	6.855	0.464
	0.119	1.185	1.768	3.644	6.845	0.454
	0.122	1.182	1.775	3.702	6.821	0.461
	0.119	1.179	1.798	3.637	6.79	0.454
	0.122	1.175	1.822	3.671	6.855	0.464
	0.122	1.179	1.853	3.725	6.848	0.461
	0.115	1.185	1.853	3.644	6.855	0.457
	0.122	1.199	1.754	3.698	6.841	0.461
	0.122	1.216	1.771	3.658	6.814	0.461
	0.119	1.304	1.795	3.671	6.78	0.457
	0.122	1.223	1.812	3.715	6.858	0.464
	0.125	1.219	1.849	3.644	6.851	0.457
	0.125	1.209	1.859	3.698	6.824	0.454
	0.122	1.202	1.758	3.705	6.777	0.464
	0.125	1.189	1.765	3.658	6.841	0.457
	0.122	1.189	1.785	3.722	6.858	0.461
	0.129	1.185	1.809	3.641	6.828	0.461
	0.129	1.189	1.839	3.912	6.787	0.457
	0.125	1.206	1.859	3.614	6.838	0.461
	0.122	1.223	1.758	3.695	6.851	0.464
	0.132	1.219	1.761	3.691	6.831	0.461
	0.135	1.199	1.778	3.647	6.801	0.467
	0.132	1.182	1.802	3.681	6.814	0.461
	0.135	1.175	1.829	3.715	6.858	0.454
	0.132	1.172	1.856	3.658	6.834	0.461
	0.132	1.185	1.788	3.708	6.804	0.464
	0.135	1.179	1.758	3.634	6.794	0.457
	0.139	1.185	1.775	3.688	6.861	0.461
	0.135	1.199	1.798	3.722	6.845	0.454
	0.149	1.216	1.829	3.647	6.814	0.461
	0.149	1.223	1.846	3.708	6.773	0.461
	0.146	1.199	1.853	3.631	6.858	0.461
	0.152	1.182	1.758	3.678	6.838	0.454
	0.163	1.172	1.768	3.722	6.814	0.457
	0.149	1.175	1.785	3.651	6.787	0.457
	0.149	1.182	1.819	3.698	6.851	0.457
	0.139	1.189	1.842	3.634	6.851	0.464
	0.139	1.189	1.856	3.671	6.821	0.457
	0.142	1.202	1.761	3.722	6.78	0.454
	0.135	1.223	1.765	3.647	6.851	0.464
	0.129	1.212	1.785	3.705	6.865	0.461
	0.129	1.196	1.812	3.644	6.824	0.464
	0.132	1.182	1.836	3.668	6.79	0.461
	0.129	1.179	1.853	3.719	6.834	0.461
	0.125	1.175	1.765	3.641	6.861	0.464
	0.129	1.179	1.758	3.695	6.831	0.464
	0.125	1.185	1.781	3.698	6.807	0.464
	0.125	1.199	1.805	3.664	6.824	0.464
	0.125	1.209	1.832	3.722	6.858	0.464
	0.115	1.301	1.856	3.641	6.834	0.457

Calculated Field

Data From Calibration Graph

K (cm/min)	1.5621	Target initial velocity (cm/d)	50
A (cm2)	4.85	Transducer Voltage to Reach it	0.341893 mV
ΔL (cm)	54.5	Expected Q (mL/min)	0.052205
n	0.31	Manifold Head (cm)	85.18
m	0.3102	Effleunt Head	84.80446
b	0.2254		

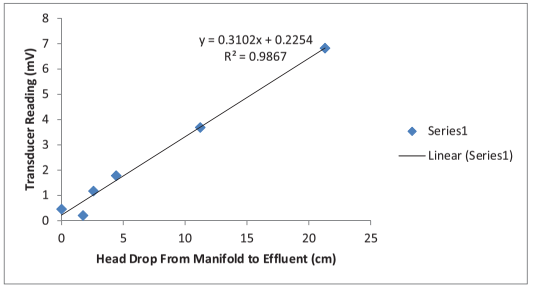

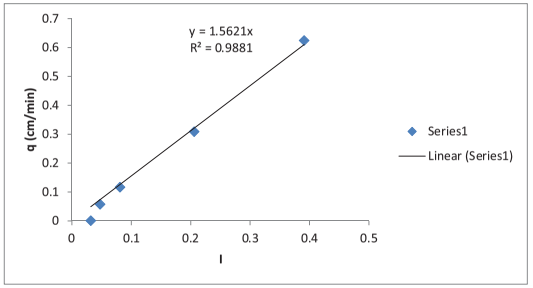

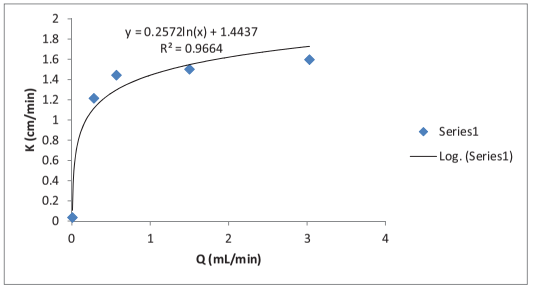

Effective pre bio K (cm/min)	0.684297
Q (mL/min) needed for desired V	0.052205

V (cm/d)	15.39519	247.4227	478.3505	1253.608	2592.99	#DIV/0!
K (cm/min)	0.102894	1.227822	1.32955	1.419671	1.553443	#DIV/0!
Q (mL/min)	0.015556	0.25	0.483333	1.266667	2.62	0
q (cm/min)	0.003207	0.051546	0.099656	0.261168	0.540206	0
Head Drop	1.73	2.33	4.16	10.21	19.3	0
i	0.031171	0.041982	0.074955	0.183964	0.347748	0
Average mV	-0.03475	0.495844	0.991079	2.732646	5.520373	-0.11445
	mV Response	mV Response	mV Response	mV Response	mV Response	mV Response
	-0.014	0.461	0.884	2.747	5.507	-0.112
	-0.017	0.464	1.074	2.743	5.473	-0.119
	-0.014	0.478	0.975	2.682	5.5	-0.112
	-0.014	0.501	1.087	2.74	5.591	-0.115
	-0.014	0.518	0.969	2.747	5.558	-0.119
	-0.014	0.528	0.969	2.686	5.514	-0.112
	-0.007	0.559	0.965	2.747	5.493	-0.119
	-0.007	0.511	0.979	2.743	5.473	-0.119
	-0.01	0.457	1.023	2.675	5.564	-0.119
	-0.014	0.444	1.08	2.747	5.581	-0.115
	-0.003	0.447	0.969	2.743	5.537	-0.112
	-0.003	0.444	0.962	2.682	5.5	-0.112
	-0.007	0.454	0.962	2.747	5.48	-0.112
	-0.003	0.467	0.986	2.747	5.476	-0.119
	-0.007	0.484	1.03	2.669	5.585	-0.112
	0	0.501	1.091	2.753	5.561	-0.119
	0.003	0.525	0.962	2.736	5.524	-0.108
	0	0.539	0.958	2.696	5.49	-0.115
	-0.003	0.569	0.969	2.747	5.473	-0.115
	0.003	0.488	0.986	2.804	5.531	-0.119
	0	0.444	1.036	2.682	5.581	-0.112
	-0.007	0.44	1.033	2.75	5.544	-0.115
	0	0.444	0.958	2.743	5.51	-0.112
	0.007	0.454	0.958	2.669	5.483	-0.115
	0	0.457	0.969	2.75	5.476	-0.119
	-0.003	0.481	0.996	2.733	5.585	-0.115
	0	0.494	1.043	2.726	5.564	-0.115
	-0.003	0.511	1.013	2.75	5.524	-0.112
	0	0.532	0.955	2.73	5.497	-0.112
	0	0.555	0.962	2.723	5.476	-0.119
	0	0.569	0.975	2.74	5.5	-0.112
	-0.01	0.471	1.003	2.716	5.591	-0.108
	0.003	0.444	1.05	2.73	5.547	-0.115
	0	0.444	1.009	2.75	5.493	-0.108
	0	0.45	0.958	2.692	5.493	-0.115
	0.003	0.461	0.958	2.736	5.47	-0.115
	0	0.471	0.975	2.74	5.568	-0.112
	-0.003	0.481	1.009	2.703	5.578	-0.108
	-0.003	0.505	1.06	2.74	5.527	-0.119
	0.007	0.518	0.992	2.747	5.493	-0.112
	-0.003	0.535	0.955	2.682	5.48	-0.115
	-0.003	0.559	0.962	2.743	5.483	-0.112
	-0.003	0.518	0.979	2.743	5.591	-0.112
	-0.003	0.454	1.016	2.696	5.558	-0.112
	-0.007	0.447	1.067	2.743	5.517	-0.122
	0	0.45	0.982	2.747	5.49	-0.108
	0	0.454	0.955	2.682	5.473	-0.112
	0	0.461	0.958	2.736	5.554	-0.108
	-0.01	0.478	0.986	2.74	5.578	-0.112
	-0.003	0.488	1.019	2.689	5.537	-0.115
	-0.007	0.501	1.087	2.736	5.5	-0.115
	-0.007	0.528	0.975	2.736	5.483	-0.112

Calculated Field

Data From Calibration Graph

K (cm/min)	1.5058	Target initial velocity (cm/d)	100
A (cm2)	4.85	Transducer Voltage to Reach it	-0.05336 mV
ΔL (cm)	55.5	Expected Q (mL/min)	0.101042
n	0.3	Manifold Head (cm)	85.18
m	0.2992	Effleunt Head	84.41214
b	-0.2831		

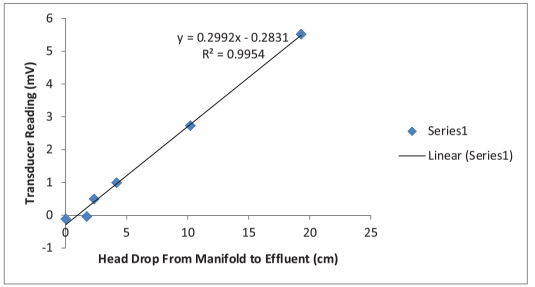

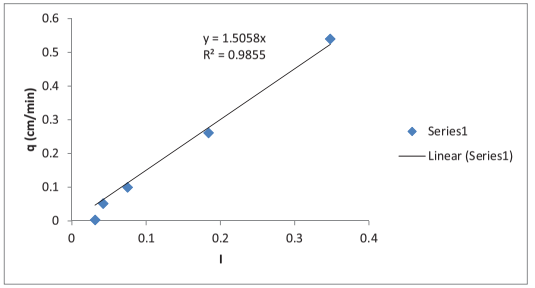

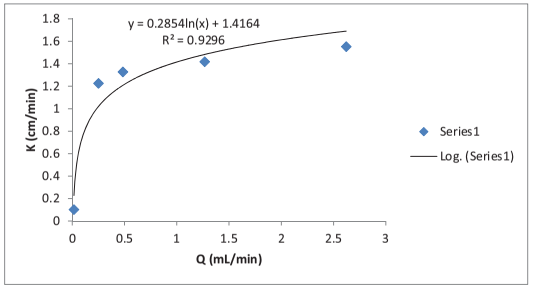

Effective pre bio K (cm/min)	0.7622
Q (mL/min) needed for desired V	0.101042

V (cm/d)	197.4383	31.49016	269.9157	1139.644	2357.263	#DIV/0!
K (cm/min)	0.66717	0.367507	1.076602	1.406882	1.519762	#DIV/0!
Q (mL/min)	0.219444	0.035	0.3	1.266667	2.62	0
q (cm/min)	0.045246	0.007216	0.061856	0.261168	0.540206	0
Head Drop	3.73	1.08	3.16	10.21	19.55	0
i	0.067818	0.019636	0.057455	0.185636	0.355455	0
Average mV	0.821826	0.403378	0.998086	3.073078	5.883292	0.256532
	mV Response	mV Response	mV Response	mV Response	mV Response	mV Response
	0.83	0.42	0.975	3.048	5.866	0.247
	0.84	0.413	1.043	3.072	5.869	0.251
	0.918	0.413	0.992	3.051	5.869	0.247
	0.877	0.42	1.009	3.051	5.913	0.254
	0.85	0.417	1.013	3.058	5.906	0.254
	0.826	0.423	1.023	3.041	5.879	0.244
	0.823	0.423	1.023	3.15	5.859	0.251
	0.806	0.42	1.06	3.038	5.862	0.251
	0.803	0.434	1.033	3.078	5.873	0.251
	0.813	0.434	1.016	3.048	5.957	0.251
	0.809	0.467	1.016	3.048	5.879	0.254
	0.813	0.518	1.009	3.062	5.869	0.244
	0.82	0.522	1.009	3.045	5.859	0.254
	0.823	0.522	1.009	3.126	5.859	0.254
	0.837	0.528	1.016	3.048	5.937	0.254
	0.921	0.481	1.023	3.062	5.903	0.251
	0.877	0.471	1.06	3.051	5.876	0.247
	0.85	0.461	1.036	3.051	5.862	0.244
	0.83	0.461	1.013	3.065	5.856	0.261
	0.816	0.444	1.006	2.984	5.869	0.247
	0.806	0.444	1.003	3.119	5.94	0.254
	0.809	0.44	1.003	3.031	5.876	0.254
	0.806	0.434	1.016	3.065	5.859	0.247
	0.806	0.427	1.023	3.058	5.856	0.247
	0.809	0.434	1.03	3.051	5.873	0.257
	0.82	0.423	1.057	3.075	5.954	0.247
	0.823	0.42	1.033	3.038	5.896	0.251
	0.837	0.42	1.016	3.078	5.876	0.251
	0.908	0.42	1.016	3.034	5.876	0.247
	0.87	0.41	1.013	3.058	5.859	0.254
	0.843	0.41	1.003	3.065	5.886	0.254
	0.826	0.413	1.009	3.048	5.917	0.251
	0.816	0.406	1.016	3.136	5.883	0.251
	0.806	0.413	1.023	3.041	5.869	0.251
	0.803	0.413	1.06	3.068	5.835	0.254
	0.799	0.406	1.047	3.048	5.862	0.261
	0.799	0.403	1.019	3.051	5.967	0.251
	0.813	0.41	1.009	3.068	5.889	0.247
	0.813	0.4	1.003	3.048	5.866	0.251
	0.813	0.4	1.003	3.146	5.866	0.257
	0.83	0.403	1.013	3.038	5.862	0.251
	0.908	0.406	1.023	3.062	5.903	0.254
	0.921	0.396	1.03	3.048	5.903	0.251
	0.85	0.396	1.063	3.051	5.879	0.257
	0.833	0.41	1.033	3.072	5.862	0.261
	0.809	0.403	1.016	3.048	5.859	0.251
	0.803	0.406	1.009	3.099	5.869	0.254
	0.806	0.403	1.013	3.041	5.95	0.254
	0.796	0.4	1.009	3.065	5.889	0.251
	0.803	0.403	1.016	3.051	5.869	0.257
	0.806	0.406	1.016	3.051	5.862	0.251
	0.813	0.4	1.026	3.092	5.869	0.251

Calculated Field

Data From Calibration Graph

K (cm/min)	1.4623	Target initial velocity (cm/d)	1000
A (cm2)	4.85	Transducer Voltage to Reach it	2.595322 mV
ΔL (cm)	55	Expected Q (mL/min)	1.111458
n	0.33	Manifold Head (cm)	85.18
m	0.2958	Effleunt Head	76.56059
b	0.0457		

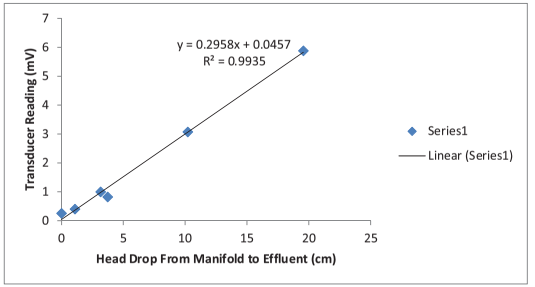

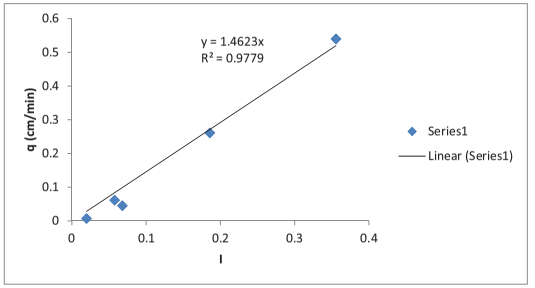

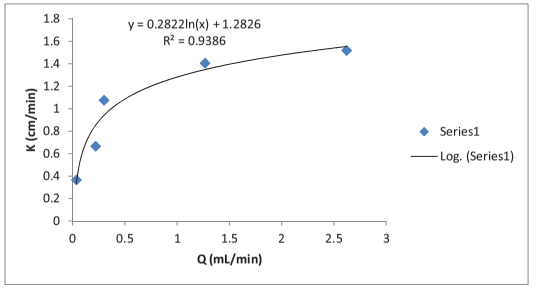

Effective pre bio K (cm/min)	1.312421
Q (mL/min) needed for desired V	1.111458

V (cm/d)	32.04713	240.3535	395.8763	1866.274	3350.81	#DIV/0!
K (cm/min)	0.375915	1.18331	1.46709	1.748525	1.708278	#DIV/0!
Q (mL/min)	0.037778	0.283333	0.466667	2.2	3.95	0
q (cm/min)	0.007789	0.058419	0.09622	0.453608	0.814433	0
Head Drop	1.15	2.74	3.64	14.398	26.46	0
i	0.020721	0.049369	0.065586	0.259423	0.476757	0
Average mV	0.101626	0.624547	0.976714	4.350403	7.90599	0.044502
	mV Response	mV Response	mV Response	mV Response	mV Response	mV Response
	0.125	0.61	0.972	4.379	7.891	0.047
	0.132	0.61	0.884	4.328	7.878	0.044
	0.122	0.613	1.074	4.335	7.881	0.044
	0.122	0.62	0.992	4.372	7.918	0.051
	0.129	0.647	0.989	4.321	7.949	0.037
	0.129	0.66	0.969	4.328	7.955	0.047
	0.122	0.63	0.972	4.372	7.878	0.041
	0.122	0.623	0.979	4.328	7.878	0.037
	0.119	0.606	0.992	4.338	7.898	0.044
	0.115	0.599	1.057	4.376	7.935	0.044
	0.125	0.606	1.003	4.332	7.972	0.044
	0.119	0.606	0.979	4.328	7.884	0.044
	0.112	0.606	0.979	4.372	7.874	0.051
	0.108	0.616	0.979	4.335	8.17	0.051
	0.119	0.627	0.982	4.335	7.878	0.051
	0.112	0.637	0.996	4.362	7.932	0.041
	0.115	0.664	1.063	4.332	7.972	0.041
	0.119	0.627	0.996	4.328	7.891	0.047
	0.108	0.633	0.975	4.365	7.881	0.044
	0.108	0.583	0.969	4.223	7.881	0.044
	0.108	0.599	0.972	4.359	7.911	0.044
	0.112	0.599	0.986	4.359	7.955	0.037
	0.115	0.613	0.996	4.328	7.942	0.044
	0.112	0.61	1.033	4.345	7.878	0.041
	0.102	0.62	0.999	4.359	7.488	0.044
	0.105	0.62	0.972	4.325	7.935	0.044
	0.112	0.644	0.969	4.345	7.925	0.047
	0.108	0.66	0.975	4.362	7.966	0.037
	0.108	0.637	0.989	4.328	7.915	0.054
	0.112	0.616	0.992	4.355	7.888	0.047
	0.108	0.61	1.043	4.362	7.881	0.041
	0.115	0.603	0.989	4.321	7.905	0.047
	0.119	0.606	0.975	4.359	7.952	0.047
	0.115	0.613	0.972	4.359	7.742	0.041
	0.115	0.613	0.979	4.325	7.898	0.047
	0.102	0.62	0.979	4.365	7.888	0.041
	0.108	0.627	1.003	4.355	7.884	0.047
	0.115	0.644	1.03	4.328	7.925	0.047
	0.115	0.65	0.986	4.376	7.979	0.044
	0.108	0.633	0.982	4.355	7.911	0.047
	0.112	0.613	0.972	4.318	7.888	0.051
	0.108	0.606	0.982	4.386	7.881	0.037
	0.112	0.603	0.986	4.352	7.905	0.044
	0.115	0.603	0.996	4.325	7.952	0.047
	0.112	0.61	1.023	4.393	7.972	0.044
	0.112	0.62	0.999	4.348	7.884	0.047
	0.115	0.623	0.979	4.315	7.874	0.041
	0.115	0.627	0.972	4.403	7.891	0.041
	0.115	0.647	0.979	4.345	7.928	0.044
	0.119	0.657	0.989	4.321	7.972	0.047
	0.108	0.633	1.003	4.409	7.918	0.044
	0.119	0.61	1.023	4.355	7.894	0.047

Calculated Field

Data From Calibration Graph

K (cm/min)	1.7077	Target initial velocity (cm/d)	50	
A (cm2)	4.85	Transducer Voltage to Reach it	-0.00239	mV
ΔL (cm)	55.5	Expected Q (mL/min)	0.058941	
n	0.35	Manifold Head (cm)	85.217	
m	0.3046	Effleunt Head	84.82204	
b	-0.1227			

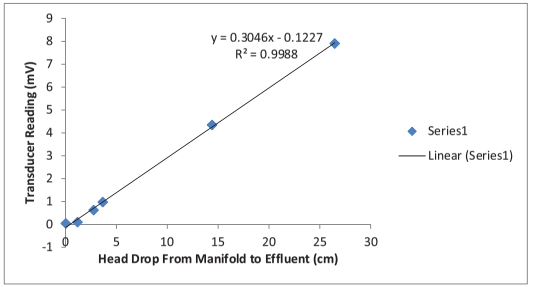

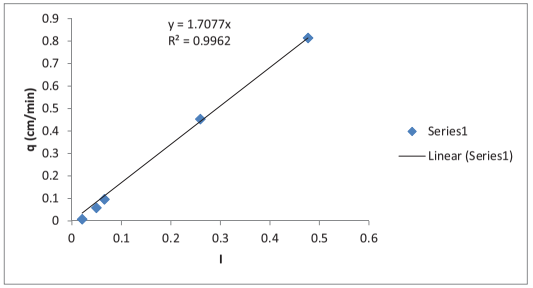

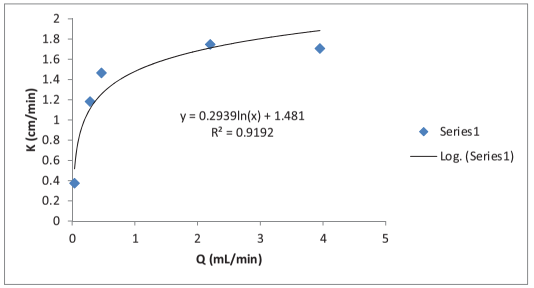

Effective pre bio K (cm/min)	0.648905
Q (mL/min) needed for desired V	0.058941

V (cm/d)	5.891016	176.7305	441.8262	1431.517	2735.788	#DIV/0!
K (cm/min)	0.096925	0.689794	1.141325	1.234818	1.302659	#DIV/0!
Q (mL/min)	0.005556	0.166667	0.416667	1.35	2.58	0
q (cm/min)	0.001145	0.034364	0.085911	0.278351	0.531959	0
Head Drop	0.65	2.74	4.14	12.398	22.46	0
i	0.011818	0.049818	0.075273	0.225418	0.408364	0
Average mV	0.163455	0.63789	1.261226	3.7026	6.777117	0.092155
	mV Response	mV Response	mV Response	mV Response	mV Response	mV Response
	0.122	0.63	1.101	3.722	6.77	0.085
	0.119	0.633	1.236	3.668	6.756	0.091
	0.112	0.64	1.287	3.725	6.845	0.088
	0.119	0.644	1.294	3.691	6.797	0.081
	0.119	0.657	1.304	3.702	6.777	0.088
	0.119	0.66	1.304	3.725	6.763	0.088
	0.119	0.681	1.287	3.678	6.767	0.085
	0.119	0.704	1.267	3.722	6.841	0.091
	0.115	0.674	1.229	3.668	6.821	0.081
	0.119	0.66	1.25	3.712	6.872	0.085
	0.115	0.647	1.28	3.705	6.811	0.091
	0.112	0.637	1.294	3.695	6.821	0.088
	0.115	0.633	1.311	3.719	6.784	0.091
	0.112	0.63	1.334	3.671	6.811	0.091
	0.115	0.633	1.277	3.725	6.763	0.081
	0.122	0.637	1.263	3.691	6.804	0.088
	0.122	0.63	1.223	3.702	6.807	0.088
	0.112	0.62	1.257	3.712	6.787	0.088
	0.115	0.65	1.287	3.681	6.767	0.085
	0.115	0.62	1.304	3.807	6.753	0.088
	0.115	0.65	1.311	3.539	6.804	0.085
	0.119	0.664	1.301	3.742	6.807	0.095
	0.115	0.701	1.284	3.698	6.777	0.091
	0.108	0.691	1.253	3.698	6.763	0.085
	0.119	0.667	1.226	3.719	6.801	0.088
	0.119	0.65	1.26	3.668	6.801	0.088
	0.115	0.644	1.301	3.725	6.794	0.091
	0.119	0.64	1.301	3.681	6.773	0.095
	0.112	0.633	1.307	3.719	6.75	0.088
	0.112	0.627	1.301	3.702	6.756	0.085
	0.119	0.637	1.28	3.688	6.838	0.088
	0.122	0.64	1.25	3.712	6.801	0.085
	0.119	0.647	1.236	3.668	6.787	0.091
	0.119	0.637	1.267	3.729	6.702	0.095
	0.112	0.644	1.294	3.702	6.733	0.085
	0.112	0.65	1.307	3.705	6.817	0.088
	0.119	0.657	1.307	3.722	6.811	0.088
	0.108	0.674	1.301	3.675	6.773	0.088
	0.115	0.711	1.287	3.719	6.76	0.095
	0.112	0.684	1.243	3.671	6.753	0.081
	0.119	0.657	1.233	3.719	6.828	0.085
	0.115	0.647	1.273	3.708	6.794	0.091
	0.119	0.64	1.29	3.702	6.784	0.095
	0.112	0.64	1.304	3.715	6.76	0.091
	0.115	0.633	1.307	3.664	6.753	0.088
	0.119	0.633	1.304	3.719	6.834	0.088
	0.108	0.627	1.28	3.681	6.797	0.085
	0.119	0.637	1.233	3.715	6.777	0.091
	0.115	0.637	1.233	3.712	6.753	0.085
	0.105	0.64	1.277	3.688	6.763	0.085
	0.115	0.647	1.301	3.719	6.841	0.091
	0.119	0.654	1.311	3.664	6.794	0.085

Calculated Field

Data From Calibration Graph

K (cm/min)	1.2759	Target initial velocity (cm/d)	100
A (cm2)	4.85	Transducer Voltage to Reach it	0.224717 mV
ΔL (cm)	55	Expected Q (mL/min)	0.094306
n	0.28	Manifold Head (cm)	85.217
m	0.3021	Effleunt Head	84.37881
b	-0.0285		

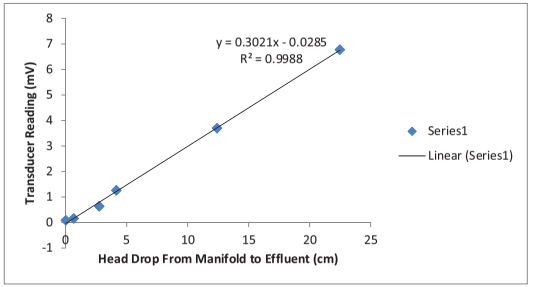

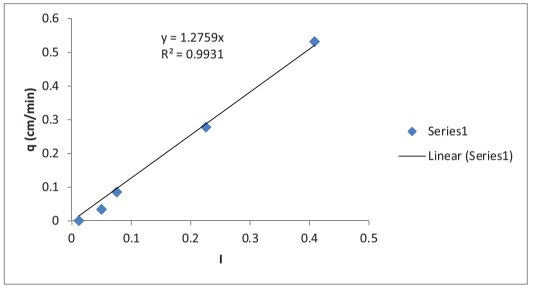

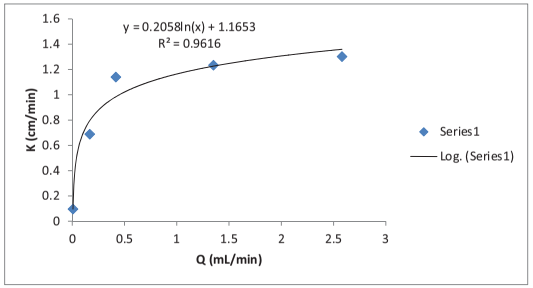

Effective pre bio K (cm/min)	0.679362
Q (mL/min) needed for desired V	0.094306

V (cm/d)	96.21993	197.9381	404.1237	1171.134	2177.32	#DIV/0!
K (cm/min)	0.780355	0.820227	0.892702	0.9743	0.990451	#DIV/0!
Q (mL/min)	0.097222	0.2	0.408333	1.183333	2.2	0
q (cm/min)	0.020046	0.041237	0.084192	0.243986	0.453608	0
Head Drop	1.4	2.74	5.14	13.648	24.96	0
i	0.025688	0.050275	0.094312	0.250422	0.457982	0
Average mV	0.105512	0.475744	1.092046	3.598332	6.946637	-0.22705
	mV Response	mV Response	mV Response	mV Response	mV Response	mV Response
	0.146	0.467	1.107	3.61	6.95	-0.234
	0.152	0.478	1.141	3.57	6.919	-0.237
	0.159	0.491	1.05	3.573	6.99	-0.24
	0.166	0.501	1.094	3.647	6.936	-0.237
	0.179	0.508	1.084	3.57	6.929	-0.24
	0.183	0.478	1.114	3.59	6.983	-0.24
	0.156	0.461	1.165	3.597	6.939	-0.234
	0.152	0.457	1.104	3.566	6.922	-0.237
	0.146	0.447	1.074	3.593	6.97	-0.237
	0.132	0.444	1.07	3.58	6.96	-0.234
	0.122	0.447	1.074	3.58	6.933	-0.237
	0.125	0.444	1.08	3.617	6.997	-0.227
	0.119	0.444	1.097	3.566	6.95	-0.24
	0.115	0.457	1.135	3.573	6.939	-0.237
	0.112	0.457	1.135	3.651	7.011	-0.234
	0.112	0.464	1.097	3.566	6.953	-0.234
	0.112	0.474	1.07	3.586	6.933	-0.234
	0.119	0.45	1.07	3.6	7.024	-0.237
	0.112	0.498	1.08	3.566	6.946	-0.24
	0.108	0.494	1.094	3.691	6.929	-0.237
	0.115	0.481	1.097	3.566	7	-0.234
	0.108	0.464	1.118	3.58	6.936	-0.237
	0.108	0.447	1.118	3.624	6.929	-0.237
	0.115	0.447	1.087	3.566	6.997	-0.23
	0.115	0.447	1.077	3.586	6.919	-0.24
	0.119	0.444	1.077	3.661	6.906	-0.23
	0.119	0.45	1.07	3.57	6.987	-0.234
	0.122	0.447	1.084	3.586	6.933	-0.234
	0.129	0.45	1.104	3.593	6.929	-0.237
	0.139	0.461	1.124	3.563	6.987	-0.237
	0.139	0.471	1.124	3.6	6.933	-0.234
	0.142	0.474	1.087	3.58	6.936	-0.23
	0.152	0.484	1.074	3.576	6.973	-0.234
	0.149	0.491	1.07	3.62	6.909	-0.24
	0.166	0.515	1.084	3.566	6.926	-0.237
	0.186	0.494	1.084	3.583	6.97	-0.234
	0.173	0.478	1.111	3.658	6.936	-0.24
	0.163	0.461	1.138	3.563	6.939	-0.234
	0.149	0.444	1.114	3.593	6.963	-0.237
	0.142	0.45	1.08	3.593	6.933	-0.24
	0.135	0.444	1.074	3.573	6.953	-0.23
	0.132	0.447	1.07	3.607	6.963	-0.234
	0.115	0.45	1.084	3.57	6.926	-0.234
	0.115	0.457	1.094	3.57	6.956	-0.237
	0.115	0.45	1.104	3.624	6.956	-0.24
	0.108	0.461	1.148	3.566	6.933	-0.237
	0.108	0.467	1.101	3.586	6.997	-0.234
	0.105	0.481	1.077	3.661	6.95	-0.237
	0.108	0.494	1.077	3.566	6.933	-0.24
	0.108	0.508	1.077	3.593	7.01	-0.237
	0.112	0.501	1.084	3.586	6.946	-0.234
	0.105	0.481	1.097	3.566	6.933	-0.234

Calculated Field

Data From Calibration Graph

K (cm/min)	0.9818	Target initial velocity (cm/d)	1000
A (cm2)	4.85	Transducer Voltage to Reach it	3.034138 mV
ΔL (cm)	54.5	Expected Q (mL/min)	1.010417
n	0.3	Manifold Head (cm)	85.217
m	0.2891	Effluent Head	73.65236
b	-0.3092		

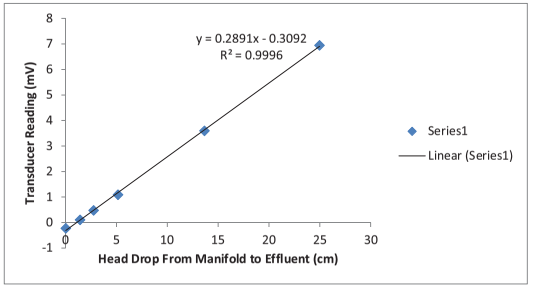

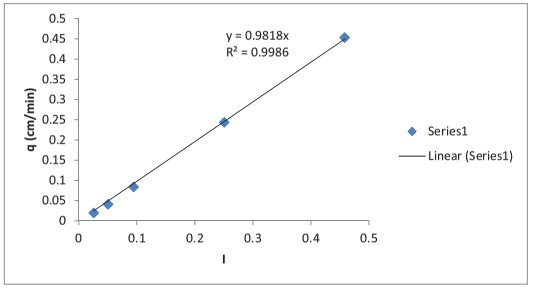

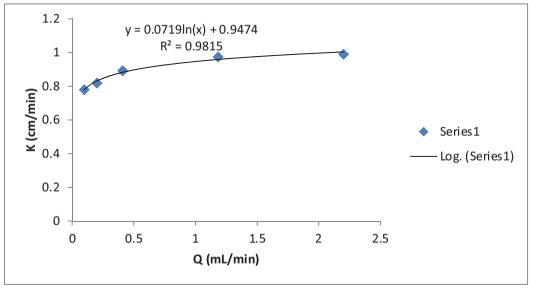

Effective pre bio K (cm/min)	0.948145
Q (mL/min) needed for desired V	1.010417

V (cm/d)	#DIV/0!	77.6228	73.68102	139.721	611.2796
K (cm/min)	#DIV/0!	0.855079	0.909992	1.238536	1.693969
Q (mL/min)	0	0.088889	0.084375	0.16	0.7
q (cm/min)	0	0.018328	0.017397	0.03299	0.14433
Head Drop	0	1.166	1.04	1.449	4.635
i	0	0.021434	0.019118	0.026636	0.085202
Average m'	-0.01722	0.199866	0.205683	0.335308	1.154167
	mV Response	mV Response	mV Response	mV Response	mV Response
	-0.027	0.186	0.179	0.315	1.141
	-0.02	0.196	0.176	0.325	1.165
	-0.027	0.2	0.176	0.318	1.185
	-0.024	0.207	0.176	0.325	1.168
	-0.024	0.22	0.173	0.322	1.145
	-0.03	0.227	0.179	0.342	1.141
	-0.017	0.247	0.176	0.339	1.141
	-0.02	0.234	0.176	0.349	1.168
	-0.02	0.227	0.173	0.369	1.178
	-0.024	0.207	0.169	0.41	1.148
	-0.017	0.19	0.173	0.366	1.131
	-0.017	0.193	0.166	0.345	1.141
	-0.017	0.176	0.176	0.342	1.165
	-0.02	0.186	0.169	0.332	1.209
	-0.017	0.169	0.173	0.328	1.155
	-0.024	0.176	0.176	0.322	1.138
	-0.017	0.176	0.176	0.318	1.134
	-0.02	0.166	0.183	0.318	1.162
	-0.017	0.173	0.176	0.315	1.172
	-0.014	0.166	0.186	0.318	1.182
	-0.02	0.173	0.19	0.318	1.138
	-0.01	0.166	0.196	0.322	1.138
	-0.02	0.166	0.193	0.318	1.151
	-0.014	0.169	0.196	0.328	1.155
	-0.02	0.166	0.21	0.339	1.202
	-0.02	0.156	0.21	0.335	1.145
	-0.014	0.159	0.224	0.342	1.134
	-0.024	0.179	0.23	0.352	1.141
	-0.014	0.19	0.24	0.383	1.151
	-0.02	0.186	0.227	0.373	1.202
	-0.014	0.193	0.213	0.359	1.158
	-0.02	0.203	0.207	0.342	1.131
	-0.017	0.207	0.196	0.339	1.138
	-0.017	0.217	0.2	0.328	1.141
	-0.02	0.217	0.183	0.325	1.172
	-0.024	0.237	0.193	0.325	1.178
	-0.017	0.264	0.183	0.315	1.138
	-0.024	0.227	0.183	0.318	1.138
	-0.02	0.21	0.179	0.332	1.141
	-0.027	0.2	0.176	0.318	1.155
	-0.02	0.196	0.179	0.315	1.253
	-0.02	0.179	0.173	0.315	1.141
	-0.024	0.179	0.176	0.325	1.145
	-0.014	0.173	0.169	0.335	1.138
	-0.024	0.169	0.169	0.332	1.148
	-0.017	0.166	0.173	0.335	1.202
	-0.02	0.163	0.169	0.356	1.155
	-0.02	0.163	0.173	0.366	1.145
	-0.014	0.166	0.173	0.383	1.131
	-0.02	0.159	0.176	0.376	1.145
	-0.01	0.169	0.186	0.359	1.175

Calculated Field

Data From Calibration Graph

K (cm/min)	1.5808	Target initial velocity (cm/d)	200
A (cm2)	4.85	Transducer Voltage to Reach it	0.367127 mV
ΔL (cm)	54.4	Expected Q (mL/min)	0.229028
n	0.34	Manifold Head (cm)	85.18
m	0.2581	Effleunt Head	83.55494
b	-0.0523		

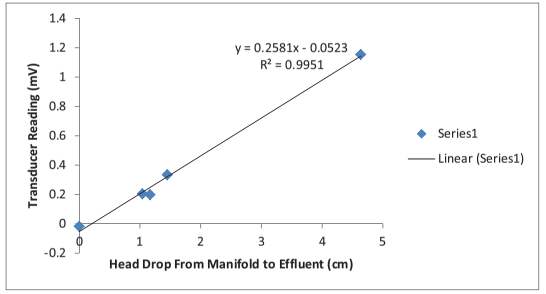

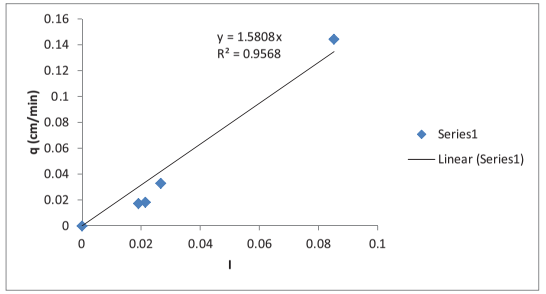

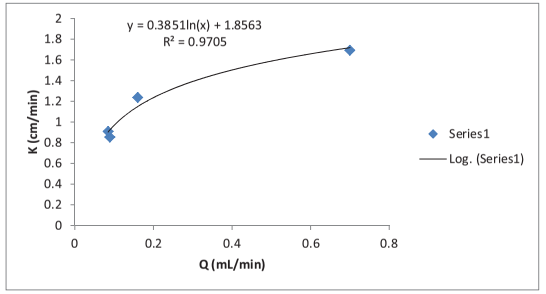

Effective pre bio K (cm/min)	1.288696
Q (mL/min) needed for desired V	0.229028

V (cm/d)	#DIV/0!	72.36448	86.79747	568.274	2131.028
K (cm/min)	#DIV/0!	0.945592	1.315085	5.672998	7.017116
Q (mL/min)	0	0.075556	0.090625	0.593333	2.225
q (cm/min)	0	0.015578	0.018686	0.122337	0.458763
Head Drop	0	0.916	0.79	1.199	3.635
i	0	0.016475	0.014209	0.021565	0.065378
Average m'	0.417876	0.509223	0.544207	0.764395	1.307377
mV	Response	mV Response	mV Response	mV Response	mV Response
	0.413	0.525	0.637	0.745	1.307
	0.413	0.498	0.572	0.772	1.294
	0.403	0.494	0.555	0.772	1.392
	0.417	0.484	0.542	0.735	1.297
	0.413	0.484	0.538	0.735	1.297
	0.41	0.481	0.528	0.752	1.344
	0.41	0.474	0.528	0.779	1.294
	0.406	0.474	0.532	0.755	1.29
	0.42	0.478	0.522	0.735	1.314
	0.41	0.471	0.528	0.745	1.297
	0.42	0.474	0.522	0.752	1.307
	0.413	0.474	0.525	0.82	1.317
	0.417	0.474	0.522	0.748	1.297
	0.417	0.481	0.522	0.742	1.368
	0.406	0.471	0.518	0.742	1.311
	0.413	0.484	0.518	0.759	1.294
	0.41	0.478	0.522	0.823	1.385
	0.41	0.484	0.518	0.745	1.304
	0.413	0.488	0.525	0.735	1.287
	0.413	0.481	0.525	0.742	1.351
	0.413	0.488	0.528	0.769	1.29
	0.417	0.488	0.528	0.779	1.294
	0.413	0.488	0.532	0.738	1.331
	0.42	0.488	0.532	0.735	1.287
	0.406	0.491	0.542	0.752	1.314
	0.417	0.488	0.538	0.772	1.311
	0.41	0.488	0.549	0.765	1.287
	0.41	0.515	0.552	0.735	1.378
	0.41	0.528	0.562	0.742	1.3
	0.41	0.538	0.589	0.748	1.287
	0.413	0.515	0.566	0.789	1.392
	0.403	0.498	0.545	0.752	1.29
	0.413	0.491	0.538	0.745	1.297
	0.41	0.484	0.538	0.721	1.338
	0.41	0.481	0.525	0.772	1.29
	0.413	0.478	0.535	0.836	1.297
	0.406	0.471	0.522	0.752	1.317
	0.413	0.478	0.528	0.731	1.29
	0.413	0.471	0.525	0.755	1.321
	0.41	0.471	0.528	0.765	1.307
	0.41	0.474	0.522	0.803	1.3
	0.41	0.474	0.522	0.742	1.375
	0.413	0.474	0.525	0.735	1.311
	0.406	0.471	0.518	0.752	1.294
	0.41	0.478	0.522	0.765	1.378
	0.41	0.474	0.518	0.776	1.297
	0.413	0.474	0.525	0.738	1.29
	0.413	0.478	0.525	0.748	1.341
	0.413	0.478	0.525	0.748	1.294
	0.42	0.481	0.528	0.776	1.287
	0.417	0.481	0.535	0.765	1.324

Calculated Field

Data From Calibration Graph

K (cm/min)	6.3602	Target initial velocity (cm/d)	200	
A (cm2)	4.85	Transducer Voltage to Reach it	0.470629	mV
ΔL (cm)	55.6	Expected Q (mL/min)	0.208819	
n	0.31	Manifold Head (cm)	85.18	
m	0.2554	Effleunt Head	84.80361	
b	0.3745			

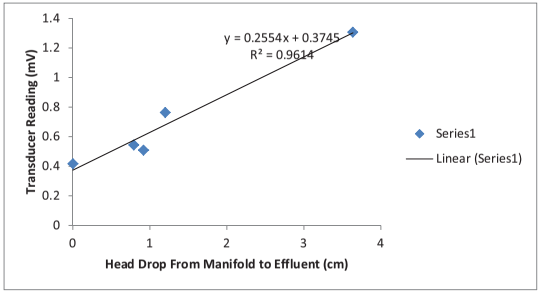

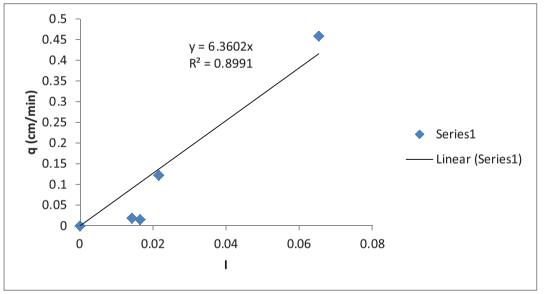

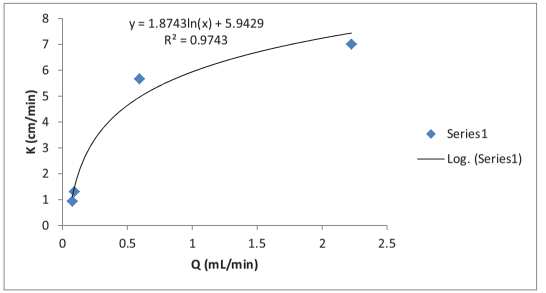

Effective pre bio K (cm/min)	3.007211
Q (mL/min) needed for desired V	0.208819

V (cm/d)	#DIV/0!	62.50678	9.766685	2422.138	6391.319
K (cm/min)	#DIV/0!	2.129262	0.477248	76.44479	79.79763
Q (mL/min)	0	0.08	0.0125	3.1	8.18
q (cm/min)	0	0.016495	0.002577	0.639175	1.686598
Head Drop	0	0.416	0.29	0.449	1.135
i	0	0.007747	0.0054	0.008361	0.021136
Average m'	0.246333	0.275841	0.30708	0.362687	0.392362
	mV Response	mV Response	mV Response	mV Response	mV Response
	0.247	0.254	0.298	0.359	0.396
	0.251	0.254	0.301	0.356	0.4
	0.247	0.254	0.295	0.352	0.393
	0.244	0.254	0.298	0.359	0.4
	0.247	0.257	0.295	0.359	0.396
	0.244	0.254	0.298	0.349	0.396
	0.247	0.261	0.295	0.356	0.403
	0.247	0.257	0.298	0.356	0.396
	0.247	0.257	0.298	0.356	0.403
	0.251	0.261	0.301	0.349	0.396
	0.247	0.254	0.295	0.356	0.4
	0.251	0.257	0.298	0.356	0.4
	0.247	0.257	0.298	0.352	0.396
	0.251	0.254	0.298	0.349	0.396
	0.247	0.257	0.298	0.352	0.396
	0.247	0.254	0.298	0.362	0.396
	0.247	0.257	0.298	0.349	0.4
	0.244	0.254	0.298	0.356	0.396
	0.251	0.261	0.295	0.352	0.393
	0.254	0.261	0.298	0.359	0.4
	0.244	0.254	0.298	0.352	0.396
	0.247	0.264	0.298	0.359	0.4
	0.251	0.257	0.301	0.359	0.403
	0.247	0.264	0.295	0.356	0.396
	0.247	0.264	0.305	0.349	0.403
	0.247	0.271	0.295	0.356	0.396
	0.254	0.271	0.298	0.359	0.4
	0.247	0.261	0.298	0.352	0.403
	0.251	0.261	0.298	0.352	0.396
	0.251	0.257	0.298	0.352	0.403
	0.247	0.257	0.298	0.356	0.393
	0.251	0.257	0.301	0.352	0.403
	0.244	0.257	0.298	0.349	0.4
	0.251	0.257	0.298	0.376	0.396
	0.247	0.261	0.295	0.352	0.396
	0.251	0.257	0.298	0.352	0.4
	0.247	0.264	0.295	0.352	0.4
	0.247	0.257	0.295	0.356	0.4
	0.251	0.261	0.301	0.362	0.396
	0.247	0.254	0.295	0.356	0.4
	0.251	0.261	0.298	0.352	0.396
	0.251	0.261	0.301	0.359	0.4
	0.247	0.254	0.298	0.359	0.396
	0.251	0.261	0.301	0.349	0.4
	0.247	0.254	0.295	0.356	0.396
	0.247	0.264	0.298	0.356	0.403
	0.251	0.257	0.298	0.356	0.396
	0.247	0.264	0.298	0.349	0.4
	0.251	0.261	0.298	0.356	0.403
	0.247	0.257	0.298	0.362	0.396
	0.247	0.257	0.298	0.349	0.4

Calculated Field

Data From Calibration Graph

K (cm/min)	67.898	Target initial velocity (cm/d)	200
A (cm2)	4.85	Transducer Voltage to Reach it	0.265363 mV
ΔL (cm)	53.7	Expected Q (mL/min)	0.255972
n	0.38	Manifold Head (cm)	85.18
m	0.1237	Effleunt Head	85.13826
b	0.2602		

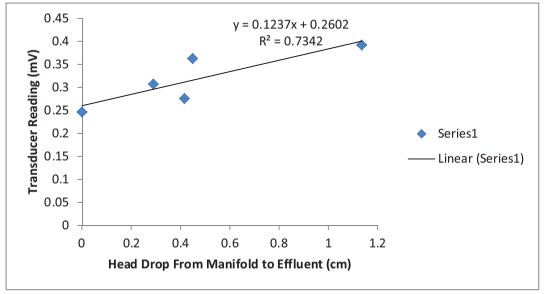

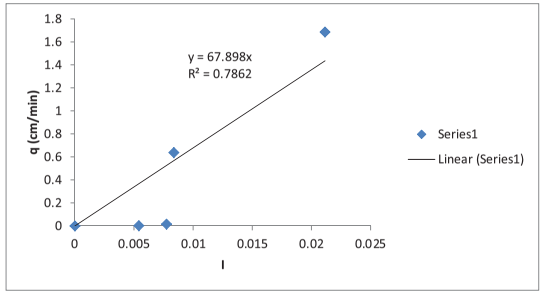

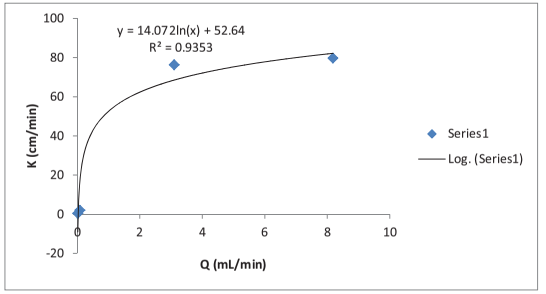

Effective pre bio K (cm/min)	33.46428
Q (mL/min) needed for desired V	0.255972

V (cm/d)	#DIV/0!	230.9278	177.8351	263.9175	1039.175
K (cm/min)	#DIV/0!	1.226892	1.287158	1.289777	2.054679
Q (mL/min)	0	0.233333	0.179688	0.266667	1.05
q (cm/min)	0	0.04811	0.037049	0.054983	0.216495
Head Drop	0	2.192	1.609	2.383	5.89
i	0	0.039213	0.028784	0.04263	0.105367
Average m'	0.594593	1.0605	1.013834	1.140721	2.211067
mV	Response	mV Response	mV Response	mV Response	mV Response
	0.589	1.179	0.992	1.114	2.181
	0.593	1.107	0.989	1.097	2.215
	0.586	1.063	1.009	1.107	2.279
	0.593	1.057	1.013	1.097	2.177
	0.586	1.04	1.104	1.107	2.201
	0.593	1.053	1.06	1.121	2.276
	0.589	1.036	1.019	1.118	2.181
	0.586	1.05	1.002	1.185	2.201
	0.589	1.084	0.985	1.219	2.232
	0.582	1.128	0.992	1.165	2.201
	0.589	1.165	0.975	1.124	2.188
	0.589	1.175	0.985	1.114	2.215
	0.589	1.107	0.982	1.104	2.269
	0.596	1.06	0.989	1.101	2.184
	0.589	1.046	0.989	1.107	2.201
	0.599	1.03	0.989	1.101	2.279
	0.589	1.046	0.999	1.124	2.194
	0.593	1.057	1.006	1.121	2.177
	0.593	1.07	1.084	1.189	2.276
	0.582	1.084	1.111	1.216	2.194
	0.596	1.131	1.04	1.162	2.174
	0.582	1.155	1.013	1.121	2.238
	0.589	1.175	0.996	1.111	2.211
	0.582	1.084	0.989	1.104	2.171
	0.593	1.03	0.979	1.101	2.215
	0.589	1.063	0.982	1.104	2.293
	0.589	1.043	0.982	1.104	2.167
	0.596	1.057	0.982	1.124	2.198
	0.589	1.053	0.985	1.121	2.299
	0.589	1.067	0.982	1.202	2.164
	0.589	1.087	0.996	1.219	2.194
	0.589	1.121	1.006	1.155	2.269
	0.593	1.151	1.026	1.118	2.174
	0.586	1.138	1.104	1.128	2.184
	0.579	1.101	1.07	1.101	2.228
	0.593	1.063	1.026	1.097	2.208
	0.582	1.05	1.006	1.107	2.177
	0.589	1.05	0.996	1.104	2.222
	0.582	1.05	0.982	1.101	2.269
	0.593	1.057	0.979	1.138	2.191
	0.589	1.067	0.979	1.165	2.194
	0.582	1.084	0.982	1.216	2.272
	0.596	1.128	0.985	1.162	2.188
	0.582	1.141	0.985	1.114	2.191
	0.599	1.148	0.992	1.111	2.238
	0.582	1.09	1.002	1.104	2.194
	0.586	1.057	1.016	1.104	2.188
	0.589	1.05	1.08	1.097	2.201
	0.586	1.043	1.104	1.118	2.266
	0.589	1.06	1.043	1.114	2.188
	0.586	1.057	1.006	1.131	2.184

Calculated Field

Data From Calibration Graph

K (cm/min)	1.8389	Target initial velocity (cm/d)	200
A (cm2)	4.85	Transducer Voltage to Reach it	0.885804 mV
ΔL (cm)	55.9	Expected Q (mL/min)	0.202083
n	0.3	Manifold Head (cm)	85.217
m	0.2772	Effleunt Head	83.95039
b	0.5347		

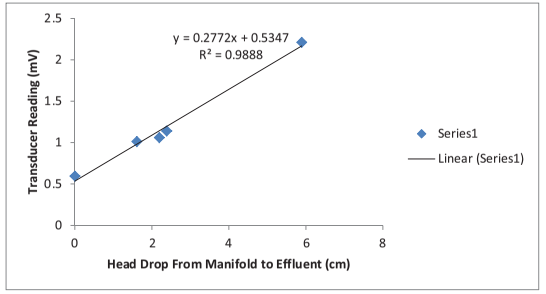

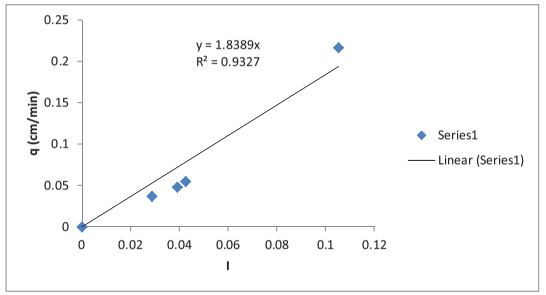

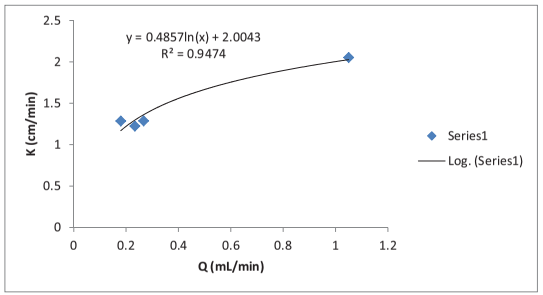

Effective pre bio K (cm/min)	1.227629
Q (mL/min) needed for desired V	0.202083

V (cm/d)	#DIV/0!	1325.409	200.1213	989.6907	2445.118
K (cm/min)	#DIV/0!	6.509977	3.080382	6.134979	7.809154
Q (mL/min)	0	1.517778	0.229167	1.133333	2.8
q (cm/min)	0	0.312944	0.047251	0.233677	0.57732
Head Drop	0	2.692	0.859	2.133	4.14
i	0	0.048071	0.015339	0.038089	0.073929
Average m'	0.471535	1.122181	0.620272	0.991668	1.480899
	mV Response	mV Response	mV Response	mV Response	mV Response
	0.471	1.172	0.633	1.04	1.453
	0.464	1.151	0.654	0.955	1.534
	0.474	1.195	0.674	0.985	1.47
	0.457	1.131	0.691	1.04	1.493
	0.471	1.172	0.596	0.948	1.517
	0.461	1.114	0.596	0.975	1.463
	0.461	1.134	0.593	1.026	1.514
	0.467	1.182	0.589	0.952	1.51
	0.461	1.124	0.593	0.965	1.456
	0.464	1.182	0.586	1.026	1.521
	0.457	1.114	0.603	0.948	1.504
	0.467	1.151	0.599	0.969	1.449
	0.467	1.202	0.613	1.019	1.521
	0.467	1.131	0.626	0.952	1.497
	0.471	1.182	0.637	0.958	1.449
	0.467	1.084	0.657	1.009	1.517
	0.467	1.158	0.667	0.945	1.483
	0.471	1.195	0.667	0.952	1.487
	0.461	1.141	0.599	1.002	1.517
	0.467	1.185	0.596	0.982	1.47
	0.464	1.118	0.593	0.958	1.517
	0.471	1.165	0.582	0.992	1.497
	0.471	1.192	0.596	1.043	1.47
	0.464	1.131	0.589	0.948	1.514
	0.474	1.162	0.599	0.996	1.497
	0.464	1.124	0.603	1.036	1.456
	0.471	1.172	0.616	0.958	1.517
	0.464	1.195	0.633	0.982	1.49
	0.467	1.145	0.64	1.036	1.453
	0.471	1.195	0.667	0.948	1.521
	0.467	1.124	0.677	0.969	1.473
	0.474	1.168	0.616	1.04	1.493
	0.467	1.162	0.596	0.938	1.507
	0.471	1.114	0.593	0.982	1.473
	0.461	1.199	0.593	1.013	1.524
	0.464	1.128	0.586	0.958	1.5
	0.464	1.179	0.596	0.958	1.463
	0.461	1.162	0.589	1.023	1.531
	0.467	1.155	0.606	0.904	1.493
	0.464	1.199	0.606	0.955	1.453
	0.464	1.128	0.62	1.013	1.527
	0.471	1.182	0.63	0.955	1.483
	0.467	1.107	0.643	0.962	1.446
	0.471	1.145	0.667	0.989	1.537
	0.471	1.172	0.681	1.036	1.463
	0.467	1.131	0.61	0.945	1.473
	0.467	1.185	0.596	0.999	1.527
	0.461	1.114	0.593	1.036	1.466
	0.471	1.158	0.586	0.955	1.504
	0.464	1.202	0.586	0.985	1.514
	0.471	1.141	0.596	1.033	1.466

Calculated Field

Data From Calibration Graph

K (cm/min)	7.1176	Target initial velocity (cm/d)	200
A (cm2)	4.85	Transducer Voltage to Reach it	0.539147 mV
ΔL (cm)	56	Expected Q (mL/min)	0.229028
n	0.34	Manifold Head (cm)	85.217
m	0.2499	Effleunt Head	84.84546
b	0.4463		

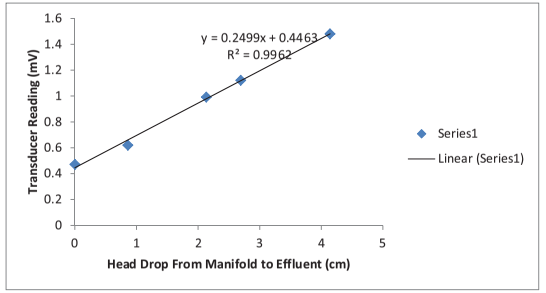

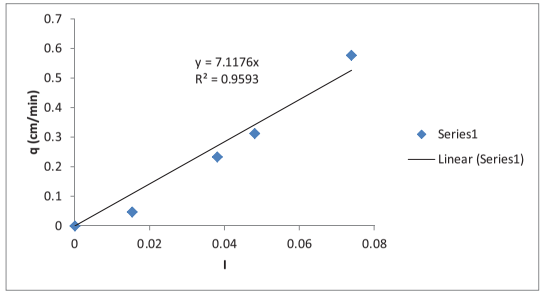

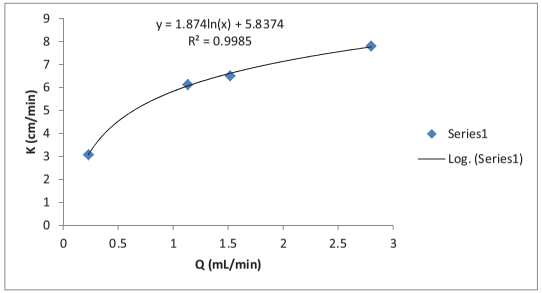

Effective pre bio K (cm/min)	3.075289
Q (mL/min) needed for desired V	0.229028

V (cm/d)	#DIV/0!	233.677	1.718213	3903.78	5443.299
K (cm/min)	#DIV/0!	4.693801	0.066527	47.8928	54.43299
Q (mL/min)	0	0.283333	0.002083	4.733333	6.6
q (cm/min)	0	0.058419	0.00043	0.975945	1.360825
Head Drop	0	0.692	0.359	1.133	1.39
i	0	0.012446	0.006457	0.020378	0.025
Average m'	0.539571	0.57594	0.650843	0.727873	0.734183
	mV Response	mV Response	mV Response	mV Response	mV Response
	0.528	0.566	0.64	0.715	0.738
	0.532	0.562	0.64	0.718	0.728
	0.532	0.562	0.64	0.715	0.728
	0.532	0.569	0.643	0.715	0.738
	0.528	0.562	0.643	0.715	0.725
	0.532	0.569	0.643	0.715	0.735
	0.538	0.566	0.64	0.711	0.731
	0.528	0.562	0.643	0.718	0.735
	0.535	0.566	0.64	0.718	0.725
	0.528	0.559	0.643	0.711	0.735
	0.532	0.569	0.637	0.718	0.728
	0.535	0.562	0.64	0.718	0.731
	0.528	0.566	0.643	0.718	0.738
	0.535	0.569	0.637	0.718	0.725
	0.528	0.566	0.647	0.721	0.735
	0.535	0.572	0.643	0.715	0.735
	0.528	0.566	0.647	0.718	0.735
	0.532	0.562	0.637	0.718	0.728
	0.538	0.566	0.643	0.715	0.735
	0.528	0.562	0.643	0.715	0.731
	0.535	0.566	0.643	0.715	0.728
	0.528	0.566	0.643	0.715	0.738
	0.532	0.566	0.637	0.711	0.728
	0.532	0.572	0.647	0.721	0.731
	0.528	0.562	0.64	0.715	0.735
	0.532	0.569	0.647	0.718	0.728
	0.528	0.562	0.64	0.715	0.735
	0.532	0.562	0.64	0.715	0.731
	0.528	0.562	0.643	0.718	0.738
	0.532	0.559	0.64	0.711	0.728
	0.532	0.569	0.64	0.718	0.738
	0.528	0.562	0.64	0.708	0.731
	0.532	0.572	0.64	0.721	0.731
	0.532	0.562	0.64	0.715	0.738
	0.532	0.566	0.64	0.725	0.728
	0.532	0.566	0.643	0.715	0.735
	0.528	0.559	0.643	0.721	0.731
	0.532	0.566	0.643	0.715	0.735
	0.532	0.562	0.64	0.721	0.728
	0.525	0.569	0.643	0.718	0.738
	0.532	0.562	0.643	0.711	0.731
	0.525	0.562	0.64	0.721	0.731
	0.532	0.569	0.647	0.708	0.742
	0.528	0.569	0.64	0.721	0.728
	0.532	0.559	0.647	0.708	0.738
	0.535	0.562	0.643	0.725	0.731
	0.528	0.562	0.643	0.708	0.735
	0.535	0.566	0.643	0.721	0.731
	0.525	0.562	0.64	0.718	0.735
	0.535	0.566	0.65	0.718	0.731
	0.532	0.566	0.64	0.718	0.728

Calculated Field

Data From Calibration Graph

K (cm/min)	44.175	Target initial velocity (cm/d)	200
A (cm2)	4.85	Transducer Voltage to Reach it	0.55852 mV
ΔL (cm)	55.6	Expected Q (mL/min)	0.2425
n	0.36	Manifold Head (cm)	85.217
m	0.1338	Effleunt Head	85.15407
b	0.5501		

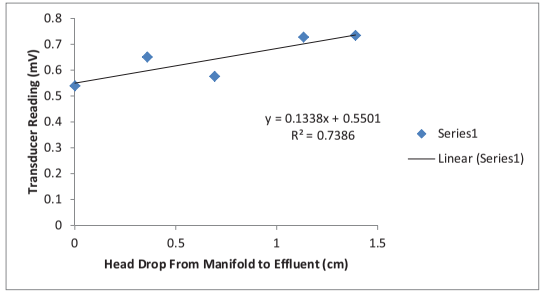

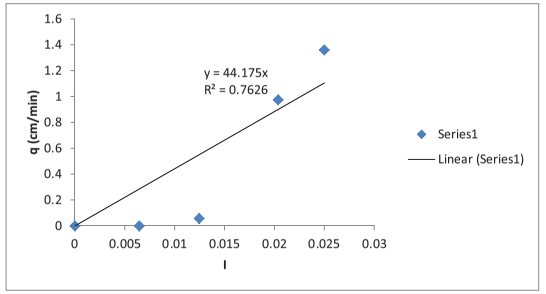

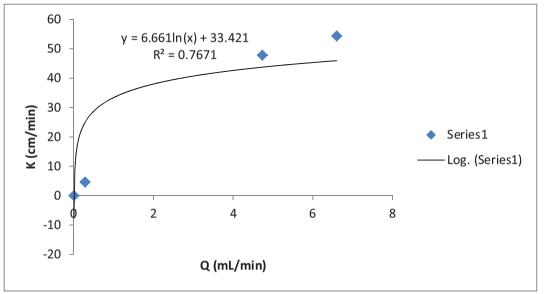

Effective pre bio K (cm/min)	23.984
Q (mL/min) needed for desired V	0.2425

Appendix 30: Total Lipid Biomass for Column Experiments

Column Experiment Biomass Analysis

Standards	Conc	Abs	Conc	Abs
	0	0.041	0	0.045
	1.5	0.068	1.5	0.065
	3	0.094	3	0.098
	6	0.137	6	0.151
	10	0.209	10	0.215

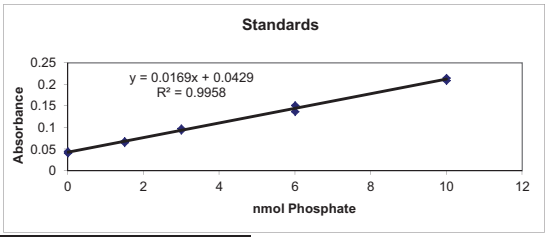

Column	Mass weighed (g dry sediment)	Absorbance	Amount of Phosphate nmol	Biomass (cells/g dry weight sed) (Dobbs&Findlay 1993)	High Value (cells/g dry weight sed)	Average (cells/g dry weight sed)
3_1	4.97	0.187	8.53	5.83E+07	3.43E+09	1.74E+09
3_2	4.97	0.189	8.64	5.91E+07	3.48E+09	1.77E+09
6_1	4.95	0.146	6.10	4.19E+07	2.46E+09	1.25E+09
6_2	4.88	0.119	4.50	3.14E+07	1.85E+09	9.38E+08
7_1	5.08	0.182	8.23	5.51E+07	3.24E+09	1.65E+09
7_2	5	0.275	13.73	9.34E+07	5.49E+09	2.79E+09
8_1	5.09	0.061	1.07	7.15E+06	4.21E+08	2.14E+08
8_2	5.1	0.065	1.31	8.72E+06	5.13E+08	2.61E+08
10_1	4.98	0.099	3.32	2.27E+07	1.33E+09	6.78E+08
10_2	5.03	0.081	2.25	1.52E+07	8.96E+08	4.56E+08
Background_1	10	0.052	0.54	1.83E+06	1.08E+08	5.48E+07
Background_2	10	0.051	0.48	1.63E+06	9.59E+07	4.87E+07

Column	Average Biomass 1	Average Biomass 2	Average Bior	Error High	Error Low
3	1.74E+09	1.77E+09	1.76E+09	1.21E+07	1.21E+07
6	1.25E+09	9.38E+08	1.10E+09	1.57E+08	1.57E+08
7	1.65E+09	2.79E+09	2.22E+09	5.73E+08	5.73E+08
8	2.14E+08	2.61E+08	2.37E+08	2.34E+07	2.34E+07
10	6.78E+08	4.56E+08	5.67E+08	1.11E+08	1.11E+08
Background	5.48E+07	4.87E+07	5.18E+07	3.01E+06	3.01E+06

Average 1200 cm/d column	1.43E+09
Average #50-70	1.16E+09

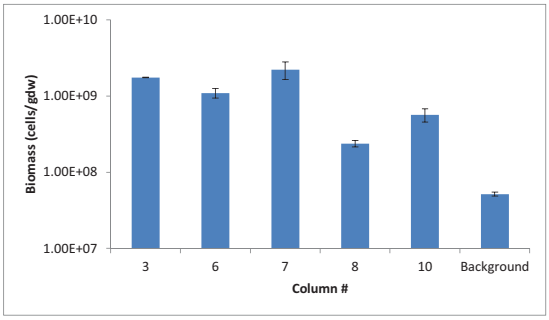

Appendix 31: Aqueous Geochemistry for Column Experiments

Manifold	Condition	pH	EC µS/cm	DO [mg/L]	Ca^{+2} [mg/L]	Na^{+} [mg/L]	Mg^{+2} [mg/L]	K^{+} [mg/L]	Sr^{+2} [mg/L]	Fe^{+2} [mg/L]
1	50 cm/d @$t_{initial}$	7.29	732	1.00	126.621	28.045	6.527	34.816	0.333	0.000
	100 cm/d @$t_{initial}$	7.29	732	1.00	127.627	28.070	6.649	34.560	0.335	0.000
	1200 cm/d @$t_{initial}$	7.34	750	1.00	128.836	27.863	6.576	34.313	0.334	0.000
	1200 cm/d DUP @$t_{initial}$	7.34	750	1.00	129.702	28.015	6.646	34.264	0.336	0.000
2	50 cm/d @$t_{initial}$	7.38	727	1.00	127.462	27.960	6.598	34.463	0.333	0.000
	100 cm/d @$t_{initial}$	7.39	727	1.00	127.583	27.951	6.581	34.317	0.333	0.000
	1200 cm/d @$t_{initial}$	7.53	748	1.00	128.655	28.087	6.615	34.278	0.336	0.000
	Manifold 1 @$t_{initial}$				129.682	28.045	6.654	34.395	0.336	0.000
	Manifold 2 @$t_{initial}$				127.770	28.472	6.628	34.363	0.337	0.000
	Method Blank @$t_{initial}$				0.855	0.000	0.000	0.040	0.000	0.000
1	50 cm/d @t_{final}	7.42	725	1.00	130.081	28.592	6.776	34.578	0.341	0.000
	100 cm/d @t_{final}	7.32	729	1.00	130.129	28.335	6.745	34.578	0.340	0.000
	1200 cm/d @t_{final}	7.57	739	1.00	129.756	28.293	6.722	34.262	0.340	0.000
	1200 cm/d DUP @t_{final}	7.57	739	1.00	129.984	28.367	6.764	34.570	0.341	0.000
2	50 cm/d @t_{final}	7.39	728	1.00	128.198	28.432	6.759	34.631	0.341	0.001
	100 cm/d @t_{final}	7.28	738	1.50	130.625	28.247	6.763	35.377	0.340	0.000
	1200 cm/d @t_{final}	7.51	730	1.00	129.624	28.246	6.759	34.514	0.340	0.000
	Manifold 1 @t_{final}	7.08	760	1.00	129.911	28.487	6.751	34.859	0.340	0.000
	Manifold 2 @t_{final}	7.12	753	1.00	129.526	28.431	6.770	34.635	0.340	0.000
	Method Blank @t_{final}				0.836	0.014	0.000	0.018	0.001	0.000
	Detection Limits				0.027	0.034	0.007	0.015	0.013	0.010

Manifold	Condition	pH	EC µS/cm	DO [mg/L]	Ca^{+2} [mg/L]	Na^{+} [mg/L]	Mg^{+2} [mg/L]	K^{+} [mg/L]	Sr^{+2} [mg/L]	Fe^{+2} [mg/L]
3	0.254 mm @$t_{initial}$	7.46	756	2.00	130.081	30.540	6.403	36.102	0.315	0.004
	0.508 mm @$t_{initial}$	7.44	767	1.00	130.213	29.637	6.305	36.365	0.317	0.000
	3.57 mm @$t_{initial}$	7.34	786	1.00	131.320	29.090	6.357	35.580	0.315	0.000
4	0.254 mm @$t_{initial}$	7.51	777	1.50	132.902	28.658	6.367	36.812	0.313	0.000
	0.254 mm DUP @$t_{initial}$	7.51	777	1.50	132.859	30.884	6.474	36.711	0.315	0.000
	0.508 mm @$t_{initial}$	7.36	783	1.00	133.543	29.725	6.419	36.546	0.315	0.000
	3.57 mm @$t_{initial}$	7.39	785	1.00	132.075	28.046	6.423	36.392	0.312	0.000
	Manifold 3 @$t_{initial}$	7.31	789	6.00	131.657	28.902	6.308	36.496	0.313	0.000
	Manifold 4 @$t_{initial}$	7.25	798	6.00	133.247	28.859	6.401	37.370	0.315	0.000
	Method Blank @$t_{initial}$				0.931	0.000	0.000	0.000	0.000	0.000
3	0.254 mm @t_{final}	7.36	677	1.50	119.354	27.042	6.284	35.054	0.300	0.000
	0.508 mm @t_{final}	7.37	688	3.00	120.324	28.648	6.521	35.489	0.313	0.109
	3.57 mm @t_{final}	7.32	688	1.00	127.818	28.463	6.352	35.841	0.312	0.000
4	0.254 mm @t_{final}	7.35	691	3.00	127.331	28.501	6.401	36.253	0.314	0.003
	0.508 mm @t_{final}	7.24	686	1.50	125.389	26.228	6.383	36.292	0.312	0.012
	3.57 mm @t_{final}	7.41	747	3.00	123.635	26.974	6.297	35.943	0.307	0.006
	Manifold 3 @t_{final}	7.41	777	1.50	133.002	27.920	6.407	36.108	0.314	0.000
	Manifold 4 @t_{final}	7.51	777	1.00	132.739	25.478	6.397	36.208	0.314	0.000
	Method Blank @t_{final}				0.978	0.000	0.000	0.000	0.000	0.000

Manifold	Condition	Mn^{+2} [mg/L]	HCO_3^- [mg/L]	CH_3COO^- [mg/L]	Cl^- [mg/L]	NO_2^- [mg/L]	SO_4^{-2} [mg/L]	NO_3^- [mg/L]	Cations meq/L	Anions meq/L
1	50 cm/d @$t_{initial}$	0.003	434.320	0.046	7.552	0.061	24.481	45.243	8.973	8.573
	100 cm/d @$t_{initial}$	0.001	445.300	0.035	7.599	0.032	26.260	47.196	9.028	8.822
	1200 cm/d @$t_{initial}$	0.001	434.320	26.455	7.054	0.429	21.422	45.151	9.067	8.950
	1200 cm/d DUP @$t_{initial}$	0.000	427.000	27.380	7.031	0.459	21.715	46.278	9.121	8.870
2	50 cm/d @$t_{initial}$	0.004	446.520	20.428	6.728	3.186	19.215	38.811	9.008	8.950
	100 cm/d @$t_{initial}$	0.002	446.520	19.536	7.936	1.220	27.247	47.465	9.009	9.233
	1200 cm/d @$t_{initial}$	0.001	434.320	23.811	7.558	2.661	25.364	44.874	9.070	9.045
	Manifold 1 @$t_{initial}$	0.000	419.680	30.083	6.839	0.078	21.414	47.608	9.126	8.797
	Manifold 2 @$t_{initial}$	0.000	422.120	29.508	7.735	0.019	28.137	52.913	9.046	9.077
	Method Blank @$t_{initial}$	0.000	10.980	0.066	0.087	0.000	0.010	0.000	0.044	0.184
1	50 cm/d @t_{final}	0.002	462.380	0.138	7.775	18.049	20.806	8.050	9.184	8.755
	100 cm/d @t_{final}	0.007	469.700	0.122	7.872	16.220	20.429	5.961	9.173	8.797
	1200 cm/d @t_{final}	0.011	174.460	0.034	8.092	19.238	24.271	7.419	9.142	4.131
	1200 cm/d DUP @t_{final}	0.008	191.540	0.023	7.730	19.067	20.483	7.305	9.168	4.317
2	50 cm/d @t_{final}	0.001	169.580	0.048	8.112	19.447	23.973	10.481	9.083	4.100
	100 cm/d @t_{final}	0.002	456.280	0.091	7.503	18.610	20.510	9.378	9.216	8.674
	1200 cm/d @t_{final}	0.004	458.720	0.163	7.740	17.648	20.907	6.985	9.143	8.671
	Manifold 1 @t_{final}	0.000	446.520	0.028	7.611	20.147	19.819	9.645	9.176	8.540
	Manifold 2 @t_{final}	0.000	445.300	0.037	7.842	20.227	24.335	12.688	9.150	8.671
	Method Blank @t_{final}	0.000	10.980	0.000	0.078	0.000	0.030	0.000	0.043	0.183
	Detection Limits	0.004								

Manifold	Condition	Mn^{+2} [mg/L]	HCO_3^- [mg/L]	CH_3COO^- [mg/L]	Cl^- [mg/L]	NO_2^- [mg/L]	SO_4^{-2} [mg/L]	NO_3^- [mg/L]	Cations meq/L	Anions meq/L
3	0.254 mm @$t_{initial}$	0.002	428.22	38.3956	8.4645	0.1941	36.7498	48.7657	9.27659531	9.46405608
	0.508 mm @$t_{initial}$	0.002	433.1	40.2894	8.2967	0.0818	37.8534	51.0295	9.24261621	9.62845619
	3.57 mm @$t_{initial}$	0.002	436.76	37.4875	9.4963	0.178	35.3907	45.823	9.25817342	9.54162923
4	0.254 mm @$t_{initial}$	0.002	428.22	41.8576	8.5039	0.0135	38.8377	52.4778	9.3505852	9.62326846
	0.254 mm DUP @$t_{initial}$	0.002	417.24	42.1071	8.5436	0.0102	39.2067	52.9179	9.45151143	9.46336487
	0.508 mm @$t_{initial}$	0.002	430.66	40.2152	8.0653	0.1764	37.062	49.07	9.42647828	9.53465203
	3.57 mm @$t_{initial}$	0.002	445.3	40.9231	8.0218	0.1479	37.8932	50.0252	9.2765731	9.81746677
	Manifold 3 @$t_{initial}$	0.002	407.48	42.3503	8.3824	0	38.3741	53.5501	9.28619915	9.29561416
	Manifold 4 @$t_{initial}$	0.002	412.36	43.2332	9.0992	0	39.3374	54.346	9.3936691	9.44367722
	Method Blank @$t_{initial}$	0.002	9.76	0.0893	0.8852	0	0.0296	0.0347	0.04643811	0.18762751
3	0.254 mm @t_{final}	0.003	435.54	0.2151	8.7772	14.5212	32.0337	0.8526	8.5521933	8.38613632
	0.508 mm @t_{final}	0.027	436.76	0.3914	8.6312	4.4226	34.5575	0.1421	8.70134357	8.22654333
	3.57 mm @t_{final}	0.010	441.64	0.1519	8.4539	16.8106	31.1712	0.8795	9.06231817	8.50817199
4	0.254 mm @t_{final}	0.004	434.32	0.011	9.114	0.6671	36.9359	28.8753	9.05433306	8.62506397
	0.508 mm @t_{final}	0.005	429.44	0.2773	8.8525	0.1957	37.5845	18.5521	8.85797207	8.37896004
	3.57 mm @t_{final}	0.014	433.1	0.0509	8.7235	0.3534	37.2491	12.6552	8.78683351	8.33279924
	Manifold 3 @t_{final}	0.002	440.42	0.2023	7.8334	29.6946	28.1816	2.1339	9.30878965	8.70961432
	Manifold 4 @t_{final}	0.002	425.78	0.0925	8.2795	0.2757	36.3819	46.6823	9.19122351	8.73011715
	Method Blank @t_{final}	0.002	9.76	0.1736	0.009	0	0.0089	0.0784	0.04881436	0.1646127

Manifold	Condition	C.B.Error	Ca (mol/L)	CO3 (mol/L)	SI Calcite
1	50 cm/d @$t_{initial}$	2.280	3.16E-03	6.49E-06	0.79
	100 cm/d @$t_{initial}$	1.153	3.18E-03	6.66E-06	0.81
	1200 cm/d @$t_{initial}$	0.652	3.21E-03	7.28E-06	0.85
	1200 cm/d DUP @$t_{initial}$	1.399	3.24E-03	7.16E-06	0.85
2	50 cm/d @$t_{initial}$	0.325	3.18E-03	8.21E-06	0.90
	100 cm/d @$t_{initial}$	-1.228	3.18E-03	8.40E-06	0.91
	1200 cm/d @$t_{initial}$	0.137	3.21E-03	1.13E-05	1.04
	Manifold 1 @$t_{initial}$	1.834	3.24E-03	3.22E-13	-6.50
	Manifold 2 @$t_{initial}$	-0.170	3.19E-03	3.24E-13	-6.51
	Method Blank @$t_{initial}$	-61.554	2.13E-05	8.42E-15	-10.27
1	50 cm/d @t_{final}	2.389	3.25E-03	9.32E-06	0.96
	100 cm/d @t_{final}	2.093	3.25E-03	7.52E-06	0.87
	1200 cm/d @t_{final}	37.750	3.24E-03	4.97E-06	0.69
	1200 cm/d DUP @t_{final}	35.979	3.24E-03	5.46E-06	0.73
2	50 cm/d @t_{final}	37.799	3.20E-03	3.19E-06	0.49
	100 cm/d @t_{final}	3.025	3.26E-03	6.67E-06	0.82
	1200 cm/d @t_{final}	2.650	3.23E-03	1.14E-05	1.05
	Manifold 1 @t_{final}	3.592	3.24E-03	4.12E-06	0.61
	Manifold 2 @t_{final}	2.687	3.23E-03	4.50E-06	0.64
	Method Blank @t_{final}	-62.033	2.09E-05	8.42E-15	-10.28
	Detection Limits				

Manifold	Condition	C.B.Error	Ca (mol/L)	CO3 (mol/L)	SI Calcite
3	0.254 mm @$t_{initial}$	-1.0002895	3.25E-03	9.47E-06	0.97
	0.508 mm @$t_{initial}$	-2.0446108	3.25E-03	9.15E-06	0.95
	3.57 mm @$t_{initial}$	-1.5077595	3.28E-03	7.33E-06	0.86
4	0.254 mm @$t_{initial}$	-1.4371527	3.32E-03	1.06E-05	1.03
	0.254 mm DUP @$t_{initial}$	-0.0626673	3.31E-03	1.04E-05	1.02
	0.508 mm @$t_{initial}$	-0.5705026	3.33E-03	7.56E-06	0.88
	3.57 mm @$t_{initial}$	-2.832788	3.30E-03	8.38E-06	0.92
	Manifold 3 @$t_{initial}$	-0.0506679	3.28E-03	6.38E-06	0.80
	Manifold 4 @$t_{initial}$	-0.2654733	3.32E-03	5.62E-06	0.75
	Method Blank @$t_{initial}$	-60.320433	2.32E-05	7.48E-15	-10.28
3	0.254 mm @t_{final}	0.9803622	2.98E-03	7.65E-06	0.84
	0.508 mm @t_{final}	2.80484059	3.00E-03	7.85E-06	0.85
	3.57 mm @t_{final}	3.15384588	3.19E-03	7.07E-06	0.83
4	0.254 mm @t_{final}	2.4280754	3.18E-03	7.45E-06	0.85
	0.508 mm @t_{final}	2.7789866	3.13E-03	5.72E-06	0.73
	3.57 mm @t_{final}	2.65212618	3.08E-03	8.53E-06	0.90
	Manifold 3 @t_{final}	3.32535186	3.32E-03	8.68E-06	0.94
	Manifold 4 @t_{final}	2.57294573	3.31E-03	1.06E-05	1.02
	Method Blank @t_{final}	-54.256634	2.44E-05	7.48E-15	-10.26

Appendix 32: Total Lipid Biomass for GPR Sandbox Experiment

Location: Sanbox
Date of Core Extraction 1-Oct
Date of PLFA Extraction 22-Jul
Date of PLFA Absorbance 31-Jul

Standards Conc	Abs	Conc	Abs
0	0.063	0	0.065
1.5	0.095	1.5	0.096
3	0.124	3	0.124
6	0.18	6	0.18
10	0.257	10	0.264
15	0.352	15	0.352

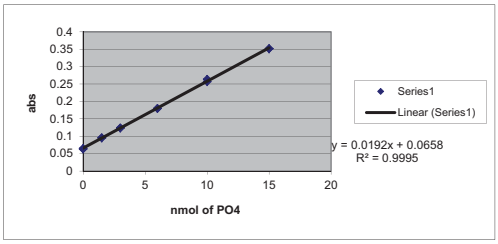

Sample	Mass weighed (g dry sediment)	Depth from surface (cm)	Absorbance	Amount of Phosphate nmol	Average normalized Phosphate (nmol)	Biomass (Dobbs&Findlay 1993)	High Value	Average
1-1	2.0076	5	0.132	3.44791667	0.93991209	5.84E+07	3.43E+09	9.55E+08
1-1D	2.0043		0.072	0.32291667		5.48E+06	3.22E+08	
1-2	2.0044	15	0.162	5.01041667	1.48538711	8.50E+07	5.00E+09	1.51E+09
1-2D	2.0069		0.084	0.94791667		1.61E+07	9.45E+08	
1-3	2.0058	25	0.106	2.09375	0.62776007	3.55E+07	2.09E+09	6.39E+08
1-3D	2.0098		0.074	0.42708333		7.23E+06	4.25E+08	
1-4	2.0018	35	0.072	0.32291667	0.10922482	5.48E+06	3.23E+08	1.11E+08
1-4D	2.0037		0.068	0.11458333		1.94E+06	1.14E+08	
2-1	2.0047	5	0.071	0.27083333	0.03115964	4.59E+06	2.70E+08	3.17E+07
2-1D	2.0069		0.063	-0.1458333		-2.47E+06	-1.45E+08	
2-2	2.0037	15	0.106	2.09375	0.44735747	3.55E+07	2.09E+09	4.55E+08
2-2D	2.0013		0.06	-0.3020833		-5.13E+06	-3.02E+08	
2-3	2.009	25	0.074	0.42708333	0.21275977	7.23E+06	4.25E+08	2.16E+08
2-3D	2.0057		0.074	0.42708333		7.24E+06	4.26E+08	
2-4	2.0063	35	0.06	-0.3020833	0.13491411	-5.12E+06	-3.01E+08	1.37E+08
2-4D	2.0086		0.082	0.84375		1.43E+07	8.40E+08	
2-5	2.004	45	0.067	0.0625	0.17400934	1.06E+06	6.24E+07	1.77E+08
2-5D	2.0068		0.078	0.63541667		1.08E+07	6.33E+08	
3-1	3.0022	5	0.189	6.41666667	1.12111508	7.27E+07	4.27E+09	1.14E+09
3-1D	3.0093		0.072	0.32291667		3.65E+06	2.15E+08	
3-2	3.0092	15	0.101	1.83333333	0.35856226	2.07E+07	1.22E+09	3.64E+08
3-2D	3.0044		0.072	0.32291667		3.65E+06	2.15E+08	
3-3	3.0081	25	0.085	1	0.2460398	1.13E+07	6.65E+08	2.50E+08
3-3D	3.0038		0.075	0.47916667		5.42E+06	3.19E+08	
3-4	3.0075	35	0.069	0.16666667	0.0554585	1.88E+06	1.11E+08	5.64E+07
3-4D	3.003		0.069	0.16666667		1.89E+06	1.11E+08	